UNIVERSITY OF GLASGOW

DEPARTMENT OF CIVIL ENGINEERING

"" FLOW IN TWO-STAGE CHANNELS WITH THE MAIN CHANNEL SKEWED TO THE FLOOD PLAIN DIRECTION ""

A THESIS SUBMITTED IN FULFILMENT OF THE
REQUIREMENTS FOR THE DEGREE OF
DOCTOR OF PHILOSOPHY
IN CIVIL ENGINEERING

BY

HASAN KADHEM JASEM B.Sc. , M.Sc.

JUNE 1990

"" To My Family ""

"Brother and Sisters"

ACKNOWLEDGEMENTS

I would like to express my appreciation to the head of department, Dr D.R. Green, and also to Professor H.B. Sutherland and Professor D. Muir Wood for the opportunity to do this work and for the use of departmental facilities.

I wish to express my sincere thanks to my supervisor, Dr. D.A Ervine, for his invaluable advice, encouragement and help throughout the course of this work. His concern for me during difficult situations is also much appreciated.

My thanks go to Dr J.G. Herbertson for his advice during the experimental work. Thanks also go to Mr. G. Irving, and to my friend Miss J. Sutherland, previous and current computer managers, for their suggestions during the development of the computer program.

I would like to thank the Chief Technician in the Soils and Hydraulics Lab, Mr W. Henderson and his Assistant Mr. T. Montgomery for building the experimental apparatus. My thanks also go to the Electrical Chief Technician in civil Engineering Department Mr. I. Todd and his Assistant Mr. A. Yuill. My thanks go to Miss M. Hoolighan (librarian in Glasgow University) for her effort in typing most of this thesis.

Many thanks also to my friends and fellow research students Dr. S. Saka, Glasgow Dental Hospital and School, Dr. S.W.T Ahmed, Mr. M. Wei, O.A. Awoleye, E. Osman, S.E. Djellab, R. Manaa, K. Belkheir, A. Bensalem, B. Famiyesin, A.R. Khan, A. Bensmail, Mr. M. Bouazza, Mr. W. Withers, Mr. J. Wark, Dr. Y.R. Fares and Mr. Lorena.

The financial support of the Iraqi Government is gratefully acknowledged.

Last, but not least, I acknowledge with humble gratitude the boundless patience and encouragement of my brother and sisters to whom I dedicate this work.

SUMMARY

The work of this thesis is an experimental study of flow in a compound or two– stage channel, where the flow in the main channel is skewed slightly to the flood plain flow direction. The purpose of the study is to investigate flow mechanisms and flow behaviour in a situation which is more complex than a straight/parallel compound channel and less complex than meandering compound channel. In other words, an element of "cross over" flow is introduced, where the flood plain flow crosses over a skewed main channel beneath. This element is absent in study of a straight and parallel channel/flood plain system.

The thesis begins by introducing the subject of two– stage channels and river flooding in Chapter 1, followed by a literature survey in Chapter 2. The literature survey attempts to draw together various strands of two– stage channel research including stage– discharge assessment, lateral turbulent shear, bend behaviour for inbank and overbank situations, and flow behaviour in the cross– over region.

Chapter 3 describes the experimental rigs used during the experiments including the main flume for the skewed compound channel flow tests, and also a smaller straight flume with a slot of variable length in the main bed, designed to simulate certain aspects of cross– over flow. This chapter emphasises the instrumentation used to measure accurate point velocities and accurate streamline angles throughout the flow field. Both these measurements were crucial in determining transverse velocity components.

Chapter 4 describes flow resistance and stage– discharge data for the skewed compound flume with both smooth and rough flood plains, and also the skewed main channel operating in isolation from adjacent flood plains. An analysis of drag coefficients for the vertical roughening rods for the flood plain is also presented.

Chapter 5 presents the experimental data of longitudinal velocities throughout

the flow field and transverse velocities within the skewed main channel, for the case of both smooth and rough flood plains. Observations are made on the asymmetry of the longitudinal velocity profile, the magnitude of transverse velocity components, as well as variations in the downstream direction.

Chapter 6 concentrates on flow measurements in a smaller flume with a slot in the channel bed, representing an idealised version of flow crossing– over the skewed main channel. Measurements are presented of variations in water surface level, energy losses at the expansion and contraction region as well as velocity measurements at various sections throughout the slot region in an attempt to produce a universal velocity profile.

Finally Chapter 7, attempts to draw together experimental evidence in Chapter 4, 5,and 6, to draw some conclusions about the behaviour of two– stage channels. This is done by putting forward ten ideas on the behaviour of two– stage channels involving stage– discharge assessment for the smooth boundary case, stage– discharge assessment for the rough boundary case, flow resistance concepts for two– stage channels, deviation of the flood plain streamlines in the cross– over region, entrainment of flood plain flow down into the main channel flow, the magnitude and distribution of secondary circulation within the skewed main channel (and how this is influenced by boundary roughness, aspect ratio and relative flow depth), the magnitude and distribution of the depth– averaged longitudinal velocity (including comparison of left and right flood plain velocities, position of maximum velocity filament, width of lateral shear layers on either flood plain), variations of flow behaviour in the downstream direction, application of the results to two– stage channel design and finally some speculations on the longer term behaviour of two– stage channels from the viewpoint of scouring and deposition of bed load and suspended sediment.

The thesis shows very clearly that flow in a skewed compound channel, even at a small skew angle of 5.84^{0}, is in many ways dissimilar to flow in the straight/parallel case. This is highlighted in the magnitude of secondary cells in the skewed main channel, deviation of flood plain streamlines, greater horizontal shear and less lateral shear between main channel and flood plain and asymmetry of the depth– averaged velocity. This thesis also reveals a very limited application of energy losses at a slot in the channel bed to a skewed cross– over flow situation.

TABLE OF CONTENTS PAGE No.

LIST OF FIGURES

CHAPTER 1

CHAPTER 2

CHAPTER 3

CHAPTER 4

CHAPTER 5

CHAPTER 6

CHAPTER 7

LIST OF TABLES

CHAPTER 4

CHAPTER 6

NOMENCLATURE

A = cross sectional area

A_1 = cross-sectional area of section 1

A_2 = cross-sectional area of section 2

A_c = main channel cross section area

A_f = flood plain cross section area

A_T = total area for compound cross section.

B = constant value

B_c = channel width

B_f = flood plain width

B_s = slot width

C = Chezy coefficient

C_d = drag coefficient

αC_d = the effective drag coefficient of rods

C_e = expansion coefficient

C_L = contraction loss coefficient

d_0 = diameter of the orifice plate

d = diameter of dowel rods

F_{tot} = total drag force

F_r = Froude Number of the flow

g = gravitational acceleration

h = bank-full depth

h_c = contraction loss

h_e = expansion loss

h_f = head loss

h_L = bend energy loss

h_s = slot depth

h_T = expansion and contraction loss

K_c = coefficient of flood plain discharge

K_e = expansion loss coefficient

K_f = coefficient of main channel discharge

K_s = the equivalent sand grain roughness size

ℓ_s = characteristic length scale

N = number of rods per unit channel length

n = Manning's roughness

n_1 & n_1 = number of rods across channel/flood plain, rows 1 and rows 2

P = wetted parameter

Q_1 = discharge of flow in section 1

Q_2 = discharge of flow in section 2

Q_c = main channel discharge

Q_f = flood plain discharge

Q_T = total discharge

R = hydraulic radius

R_c = the hydraulic radius of main channel

R_f = the hydraulic radius of flood plain

R_e = Reynold's Number

r = radial direction

r_m = bend radius

S = longitudinal slope of the channel

S'' = bend losses due to secondary current

S_r = radial water surface slope

U = the mean velocity over flow depth

U_c = the mean channel velocity

U'_c = mean channel velocity during the interaction

U_f = the flood plain velocity

U'_f = flood plain velocity during the interaction

u_n = normal velocity approaching the slot

u_s = averaged velocity for main channel and flood plain velocity during the interaction.

u' = fluctuation velocity components in x direction

u_* = shear velocity

V = mean velocity upstream the slot

V_m = maximum velocity

V_r = the recirculation velocity

v' = fluctuation velocity component in y direction

Y_b = normalising depth

Y_c = main channel depth

Y_f = flood plain depth

W = width of the shear layer

Z_* = the ratio of flow depth to rod diameter

α = velocity distribution coefficient

β_1 & β_2 = the blockage effect.

ϵ = turbulent eddy viscosity

ϵ_{yx} = is the depth averaged lateral eddy viscosity

λ = friction factor

λ_b = friction factor rising from the drag at the solid surface.

λ_e = equivalent friction factor value

λ_w = friction factor values for the wall material

ρ = specific mass of fluid

τ_a = apparent shear force

τ_{yx} = shear stress in y direction

τ_{zx} = shear stress in z direction

δ = Prandtl mixing length

θ = skew angle

Φ_c = correction factor for main channel

Φ_f = correction factor for flood plain

Φ = deviation angle

ν = kinematic viscosity

CHAPTER ONE

INTRODUCTION

CHAPTER 1

INTRODUCTION

1.1 RIVER AND FLOOD PLAINS.

The relationship between human civilisation and rivers has always been close, simply because water is such an essential natural resource. Most early civilisations depended on the farming of crops and animals, so that people tended to settle in areas where there were good supplies of both fresh water and fertile land. The result was that many of the large early civilisations developed in or near large river valleys, such as the Tigris and Euphrates, the Nile and the Yellow River.

As civilisation has developed and the world population has increased, the demands on the world river systems to satisfy our needs has also increased. In the modern worlds, rivers are used for many purposes which are often not complimentary to each other. These uses include navigation, hydro– electricity generation, irrigation, water supply for consumption and industrial applications and the disposal of wastes. In the past the use of rivers as a resource has not been adequately planned or managed, with the result that many rivers have become unfit for many or all uses.

Many communities have developed alongside rivers, in areas which tend to be on the low lying flood plain areas adjacent to the river, as they usually provide good access to water supplies, transportation, waste disposal, river crossings and/or fertile soils. Flood plains are a product of the natural environmental processes of erosion and sedimentation and at times when the flow in the river exceeds the capacity of the main channel, the excess water flows onto the flood plain.

The floods which occur at these times of high flow can have serious consequences, resulting in the loss of life and damage to property. The financial costs to the community from flooding can be very high due to the disruption to industries and services, such as water supply, electricity and communications. Flooding also poses a serious health risk as water supply systems become contaminated with sewage and other wastes. In order to decrease the adverse impacts to the community from flooding, it is important that land use and development on flood plains are effectively managed. As well as providing direct community benefits, river and flood plain management is important in the protection of the natural environment. Flood plains, which are low lying areas,

naturally provide flood storages which form wetland environments. With the increase in development of rural areas, these wetland environments are increasing in the conservation significance and it is important that effects on these environments from development and land uses are adequately controlled. Management is also important in controlling contamination of river waters by sewage and other hazardous wastes.

In the management of rivers with flood plains, it is important to understand the flow conditions which exist in the natural river, as well as those which will exist after the planned development. In some natural rivers it may take many years for the full impact of these flow conditions to become apparent after development.

1.2 FEAR OF FLOODS.

The floods of January and February of 1990 have reminded the British public once more that rivers exist, that occasionally rivers over flow their banks unto adjacent flood plains, and that river floods have devasting power to endanger human life, damage property and agricultural land.

Such perception has been intermittent in the mind of the public since the end of World War II. On March 16th, 1947, melting snow swelled the rivers in the Fenland region of England near the Wash. Many rivers burst their banks causing several hundred thousand acres to be inundated with water, and families made homeless. It was thought to be the worst fen flood for 300 years, and it sparked off a programme of dredging and clearance in rivers which according to Purseglove (1989) has been an ecological disaster, in the sense that rivers have been turned into drains.

In February 1953 floods struck Britain again mainly on the East coast. A total of 307 people were killed along a length of coast from Northumberland to Kent, and many thousands left homeless.

The Lynmouth flood in Devon occurred on 15th August 1953. In a 24 hour period an average of 143mm of rainfall fell on the catchment. The flood killed 37 people and swept away various buildings and bridges. The flooding problem was thought to have been exacerbated by fallen trees blocking bridges in narrow valleys upstream. It sparked off a programme of tree clearance in upstream catchments in case of duplication of such an event.

In more recent times the public perception of river floods has been heighened in the international scene by the massive floods in Banghaladesh in 1988 when the river burst its banks in several locations causing 25 million people to be made temporarily homeless. In this instance the problem was greatly exacerbated by a large scale tree harvesting programme in the upland reaches of the river.

Removal of trees had the dual effect of absorbing less rainfall as well as causing more soil erosion, which in turn silted up the river bed causing further rises in river water level. An international effort is now under way to resolve the crisis.

On entering the final decade of the twentieth century a new and more potentially damaging scenario is being discussed. That is, global warming and the possibility of rising sea water levels. Global warming is already under way, mainly due to burning carbon products, such as coal and gas, which is producing gases which rise high into the upper atmosphere causing a halo effect around the earth and producing a sort of global greenhouse.

The fear is that rising temperatures will result which will melt the ice caps to cause rising sea levels. Sea level rises between 0.5 and 1.0 metre are predicted for the year 2030. Rising sea levels will in turn increase the possibility of river floods, especially in low lying urban areas near estuaries.

It becomes important, therefore, to control existing or future river floods in a way that will not be damaging to the river environment. This is the background to carrying out the work on two– stage channels in this Thesis.

1.3. CONTROLLING FLOODS.

It is clear that if mankind continues to gravitate towards flood plain areas, then some degree of flood control is necessary if damage to human life and property is to be avoided. We are becoming increasingly aware, however, that certain forms of river flood control management are damaging to the environment. For instance, one of the most common types of flood control is to form higher banks at the edge of rivers.

These are known sometimes as levees and are usually in the form of earth dykes, although in urban areas they may be concrete walls. Their purpose is to prevent overtopping and lateral flood flow into riverside communities.

Purseglove (1989) shows in Fig (1.1a) overleaf how this problem is typically

handed by River Engineers. The new banks are placed too close to the rivers edge, trees near the rivers edge disappear, wetlands at the rivers edge disappear, new banks are sown with expensive grasses, and above all, the flooding problem is often transferred downstream. The latter effect is due to less attenuation of the flood peak because part of the flow does not go into temporary storage on adjacent flood plains.

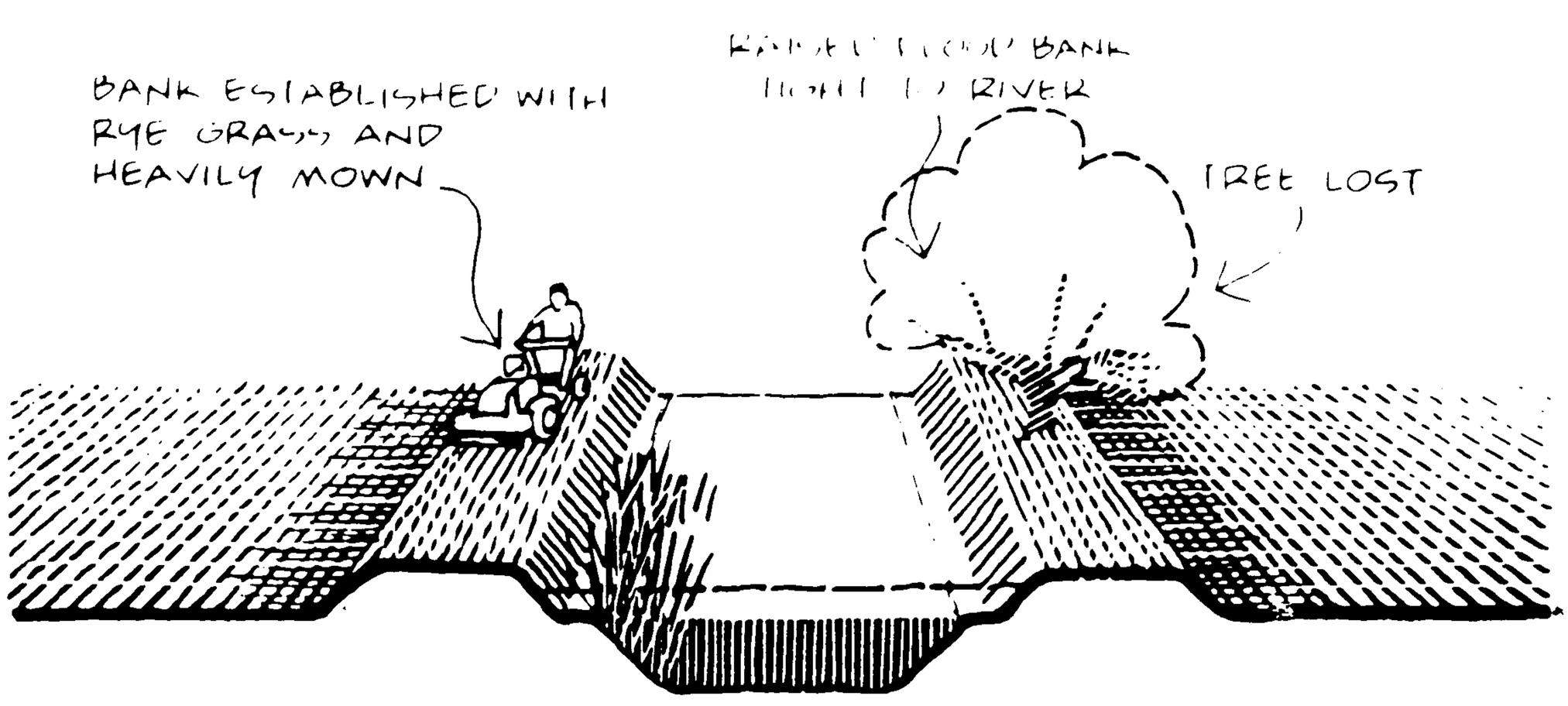

Fig (1.1a) Poor River Management.

Many of the negative points introduced by the higher banks in Fig(1.1a) above can be overcome by a simple expedient shown in Fig (1.1b) below. The new raised flood bank is set behind the line of existing trees, + a wetlands region is created in the form of a side berm with grass planted. The berm region now provides some extra storage, a certain degree of flood wave attenuation and the line of trees remains intact.

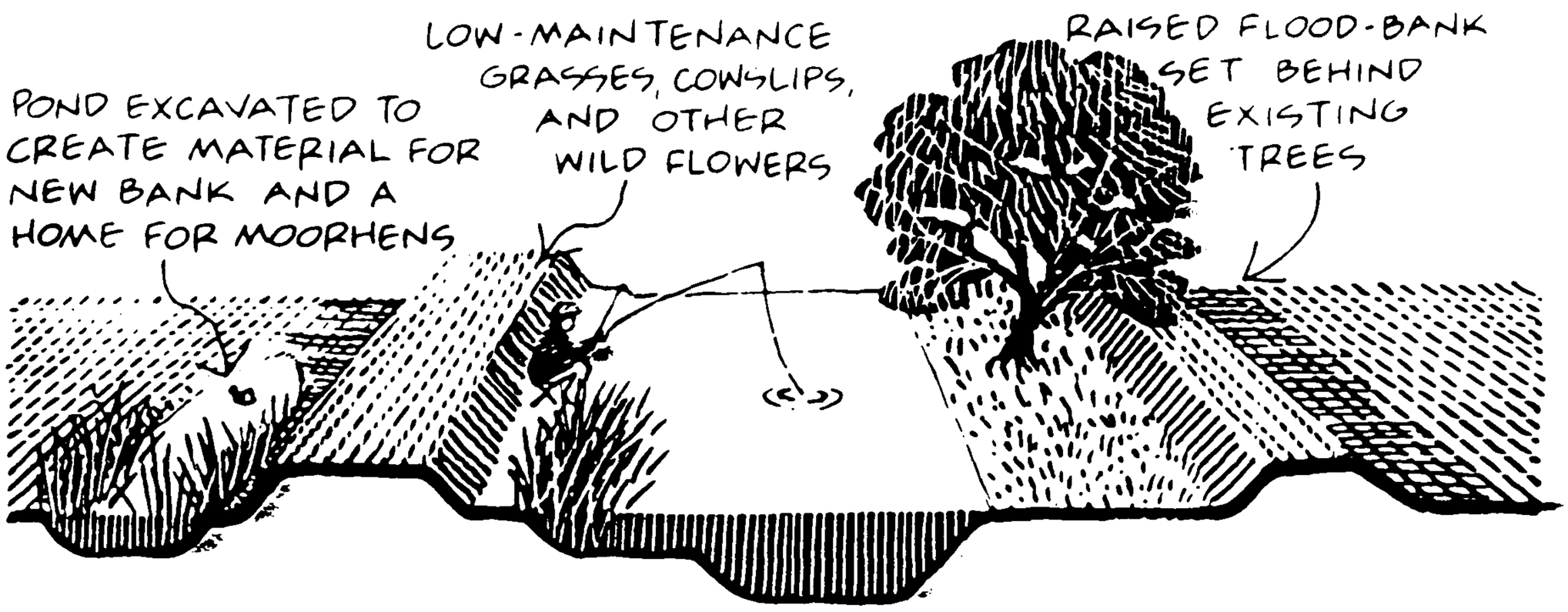

Fig (1.1b) Better River Management Practice.

Another example of flood control concerns the deepening, (dredging), widening and straightening of meandering rivers which cause occasional flooding problems. This is sketched below in Fig (1.2), illustrating a flood control or flood prevention technique which solves the flooding problem by changing the natural meandering system into an efficient drain. The river is canalised, and in doing so the natural ecological system is profoundly disturbed perhaps irreversibly so. This effects plant life, weeds on the river bed, wetlands at river edge, fish life, sediment transport rate along the new efficient canal section, as well as removal of trees. It raises a question of conflict between solving a flooding problem and causing damage to the environment.

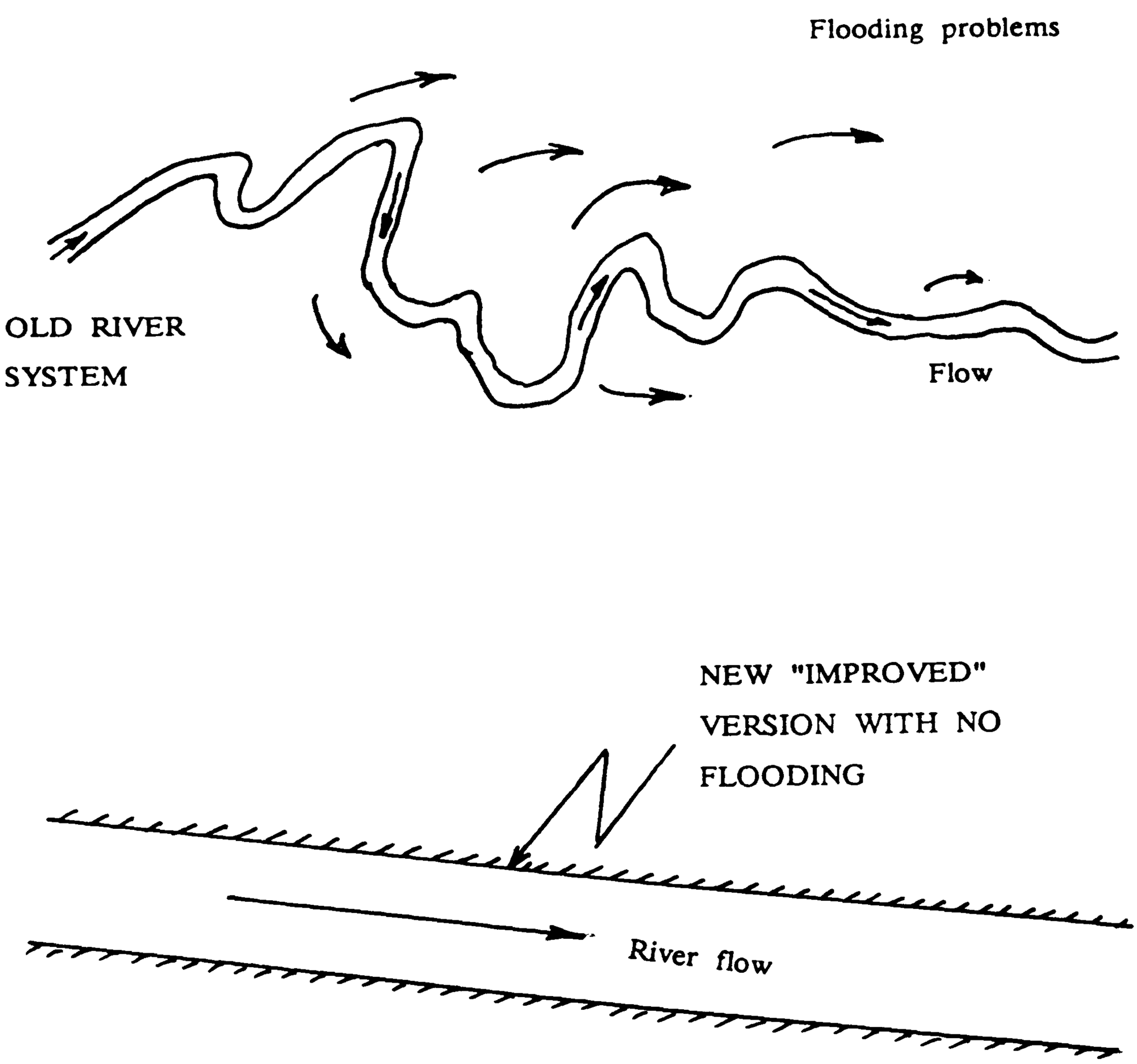

Fig (1.2) The Old and New River System.

The challenge is to provide better solutions to the flooding problem above. Solutions which will reveal a more sensitive approach by Engineers, solutions which will allow local people to feel that their stretch of river has not been desecrated, solutions which will allow anglers continued fishing in the pool/riffle bed forms of the original river and solutions which will allow the natural habitat to be preserved as much as possible. Two stage channels are one such possible solution. Before discussing two– stage channels, it is worth mentioning another common method of flood control. That is the use of reservoirs and flood plain detention basins to provide temporary storage of flood waters.

Perhaps the simplest example of this method of flood control is the construction of a regulating reservoirs in the catchment river upstream of the flood protected zone.

Normally the level of water in the reservior upstream of the dam is maintained at a depth which would enable the reservoirs to act as a storage basin during times of extremely high rainfall. Occasionally due to the flat topography of the catchment, it is not always possible to construct a regulating reservoir and on such occasions the construction of the smaller detention basin adjacent to the flood plain, (upstream of the flood protected area) is a feasible alternative. Such detention basins are constructed at such an elevation as to allow flow laterally into the basin as extreme flooding occurs. As the water level rises, the peak of the flood wave is diverted to the detention basin, and later on, as the flood diminishes, the excess volume is released back into the river. Sometimes the flood plain can be improved to act more efficiently as a storage basin and thus attenuate the flood peak by temporary storage.

1.4 TWO– STAGE CHANNELS – AN ENVIRONMENTAL SOLUTION.

A new more environmentally sensitive method of coping with river floods is the two– stage channel. A good example is the river roding in Essex sketched in Fig (1.3a). The existing river may be causing flood problems, and a normal solution would be to straighten, widen or deepen the river. Instead, a two– stage channel solution was adopted. In this case, the river is kept meandering more or less as before, allowing the retention of fish, insects and water voles. Berms were cut back over the dotted area shown, out as far as the edge of the meanders. The dotted area (overleaf) was then planted as grassland, and was

and was designed so that the existing river would cope adequately with lower flows, and the upper berms would inundate only during high winter flows. It would be common for flow depths on this side berms to exceed 1m giving a relative flow depth (depth on the berm to depth in the main channel (Y_f/Y_c) ratio) of the order of 0.5. This is the upper limit set for experiments in this Thesis. Another example is shown in Fig (1.3b) overleaf of the River Ray in Oxford shire. In this case it was felt desirable to retain the row of trees on the left side of the river.

Hence a side berm was constructed only on the right side, and was designed to cope with the highest floods.

In the same year as the River Roding scheme was carried out (1980) a similarly pioneering two–stage channel design was executed on the Herefordshire Lugg near Leominster by the Welsh Water Authority. Over a length of several miles, the meandering source of the river was retained with flood banks which were set well back from the river. The spoil, from creating lowered berms, was used to build the new raised flood–banks. See Purseglove (1989).

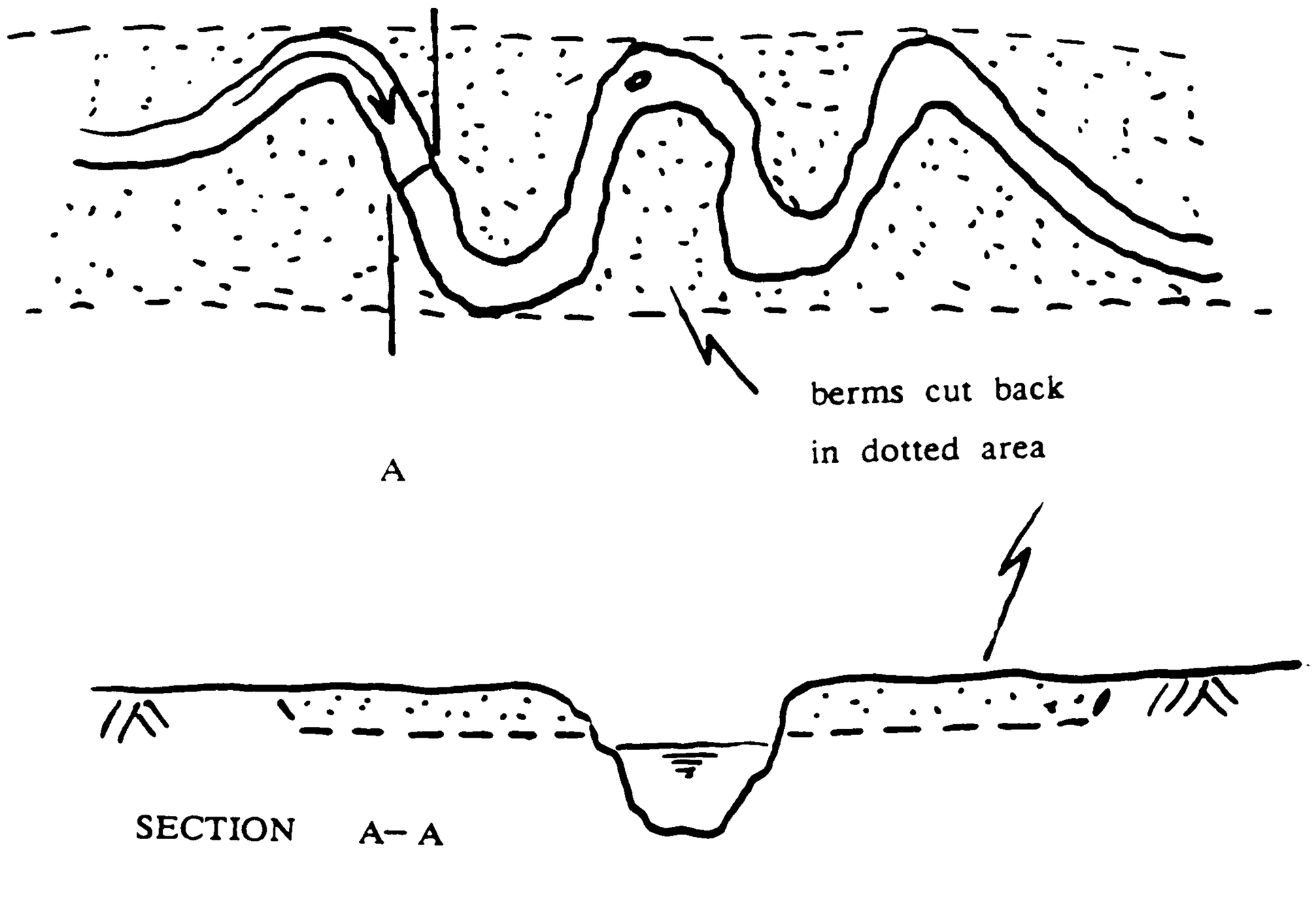

Fig (1.3a) River Roding in Essex.

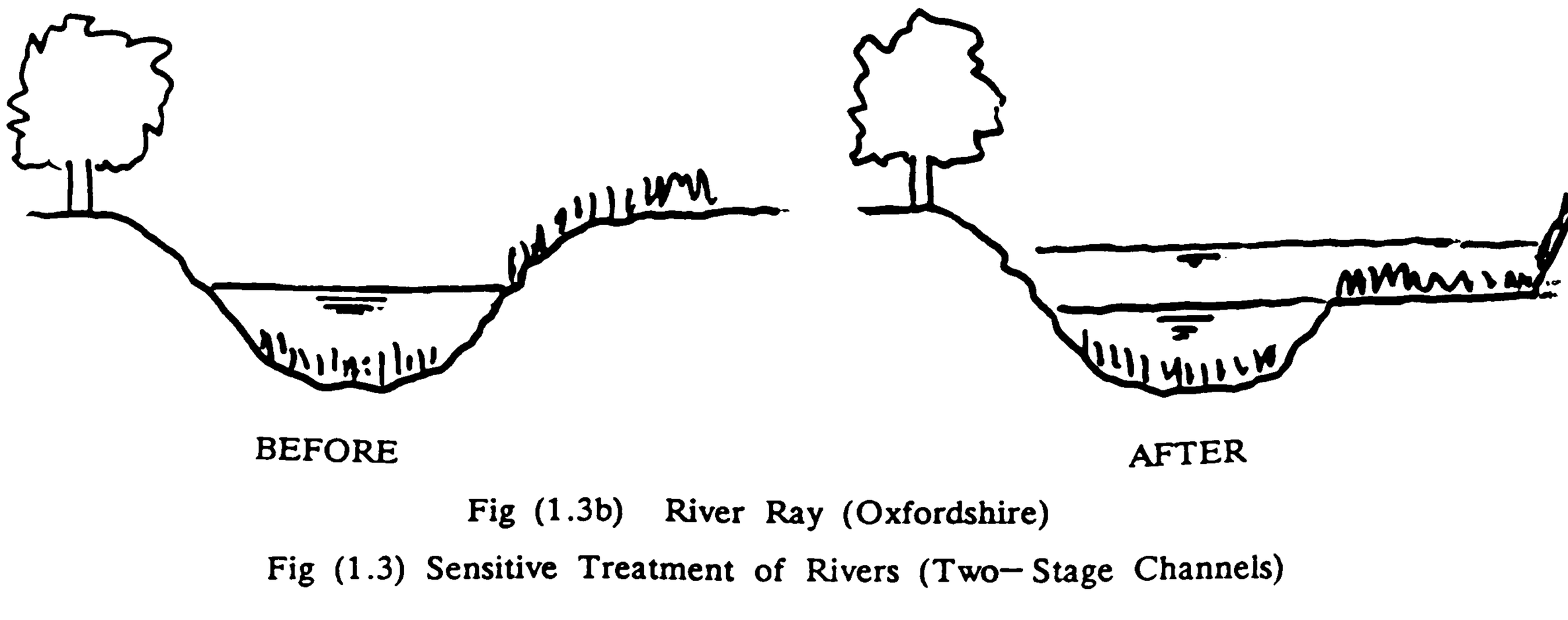

Fig (1.3b) River Ray (Oxfordshire)

Fig (1.3) Sensitive Treatment of Rivers (Two– Stage Channels)

1.5 THE PURPOSE OF THIS RESEARCH WORK.

The purpose of this research work is to investigate the flow behaviour in two–stage channels, with relative flow depth up to around 0.5. It should be noted that a choice was available as to the nature of the main river channel to be investigated. The three possible choices are shown sketched below in plan view.

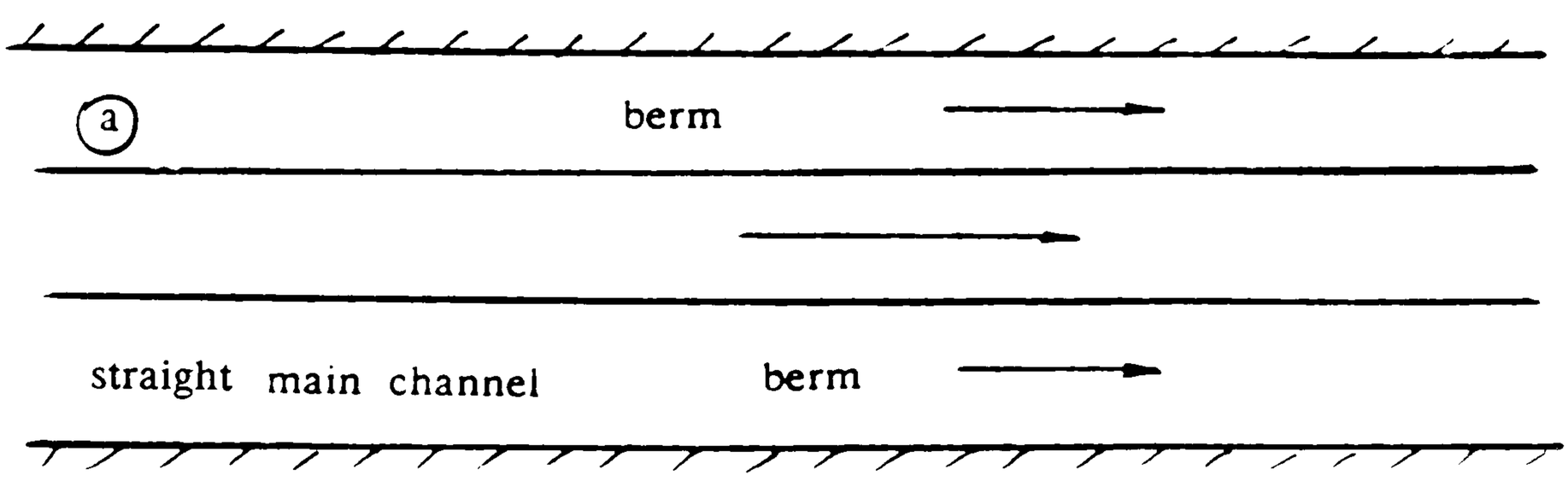

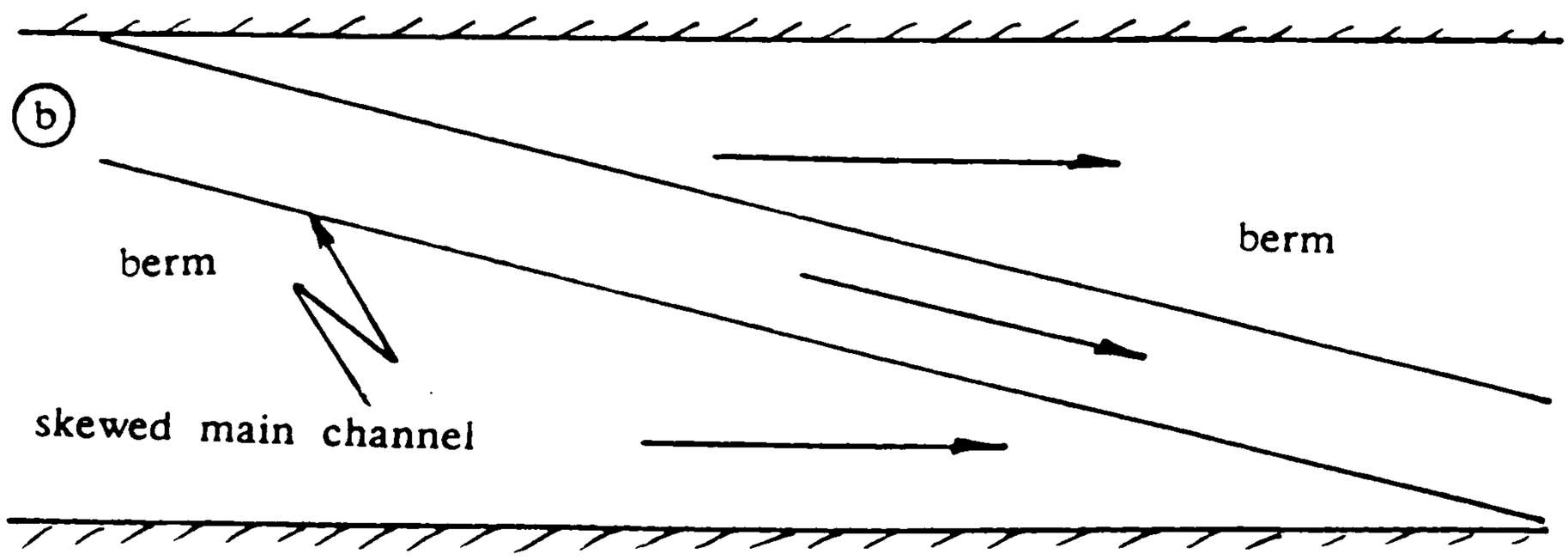

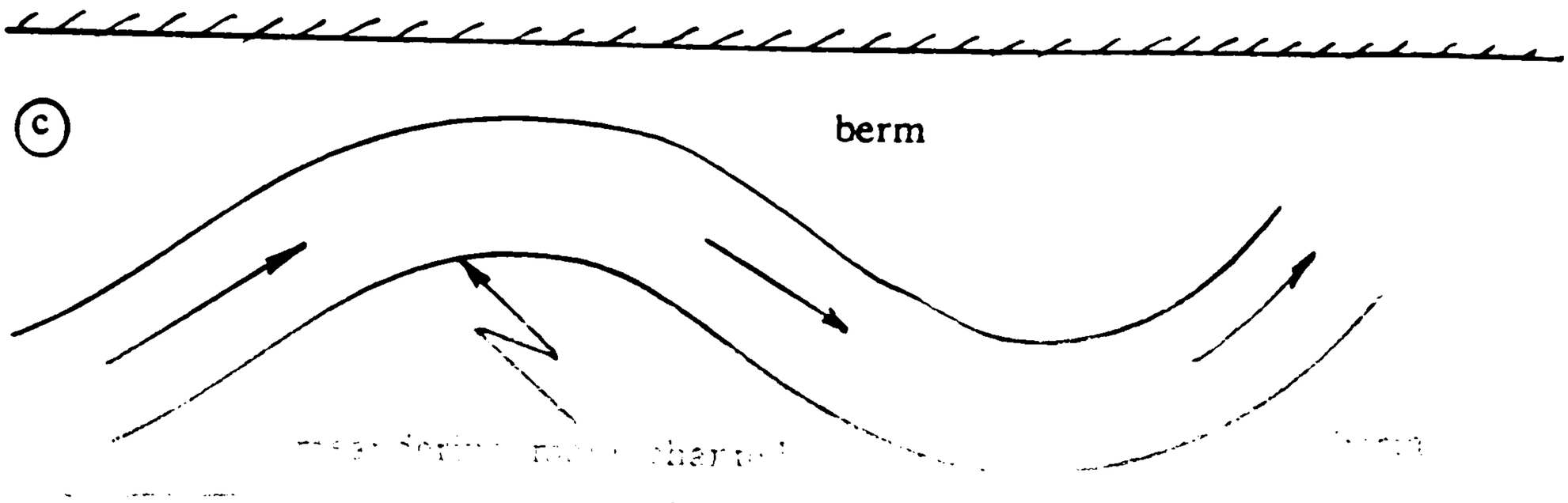

Choice (a) with a straight main channel parallel to berms offers the least complexity because the main channel/flood plain interaction will be mainly in the form of lateral shear and lateral momentum transfer. This has been investigated extensively.

Choice (b) with the main channel skewed to the flood plain (berm) direction offers one degree extra of complexity. In this case, lateral shear between main channel and side berm still exists, but it is accompanied by horizontal shear where the flood plain berm flow passes over the main channel flow beneath.

Choice (c) with the meandering main channel and side berms is closest to reality but the most complex. It contains an additional degree of complexity above choice (b), in the sense that main channel bends introduce additional circulation and interaction with the flood plain, to add to the other two already mentioned in (a) and (b) above.

At the time of commencing this work in 1986, it was decided to pursue choice (b), and as such, was a smaller scale version of work to be under taken on the SERC flume as part of the flood channels Initiative (Series A).

Having decided to opt for the skewed main channel cases, the main points of research were to be:—

(a) Stage— discharge for skewed main channel/flood plain flows.

(b) Energy loss distribution in such flow systems.

(c) Fundamental flow mechansims, such as lateral shear layers, secondary cells in the main skewed channel and horizontal shear where the berm flow passes over the main channel.

(d) Effect of the skew angle, and other geometrical parameters such as aspect ratio of the main channel, berm width to main channel width, etc.

(e) Effect of flood plain roughness.

(f) Scale effects when compared with data from the much larger scale SERC flume at Wallingford. (Series A).

(g) Flow development effects in moving in the downstream direction.

(h) Discharge assessment errors in skewed channel/flood plain systems.

In fact all the areas except (d) have been investigated in this work. It is hoped that the results of this work will be used in the design of two— stage channels as well as the varification of two— dimensional numerical models of such a system.

1.6 RELATED RESEARCH WORK.

The work of this Thesis is not an isolated piece of research but inter– related to (a) An integrated programme at the University of Glasgow (b) A national SERC funded programme of HR Ltd, Wallingford and (c) A wider international programme.

(a) Research at the University of Glasgow.

Fig (1.4a) overleaf shows the sub– division of work at the University of Glasgow. It includes this study of a skewed river channel with side berms. A study of one river bend with flood plains (or berms) is also being under taken by Lorena (1990) as part of the SERC funded Flood Channels Programme (Series B).

A computational (numerical) study is also being carried out by Wark (1988), using a two– dimensional finite element model for meandering channels and flood plains. This work is also funded by SERC through the CASE award scheme, jointly with Dr. Paul Samuels of HR Ltd, Wallingford.

(b) National SERC Funded Programme.

In 1985 the Science and Engineering Research Council decided to invest substantial research funding into river flooding, and two– stage channels in particular. It was decide to construct a large central flume facility at Hydraulics Research Limited, Wallingford. This flume is 56m long and 10m wide and carries flows up to 1 m^3/sec., as shown in Fig (1.4b) overleaf. In October 1986 the first teams of researchers were operating the flume with emphasis on straight/parallel channels with flood plains. One study by Bristol University, Sellin and Elliot (1988), however, investigated a skewed main channel with flood plains. Their work is essentially a large scale version of the work in this Thesis. It was hoped that the two separate studies Bristol and Glasgow, would complement each other, with a two– way flow of information and ideas.

(c) On a wider international level it was hoped to relate this work to research work at University College, Cork, Ireland; University of Aachen, West Germany, as well as work at work at Monash University, Australia.

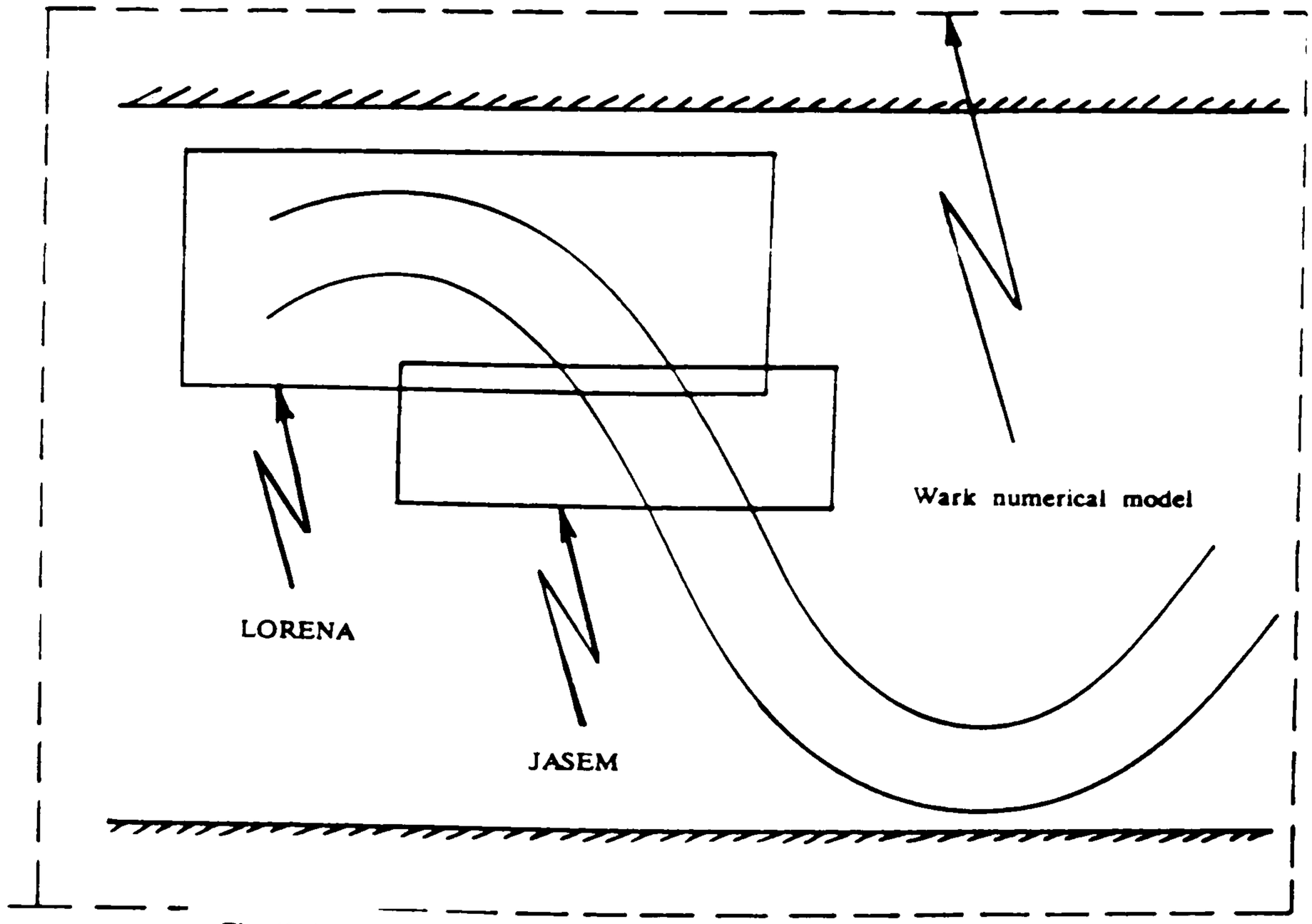

Fig (1.4a) Integrated Research Programme at University of Glasgow

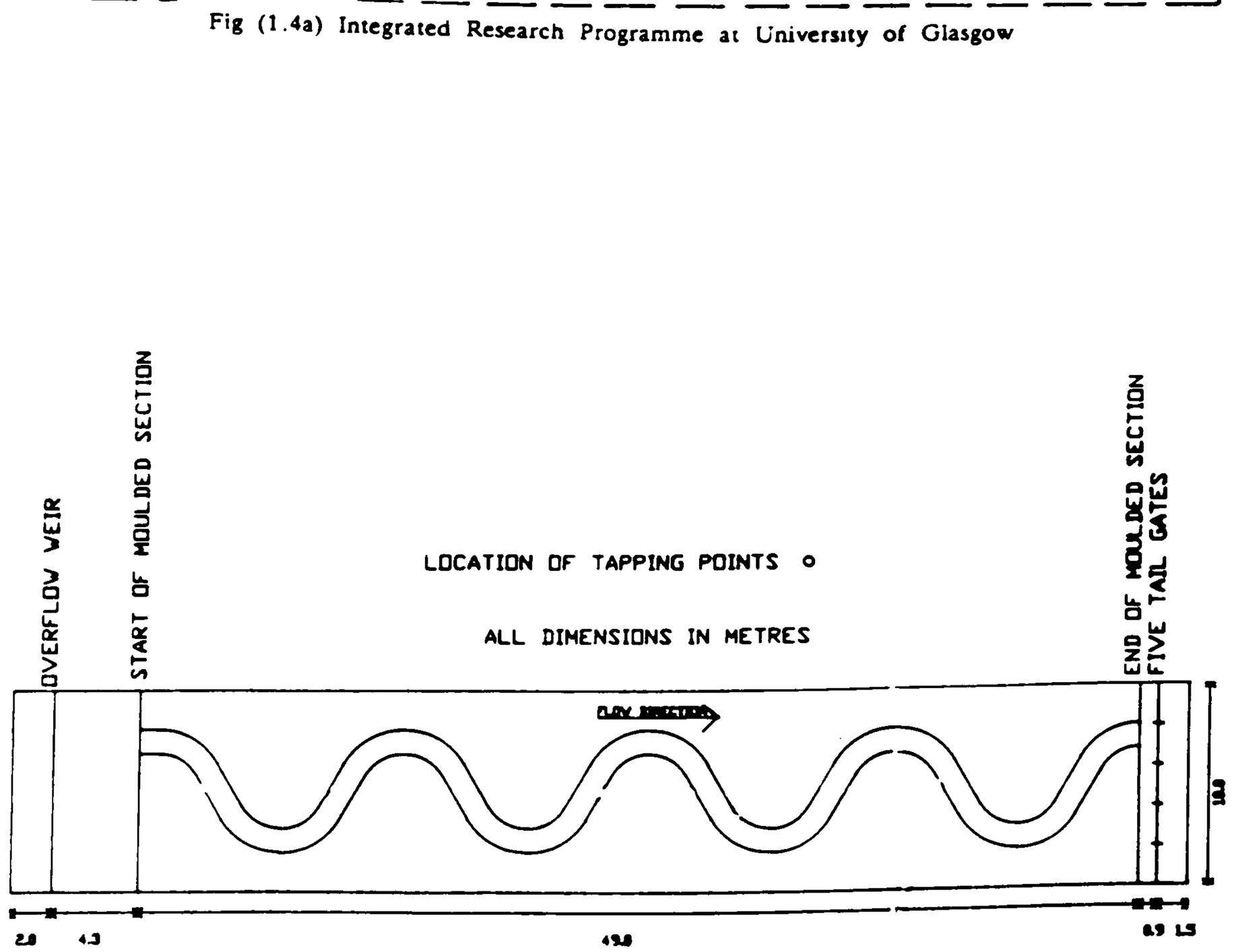

Fig (1.4b) SERC Flume Facility at Wallingford Plan View

CHAPTER 2

LITERATURE SURVEY

2.1 INTRODUCTION

2.2 FLOW MECHANISM IN A STRAIGHT MAIN CHANNEL WITH ADJACENT FLOODPLAIN.

2.2.1 The Flow Mechanism In a Straight Compound Channel .
2.2.2 The Stage Discharge Relationship .
2.2.3 Area and Depth Averaged Velocities in a Straight Compound Section.
2.2.4 The Role of Secondary Currents in Straight Compound Channels.
2.2.5 Apparent Shear Force in Straight Compound Channels.
2.2.6 Numerical Modelling of the Interaction Effect in Straight Compound Channel.

2.3 MEANDERING CHANNELS WITH FLOODPLAIN FLOW.

2.3.1 Introduction
2.3.2 Bend Behaviour For Inbank Flows.
2.3.3 Bend Behaviour For Overbank Flow.
2.3.4 Flow Behaviour at the Cross– Over Region.
2.3.5 Stage– Discharge Relationships in Meandering Channels with Floodplain Flows.
2.3.6 Velocity Distributions in Overbank Meandering Channels.
2.3.7 Numerical Models of Meandering Channel With Overbank Flow.

2.4 SUMMARY .

CHAPTER 2

LITERATURE SURVEY

2.1 INTRODUCTION

An attempt has been made in this chapter to draw together various aspects of past research in hydraulic engineering concerning the behaviour of rivers and channels during overbank flow. Apart from initial work by Zheleznyakov (1965) prior to the early sixties, very little was known of the complex flow patterns which exist between a channel and its flood plains. Recent developments have led to a clearer understanding of the hydraulic mechanisms between a straight channel and its floodplain, but still little is known about the hydraulic mechanisms in meandering channels with floodplain flow. The reason for this is not difficult to find. A meandering channel with overbank flow involves complex three dimensional flow patterns as shown in **Fig (2.1)**. The turbulent shear interaction between main channel and floodplain, which shows up clearly in the straight/parallel case is now mixed in with river bends with associated secondary currents as well as "cross–over" regions where the main channel flow is skewed in the direction of the floodplain flow. Added to this is the very wide range of meander patterns which may be chosen for investigation.

The purpose of the work in this thesis is to investigate experimentally physical flow mechanisms in the "cross–over" region of skewed main channel/floodplain flows. It should be appreciated that this represents only a sub–section of meandering overbank flow channel mechanisms, but nevertheless an important sub–section, and a substantial deviation from the straight parallel case. There appears to be four major reasons why consideration should be given to the hydraulic behaviour of the skewed and meandering channels with floodplain flow.

1. To obtain a deeper understanding, and to derive a method of predicting the nature of rating curves, or stage–discharge relationships, during the interaction of the flow between skewed or meandering channels with overbank flow.

2. To produce an understanding of how river bends behave during overbank flow, including the effect on the bend secondary currents and energy loss mechanisms (These secondary currents are in effect a large scale turbulent eddy occupying most of the cross–sectional area, giving rise to the energy loss, both in the form of internal flow friction and also boundary resistance due to transverse shear).

3. To obtain an understanding of the complex behaviour of the flow mechanisms during the flood plain flow passing over the top of the main channel flow at a given of angle skew. This behaviour is akin to a horizontal shear layer, possibly generating recirculation regions under the shear layer **(Fig (2.2))** and also losing energy in the horizontal interaction. **(Ervine and Eills 1987)**.

4. To obtain an understanding of the influence of floodplain boundary roughness. According to Sellin (1987) the floodplain roughness dominates the stage–discharge relationship during overbank flow. What effect does it have on bend flow mechanisms and cross over flow mechanisms?

In a sense, an investigation of all four areas is too broad for a single thesis, thus it was decided at an early stage of the work to concentrate on areas 1, 3 and 4, omitting a study of river bends. The latter is at present the subject of two separate studies at the University of Glasgow including Wark's two–dimensional numerical study and Lorena's experimental study of river bends during overbank flow.

2.2 FLOW MECHANISMS IN A STRAIGHT MAIN CHANNEL WITH ADJACENT FLOOD PLAINS.

2.2.1 The Flow Mechanism in a Straight Compound Channel.

The behaviour of the flow in a straight main channel with parallel flood plains has been investigated in detail over the last forty years. A summary of relevant research papers is to be found in a report **Hollingrake (1987)**.
The straight parallel work culminated in an SERC intiative in 1986, in the construction of a large flume facility at HR Ltd. Wallingford, the flume measuring 56m long and 10m wide. **Knight (1986), Sellin (1986), Myers (1986), and Wormleaton (1986)**, have been the main investigators of the flume facility to date.

The main flow mechanism during uniform steady state flow is the well–known turbulent shear interaction between the faster moving main channel section and the slower moving floodplain flow. This phenomenon is best visualised as a vertical shear layer at the channel/floodplain interface as shown in **Fig (2.3)**. Vortices with vertical axes are considered to form causing a substantial energy loss and transferring momentum usually from main channel to floodplain.

Essentially this is a turbulent diffusion process with a mixture of bed generated turbulence (due to the roughness) and lateral shear generated turbulence (due to change in cross–sectional geometry). The process near the interface is complex and three dimensional. This has been reinforced recently by Tominaga and **Ezaki (1987), Kawahara and Tamai (1988)**, and **Tominaga and Nezu (1988), (1989)** who studied the momentum transfer between the main channel and its floodplain both experimentally and numerically, and found that secondary currents were an important factor in the interaction process, particularly at higher relative depths of flow. This is illustrated in **Fig (2.4)** and will be discussed in more detail in 2.2.4.

2.2.2 The Stage Discharge Relationship.

It is not applicable to use Manning's equation for stage– discharge estimation in a compound cross– section as shown in **Fig (2.5)**. At low floodplain depths, the hydraulic radius **R (A/P)** suddenly increases, and if the discharge is estimated as a single channel then great errors will ensure. The commonest method to overcome this is to insert imaginary vertical walls with friction, and to compute the discharge in each sub– section of the flow, as shown in **Fig (2.6)**. This method has been advocated by **Chow (1959)** and has the advantage of enabling different boundary roughnesses in each sub– section to be taken into account. Thus the total discharge might be given by,

$$Q = \frac{1}{n} A_1 R_1^{2/3} S^{1/2} + \frac{1}{n} A_2 R_2^{2/3} S^{1/2} + \frac{1}{n} A_3 R_3^{2/3} S_{1/2}$$

---------- (2.1)

Equation 2.1 is not accurate, especially at lower values of relative depth Y_f/Y_c (Y_f/Yc = floodplain depth/ main channel depth), due to turbulent interaction effect.

The **U.S Army** Engineers Report **(1956)** was one of the earliest to investigate the stage discharge relationship as the flow exceeds bank full depth, although it was not until the work of **Sellin (1964) and Zheleznyakov (1965)** that the interaction effect between channel and floodplain showed up distinctly as a discontinuity in the stage– discharge relationship, revealing that Manning's equation was not applicable directly to the overbank flow situation.

Zheleznyakov (1965) found that the effect of the interaction increases to a maximum at low flood plain depth, and decreases with subsequent increases in the flood plain depth. He stated the value of the relative depth, Y_f/Y_c (where Y_c is the channel depth and Y_f is the flood plain depth) at which the reduction in channel velocity was maximum, increased with B_c/B_f, where B_c is the channel width, and B_f is the flood plain width. He found from the experiments that the channel flood plain interaction plays a significant role in the estimation of discharge velocity and resistance to flow, especially at low floodplain depths. For

shallow flood plain depths ($Y_f/Y_c = 0.166$) for instance, the channel discharge could be reduced by as much as 32% compared with the bankfull discharge. Zheleznyakov attempted to quantify the reduction in discharge due to the channel/flood plain interaction and suggested the following relationship:

$$Q = K_c\ Q_c + K_f\ Q_f \qquad (2.2)$$

where Q_c and Q_f are the discharges in the channel and the floodplain respectively, under non-interacting conditions, K_c and K_f are coefficients for the channel and the flood plain respectively. The value of K_c was found to vary between 0.6 and 1.05 and K_f was found to vary between 1.0 and 1.2.

Posey (1967) has outlined four possible methods which might be used to calculate the main channel and floodplain discharge:-

(i) Consider the whole cross-sectional area of the compound channel and divide it by the total wetted perimeter (single channel method).

(ii) Divide the channel and flood plains by imaginary walls at the channel/flood plain junction and compute the discharge for each section, not including the vertical imaginary walls for the calculation of the hydraulic radius for each section. Posey neglected the turbulent shear interaction and momentum transfer which occurs across each division .

(iii) This method is similar to method two except that the imaginary walls are considered in the calculation of the hydraulic radius for each section.

(iv) This method is the most complicated approach and involves the introduction of the imaginary walls inclined towards the centre of the channel from the channel bank.

Posey found that method (ii) was the most accurate at low flood plain depths, and method (i) became more accurate at greater depths. He neglected the interactive turbulent shear mechanism, but none of the four methods satisfactorily predicted the discharge of low flood plain depths.

The first real attempt to include the interaction effect in stage-discharge computations was made by Radojkovic (1976,1985) with the introduction of Φ indices. These indices were used to calculate the interaction effect by

sub– dividing the main channel from floodplains as in **Fig (2.7)**, and determining the net force balance on each sub– division. The term Φ_c for the main channel represents the integrated boundary shear to weight component ratio, whilst the term Φ_f represents the floodplain ratio of boundary shear force to weight component. Rodojkovic related his Φ indices to the ratio of the mean velocity in each subsection during interaction with a floodplain, and to the mean velocity in each subsection isolated from neighbouring sub– sections. Thus he defined:

$$\text{/ } \Phi_c = V'_c \text{ / } V_c \qquad \text{and / } \Phi_f = V'_f / V_f \qquad (2.3)$$

where V'_c and V'_f are mean velocities in the main channel and floodplain respectively during interacting flows, whilst V_c and V_f are these velocities when the subsections are isolated from each other. A knowledge of Φ_c and Φ_f will allow the discharge to be computed:

$$Q = A_c V'_c + \Sigma A_f V'_f \qquad (2.4)$$

This theme was continued by **Ervine and Baird (1982)** who related the Φ factor to the apparent shear stress acting at a vertical interface as shown in **Fig(2.7)**. The out of balance force on the main channel for example is given by:

$$\rho g A_c S - \tau'_c P_c = \tau_a Y_{fp} \qquad (2.5)$$

whereas on the floodplain it is given by:

$$\tau'_f P_f - \rho g A_f S = \tau_a Y_{fp} \qquad (2.6)$$

Ervine and Baird showed that the apparent shear force could be given by:

$$\tau_a Y_f = \int_0^{y_c} \rho u'v' d_y + \int_0^{y_c} \rho uv \, dy \qquad (2.7)$$

Representing both turbulent diffusion and advection terms. A crude estimate of τ_a was advanced, approximated to:

$$\tau_a \approx 50\ (V_c - V_f)^2 \qquad (2.8)$$

which enabled Φ_c and Φ_f to be calculated and hence the total discharge.

This method was further developed by **Wormleaton and Merrett (1988)** based on their experimental work on the SERC flume at HR Ltd Wallingford. This set of experiments was carried out at constant bed slope but with varying cross–sectional geometry and two values of floodplain roughness. The importance of the SERC flume data is that the scale of the model is an order of magnitude greater than most University scale models and also it gives less vertical distortion than University type models. Wormleaton and Merrett considered vertical, diagonal, and horizontal imaginary walls for sub–division, showing that all three methods were inaccurate to varying degrees. They provided an estimate for the vertical depth–averaged apparent shear stress in the form,

$$\tau_a = 3.325\ \Delta V^{1.451}\ (H-h)^{-0.354}\ B_f^{0.52} \qquad (2.9)$$

which was used to determine estimates of the Φ indices and hence the discharge in each subsection of the flow. The accuracy of the stage–discharge estimates was greatly improved. Typical values of the Φ indices for the case of smooth floodplains are shown in **Fig (2.8)**.

Other authors who investigated stage–discharge relationships include **Sellin (1964), Toebes** and **Sooky (1967), James** and **Brown (1977), Bhowmik** and **Demissie (1982), Ervine** and **Baird (1984), Myers (1987), Mckeogh E.J** and **Kiely G.K (1989)** and **Kiely (1989)**. They found generally that the discharge reduction in the main channel increased with increasing the width ratio (B_f/B_c) and at a lower relative depths (Y_f/Y_c). In the main channel section, the discharge can be reduced by as much as 30% relative to the non–interacting case, and as the overbank depth increases the discharge again begins to increase. Typical stage discharge curve obtained by **Kiely (1989)** for the straight main channel with floodplain is shown in **Fig (2.9)**.

The most promising method of discharge estimation to date lies in the solution of the depth–averaged steady state, uniform flow solution to the dynamic

equation for compound sections. This is discussed in some detail in section 2.2.6 so will be mentioned only briefly at this point.

Considering the normal convention of u,v,w, being the velocities in the x,y, and z directions respectively, then the Navier– Stokes equation for a fluid element in steady uniform flow is given by **Knight et.al (1988)** as

$$V\frac{du}{dy} + W\frac{du}{dz} = \rho g \sin\theta + \frac{d\tau_{yx}}{dy} + \frac{d\tau_{zx}}{dz} \qquad (2.10)$$

where secondary flows are negligable, and when the slope is shallow $\sin\theta = S_o$, then the depth integrated version of equation (2.10) gives

$$0 = gS_o + \frac{d}{dy}\left(\epsilon_{yx}\frac{du}{dy}\right) - \frac{f(u)u}{8h} \qquad (2.11)$$

where h is the flow depth, where the bed friction is given by the Darcy– Weisbach equation and where the turbulent shear stress τ_{yx} is approximated by an eddy viscosity model.

Equation (2.11) has been solved by **Wark (1988)** numerically using a finite difference technique, with suitable boundary conditions, and in terms of unit discharge q rather than depth averaged velocity u in the longitudinal direction. The model has now been applied to many real rivers with a typical example of measured stage– discharge for both inbank and overbank flows shown on **Fig(2.10)** for the case of the River Severn. It can be seen from **Fig (2.10)** that the best estimate for the kinematic eddy viscosity ϵ_{yx} (depth averaged) is approximately 0.16 u_*h., where u_* is the shear velocity $\surd ghS_0$.

Perhaps the biggest effect on the stage– discharge relationship in a straight compound channel, is the degree of boundary roughness on the floodplain. Many experiments in the past have been carried out with smooth floodplains, which is not representative of many real rivers which typically have Manning's n of 0.035 for the main channel and 0.07 for the floodplain.

A roughened floodplain will provide greater flow retardation on the floodplain and hence greater turbulent shear between main channel and floodplain, and therefore greater momentum transfer from main channel to floodplain.

The effect of floodplain roughness has been investigated by **Sellin (1964), Pasche and Rouve (1985), Nalluri and Judy (1987), Sellin and Searle (1987), Knight and Shiono (1988) and Sellin and Elliot (1989).** The latter piece of work was carried out on the SERC flume facility at Wallingford, with typical stage– discharge curves shown on **Fig (2.11)** comparing the effect of smooth and rough floodplain boundaries.

An extensive study of the effect of the floodplain roughness was carried out by **Nalluri and Judy (1988)** in which a range of flexible and rigid floodplain roughness elements were investigated in a compound channel with both rectangular and trapezoidal main channel cross sections. The findings revealed that greater floodplain roughness increases the ratio of apparent shear force to the main channel body weight component, meaning that much greater momentum transfer occurs compared with an equivalent smooth boundary case. As well as that the main channel carrying capacity decreases significantly, as if the floodplain roughness elements were retarding the main channel as well as the floodplain.

2.2.3 Area and Depth Averaged Velocities in A Straight Compound Section.

The sketch below shows typical distribution of depth averaged velocity across a compound section compared with u_∞ for each sub– section ($u_\infty = \sqrt{(8gRS/f)}$ for a wide rectangular channel).

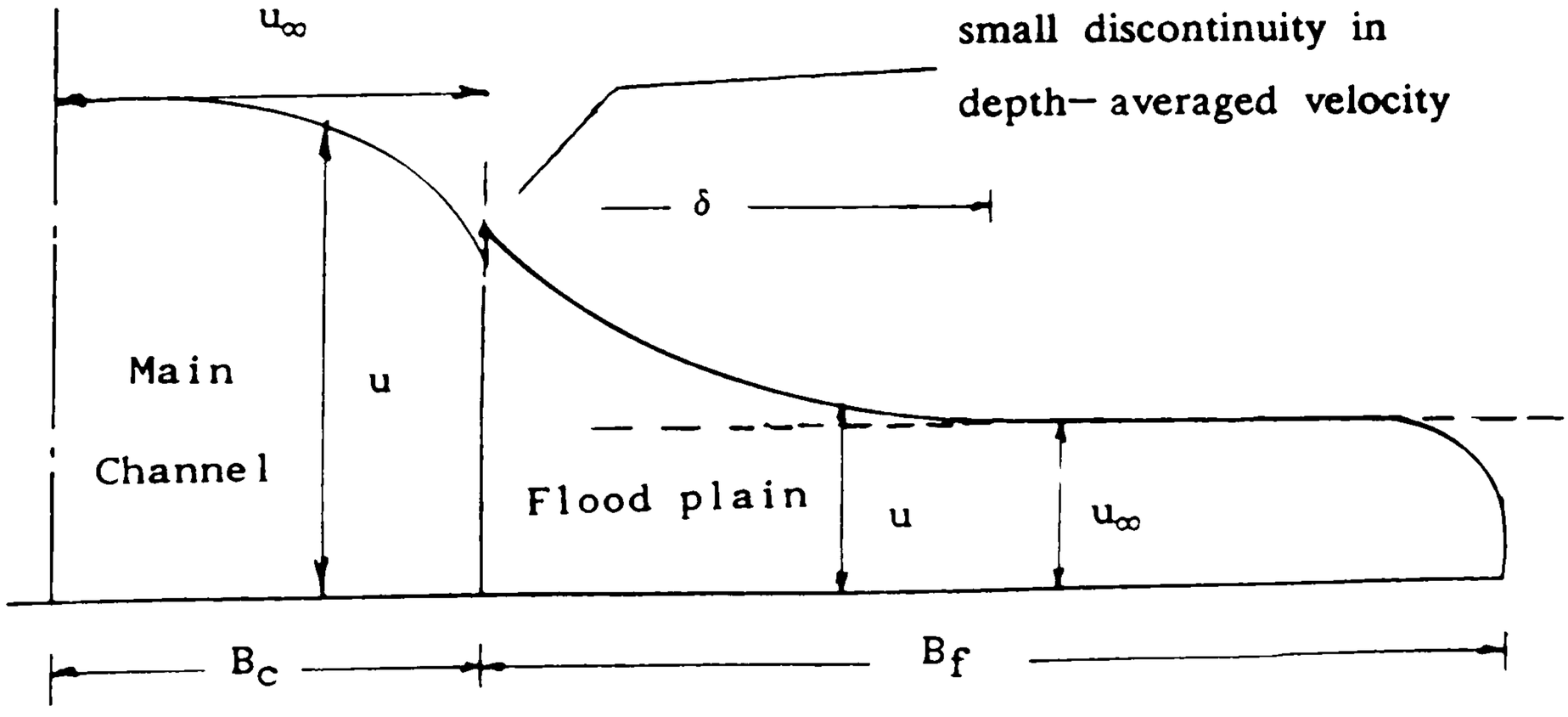

It is clear that if the depth averaged flood plain velocity is increased on the floodplain due to the interaction effect, then the depth averaged velocity in the main channel must have decreased due to the same effect.

Spitsin (1961) compared the flow in the main channel under interacting and isolated conditions, by inserting a glass wall at the channel/flood plain junction. He was able to calculate the energy existing in the channel and flood plain under isolated and interacting conditions. Spitsin found the amount of energy transmitted to the floodplain from the channel was never greater than 25% of the total energy lost from the main channel, suggesting that at least 75% of the energy lost from the main channel was dissipated in the formation of eddies and vortices in the turbulent shear layer at the channel/flood plain interface. The energy transfer to the floodplain increased floodplain velocities, and the energy loss in the main channel decreased the main channel velocities. **Sellin (1964)** carried out his investigation of the interaction between channel and flood plain and noted that during interacting conditions, the maximum velocity filament in the main channel was depressed below the water surface and away from the interacting regions. Another effect of the interaction mechanism was the reduction of velocities in the main channel, especially near the channel/floodplain junction .

Zheleznyakov (1965) observed the formation of turbulent eddies and large scale vortices with vertical axes at the channel/flood plain junction, and also noted that the interaction mechanism or "kinematic effect" was characterised by a reduction in the main channel velocities and an increase in flood plain velocities close to the main channel junction. He presented field test results as shown in **Fig (2.12)**, and observed significant reductions in main channel velocities at low flood plain depths due to the interaction effect. Zheleznyakov identified three stages of interacting flow:

1. The main channel velocity is decreasing with increasing flood plain depths.

2. The main channel velocity is reduced to a minimum at the point where the interaction effect is maximum. Usually $Y_f/Y_c = 0.2$ to 0.3.

3. The main channel velocity increases with further increases in floodplain depths.

Zheleznyakov's results have been confirmed by numerous investigators who have studied the interaction between a straight main channel with floodplain experimentally, including **Myers (1978), Rajaratnam and Ahmadi (1979), Ervine and Baird (1982) and Crory (1982), Bhowmike and Demissie (1982), Knight and Demetriou (1983),** Ervine and Baird (1984), Baird (1984), Wormleaton and Hadjipanos (1985), Myers (1987), Tominaga (1989) and McKeogh and Kiely (1989). The general consensus amongst the authors above is:—

(1) The turbulent mixing shear layer generated at the channel/floodplain interface spreads over part of the main channel and floodplain.

(2) According to **Samuels (1985)** the width of the shear layer in the main channel and floodplain can be approximated (separately) by the relationship:

$$\delta = 5.7\ (ghS/f)^{1/4}\ \epsilon^{1/2} \qquad (2.12)$$

where h is the local flow depth and f the Darcy— Weisbach friction factor. ϵ is the turbulent eddy viscosity which may be roughly approximated (considering bed generated shear only) as $\epsilon = C\ u_*\ h$

(3) The greatest turbulent shear stress at the interface region occurs when the velocity gradient from main channel to floodplain is greatest i.e.
$\tau = \rho \ell^2 (du/dy)^2$. This does not necessarily coincide with the highest momentum transfer, as the latter is proportional to the turbulent shear stress times the area it is acting over.

(4) At higher relative depths and smooth floodplains, it is possible to have little or no variation in velocity between main channel and floodplain, meaning little momentum transfer. This is not true for rough floodplains, which exhibit large transfer at relative depths even in excess of 0.5.

(5) The velocity difference from the main channel to floodplain appears to be a function of the relative depth Y_f/Y_c, relative roughness n_f/n_c, relative widths of the channel B_f/B_c, side slopes of the main channel as well as the longitudinal bed slope S_0.

(6) The depth— averaged velocity for the channel/floodplain width can now be computed numerically from Equation (2.11) at least for reasonably straight

compound sections. This method will be discussed further in section 2.2.6., but it has been applied to real rivers as shown by the work of **Knight, Shiono and Prit (1988)** on **Fig (2.13)** in the case of the River Severn at Montfort.

2.2.4 The Role of Secondary Currents in Straight Compound Channels.

In open channel flows there are two basic types of secondary currents.

i) Skew induced secondary currents that derive their origin to changes in channel plan geometry. River bends are a classic case of the phenomenon with secondary flows stemming from non– uniform centrifugal pressures.

ii) Stress induced secondary currents. These usually stem from non– uniform shear stress distribution with the resultant momentum transfer to lower velocity and shear stress regions often towards the lower two corners of a channel base.

Straight compound channels until recently were thought to have only weak secondary currents of type (ii) above. However these "weak" secondary currents have been shown to cause as least as much mixing as turbulent diffusion and to cause comparable levels of energy loss.

Noat and Rodi (1982), Nezu and Rodi (1985), Tominaga and Ezaki (1985), and **Nezu and Nakagawa and Rodi (1989)** have presented a mathematical model to determine the magnitude of secondary currents in straight open channel flows by using the Reynolds stress equations. They found the maximum secondary current velocity is 3% of the mean longitudinal velocity for open channel flow.

Taminaga and Ezaki (1987,1988), Larsson (1988), Taminaga and Nezu (1989), Kawahara and Tamai (1988,1989) measured secondary flow in compound channels experimentally, and found the secondary currents generated near the junctions to be about 3% – 4% of the streamwise velocity. Taminaga's results are shown in **Fig (2.4).**

1– The secondary current in compound open channel flows is mainly composed of the floodplain and the main channel vortex which are separated by co– flowing at the junction

2– For high floodplain depths the distributions of the streamwise velocities are affected considerably by the secondary currents.

2.2.5 Apparent Shear Force in Straight Compound Channels.

When a straight compound channel is sub–divided into its various sub–sections, there is an out of balance force now known as the apparent shear force. This has been sketched in Fig (2.7) with the out of balance force considered to act in this case, along a vertical interface along a unit length and a depth equal to the floodplain depth Y_f. Thus the apparent shear force is given by,

$$ASF = \tau_a \times Y_f \times 1 \qquad (2.13)$$

where τ_a is the depth–averaged apparent shear stress. The apparent shear force at any vertical section is thus equal to the momentum transfer across that section, composed of the turbulent diffusion and secondary current advection. This phenomenon has been studied in detail by **Creff (1965), Myers (1975), Wormleaton (1982), Knight (1983), Ervine and Baird (1984), Tominaga (1989) and Kawahara (1989).** Most of the authors mentioned have produced an empirical relationship describing the apparent shear stress related to the geometrical and flow parameters involved. Typical examples include:–

Wormleaton (1982)

$$\tau_a = 13.84\ (\Delta V)^{0.882}\ (h/Y_c)^{3.123}\ (B_c/B_f)^{0.727} \qquad (2.14)$$

Baird and Ervine (1984)

$$\frac{\tau_a}{\rho g Y_f S_0} = 1.12\ \left(\frac{Y_c}{Y_f} - \psi\right)^{1.5}\ \left(\frac{B_c}{h}\right)^{0.5}\left[\,1 - e^{-0.53 B_f/h}\right] \qquad (2.15)$$

Such relationships can be used to determine the mean boundary shear stresses in each sub–section of the flow, which for steady uniform flow can be related to the mean velocity in each subsection of the flow, finally estimating the total discharge as outlined in section 2.2.2.

More recently **Kawahara** (1988,1989), **Tominaga and Ezaki** (1988) and **Tominaga and Nezu** (1989) have investigated the mechanism of lateral momentum transfer from a straight main channel to the floodplain using three dimensional numerical models. **Tominaga** (1988,1989) investigated the structure of turbulent shear in compound open channel flows with rectangular and trapezoidal main channel cross section . He found the apparent shear stress on the junction interface smaller in the trapezoidal main channel case. Kawahara's results are shown in **Fig (2.14)** for a range of relative depths, floodplain roughnesses and main channel aspect ratios. The apparent shear stress is subdivided into its diffusion and advection components revealing:—

1— The apparent shear stress decrease with the increasing floodplain depth .

2— The increase of the apparent shear stress with increment of the floodplain roughness is mainly due to the enhancement of diffusion although advection also increases slowly .

3— The change of the apparent shear stress with the main channel width is due to the variation of advection rather than diffusion.

2.2.6 Numerical Modelling of Interaction Effect in Straight Compound Channels.

The development of successful mathematical models to calculate flow characteristics in straight compound channels has now reached a stage where other methods are becoming obsolete. The interaction effect has been investigated numerically by **Cunge** (1980), **Vreugdenhill and Wijbenga** (1982), **Samuels** (1985), **Wormleaton** (1986) (1988), **Knight and Shiono** (1988) (1989), **Samuels** (1988), **Killer and Rodi** (1988), **Arnold and Rouve** (1989), **McKeogh and Kiely** (1989) and most recently by **Wark and Samuels** (1989).

The basis of the method has been discussed already in section 2.2.2 considering the balance on a fluid element in steady (du/dt = 0), uniform (du/dx= 0), flow. The resulting equation (2.11) is simplified for the case of zero secondary motion (not correct) into,

$$\frac{f\ u|u|}{8h} = \frac{d}{dy}\left(\epsilon_{yx}\frac{du}{dy}\right) + gS_0 \qquad (2.16)$$

where u is the depth averaged velocity.

h is the local flow depth.

f is the Darcy Weisbach friction factor.

S_0 is the longitudinal bed slope.

ϵ_{yx} is the depth averaged lateral eddy viscosity.

There are various problems in solving Equation (2.16) above, namely, that for compound sections the flow depth h varies in the lateral direction. Also the lateral turbulent exchange parameter ϵ_{yx} varies in the lateral y direction as it reflects various levels of turbulent shear stress across the width. A third problem concerns the fact that there is a discontinuity in u at the channel floodplain interface. **Samuels (1985)** has shown that this can be overcome by solving Equation (2.16) in terms of discharge per unit width q, which is continuous across the interface.

Various methods and techniques have been proposed for solving Equation(2.16). The most common is a finite–difference numerical technique using a Newton Raphson iterative scheme with suitable boundary conditions at walls, discontinuities and point of symmetry.

The most fascinating aspect of the solution of Equation (2.16) has been concerned with the estimation of the lateral depth–averaged kinematic eddy viscosity ϵ_{yx}. This term is attempting to simulate the turbulent shear stress which in the case of a compound section includes;

1– bed generated turbulent shear.

2– lateral velocity gradient generated shear.

Both these are mixed together in the interface region together with momentum transfer due to secondary currents which has been omitted from equation (2.16) for ease of solution. **Lean and Weare (1979)** estimate the eddy viscosity for lateral momentum transfer is

$$\epsilon_{yx} = 0.16\ u_*\ h \qquad (2.17)$$

For bed generated shear only, when u_* is the shear velocity and h the flow depth. For velocity difference generated shear, Lean and Weare suggest

$$\epsilon_{yx} = 0.01 \; |\Delta u| \; \delta \qquad (2.18)$$

where Δu is $(u_{max} - u_{min})$ across the shear layer and δ is the shear layer width. **Samuels (1988)** has provided estimates for the value of (δ). **Wormleaton(1988)** has proposed a cumulative eddy viscosity describing both flow phenomena, in the form,

$$\epsilon_{yx} = 0.16 \; u_* \; h + \lambda_s u_s \ell_s \qquad (2.19)$$

where $\lambda_s = 0.013$ and $u_s = (u_{mc} + u_{fp})/2$. ℓ_s is a characteristic length scale which can be estimated from Townsend (1976).

$$\ell^2_s = \int \frac{du}{dy} y^2 \, dy \; / \; \int \frac{du}{dy} \, dy \qquad (2.20)$$

Research continues in this area, especially the incorporation of secondary currents into the eddy viscosity term, which simply makes ϵ_{yx} a type of correction factor. Some comparisons between theory and experiment are shown on **Fig (2.15)** for the SERC flume data.

2.3 MEANDERING CHANNELS WITH FLOOD PLAIN FLOW.

2.3.1 Introduction

The flow behaviour in a meandering river channel with flow in adjacent floodplains is a highly complex three–dimensional chaotic system, which is only now receiving serious attention from researchers. At the time of writing this thesis, meandering overbank flow is being investigated at the SERC flume Wallingford as part of the on going SERC initiative.

The situation has been investigated experimentally in various stages by the **U.S Army Corps of Engineers (1956), Toebes and Sooky (1967), Rajaratnam and Ahmadi (1979)(1983), Yen and Yen (1983), Ervine and Eills (1987), Sellin and Giles (1989), Sellin and Elliot (1989), Kiely (1989), McKeogh and Kiely (1989), Stein and Rouve (1989a)(1989b)**, and most recently by researchers at the **Universities of Aberdeen, Bristol and Glasgow as part of the SERC** initiative.

The complexity of a meandering overbank flow is seen in a schematic plan sketch by **Ervine and Ellis (1987) Fig (2.16)** showing the additional complexities of :–

(i) river bend during overbank flow with secondary currents, superelevations and energy dissipation all profoundly modified by overbank flow.

(ii) The cross over region where the floodplain crosses over the main channel flow passing underneath but at a skew to the floodplain flow.

(iii) Co– flowing turbulent shear which may still exist especially near the apex of each bend and especially at lower depths of flow on the floodplain.

Stein and Rouve (1989) have captured some of the complexity of the flow pattern in a 3– dimensional sketch in **Fig (2.17)** showing a complex system of counter rotating secondary cells at the cross– over region. At this stage it may be instructive to have a more detailed look at the behaviour of bends and cross– over sections during overbank flow.

2.3.2 Bend Behaviour for Inbank Flows.

The physical behaviour of river bends has been the subject of much study, mainly since **Thompson (1876)**. If the flow is subcritical then in a curved channel, (plan), centrifugal pressures will be acting producing a unique feature known as superelevation, which is a rise in water level around the outer bank of the flow. This is sketched in **Fig (2.18)**.

Centrifugal pressures are proportional (u^2/r) (where u is the local longitudinal velocity and (r) the local bend radius) and hence fluid elements near the free surface will be subject to higher centrifugal pressures compared with near the channel bed, and hence a secondary motion or helical swirl will be produced.

Such secondary motions often dominate bend flow in the sense of sediment deposition and scour, transfer of momentum from the inner bend to the outer bend and also the degree of energy loss that exists in the bend over and above bed friction.

Fares (1989) has shown that the entrance conditions to a bend often resemble free vortex flow. That is, the application of Bernoulli's equation to streamlines produces much higher velocities at the inner bend because of the shallower flow depth. The application of this theory in the radial direction produces a hyperbolic shaped convex upwards superelevation. **Ippen etal (1962)** showed that momentum transfer from the inner to outer part of the bend produced almost forced vortex conditions in the downstream part of the bend, with higher velocities at the outer part of the bend.

This is reflected in distributions of bed shear stress in the region of bends such as shown in **Fig (2.19)** from the work of **Nouh etal (1979)** clearly indicating highest shear stresses at the bend inner entrance and outer exit.
Another feature is that of inner bend separation when fluid particles near the wall have insufficient kinetic energy to overcome the pressure gradient. The result is separation as noted by **Shukry (1949), Rozovskii (1961) and Ippen etal (1962).**
Separation effects are dependent on the ratio of mean bend radius r_m to channel width B, and also the Froude Number of the flow $u/\sqrt{gh}$. This is shown by the work of **Leeder etal (1975)** shown on **Fig (2.20)** clearly flow separation at the inner bend would transfer streamlines to the outer bend, further explaining high shear stresses near the outer bend near the bend exit.

In real rivers, work by **Thorne and Hey (1979), Thorne and Rais (1983) and Thorne etal (1985)** have produced more detailed results of secondary currents. An example is shown in **Fig (2.21).** Here it is clearly seen that the bend apex produces two counter rotating secondary cells, the inner clockwise cell being more dominant. **Hey (1979)** concludes that the outer bend counter clockwise cell almost always happens with steep outer banks and is not found on more gradual shelving outer banks.

The energy loss at a river bend appears to be more complex than for the case of straight channels. As well as normal bed friction, energy losses stem

from internal fluid mixing due to the large secondary currents developed at the bends, additional radial boundary shear stress due to these currents and also flow separation when it occurs. The phenomenon has been investigated by **Mockmore (1944), Shukry (1949), Chow (1959), Leopold etal (1960), Rosovskii (1961), Ippen etal (1962), Yen (1965), Soliman (1968) and Chang (1983) (1984a).** The simplest model for bend energy loss is of the form,

$$h_L = C_e \ (u^2/2g) \qquad (2.21)$$

where C_e is a bend loss coefficient and $u^2/2g$ the mean kinetic energy in the flow. The work of **Shukry (1949)** shown on **Fig (2.22)**, reveals that the bend loss coefficient depends on the Reynolds Number of the flow, the channel aspect ratio h/B, the bend tightness r_m/B and the total bend angle $\theta_b/180^0$.

More recently **Chang (1983) (1984a)** has developed an analytical model to compute the rate of energy dissipation in subcritical fully developed bend flow. Chang's expression for bend losses due to secondary currents and other transverse phenomena is given by the energy gradient S",

$$S'' = F_r^2 \left(\frac{h}{r_m}\right)^2 \left(\frac{2.86\sqrt{f} + 2.07f}{0.565 + \sqrt{f}}\right) \qquad (2.22)$$

where F_r is the flow Froude Number, h/r_m the depth of flow to bend radius and (f) the Darcy Weisbach friction factor. **Fig (2.23)** shows the ratio of the bend transverse energy losses to the total bend energy losses, S''/S. It is significant to note for "tight" bends with r_m/h of the order of 20 to 25, the value of S''/S is of the order of 0.5, meaning that energy losses transversely are of the same magnitude of energy losses longitudinally usually due to bed friction.

Mathematical models of inbank river bend flows have been investigated by several authors including **Rosovskii (1961), De Veriend (1983), Kalkwiijk (1986), Smith and Hussein (1986)** and most recently by **Herbertson and Fares (1989).** The main emphasis has been on the estimation of the magnitude of the transverse secondary currents, as well as predictions of the superelevation around the bend. The most recent two dimensional numerical bend model has been

investigated by **Fares (1989)** and **Herbetson etal (1988)**, for the case of wide gentle rectangular bend as sketched in **Fig (2.24)**. The radial (transverse) secondary currents velocities were computed first using simplifications of steady state, width averaged, with r defined as the radial direction, s the tangential direction and z the vertical direction. The simplified dynamic equation becomes,

$$gS_r = \frac{u^2_s}{r} + \frac{d}{dz}\left(\epsilon \frac{du_r}{dz}\right) \qquad (2.23)$$

where

S_r is the radial water surface slope

u_s, u_r the longitudinal and radial velocities

ϵ the kinametic eddy viscosity.

Equation (2.23) was solved analytically to produce values of radial velocity u_r in terms of the radial (r/h), and mean longitudinal velocity (u_m). **Fig (2.25)** shows a typical comparison between theory and experiments. Fares then proceeded to formulate and solve a two dimensional depth–averaged bend model which predicted the longitudinal components of depth averaged velocity around a complete bend, as well as free water surface elevations. This was combined with the earlier model of the radial velocity components around a bend.

2.3.3 Bend Behaviour for Overbank Flow.

Much less is known of the behaviour of river bends during overbank flow, although the situation is currently being investigated experimentally at the SERC flume facility, Wallingford and also numerically by Wark at the University of Glasgow.

The first serious investigation was by Toebes and Sooky in a small experimental flume 7.32m long and 1.185m wide, with a continuous series of meanders with overbank flow. A low value of sinuosity of 1.135 was used. The plan geometry is shown on **Fig (2.26)** with X/L of 0.25 corresponding to the upstream bend apex, X/L= 0.75 the downstream bend apex and X/L= 0.5 the inflexion point at cross over. It is clear from **Fig (2.26)** showing inferred

secondary currents, that the secondary currents at the bend apex (at both bends) are moving in the opposite direction to the inbank flows. i.e. the main secondary current is moving to the inner bank at the free surface rather than the outer bank. At the inflexion point X/L= 0.4 to 0.6, there appear to exist two counter rotating cells, one driven by the floodplain flow crossing over the main channel flow and the other appearing to be a remnant of the previous bend.

This is reiterated in the experiments of **Stein and Rouve (1989)** shown as a 3– dimensional sketch in **Fig (2.17)**. At both bends the main secondary current is again in the opposite direction to the inbank flows. The reason for this may simply be connected with the use of smooth floodplains and the relatively high velocities which exist outwith the meander belt width. This often results in a momentum transfer from the outer floodplain regions to the inner meander belt width floodplain region. It can also be seen at the cross over inflexion region, that again two counter rotating cells exist, one decaying from the previous bend and the other growing and driven by floodplain flow crossing over the main channel.

Kiely (1989) has carried out an exhaustive study of meander bends, for a continuous series of meanders, using a laser doppler system to measure longitudinal and transverse components of velocity. A schematic of his secondary current distribution at bend apices and cross over is shown in **Fig (2.27)**.

2.3.4 Flow Behaviour at the Cross– Over Region.

The mechanics of the flow at the cross– over region near the inflexion point of a meander represents a flow situation as complex as bend flow, because the floodplain flow is moving approximately longitudinally whereas the main channel flow is passing underneath the flood plain flow with a large angle of skew between the two flows. This area of flow behaviour is the purpose of the work of this thesis, although limited to a small skew angle (5.843^0) and to the absence of upstream and downstream bends.

Even for inbank flows the inflexion point represents a complex flow situation as seen in the measurements by Thorne and Hey on Fig (2.21). The upper cell

is a relic cell from the upstream bend which is decaying, and giving way to the underneath cell growing in strength and size to reach its maximum at the downstream bend.
Similar patterns have been observed in section 2.3.3. for overbank flow inflexion points except in this case the growing cell is driven by floodplain flow crossing over the main channel flow below.

Experiments on cross over type flow have been limited in number, the first major work being carried out by **James and Brown (1977)** for three different skew angles, two of which are shown on **Fig (2.28)**. Although James and Brown produced mainly stage–discharge data, there is clear evidence of cross–flows in **Fig (2.29)** because of higher velocities on the diverging floodplain than on the converging floodplain.

More recent work has been carried out by **Elliot and Sellin (1990)** on the SERC flume, where the main channel is kept straight but the floodplain skews at angles of 5.1^0 and 9.2^0 which is around the same order of magnitude of the work of this thesis. **Sellin and Searle (1987)** reveal fascinating flow mechanisms in **Fig (2.30)** showing strong secondary currents driven by the crossing–over floodplain flow, all rotating in the same direction as the floodplain flow. This phenomenon occurs along the length of the flume and more clearly distinguishes the crossing over flow mechanism in the complete absence of any upstream bends. Clearly such intense secondary cells are responsible for significant energy loss over and above bed friction and co–flowing shear.

Ervine and Ellis (1987) considered the cross–over flow to be analogous to a sudden expansion and contraction or flow passing over a slot in the channel bend. This is not a complete parallel because of the angle of the skew and because there is flow in the main channel beneath, rather than simple stagnant recirculation. They argued that flow passing over a slot generates a recirculation region in the main channel beneath. This is sketched in **Fig (2.2)**.
The recirculation region length is approximately $6H_s$, where H_s is the step height or bankfull depth. Flow passing over the slot generates therefore a horizontal shear layer (as sketched) in the region of sudden expansion and a further separation and shearing zone downstream in the area of sudden contraction. The energy losses in both regions can therefore be approximated to sudden expansion and sudden contraction losses. The sudden expansion loss as approximated by

Chow (1959) can be given by,

$$h_e = (1 - Y_f/Y_c)^2 U_n^2/2g \qquad (2.24)$$

where Y_f/Y_c is the ratio of the upstream and downstream depths and U_n the normal velocity approaching the slot. Similarly the contraction loss can be approximated by,

$$h_c = C_L U_n^2/2g \qquad (2.25)$$

where values of C_L can be obtained from **Yen and Yen (1983)** and U_n is the normal downstream flow velocity. Equations (2.24) and (2.25) represent an approximation of the head losses in this region, although the work of Elliott and Sellin does reveal more complex flow patterns in the cross over region.

A more sophisticated study by **Barbarutsi and Chu (1987)** is shown on **Fig(2.31)**. The magnitude of the recirculating current is shown to be dependent on whether bed friction is dominating the process or whether the shear layer dominates.

2.3.5 Stage– discharge Relationships in Meandering Channels with Flood plain Flows.

The **US Army Corps of Engineers (1956)** produced stage– discharge measurements in meandering compound sections with floodplains varying in roughness from Manning's "n" of 0.012 to Manning's "n" of 0.035. The sinuosity (curved main channel length/ straight valley length) varied mainly in the range 1.0 to 1.57, with resulting stage– discharge curves shown in **Fig (2.32a)** for the case of smooth floodplains (n = 0.012) and sinuosities 1.00 to 1.57 and also the case at rough floodplain, (n = 0.035), over the same range of sinuosity. It is clear from **Fig (2.32b)** that increasing sinuosity reduces discharge dramatically. This is due to additional bend head losses and possibly greater cross– over losses. The reduction is most noticable in moving from straight channels to mildly sinuous r= 1.2, and less pronounced as the value of sinuosity increases. It is also clear from **Fig (2.32b)** that for high flood plain roughness, not only is the total discharge greatly reduced but the impact of greater sinuosity is significantly less

than the smooth floodplain case. The US Army work did report that the effect of sinuosity on the total flow capacity is small when the meander belt width is substantially smaller than the total floodway width.

Toebes and Sooky (1967) investigated the stage–discharge relationship in a very mildly sinuous compound channel. They concluded from experimental studies of smooth boundaries and sinuosity r = 1.135 that the energy losses were 2.5 times greater compared with those of a uniform channel at the same discharge. This has a significant effect on the stage–discharge relationships showing that the bed friction alone will not provide good estimates. Toebes and Sooky recommended a sub–division method using a horizontal division at the level of bankfull.

Elliot and Sellin (1989) carried out extensive stage–discharge testing of the skewed SERC flume, with skew angles 5.1^0 and 9^0. The results are shown in **Fig (2.33)** and compared with the stage–discharge curve of equivalent straight compound section. The percentage difference in discharges reveals that even a very small angle of skew of 5^0– 9^0 will reduce the discharge carrying capacity by up to 12% compared with a straight compound overbank flow section. It is significant that despite the reduction in co–flowing shear because of the skew, there is still greater energy loss presumably attributed to the generation of secondary currents and a horizontal shear layer along the main channel/floodplain horizontal interface.

This theme is repeated for the meandering channels of **McKeogh and Kiely (1989) and Kiely (1989).** **Kiely's** flume used only smooth boundaries, but the stage–discharge relationship was investigated for a straight compound section, a single meander compound section and finally multiple meander compound section. The result is shown on **Fig (2.34)** revealing reductions of the order of 20% in discharge when comparing straight with multiple meanders of sinuosity 1.25.

The effect of floodplain roughness on the stage–discharge curve is shown in **Fig (2.35)** for the single meander flume of **Stein and Rouve'(1989).** In this case the floodplain roughness varied from 0.01 to 0.035 with a marked effect.
Fig (2.35) also shows a marked discontinuity around the bankfull level and in fact brings into question the definition of the bankfull level. This is because at inbank levels below bankfull it is possible to get overbank flow because of

superelevation at the crown of each bend.

The influence of floodplain roughness has been illustrated dramatically for the case of the River Roding which is a two–stage channel investigated for Thames River Authority by **Searle and Sellin (1986)**. Both filed measurements and a vertically distorted model was used to investigate the flow situation. **Fig (2.36)** reveals the effects of floodplain vegetation.

2.3.6 Velocity Distributions in Overbank Meandering Channels.

Work in this area has been mainly experimental in nature and has covered both fully meandering and also skewed channel situations. The main investigators have been, **Toebes and Sooky (1967), James and Brown (1977), Ahmadi (1979), Rajaratnam and Ahmadi(1983), Yen and Yen (1983), Samuels (1985), Stein and Rouve (1985), Ervine and Ellis (1987), Searle (1986), Sellin and Elliot (1989), Sellin and Giles (1989), Smith (1989), Mckeogh and Kiely (1989) and Kiely (1989).**

James and Brown (1977) and Sellin and Elliot (1989) carried out experimental studies on a skewed main channel with floodplain, and concluded that the maximum velocity filament occurs in the main channel section, but displaced sideways in the same direction as the cross flow, usually from the converging floodplain towards the diverging floodplain. This is clearly shown in **Fig (2.29) and Fig (2.37)** from James and **Brown and Sellin and Elliot** results. **Toebes and Sooky (1967)** were the first to note the velocity movement through a meandering channel with floodplain. They found that the maximum filament of the velocity occurs closest to the inner bends. **James and Brown (1977) and Ahmadi (1979)** confirmed Toebes and Sookys results.

Stein and Rouve (1988,1989) studied overbank flow in single meander compound channel experimentally and numerically. They noted that the main direction of the flow on the floodplain is streamwise, while that in the main channel is between partially longitudinal and partially of primary direction, and there is a wake effect downstream of the cross–over sections where the velocities are reduced.

The most comprehensive study to date on velocities in meandering channels

with overbank flow, has been carried out by Kiely (1989) and McKeogh and Kiely (1989). Their experimental flume facility is shown in **Fig (2.38)**. The flume is constructed in glass, with bankfull depth 50mm, main channel width 200mm, with a 'tight' bend radius of R_c/B_c of 2, a sinuosity of 1.25, cross over angle of 45^0 and with velocities measured using Laser Doppler Anemometry.

The depth–averaged longitudinal velocity at the apex of a bend and for a relative depth of 0.38 is shown in **Fig (2.39)**. The highest velocity filaments are on the smooth floodplain outside the meander belt.
A smaller peak exists in the region of the inner bend apex and the floodplain region just adjacent to the inner bend. A "wake effect" is shown at a lateral distance of 0.7 to 0.8, thought by Kiely to be stemming from the previous cross over region. This is analogous to a bluff body effect. There has been no work done yet on rough floodplains with meandering overbank flow.

Regarding the maximum velocity filament, the author of this thesis believes that for very shallow overbank flow depths the maximum velocity filament more or less follows the path of the main channel, as sketched below. For very large overbank flow depths the maximum velocity filament will follow the centre–line of the entire flume as the main channel has less and less effect. For intermediate flow depths the maximum velocity filament will tend to hug the inner bends in a flow path somewhere between the two extreme cases.

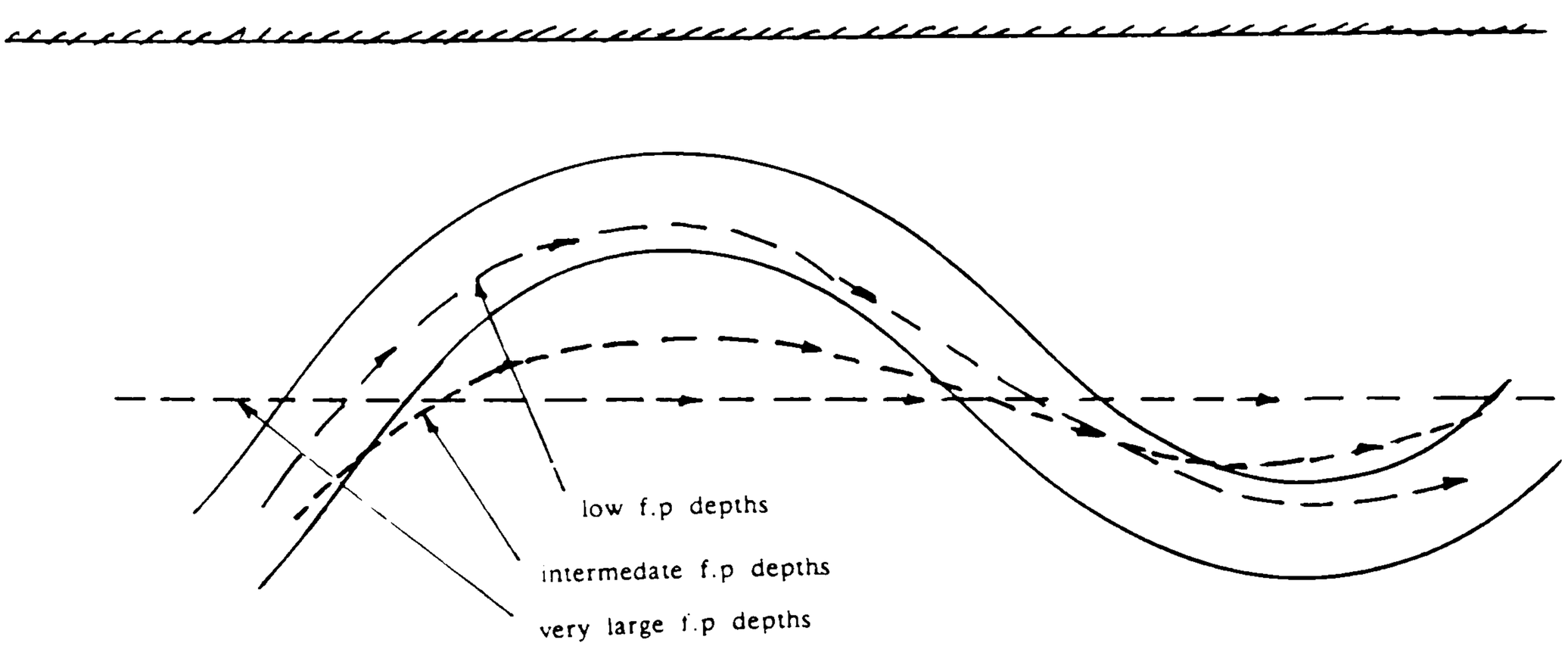

2.3.7 Numerical Models of Meandering Channel with Overbank Flow.

Very few serious numerical models have been attempted for meandering channels with overbank flow.

Pender (1985) used a quasi one– dimensional model to simulate side flows into adjacent floodplain and subsequent side flows back into the main channel some distance downstream. This approach does not allow for any lateral shear interaction between main channel and floodplain.

Samuels (1985) used a finite element technique to discretize the two– dimensional flow equations excluding turbulent shear stress terms.
The results of Samuels model gave reasonable correspondence with experimental data of **Toebes and Sooky (1967)**, but his work is now being extended by Wark(1989) of University of Glasgow with lateral turbulent shear included.

A recent 2– D model by **Stein and Rouve' (1989)** successfully predicts transverse water surface profile but has difficulties predicting velocity profiles.

Ervine and Ellis (1987) presented a one– dimensional model based on summating the total energy loss in the meandering overbank flow system. Transverse shear was excluded. Main channel and floodplain bed friction was estimated from the Darcy– Weisbach equation, secondary current losses at bends were estimated from Chang's equation (2.22), and floodplain flow passing over main channel flow losses were estimated from sudden expansion and contraction losses given by Equations (2.24) (2.25). The output from this one– dimensional approximation was compared with experimental data from **US Army Corps of Engineers (1956)** and shown on **Fig (2.40)**. Reasonable correspondence was achieved. This model will be discussed in more detail in Chapter 7.

2.4 SUMMARY .

An attempt has been made in this literature review to draw together diverse strands of open channel flow research including straight channels with parallel floodplains, meandering and skewed channels with adjacent floodplains, flow behaviour at river bends as well as cross–over regions.
In each case an attempt has been made at investigating the flow mechanisms involved, secondary currents, turbulent interaction, stage–discharge relationships velocity distributions across the channel width, as well as the most recent numerical investigations.

The conclusion to be drawn is that a great deal is now known about the straight–parallel channel floodplain case but little is known about meandering channels with floodplains. It was decided therefore that this thesis would be a contribution towards meandering channels, by concentrating on the cross–over region where the main flow passes under the floodplain flow above, both flows at a skewed angle θ to each other. The reason for choosing this area of study can be summarised as:–

(i) The skew represents an idealisation of part of meandering channel flow.

(ii) It presents an opportunity to investigate flow mechanism in a situation akin to the straight/parallel case but with an element of cross–over.

(iii) It presents an opportunity to investigate energy losses in a skewed cross–over section and hence to build up a more realistic stage–discharge relationship.

(iv) By studying this skew geometry separately from the influence of the upstream bends, this will enable bend effects and cross–over effects to be separated in future meandering studies.

Thus the overall theme of this thesis is to establish the flow mechanisms, determine the energy losses and to produce realistic stage–discharge predictions for a skewed main channel with floodplain.

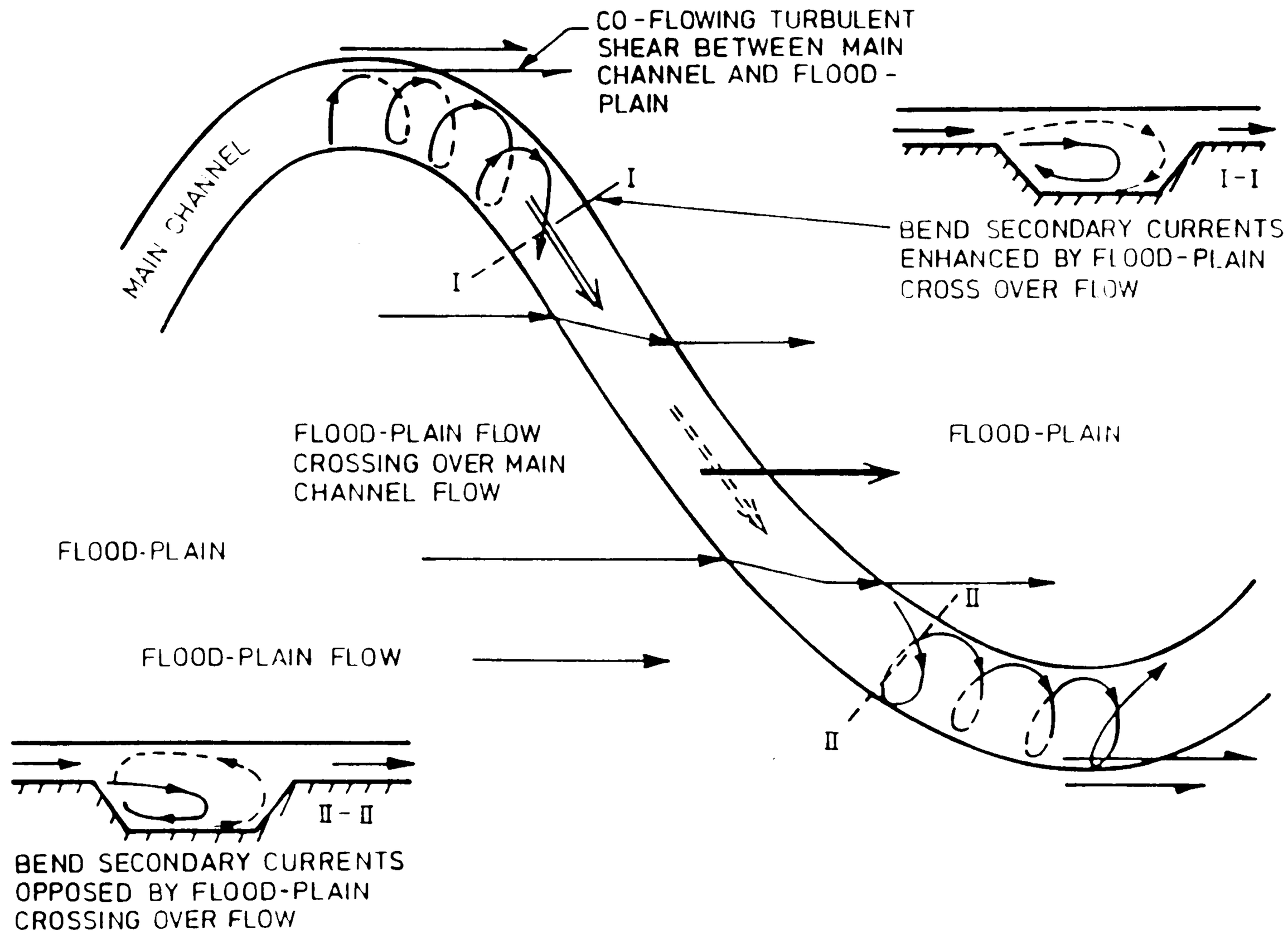

FIG (2.1) Flow Mechanisms in Meandering Channel With Flood Plain Flows. (**Ervine and Ellis (1987)**.

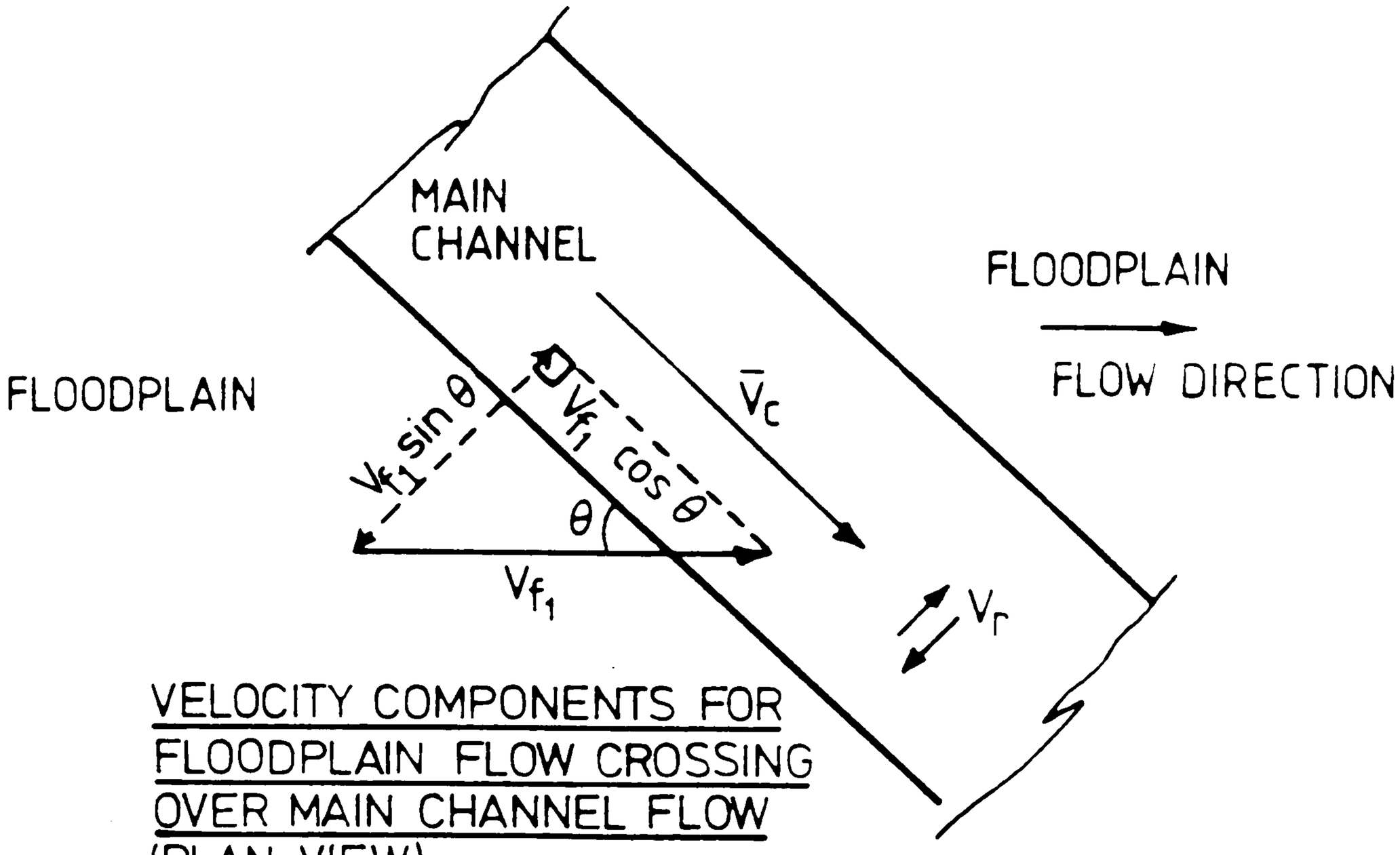

VELOCITY COMPONENTS FOR FLOODPLAIN FLOW CROSSING OVER MAIN CHANNEL FLOW (PLAN VIEW)

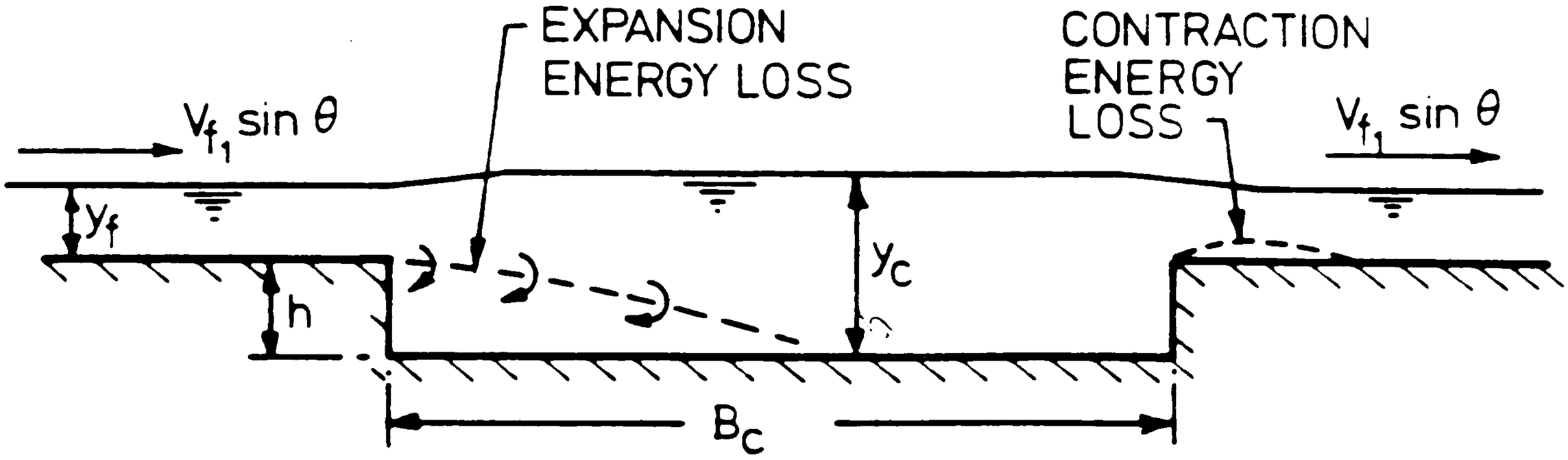

EXPANSION AND CONTRACTION LOSSES AT A SECTION NORMAL TO MAIN CHANNEL FLOW.

FIG (2.2) The Flood Plain Flow Velocity Passing Over Over Main Channel. (Ervine and Ellis 1987)

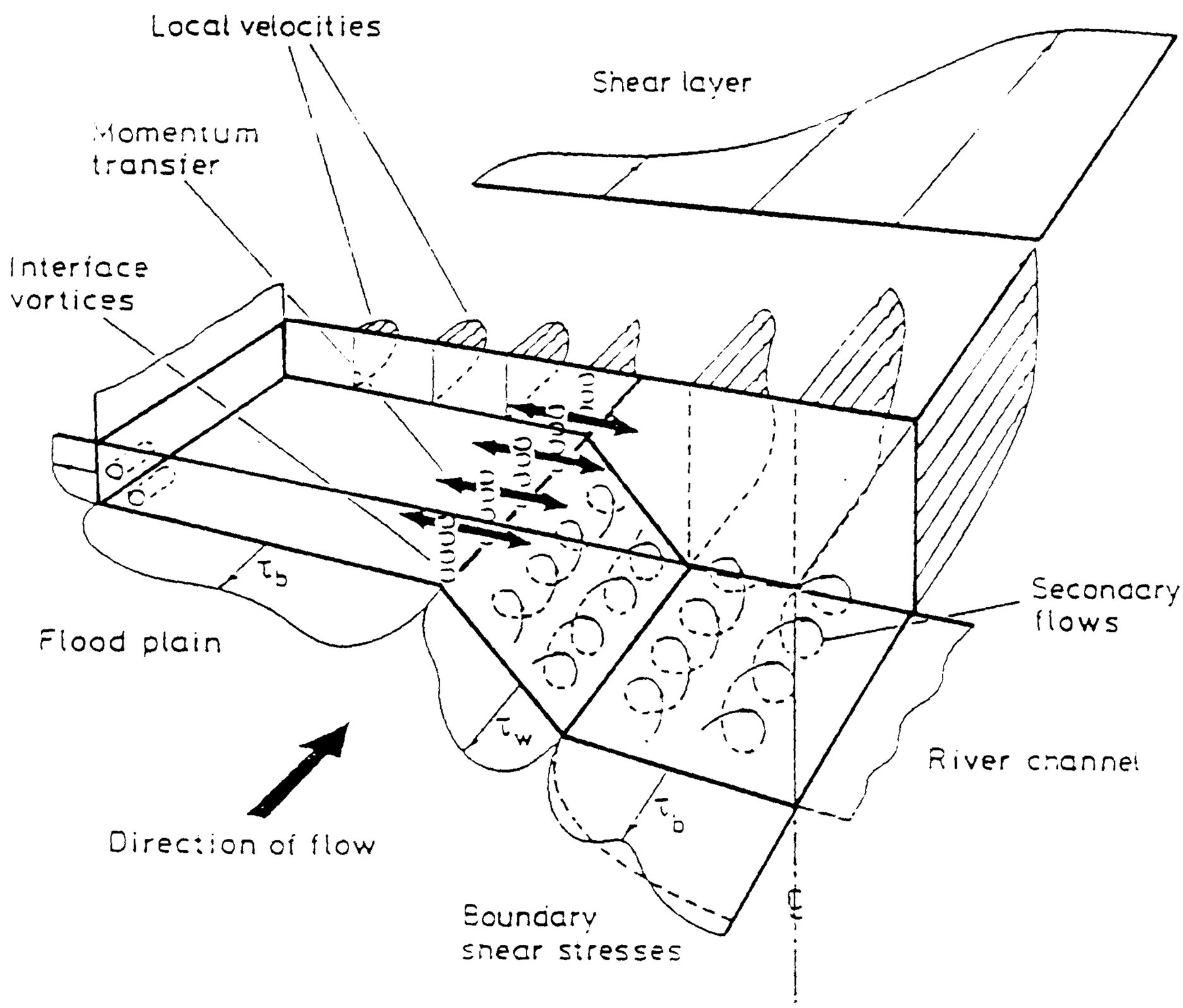

FIG (2.3) The Flow Mechanisms in Straight Main Channel With Overbank Flow. (Knight 1983)

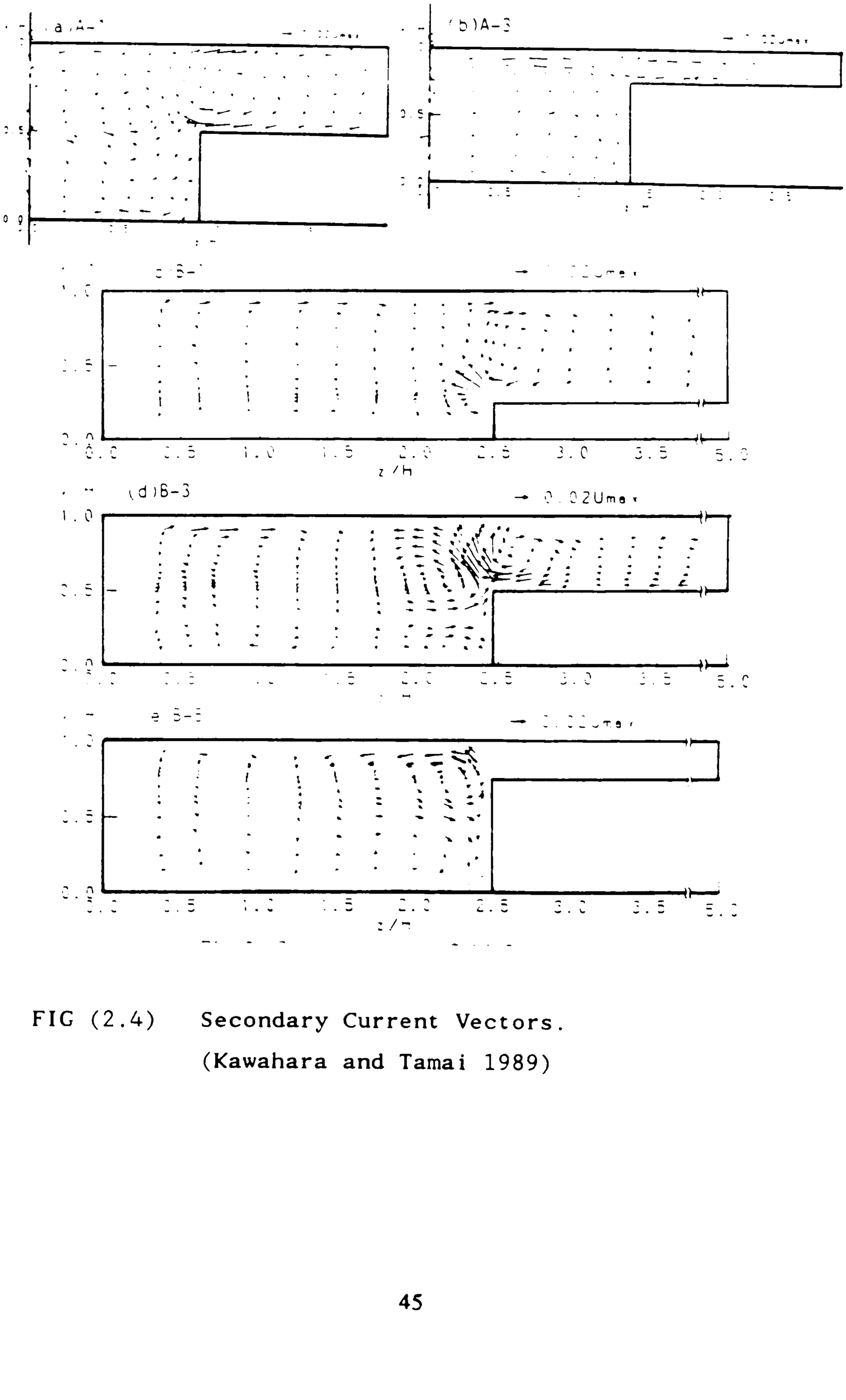

FIG (2.4) Secondary Current Vectors.
(Kawahara and Tamai 1989)

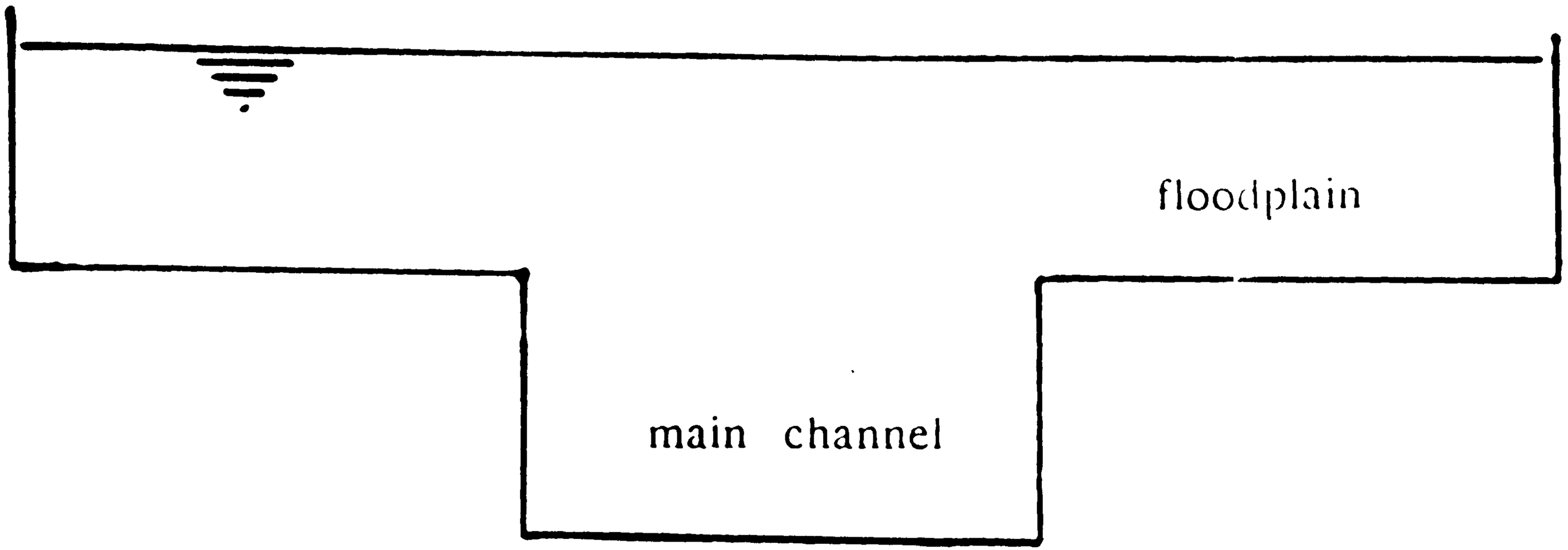

FIG (2.5) The Compound Cross Section

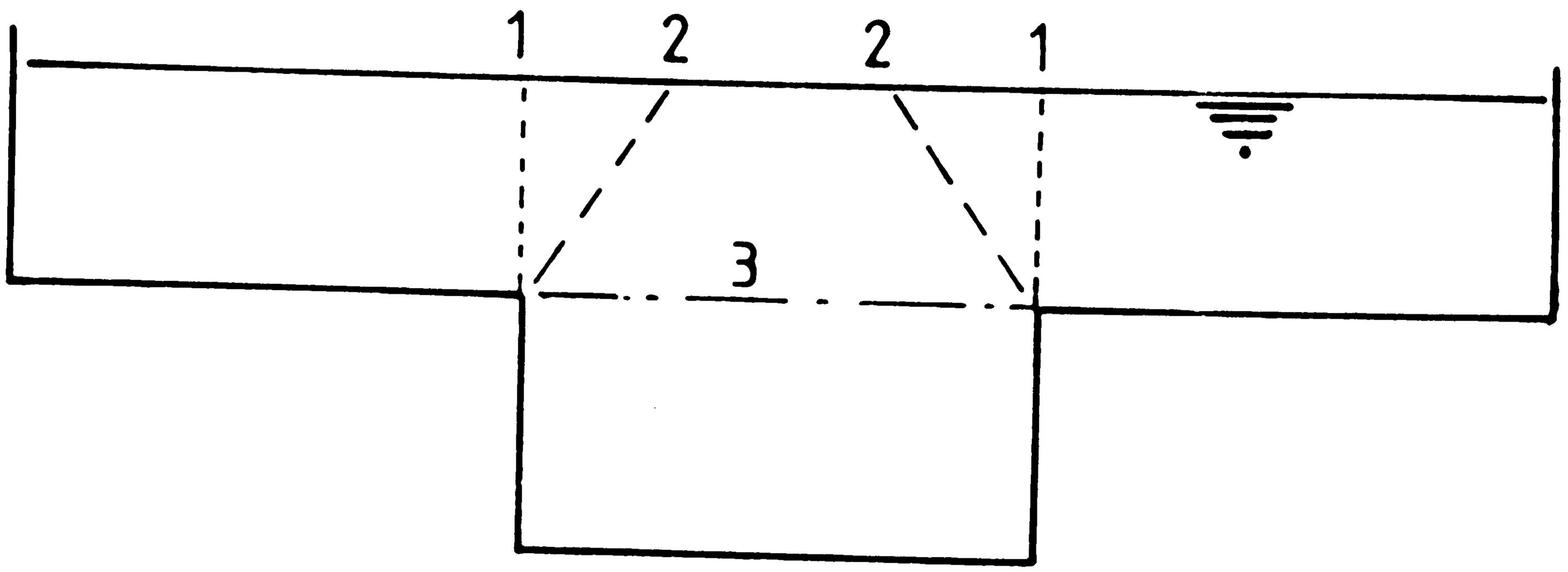

FIG (2.6) Sub-divided Channel Methods

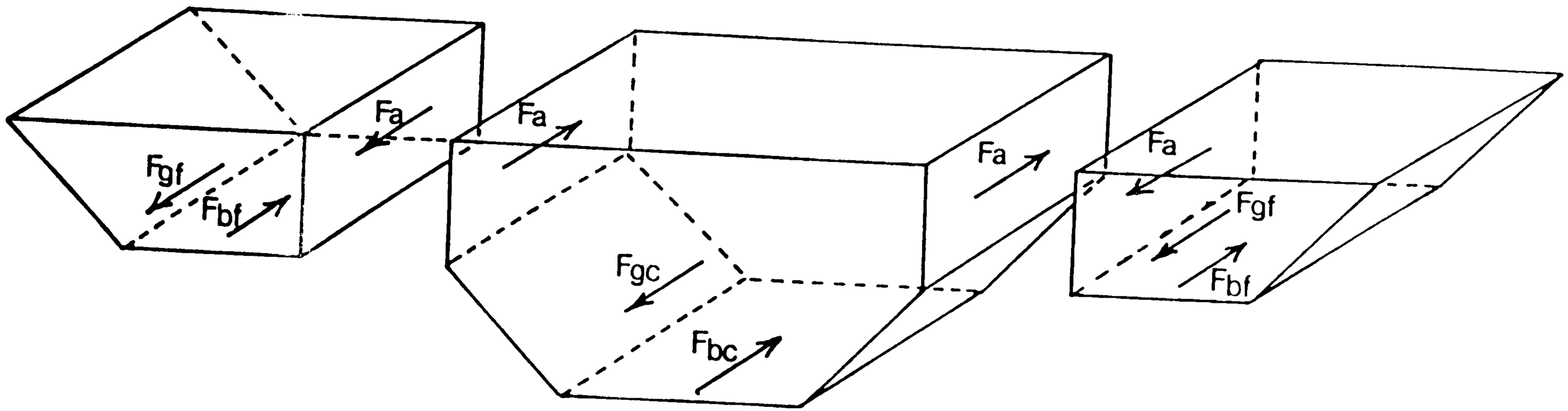

Fig (2.7) The Out Balance Forces in Compound Cross Section.

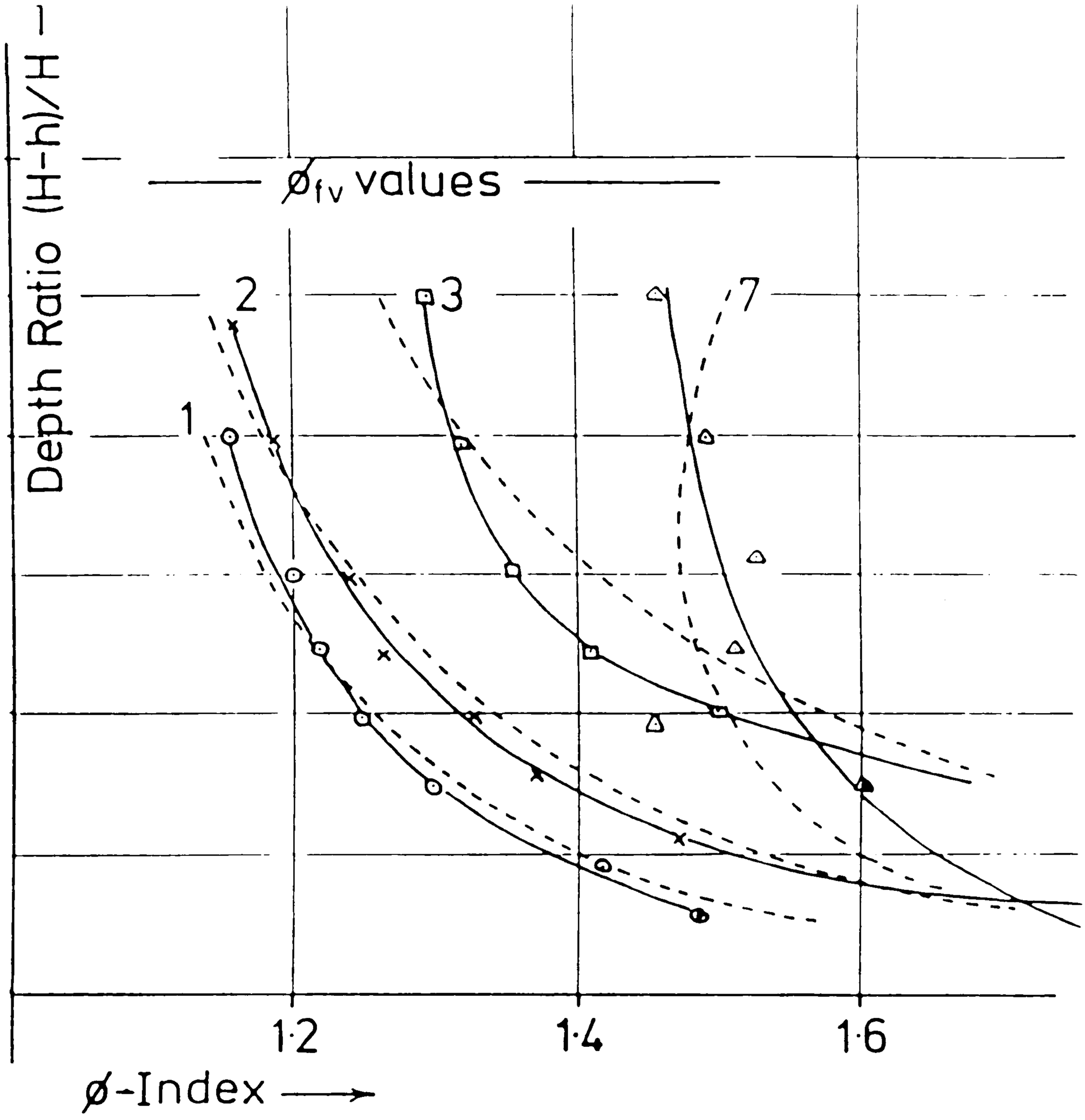

FIG (2.8) The Relationship Between Φ and Relative Depth
(Wormleaton and Merrett 1988)

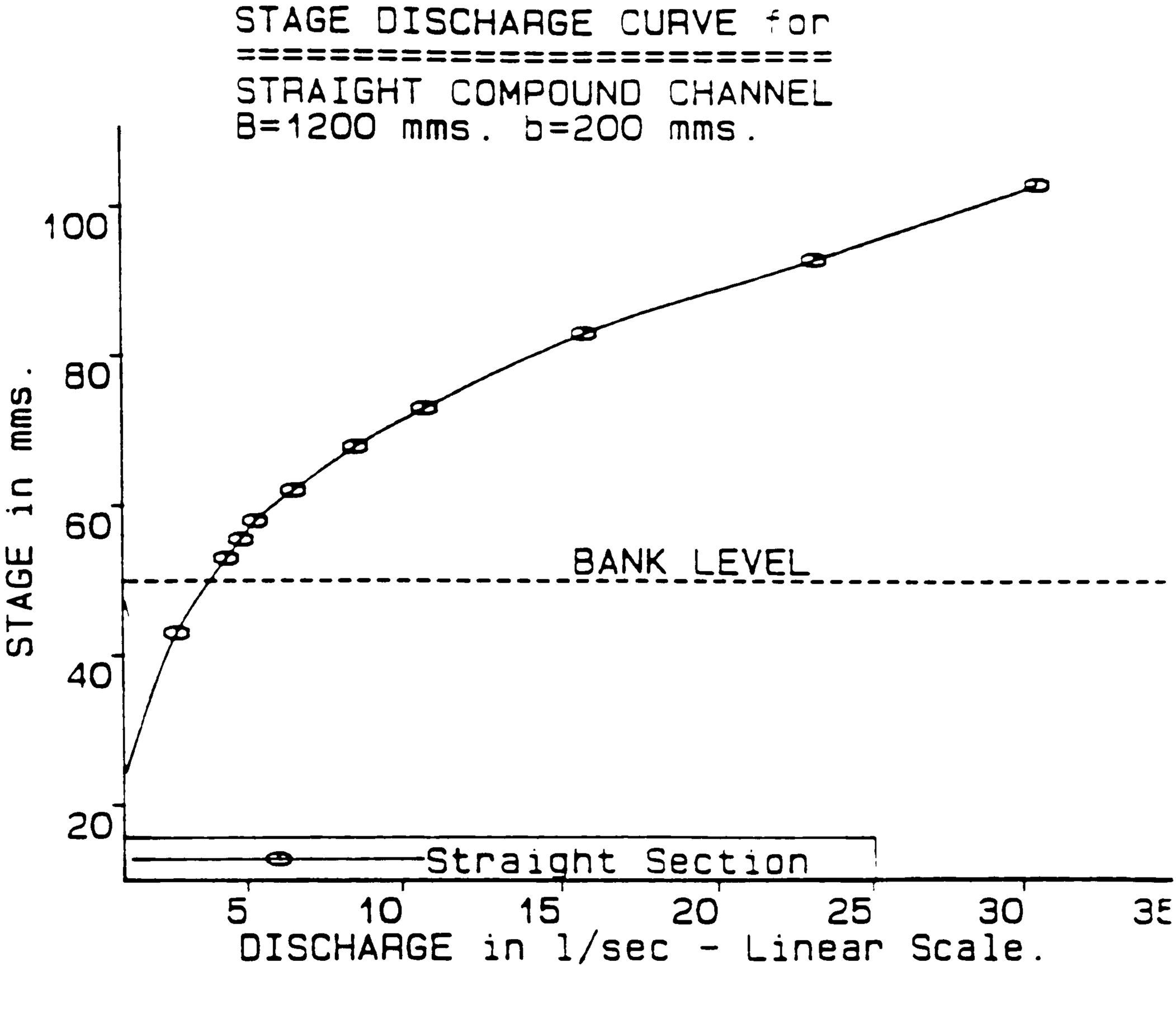

FIG (2.9) Stage Discharge Curve For Straight Main Channel With Flood Plain. (Kiely 1989)

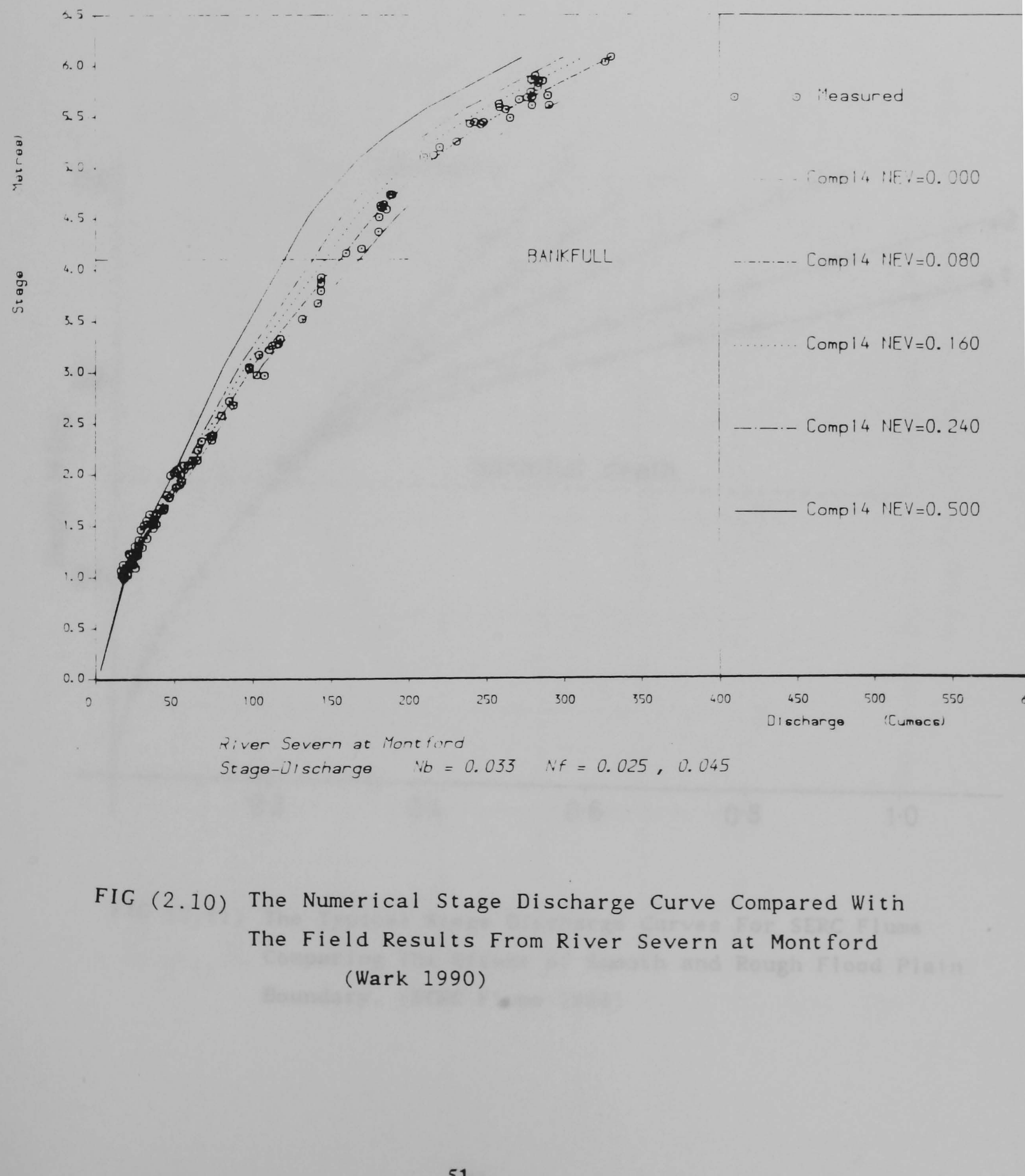

River Severn at Montford
Stage-Discharge Nb = 0.033 Nf = 0.025 , 0.045

FIG (2.10) The Numerical Stage Discharge Curve Compared With The Field Results From River Severn at Montford (Wark 1990)

B_f/b_c = 5.47 for Geo.1
B_f/b_c = 3.0 for Geo.2
B_f/b_c = 1.0 for Geo.3
B_f/b_c = 0 for Geo.4
B_f/b_c = 3.0 for Geo.7

b_c= 1/2 B_c =0.75
S_0 = 1.027×10^{-3}

Geo.7 (flood plain roughned
by 25mm wooden dowels
12 dowels/m^2)

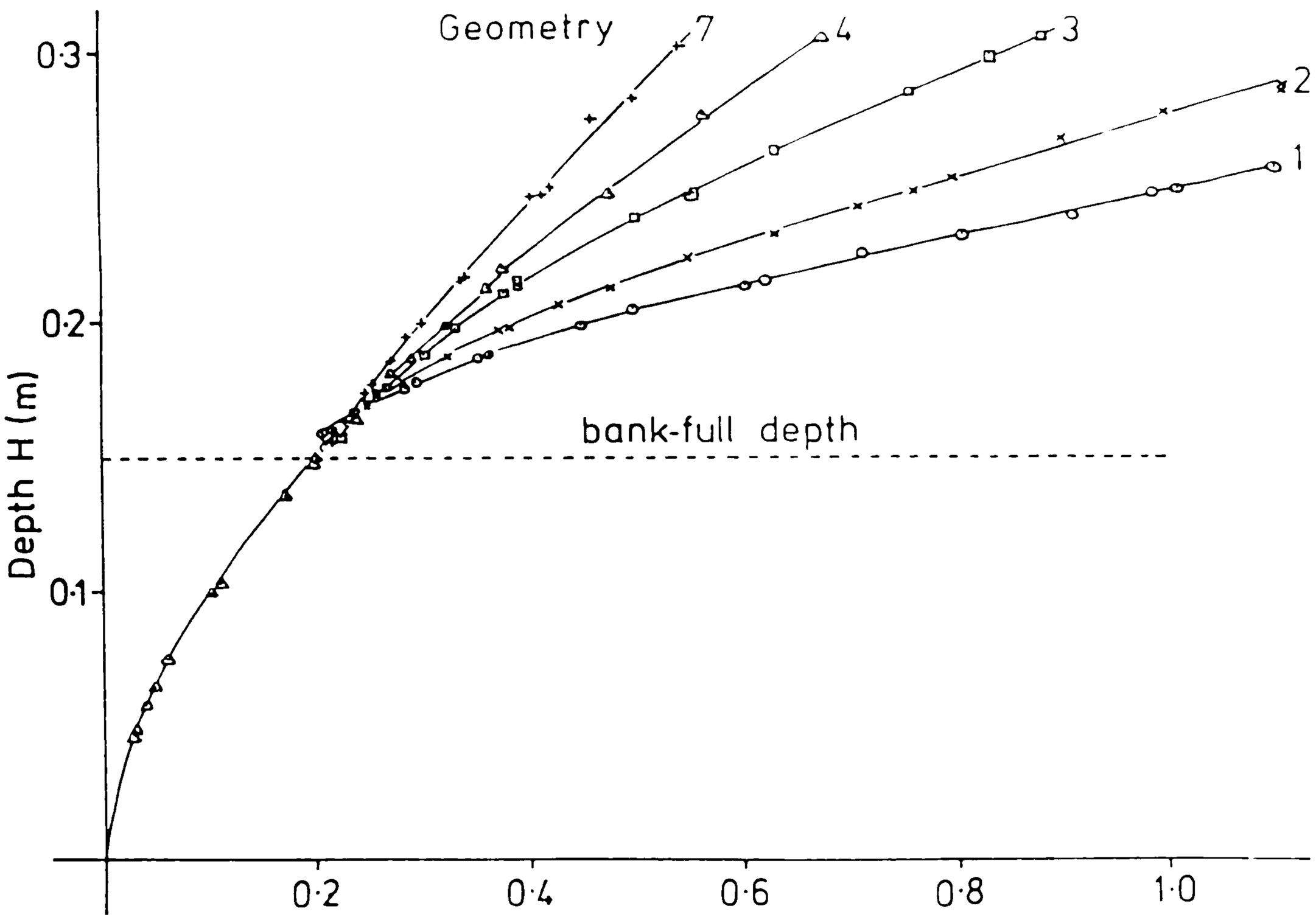

FIG (2.11) The Typical Stage Discharge Curves For SERC Flume Comparing The Effect of Smooth and Rough Flood Plain Boundary. (SERC Flume 1988)

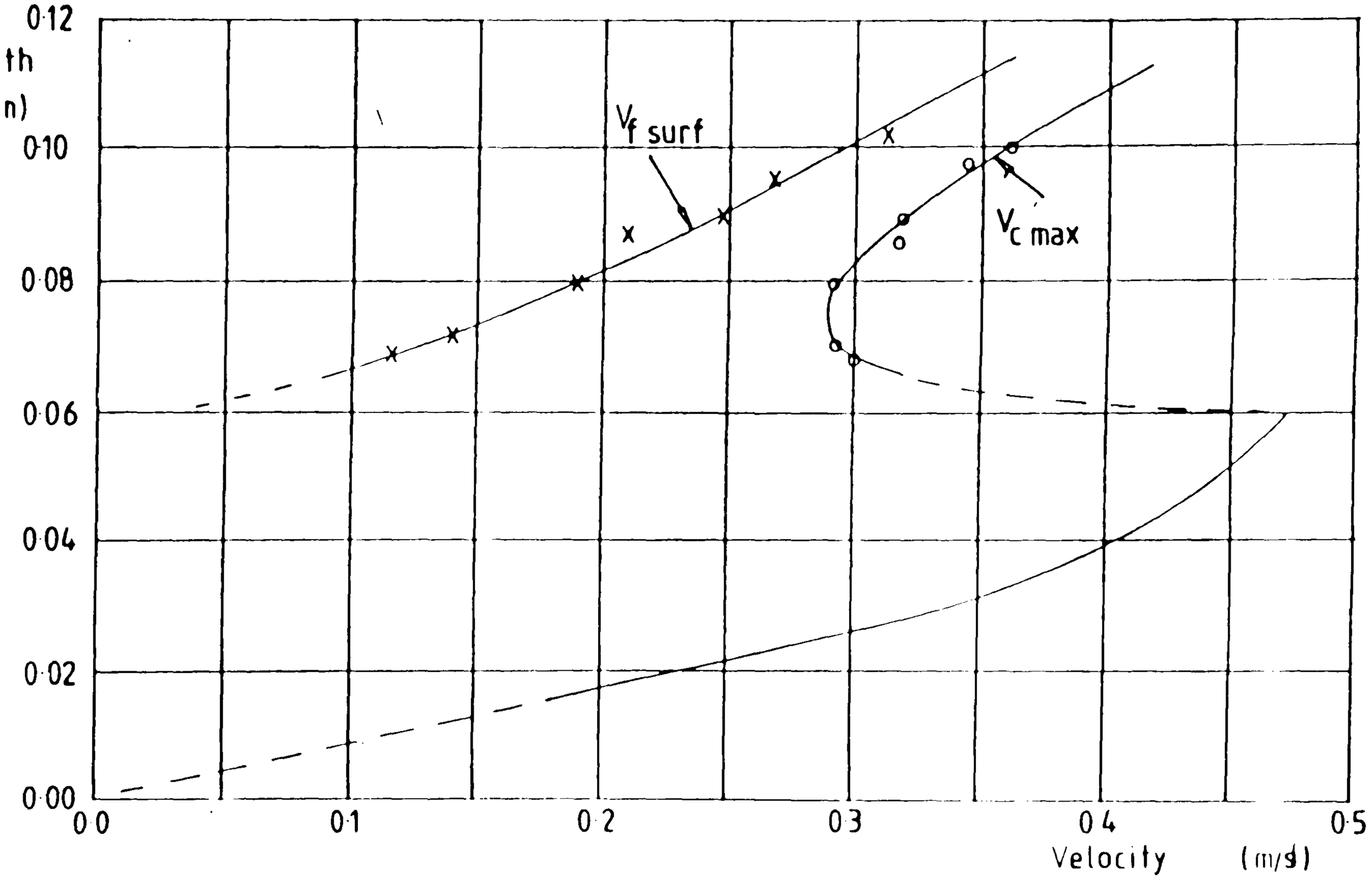

FIG (2.12) The Velocity Magnitude in Channel and Flood Plain During Interaction Flow. (Zhelezyakove 1965)

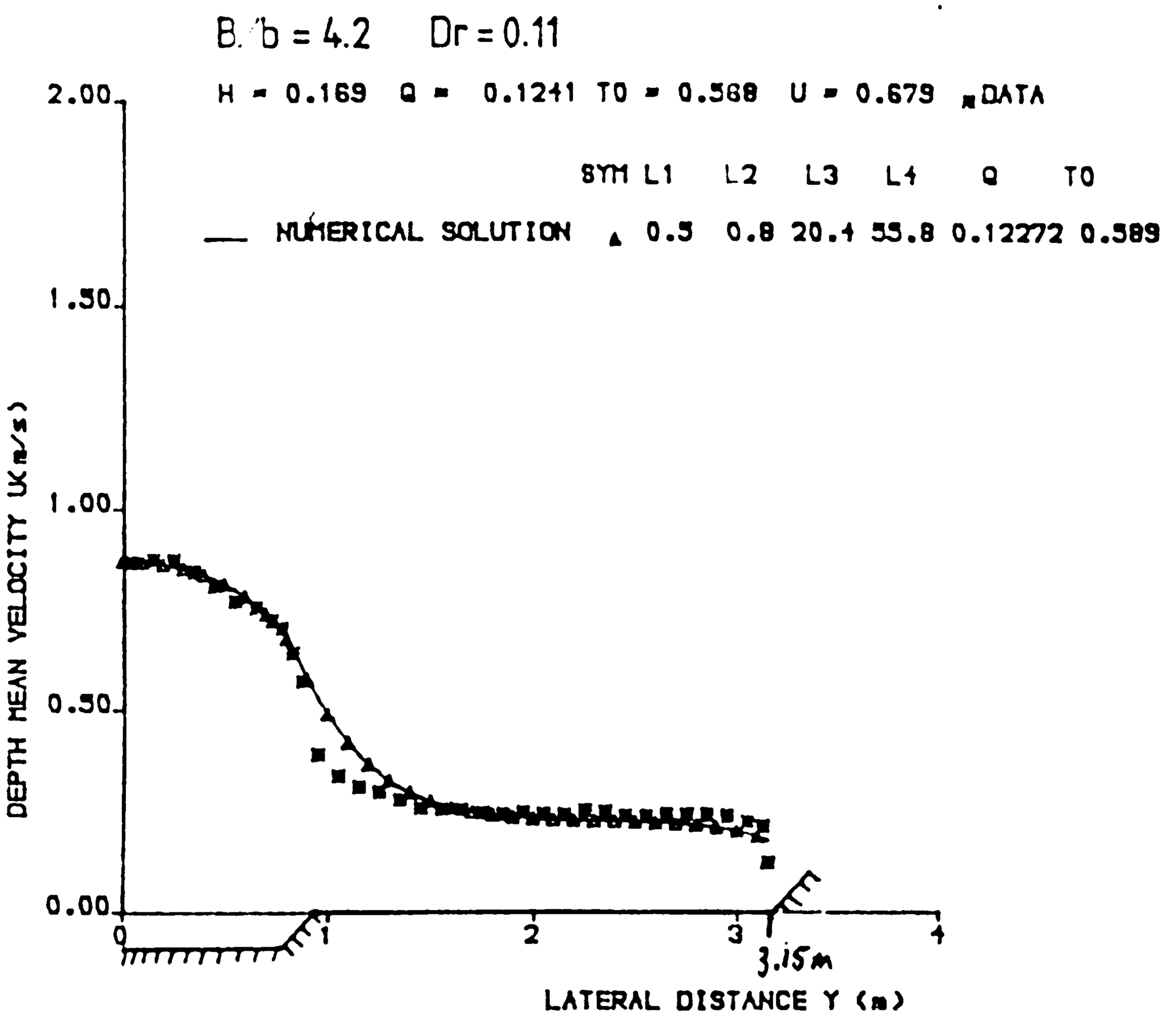

FIG (2.13) The Numerical Depth Averaged Velocity Compared With Experimental Results. (Knight, Shiono and Prit 1988)

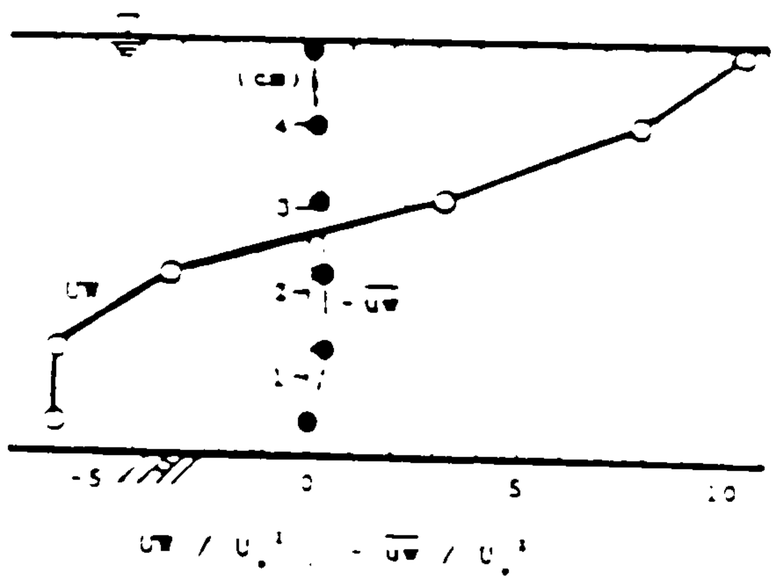

Momentum transfer

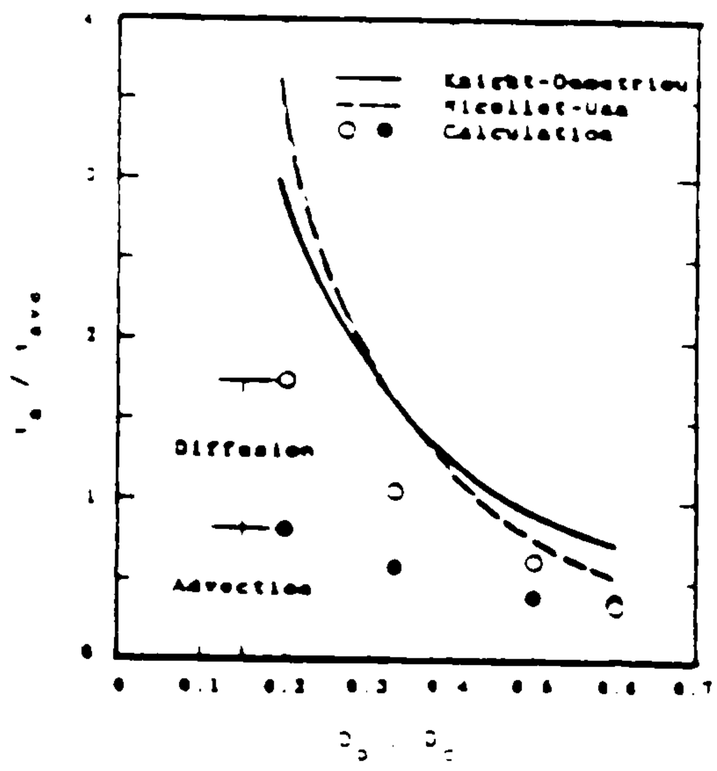

Effect of water depth
on apparent shear stress

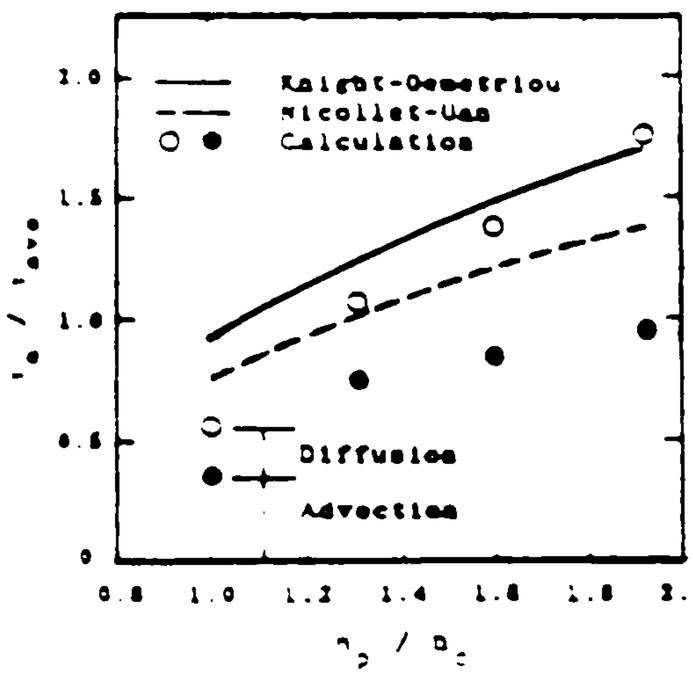

Effect of flood plain roughness
on apparent shear stress.

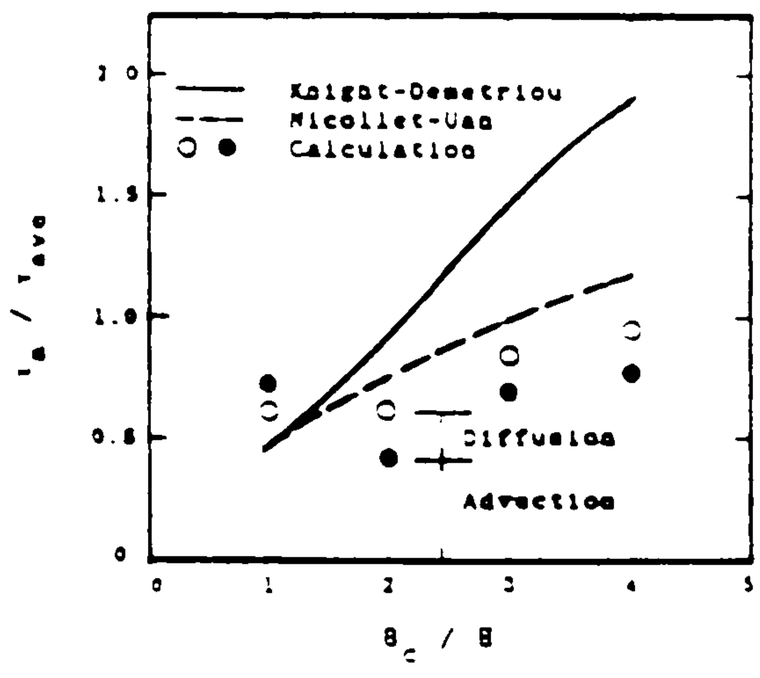

Effect of main channel width
on apparent shear stress.

FIG (2.14) Kawahara et al. (1989)

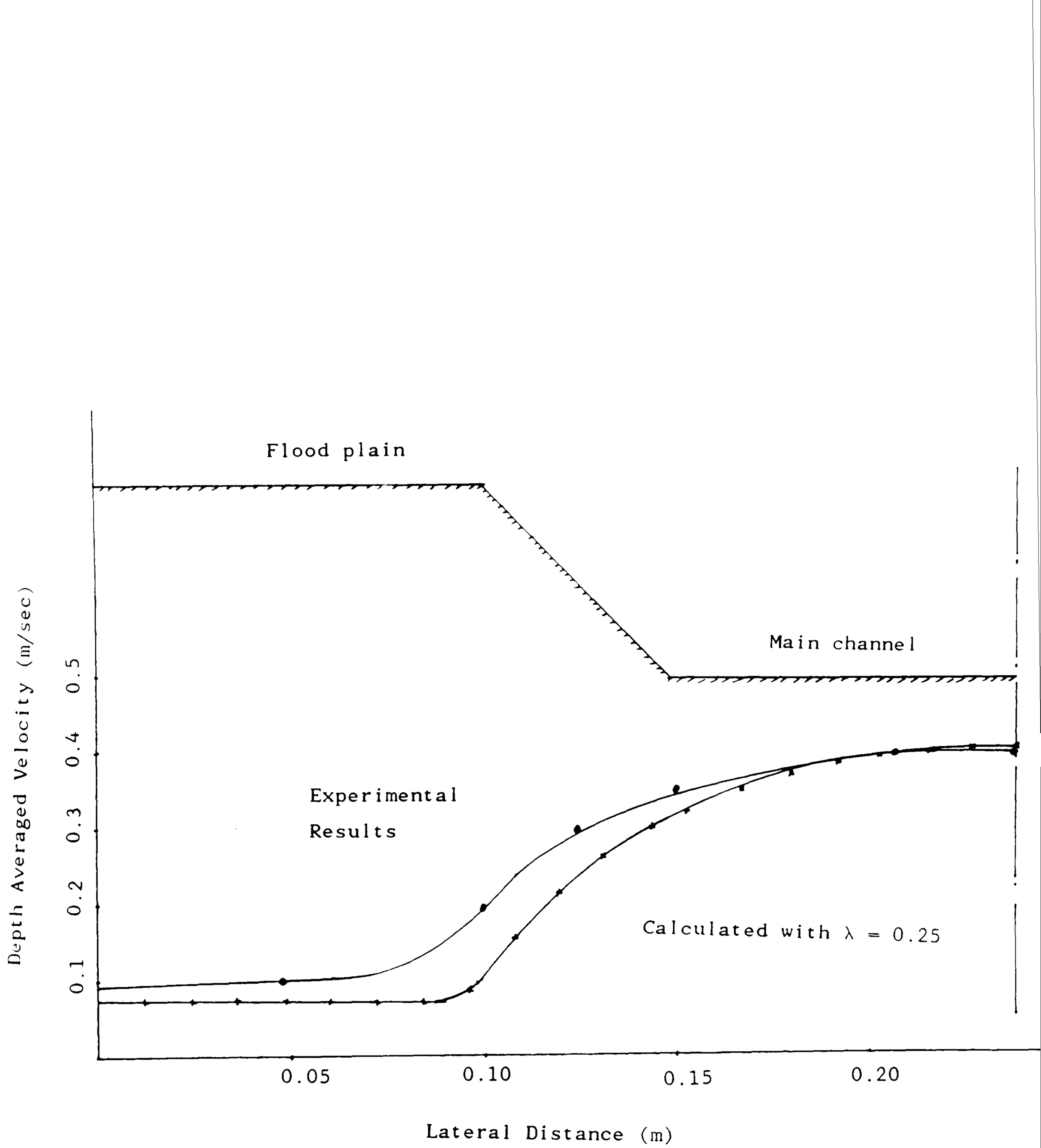

FIG (2.15) The Numerical Depth averaged Velocity Compared With The SERC Flume Data.(Wormleaton 1988)

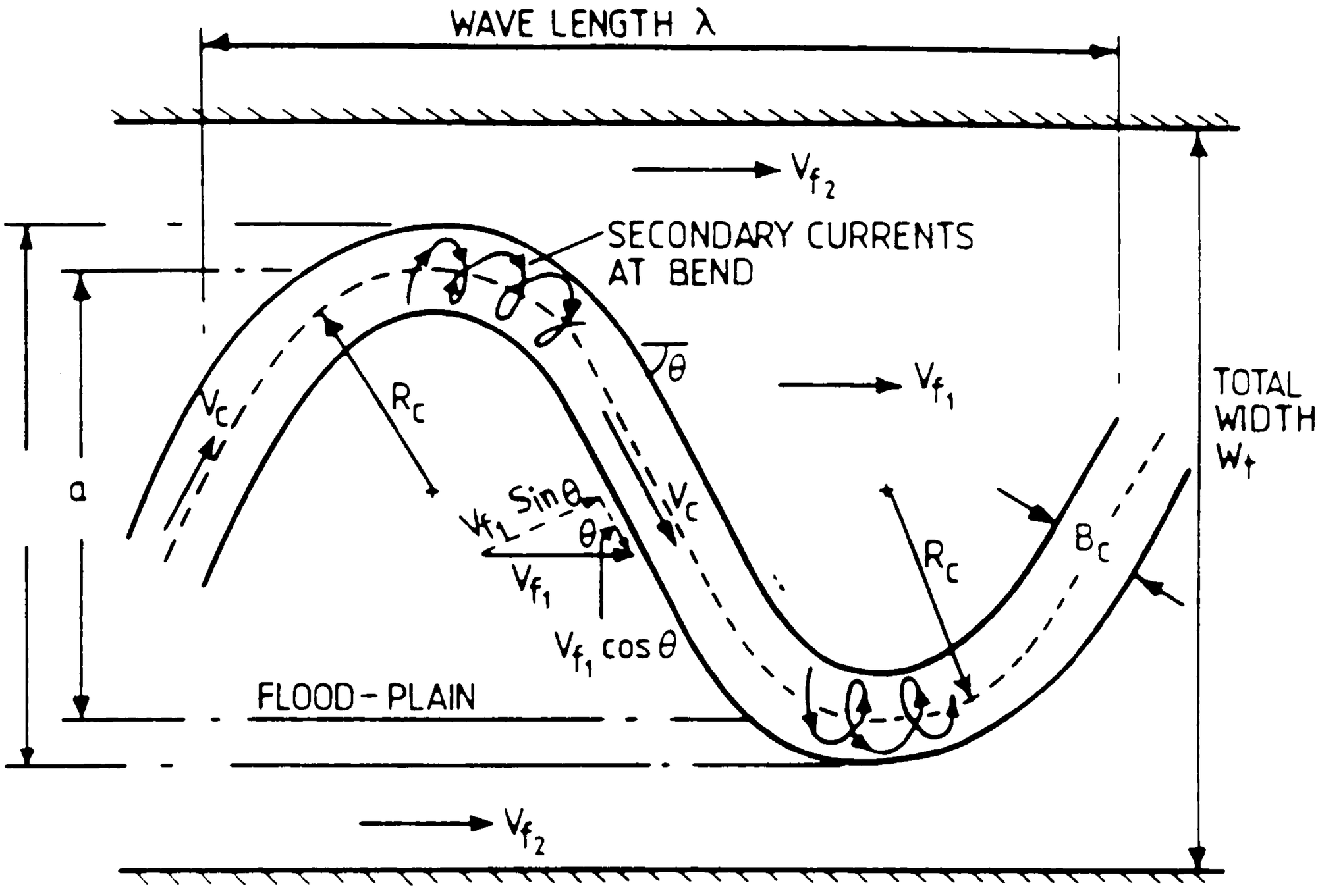

FIG (2.16) The Flow Mechanisms For Meandering Channel With Flood Plain. (Ervine and Ellis 1987)

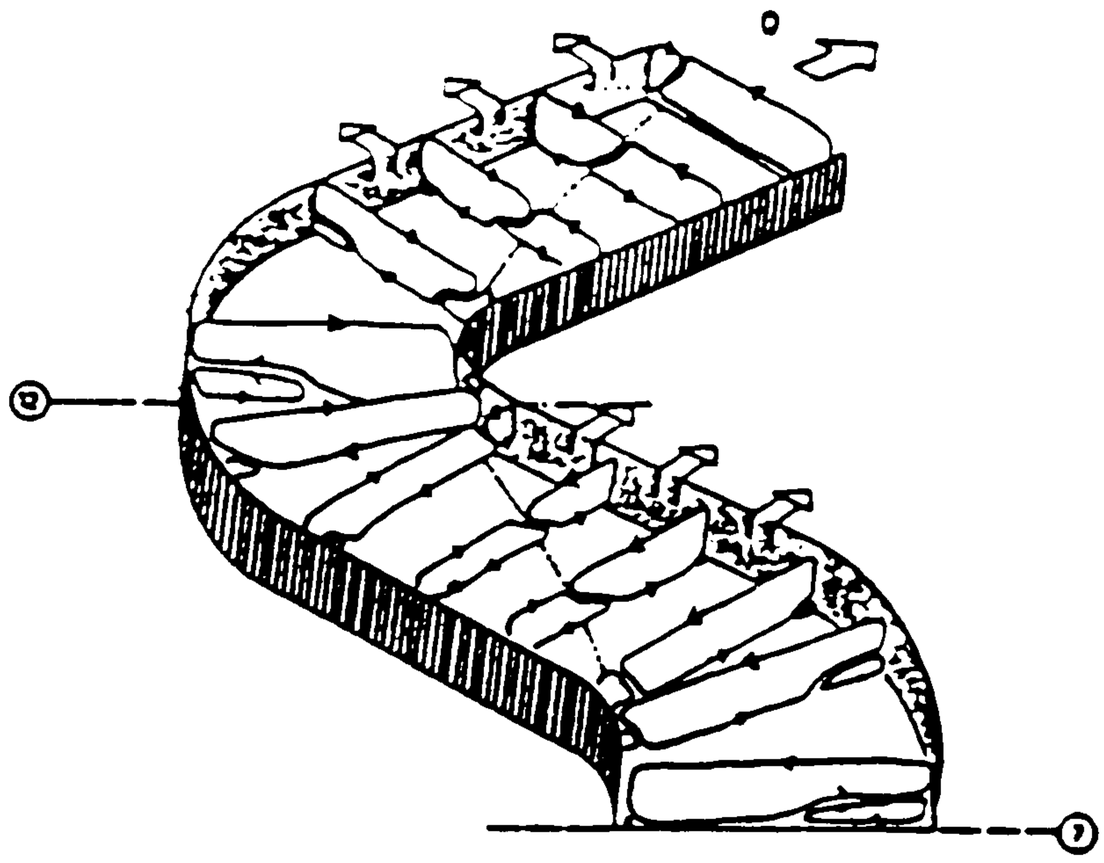

Secondary motion in the bend

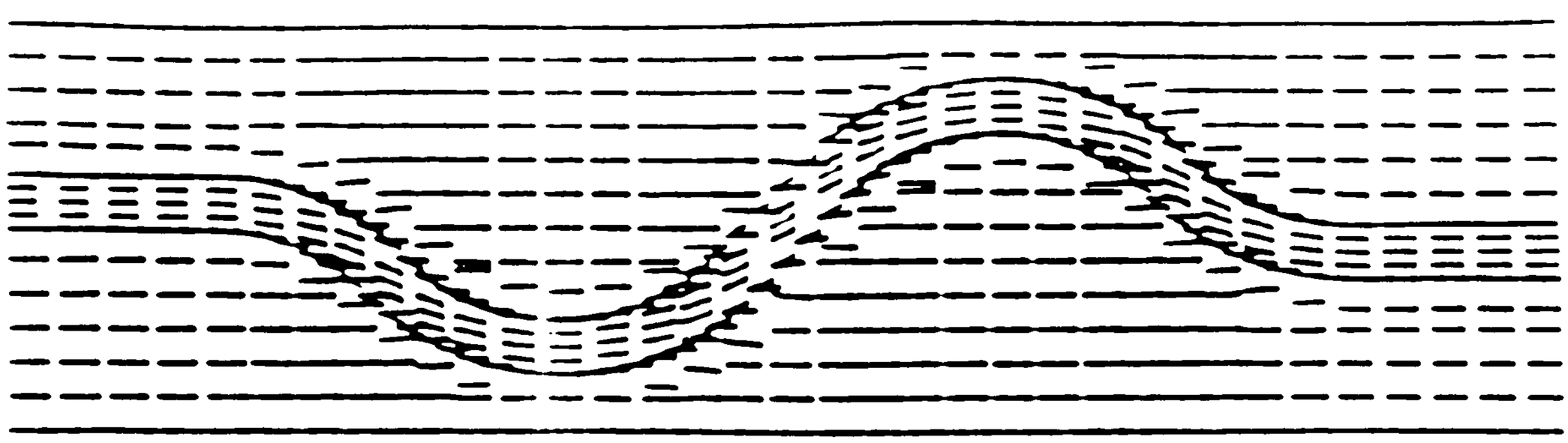

Vectors of Depth Averaged Velocities

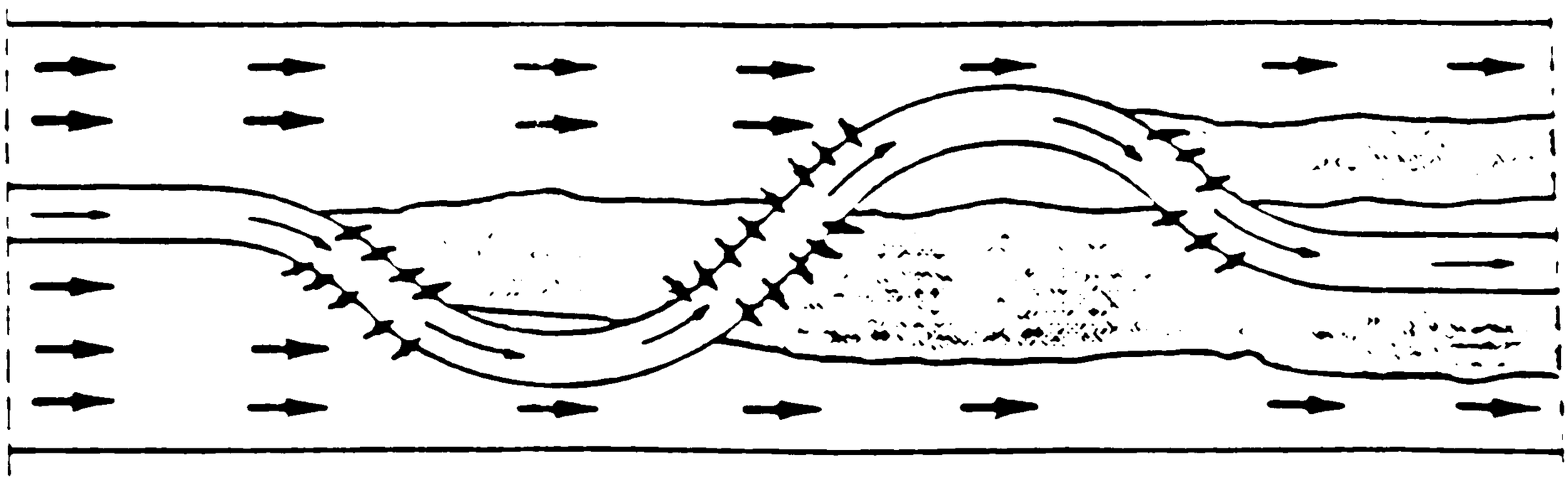

Qualitative Distribution of Discharge

FIG (2.17) Stein and Rouve (1988).

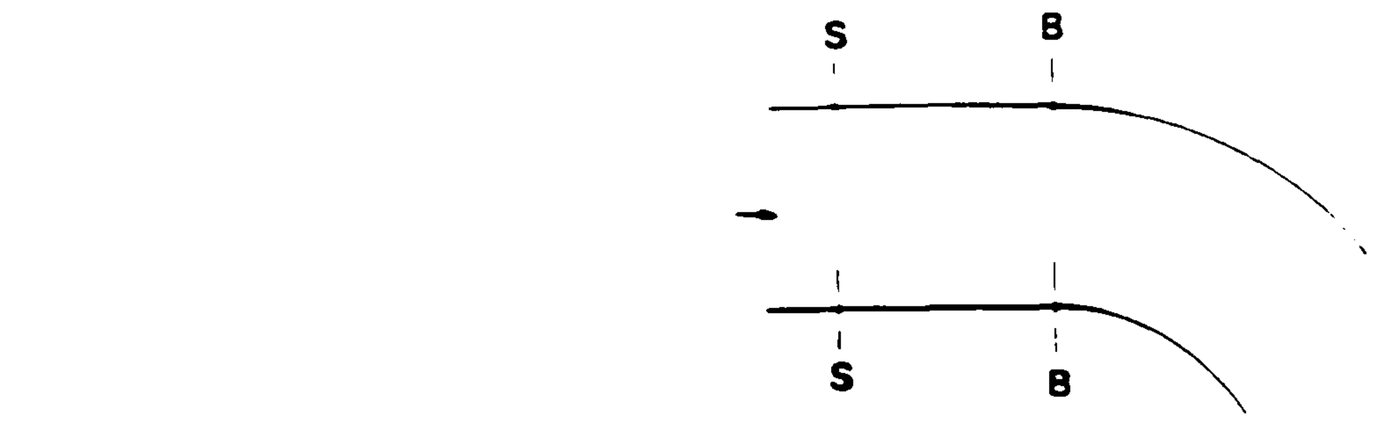

Plan

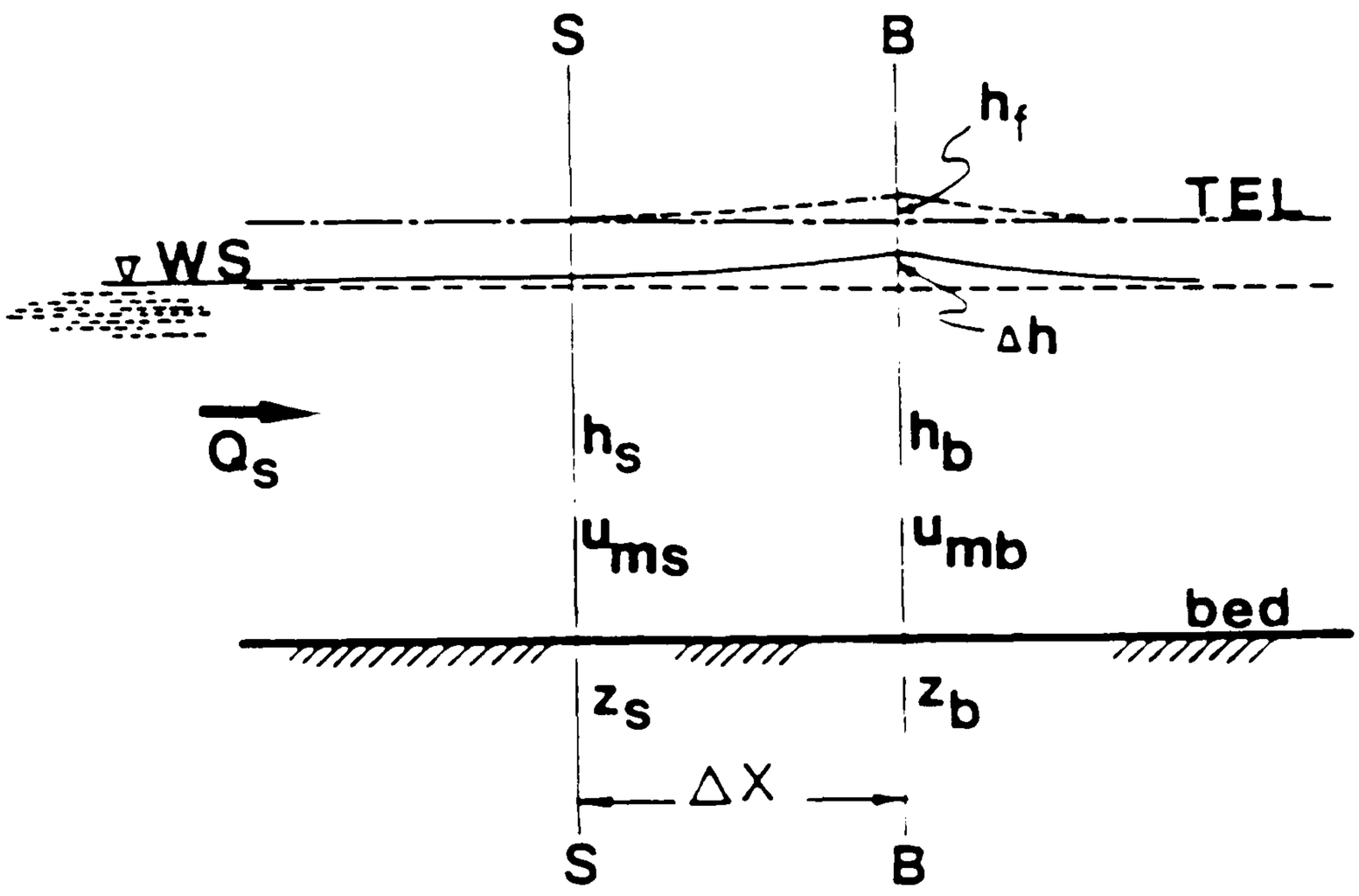

Long. Sec.

FIG (2.18) **Profiles of Flow Surface and Energy at the Bend Entrance**

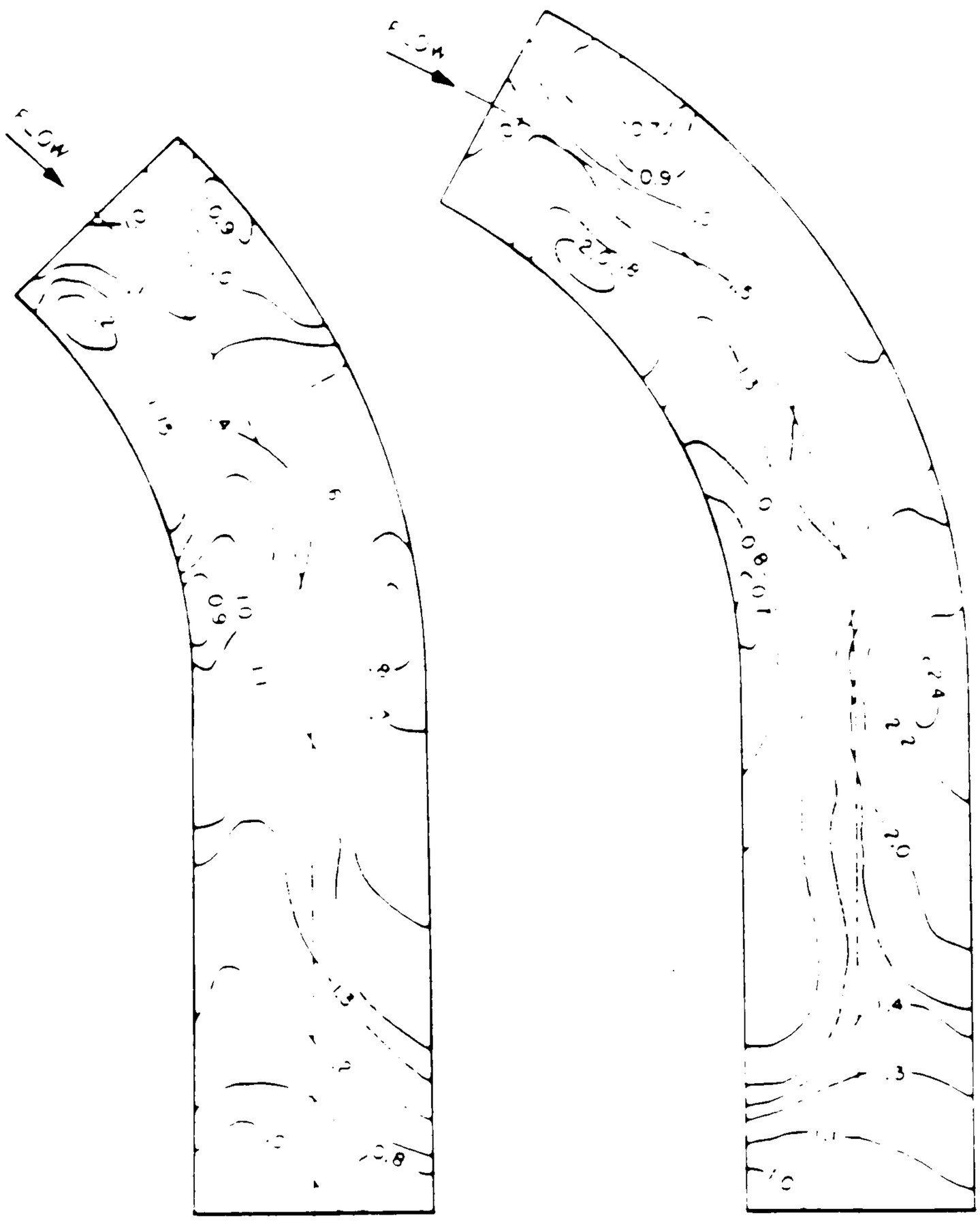

a b

FIG (2.19) Observed Dimensionless Shear Stress Distributions
(a) $\theta_b = 45^\circ$
(b) $\theta_b = 60^\circ$
(after Nouh et al (1979))

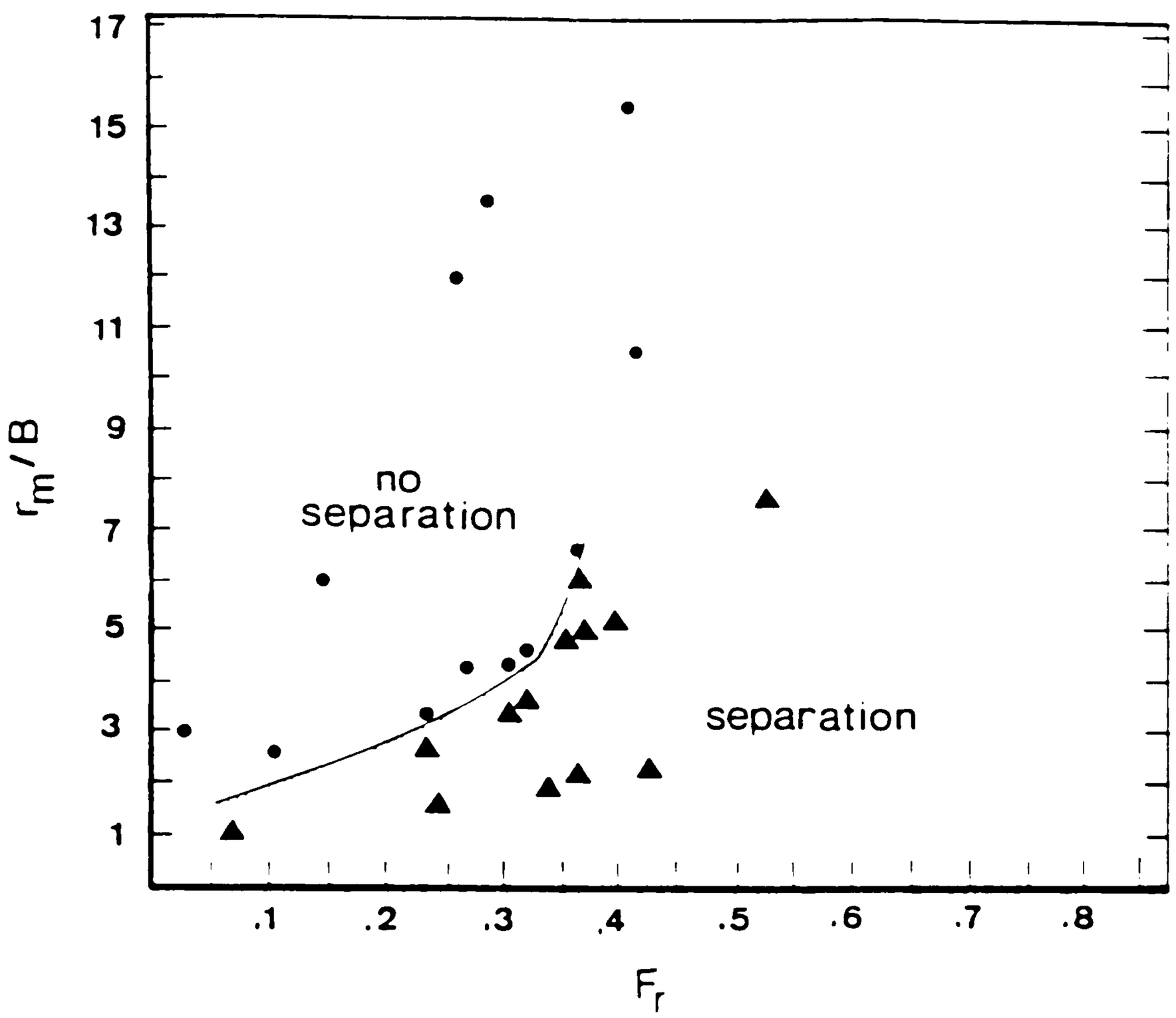

FIG (2.20) Occurrence of Flow Separation in River Bends
(●) No Flow Separation
(▲) Flow Separation
(after Leeder et al (1975))

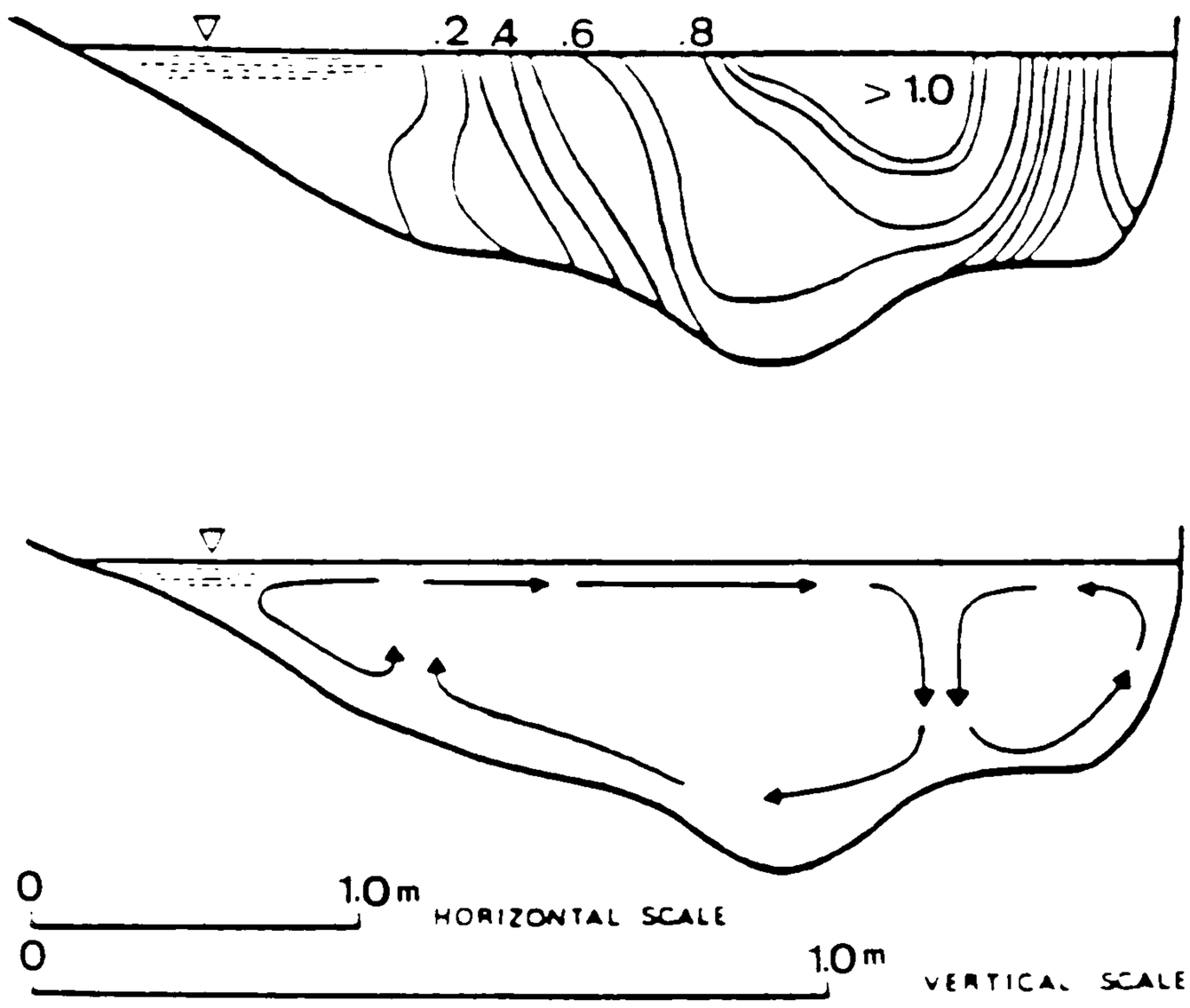

FIG (2.21) Velocity Distribution and Secondary Flows at Meander Apex, River DOVE. ($\theta_b = 90^\circ$, $r_m = 62.5$m , Velocities in m/s) (after Hey et al (1975))

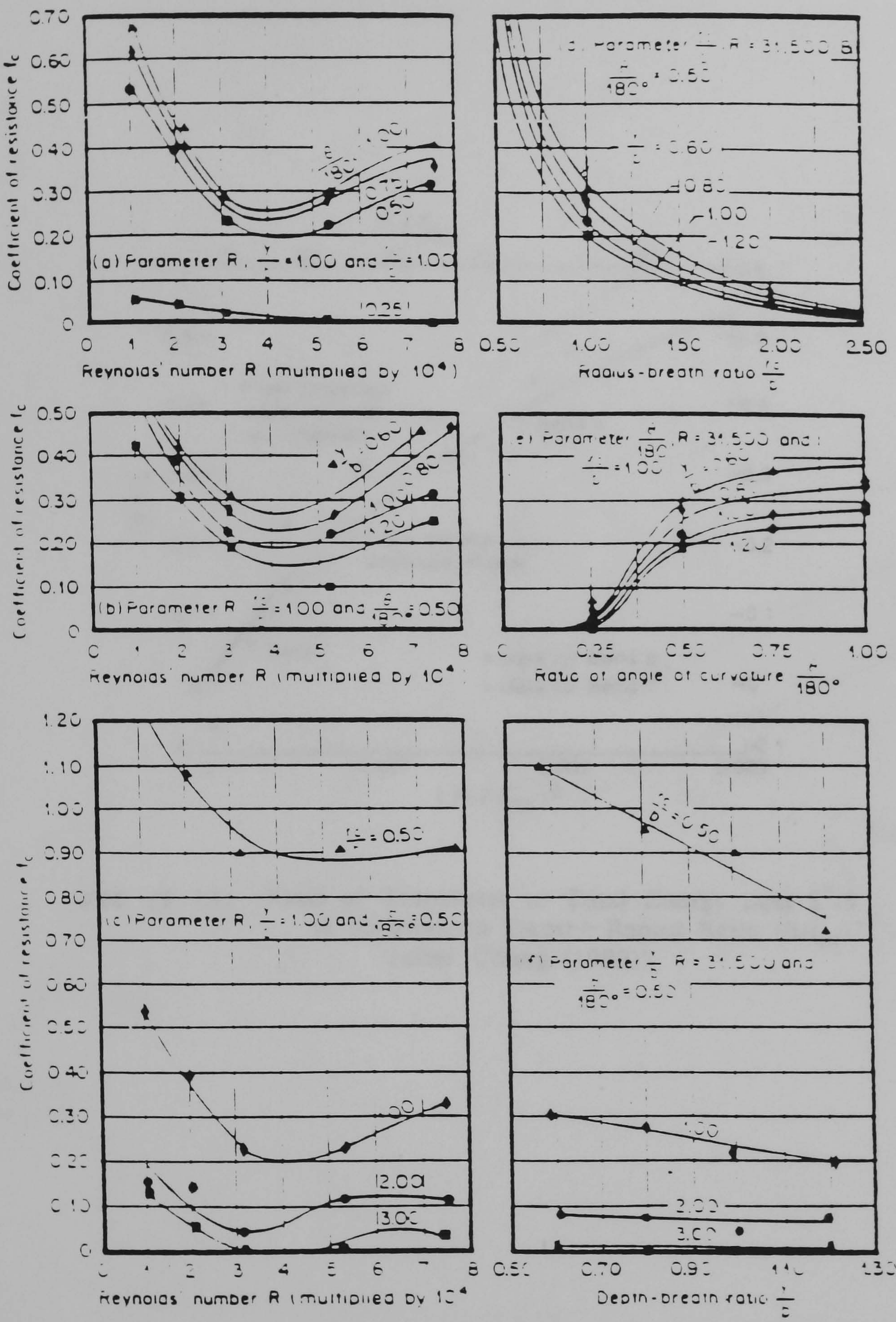

FIG (2.22) Experimental Parametric Functions of the Coefficient of bend resistance (after Shukry (1949))

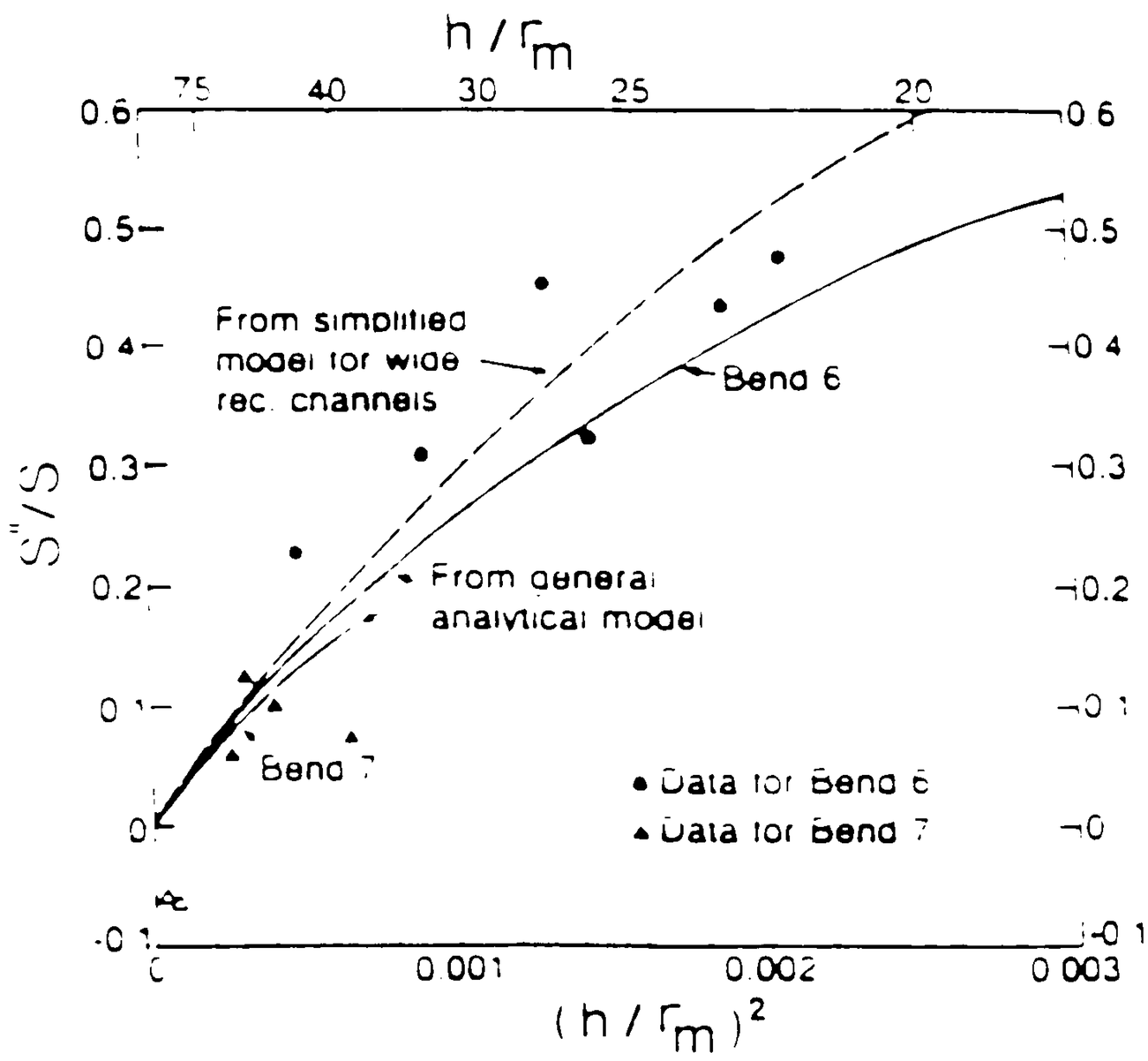

FIG (2.23) Ratio of Transverse to Total Energy Loss S''/S in Relation to Depth–Radius Ratio $(h/r_m)^2$ (after Chang (1983))

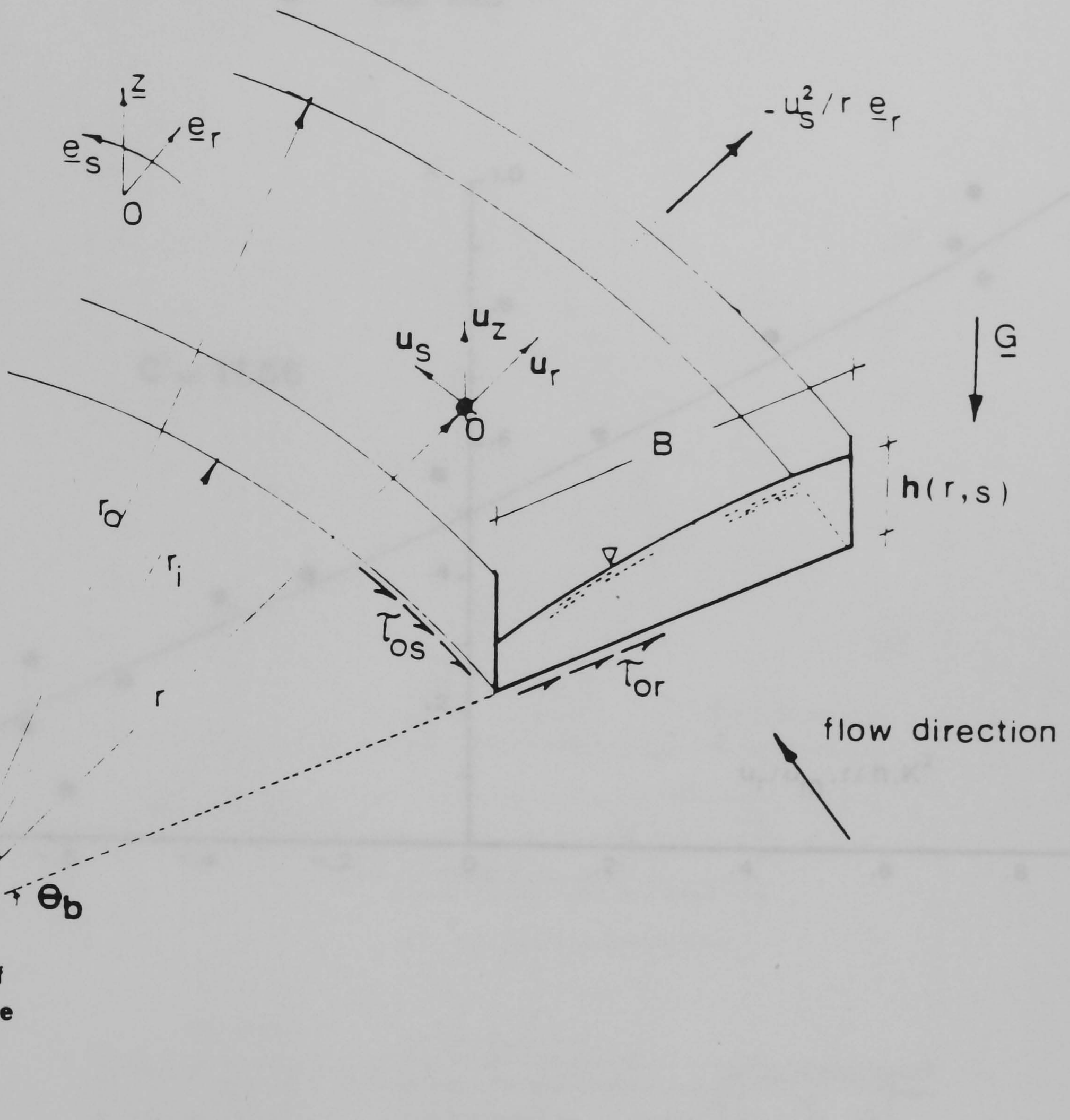

FIG (2.24) The Gentle Rectangular Bend
Used by Fares and Herbetson 1988.

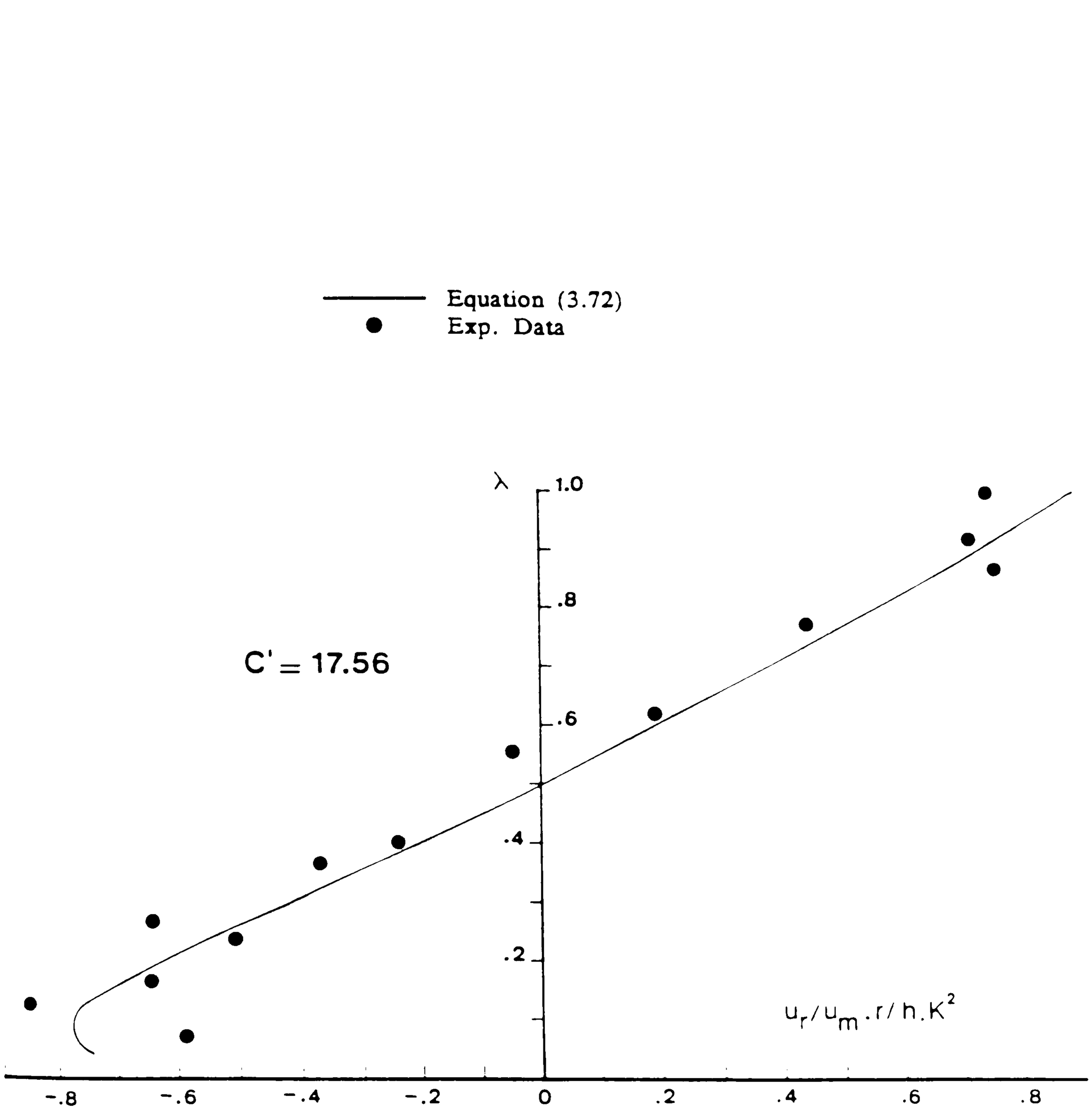

FIG (2.25) Comparison of the Predicted Profile of $u_r(\lambda)$ with the Experimental Data obtained from Kondrat'ev et al (1959)

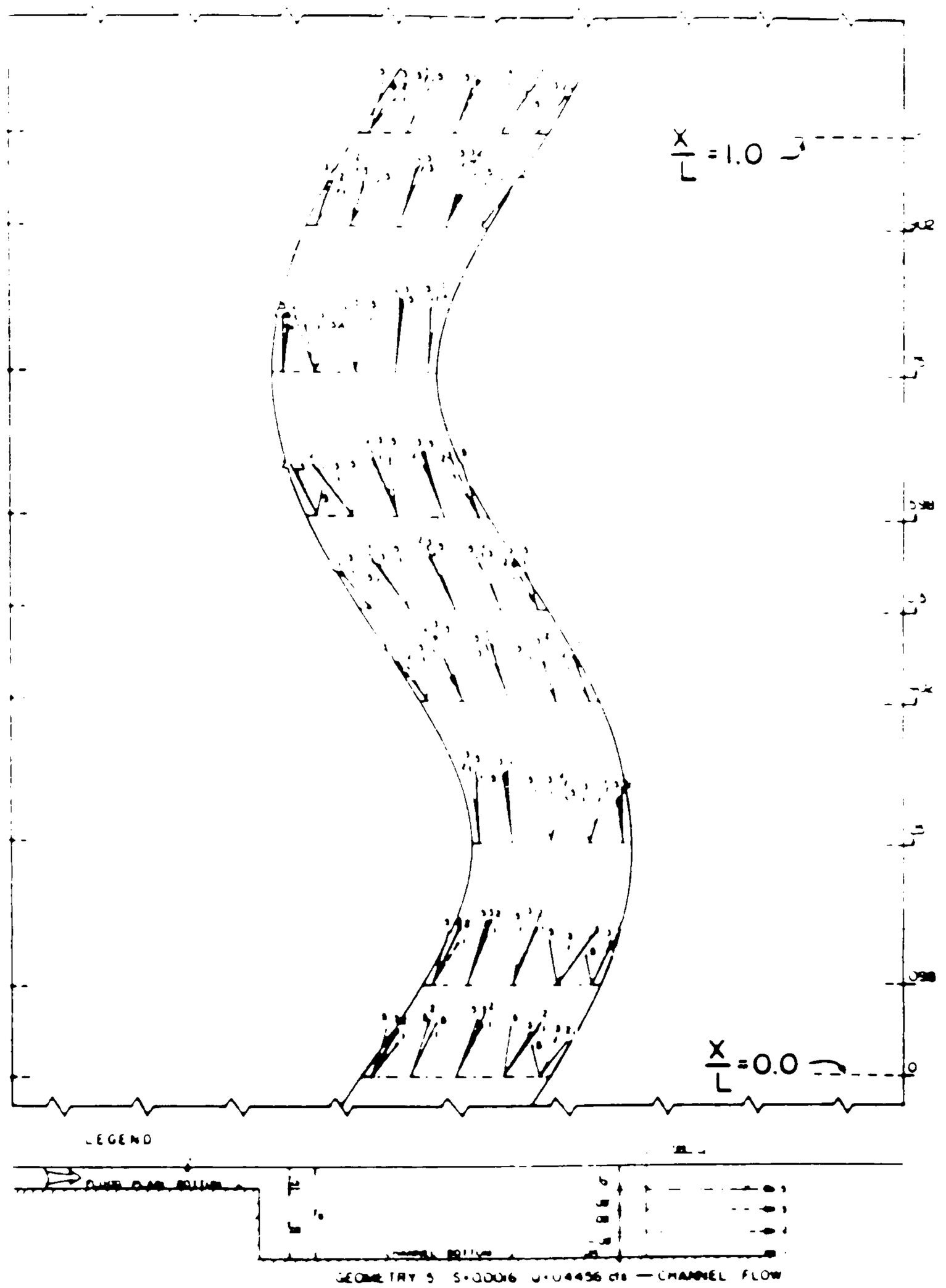

FIG (2.26) The Plan Geometry and Secondary Current For Meandering Channel With Flood Plain.
(Toebes and Sooky 1967)

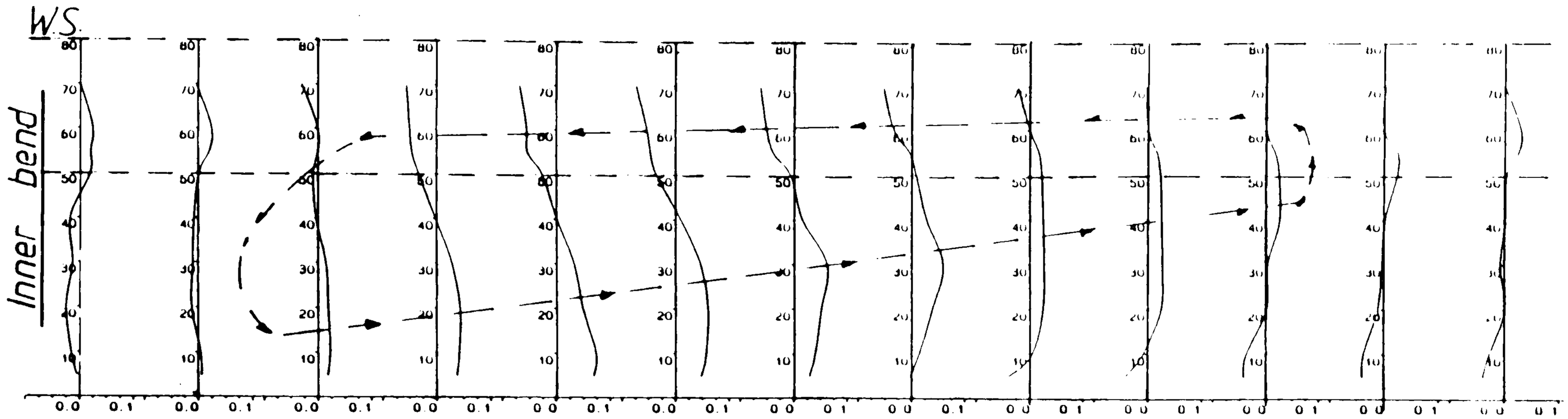

VERTICAL PROFILES of SECONDARY VELOCITY, m/sec, SECTION S1, for 200mm WIDTH of MAIN CHANNEL only

5mms 10mms 20mms 40mms 60mms 80mms C/LINE 120mms 140mms 160mms 180mms 190mms 195mms

FIG (2.27) The Secondary Current Recirculation in Meandering Channel With Overbank Flow (Kiely and McKeogh 1989)

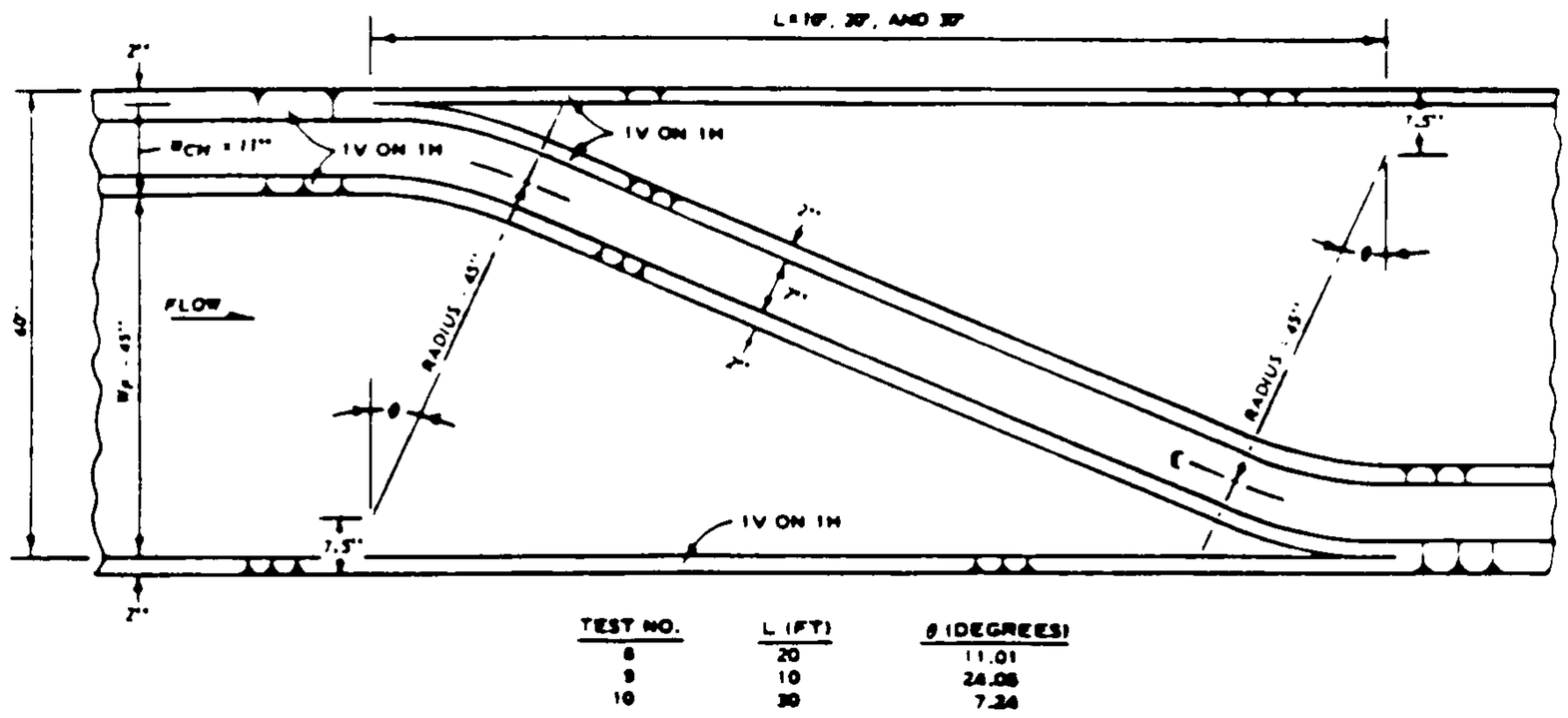

Figure 3. Plan view of single crossover configurations

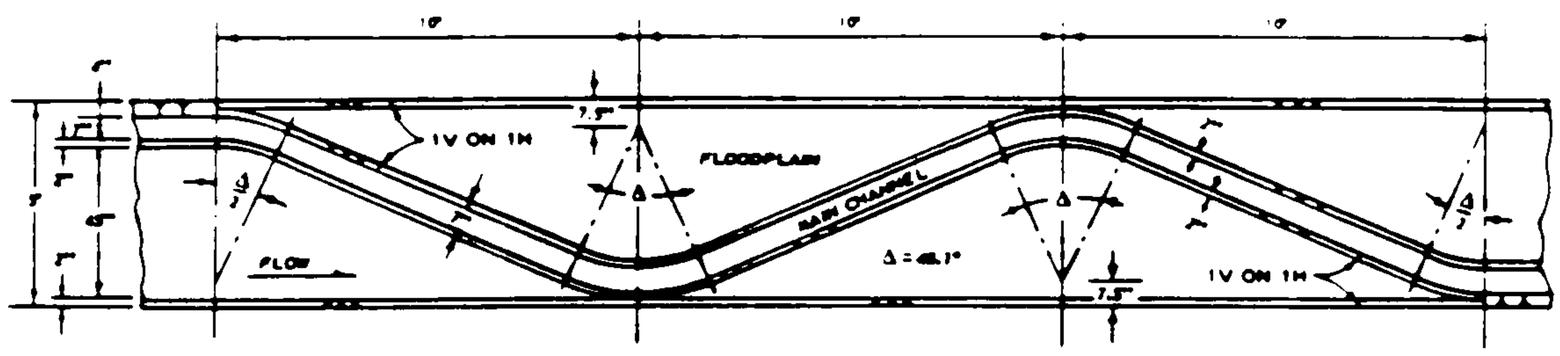

Figure 4. Plan view of three consecutive crossovers, Test 11

FIG (2.28) James and Brown Models (1977)

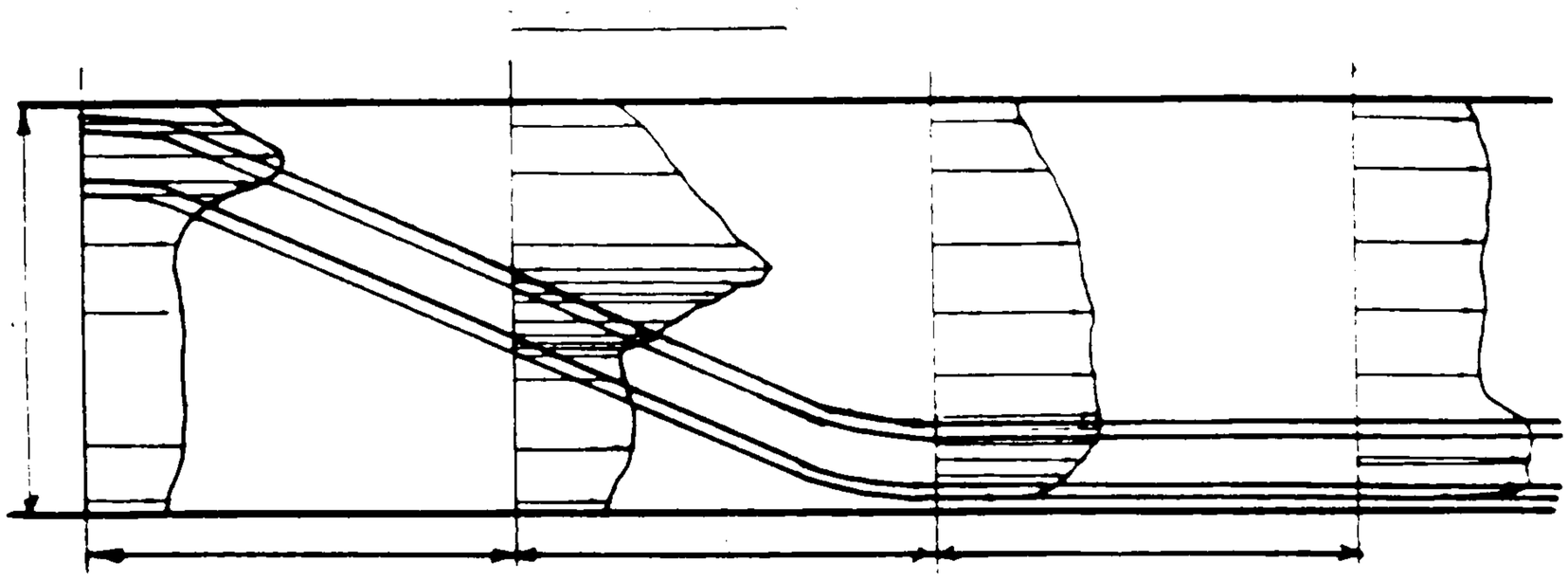

Test Conditions
aspect ratio 4.09
depth 0.21ft.
slope 0.001
$\bar{V}$ average velocity
$\bar{\bar{V}}$ Discharge/area

VELOCITY PROFILES
ON PLAN
MEANDERING CHANNEL WITH
0-FT CROSSOVER

FIG (2.29a) James and Brown (1977)

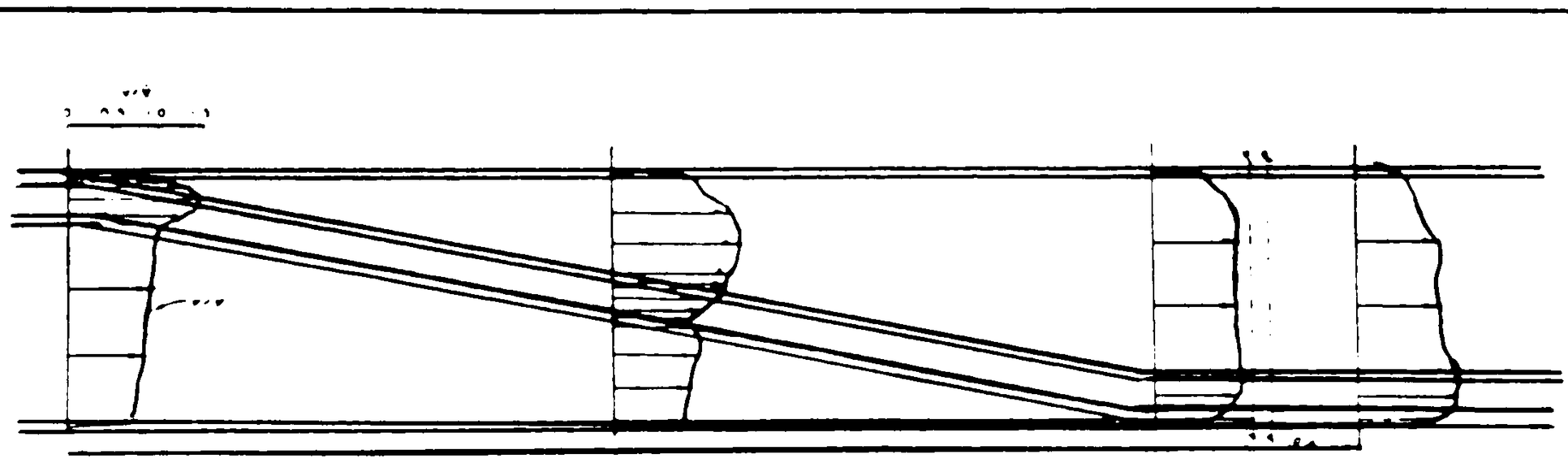

Test Conditions
aspect ratio 4.09
depth 0.21ft.
slope 0.001
$\bar{V}$ average velocity
$\bar{\bar{V}}$ Discharge/area

VELOCITY PROFILES
ON PLAN
MEANDERING CHANNEL WITH
20-FT CROSSOVER

FIG (2.29b) James and Brown (1977)

FIG (2.29) The Velocity Profile For Skewed Main Channel With Flood Plain. (James and Brown 1977)

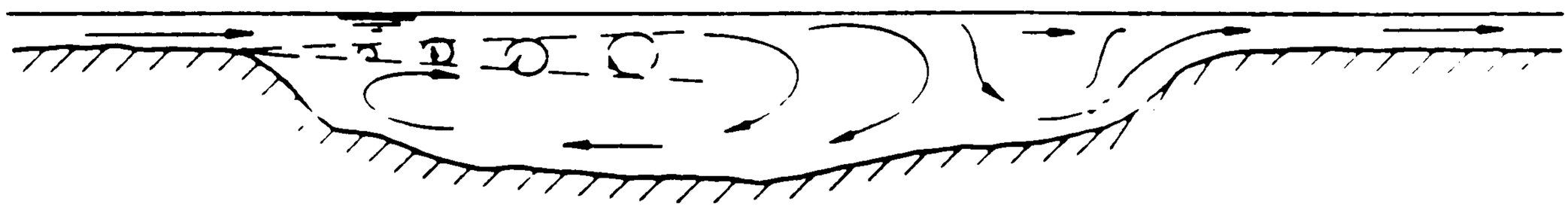

FIG (2.30a) Inferred recirculation pattern in the lower channel at cross-over region. Shallow overbank depth.

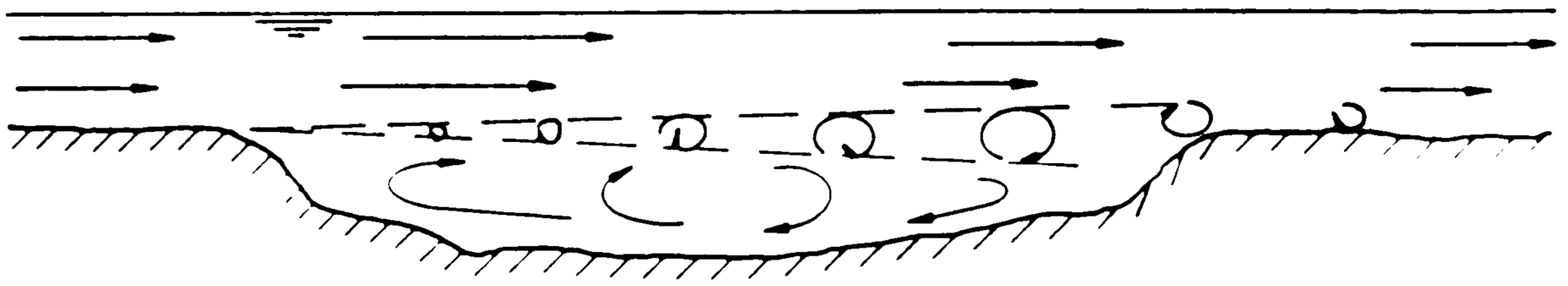

FIG (2.30b) Inferred recirculation pattern in the lower channel at cross-over region. High overbank depth.

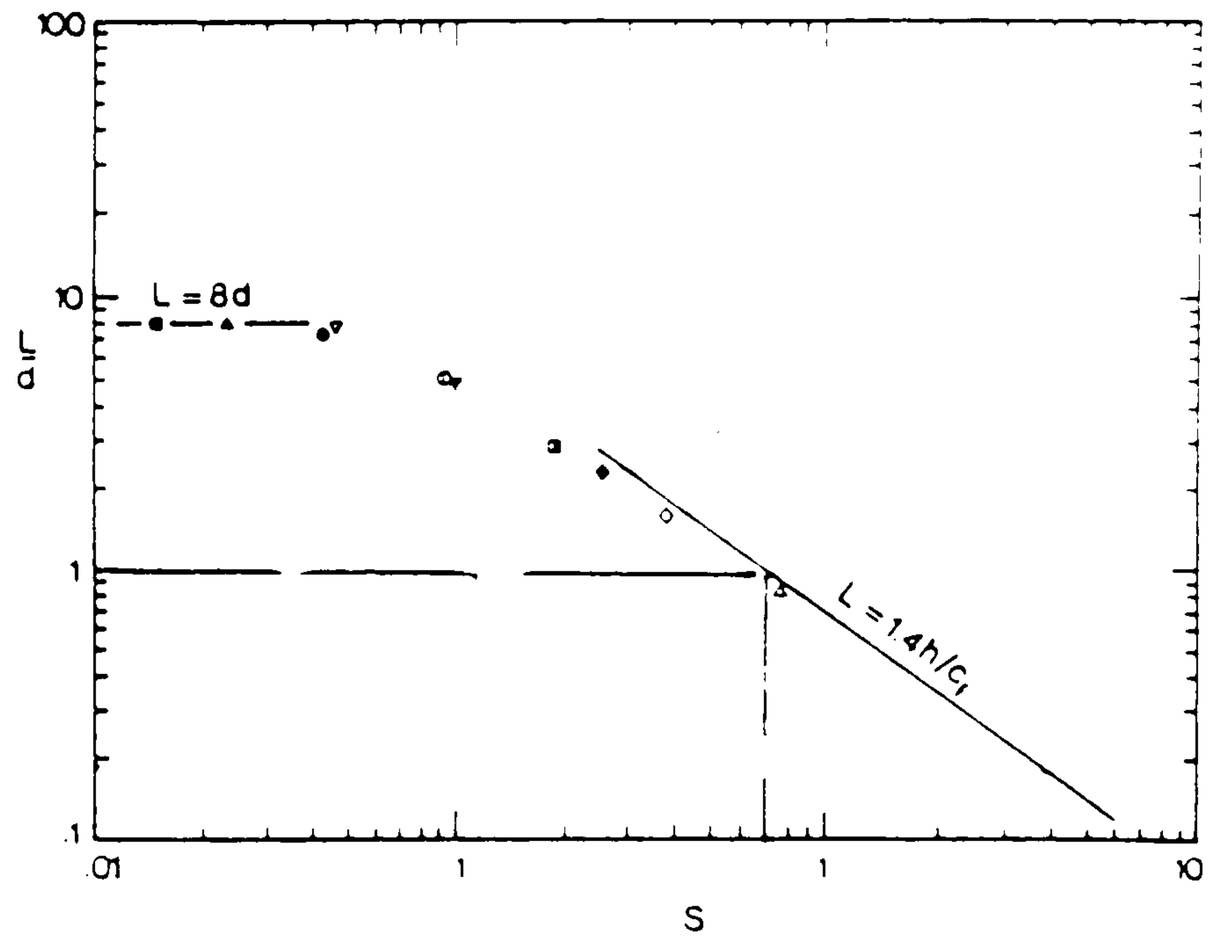

Length of the recirculating eddy.

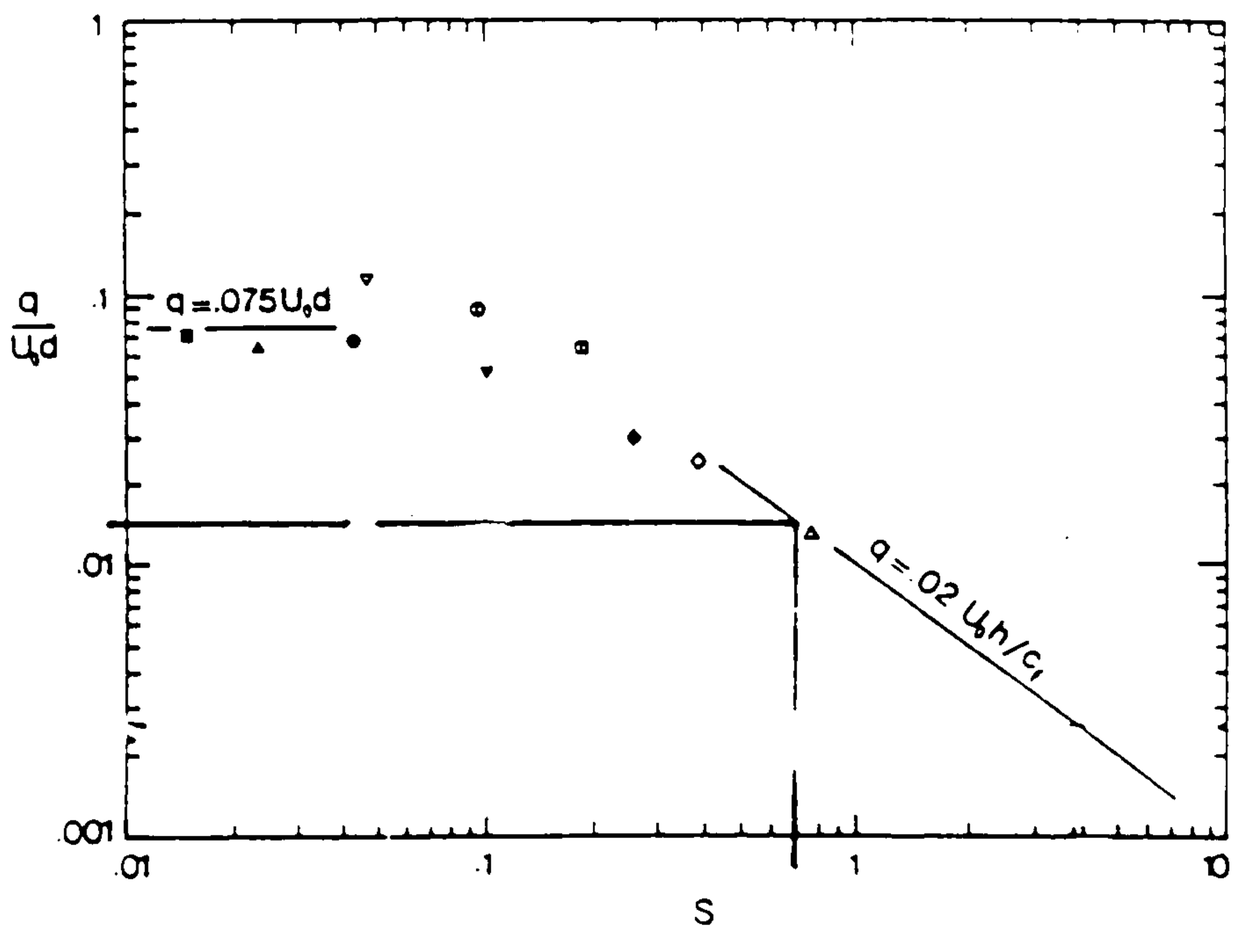

Recirculating flow rate.

FIG (2.31) Barbarutsi and Chu (1987)

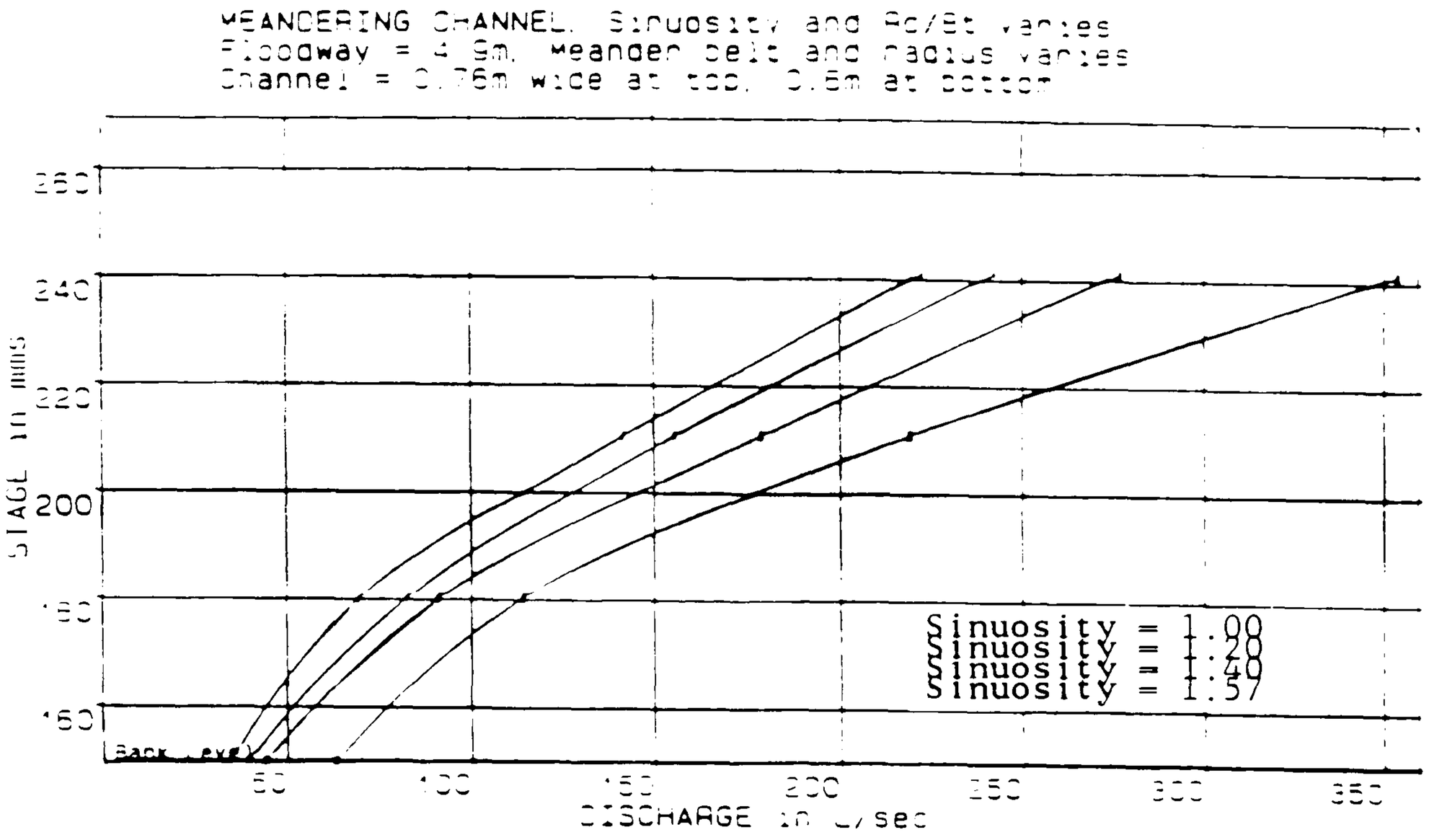

FIG (2.32a) Stage Discharge Curves For Meandering Channel With Flood Plain With Various Sinuosity.
n = 0.012 (US Army Engineer 1956)

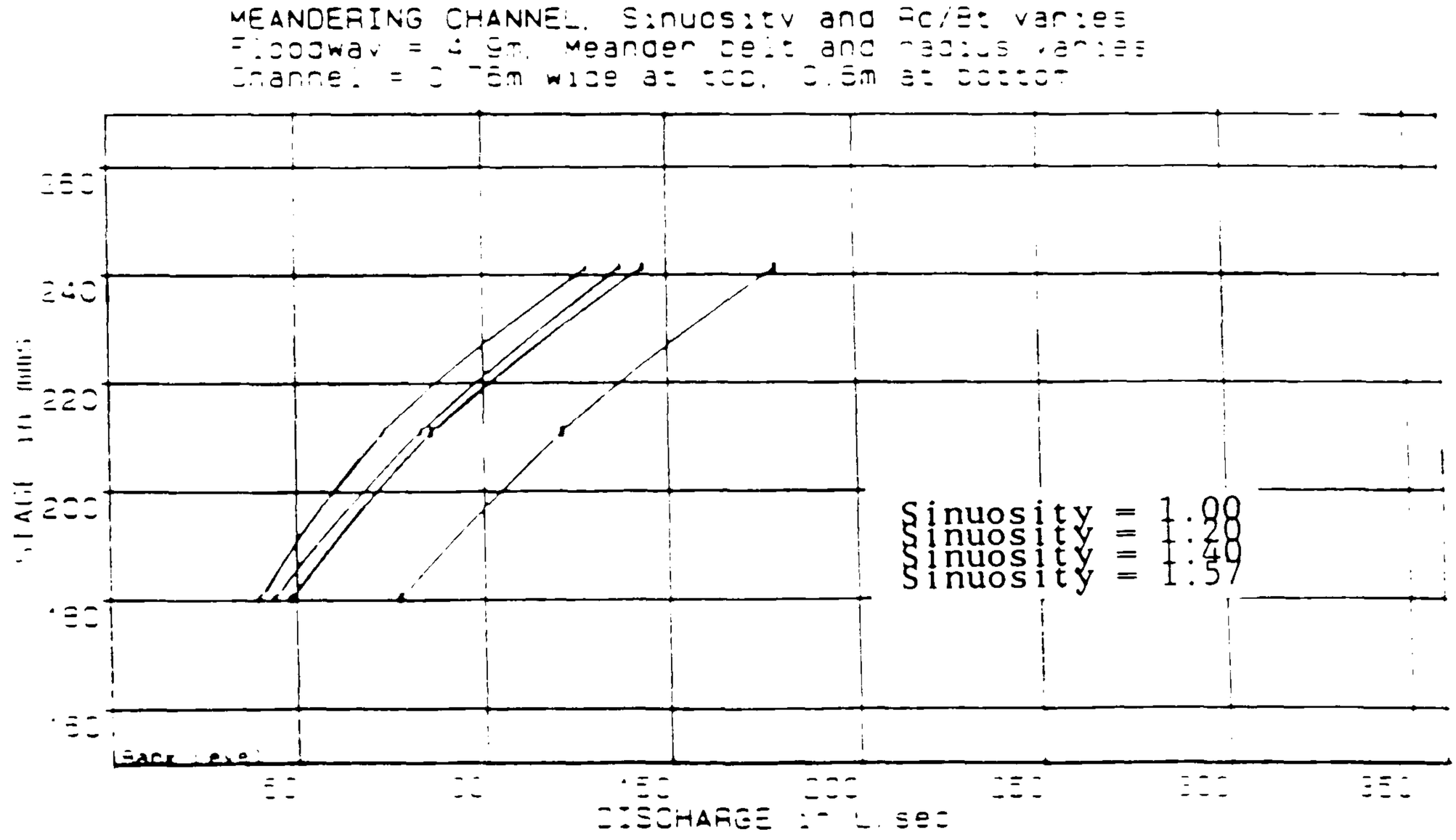

FIG (2.32b) Stage Discharge Curves For Meandering Channel With Flood Plain With Various Sinuosity.
n = 0.035 (US Army Engineer 1956)

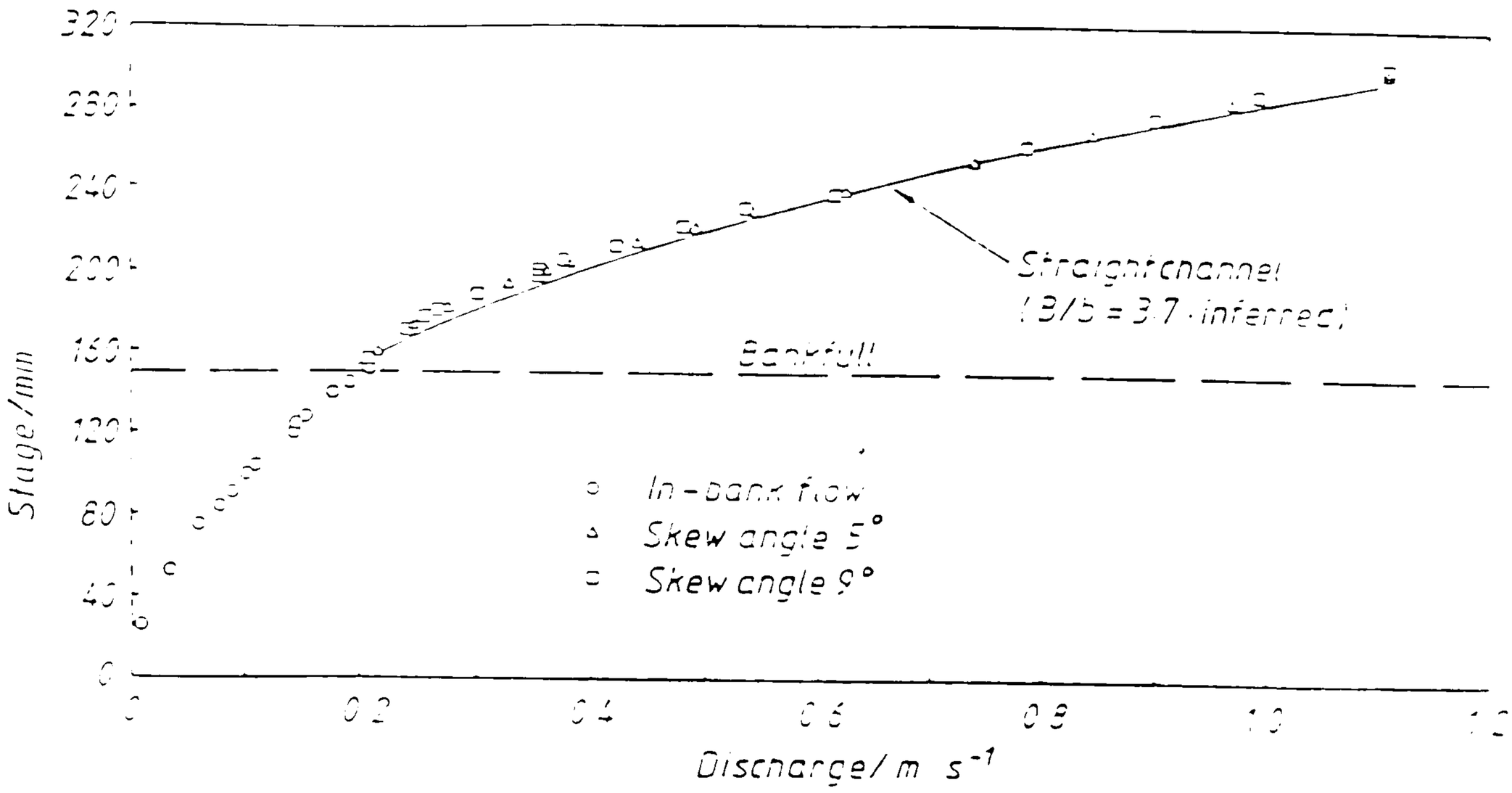

FIG (2.33) Stage Discharge Curves For Skewed Main Channel With Flood Plain. (Skew angle 5° and 9°)

(Elliot and Sellin 1990)

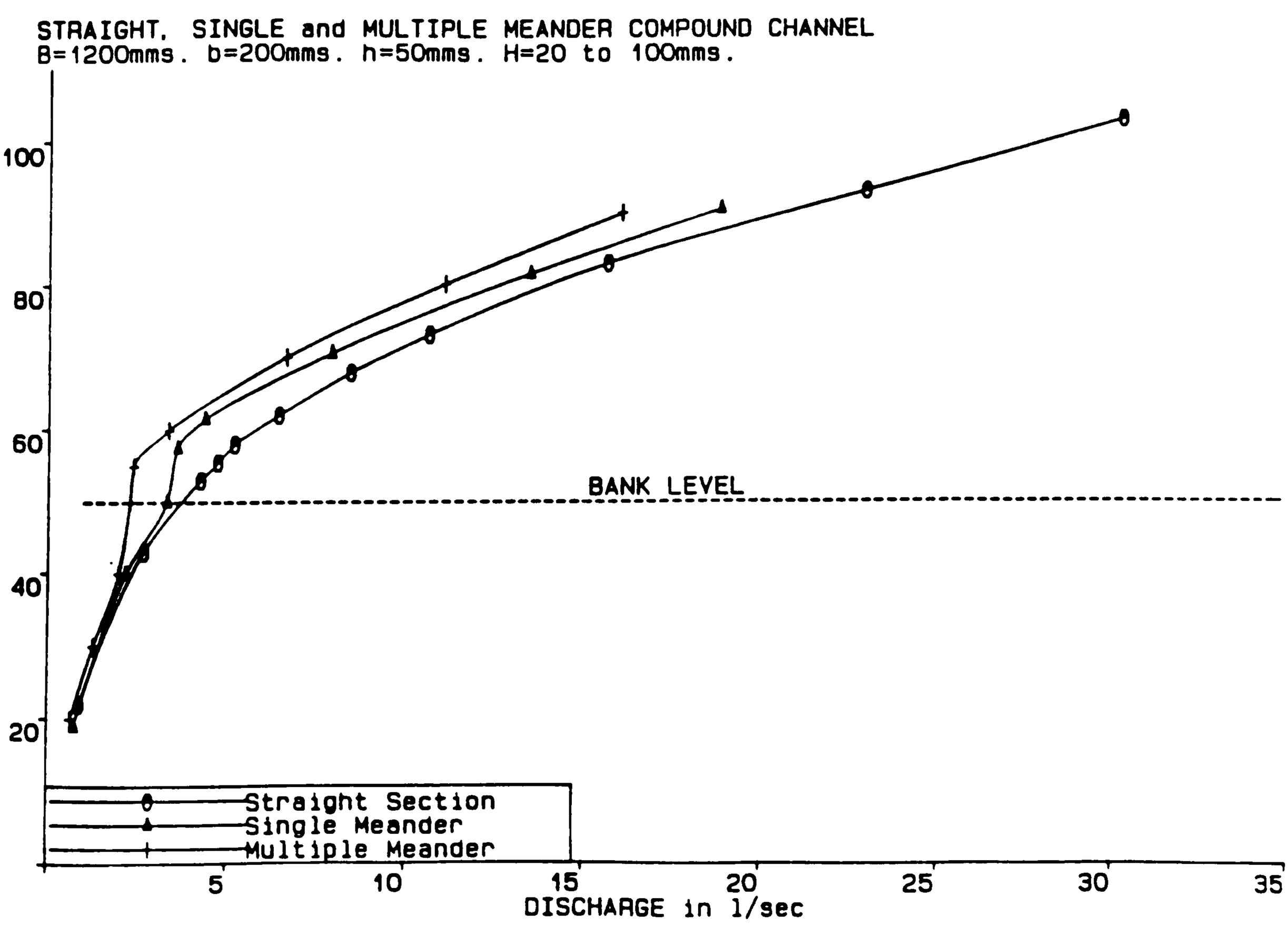

FIG (2.34) Stage Discharge Curves For Straight, Single Meander and Muliple Meander Channel With Flood Plain

(Kiely and McKeogh 1989)

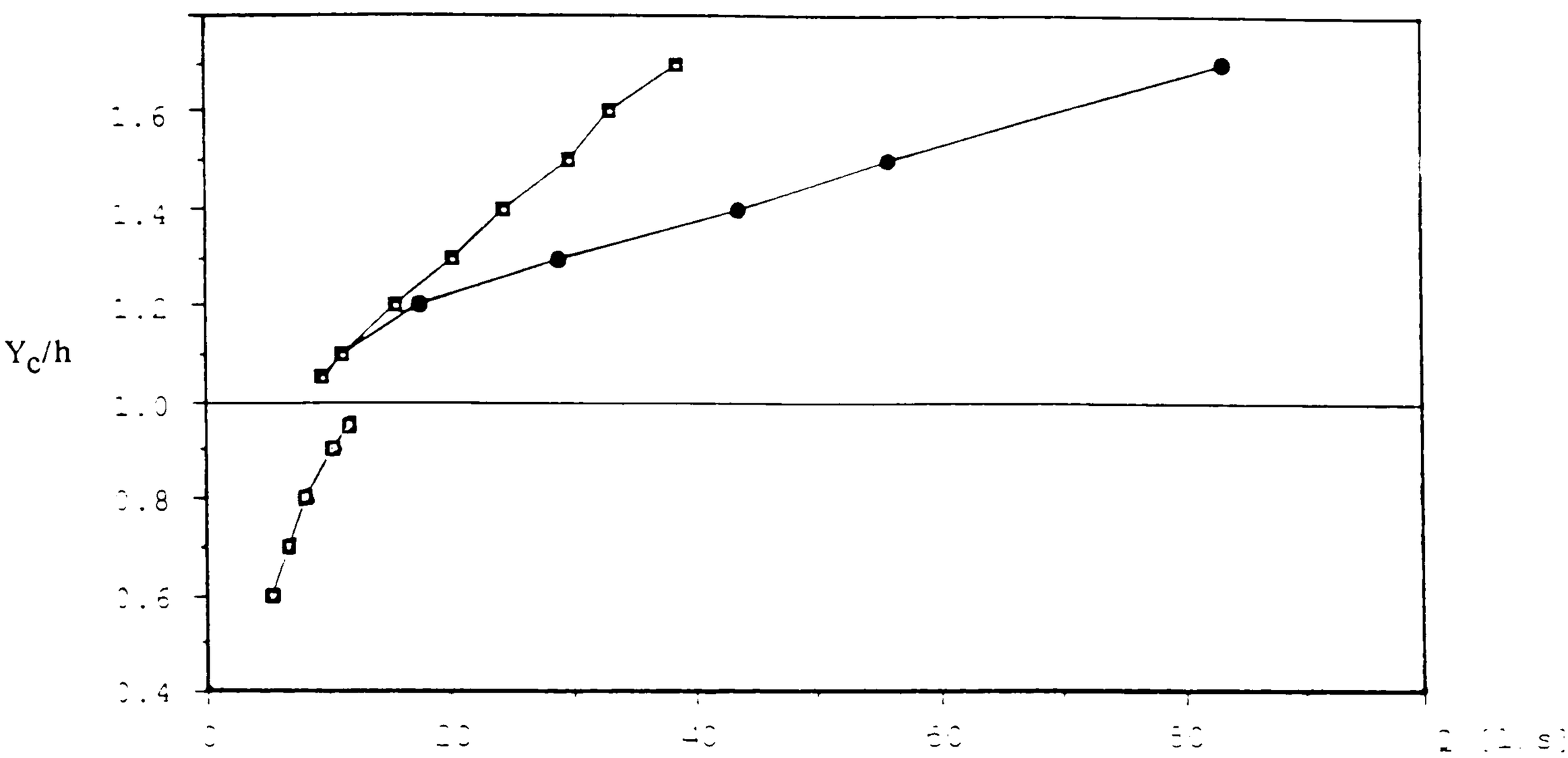

FIG (2.35) The Stage Discharge Curves For Meandering Channel With Smooth and Rough Flood Plain Areas. (Stein an Rouve 1989).

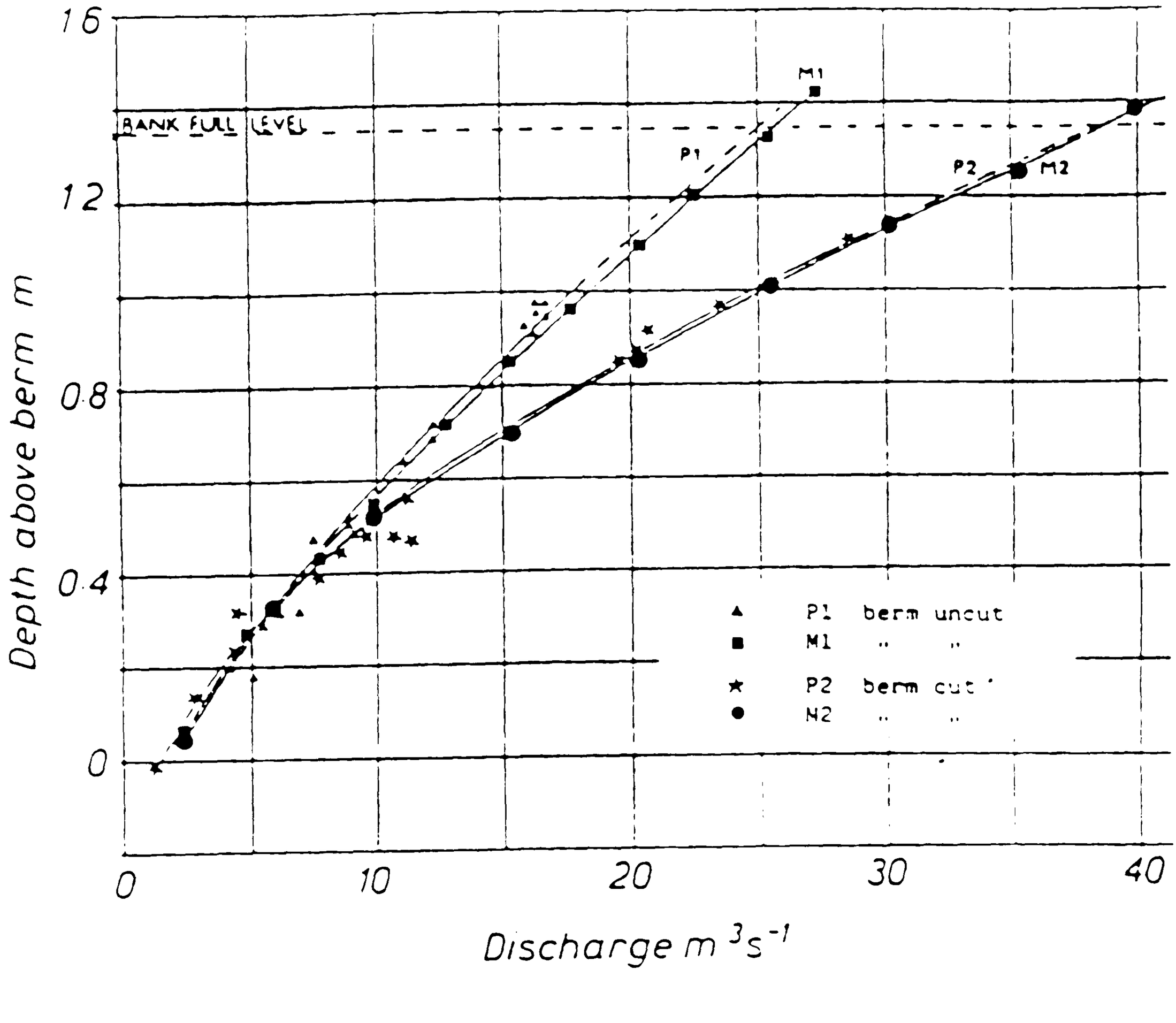

FIG (2.36) Stage Discharge Curves For Meandering Channel With The Smooth and Rough Flood Plain Area.
(Sellin and Searle 1987)

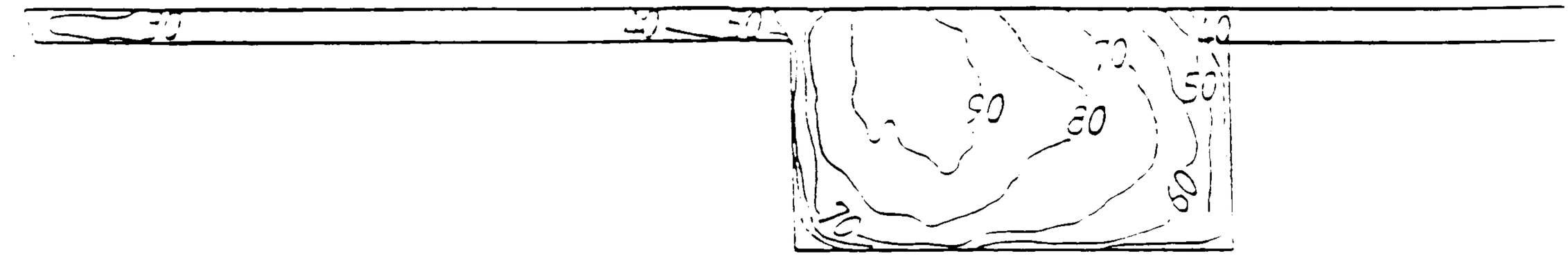

CODE : 0/5°/0.15/2

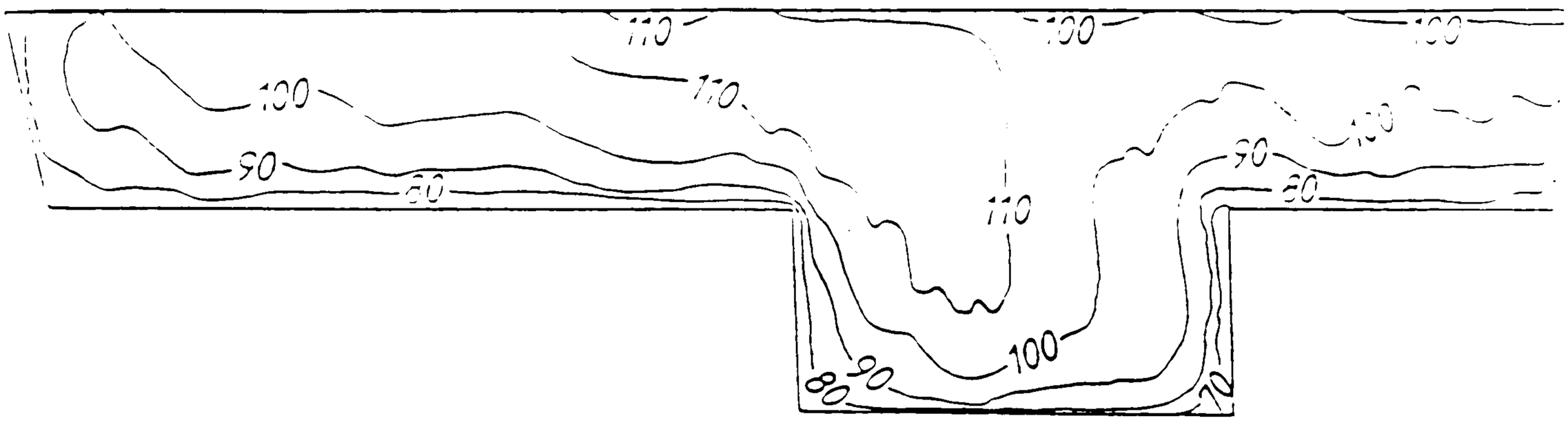

CODE : 0.5°/0.5/2

FIG (2.37) The Velocity Profile For Skewed Main Channel With Flood Plain (skew angle 5°) Elliot and Sellin 1990.

MULTIPLE MEANDER COMPOUND CHANNEL

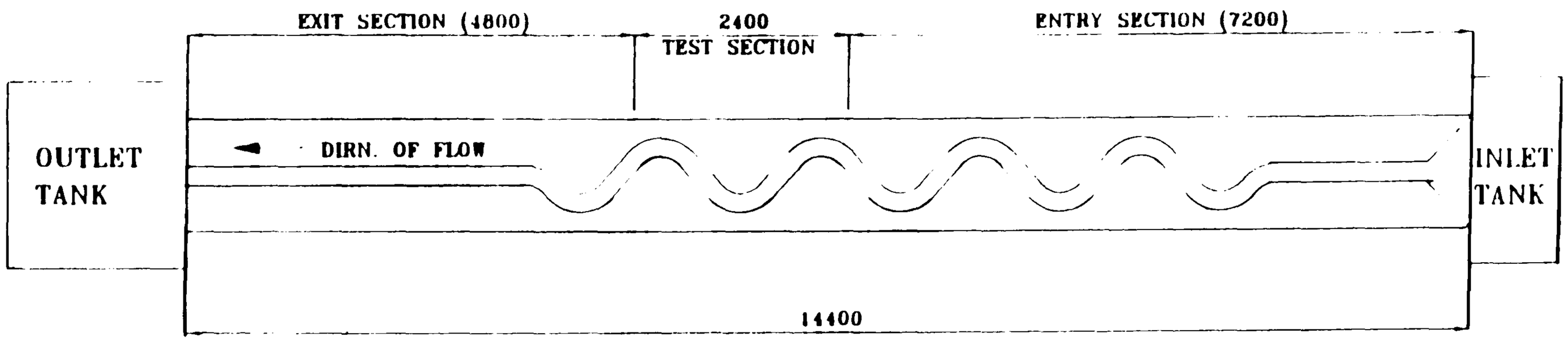

l	2400
W	1200
Bc	200
Rc	400
h	50
Ls	4.5
M	1800
A	570
Rc/B	2
W/Bc	6
r	L/M 1.25
L	2250
α	45
θ	90

ALL DIMENSIONS ARE IN MILLIMETERS

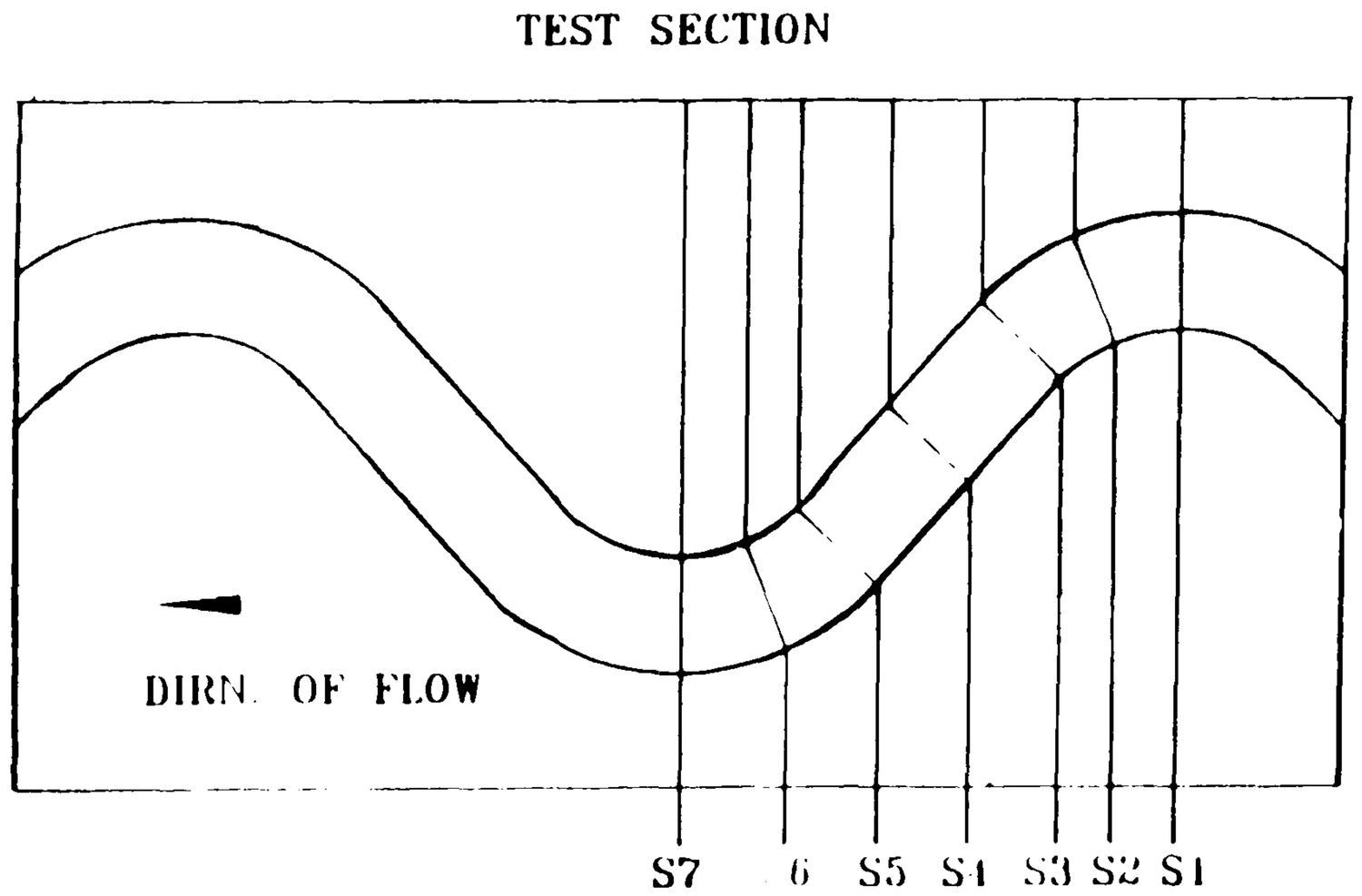

l	Length of test section
M	Meander Wavelength
Rc	Radius to centerline
Bc	Width of Main Channel
A	Double Amplitude
α	Angle of crossover
h	Height of Flood Plain
Ls	Straight length of tangent between curves
L	Curved Length of Meander along centerline
M	Straight Length 1800
r	Sinuosity
θ	Angle of arc

FIG (2.38) Kiely and McKeogh Model Flume (1989)

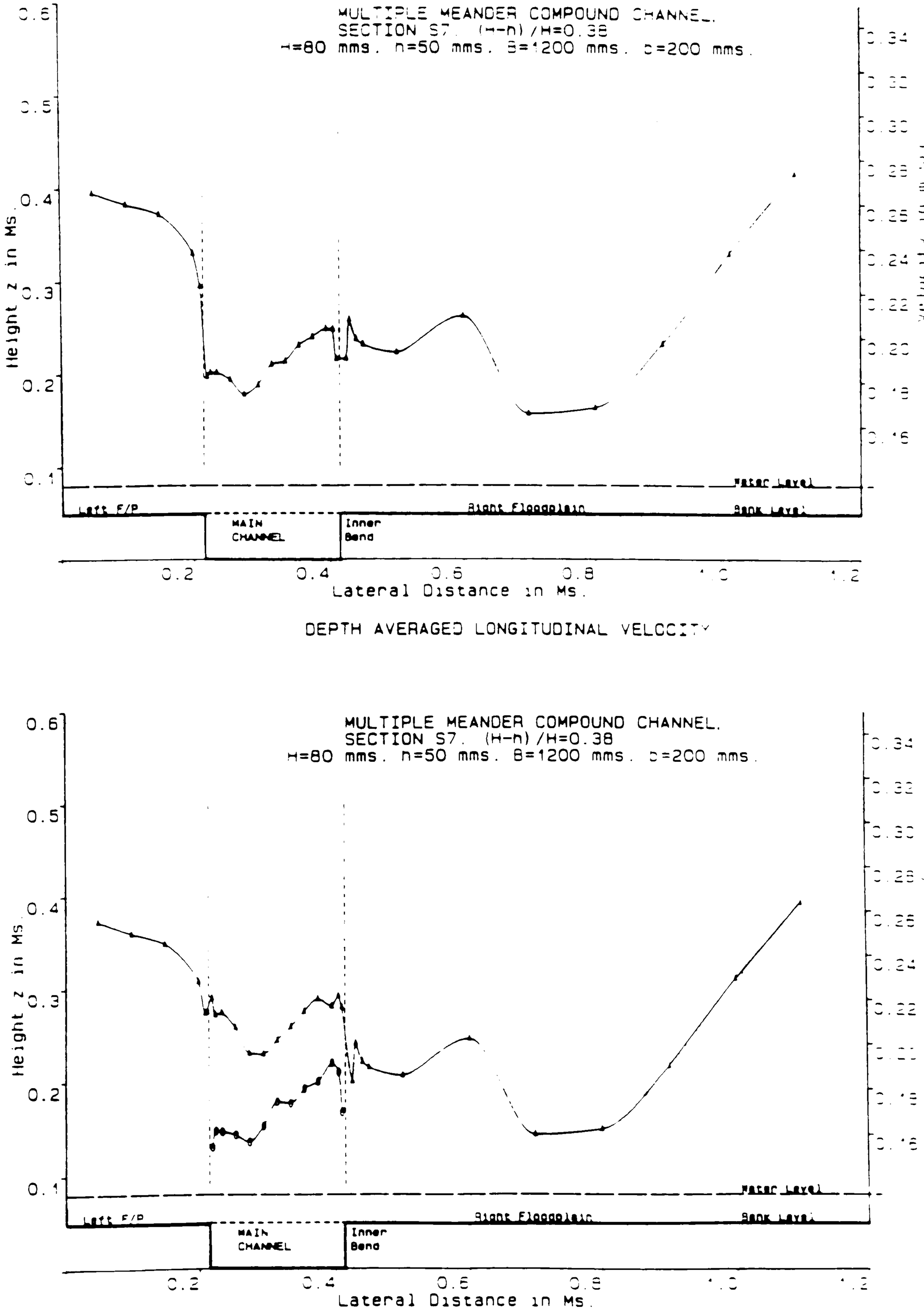

FIG (2.39) The Depth Averaged Velocity For Meandering Channel and Flood Plain (Kiely and McKeogh 1989)

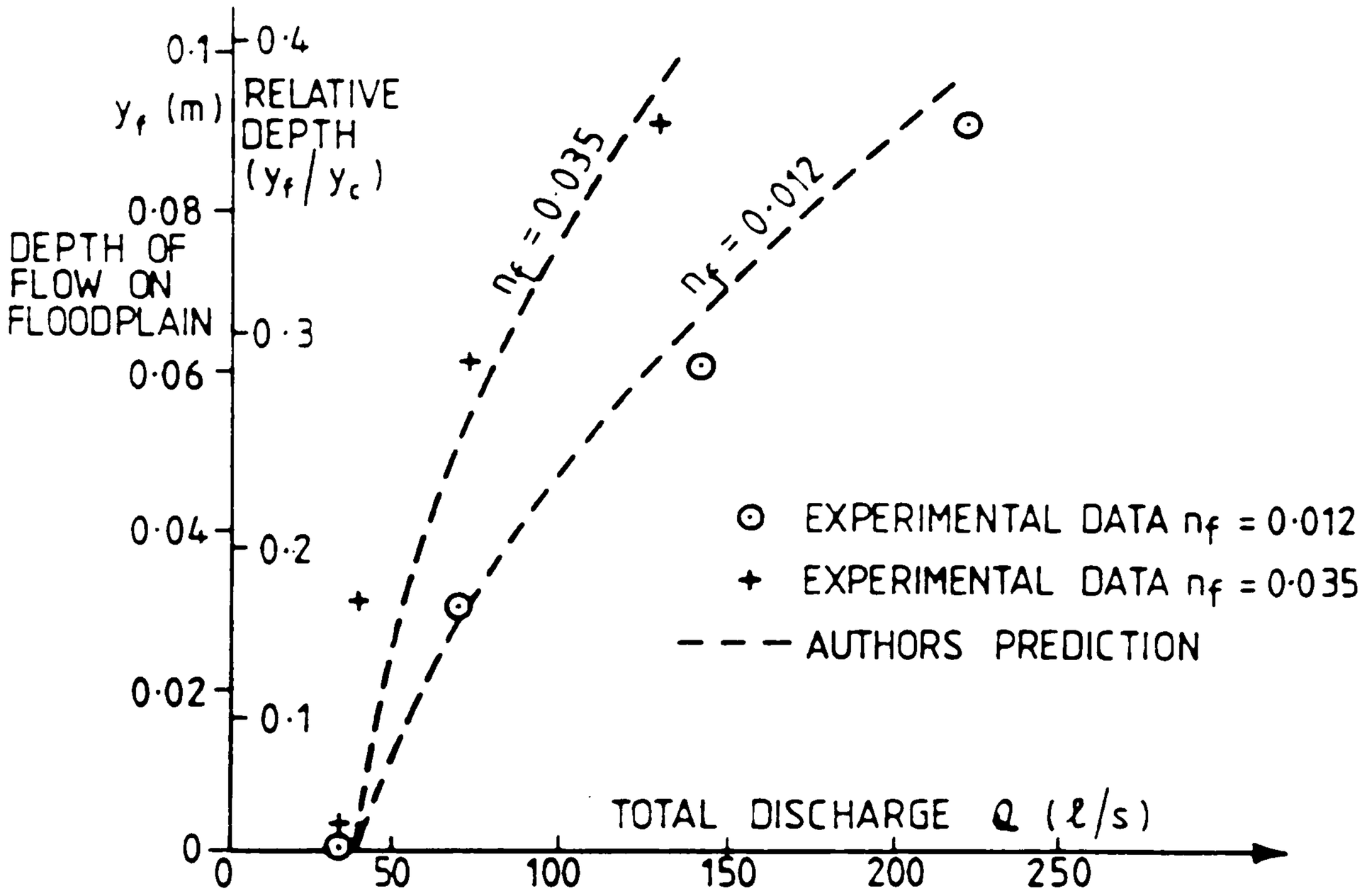

FIG (2.40) COMPARISON BETWEEN EXPERIMENTAL DATA AND THEORY FOR STAGE / DISCHARGE RELATIONSHIP (r = 1·57) (U.S. CORPS OF ENGINEERS DATA)

CHAPTER (3)

THE EXPERIMENTAL APPARATUS AND INSTRUMENTATION

3.1 INTRODUCTION

3.2 THE DESIGN AND CONSTRUCTION OF THE SKEWED MAIN CHANNEL WITH FLOOD PLAIN.

3.2.1 Range of Parameters Investigated.

3.2.2 The Range of Experiments Carried out

3.2.3 Experimental Flume Details and its Modifications.

3.2.4 Construction of the Flood plains.

3.2.5 Design of the Flood plain Roughness Elements.

3.3 INSTRUMENTATION and CALIBRATION FOR THE MAIN FLUME.

3.3.1 Introduction

3.3.2 The Orifice Plate And Its Calibration

3.3.3 Setting Normal Depth and Slope Measurements.

3.3.4 The Pitot Static Tube and Pressure Transducer.

3.3.5 The Angular Measurement Transducer and its Calibration.

3.3.6 Recording and Storing Experimental Data by Computer.

3.3.7 A Note About Longitudinal and Transverse Velocity Components.

3.4 EXPERIMENTAL PROCEDURE FOR TESTS IN THE SKEWED MAIN CHANNEL AND FLOOD PLAIN.

3.5 SLOT APPARATUS FOR SERIES F TESTS.

3.5.1 Introduction

3.5.2 The Experimental Flume For Series F Tests.

3.5.3 The Initial Series of Tests Series F_1.

3.5.4 Measurements Carried Out.

3.5.5 Experimental Procedure For Tests F_2 to F_5.

CHAPTER (3)

THE EXPERIMENTAL APPARATUS AND INSTRUMENTATION

3.1 INTRODUCTION

At the commencement of this research work it was generally agreed that overbank flow studies using straight parallel main channel/floodplain flumes had been investigated by so many experimenters, that the time had come to move to meandering channels with overbank flow. The latter situation was thought to be extremely complex, so an intermediate case was considered, which consisted of a main channel skewed to the direction of the floodplain flow, representing an idealised version, perhaps, of a section of a meander which crosses–over to the next bend. Such a skewed overbank situation was chosen as the subject of this study.

Having decided the broad subject area, it was then considered whether to concentrate on experimental studies, field tests or computational modelling. The latter area was ruled out because of the complexity of the flow and the fact that the mechanisms of the flow in the skewed channel/floodplain were as yet unknown. A suitable site was not found for field measurements, so a decision was made to concentrate on experimental studies.

In choosing experimental studies it was decided to investigate the following broad areas in the skewed channel/floodplain situation:–

(i) The fundamental flow mechanisms and how they differ from the straight parallel case of overbank flow.

(ii) The energy loss mechanisms in skewed overbank flow, with an investigation of how they can be quantified.

(iii) An investigation of stage–discharge relationships for skewed channels, looking at possible methods of discharge assessment.

(iv) The development of flow in the longitudinal direction.

(v) An investigation of scale effects. In the absence of field data it was hoped to compare the Glasgow data with that of skewed channels in the SERC flume, to obtain some ideas of scale effects.

Each of these five areas will be dealt with in some detail throughout this

thesis. In order to investigate the above areas in detail, experimentally, it was agreed that the three dimensional nature of the flow would require measurement of at least two components of velocity, angles of streamlines to a given reference direction, as well as stage, discharge, and perhaps most important, the flow development along the length of the flume. Such measurements might be required for a range of geometries and boundary roughness. It was decided at an early stage that this investigation would not include boundary shear stress measurements. This was because of the time element involved. The author thus accepted that any study of force balance and apparent shear stress would therefore be severely curtailed.

3.2 DESIGN AND CONSTRUCTION OF MAIN CHANNEL AND FLOOD PLAIN

3.2.1 Range of Parameters Investigated

The majority of the experiments were carried out in a previously constructed fibre–glass flume, measuring 0.8m wide, 0.3m deep and 8.5m long, to be discussed in detail in section 3.2.3 and shown in **Fig (3.1)**. The flume required extensive modifications before it could be used in the research work. The main purpose of work in this flume was to investigate the fundamental mechanisms of flow and energy loss in a channel which is skewed at an angle θ to the adjacent floodplains, with the emphasis on the overbank flow scenario.

It was clear from the preceding literature review section, that the flow patterns, even for the skewed overbank flow case were going to be complex and highly three–dimensional. It was becoming clear that as well as lateral shear between the main channel and floodplain, there was also likely to be significant horizontal shear where the floodplain passes over the skewed main channel below. The non–dimensional parameters which were thought to have most effect in this complex flow situation include:–

$$\frac{n_c}{n_f}, \frac{Y_c}{Y_f}, \frac{v_c}{v_f}, \frac{B_c}{B_f}, \frac{B_c}{h}, \frac{B_f}{h}, S, \theta \qquad (3.1)$$

where n_c is the main channel Mannings 'n' value, n_f, the floodplain Manning's

'n' value, Y_f/Y_c, the main channel to floodplain depth ratio, B_c/B_f, the main channel to floodplain widths, h is the bankfull depth, S the longitudinal bed slope and θ the angle of skew.

It was decided at the outset to vary the floodplain roughness but to retain a "smooth" main channel. Two values of floodplain roughness were used, the first relatively smooth and the second using vertical, rigid, fixed rods to generate additional turbulence over the full depth of flow, and hence to increase the floodplain roughness. The values of relative depth Y_f/Y_c were also to be varied over the usual range of 0.0 to 0.5, the lower end of the range representing a river with shallow flood plain depths, and the upper end of the range representing more a two–stage channel as in the case of the River Roding Sellin (1987).

It was decided to keep the longitudial bed slope S_0, fixed as near 1/1000 as possible, thus tying in with experimental work on the SERC flume at HR limited, Wallingford.

Initially it was hoped to vary the skew angle θ, but this eventually proved such a time consuming exercise that only one θ value was investigated. This was designed to be the optimum θ value considering the length and width of flume. From previous experience it was decided that the bankfull depth should be at least 50–60 mm thus insuring reasonable inbank measurements. Of course this meant that a realistic aspect ratio for the main channel in the region of B_c/h = 5 to 20 was not possible, as the main channel would then have occupied too much of the flume width (0.8m), leaving very narrow flood plains.

It was also considered important that the flood plains, at least at the point of symmetry, should be wide enough to allow fully developed lateral shear layers. This usually requires a value of B_c/h, floodplain width to bankfull depth, of the order of 4 to 5. With a bankfull depth of the order of 50–60 mm this would require floodplains of the order of 200–300 mm wide on either side of the main channel. Of course this would not always be possible on the side of the tapering flood plain, which of necessity was to be tapered down to zero width. Considering the constraints of the flume dimensions, and the desire to meet as many of the criteria above as possible, the final choice of design is shown in Fig (3.1). The angle of skew of the main channel was fixed at 5.84^0, which

represented a low skew angle but similar to work on the SERC flume. The bankfull depth was finalised at 0.061m, the main channel width at 0.15m, giving a main channel aspect ratio of only 2.46. This is considerably less than the natural range of 5⟶ 20 and thus represents a considerable vertical distortion in the model tests. The total width of floodplain (both sides) was 0.614m, representing 0.307m for each floodplain at the point of symmetry, shown as Section I in **Fig (3.1)**. The longitudinal bed slope was fixed at 0.001.

Fig (3.1) also shows measurements which were taken at three different cross sections along the length of the flume. This was primarily a device for looking at flow development along the flume length and how the fundamental flow mechanisms change in the downstream direction. It was important therefore, to establish that the flow was more or less fully developed at the first measurement cross– section.

In the design of any channel or flood plain it is important to achieve fully developed turbulent flow before the measurement test section is reached. That is, the boundary layer depth (d) should have reached a value equal to the depth of flow. Baird (1984) used the relationship between the value of (d) the distance downstream from the channel entrance (x), and the mean velocity, (u) for fully developed turbulent conditions and is shown in this equation :

$$d = 0.37 \times [\ \upsilon\ /\ (ux)\ ]^{0.2} \qquad (3.2)$$

where

d is the fully developed turbulent flow depth

υ is the kinematic viscosity of the water

u is the velocity through the fully turbulent flow condition

x is the distance downstream from the channel entrance

all of the dimensions of the parameters in the equation above are in metres.

Applying the typical flood plain velocities and depths of flow, it was clear that most of the experimental data (although not all) on the flood plain flow would be fully developed by the first measurement test section midway along the flume.

As a result, Section I was accepted as the upstream section for detailed measurements, being a point of symmetry and 4.5m from the flume entrance. Section II **Fig (3.1)** was placed 1 m downstream at 5.5m from the entrance and Section III at 6.5 m from the entrance. This produced floodplain widths of 307mm at the point of symmetry Section I, 409mm and 205mm widths at Section II and 509mm and 105mm widths at Section III. Photographs of the flume are shown in **Fig (3.2)**.

3.2.2 The Range of Experiments Carried out

It was decided that in order to optimise information about flow mechanisms and energy loss mechanisms in a skewed channel/floodplain situation that a range of five experiments be carried out in the main flume plus a further range of experiments in a subsidiary flume. In the main flume the following tests were carried out:—

SERIES A consisted of experimental work with the smooth skewed main channel and smooth floodplains as shown in **Fig (3.3a)**. This involved stage, discharge, two components of velocity, streamline angles all at three different cross sections along the flume length.

SERIES B tests are shown in **Fig (3.3b)** and consist of the main channel being infilled to produce a flood plain 0.764m wide. The main purpose of this was to establish the boundary roughness of the floodplain, and stage—discharge, with the flood plain isolated from main channel effects.

SERIES C tests are shown in **Fig (3.3c)**, consisting of tests in the main channel isolated from the flood plain by small vertical walls. These tests included stage, discharge, two components of velocity and streamline angles at 3—different cross sections. The purpose here is to establish the difference in the main channel behaviour between isolated and interacting with flood plain flows, as well as determining the boundary roughness for the main channel alone. Thus velocities, secondary currents, energy losses, etc could all be compared, between interacting and isolated main channel flows.

SERIES D tests are shown in **Fig (3.3d)** and consist of a skewed main

channel with flood plain extensively roughened using 10mm diameter dowels. Again, stage, discharge, 2– component velocities, and streamline angles at three different cross sections were measured.

SERIES E tests are shown in **Fig (3.3e)**, consisting of the main channel infilled, with the entire width of 0.764 m covered in flood plain roughness. The purpose of this test was to establish the roughness characteristic of dowel bars, to do a fundamental study of separating skin friction from dowel bar friction and hopefully relating to the SERC flume dowel bar work.

SERIES F tests were carried out in a completely separate **ARMFIELD** flume, sketched in longitudinal section in **Fig (3.3f)**. The purpose of this work was to investigate flow over a slot in the channel bed of varying aspect ratio, representing an idealised region of flood plain flow passing over a main channel. The results of SERIES F tests were to be used to determine the energy losses associated with expansion and subsequent contraction over a slot in a channel bed, as well as investigating the magnitude and extent of recirculating velocities in the slot region, representing the magnitude of reciculations driven in a main channel by flood plain flow passing over the top.

The table below shows the range of measurements made in each test series and how these relate to the wider aims of the thesis.

	Discharge $Q_{(L/Sec)}$	Stage $H_{(m)}$	Velocity $U_{(m/Sec)}$	Streamline Angle θ	Distance Along Flume $\Delta X_{(m)}$
SERIES A	x	x	x	x	x
SERIES B	x	x	0	0	0
SERIES C	x	x	x	x	x
SERIES D	x	x	x	x	x
SERIES E	x	x	0	0	0
SERIES F	x	x	x	x	x
	Discharge assessment + Energy loss mechanism		Flow mechanisms U_x , U_y		Flow development along length

x Investigated parameter

3.2.3 Experimental Flume Detail and Modifications

As already described, a flume existed in the Department of Civil Engineering, which was reasonably suitable for model studies. This is shown in **Fig (3.4)** both in the longitudinal section and plan view.

It can be seen from **Fig (3.4)** that the system is recirculating, with a centrifugal pump capable of delivering 55 L/sec through a 0.152m diameter pipe containing an orifice plate for flow measurement. The inlet tank to the flume is a cubic with sides 1.22m, and the flume itself being an 8.5m long, fibre–glass construction, 0.8m wide and 0.30m deep, resting on a heavy jacking arrangement. A tail–gate at the downstream end controlled the flume water levels and led the flow directly to the outlet sump which was 2.44m x 1.86m in plan area. The outlet from the Myson Msk 150–4210 pump incorporated a 150mm gate–value for flow control.

The first and most major modification concerned the fibre glass U–shaped flume itself. Initial surveys were carried out on the base of the flume using a surveyors level to determine undulations and discrepancies. These were of the order of _ 2mm, and following extensive rearrangement of the underside of the flume structure, no real improvement was achieved. It was decided at this stage to insert a new flume liner constructed of varnished marine plywood, both base and sides. Great care was taken to insure bonding and water tightness of the new flume "within a flume", the new cross section geometries shown on **Fig (3.5)**. This operation greatly increased the stiffness of the entire flume structure and also significantly reduced the magnitude of undulations of the flume bed. After a further survey, the flume bed is shown in **Fig (3.6)** showing a longitudinal bed slope of 1 in 1000, and with maximum undulations of the order of _ o.5mm, which is acceptable for this scale of model. The only drawback from this procedure is that the revised flume internal width was reduced to 764mm following insertion of the 18mm thick marine plywood.

One advantage of the introduction of a marine plywood liner concerned the tailgate at the downstream end. The tailgate was necessary to act as a control for the water level in the flume, and consisted of a brass plate 800mm wide, 200mm deep and 5mm thick hinged to the fibre glass flume base in the inside of the flume as shown in **Fig (3.7)**.

Rubber seals prevented any leakage either under of round the sides of the tailgate. A screwed rod arrangement was attached to the weir allowing raising or lowering of the tailgate. Introduction of the marine plywood now enabled the base of the weir to be located below the new bottom of the flume as shown in the sketch below thus enabling stage– discharge measurements in the main channel down to lower normal depths than before.

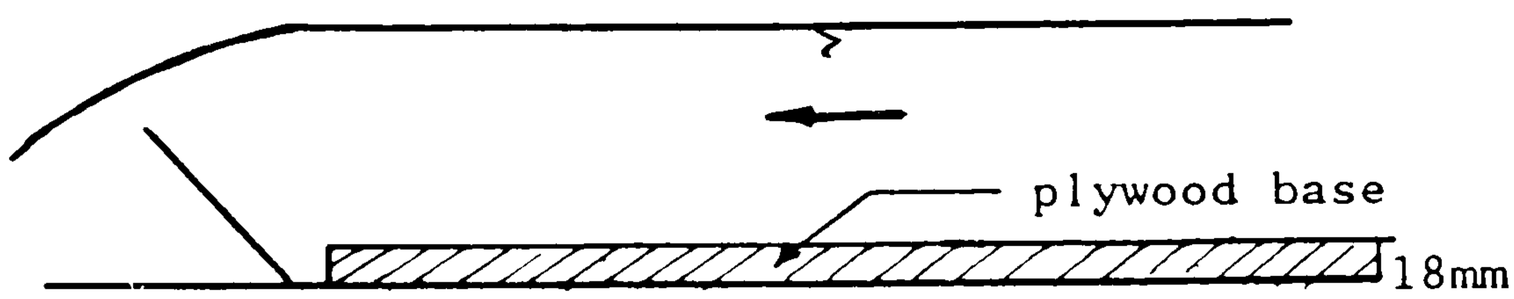

The next modification to the flume concerned accurate measurements of normal depth and the best method of ensuring uniform flow along the channel length. It was decided to introduce permanent pointer gauges at 1m intervals along the flume length giving a total of seven pointer gauges. Eeach pointer gauge is referenced to the channel bed at its own cross section then each gauge it raised the same height one can easily determine if uniform flow is occurring or not, or whether an M1 backwater profile or whether an M2 drawdown profile. The technique of establishing uniform flow involved setting up a deliberate M1 profile and by successive lowering of the tailgate, each time measuring the water surface profile and plotting to test if parallel with the bed at a slope of 0.001. Great care was taken in this procedure to allow time for the flume flow to settle, between alterations of the tailgate.

The next modification concerned the instrument carriage, which had to be modified to carry a movable pointer gauge, for water surface levels across the flume width. The Pitot static tube and ultra– low head pressure transducer for point velocity measurements, as well as a special angular measurement transducer with freely rotating tailfin for streamline angle measurement were used. The tailfin arrangement was designed by **Dr. Ervine.**

A photograph of the instrument carriage is shown in **Fig (3.8)**, showing the transverse screws for movement of pointer gauge and Pitot tube.

It was decided to measure streamline angle and point velocity separately, hence the same transverse screw could be used for Pitot static tube and angular measurement transducer. The latter device required to be zeroed very sensitively along the length of the flume, x direction, which in turn required that the transducer should not rotate even a fraction of an angle when moving from one location to the next. This was achieved by two means:—

(i) To build a rigid brass housing for the transducer.

(ii) To building a square section rod at the clamping position to ensure no rotation.

These measures are shown sketched below.

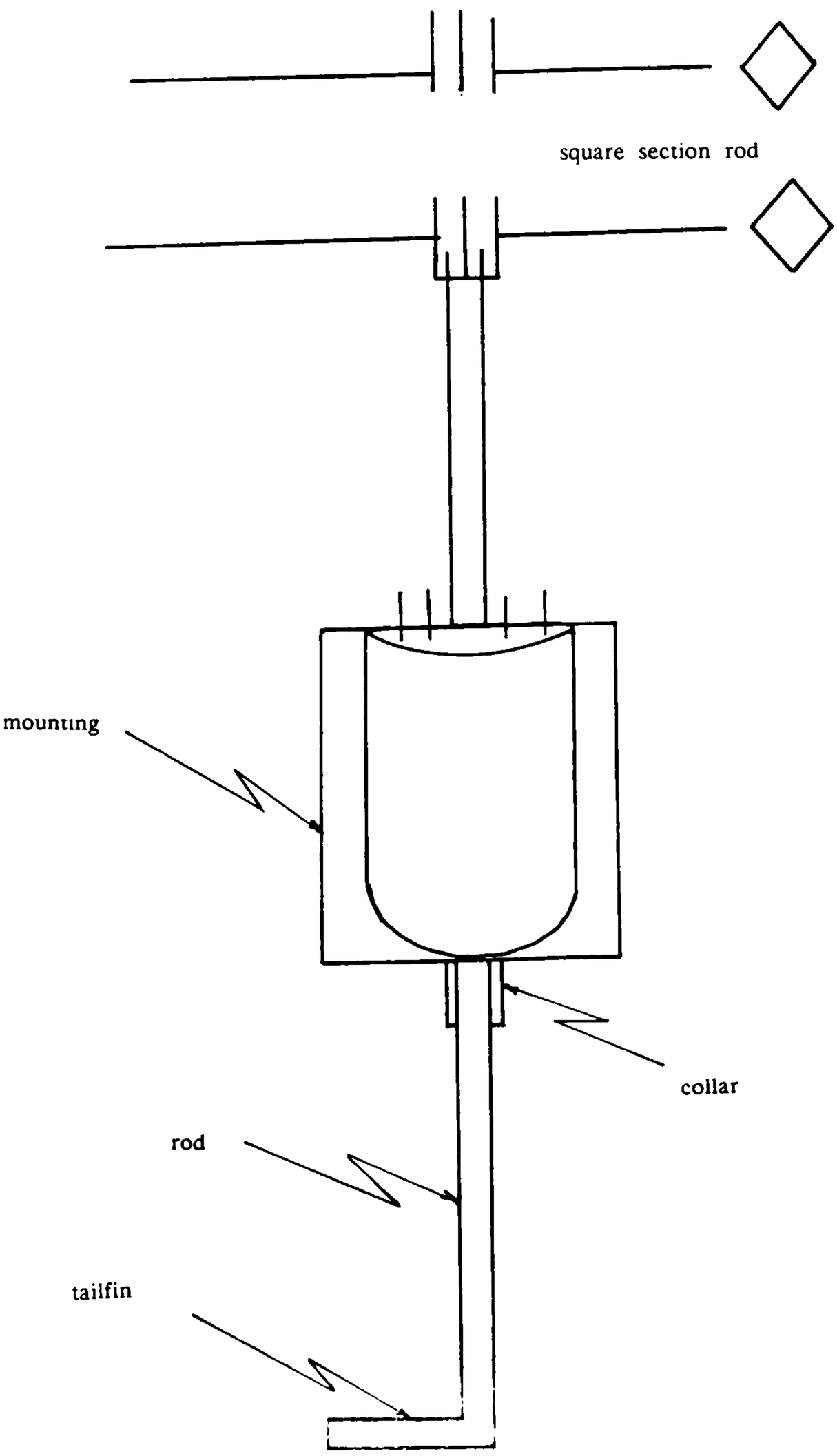

3.2.4 Construction of Flood plain

Referring back to **Fig (3.1)** it is clear that flood plains of varying width would require to be constructed for the experimental tests. Initially it was envisaged to change the skew angle θ, several times, and hence, the first resort was made to polystyrene flood plains which are light, easy manoeuvre and easy to change plan geometry. This approach was attempted with little success, because irrespective of the glue used, or the technique employed to keep the polystyrene stuck to the marine plywood, the flood plains kept lifting due to buoyancy.

The final solution arrived at consisted in constructing flood plains in varnished marine plywood, the same material as the new base and sides of the flume. Although these flood plains were more difficult to construct than polystyrene, it was a straight forward matter to fix them to the existing base and sides by screws. The dimensions of the marine plywood are 2.44m long, 1.22m wide, and 18mm deep. The flood plain construction and arrangement is shown in **Fig (3.9)**.

3.2.5 Flood plain Roughness Elements

It has been noted in section 3.2.2 that SERIES D and SERIES E tests involved extensive roughening of the floodplains so as to effectively increase Manning's "n" or Darcy Weisbach friction factor by a factor of at least two. A review of main channel and floodplain roughnesses for real rivers had been carried out by Dr. Ervine to reveal that flood plains are typically two or three times rougher than the main channel. For instance, main river channels have a typical Manning's n of 0.03, whereas flood plains are more likely to have 'n' values 0.05 to 0.1. It was decided in this work, to retain a "smooth" main channel ($n_c \simeq 0.01$) and to attempt to roughen the flood plains to give, $n_f \simeq 0.02 \longrightarrow 0.03$, giving a ratio of n_f/n_c similar to nature.

A visit to Dr. Sellin at Bristol University was undertaken to establish the most effective method of roughening the flood plain to ensure a Manning's 'n' value of the order of 0.03. Follwing discussions at Bristol and using expereience from the SERC flume flood plain roughening programme at Wallingford, it was decided to follow approximately the Wallingford model. This consisted of using

vertical, rigid, smooth circular rods, which occupied the full flow depth and were placed in a diagonal pattern as sketched below.

S_1 is the longitudinal distance, S_2 is the lateral distance and dowel diameter is 10mm.

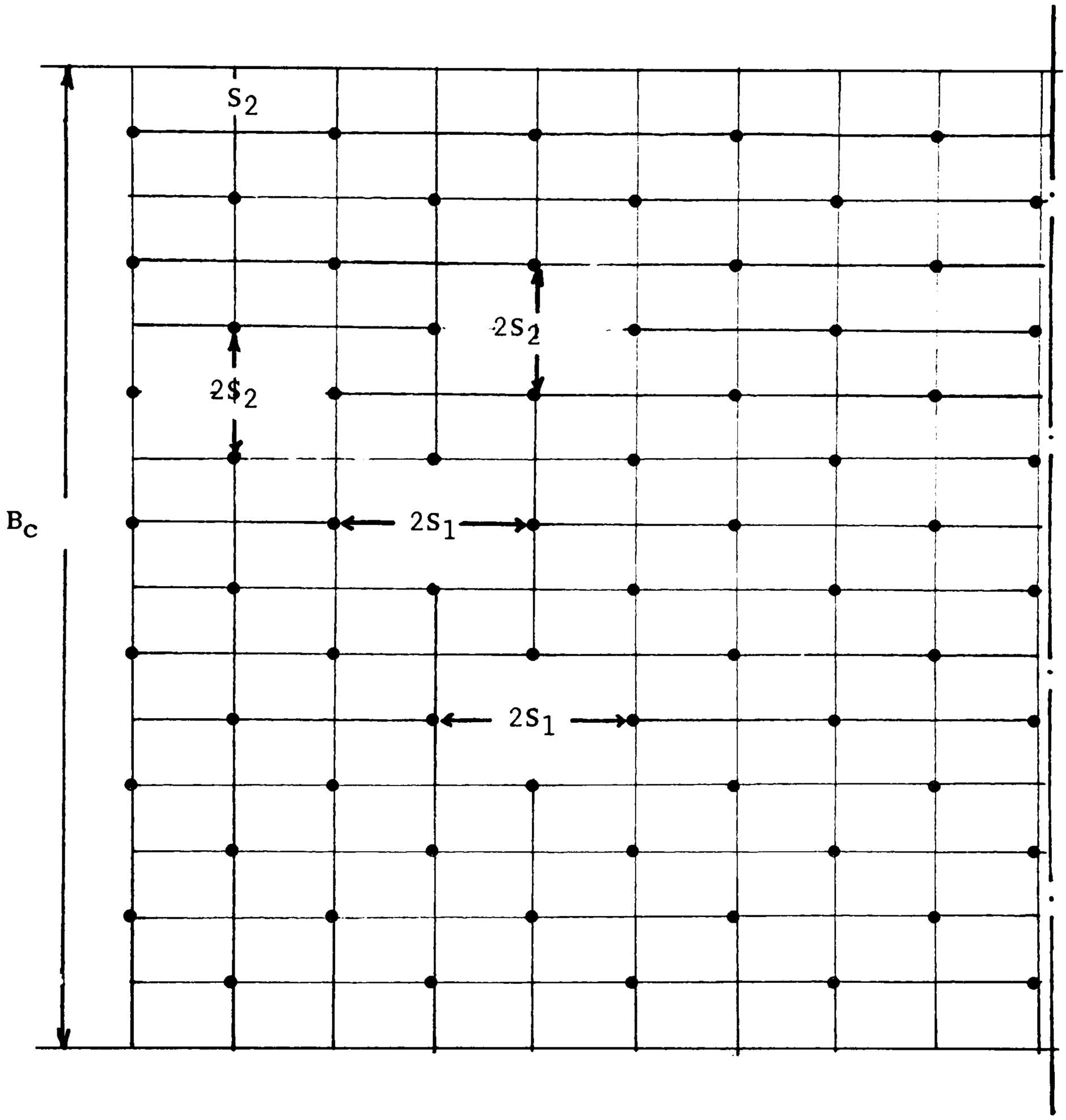

B_c = 0.764m , S_1 = 100mm , S_2 = 100mm

- rod diameter (d) and equal 10mm.

The Wallingford roughening rods were of diameter 25mm, bankfull depth h of 150mm, lateral spacing 456mm and longitudinal spacing 300mm. This gave non–dimensional ratios of d/h of 0.166, S_1/d of 18.24 and S_2/d of 12, with an approximate Manning's "n" value of 0.035 in SERC flume floodplains. It was

decided thus at Glasgow to use circular galvanised steel dowels 10mm diameter, giving a d/h of 0.1667. The lateral spacing was established at 100mm centres, giving S_1/d of 10. The longitudinal spacing was also established at 100mm centres, giving an S_2/d of 10.

A photograph of the roughness rods is shown in **Fig (3.10a)**. The arrangement for SERIES D tests (channel/flood plain) is shown in **Fig (3.10b)** for the three measurement cross sections along the flume length. SERIES E tests are indicated in **Fig (3.10c)** showing 7 dowels across the flume width. This series of tests involved filling of the main channel, thus providing detailed resistance data for floodplain roughness elements without the main channel interaction effect.

A theoretical model for dowel bar roughness was also developed. This is based on separating boundary skin friction from vortex generation and free surface effects due to the rods. This aspect will be discussed in more detail in chapter7

3.3 INSTRUMENTATION AND CALIBRATION FOR THE MAIN FLUME

3.3.1 Introduction

The most important consideration in the experimental test programme was the accuracy and detailed calibration of the various measurement devices used. The test runs covered test SERIES A to F as described in Section 3.2.2, Six series of tests, each series containing measurements at various discharge rates, and various cross sections along the flume length. Each test run involved at least the measurement of stage and discharge, and usually measurements of the streamline angle θ as well as the velocity component. At any given cross section approximately 50−100 measurements of u and θ were taken. The experiments ran continuously for two years, and because of the large volume of data, required careful notation, and storage of each data point for analysis through the mainframe computer ICL 2900 and subsequent plotting in graphical form.
The following areas of accuracy and calibration will be discussed:−

(i) Discharge measurement and orifice calibration.

(ii) Normal depth of flow and tailgate usage and longitudinal water slopes.

(iii) Pressure transducer, Pitot– static tube and point velocities.

(iv) Angular transducer and measurement of streamline angle.

3.3.2 The Orifice Plate and its Calibration

The flow in the recirculating flume was measured by using the orifice plate. The orifice plate is inserted into the pipeline acting as a contraction to the flow, and producing an energy or head loss as the flow passes through the throat of the orifice plate. This energy loss can be measured on a manometer by measuring the pressure difference between the pressure tapping upstream and downstream of the orifice plate.

According to BS1042:Part 1:1964 the discharge through the orifice is given by,

$$Q = 0.01252\ C\ Z\ E\ \epsilon\ d^2\ \surd\ (h/\rho_w) \qquad (3.3)$$

Provided the correct number of pipe diameters upstream and downstream of the device are adhered to.

Q is the orifice discharge in (m /hr)

C is the basic correction coefficient equal (0.608)

Z is the correction factor of Reynolds number equal (1.058)

ϵ is the expansibility factor which for incomprehensible flow can taken as (1.0)

E is the factor of the approach velocity equal (1.207)

h is the difference in pressure between the upstream and downstream at the orifice plate in (mm).

ρ_w is the density of the water and normally is taken (998Kgm)

d_1 is the inner diameter of the orifice throat and equal to 120mm.

then equation (3.3) becomes

$$Q = 4.4309 \surd h \qquad (3.4)$$

where Q in (m^3/sec), or equation (3.4) becomes

$$Q = 1.2308 \surd h \qquad (3.5)$$

where

Q is the discharge through the orifice plate in (L/sec)

h is head difference in manometer tubes (mm)

Equation (3.5) is the theoretical formula used to measure the discharge through the orifice plate.

It will be appreciated that an orifice plate already existed in the flume system as indicated in **Fig (3.3)**. It was decided not to simply accept the B.S.1042 estimate, because the statutory number of pipe diameters upstream and downstream had not been met. It was decided to recalibrate the orifice. This is difficult in an enclosed recirculating flume system, so two methods were adopted:—

(i) Because of the relatively large pump sump area, the first method involved turning on the pump, pumping into the empty inlet tank and measuring the rate of fall of water level in the pump sump. The manometer was read by an assistant at the same time as the measurement of change of sump water level. This method has the inherent difficulty of a continually changing static pump head and thus could not be considered very accurate. The measured discharges (Q_{tank}) are shown plotted in **Fig (3.11)**, against the BS1042 estimates from measuring the manometer head difference, $Q_{orifice}$, showing good agreement but excessive spread. It was decided to use a more accurate method.

(ii) The second method was much more time consuming and involved integrated point velocities over the flume width. For this exercise the flume was run at uniform flow under the initial condition of having the new plywood liner inserted and a flume width of 0.764m. Velocities were measured at three cross sections along the flume using the Pitot static tube with each section sub— divided into an array of grid points.

The discharge was integrated at each cross section and averaged over the three cross–sections to give the integrated discharge, Q_{integ}. This is plotted against the orifice discharge in **Fig (3.12)** showing good agreement and the spread confined to about ± 5%. The final result for the tank and integrated discharge measurement gave a correlation of,

$$Q = 1.238 \sqrt{h} \qquad (3.6)$$

where

Q is the discharge in (L/Sec)

h is the head difference at the manometer in mm

This was accepted because of its proximity to the BS correlation of $1.235\sqrt{h}$ from Equation 3.5. **Fig (3.13)** shows the correlation graph for Equation 3.6 above for use in translating from manometric head differences to discharge rates.

The manometers themselves were vertically mounted on an adjacent wall. Two manometers were used, one using water/air for low discharges and the other using mercury/water for higher discharges. A special valving arrangement allowed easy switch over from one manometers to the other.

3.3.3 Setting Normal Depth and Slope Measurement

As already mentioned in section 3.2.3, the most important aspect of the water level (or stage) measurement is the establishment of the uniform flow, combined with the use of pointer gauges with suitable vertical scales and vernier scales if possible. Using vernier scales an accuracy of ± 0.1mm in water level can be achieved, although this is of theoretical value only in view of the fact that small waves on the free surface often mean that the "average" water level is guessed at, by the tip of the pointer gauge being submerged 50% of the time and open to the air 50% of the time.

In this work uniform flow was established by first setting up a backwater profile. Water levels were measured at seven sections along the flume using seven pointer gauges fixed at 1m intervals. The results for the free surface were

plotted on graph paper where the slope is obviously less than 0.001. The tailgate is lowered, the flow settles (20 minutes) and the same graph plotting procedure is followed. This iterative process continues until an average longitudinal water slope of 0.001 is achieved. A typical example is shown in **Fig(3.14)**, in this case showing both the bed and free water surface sloping at 0.001. The normal depth is measured.

This process is straightforward for measurements in a single channel. For measurements in the skewed channel/flood plain arrangement, the water level was measured at three points across the flume width and averaged. This is necessary because of significant variations in water level in the region of the skew.

3.3.4 The Pitot Static Tube and Pressure Transducer

The measurement of velocities throughout a cross section of flow necessitated an accurate velocity measurement device, because of the low velocities in the channel and flood plain (typically 0.2 to 0.30m/sec). The choice was between a miniature propeller meter device or a Pitot static tube linked to an existing ultra−low head pressure transducer. It was decided in view of the relatively large diameter of the propeller meter (10−15mm) and relatively shallow flow depths, to use a Pitot static tube, as it had the advantage of being only 4mm external diameter which means that averaging of velocity is over a much smaller area, plus the fact it is more suitable for shallow flood plain work. The Pitot static tube is shown in **Fig (3.15)**.

A Pitot static tube is generally an "L" shaped hollow tube used to measure the dynamic energy of a flow. Two tubes run up the stem of the Pitot static tube. The inner tube measures the dynamic energy of the flow ($Y + V^2/2g$), while the other tube leads to small holes in the wall of the Pitot tube and so measures only the static energy of the flow (Y). The difference in pressure between the static tube and the dynamic tube is equal to the velocity head, ($V^2/2g$). If both tubes are connected to the pressure transducer, a quick method is available for measuring the local velocities.

The pressure transducer used was a Validyre DP103 type which already had

been used for previous research work but required recalibration. A photograph of the transducer is shown in **Fig (3.16)**. The tubes from the Pitot static tube enter either side of the pressure transducer and the head difference ($V^2/2g$) deflects a thin diaphragm. The thin diaphragm is supported by two symmetrical assemblies and embedded in each assembly is a small magnetic E– core. The diaphram completes the magnetic circuit in each E– core. The application of pressure to either side of the transducer increases or decreases the gap between the diaphragm and the E– core varying with the gap, thus determining the induction. This ratio is measured in an AC bridge circuit in which the output voltage is proportional to the pressure difference. The diaphragm chosen gives a linear relationship between the output voltage and the differential pressure up to the pressure difference of 35 mm head of water.

In use the pressure transducer is very simple: a reading of (10) on the digital output display is equivalent to a head difference of 1 mm of water for the chosen membrane and calibration. It was decided to calibrate the transducer as follows:

Using the equipment shown in **Fig (3.17)**, two graduated cylinders were connected together via a valve each side of the pressure transducer and also to a tilting manometer set a 19.5^0 to the horizontal giving a 3 to 1 "magnification" of the head difference. A difference of 3mm in water level in the two manometer tubes was equivalent to 1mm vertical head difference. It was important to remove all traces of air on either side of the transducer diaphragm.

1. With valve A open the water levels in both beakers were equal and the differential pressure between the two sides of the transducer was zero. The reading on the demoducator was set at zero (000) using the zero control.

2. Valve A was shut and the water introduced into one of the beakers until the difference in the manometer readings was 90mm corresponding to a differential pressure of 30mm of water.

3. The reading on the output demodulator was set at 300 using the gain control. Valve A was opened and the water levels allowed to equalise. Steps one and two were repeated until the reading on the demodulator automatically returned to zero (000.0) when the water levels equalised.

4. At this point the calibration proper could proceed in increments of head difference of the order of 2–3mm, to obtain the complete calibration. The relationship between the display obtained from the pressure transducer and the readings from the inclined manometer is shown in **Fig (3.18)**. It can be seen that the transducer results agree very favourably with the results obtained from the inclined manometer.

3.3.5 The Angular Measurement Transducer and its Calibration

It was decided to use an angular position transducer to measure the direction of the maximum filament of the streamline in the skewed main channel and on the floodplain. The angular measurement transducer is basically a transformer in which the output is governed by the angular position of the input shaft in relation to the transducer body. The tranducer is connected to a tailfin which dips into the flow and follows the streamline direction. A photograph is shown in **Fig (3.19)**, with the transducer supplied by Penny and Giles Type DS 3810/300. This transducer should have a linear relationship between angle and output reading over a range of 300^0. It cannot therefore be used over a 60^0 segment. The detailed specifications are as follows:–

1) The effective electrical angle is 300^0.
2) Output sensitivity per degree– nominal 33 mv.
3) Residual voltage maximum at 0^0 arc 50 mv.
4) Linearity – deviation from best straight line + 0.5%.
5) Resolution infinite.
6) Output ripple (> 1.2 KH_z) is 0.05% FS + 0.4% output.
7) Input current nominal is 50 mA of 10.00 V d.c.
8) Mean temperature coefficient of output + 10 C^0 to + 40 C^0
   + 0.8 mv/C^0.
9) Frequency response at 40 H_z output 1% down.
10) Temperature range operational – $20C^0$ to + $60C^0$.
    storage – $40C^0$ to + $100C^0$.

It was decided to calibrate the angular transducer by using a large protractor to check the angular device readings against protractor angles. The tailfin of the

angular device was fixed on 0.00^0 on the protractor, and the voltmeter was recorded as a datum. The fin was moved 10^0 in the clockwise direction and recorded the voltmeter reading. The second step was moving the fin 20^0 from 0.00^0 and recording the voltmeter again. The procedure was carried out in 10.0^0 increments in a clockwise direction up as far as a total deviation angle of 90.0^0. The same procedure used counter clockwise from 0.00^0 to -90.0^0. From these measurements, it was found that the correlation or calibration factor to transfer the voltmeter readings to the angular readings was 28.14. The results are shown in **Fig (3.20)**. The figure shows the relationship between the actual angles from the protractor compared with the angular device readings revealing a linear relationship. The calibration was repeated many times to check the correction factor and the results were the same. The use of the pressure transducer and tailfin in flowing water required a further series of checks and calibration. The first of these checks concerned the verticality of the rod attached to the transducer at one end and the tailfin at the other as shown in **Fig (3.18)**. If the rod is not exactly vertical then the tailfin will have an inbuilt bias and will tend towards a given direction even when submerged in flowing water. A method used to overcome this problem is simply to spin the tailfin in the air and record the angle where the tailfin comes to rest. If this procedure is repeated say, 100 times, then there should be a random distribution of angles where the tailfin comes to rest. If there is a preponderance of tailfin stopping angles in one region, then the bias needs to be removed. This procedure was followed in an initial set of tests to reveal a slight bias in one direction. This was connected by the Technician in charge and the tests repeated to reveal zero bias.

At the start of angular measurement tests each day, it was crucial to ensure that the zero reading on the voltmeter corresponded exactly to the 0^0 direction in the flume, which was chosen to be longitudinally in the direction of the flow. This was achieved by having a permanently marked line on one flood plain which was thought to be exactly longitudinal in the 0^0 direction. This line was set up by measuring out a given distance from either flume wall along a part of the length of the flume. The best fit line was drawn, representing the zero direction. The tailfin is then placed exactly along this line, say at three or four different positions, and the average reading should be 0^0 on the voltmeter.

3.3.6 Recording and Storing Experimental Data by Computer

Section 3.3.4 and 3.3.5 have described the calibration of the instruments used in the velocity and streamline angle experiments. These are known as the u, θ tests, and in each case the object is to measure the mean velocty u, and the mean velocity filament angle θ at any given point in the flow. The location of both the u and θ measurements is shown in **Fig (3.21a)** to **Fig (3.21c)** for series A and series D tests, and in **Fig (3.21d)** for series C tests. In each series of tests, values of u and θ were measured at three different cross–sections as already described, the first cross section being at the point of symmetry in the flume arrangement. It can be noted from **Fig(3.21)** that u, θ readings were taken at 40mm intervals across the flume width and at 20mm intervals with flume depth and this was repeated at all three cross–sections for each test run. It is clear that choice of spacing for measurements is a balance between enhanced accuracy and the amount of time the process is taking up. It was felt that depth spacing should be more refined than width spacing which in turn should be more refined than longitudinal spacing (1m).

Fig (3.22) shows a schematic view of the Pitot tube and angular measurement transducer. These two sets of data readings were carried out at separate times, but the location of the points coincided in the x, y, z are work. The Pitot–Static tube and the angular measurement transducer were connected to a multi–meter as shown in **Fig (3.23)**.

This device was capable of taking 10 readings per second, which were then transmitted in a digitised form to the micro computer. A computer program was written (Appendix C and D) to accept 10 readings per second over any specified time interval, and thereafter to give the mean value of velocity or angle over the period concerned. Typically a 50 sec sample gave 500 hundred readings to produce one value of u and θ. Values of u and θ were then transferred to the ICL 2988 mainframe computer for storage, analysis and eventual plotting, in the x, y, z framework. **Fig (3.23)** shows the work–station for the multimeter and micro–computer arrangement.

3.3.7 A Note About Longitudinal and Transverse Velocity Components

It has been already noted that the longitudinal velocities u were measured in the x– direction in both the floodplains and in the skewed main channel. The angle of the maximum velocity filament to the longitudinal direction θ was also measured, also on both main channel and flood plains. From these two sets of measurements the transverse velocity component was calculated, v. The method of calculation was straightforward and is sketched below:–

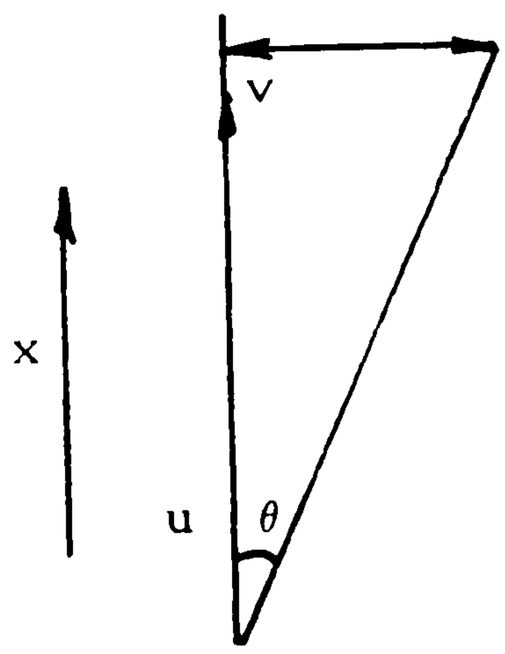

$v = u \tan\theta$

Above bank full

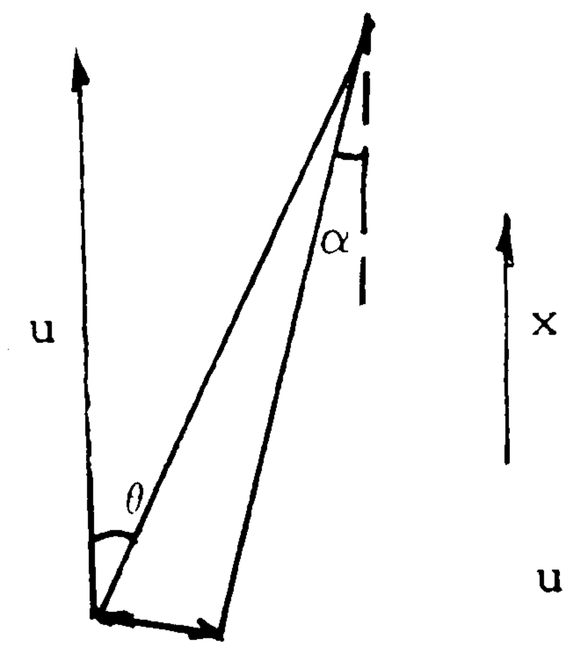

$$v = \frac{u \sin(\theta-\alpha)}{\cos\theta}$$

Main channel below bank full level

Above bank– full level the flow is guided by the two parallel flume walls in the longitudinal direction. Transverse velocity components are simply normal to this direction, $u\tan\theta$.

Below bank– full level transverse velocity components are guided by walls at a skew angle 5.843^0 to the longitudinal direction. The maximum velocity filament sketched above has a velocity of $u/\cos\theta$, but is acting at angle $\theta - 5.843^0$ to the skewed main channel direction. This produces a transverse velocty component normal to the skewed main channel walls of $v = u \sin(\theta - 5.843^0)/\cos\theta$.

3.4 EXPERIMENTAL PROCEDURE FOR TESTS IN THE SKEWED MAIN CHANNEL AND FLOOD PLAIN

The majarity of tests in SERIES A to E involved measurement of the bed and water slope, stage, discharge, velocity and streamline angle variation with width, depth, and in the longitudinal flume direction.(x, y, z). Several hundred test runs were carried out and the summary below gives a typical step–by–step procedure for one test run.

1. The bed slope of the flume was adjusted to give a (1/1000) slope using the screw jack arrangement under the flume. The bed level was read at one metre intervals along the flume length and at three different lines down the flume length. A surveyors level was used for this purpose. Once the entire flume was set at S_b= 1/1000, then it was checked only occasionally thereafter.

2. The pump was switched on and the discharge measured from the manometers combined with the orifice plate calibration.

3. The normal depth was established by a method already described whereby a deliberated backwater slope is set up, the water surface slope measured at 1m intervals along the flume length, and the tailgate successively lowered until the average water slope is also 1/1000, thus being parallel with the average bed slope.

4. The main channel depth Y_c and flood plain depth Y_f are thus measured at sections I, II, III along the flume length and averaged.

5. The Pitot static tube was connected to the pressure transducer by means of the clear plastic tubing, and the complete bleeding–out of any air in the system was required, as air bubbles would seriously affect the transducers response.

6. The Pitot static tube was placed in a beaker of water to give a zero pressure difference across the static head and the dynamic head. The carrier demodulator was checked for a zero reading and if not, was adjusted accordingly.

7. The Pitot static tube was then removed from the beaker into the flow and placed at known positions throughout the cross–sectional area of the channel and flood plain flow to give a velocity transverse. U(x, y, z). When a complete

traverse was completed in the y, z plan, then the instrument carriage was moved to the next cross– section downstream.

8. The Pitot static tube was then removed and replaced by the angular measurement device to measure the direction of maximum velocity filament of the stream flow. The angular measurement device was connected to the demodulator in the same way as the Pitot static tube. The angular measurement device was checked to ensure that a zero voltmeter reading coincided with the 0^0 longitudinal direction.

9. The angular measurement was then placed into the flow at the same position as the Pitot static tube to obtain the angular measurement reading (θ).

10. Point velocity and the angular measurements were taken over a grid at intervals of approximately (20mm x 40mm) in the vertical and lateral directions respectively, and at intervals of 1m in the longitudinal direction.

11. The point velocity and the angular measurement readings were transferred to the microcomputer continuously via the multi meter giving values of mean longitudinal velocity u and mean angular readings θ over the three sections already described. The velocity and the angular readings were entered on the ICL 2988 mainframe computer and processed by the program in Appendix A into a graphical representation of contours of longitudinal velocity, depth averaged velocities across the channel and flood plain, as well as the transverse velocity across the skewed main channel sections.

12. The longitudinal mean velocities were then integrated using another program in Appendix B to give a total discharge. This was for comparison with discharges from the orifice plate calibration.

13. At the end of each test run the recorded data would include the following parameters:–

1) Total discharge Q_t
2) Bed slope S_b and water surface slope S_w
3) Channel depth Y_c and flood plain depth Y_f
4) Point velocities u and angular measurements θ in the x, and y directions.

5) Bankfull depth h, channel and flood plain widths B_c and B_f. The overall testing programme is summarised in **Fig (3.24)** with a flow chart illustrating all the activities clearly.

3.5 SLOT TEST APPARATUS

3.5.1 Introduction

At an early stage of this work it was thought that an important feature of the flow would be the "horizontal shear" problem, where the floodplain flow passes over the skewed main channel flow as sketched below.

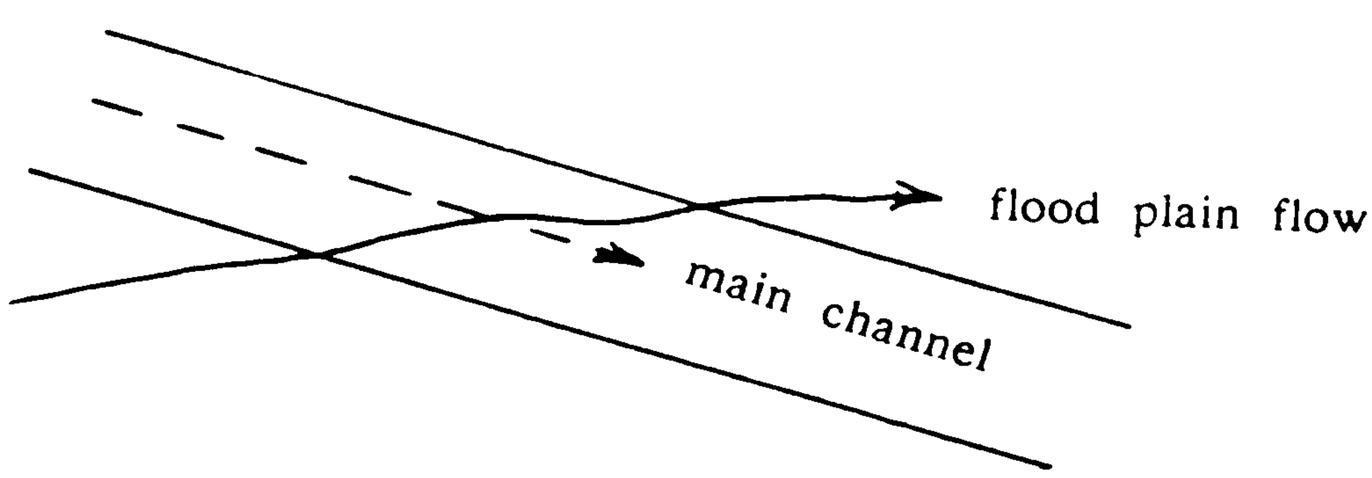

In some respects this is akin to the floodplain flow "feeling" a sudden expansion followed by contraction, albeit with a flow passing underneath at a skewed angle θ. It was decided to carry out a series of tests (SERIES F) investigating the mechanics of flow over a slot in the channel bed, representing an idealised version of the sketch above. The idealisation occurs in the sense that the slot flow tests did not have a flow passing underneath in the deeper part of the channel, and also the floodplain flow always passed over the main channel at 90^0 rather than a range of skews from 0^0 to 90^0.

It was felt that the fundamental slot tests would nevertheless reveal very valuable information regarding the flow mechanics at a sudden expansion/contraction of the channel bed. The results of this work are presented

in Chapter 6 and discussed in detail in Chapter 7. It was hoped that the slot tests would reveal information about the following items:—

(i) Variation of free water surface levels in the region of a sudden expansion and contraction.

(ii) Energy losses in both the expansion and contraction regions for a range of slot width/depth ratios.

(iii) Details of the horizontal shear layer and recirculation zone including any secondary currents generated.

(iv) Velocity distributions throughout the expansion and contraction regions. These measurements allowed accurate calculation of the energy level at each section along the flow, and also details such as magnitude of recirculating currents. These items are sketched below.

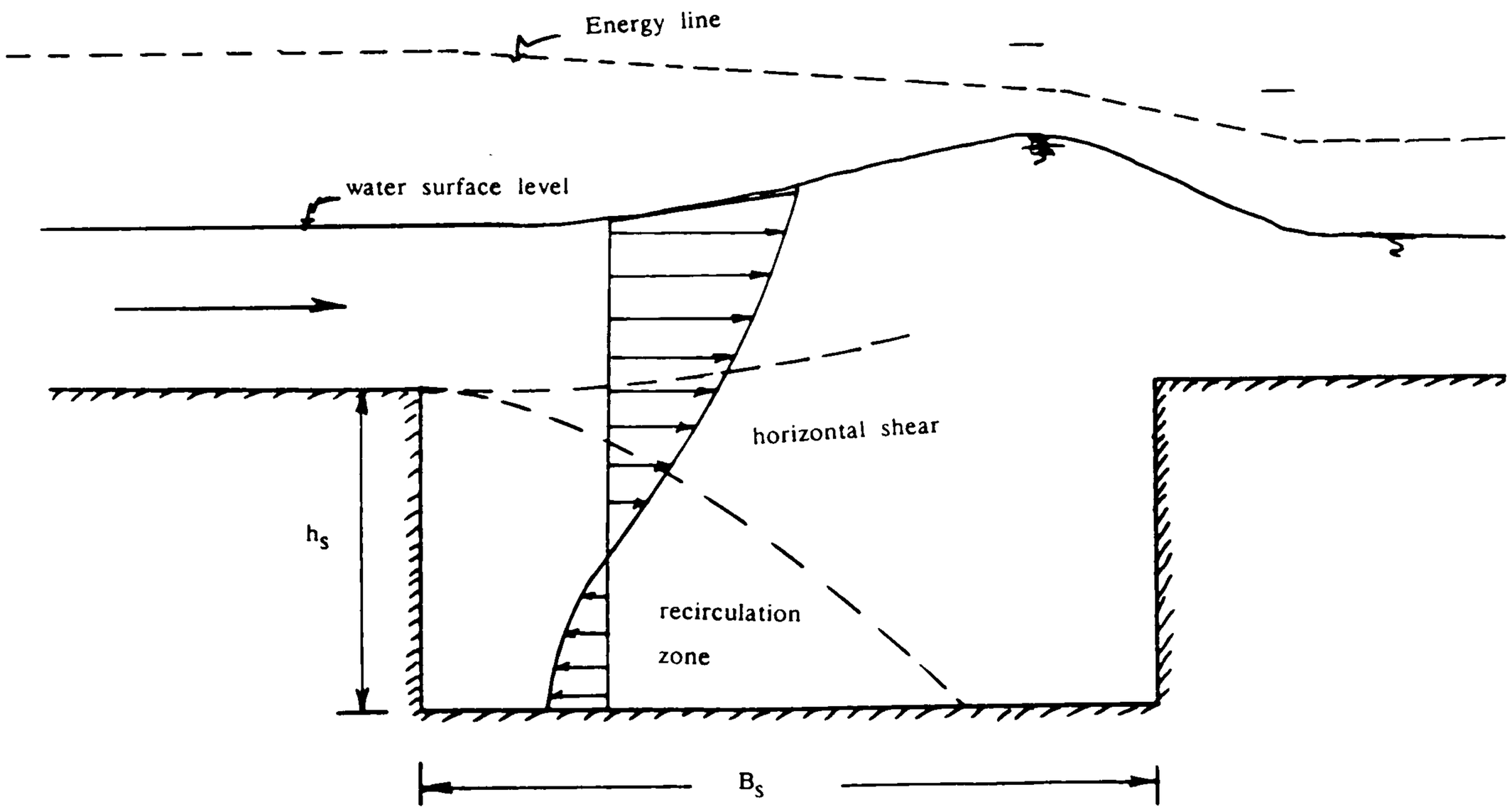

3.5.2 The Experimental Flume For Series F Tests

The experimental flume used for the slot tests was a standard Armfield 5m long flume of width 80mm, depth 300mm, recirculating discharge, and with a tilting mechanism. A slope of 1/1000 was used throughout to link with the experiments in the main flume. The flume is shown in **Fig (3.25)**.

Fig (3.26) shows a schematic of the flume and slot in plan and longitudinal section. The flume base was made up of removable concrete blocks which could be altered to give any required slot width B_s shown in **Fig (3.26b)**. The blocks were 53.0 mm high, giving a constant step height throughout all the test runs. The slot width B_s was varied over a range of four values, namely, 1060mm, 530mm, 265mm and 106mm. This produced a variation of the ratio of B_s/h_s, slot width to step height, of 20, 10, 5 and 2 respectively. This range is representative of aspect ratios in natural rivers and also covers the aspect ratio of the main channel section in the main flume.

3.5.3 The Initial Series of Tests SERIES F_1

Before the slot tests commenced, it was decided to carry out test runs in the flume with the slot infilled with a concrete block so that the whole length of the base was composed of concrete blocks. The purpose of test SERIES F1 was to establish uniform flow depth at various discharge rates and also to determine the roughness coefficient Manning's "n" and roughness size 'k_s' for the concrete block base with perspex walls. The results of this work will be discussed in chapter 6. A second purpose of this tests was to calibrate the rotameter flow meter attached to the Armfield flume. This was achieved by using a miniature propeller meter to measure velocity throughout a cross section at uniform flow. Discharge was determined from integrated velocity measurements and compared with the rotameter. The calibration curve is shown in **Fig (3.27)**.

3.5.4 Measurements Carried Out

The test runs already discussed F_1 and the slot test runs F_2 to F_5 all required the longitudinal bed slope to be set accurately at 1/1000. This was done by altering the Armfield screw jack arrangement and using a surveyors level to take bed level measurements along the flume length. A typical result is shown in **Fig (3.28)** giving an average longitudinal slope of 1/1000.

A tailgate arrangement at the downstream end was used to set normal depth. The procedure followed was again deliberately setting a backwater curve, M_1 profile, and by gradually lowering the tailgate, producing uniform flow. This procedure was straight forward in test series F_1, but series F_2 to F_5 with the slot, normal depth measurements were not taken in the region of the slot because of large level variations. In these runs, the normal depth measurements were taken some distance upstream and downstream from the slot. The normal depth was measured at 1m intervals along the flume length, by using pointer gauges.

Detailed water surface measurements in the region of the slot were carried out by a moveable pointer gauge with vernier scale. An example is shown in **Fig (3.29)** of the large variation in free water surface in the region of the slot. Accurate depth measurement was required to obtain accurate assessments of the energy level and energy losses over each section. It was decided to use a miniature propeller meter for velocity measurements in the region of the slot. Only longitudinal velocities were measured. **Fig (3.30)** shows the instruments for measuring the point velocity in the expansion and contraction flows. The propeller consists of a circular ring with five blades inside.

It was connected by a co– axial cable to a frequency meter. There are two switches on the frequency meter, the first one is used to turn the power on or off, and the second is used to change the measurement scale. Two alternative readings of frequency meter, the first one was used for low velocity readings and the second was used for high velocity readings. The frequency meter was calibrated by the manufactures and the result was a flow chart enclosed with the propeller. The flow chart consists of two curves one was used for high readings and the second was used for low readings and is shown in **Fig (3.31)**. A large array of velocity measurements were carried out for each tests run. An example is shown in **Fig (3.32)** for the case of $B_s/h_s = 20$. This shows the points and

sections at which velocity was measured. At each cross section shown there were 5 sets of readings with channel width. All this information was required to produce very accurate values of velocity head ($\alpha V^2/2g$), so that accurate energy profiles could be obtained.

3.5.5 Experimental Procedure for Tests F_2 to F_5

The four dimensions were tested over five to six flow depths each, giving a total number of test runs of 20. Each of 20 test runs involved water level and point velocity measurements at more than 20 cross sections giving an large volume of data for detailed analysis (Chapter 6). The outline of the experimental procedure for each test run is below:—

1. The slot model was inserted into the flume by using the concrete block material upstream and downstream of the slot.

2. The bed slope of the flume was adjusted to give a (1/1000) slope. The slope was obtained by adjusting the flume from the driving wheel, and reading the bed level every 1.0 metre down the flume, using the surveying level and the scale gauge.

3. The pump was switched on and the depth of the flow was selected. With reference to the calibration curve.

4. Several point gauges were used to set the flow depths upstream and downstream of the slot to get uniform flow. Very detailed water level measurements were carried out in the slot region.

5. The streamflow probe (propeller) was used to measure the point velocities during the tests.

6. The point velocity measurements were transferred to the main frame computer.

7. The point velocity measurements were taken over a grid at intervals of

approximately (20mms x 50mms) in horizontal and vertical directions respectively.

8. The point velocities were integrated to give the total discharge.

9. At the end of each test the recorded data would include the following parameters:

1) The total discharge Q_t.
2) Bed slope S_b and water surface slope S_w.
3) Upstream, downstream and the slot water level measurements.
4) Point velocity measurement with depth, distance along flume and with flume width, of approximately 20 cross sections. The overall testing programme is summarised in **Fig (3.33)** with a flow chart illustrating all the activities clearly.

FLUME DIMENSION IS (8.2 X 0.764 X 0.3) METRE.

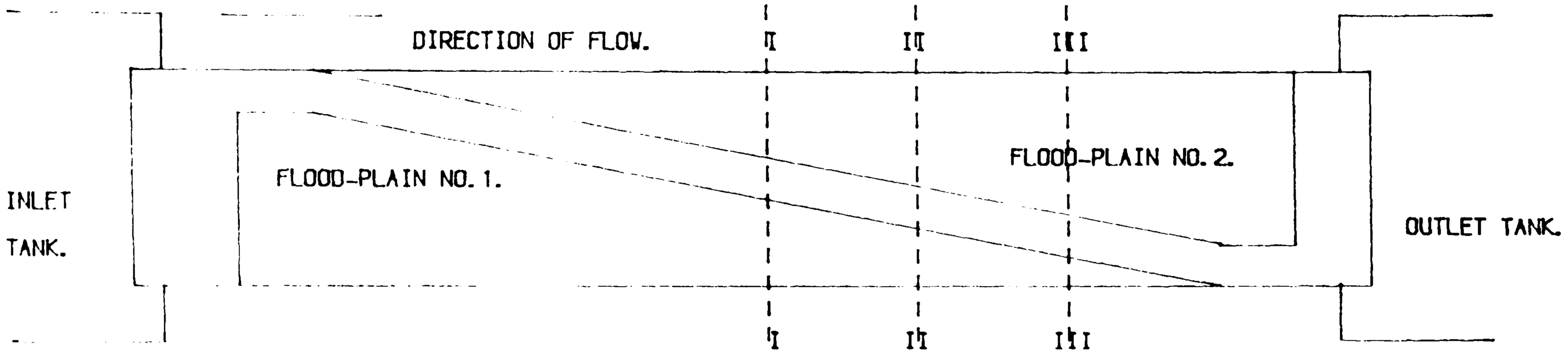

PLAN VIEW OF THE FLUME.

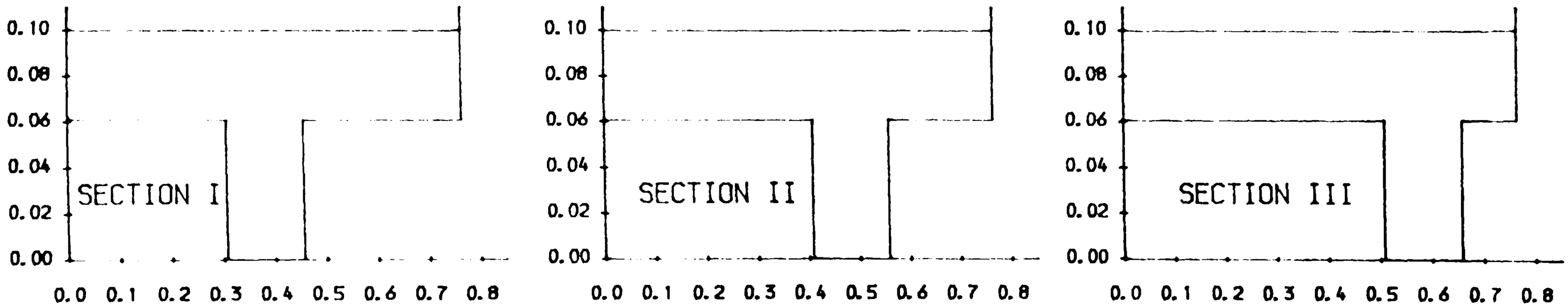

EXPERIMENTAL CROSS SECTIONS.

FIG (3.1) THE FLUME AND THE CROSS SECTIONS IN PLAN.

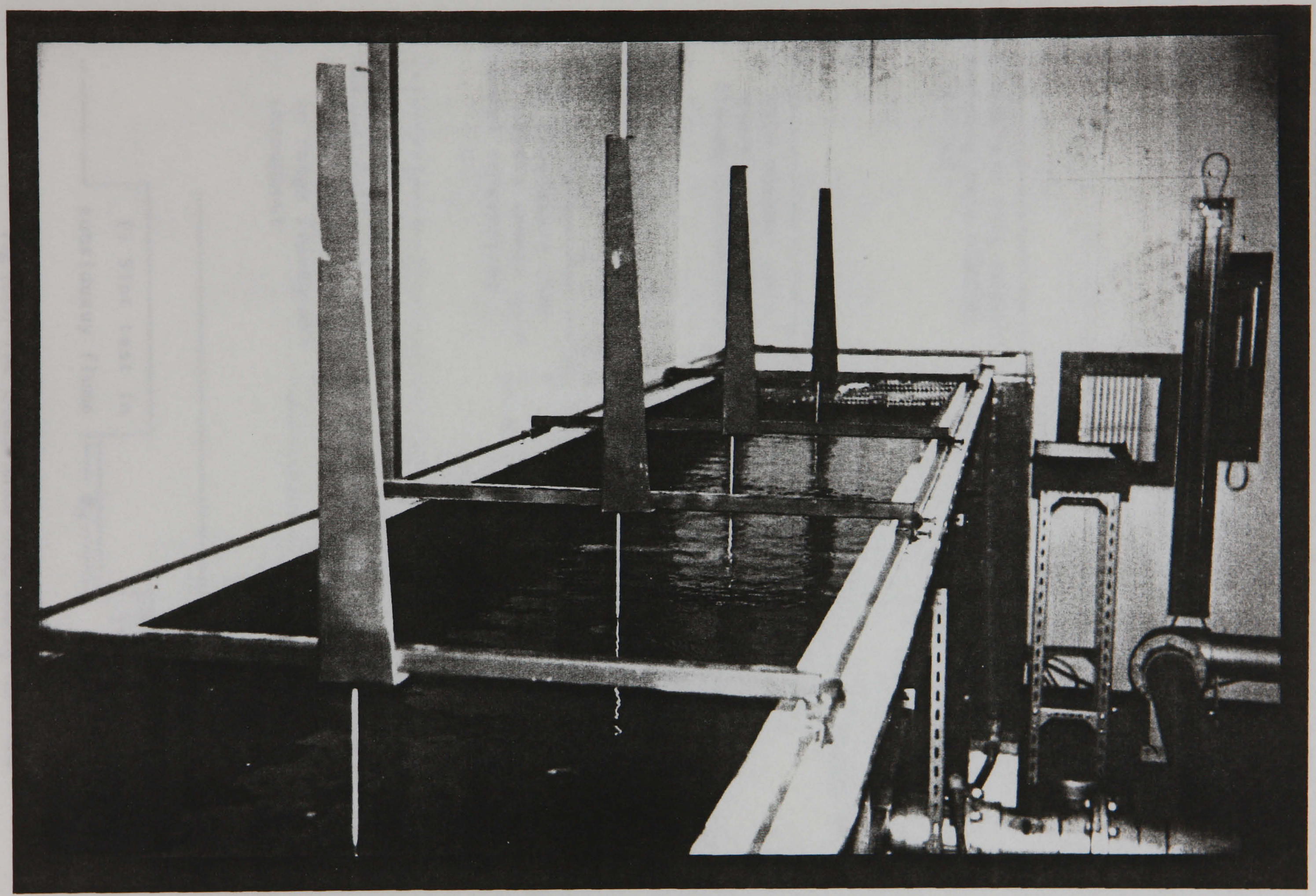

Fig (3.2) The Main Flume Used to Test Skewed Main Channel With Flood Plain.

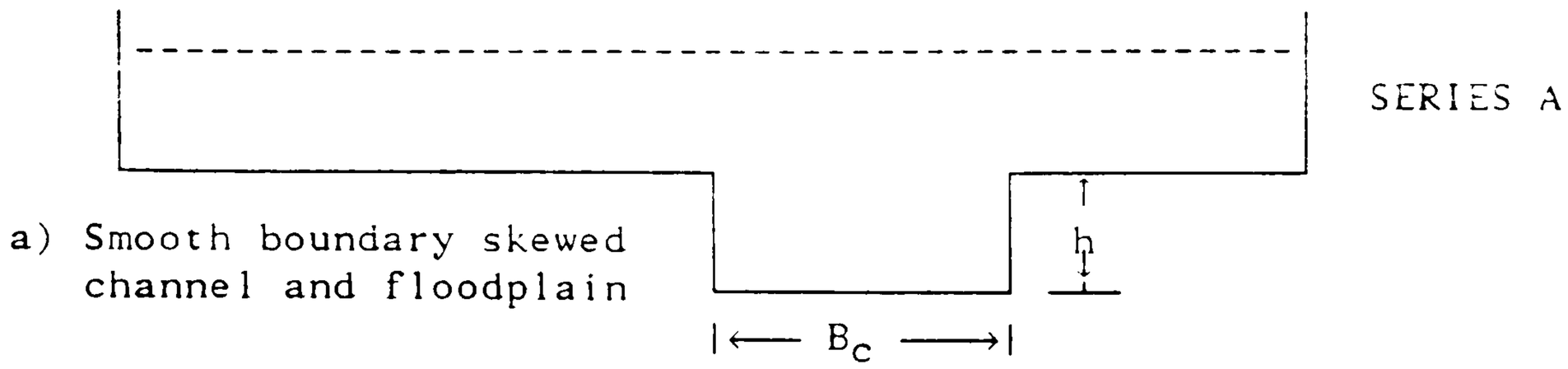

a) Smooth boundary skewed channel and floodplain

b) Floodplain only smooth boundary main channel infilled.

c) Main channel only smooth boundary floodplain isolated

d) Rough floodplain 10mm dia. dowels smooth main channel interacting

e) Main channel filled in rough floodplain throughout.

Fig (3.3) The Geometeries Used During the Tests.

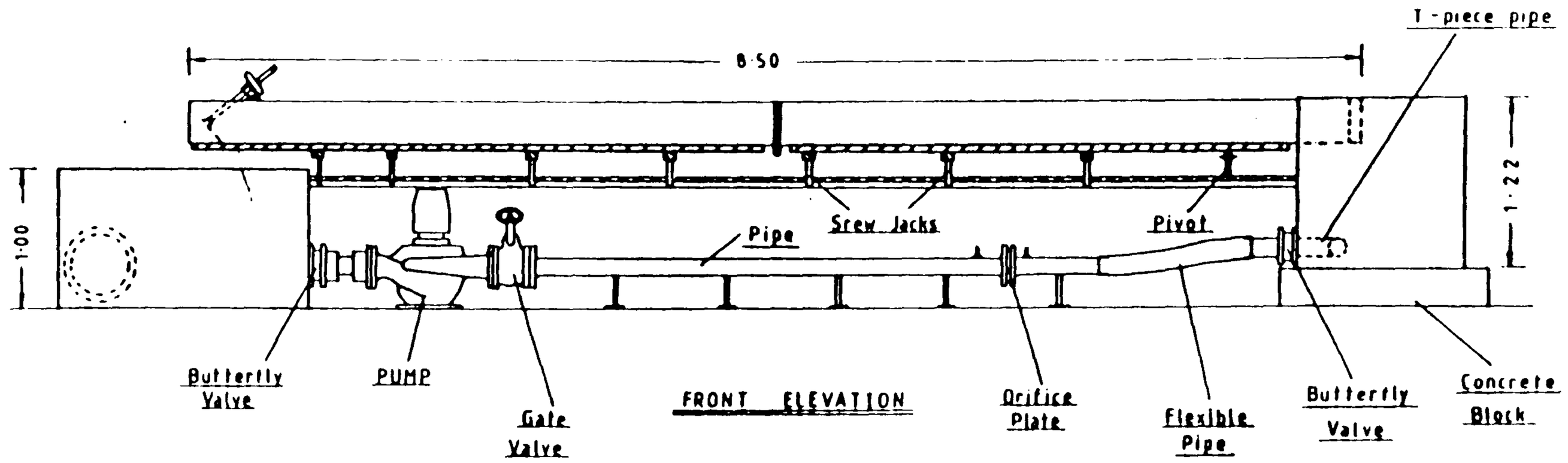

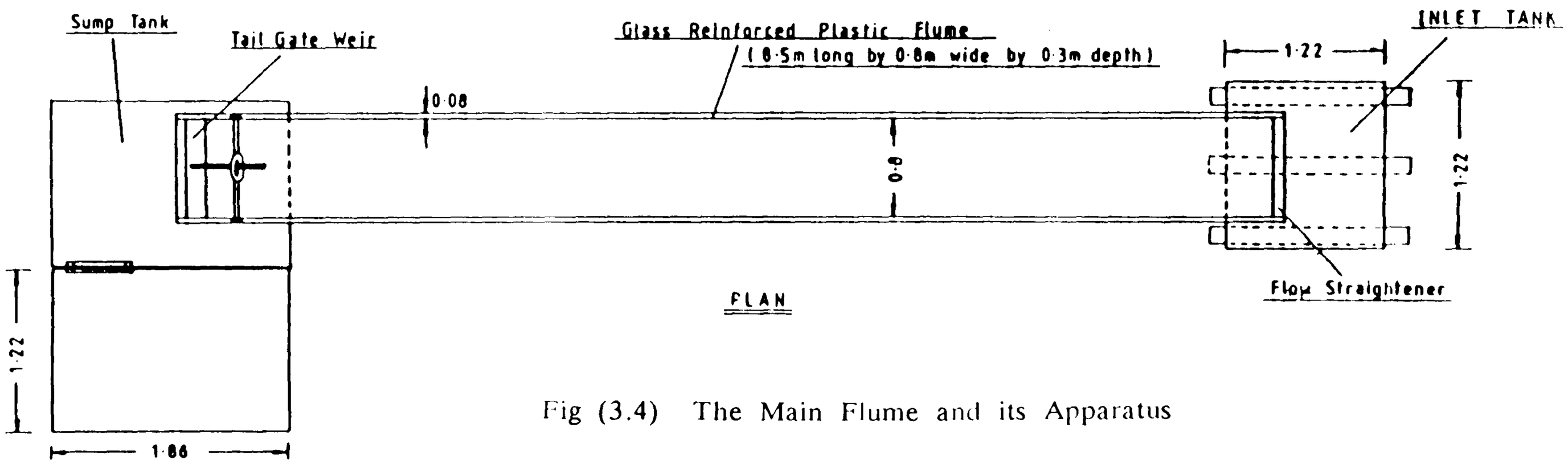

Fig (3.4) The Main Flume and its Apparatus

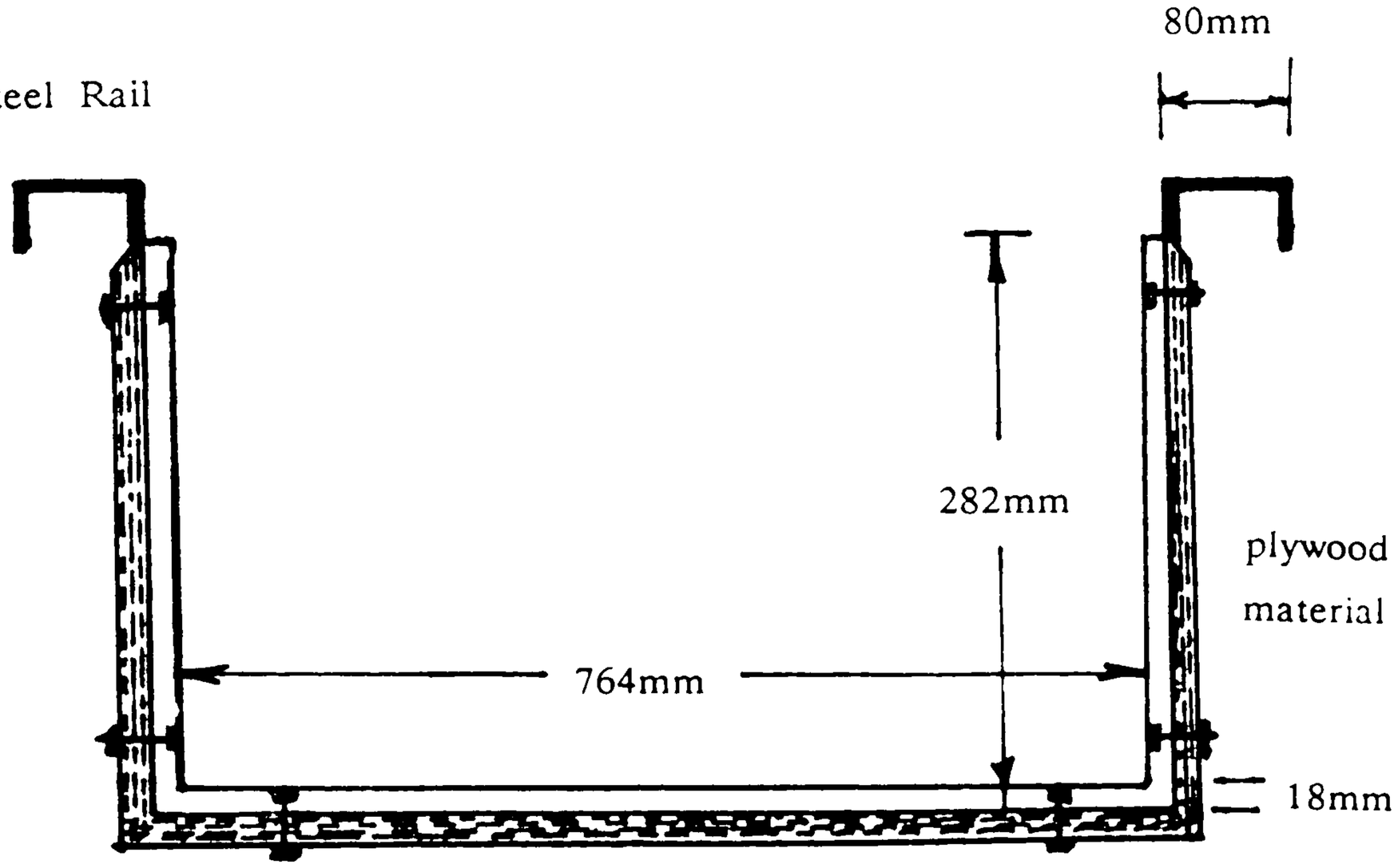

Fig (3.5) Cross Section of the Flume

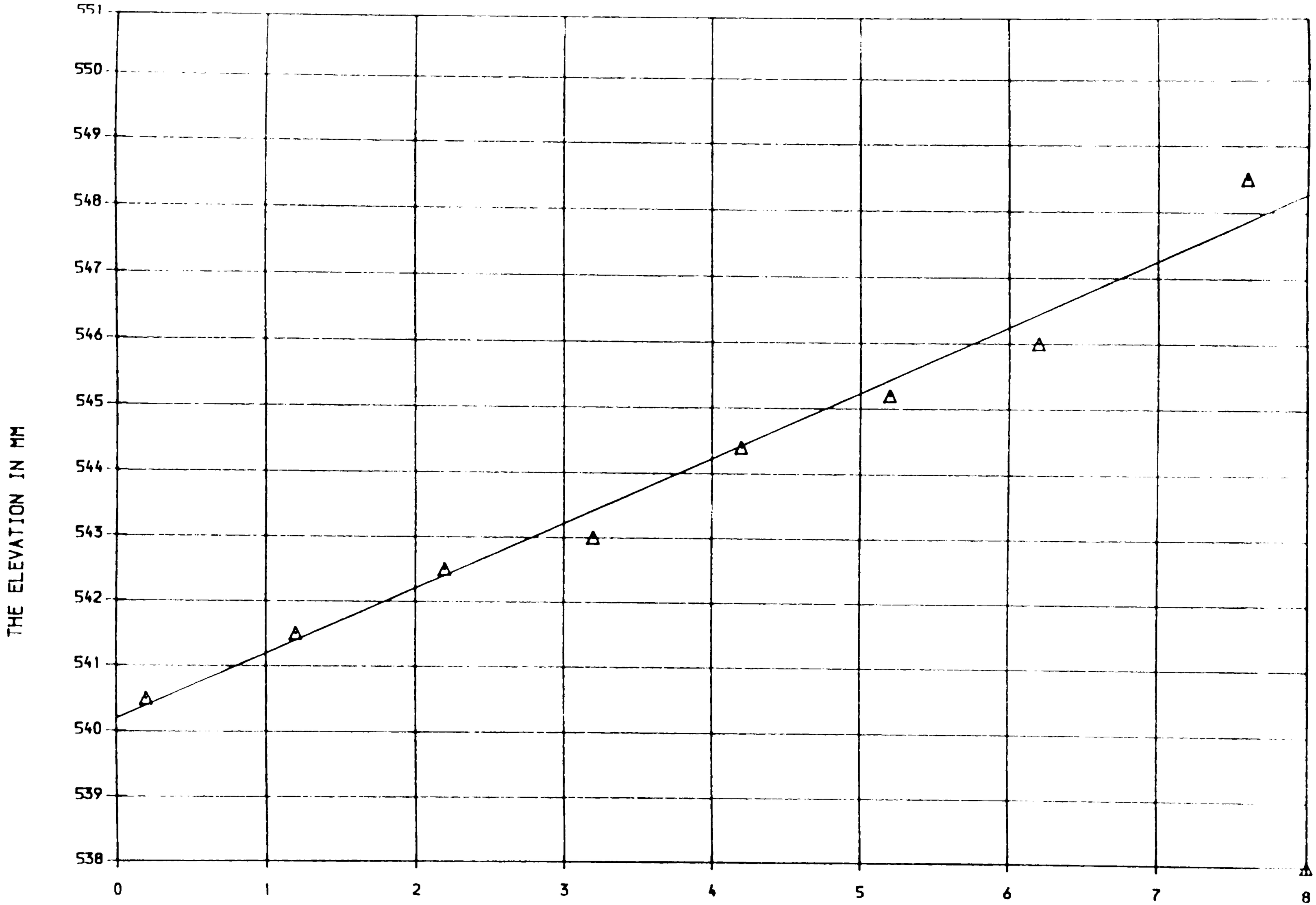

FIG (3.6) The Flume Bed Level After Modification

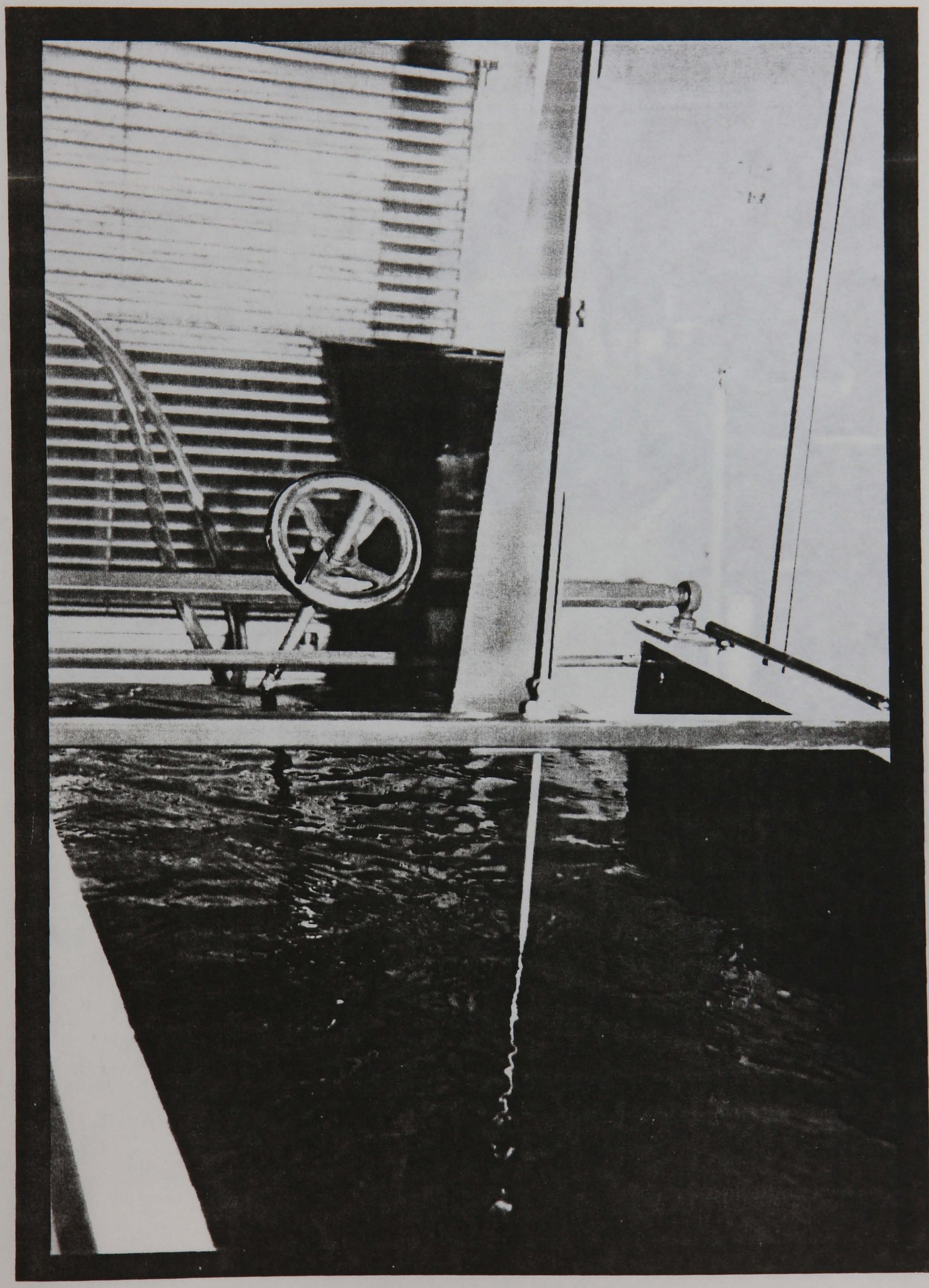

Fig (3.7) The Tail– Gate Weir

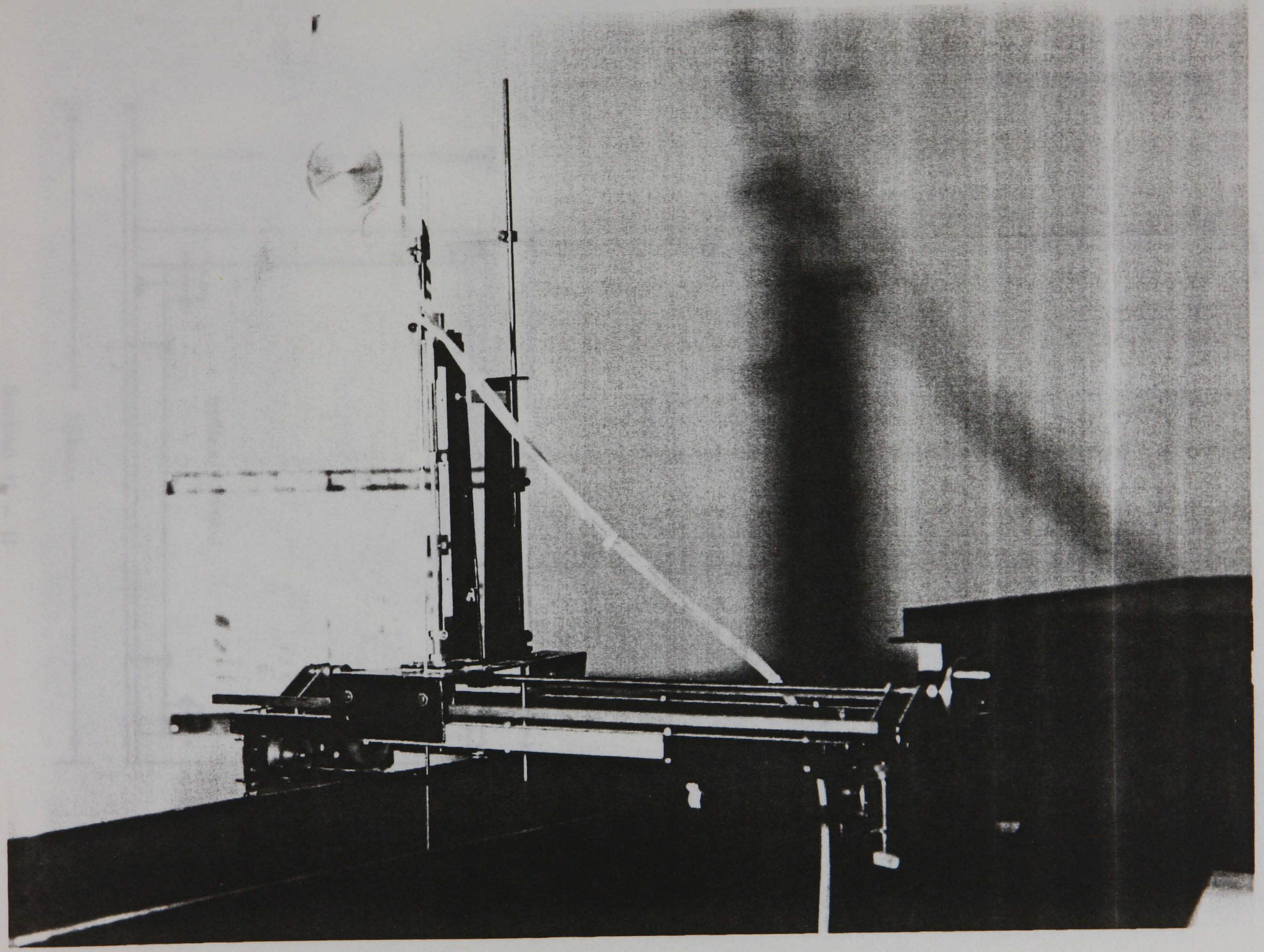

Fig (3.8) The Carriage Instrument Used to Carry The Pitot– Static Tube,

The Angular Measurement Transducer and Pairs of Gr

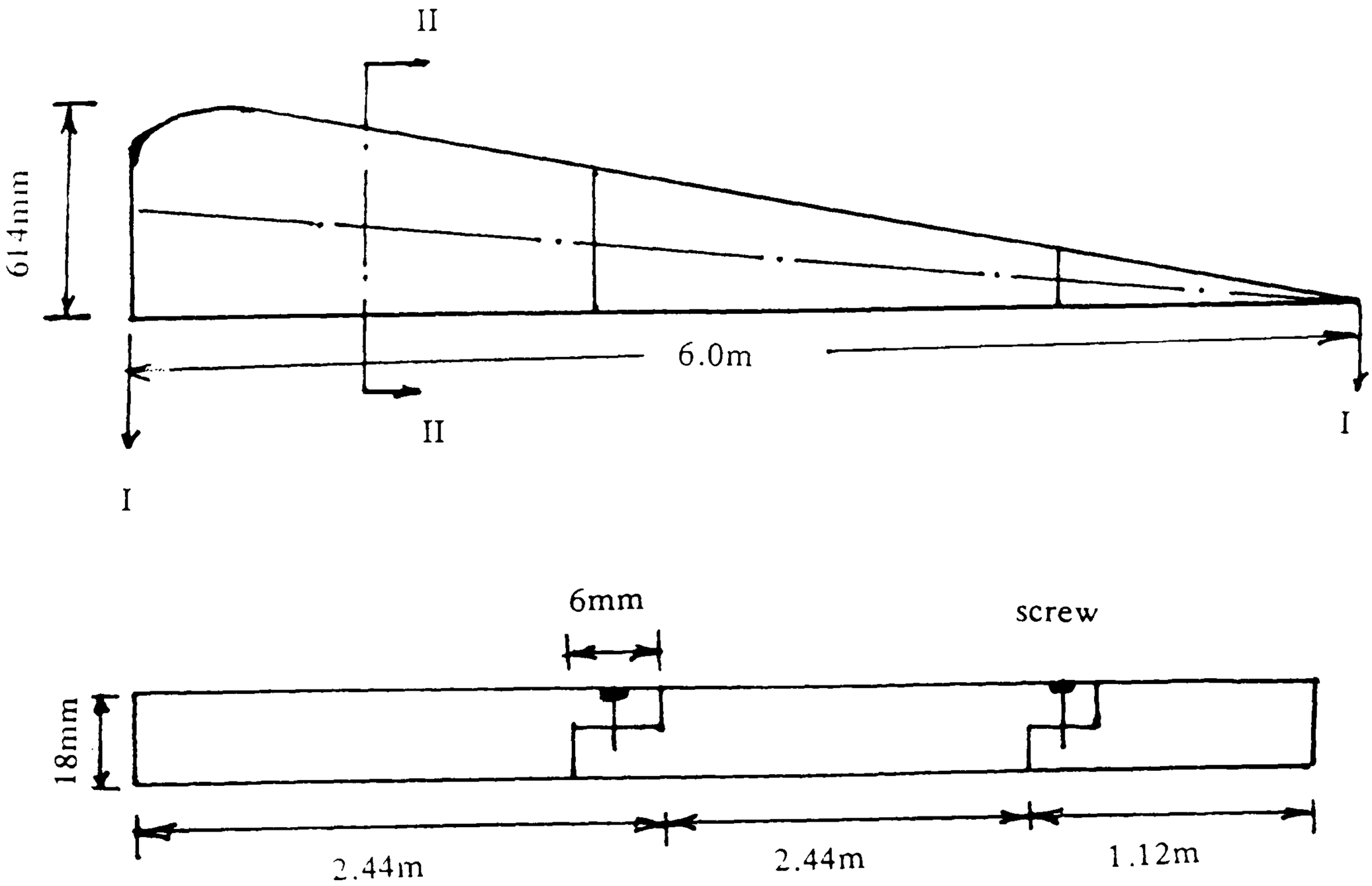

Section I – I

Section II – II

FIG (3.9) The Flood Plain Construction

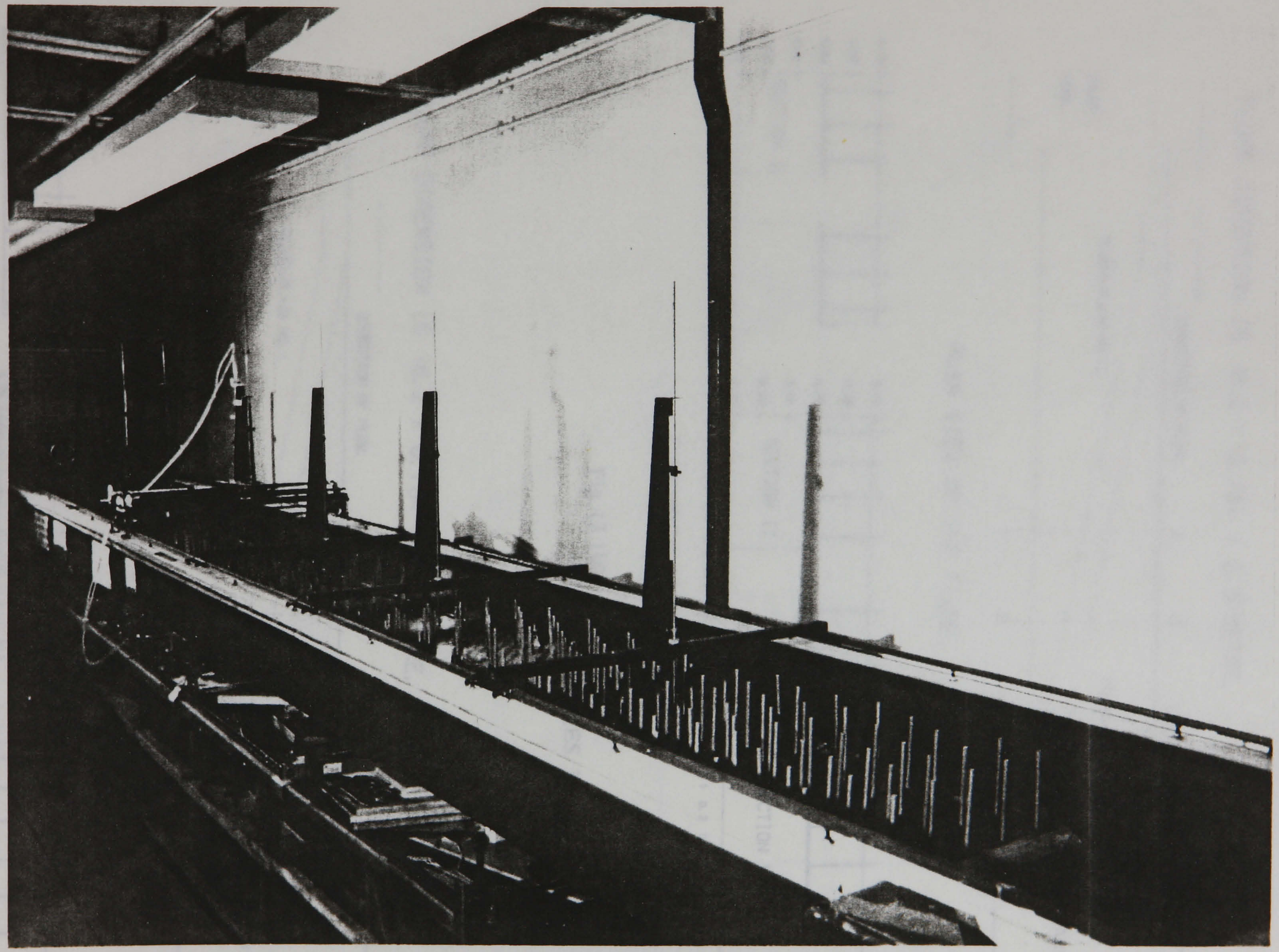

Fig (3.10a) The Roughness Elements Distribution Along the Flume.

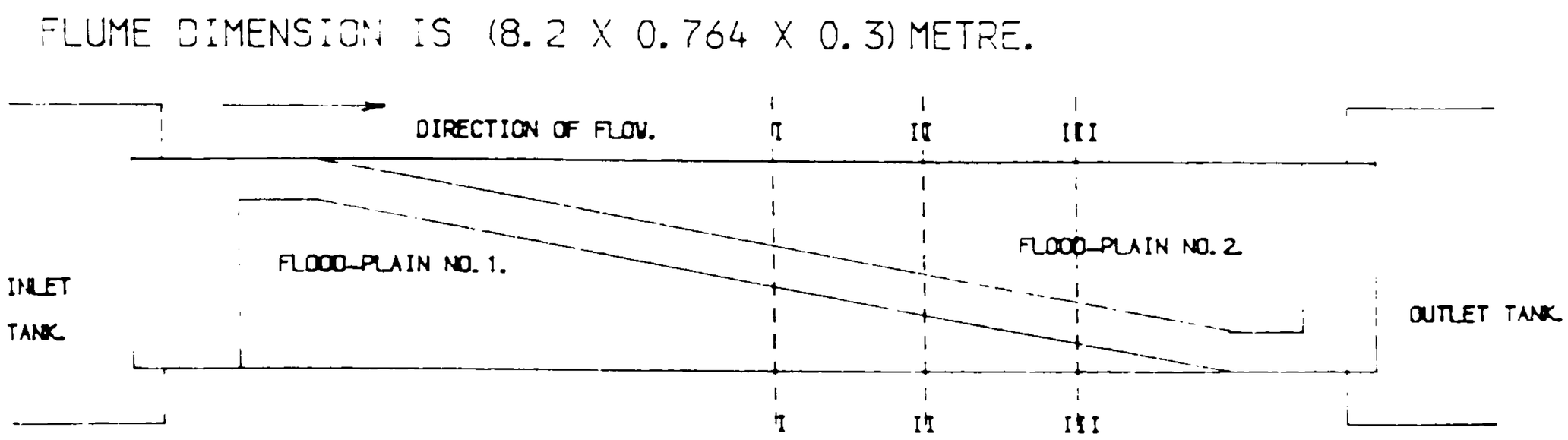

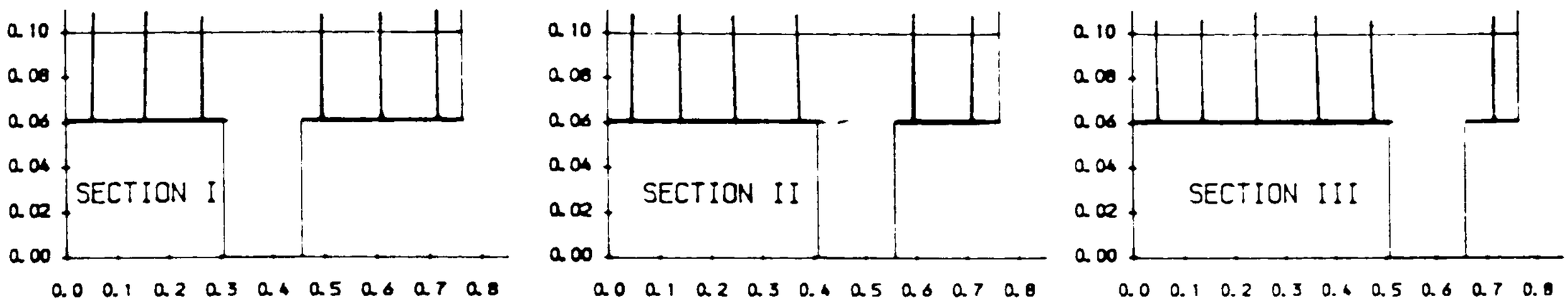

Fig (3.10b)

SERIES D tests

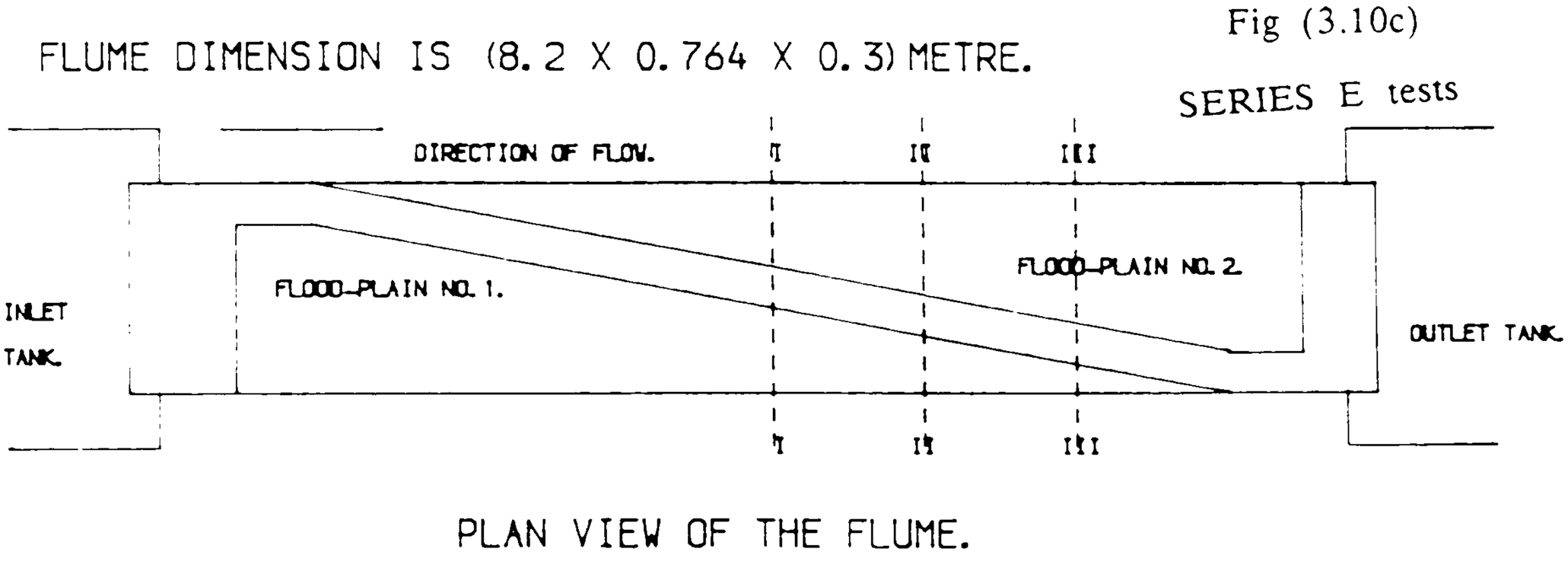

Fig (3.10c)

SERIES E tests

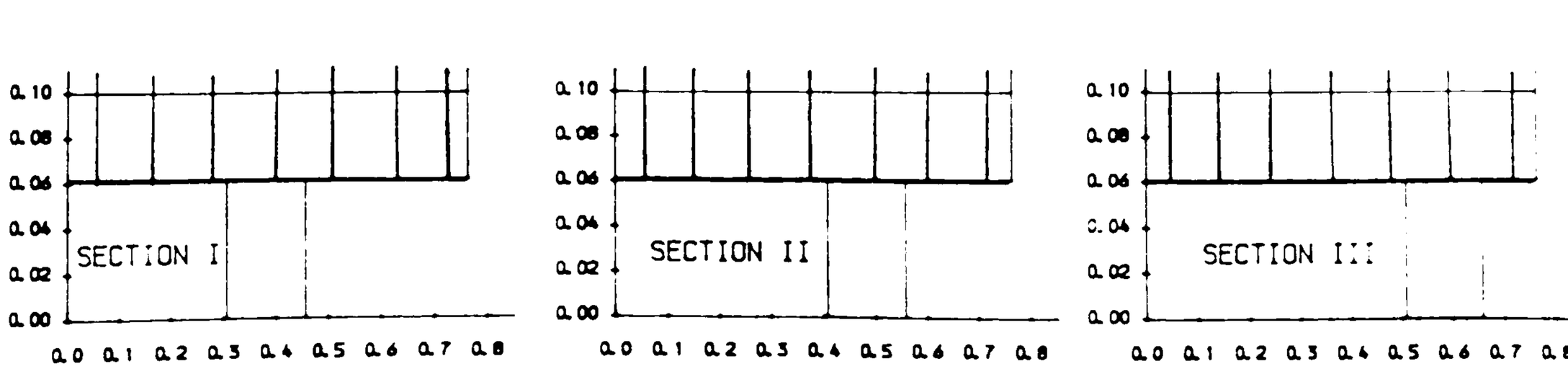

Fig (3.10) The Roughness Elements Distribution Along the Flume.

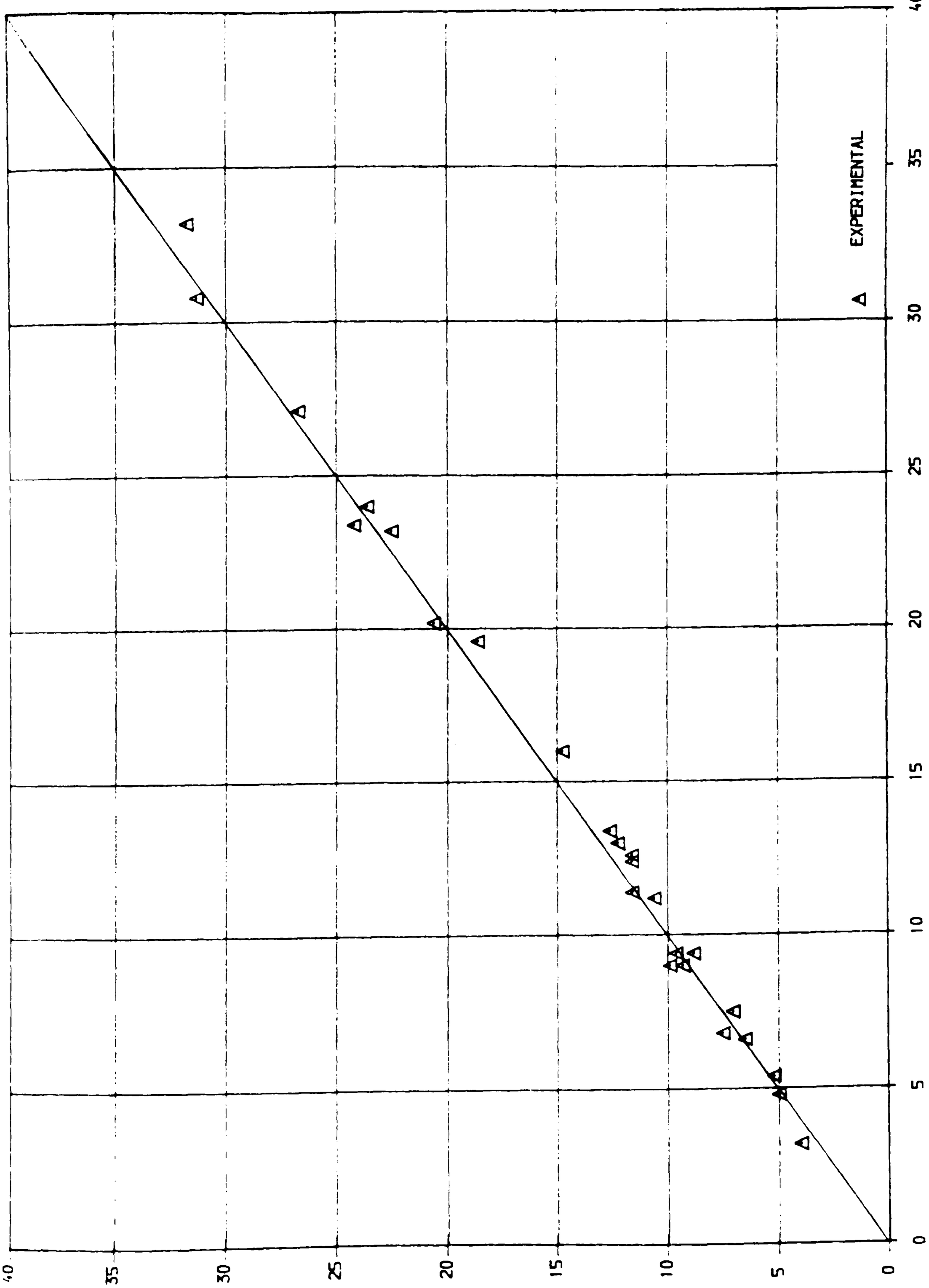

FIG (3.11) The Relationship Between Q_{tank} And $Q_{orifice}$

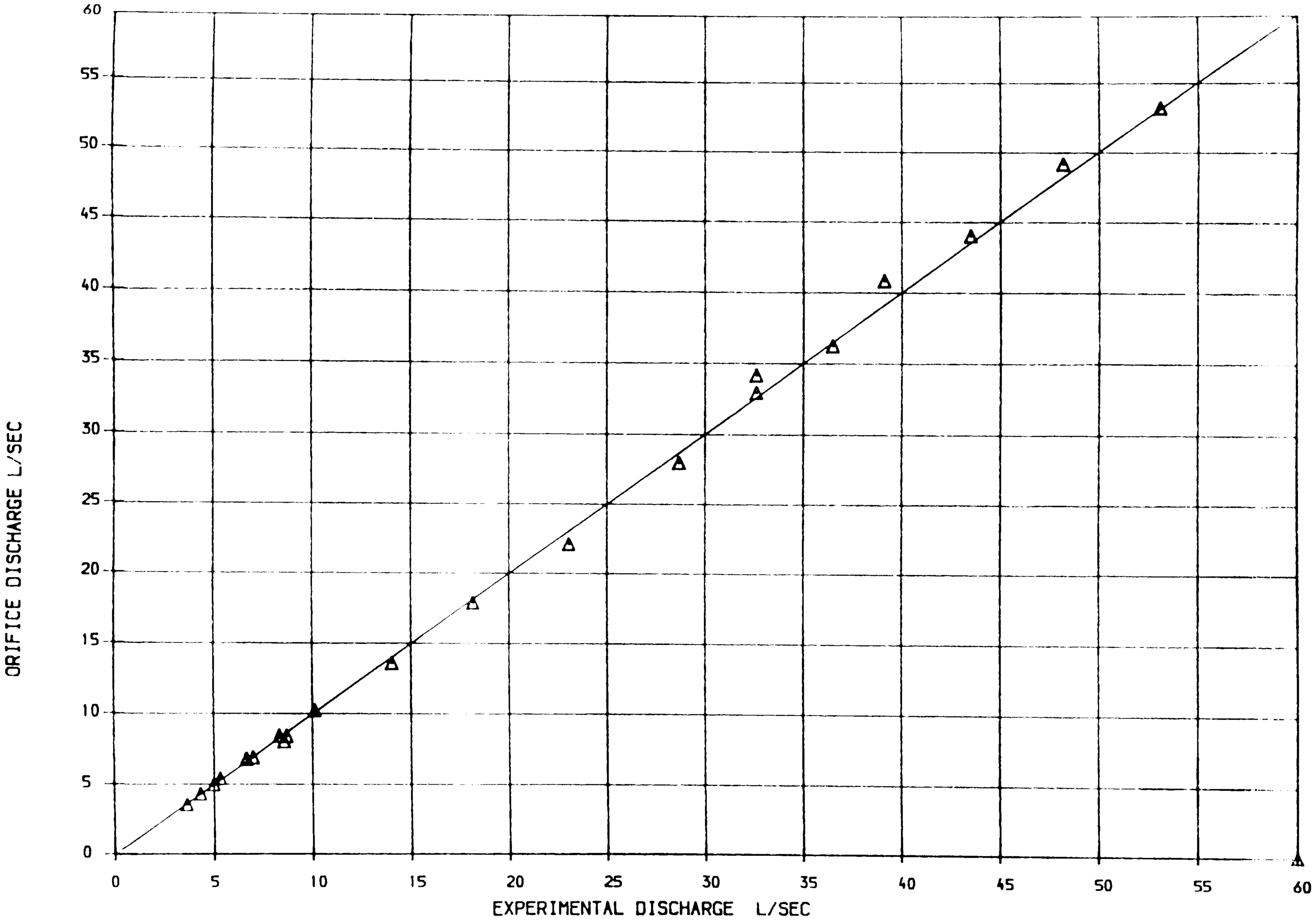

FIG (3. 12) THE RELATIONSHIP BETWEEN THE ORIFICE DISCHARGE AND THE EXPERIMENTAL DISCHARGE (INTEGRATED DISCHARGE)

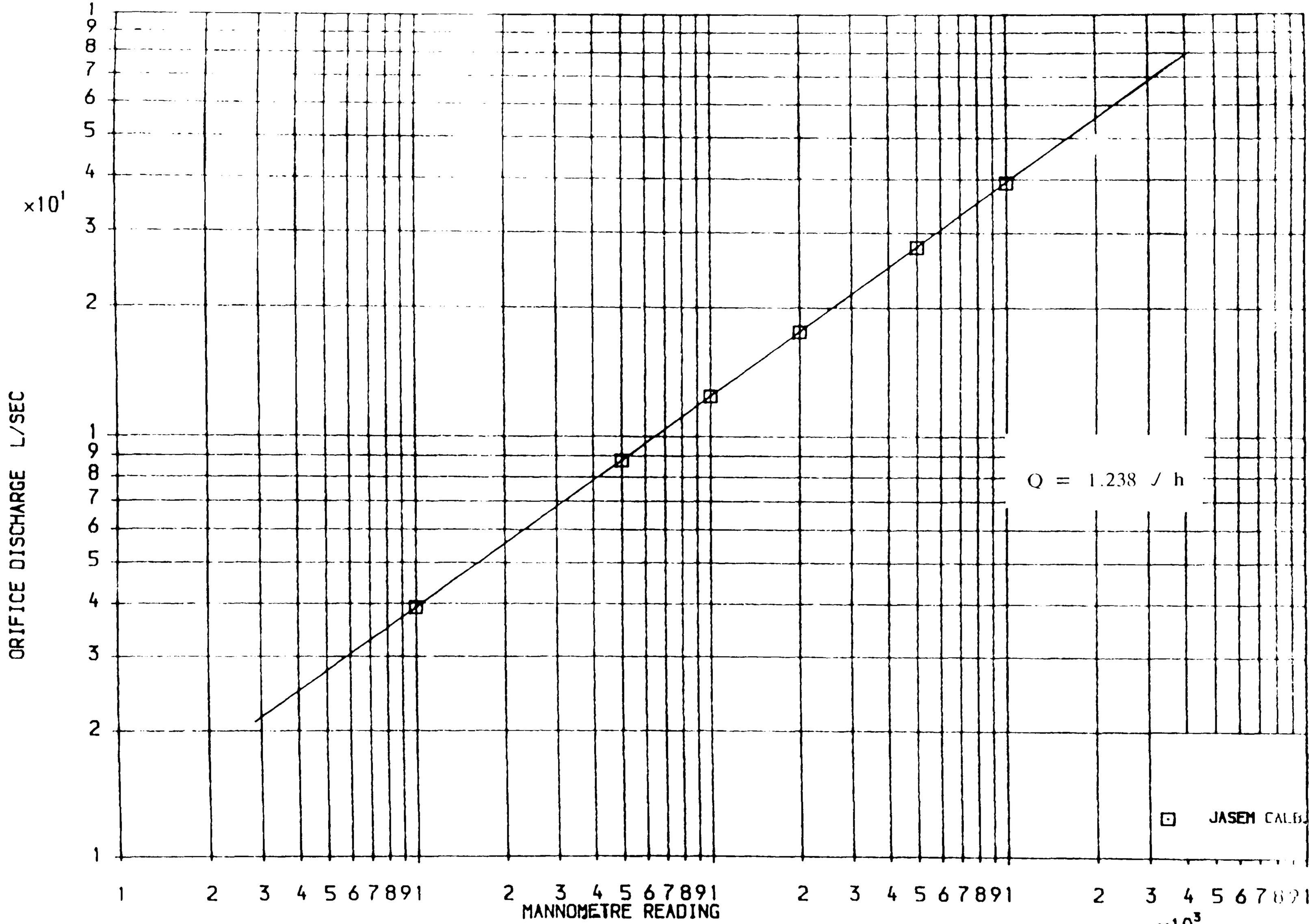

FIG (3.13) THE RELATIONSHIP BETWEEN THE MANNOMETRE READING AND THE ORIFICE DISCHARGE

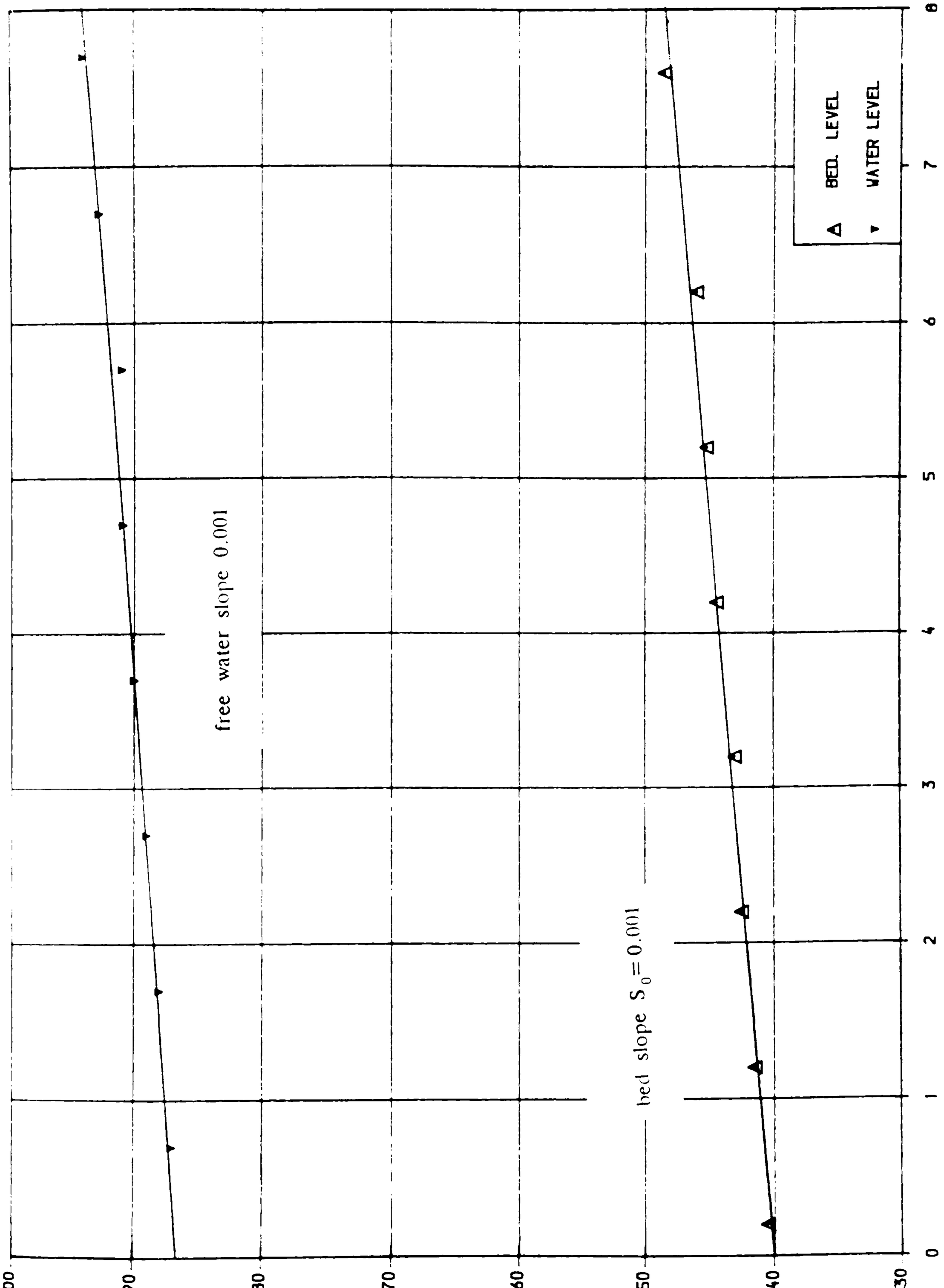

FIG (3.14) THE FLUME BED LEVEL AND FREE WATER SURFACE

Fig (3.15) The Pitot– Static Tube Device.

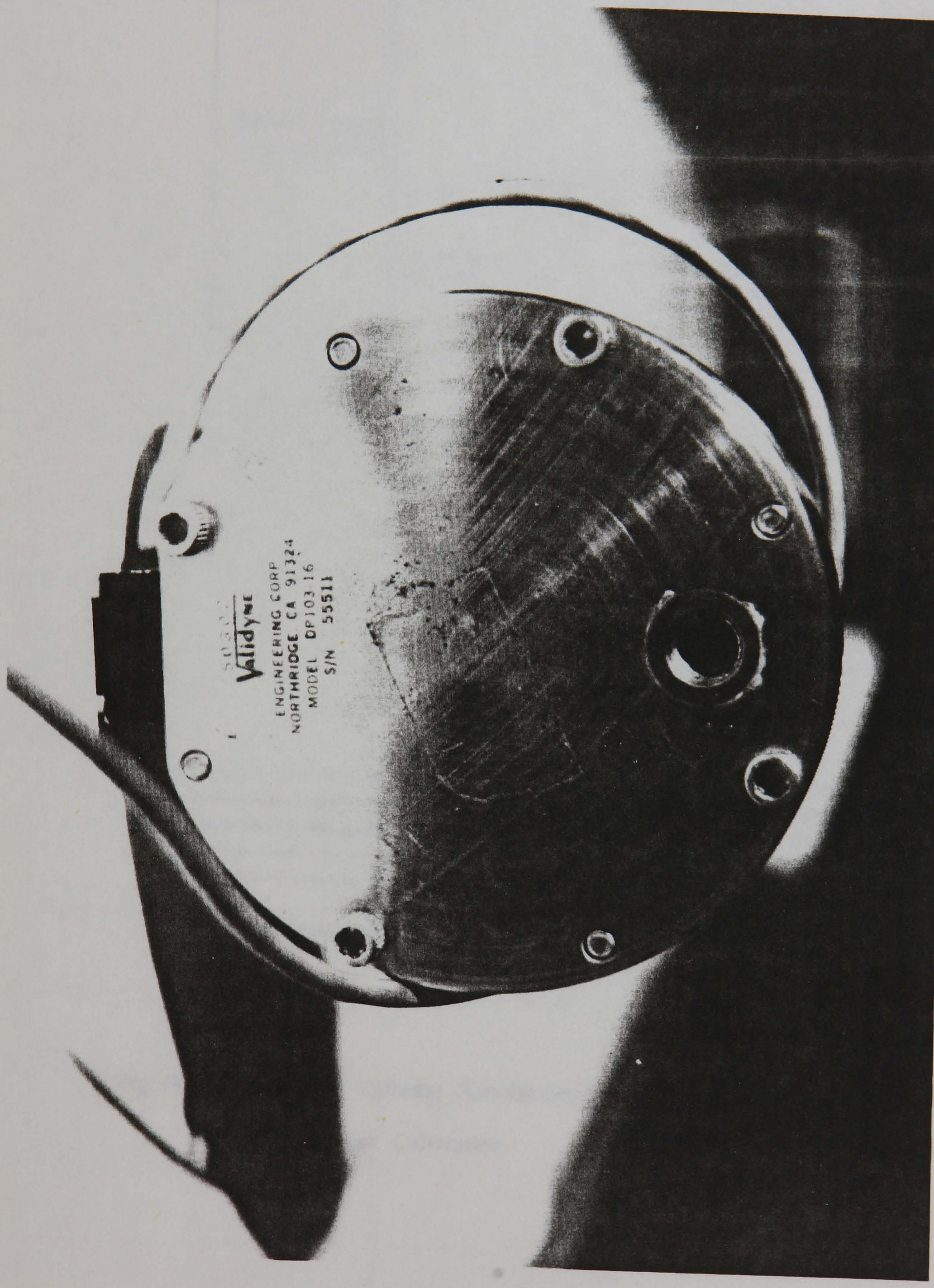

Fig (3.16) The Pressure Transducer

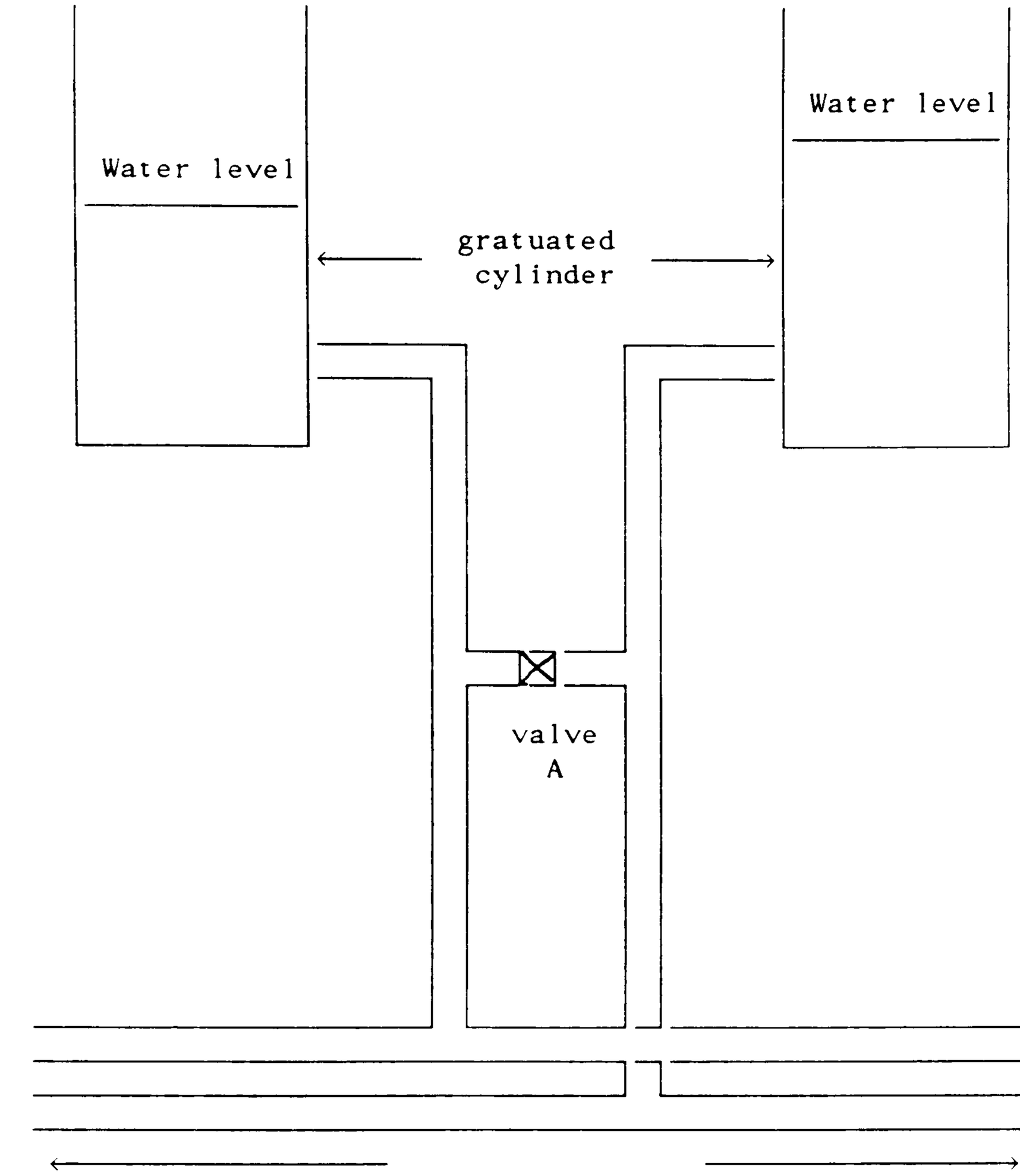

Fig (3.17) Graduated Cylinder Arrangement Used for Pressure Transducer Calibration.

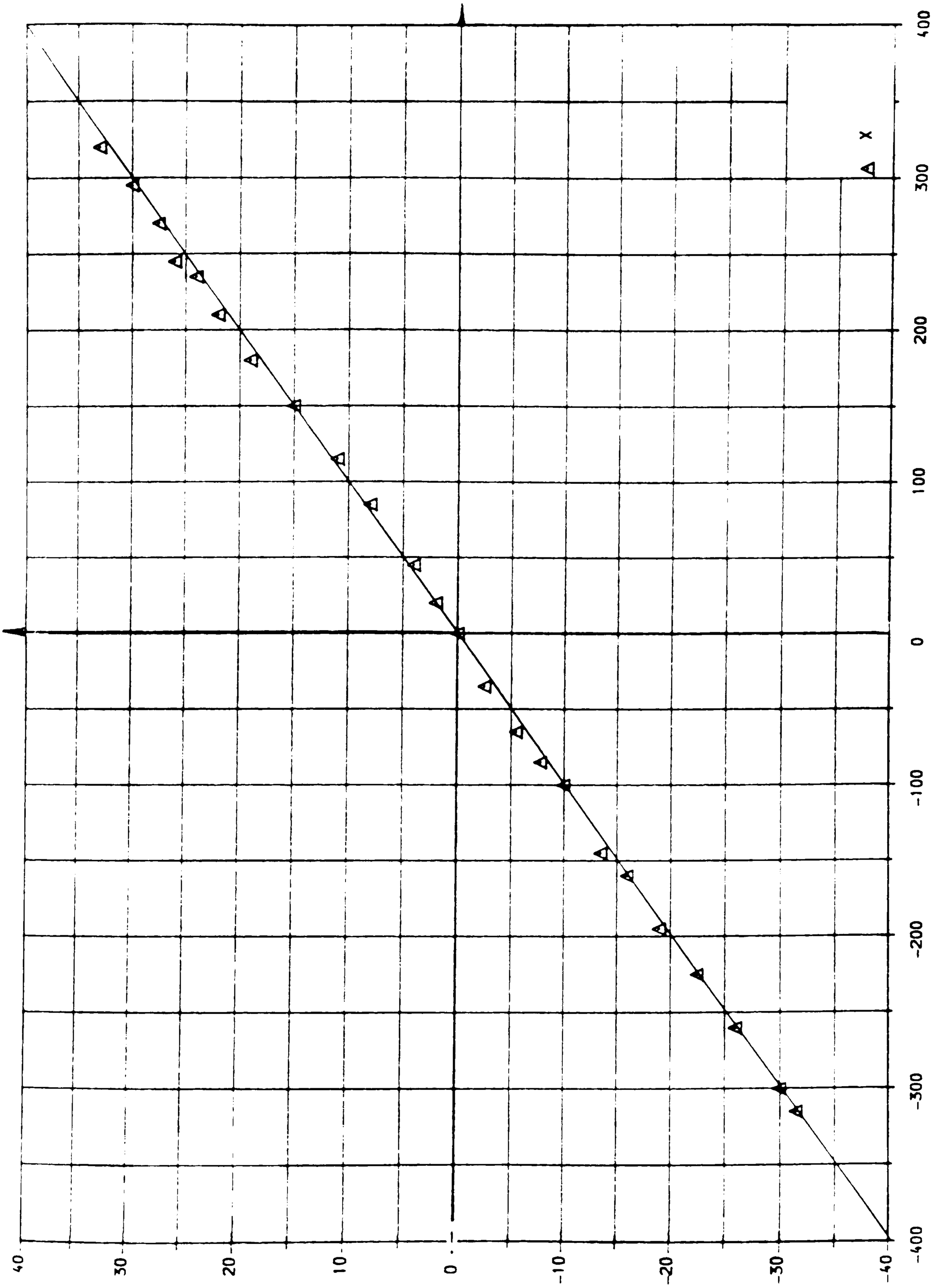

FIG (3.18) PRESSURE TRANSDUCER CALIBRATION SHOWING LINEAR RELATIONSHIP BETWEEN READING AND PRESSURE DIFFERENCE.

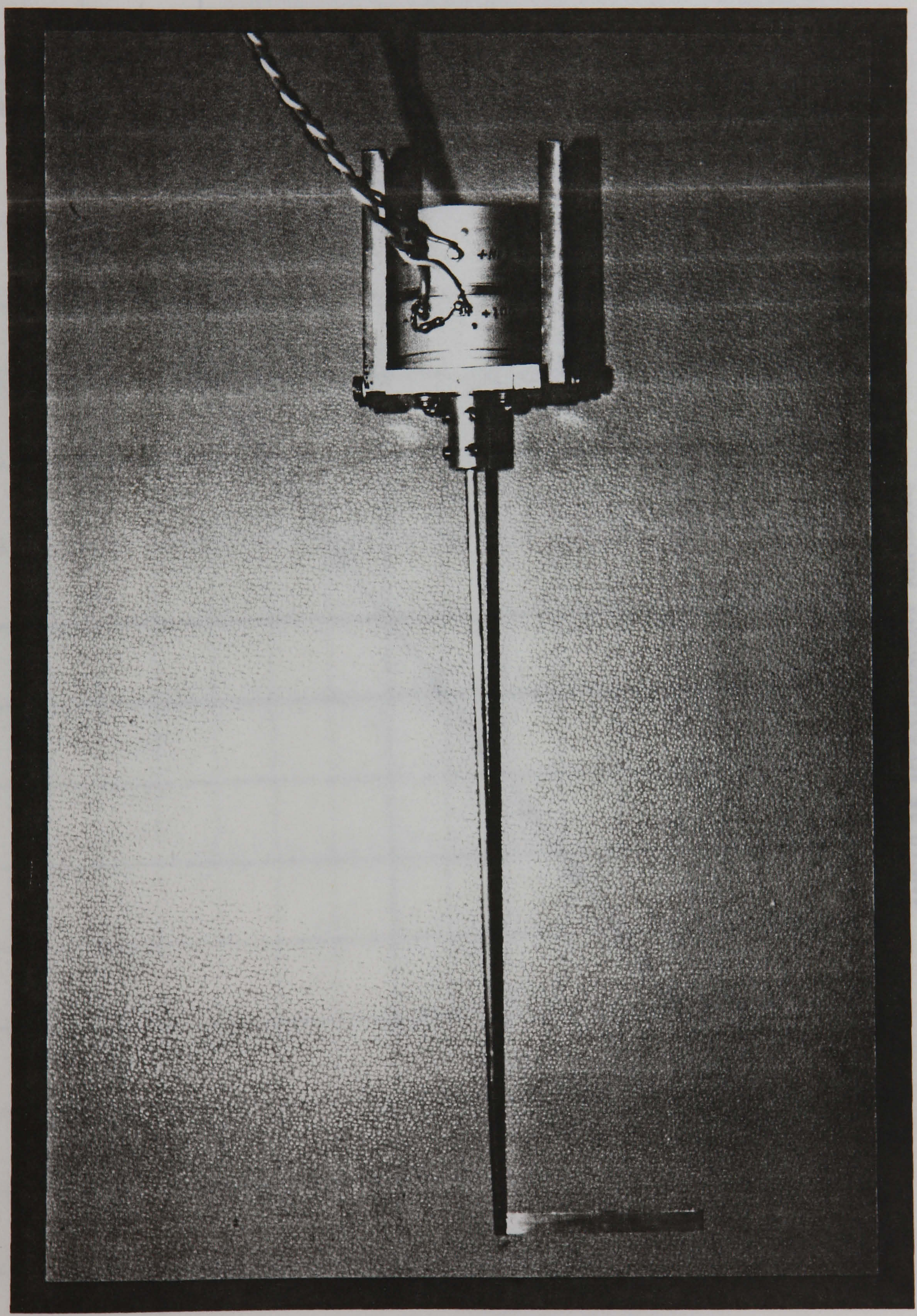

Fig (3.19) The Angular Measurement Device.

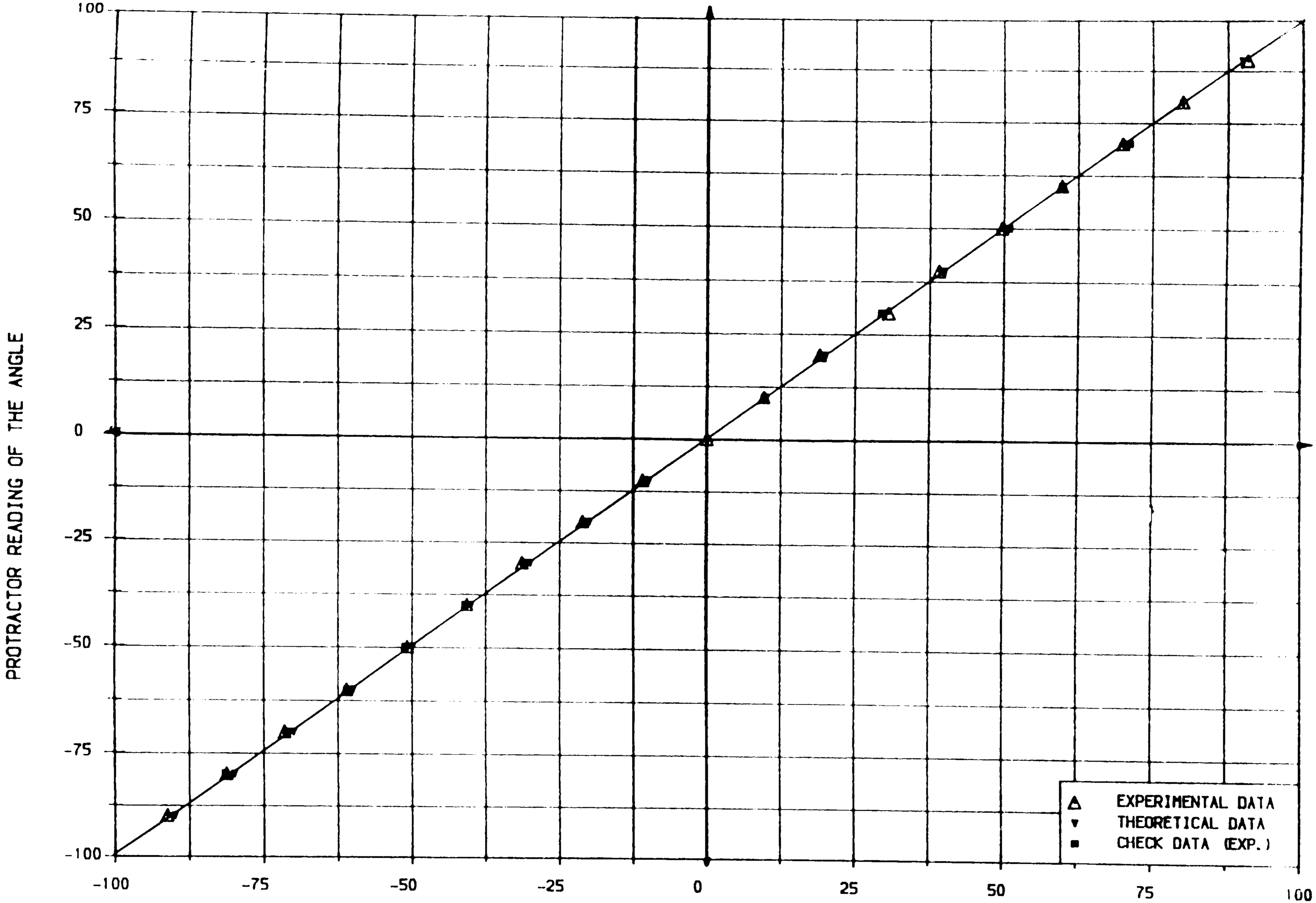

FIG (3.20) THE RELATIONSHIP BETWEEN THE ACTUAL PROTRACTOR READING AND ANGULAR MEASUREMENT DEVICE READING

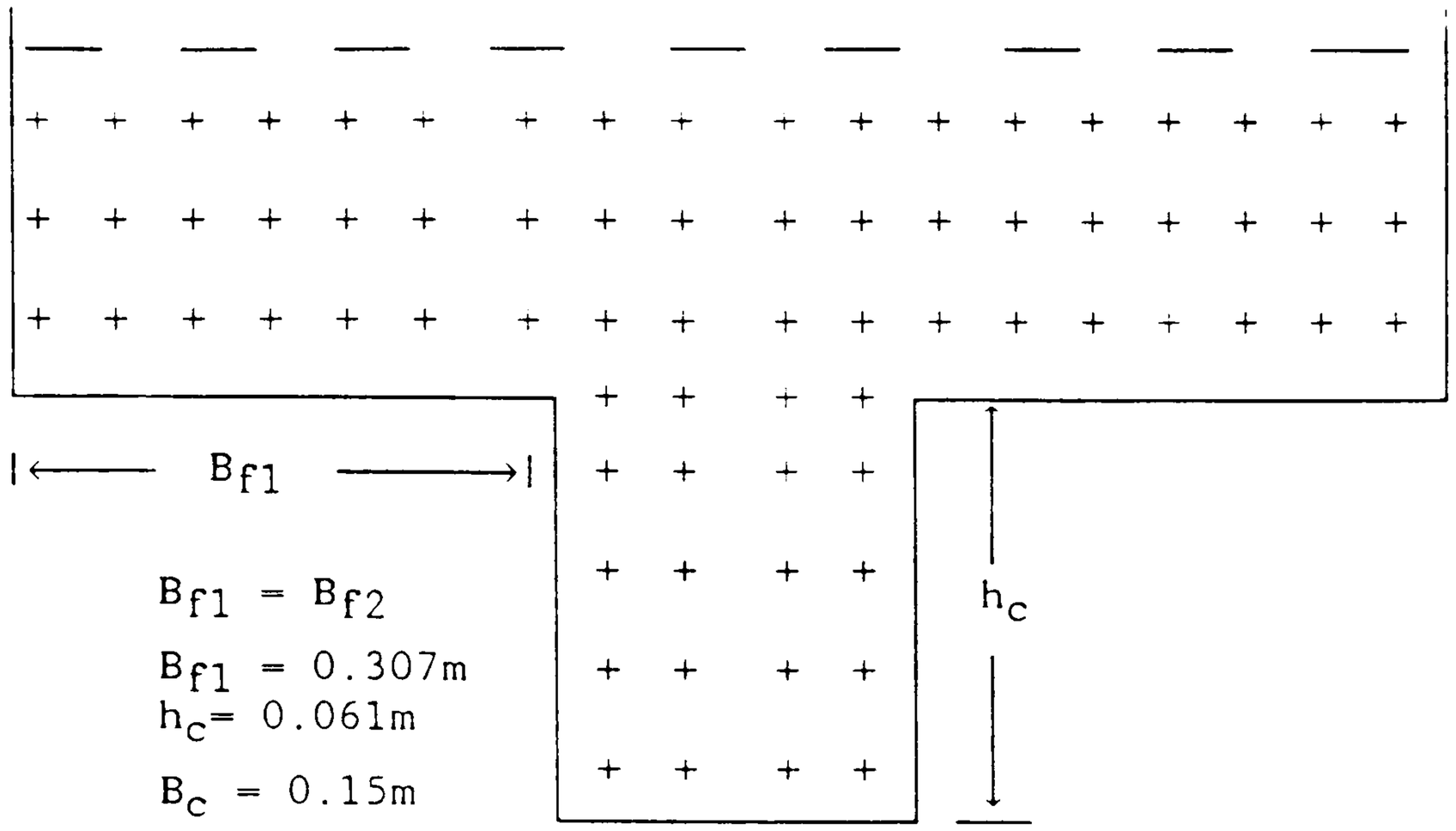

Fig (3.21a) Symmetrical Cross Section (Section 1)

(Skewed Channel With Floodplain) SERIES A, D

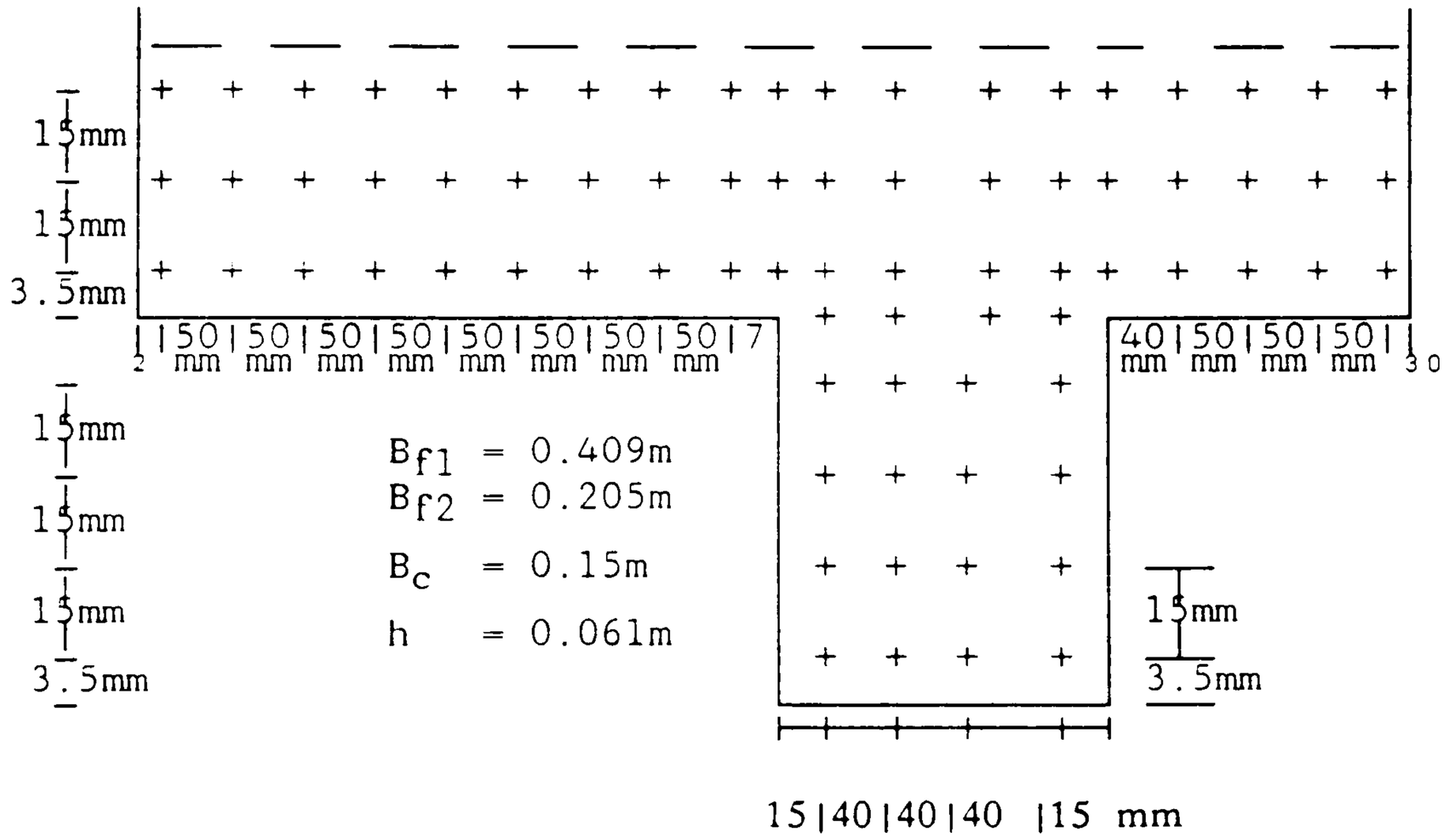

Fig (3.21b) Asymmetrical Cross Section (Section 2)

(Skewed Channel With Floodplain) SERIES A, D

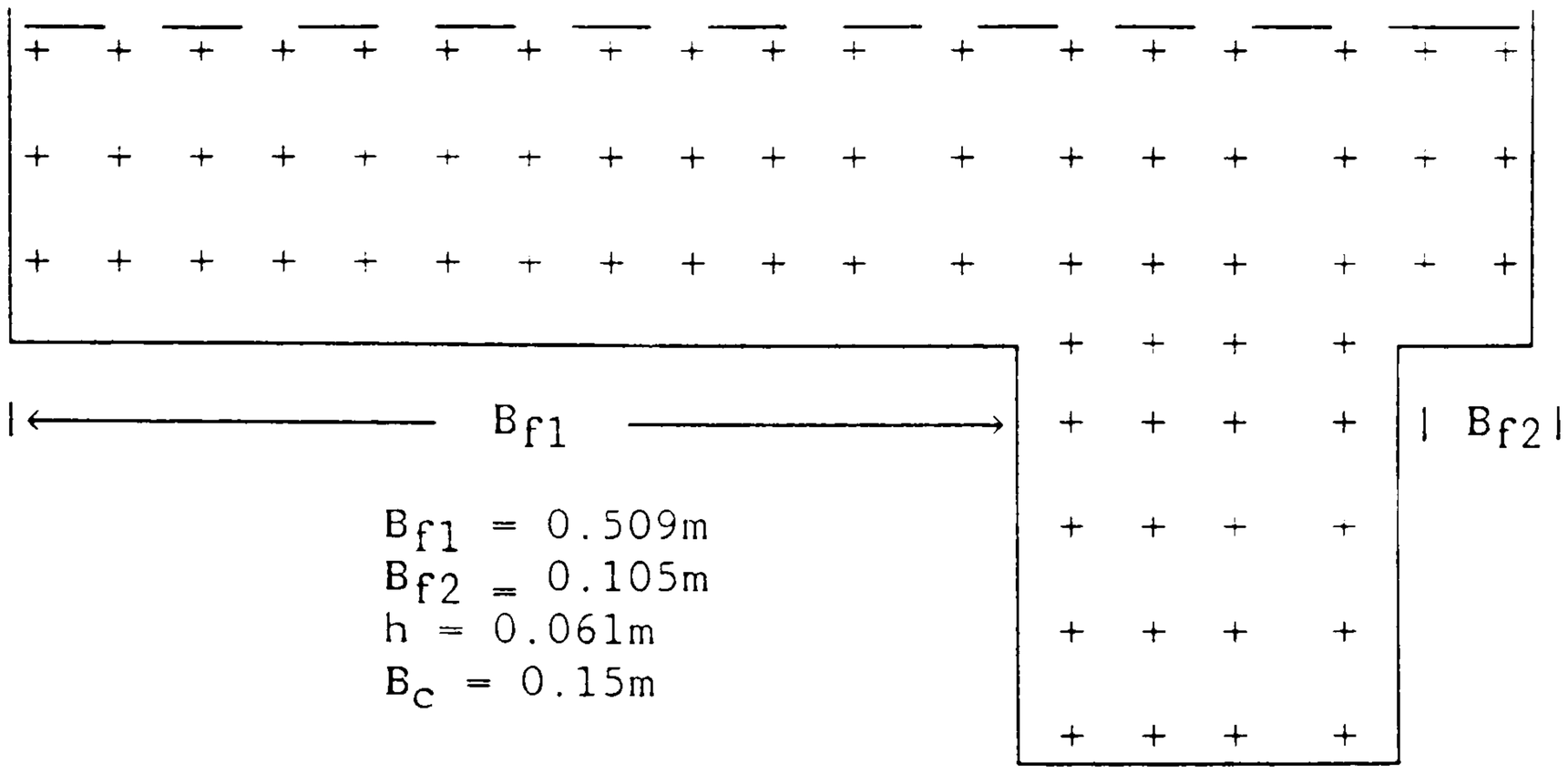

Fig (3.21c) The Asymmetical Cross section For The Skewed Main Channel With Floodplain (Section 3) SERIES A, D

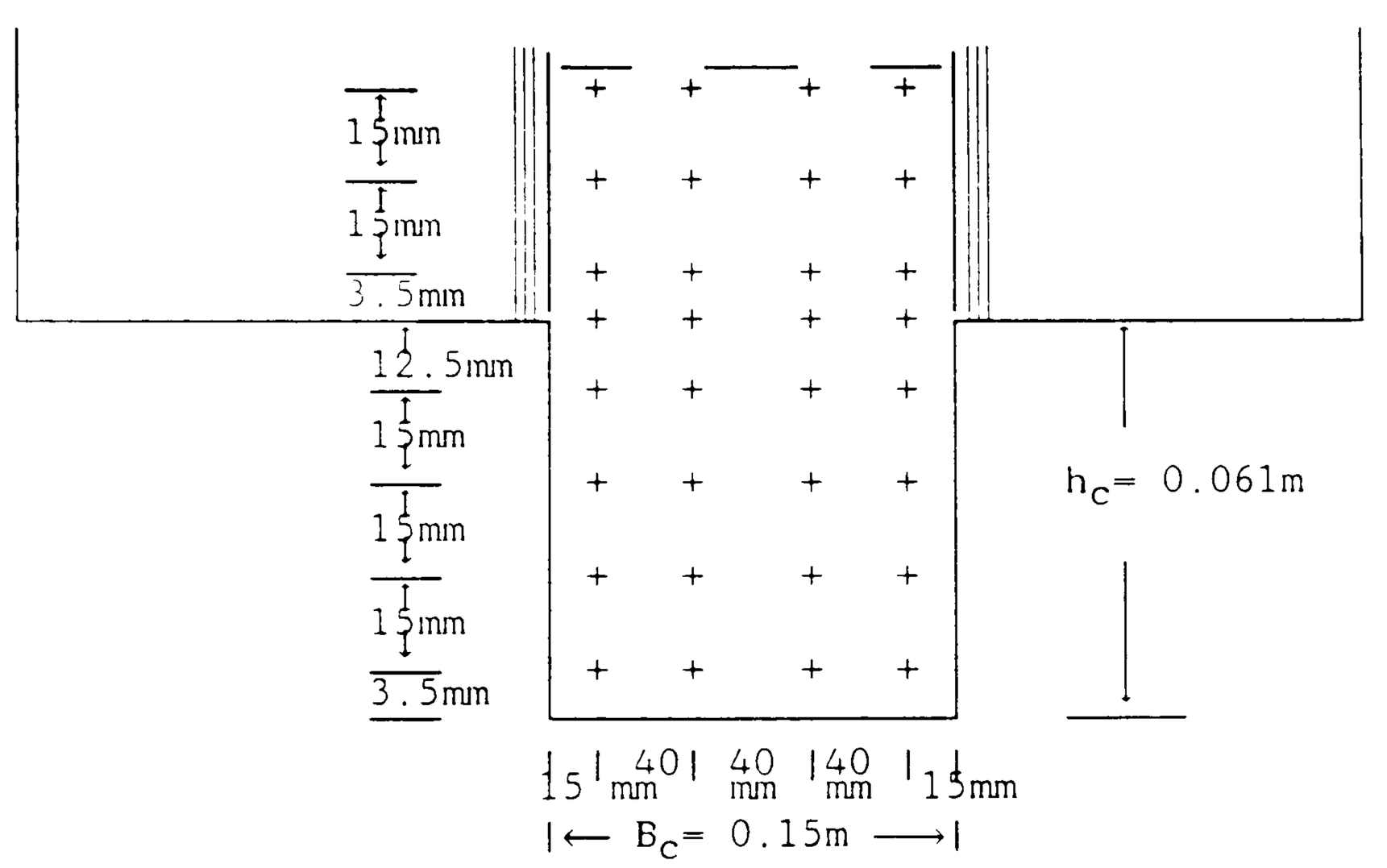

Fig (3.21d) Skewed Main Channel Isolated From The Floodplain. SERIES C

Fig (3.21) The geometry Section During The Test .

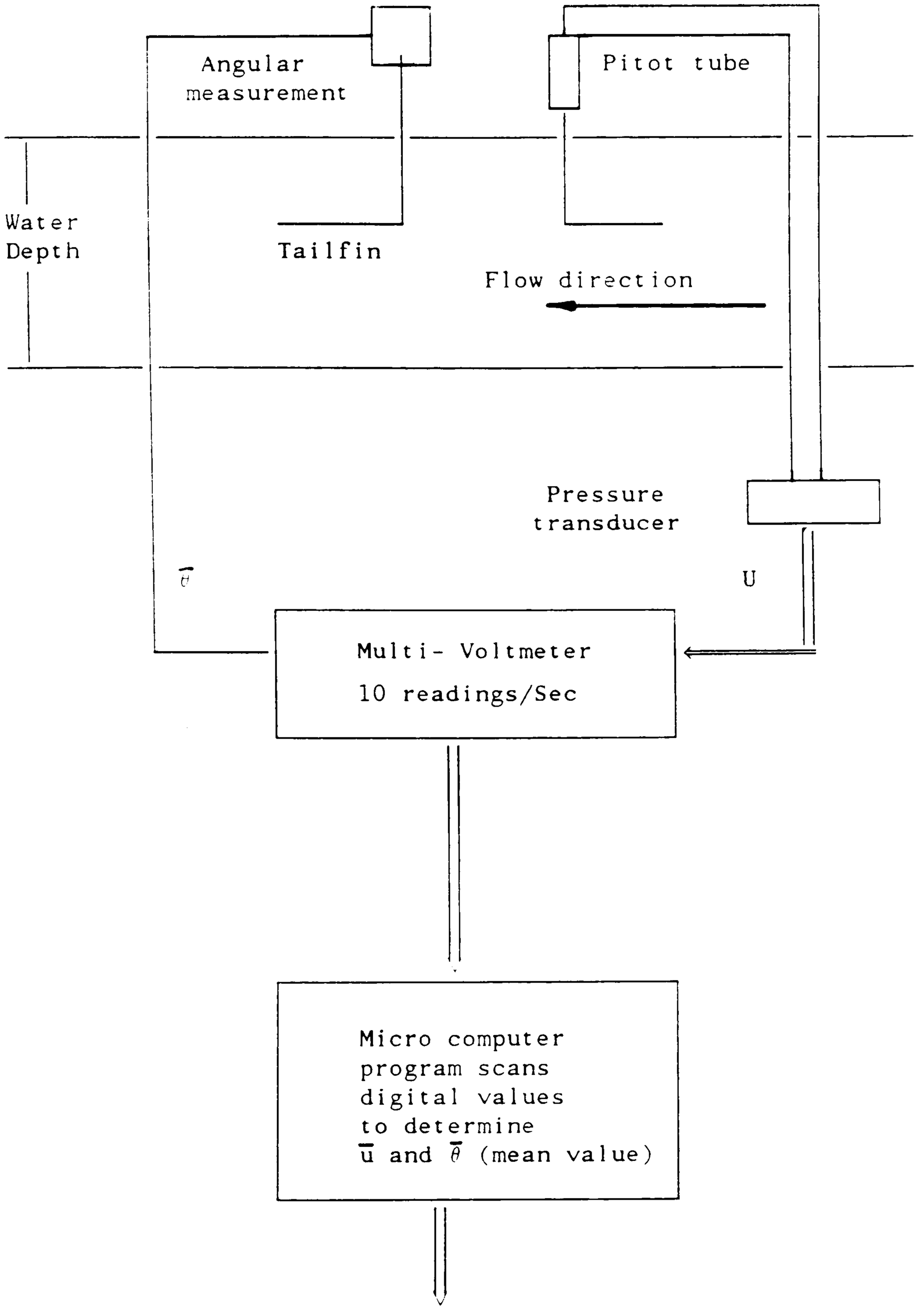

Fig (3.22) The Pitot Tube and Angular Measurement Connection.

PAGE NUMBERING AS ORIGINAL

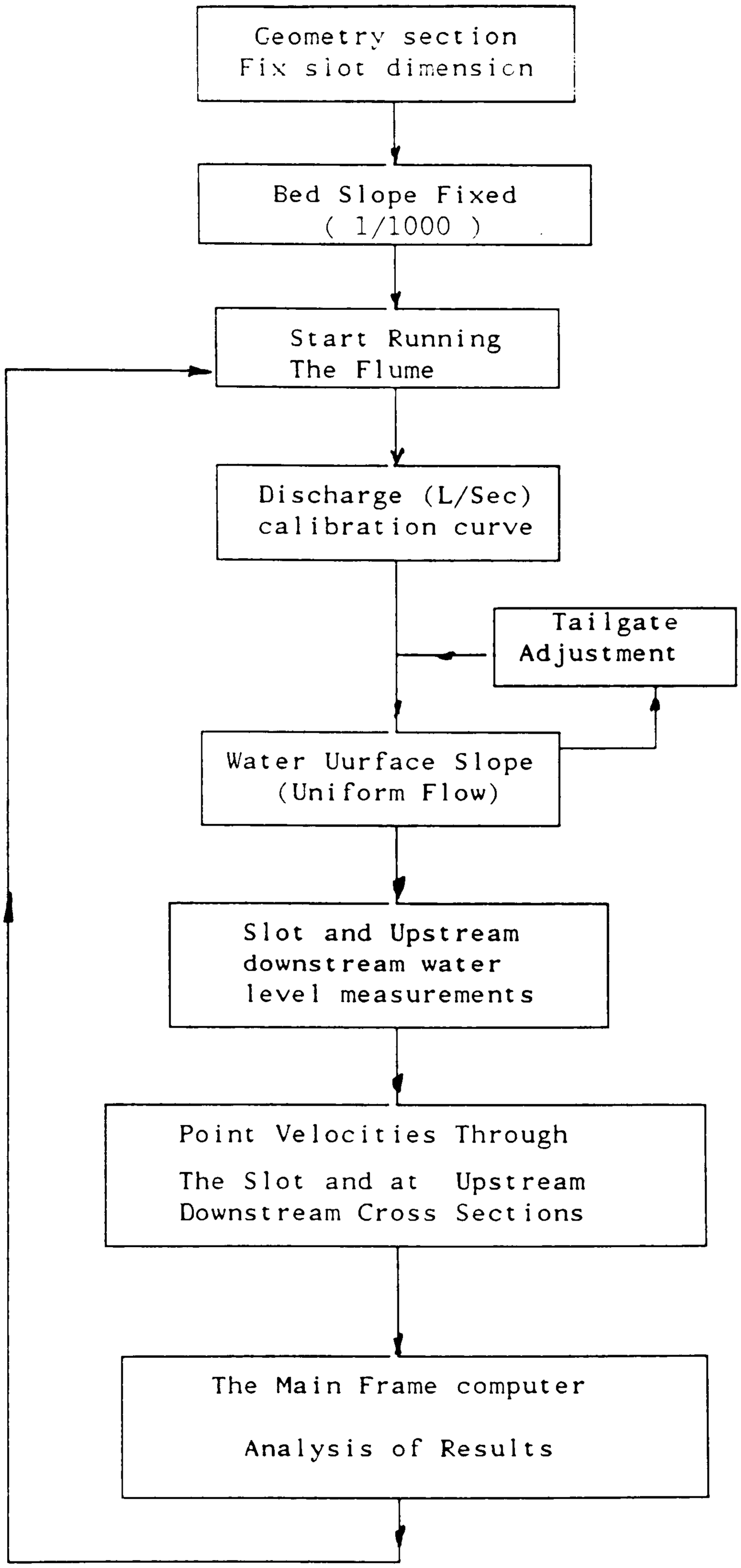

Fig (3.33) The Flow Chart Showing The Experimental Procedure (Slot)

SERIES F Tests.

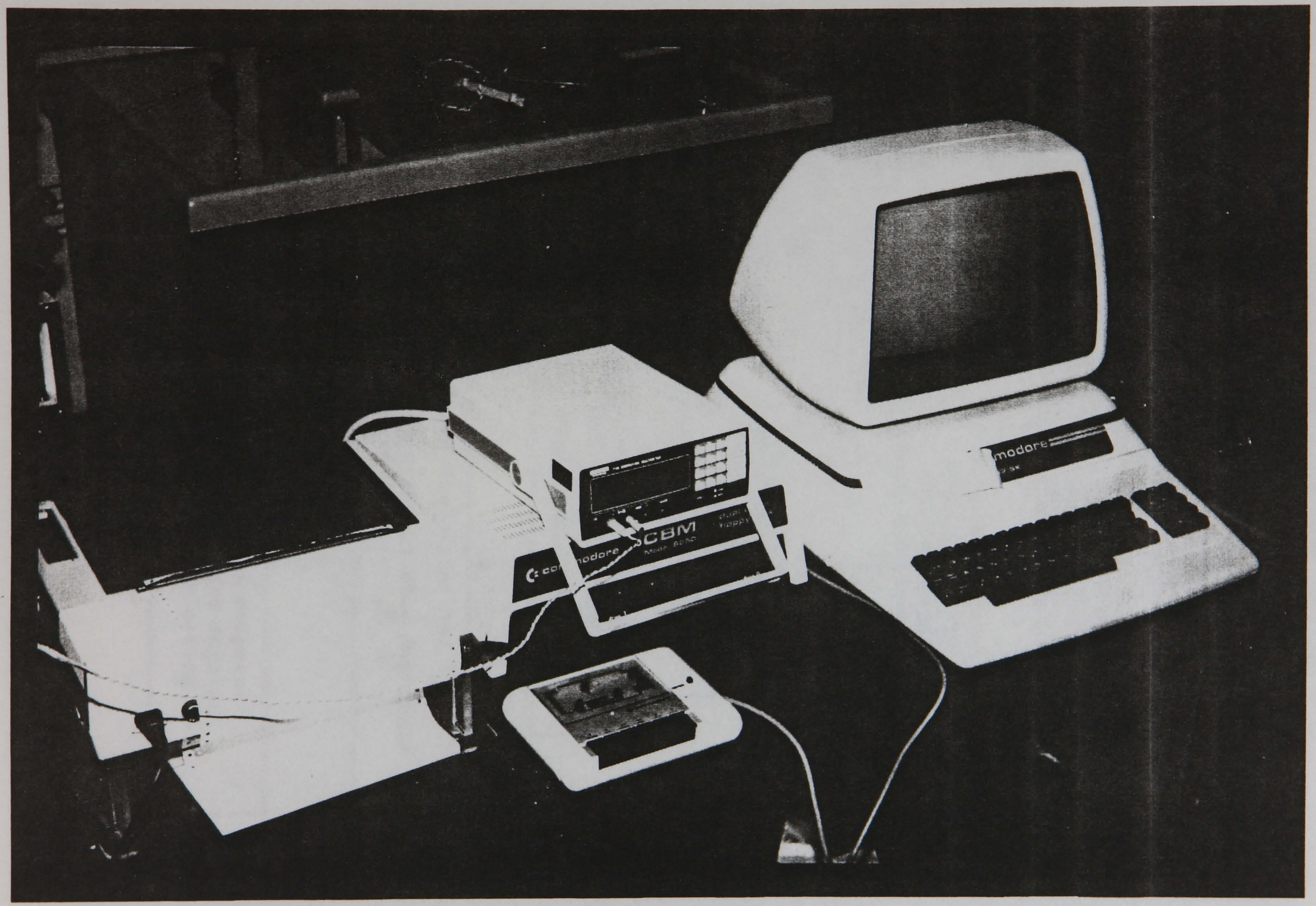

Fig (3.23) Micro computer and Multimeter Used to Measure the point Velocity and the Direction of the Flow.

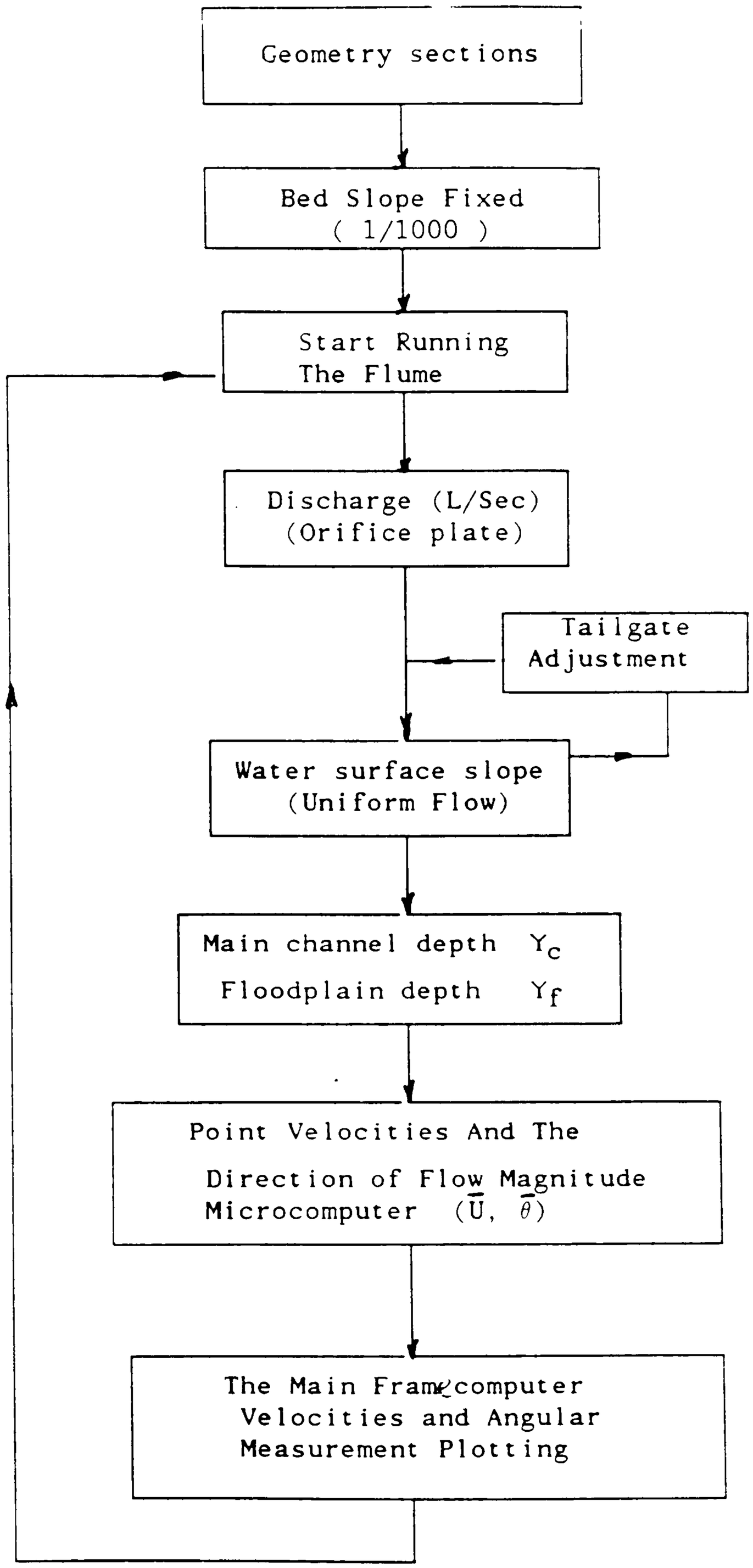

Fig (3.24) The Flow Chart Showing The Experimental Procedure

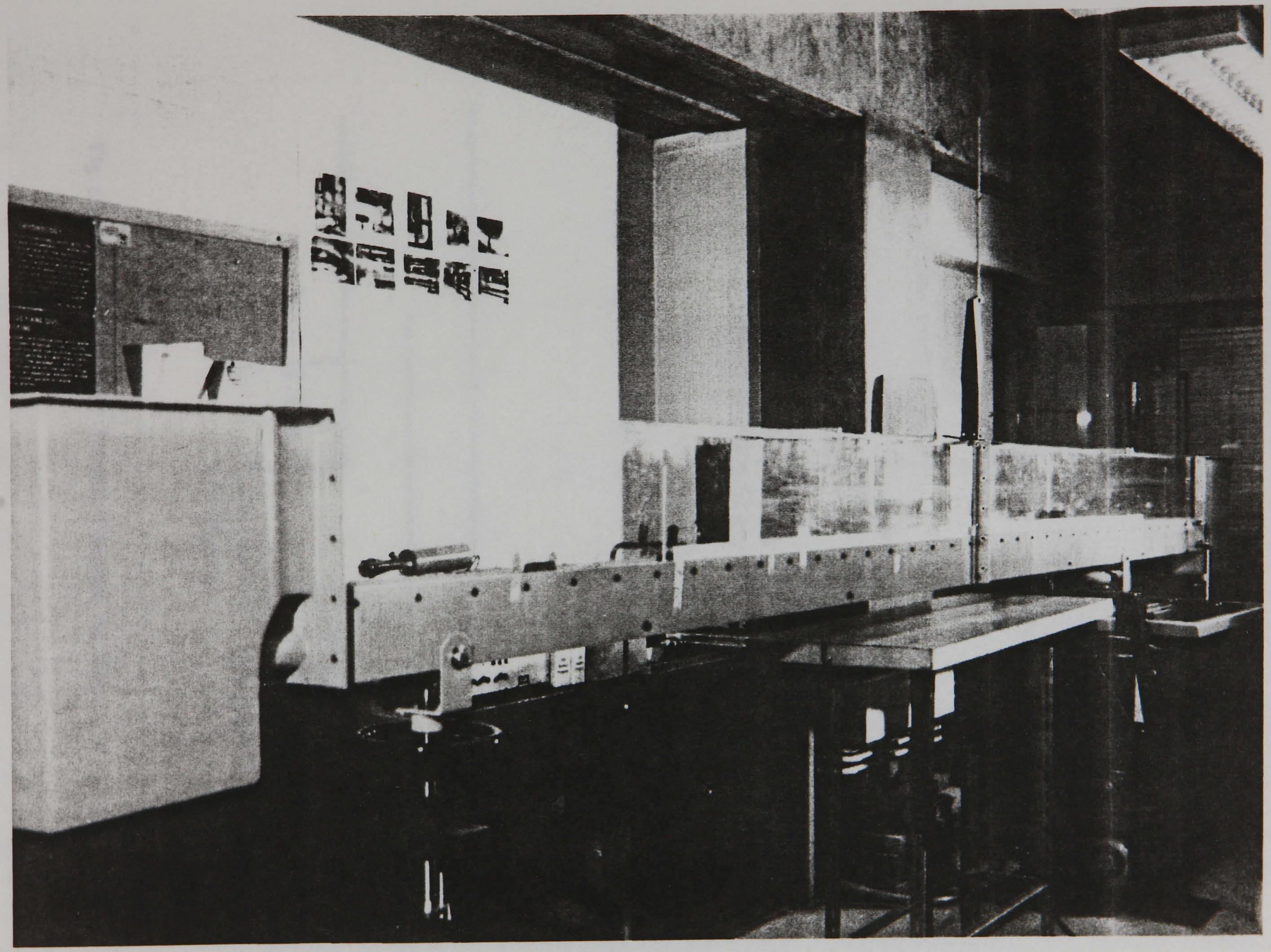

Fig (3.25) The Flume Used For the Expansion and Contraction Tests.
SERIES F

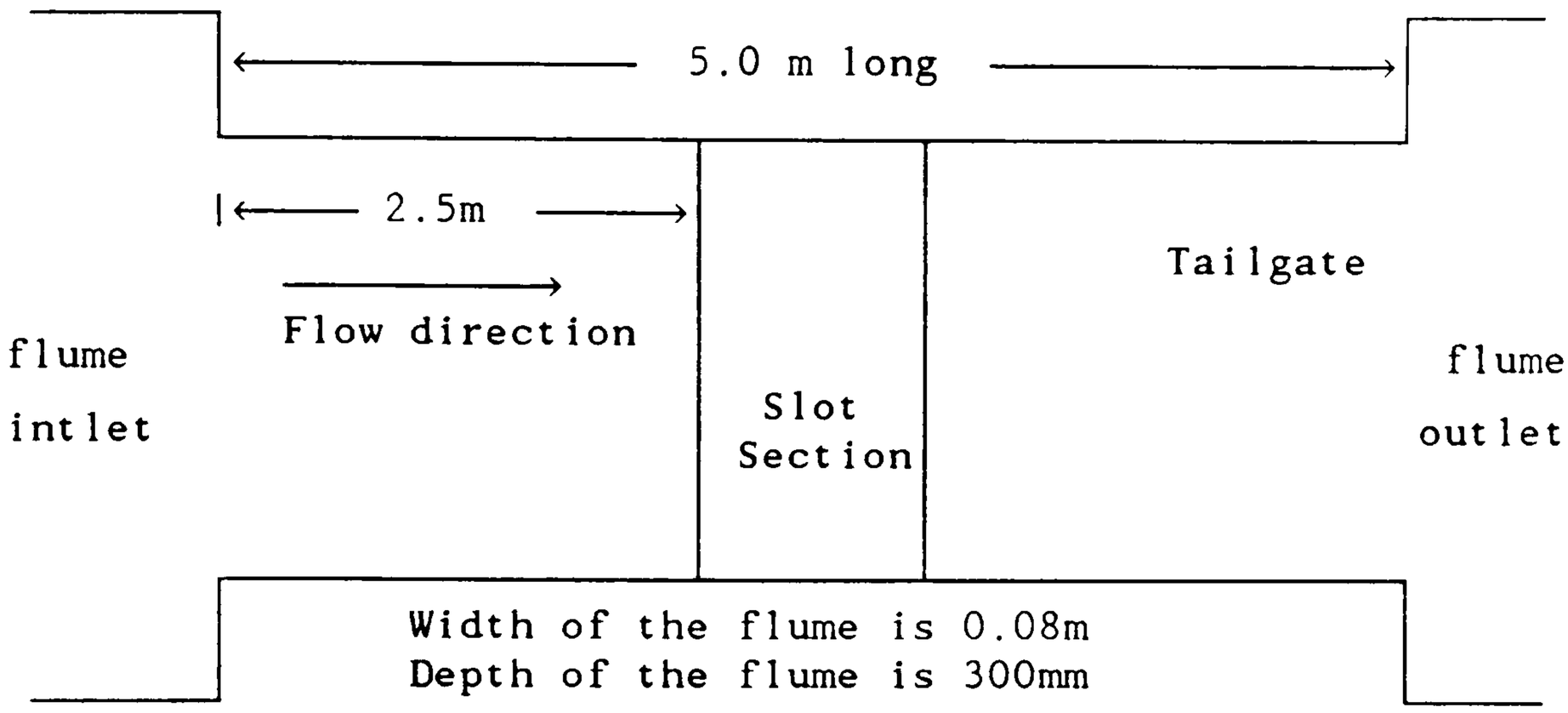

Fig (3.26a) Plan Sketch of Flume and Slot

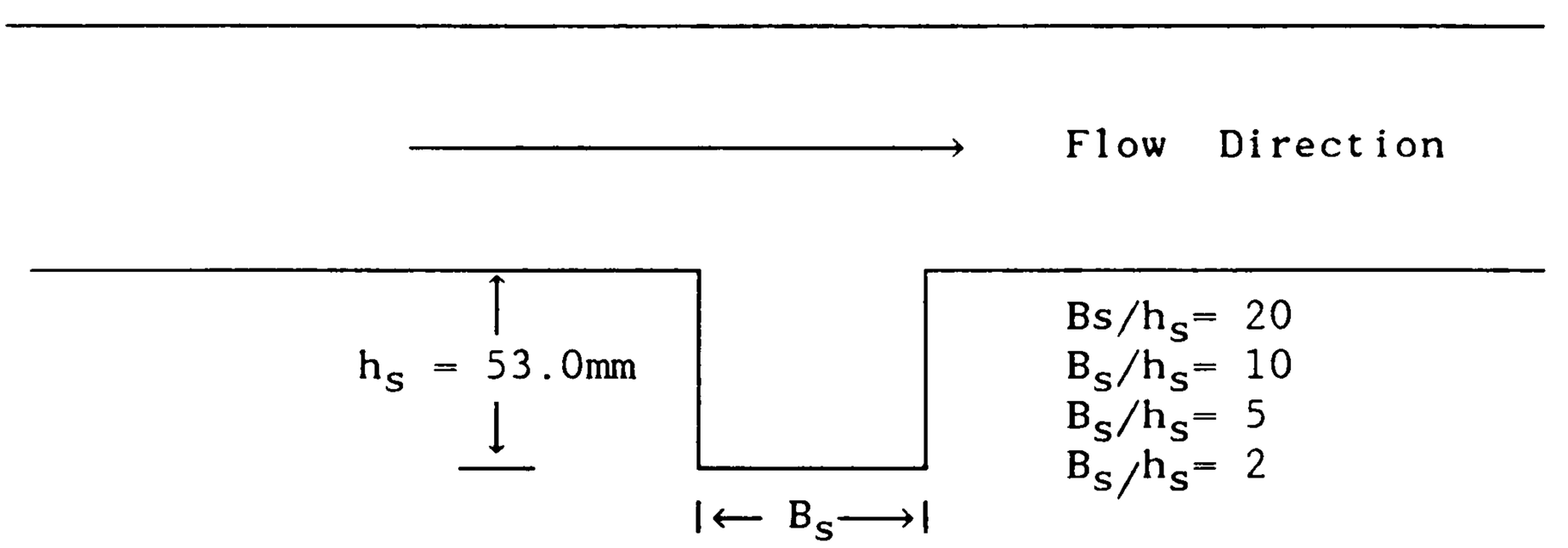

Fig (3.26b) Longitudinal Section Through the Slot.

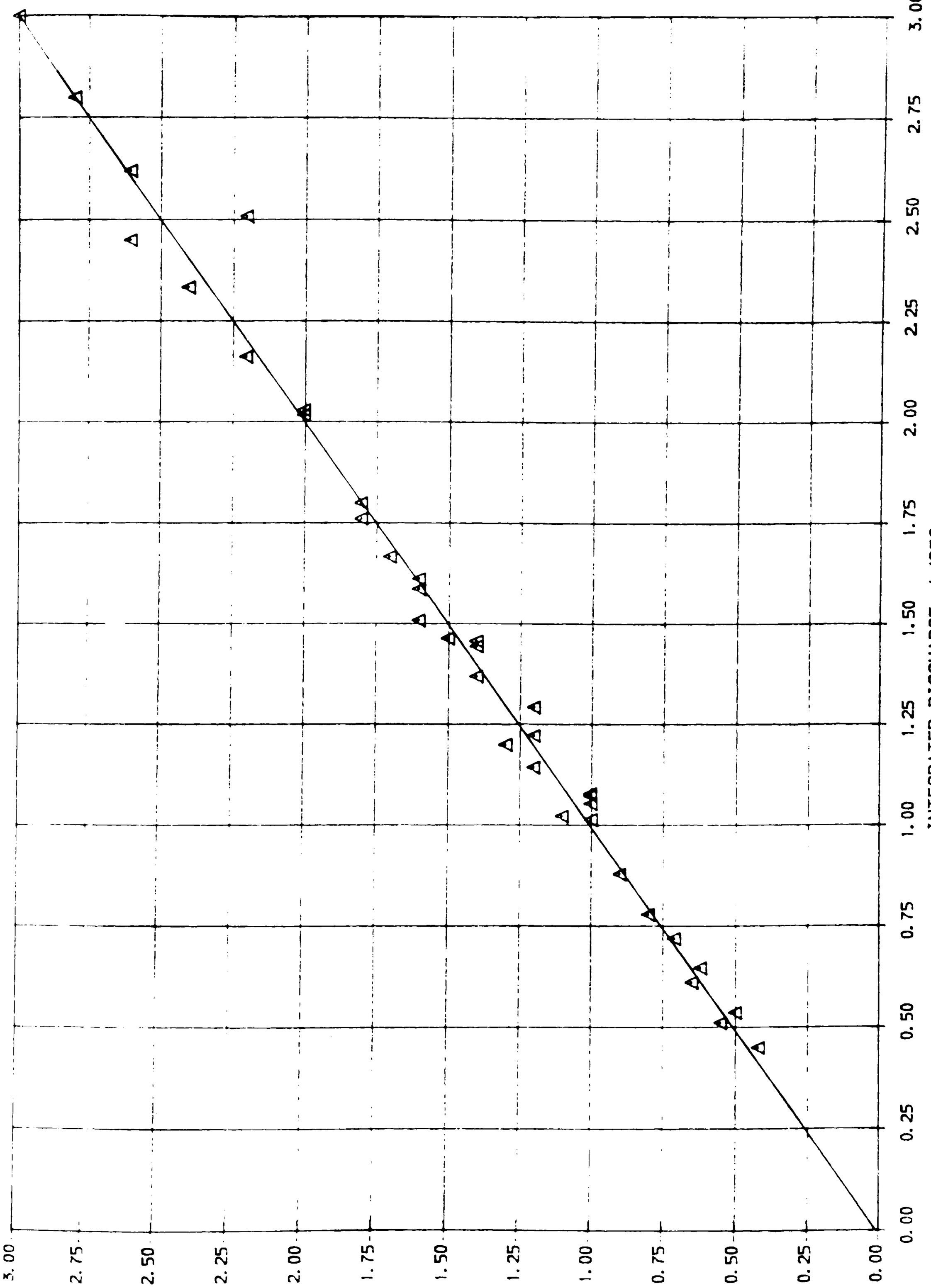

FIG (3.27) CALIBRATION FOR ARMFIELD FLUME FLOW ROTAMTER.

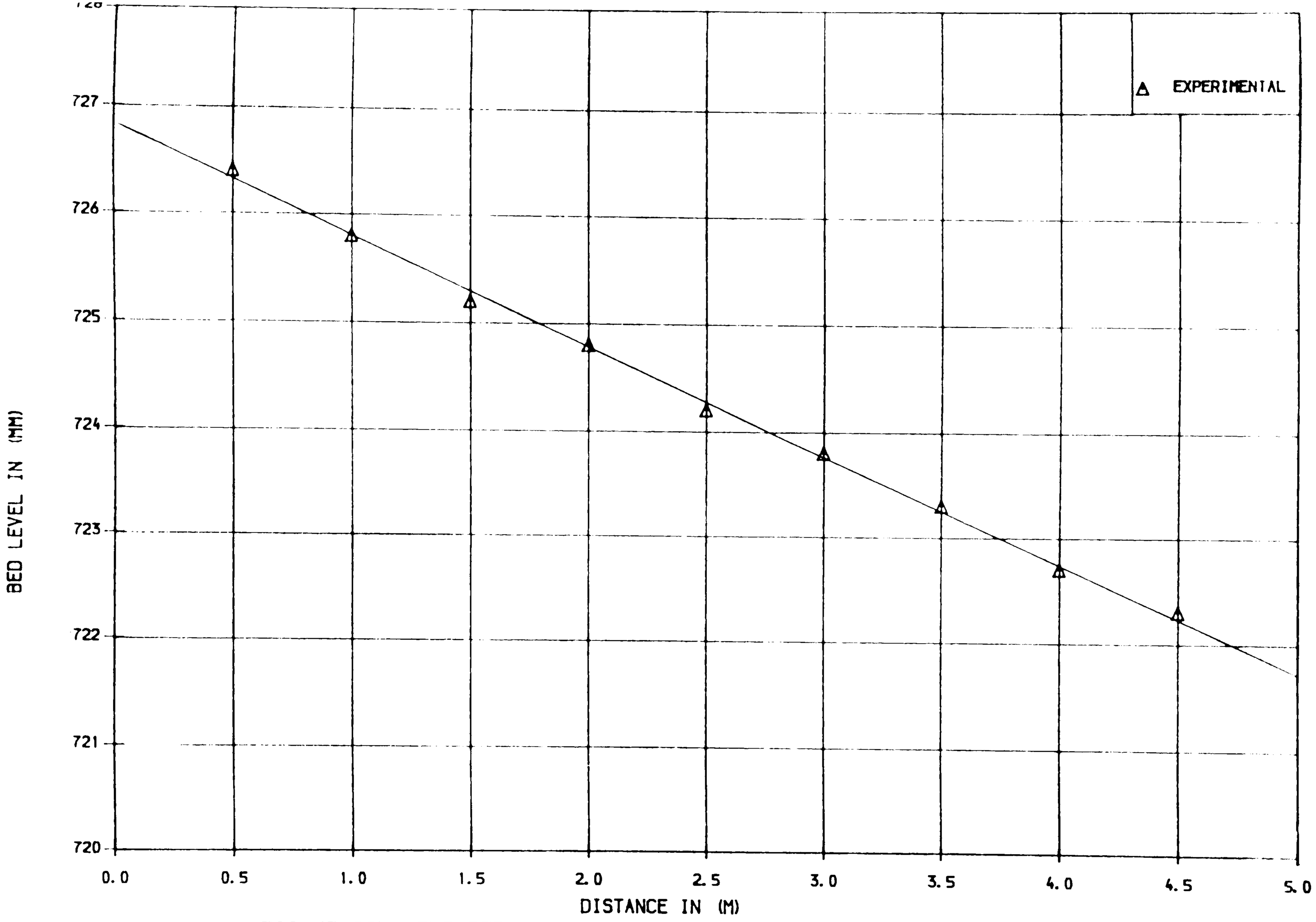

FIG (3.28) THE BED LEVEL OF THE FLUME USED TO TEST THE EXPANSION AND CONTRACTION FLOWS. (SERIES E)

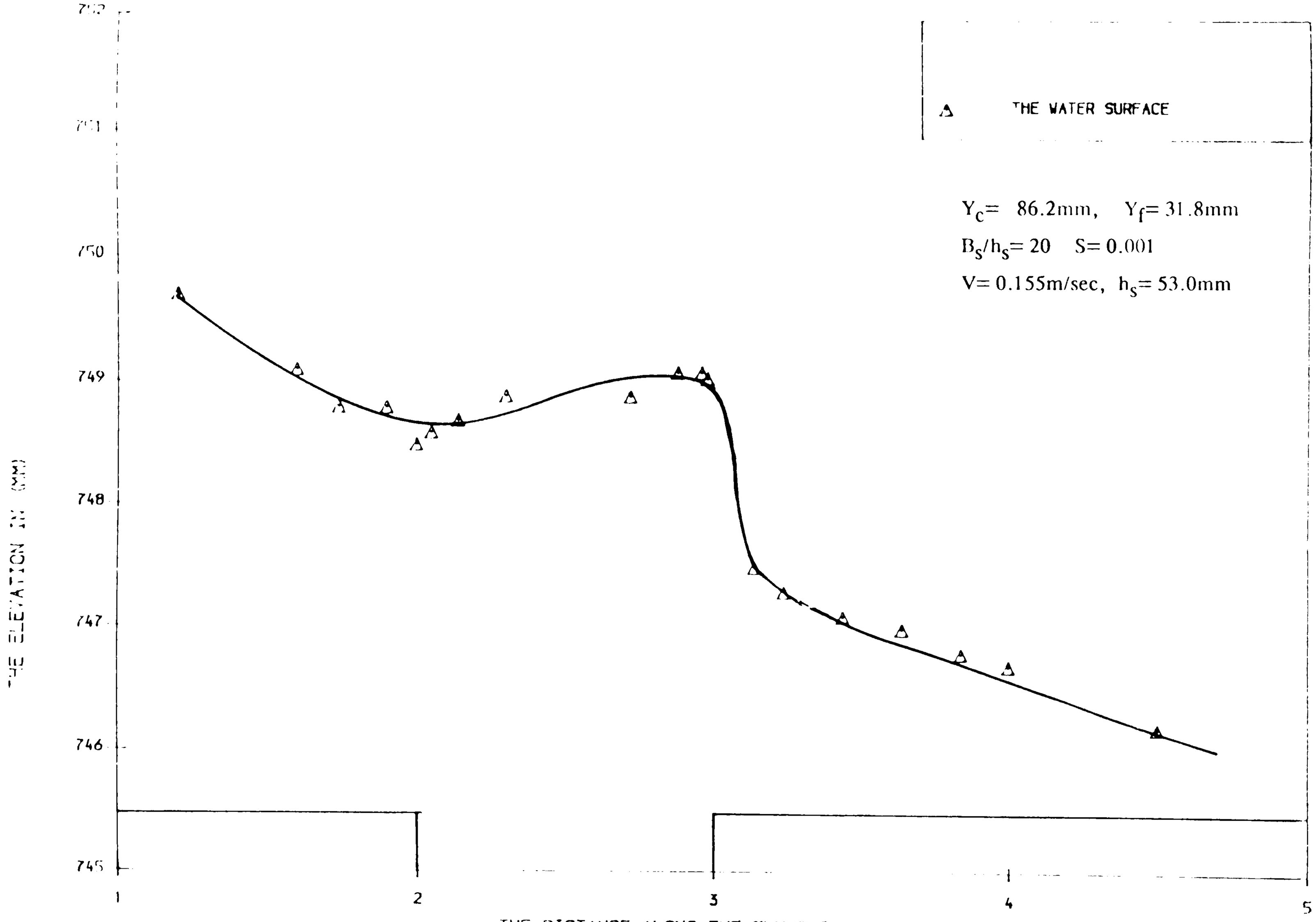

FIG (3.29) WATER SURFACE PROFILE THROUGH SUDDEN EXPANSION AND CONTRACTION REGION

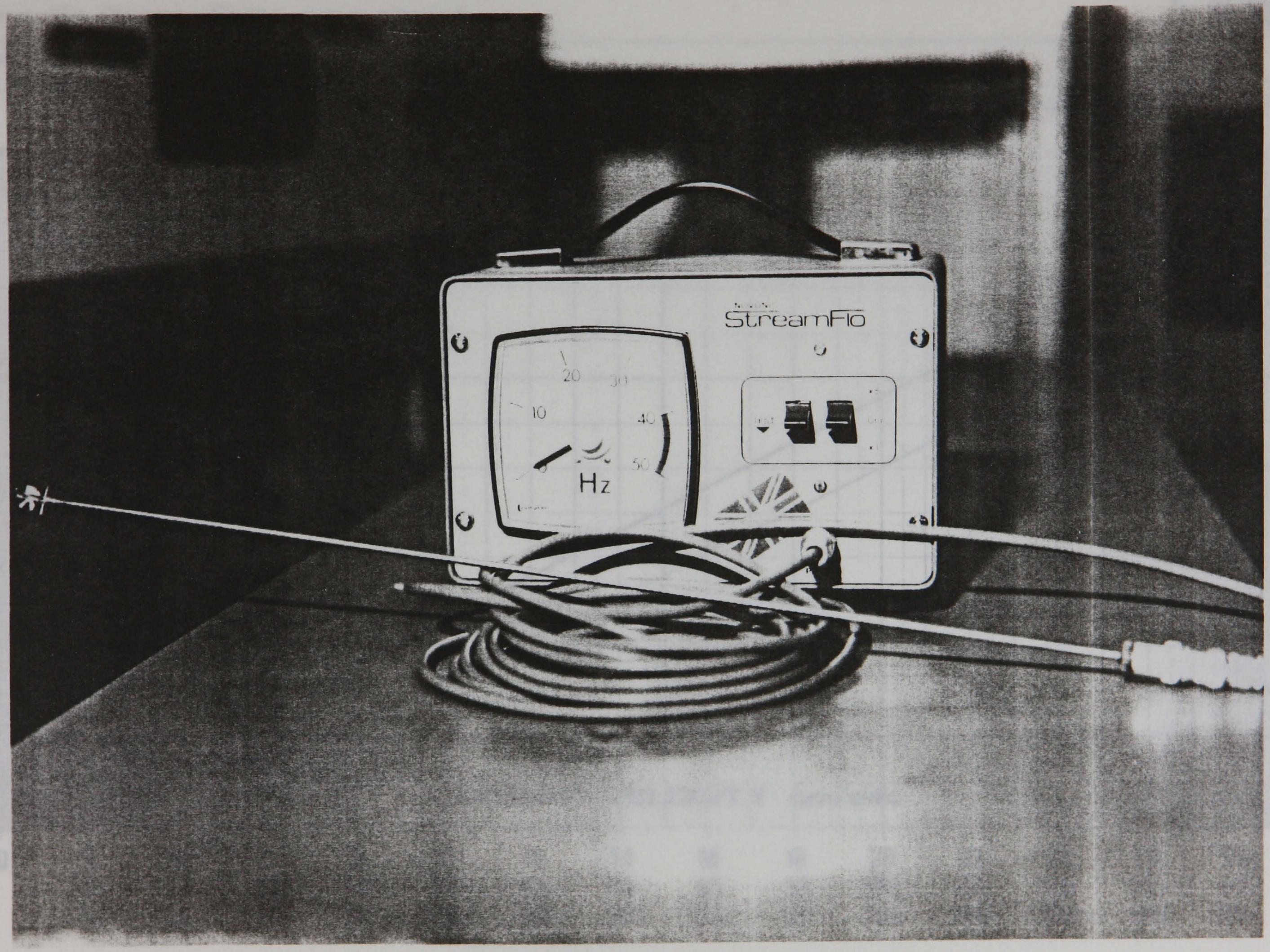

Fig (3.30) The Instrumentation Used to Measure the Point Velocity During the Expansion and Contraction Tests

NIXON INSTRUMENTATION LIMITED

Streamflo Probe Calibration Chart

Use green figures for high speed probes

Use red and black figures for low speed probes

Serial no. 817	type 423	Date 5/3/82	Engineer

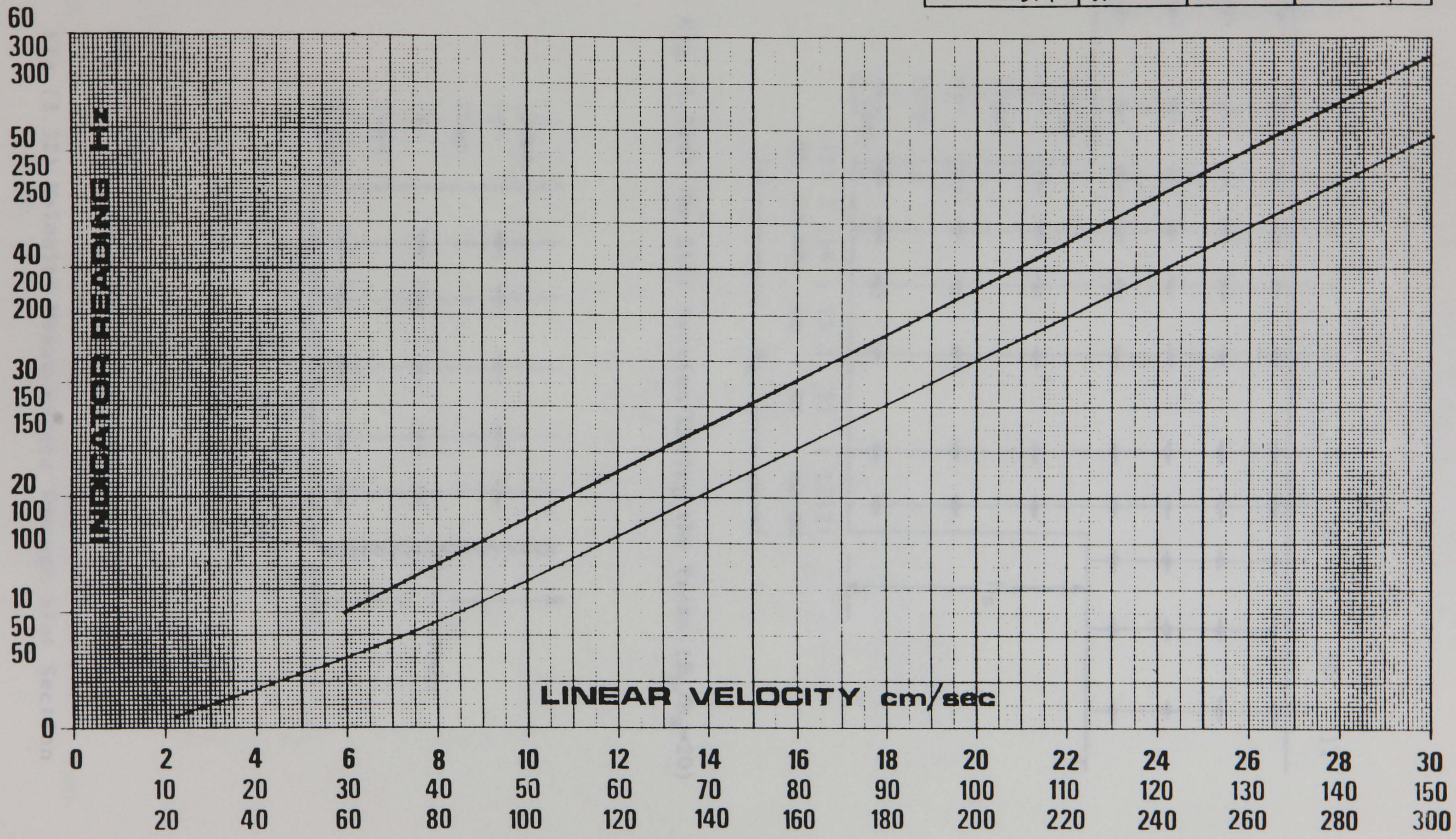

Fig (3.31) Shows the Graph Used to Find the Velocity Magnitude.

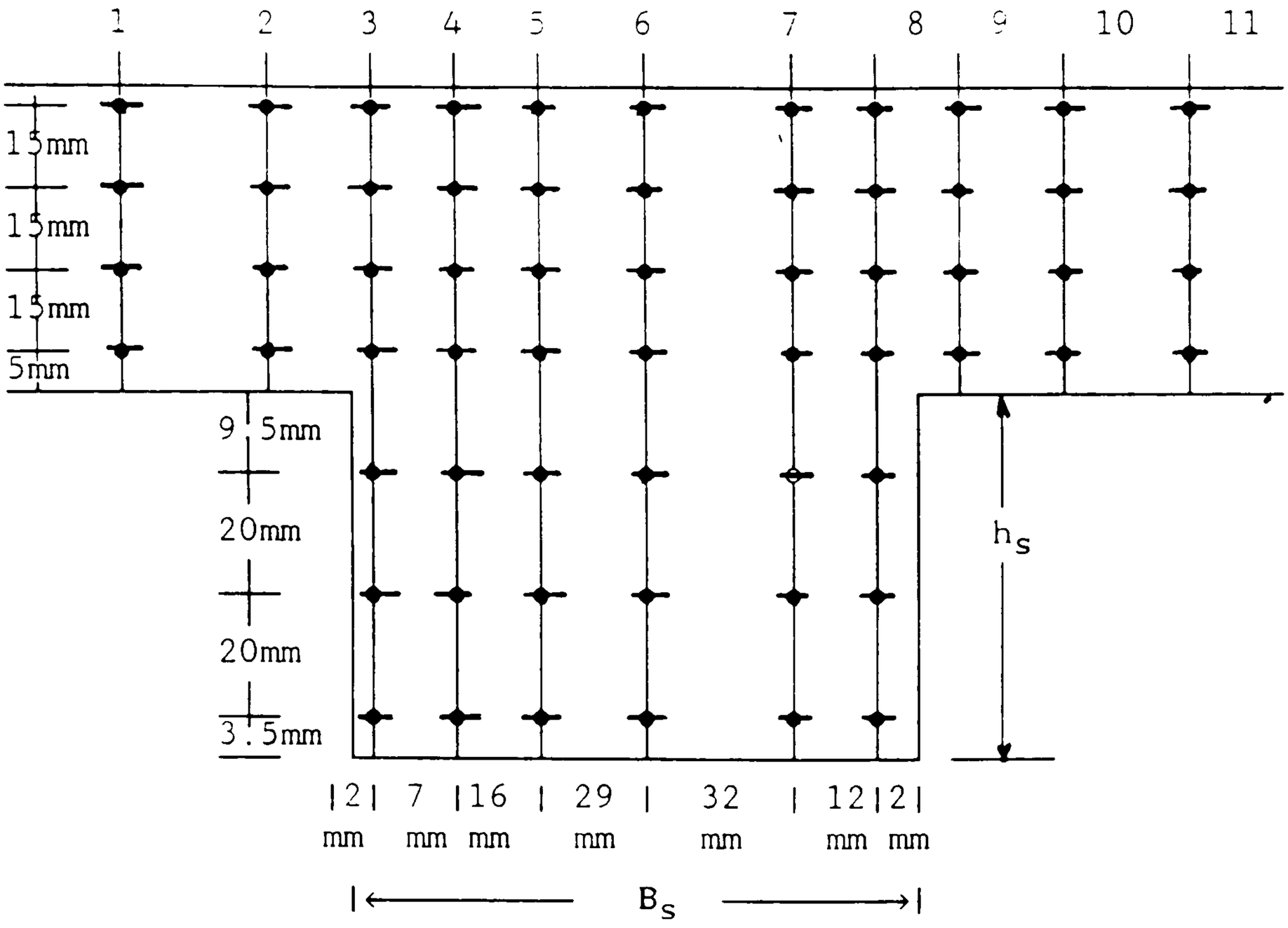

Fig (3.32a) The Slot Section During the Tests. (B_s/h_s=20)

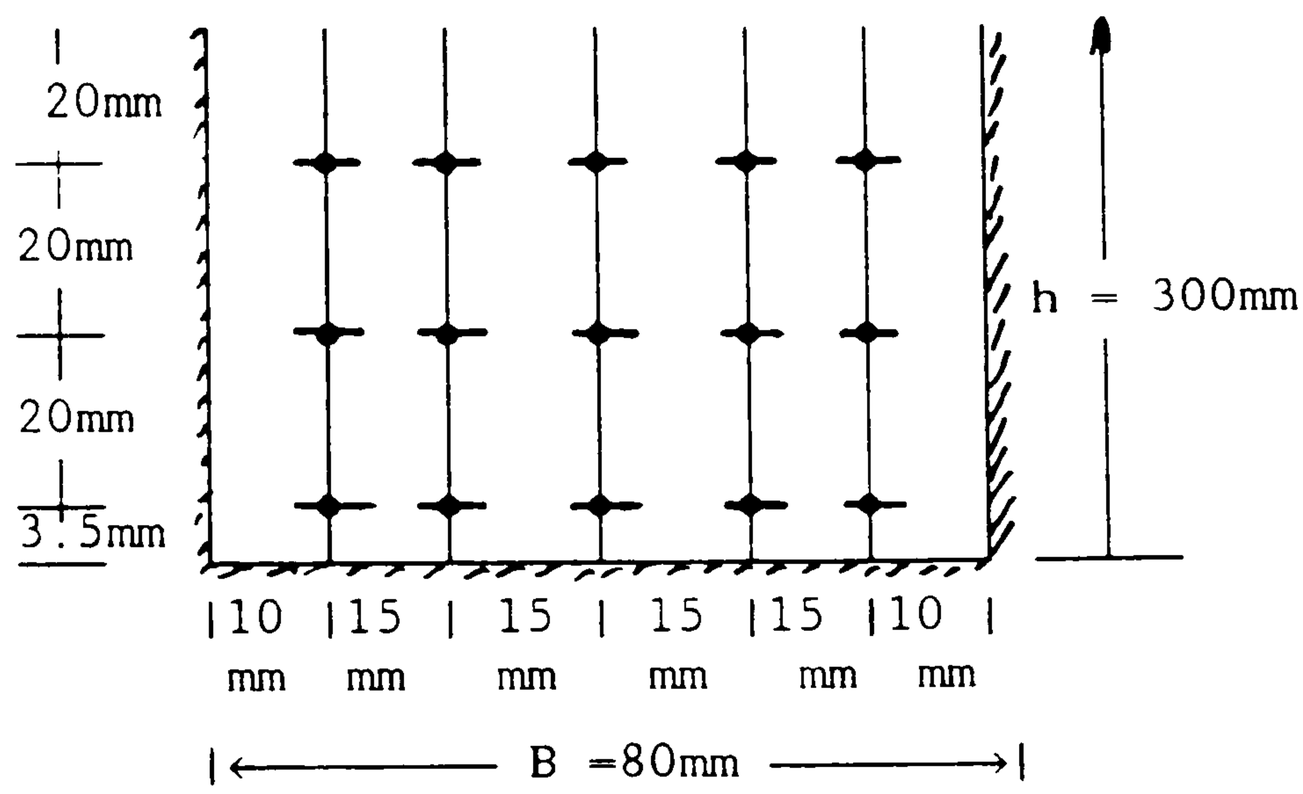

Fig (3.32b) The Armfield Flume Section.

Fig (3.32) Velocity Measurements Through Slot Section

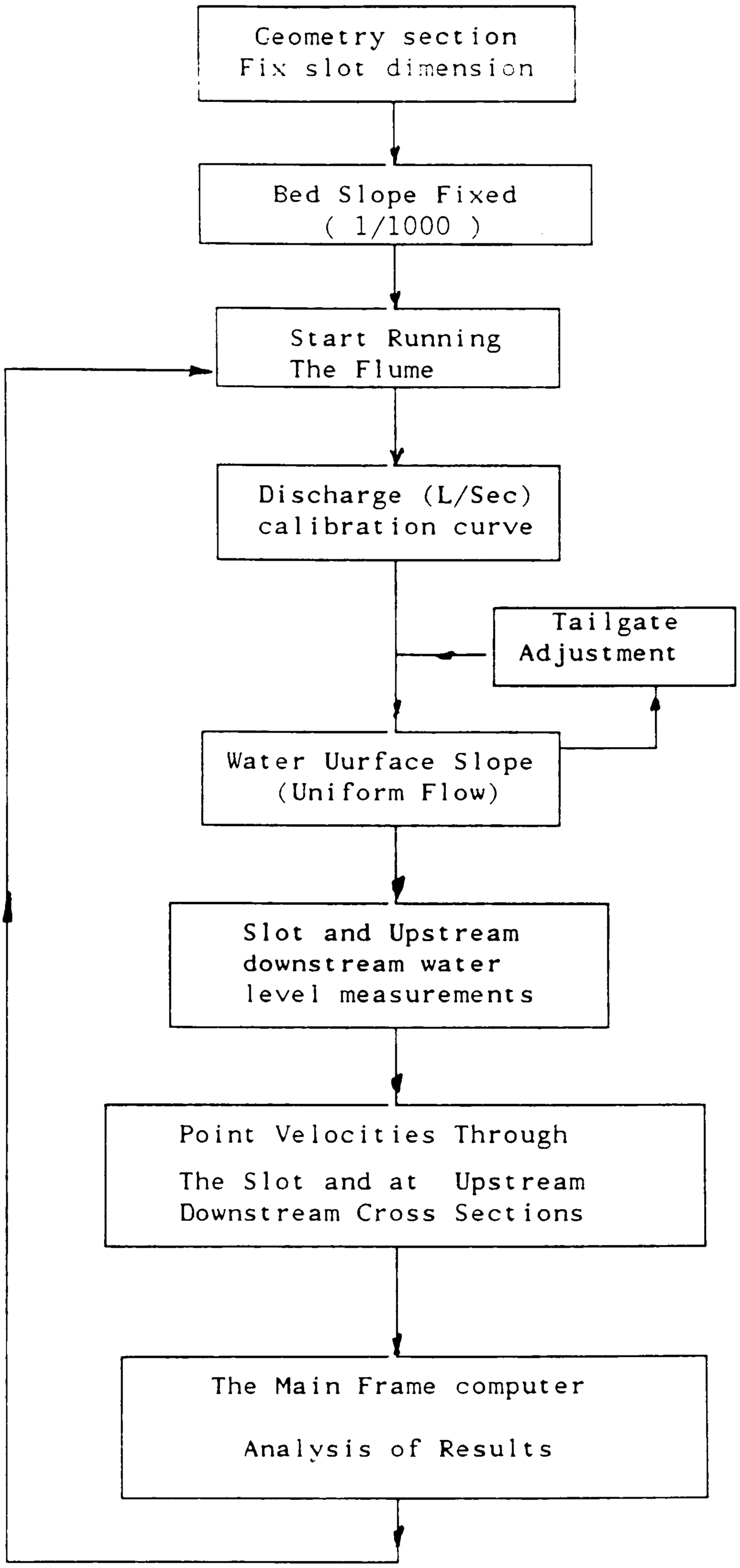

Fig (3.33) The Flow Chart Showing The Experimental Procedure (Slot) SERIES F Tests.

CHAPTER 4

FLOW RESISTANCE AND STAGE– DISCHARGE DATA FOR TESTS IN THE MAIN FLUME.

4.1 INTRODUCTION

4.2 A NOTE ON FLOW RESISTANCE COEFFICIENTS

4.3 STAGE– DISCHARGE AND RESISTANCE COEFFICIENTS

4.3.1 SERIES B – Smooth Flood plain Alone.

4.3.2 SERIES C – Smooth Main Channel Alone.

4.3.3 SERIES A – Smooth Main Channel and Flood plain Interacting.

4.3.4 A Note on Discharge Assessment for the Skewed Main Channel During Overbank Flow.

4.4 FLOW RESISTANCE AND STAGE– DISCHARGE FOR THE ROUGH FLOOD PLAIN.

4.4.1 Introduction

4.4.2 A Note on Flow Resistance Due to Vertical Rods

4.4.3 Flow Resistance for the SERIES E Tests

4.4.4 SERIES D – Rough Flood plain/Smooth Channel Interaction

4.4.5 Main Channel Behaviour Under Various Regimes.

4.5 CONCLUSIONS

CHAPTER 4

FLOW RESISTANCE AND STAGE– DISCHARGE DATA FOR TESTS IN THE MAIN FLUME.

4.1 INTRODUCTION

Chapter 4 presents the basic stage– discharge data as well as the flow resistance data for all the work carried out in the main flume, already described in chapter 3. The test series are annotated SERIES A, B, C for the smooth main channel/smooth floodplain cases, and SERIES D, E for the smooth main channel/rough floodplain cases.

For the smooth floodplain cases, SERIES B is presented first, representing the floodplain acting alone and isolated from any interaction from a skewed main channel. This is followed by a presentation of SERIES C data, representing flow in the skewed main channel completely isolated from the floodplain. Finally, data for SERIES A is presented, representing compound flow in a free interacting skewed main channel with floodplains on either side. Using this technique of building up in complexity, we are able to determine the flow carrying capacity of each sub section, the flow resistance coefficient of each sub– section as well as being able to isolate the interaction effect between a skewed main channel and its adjacent floodplains.

The second part of the chapter deals with the case of rough floodplains where the Mannings roughness coefficient is at least two or three times greater than the main channel. The experimental results of stage– discharge and roughness coefficient are this time preceded by an analysis of the resistance to flow by vertical rods. This analysis attempts to separate skin friction from the effects of vortices and turbulence shed behind each resistance element.

The SERIES E results are presented first, representing flow in the rough floodplain completely isolated from the skewed main channel. Finally SERIES D results are presented with the skewed main channel interacting with the rough floodplain.

4.2 A NOTE ON FLOW RESISTANCE COEFFICIENTS

The estimation of discharge capacity and resistance to flow represents a considerable challenge to hydraulic engineers, especially in the area of open channel flow. The reason for additional complexity in open channel flows compared with pipe flow is that flow resistance is affected not only by boundary roughness or smoothness, but is also greatly influenced by the cross–sectional channel shape. Form resistance such as meanders, bends, pools and riffles cause an even further complexity in flow resistance. A summary of resistance coefficients for open channels has been given by Chow (1959).

The influence of cross–sectional channel shape is of prime importance. A circular pipe, for instance, has essentially axi–symmetric flow patterns giving a uniform boundary shear stress and velocity distribution around the wetted perimeter. A rectangular shaped channel, on the other hand, has low boundary shear and low velocity at the base corners of the cross section as sketched below.

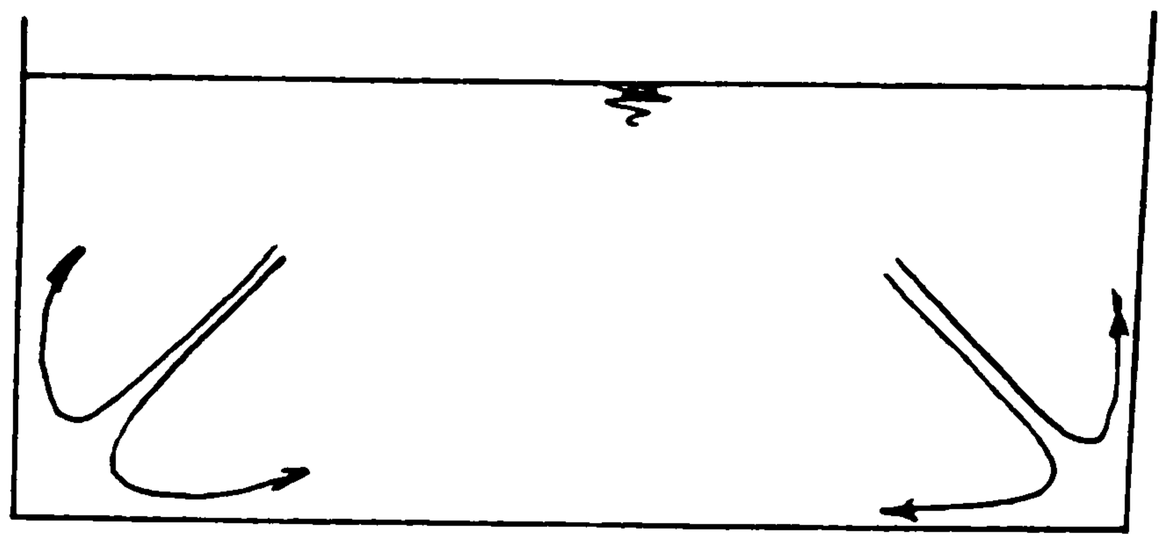

This means that momentum will be transferred from higher velocity regions to the low velocity corner regions thus giving rise to weak secondary currents. Such secondary currents have transverse velocities of the order of only 1 or 2% of the longitudinal velocity components, but because of lateral mixing often generate energy losses of the order of 10% of bed friction. This is why the friction factor λ, is higher in rectangular channels compared with circular pipes. Myers (1976), Tracy and Lester (1961), Kazemipour and Apelt (1982).

A compound cross–section channel therefore contains the further degree of complexity involving large quantities of momentum transport from the fast moving deep section to the slower moving shallow section. Such transport is achieved by a combination of turbulent diffusion and advection as already discussed in chapter two and can give rise to flow resistances as high as 30% greater than the simple rectangular channel case Baird and Ervine (1984), Knight (1982) and Rajaratnam (1981).

This leads naturally to the inter relationship between discharge assessment and resistance to flow. This has proved a difficult task in the case of compound shaped channels simply because of large lateral momentum transport and shear, and also the discontinuity in hydraulic radius at flow depths just over bank–full.

The three simplest relationships for discharge in an open channel are Chezy, Manning and Darcy–Weisbach equations.

Chezy's Equation is given by

$$Q = C A \sqrt{RS} \qquad (4.1)$$

where C is Chezy coefficient for frictional resistance.

Manning's Equation is given by :–

$$Q = \frac{1}{n} R^{2/3} S^{1/2} A \qquad (4.2)$$

where

Q is the discharge of flow

R is the hydraulic radius

A is the cross section area

S is the longitudinal slope of the channel

n is the Manning's co–efficient.

Manning's equation is often chosen to give a quick and reasonably accurate prediction of the stage–discharge relationship especially for uniform flow conditions. The main drawback of equation (4.2) is assumption of a constant "n" value for all flow depths. The third relationship is the Darcy–Weisbach equation.

$$Q = A \sqrt{\frac{8gRS}{\lambda}} \qquad (4.3)$$

where

λ is the Darcy– Weisbach coefficient.

The three expressions are related by

$$C = (8g/\lambda)^{1/2} = R^{1/6}/n \qquad (4.4)$$

The Darcy– Weisbach equation is now the most widely used relationship in the research field, following advice from the ASCE Task Force on friction factors in open channels (1963). The reason for this is because the friction factor λ, is non dimensional, and also it can be related directly to flow resistance in circular pipes.

The value of the friction factor λ is most commonly evaluated from the Colebrook– White equation for pipes,

$$\frac{1}{\sqrt{\lambda}} = -2.0 \text{ Log } \left[\frac{K_s}{14.81\ R} + \frac{2.51}{Re\sqrt{\lambda}} \right] \qquad (4.5)$$

where

λ is the friction factor

R_e is the Reynolds number

R is the hydraulic radius

K_s is the equivalent sand grain roughness size.

Ackers (1958) suggests a modification to the circular pipe equation for the value of the friction factor λ in wide open channels.

$$\frac{1}{\sqrt{\lambda}} = -2.0 \text{ Log } \left[\frac{K_s}{12.3\ R} + \frac{3.02}{Re\sqrt{\lambda}} \right] \qquad (4.6)$$

In this case both the smooth and rough parts of the equation are modified. When the boundary is smooth and sand grain roughness can be considered zero,

then the Keulegan form (1938) of the friction factor is often adopted. For the case of circular pipes this becomes,

$$\frac{1}{\sqrt{\lambda}} = 2.0 \text{ Log } [R_e \sqrt{\lambda}] - 0.8 \qquad (4.7)$$

Many experiments have been carried out in attempting to establish the significance of equation (4.7) when applied to open channels rather than smooth pipe flow.

Henderson (1966) suggested it could be used quite satisfactorily. Most investigators agree with the general form of equation (4.7) for smooth open channels.

$$\frac{1}{\sqrt{\lambda}} = A \text{ Log } [R_e \sqrt{\lambda}] - B \qquad (4.8)$$

but disagree somewhat on the values of the constants A and B. The variation in the constants A and B are presented in Table (4.1). It can be seen that there is significant disagreement over the value of (B). It was decided to look at the relevance of such a relationship and establish the value of (B) for a series of tests for floodplain alone and skewed main channel alone.

The use of Manning's 'n' value has been denigrated in some quarters as a very crude resistance coefficient. This is primarily because it is only applicable in the rough turbulent zone independent of Reynolds Number. Ackers (1958) has shown why Mannings 'n' is also successful even for the case of smooth transitional and turbulent flow.

The relationship for smooth pipe flow, for instance, is given by Blasius (1913) as:

$$\lambda = 0.08 \ R_e^{1/4} \qquad (4.9)$$

This can be put in the general form

$$\lambda = B\ R_e^{-b} \qquad (4.10)$$

which in turn is given by

$$\frac{8gRS}{V^2} = B\left(\frac{4\ R\ V}{\nu}\right)^{-b} \qquad (4.11)$$

For the hydraulic radius R to have a 2/3 power as in Mannings Equations, then Equation (4.11) can be rearranged into the Manning form

$$V = [(8g/B)^{5/9}\ (4/\nu)^{1/9}\ S^{1/4}]\ R^{2/3}\ /\ S \qquad (4.12)$$

meaning that for a constant fluid viscosity and bed slope, the value of Manning's 'n' is constant.

4.3 STAGE– DISCHARGE AND RESISTANCE COEFFICIENTS

4.3.1 SERIES B Tests (Smooth Flood Plain Alone).

The first set of experimental tests were designed to determine the resistance coefficients for the smooth floodplain (varnished marine plywood) when isolated from the main channel. The flood channel facility consists of a fixed bed model with a uniform slope of 1/1000. Usable flume length was 8.5m and maximum width was 0.764m. The pump was switched on and uniform flow was obtained by adjusting the tailgate weir until the water surface slope was equal to the bed slope. The water depth and the discharge were recorded. The results are shown in Table (4.2) which are represented as SERIES B.

Fig (4.1) shows a plot of stage and discharge for the smooth floodplain

alone. The channel bed was considered "smooth" in the sense that it contained no roughnesses and was varnished wood. In the hydraulic sense it should be termed quasi– smooth.

As mentioned before in this chapter, the main object of this set of results is to establish the Darcy– Weibach friction factor and the Manning's "n" for bed material used for the floodplain area. It has been shown for smooth channels that the friction factor λ, is depending on the Reynolds Number (R_e) alone in the generalised form:

$$\frac{1}{\sqrt{\lambda}} = A \text{ Log } [R_e \sqrt{\lambda}] - B \qquad (4.13)$$

where

$$R_e = (4 R_C V_C)/ \nu \qquad (4.14)$$

and

$$\lambda = (8gR_CS)/ V_C^2 \qquad (4.15)$$

where R_C is the hydraulic radius, V_C is the mean channel velocity, S is the longitudinal slope, ν is the kinematic viscosity. From table (4.1) most researchers have found the value of A to be approximate to 2.0, therefore it was decided to fix A at 2.0 and to use equation 4.13 to find an average B value. The value of B from this set of experiments was found to be 1.487. Then equation (4.13) becomes,

$$\frac{1}{\sqrt{\lambda}} = 2.0 \text{ Log } (R_e \sqrt{\lambda}) - 1.487 \qquad (4.16)$$

This result is shown in Fig (4.2) giving a reasonable correlation with a limited number of results. Equation (4.15) was used to find the theoretical prediction of the Manning's "n" values by using the equation below:–

$$n = \frac{R^{1/6}}{(8g/\lambda)^{1/2}} \qquad (4.17)$$

The resulting theoretical Manning's 'n' values were then plotted against experimental values and are shown plotted against flow depth in Fig (4.3). The experimental values of Manning's 'n' show an apparently large spread but this is more a function of the choice of scale for the 'n' values. As expected, the value of n increases near the solid boundary, but approaches an asymptote at large depths of flow. The asymptotic value is around 0.0101. It was also decided to attempt a correlation of the smooth floodplain friction factor using the Colebrook– White circular pipe function and by determining an average sand grain roughness size k_s. The results are shown plotted in Fig (4.4) with the best fit giving a k_s value of o.162mm. The correlation was not as successfull as the quasi– smooth friction factor in Fig (4.2) and therefore Equation (4.5) for the value of λ was hence forth adopted for all calculations on the smooth floodplain.

4.3.2 SERIES C (Smooth Main Channel Alone)

The second set of experimental data concerned the case of the skewed main channel artificially separated from the floodplain by the construction of small vertical walls at the main channel/floodplain interface. The data for the stage and discharge are given overleaf in Table 4.3 and also shown graphically in Fig (4.5).

The purpose of this experiment was essentially to obtain an accurate assessment of the resistance to flow in the 0.15m wide main channel without any influence from adjacent floodplains. The channel material was again varnished plywood, (the same as the floodplain) and was again considered quasi– smooth. These separate tests were carried out to establish the effect of a different aspect ratio (B/h) compared with the series A work, and perhaps more importantly the channel was skewed. It can be seen from Fig (3.1) that the skewed channel has a very slight bend at its upstream end which may well give rise to a weak secondary current propagating along the skewed main channel and hence giving rise to a slightly higher resistance coefficient.

The best correlation for the Darcy– Weisbach friction factor λ was again given by the quasi– smooth form of the equation (4.8). It was decided to fix the A value in equation (4.8) at 2.0, and to use experimental Reynolds Numbers and

friction factor values to estimate B values. The average value of B was found to be 1.76. The correlation is shown plotted in Fig (4.6), showing a good fit to the experimental data and producing a relationship for the skewed main channel,

$$\frac{1}{\sqrt{\lambda}} = 2.0 \, \mathrm{Log}(R_e \sqrt{\lambda}) - 1.76 \qquad (4.18)$$

Equation 4.19 is essentially the best– fit Darcy– Weisbach friction factor and hence can be used to determine a theoretical value of Manning's 'n' according to Equation 4.19 already discussed. These values are now compared with experimental values of Manning's 'n' and the comparison shown in Fig (4.7). The experimental values of 'n' appear to have a large spread, but this is again a function of the expanded scale on the horizontal axis.

For large depths of flow the value of Manning's 'n' for the main channel approaches an asymptote around 0.01062 whereas at a depth of 0.061m which corresponds to bank full depth, the 'n' value is of the order of 0.0108. It was decided also to determine an equivalent sand grain roughness size for the skewed main channel. The Colebrook White equation for circular pipes was also used to find the equivalent grain roughness values k_s for skewed main channel isolated from floodplain area. The average value of k_s was establish as 0.3389mm. The results are shown in Fig (4.8). Fig (4.8) represents friction factor plotted against the Reynolds Number values, also the figure shows the experimental values which are calculated by equation 4.14 and 4.15. The correlation is not as good as the modified smooth law in Fig 4.6 especially at higher values of reynolds Numbers. The modified smooth law (A= 2, B= 1.76) was used for all future calculations for the isolated skewed main channel.

4.3.3 SERIES A (Smooth Main Channel and Flood Plain Interacting).

The Series A tests were concerned with a skewed main channel with overbank flow onto adjacent floodplains, with the total flume width remaining constant at 0.764m as outlined in Chapter 3. The floodplain sections were positioned in the flume to give the skewed main channel width of 0.15m, 0.061m deep and skew angle at 5.9^0 to the longitudinal axis. The longitudinal flood

plain and the main channel bed slope was kept fixed at 0.001. The maximum discharge through the system being 60 litres/sec.

Experiments were carried out to establish the stage discharge relationship for the skewed main channel with smooth floodplain. For each test the bed slope remained fixed. A discharge was chosen, the tailgate weir altered many times by trial and error to establish uniform flow along the channel. The flow depth and the discharge were then recorded. The discharge was then varied and new uniform flow conditions set up. Fourteen results were recorded to establish the stage– discharge relationship for skewed main channel with smooth floodplain conditions and these results are tabulated in Table (4.4). The results are shown graphically in Fig (4.9). The lowest overbank flow depth tested was 12mm corresponding to a relative depth (Y_f/Y_c) of 0.164 whilst the largest depth tested was 84mm corresponding to a relative depth of 0.58. The upper end of the scale might produce useful data for 2– stage compound channels, where relative depths of 0.5 or 50% are now common– place especially during winter floods.

It was decided not to investigate overbank flood depths less than 12mm in view of the fact that the floodplain flow at that depth is approaching laminar flow ($R_e < 3000$) and hence not representative of very much in nature.

The values of the resistance coefficient during inbank and overbank flow are shown plotted in Fig (4.10). For the sake of clarity these are presented in the form of Manning's 'n' values only. Below bank– full the values of Manning's 'n' are as already described in Fig (4.7). Above bank– full the 'n' values have been calculated for the compound channel treated as a single unit and thus will reflect the sudden reduction in hydraulic radius R just above bank full level. It is clear from Fig (4.10) that because the main channel and floodplains have very similar Manning's 'n' values, therefore at larger flow depths on the floodplain the 'n' value will approach an asymptote dominated by the floodplain roughness.

Also show in Fig (4.10) is the effective Manning's 'n' value for the main channel sub– section. This has been computed by point velocity measurements in the main channel sub– section integrated over the area (B_c * $Y_{c)}$ to give the discharge in the main channel during interaction. As expected, the effective 'n' is high for low relative depths reducing to an asymptote as the interaction effect becomes negligible.

4.3.4 A Note on Discharge Assessment for the Skewed Main Channel During Overbank Flow

The normal method of assessing discharge in a compound cross–section channel is to subdivided the section using imaginary walls at the main channel floodplain junctions. This technique overcomes the problem of discontinuity of hydraulic radius R, and discontinuities in boundary roughness, but excludes the turbulent interaction effect. In most calculations the imaginary walls are considered to be vertical and to have zero friction, as shown in the sketch below, although Wormleaton (1987) investigates other sub–division methods.

Discharge assessment by sub–division methods will be investigated further and in some detail in Chapter 7. The subject is introduced at this stage mainly to familiarise the reader with the concept of errors in discharge assessment by neglecting the interaction effect.

The Series B correlation of resistance factor outlined in Section 4.3.1 allows accurate discharge assessment on the smooth floodplain. Series C correlations in Section 4.3.2 allow accurate discharge assessment in the main channel. When both are combined, an estimated stage–discharge curve can be obtained for the compound section using the sub–divided channel method. This estimate is shown in Fig (4.11) and compared with the experimental stage–discharge data for overbank flow in the skewed channel.

The small difference between the overall hydraulic resistance of these channels, barely visible in stage discharge curves (Fig 4.11), can be better appreciated if shown as percentage change in discharge, % ΔQ. Fig (4.12) shows values of $\%\Delta Q$ plotted against relative depth Y_f/Y_c for the skew angle of 5.843^0. The $\%\Delta Q$ is the percentage error between estimated and experimental discharge for same depth of flow as,

$$\%\Delta Q = \frac{Q_{est.} - Q_{exper.}}{Q_{exper.}} \times 100 \qquad (4.20)$$

It is clear from Fig (4.12) that for a small skew angle main channel with compound flow, there are substantial errors in discharge assessment, up to 25% in

this case. The reasons for this may not be difficult to imagine but may be more difficult to prove. For instance, a small skew angle of 5.843^0 will ensure there is substantial co–flowing lateral shear. The flood plain flow passing over the main channel below will ensure some horizontal shear. Both these sources of energy loss exist but are not included in bed friction terms. Thus the value of ΔQ in Fig (4.12) must contain both elements of additional energy loss. One aim of this work is to separate the two additional sources of loss, and will be discussed more fully in Chapter 7. The purpose therefore of using a skewed straight channel rather than a meandering channel is so that the picture is not further complicated by bend flows.

4.4 FLOW RESISTANCE AND STAGE–DISCHARGE FOR THE ROUGH FLOOD PLAIN

4.4.1 Introduction

A survey of flood plain roughness by Ervine revealed that Manning's 'n' for typical British river is of the order of 0.03 to 0.035, whilst the corresponding values of the adjacent flood plains is of the order of 0.05 to 0.1. The flood plain in nature thus has a Manning's 'n' value two or three times greater than the main river channel.

The roughness elements on the flood plain in nature tend to be grass, trees, hedges, and walls, and the problem arose as to how to best simulate such roughness in a small scale model. A visit to Bristol University (Dr. Sellin) revealed that roughness elements stuck to the flood plain floor did generate some turbulence, but that the turbulence did not penetrate far in the vertical direction for deeper flood plain flows. The recommendation from Bristol University was the use of circular dowel rods extending vertically throughout the full flood plain flow depth, which had the effect of generating turbulence almost uniformly over the full flood plain depth of flow. Such rods were adopted for Series A tests on the SERC flume at Wallingford, using 25mm diameter dowels, spaced at 310mm centres in the lateral direction and 268.5mm centres in the longitudinal direction. The rods were placed in a staggered grid section so that any three dowels make

an equilateral triangle in plan view. The same procedure was to be adapted for the Glasgow flume but with scaled down rod diameters and spacings.

4.4.2 A Note on Flow Resistance Due to Vertical Rods

Having decided to adopt the Bristol procedure to use vertical rods to simulate flood plain roughness, it should be pointed out that half the tests in Glasgow flume were carried out with a roughened flood plain SERIES D and E. This represented the nearest simulation to nature, or a real two–stage channel, although the aspect ratio of the main channel of 2.5, represented a vertical distortion of the order of three to one. It was realised at any early stage that use of the rods was likely to give increases in Manning's 'n' value with increasing flood plain flow depths. The alternative of using stick–on roughness elements produces decreasing Manning's 'n' values with increasing flood plain flow depth. In reality the 'n' value can either increase or decrease with depth on flood plains, depending on the degree of submergence of grass, trees, hedges, etc.

In the Glasgow flume it was felt important to use the vertical rods to generate a Manning's 'n' value around 0.03; to use scaled down rod diameters, and scaled down lateral and longitudinal spacings relative to the SERC flume, and finally to produce a method of determining what the flume resistance is going to be for any rod pattern, or rod diameters. The latter aim is the purpose of this section.

Is it possible to separate boundary friction from the effect of vortices shed behind the dowel rods? Is the drag coefficient C_d known for such an experimental test? What is the component of free surface effects?

It is quite likely in terms of the physical behaviour that there are 4 effects listed and sketched below.

a) free surface drag

b) internal vortex street drag

c) skin friction drag

d) interaction with other rods

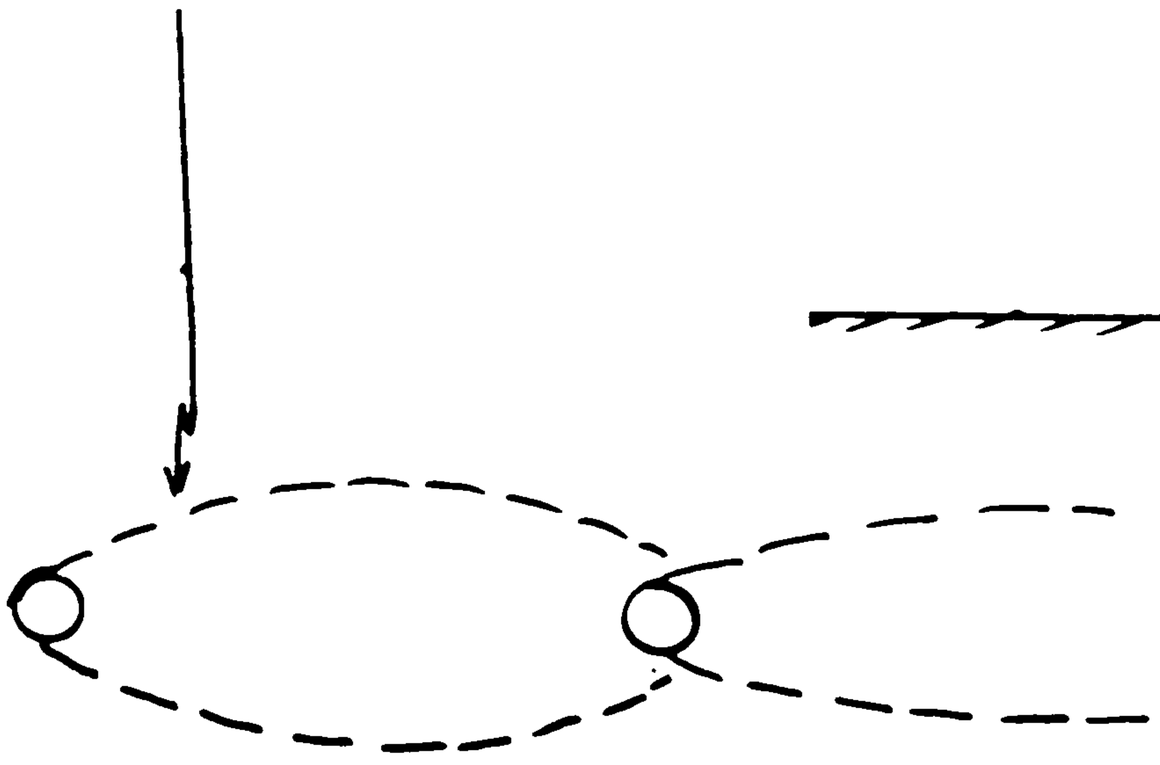

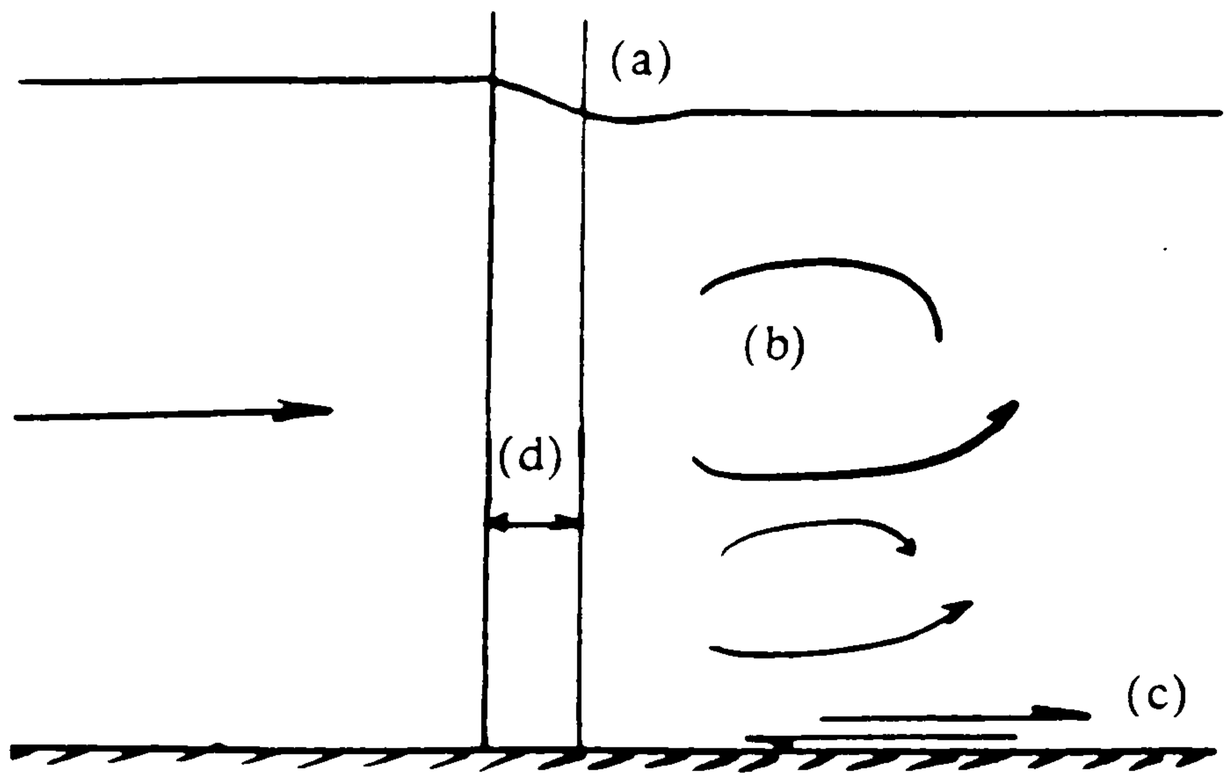

a) Free surface effect.

This effect will be important for shallower flow depths and smooth boundaries. Froudes work on C_d (for free surface) is sketched below. It is quite possible that the Glasgow dowels are around the first peak which means an increase + then decrease in C_d whether the Froude Number is increasing or decreasing. At large flow depths this effect will becomes negligible (relative to other effects).

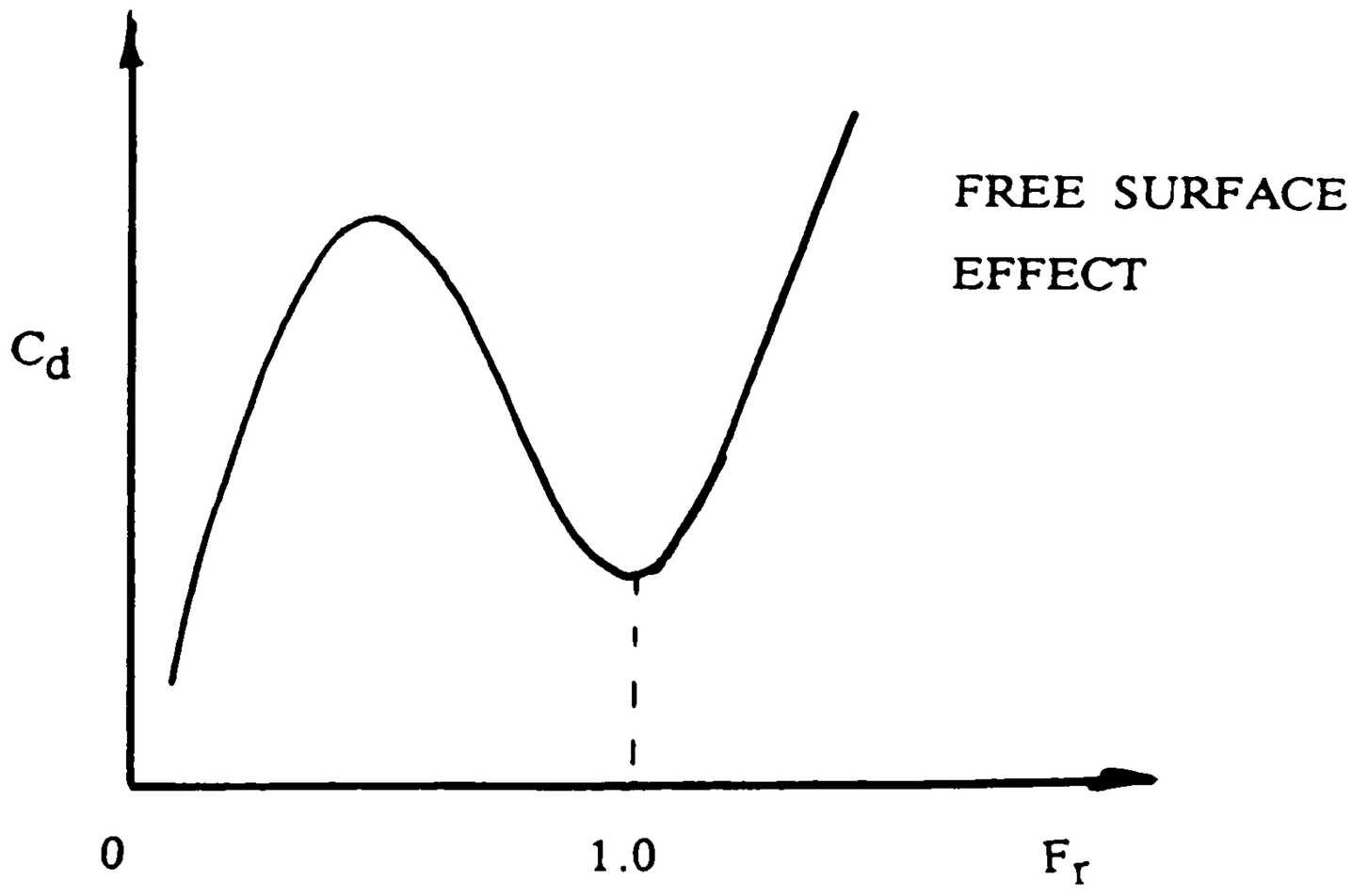

b) Internal drag by production, convection and dissipation of turbulence and shedding of vortices produces a C_d which is sketched below. During the tests however, R_e is more or less constant which means that this effect does not account for the variation of C_d for $R_e = 4 \longrightarrow 5x10^3$, $C_d \simeq 0.95$ for a single cylinder.

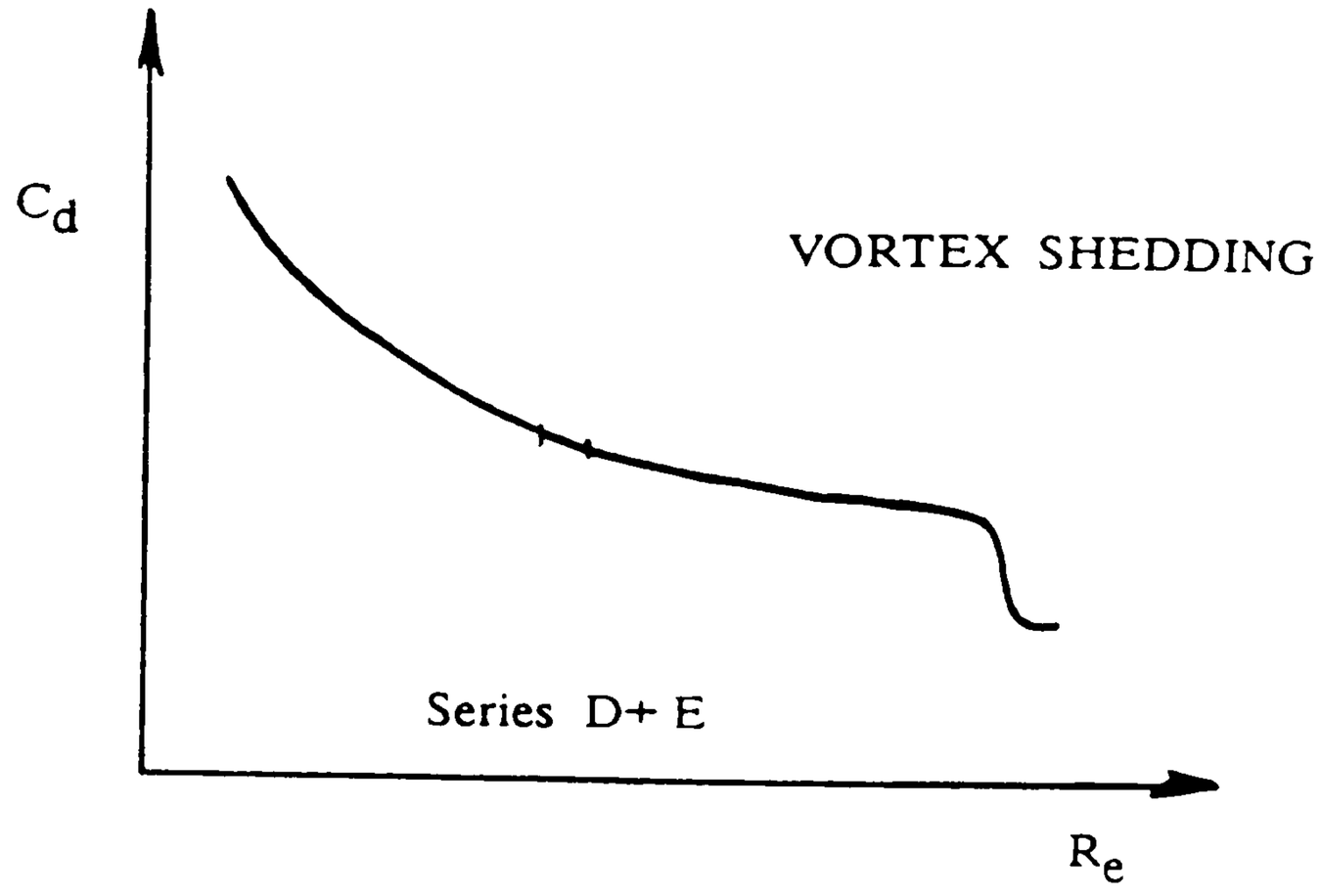

c) The skin friction drag coefficient.

For a smooth boundary this has relatively small effect. By definition $S_f = \lambda_s u^2/8gR$, the skin drag coefficient must be proportional to the Drag friction factor λ_s and hence it will also be decreasing with R_e.

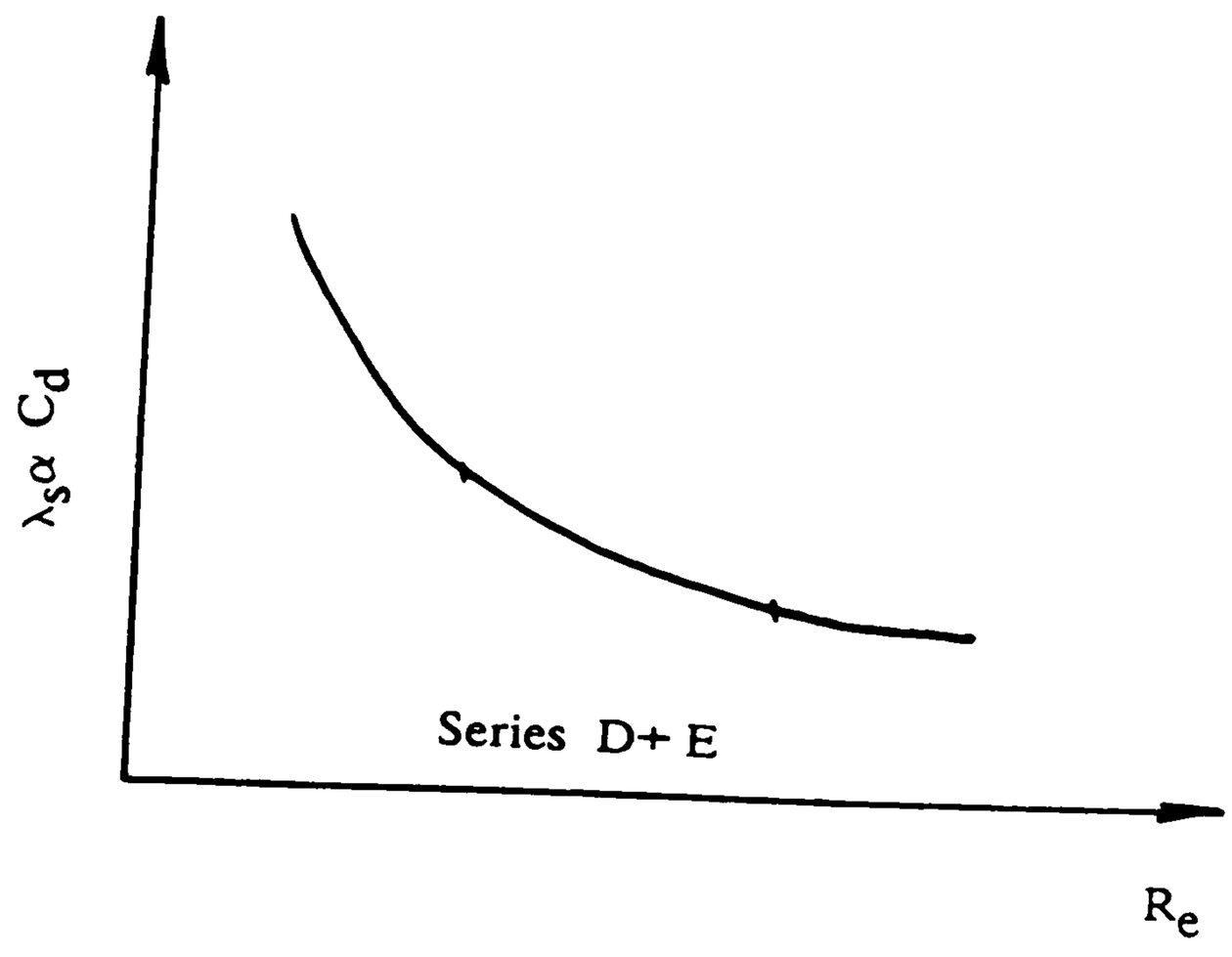

d) Perhaps the most difficult area to quantify is the interaction effect. It has the effect of producing both lower mean velocities (wakes) behind each bar but greater turbulence coming up to the start of the next bar.

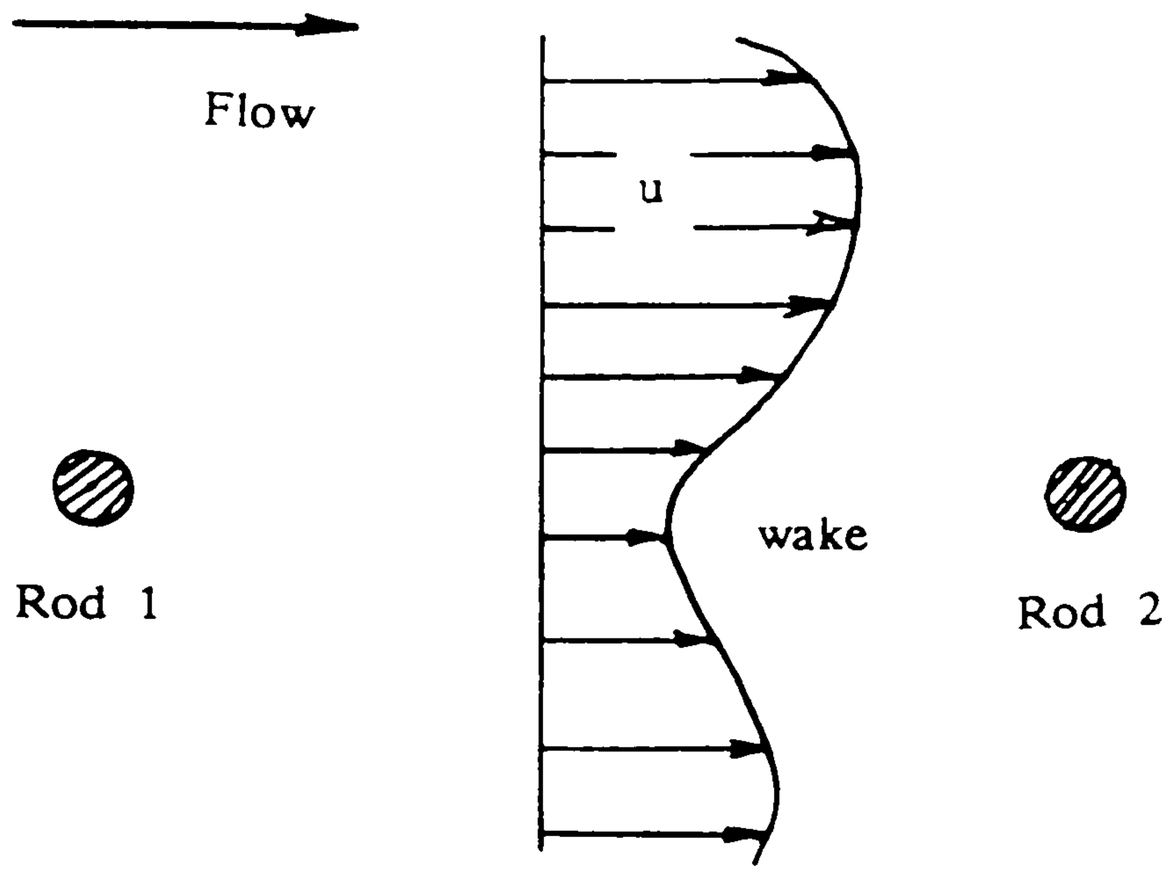

In terms of momentum flux Rod 2 "feels" a greatly reduced mean momentum flux $\rho A u^2$. But a greatly <u>increased</u> turbulent momentum flux $\rho A(u')^2$. The net effect at Rod 2 may well be the production of less NEW turbulence than would be the case if Rod 2 was isolated by itself.

This means that the interaction effect may well effectively reduce the value of C_d as sketched below simply because in terms of turbulent production the total generated will be less than the sum of the individual components added together as if they were isolated.

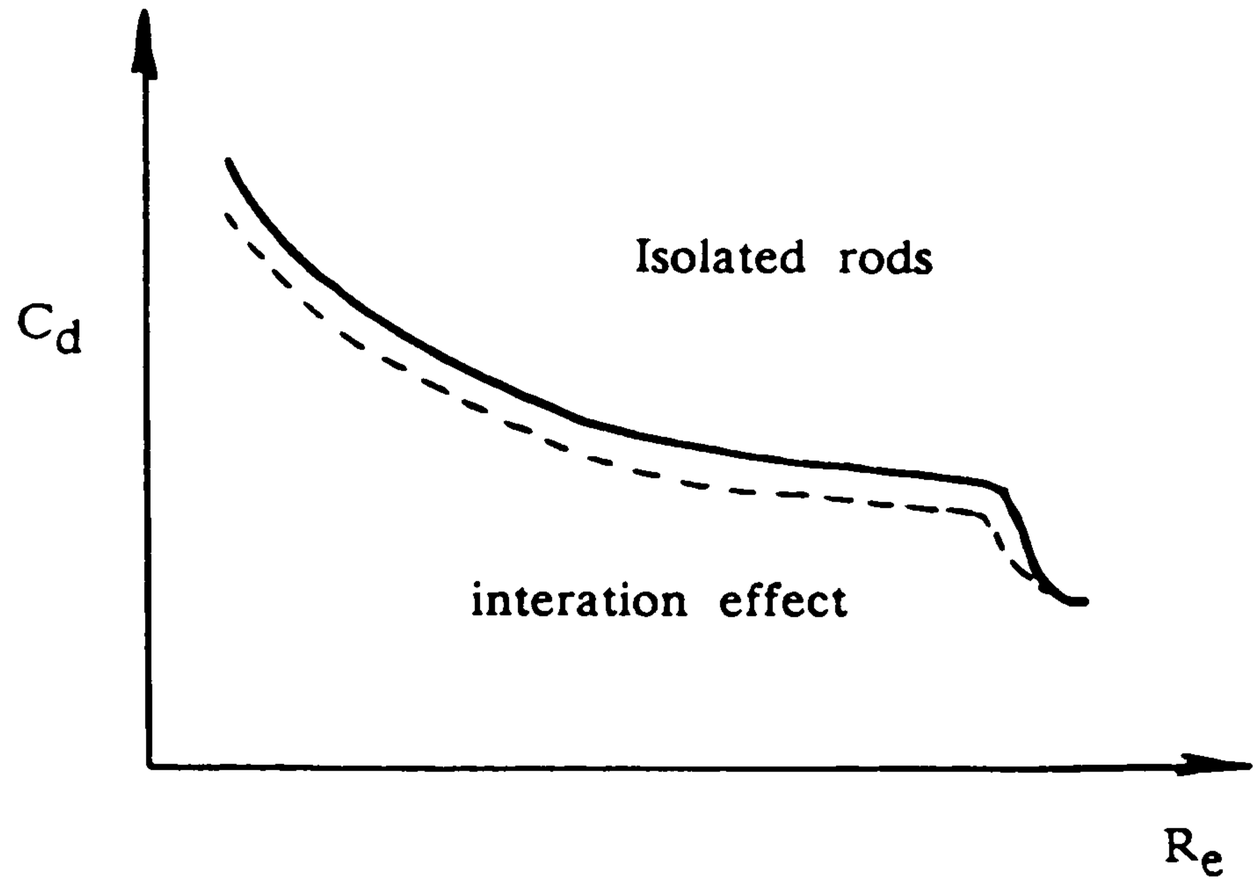

It is quite likely therefore that a combination of all four effects (a) to (d) will produce a generally reduced drag coefficient with increasing Reynolds Number but may contain an upward "blip" due to the free surface effect. This is sketched below

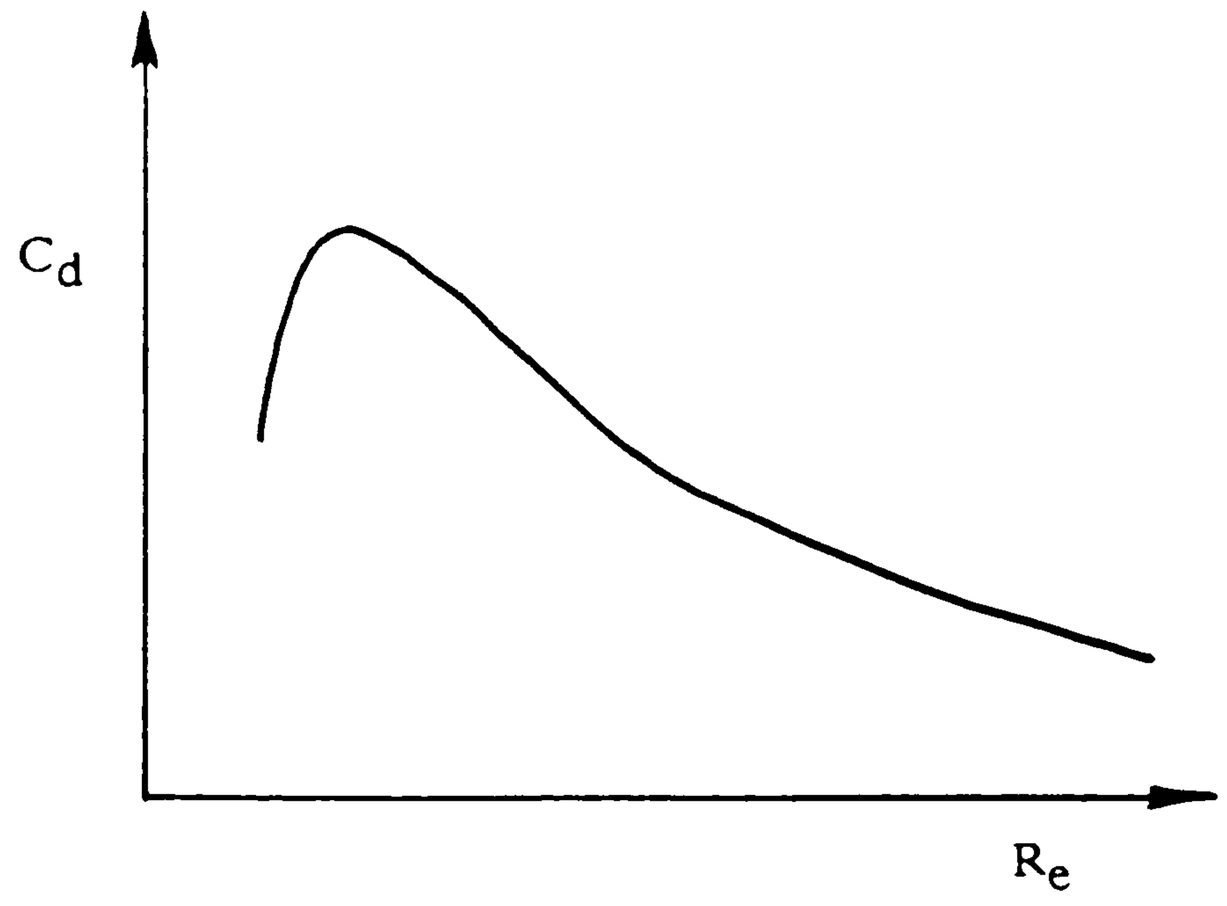

In terms of mathematical formulation we can attempt a separation of skin (boundary) drag from the vertical bar effect, C_d, with the value of C_d incorporating a mixture of free surface, internal drag and interaction effects.

Assuming a rectangular cross–section (as sketched below) and uniform flow, then over a length L of channel,

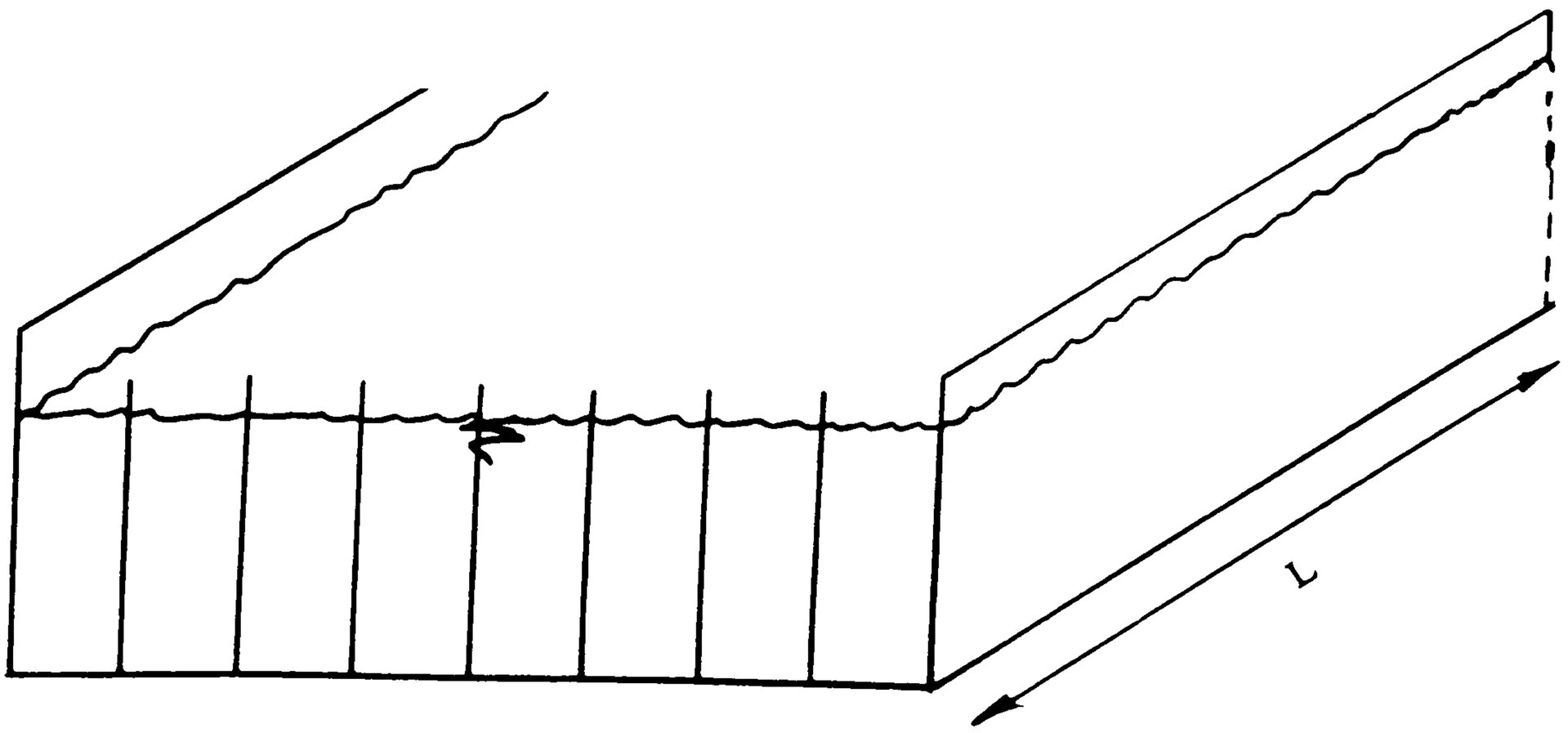

The total forces producing flow can be equated to the total forces resisting flow, therefore

Drag force + Skin Friction force = Weight component Fluid in Control Volume

then

1) The best equation for the drag at the solid surface was derived by Ackers (1987), as followed:

$$1/\sqrt{\lambda_b} = 2.0 \text{ Log } (R_e \sqrt{\lambda_b}) - 1.478 \qquad (4.21)$$

where

λ_b is the friction factor rising from the drag on the channel perimeter.

R_e is the Reynolds Number of the flow.

2) The drag arising from the rods is given by:

$$F_{rod} = 0.5\ C_d\ N\ d\ Y_c\ \rho\ \alpha\ U^2 \qquad (4.22)$$

where

F_{rod} is the form drag of the rods per unit length of channel.

C_d is the drag coefficient.

N number of rods per unit channel length.

d dia. of rods.

Y_c flow depth.

ρ specific mass of fluid.

α velocity distribution coefficient.

U the mean velocity over the flow depth.

The velocity distribution coefficient α allows for the variation of velocity over the length of the rod, i.e. the depth of flow. The depth mean velocity U is calculated allowing for the blockage of the transverse rows of rods:

$$U = Q / (A - n\ Y_c\ d) \qquad (4.23)$$

where

Q is the discharge

A is the channel cross– section.

n number of rods in each row

A blockage coefficient, β, may be defined as:

$$\beta = (U/V) = (1 - nY_c d/A)^{-2} \qquad (4.24)$$

the total drag per unit length of channel is then given by:

$$F_{tot} = \beta \rho V^2 (0.5 \alpha N d Y_c C_d + \lambda_b P/8) \qquad (4.25)$$

where P is the wetted perimeter of the channel

The drag equation can be converted into a conventional form of resistance equation using the force balance equation:

$$F_{tot} = \rho g A S = \rho g R S P \qquad (4.26)$$

where

g is acceleration due to gravity, A is the cross sectional area of flow.

S is the channel slope and R is the hydraulic mean depth, A/P

then

$$F_{tot} = 8gRS/V^2 = \beta[4 (N d Y_c/ P) \alpha C_d + \lambda_b] \qquad (4.27)$$

where F_{tot} = overall friction factor

then

$$\alpha C_d = 1.578 - 0.206 Z_* + \sqrt{} (0.209 Z_* - 0.369) \qquad (4.28)$$

where Z_* is flow depth/rod diameter

Ackers (1989) used the blockage effect (β) to find the overall friction factor as below:

$$F_{tot} = 8gRS/V^2 = 4\ \alpha\ C_d(\beta_1 N_1 + \beta_2 N_2)d\ Y_c/P + (\beta_1+\beta_2')\lambda_b/2 \qquad (4.29)$$

Equation 4.29 is used for $1.75 < Z_* < 6.6$

$$\beta_1 = (1 - n_1 Y_c\ d/A)^{-2} \qquad (4.30)$$

$$\beta_2 = (1 - n_2 Y_c\ d/A)^{-2} \qquad (4.31)$$

where

β_1, β_2 are the blockage effect, i.e. square of area ratios for alternate rows.

n_1, n_2 are number of rods of diameter (d) across across channel/floodplain, rows 1 and rows 2.

N_1, N_2 are the number of rods per unit length of main channel/floodplain.

A is the gross cross sectional area of zone under consideration

αC_d is the effective drag coefficient of rods.

4.4.3 Flow Resistance for the SERIES E Tests

The Series E tests were essentially the whole flume width acting as a flood plain, with vertical dowel rods over the full width and length. The purpose of this test series was to determine the proper resistance functions for the vertical rods, thus representing flood plain behaviour when it is not interacting with the main channel.

The model for this series of tests was described in Chapter 3. Seven dowels, each 10mm diameter, and 100mm lateral spacing were placed across the flume width. Each dowel was 160mm high, meaning that the dowels were never completely submerged as the highest flow depth tested was 145mm. The dowel bars were also placed at 100mm spacing longitudinally in a staggered grid pattern.

The results of the stage–discharge relationship are shown in Fig (4.13) and also are given in tabular form overleaf in Table (4.5). Values of the roughness

coefficient Manning's 'n' were computed from the stage– discharge graph, and the results plotted in Fig (4.14). It is clear from Fig (4.14) that the 10mm diameter dowels at 100mm centres (both laterally and longitudinally) produce Manning's 'n' values 2 to 4 times that of the smooth case. This was the range required for the roughened experimental flood plain. It is also clear that the 'n' values increase with increasing flood plain depth which was expected with the use of vertical dowel rods. The use of wire mesh at the boundary to generate roughness would have produced a greatly decreasing 'n' value with increasing flood plain depth.

It is also of interest to determine the experimental values of the drag coefficient C_d for the vertical rods, and derived from the force balance in section 4.4.2. The results are shown in Fig (4.15) for C_d plotted against the non– dimensional flow depth Y_c/d, (flow depth/dowel diameter) and again in Fig (4.16) for C_d plotted against Reynolds Number. It appears from these graphs that the range of C_d 0.75 to 1.2 is in the correct range although a little lower than expected, probably due to the interaction effect.

There is no peak due to free surface effects. This will be discussed in more detail in Chapter 7 when C_d values are compared with those obtained on the SERC flume.

4.4.4 SERIES D Tests– Rough Flood Plain/Smooth Main Channel Interaction

The Series D experiments were carried out to establish the stage discharge relationship for the skewed main channel with rough flood plain. The same procedures are used to establish the stage discharge curve, with eighteen results recorded and shown in Table (4.6). These results are also shown in Fig (4.17). From Fig (4.17), the minimum discharge recorded was 4.3 L/sec at flood plain depth Y_f of 16mm and channel depth Y_c was 77mm. The maximum discharge recorded was 23.1608 L/sec at Y_f of 140.3mm and Y_c was 201.3mm.

It was then decided to investigate the errors in discharge assessment using various methods of sub– division. This exercise was made possible from the accurate knowledge of the smooth skewed main channel friction factors (SERIES

C) as well as the roughened flood plain friction factors (SERIES E). Three methods of sub– division were attempted:–

i) Imaginary vertical walls at the main channel/flood plain junction, with the imaginary walls carrying zero friction.

ii) Imaginary vertical walls at the main channel/flood plain junction, with the imaginary walls carrying roughened flood plain friction.

iii) A horizontal sub– division at bank full level, with the imaginary sub– dividing wall carrying roughened flood plain friction.

(iv) A fourth method of sub– division produced almost zero errors in discharge assessment at all relative– depths. The method represents an imaginary horizontal wall, placed at a distance of one third of bankfull depth below bank full depth. The imaginary wall carries flood plain friction on its upper side only, but flood plain friction is also added to the main channel walls above this imaginary subdivision.

All four methods are shown in Fig (4.18) when compared with the experimental results. It is clear from Fig (4.18) that the estimate discharge using zero friction vertical walls is completely inaccurate and becoming worse with increasing depth. The roughened vertical wall method is also inaccurate but improves with increasing flood plain depth. Finally, the roughened horizontal sub– division method is shown to be the most accurate, by far and may be a pointer to the best method of discharge assessment when the flow is dominated by flood plain roughness as is the case in Series D tests.

The percentage error in ΔQ is shown in Fig (4.19) for all four discharge assessment methods showing the magnitude of error in each of the four methods attempted and again showing the horizontal rough sub– division method which is by far the best.

The reason for this is due to the fact that flow below bankfull is dominated by the smooth flood plain walls, whereas, flow in the MAIN CHANNEL above bank– full level is so heavily dominated by flood plain friction that the main channel behaves almost like a part of the flood plain. It is not certain if this would apply for wide main channels with more realistic aspect ratios (around 10).

4.4.5 Main Channel Behaviour under Various Regimes

Series C tests have established the stage–discharge behaviour in the skewed main channel when completely isolated from the flood plain.
This can be used as a bench mark for the stage–discharge behaviour in the main channel section when interacting with the flood plain. The main channel section means the total flow below bank full level plus the flow in the main channel above bank–full. During interacting conditions this is measured using point velocity data in the deep main channel section and integrating over the area $B_c x Yc$ to obtain the component of discharge which is operating in that sub–section of the flow.

Fig (4.20) shows the discharge in the deep skewed main channel under the conditions of, isolated from the flood plain, interacting with smooth flood plain, and, interacting with the rough flood plain. The case of the smooth flood plain produces the classic reduction in main channel discharge as shown by the dashed line. This is a lateral and horizontal shear problem as outlined in section 4.3.4. At higher depths of flow this behaviour approaches that of a single channel again, with Manning's 'n' for both main channel and flood plain approximately equal.

The interesting point from Fig (4.20) is the case of the rough flood plain, which appears to produce a very small turbulent interaction effect at low flood plain depths. The apparently large interaction at larger flood plain depths is due to the fact that the flow is beginning to behave like a single channel were most of the boundary is rough n ≃ 0.03 to 0.04, giving greater deviations from the smooth main channel case where the boundary is smooth (n ≈ 0.01).

4.5 CONCLUSIONS

(1) The resistance coefficient of the flood plain material is best described by the Darcy Weisbach quasi–smooth function

$$1/\sqrt{\lambda} = 2 \text{ Log } (R_e \sqrt{\lambda}) - 1.487$$

(2) The resistance coefficient for the skewed main channel is given by

$$1/\sqrt{\lambda} = 2 \text{ Log } (R_e \cdot \lambda) - 1.76$$

(3) At present we are unable to predict stage and discharge for a skewed main channel interacting with flow on smooth floodplains. The errors in discharge assessment are of order of 25%, because of both lateral shear (coflowing) and horizontal shear.

(4) An attempt has been made to separate drag due to vertical rods, from skin friction, and also to estimate drag coefficients C_d for the experimental set– up. The trends and values of C_d are shown in Fig (4.15) and Fig (4.16).

(5) 10mm rods at 100mm centres both laterally and longitudinally produce Manning's 'n' values around 0.02 to 0.04, increasing with flow depth.

(6) At present we are unable to predict stage and discharge for a skewed main channel with rough flood plains. This best sub– division method appears to be a horizontal sub– division at bank full level with the sub division having the same roughness as the flood plain see Fig (4.18) and Fig (4.19).

(7) For the rough flood plain case, flow in the main channel becomes completely dominated by the flood plain roughness Fig (4.20) rather than the classical interactive lateral shear which is more the case for smooth flood plains.

Table (4.1) Comparison of constant in open channel flow equation.

(Myers

Investigation	Value of A	Value of B
Smooth pipe 1966	2.0	0.80
Keulegan 1938	2.03	1.08
Reinus 1961	2.0	1.06
Tracy 1961	2.03	1.30
Rao 1967	2.12	1.83
Myers 1982	2.12	1.56

Table (4.2) The Experimental Stage Discharge Results Floodplain Area Isolated From Skewed Main Channel

B_c = 0.764m S = 0.001

SERIES B Tests

Channel depth Y_c (m)	Discharge Q (L/Sec)
0.0347	8.1181
0.0465	13.276
0.0543	17.019
0.0666	23.07
0.0764	28.6725
0.0.083	32.62
0.088	36.505
0.0913	39.1346
0.099	43.5156
0.1079	48.20
0.1123	53.107

Table (4.3) The Experimental Stage Discharge Results For Skewed Main Channel Isolated From Floodplain

B_c = 0.15m S = 0.001

skewed angle = 5.843°

SERIES C

Stage Y_c (m)	Discharge Q (L/Sec)
0.046	1.9035
0.058	2.6365
0.0631	2.955
0.0710	3.400
0.0714	3.440
0.0770	3.8140
0.0826	4.200
0.0840	4.330
0.09	4.680
0.0940	5.0046
0.0976	5.20
0.106	5.80
0.1180	6.680
0.1260	7.280
0.1330	7.80
0.145	8.70

Table (4.4) The Experimental Stage Discharge Results For Skewed Main Channel With Smooth Floodplain

B_c = 0.15m B_f = 0.614m S = 0.001

skewed angle = 5.843°

SERIES A tests

Main channel depth Y_c (m)	Flood plain depth Y_f (m)	Discharge $Q_{exp.}$ (L/Sec)
0.073	0.012	4.01157
0.0751	0.0141	4.300
0.081	0.020	5.910
0.0825	0.0215	6.670
0.084	0.023	7.00
0.0935	0.0325	10.36
0.094	0.033	10.577
0.103	0.042	14.45
0.1042	0.0432	15.60
0.107	0.046	16.40
0.114	0.053	20.1
0.126	0.065	25.91
0.131	0.070	29.0
0.145	0.084	36.62

Table (4.5) The Experimental Stage Discharge Results For Rough Floodplain Isolated From Skewed Main Channel.

B_c = 0.15m S = 0.001

skewed angle = 5.843°

SERIES E Tests

Depth of flow Y_c (m)	Discharge Q (L/Sec)
0.025	1.918
0.034	2.90
0.0485	4.63
0.053	5.23
0.062	6.313
0.069	7.324
0.0771	8.40
0.0865	9.60
0.096	11.0
0.10	11.48
0.1089	12.686
0.11507	13.45
0.1259	15.213
0.135	16.70
0.145	18.3

Table (4.6) The Experimental Stage Discharge Results For The Skewed Main Channel With Rough Floodplain Area.

B_c = 0.15m B_f = 0.614m S = 0.001

skewed angle = 5.843^0

SERIES D Tests

Main channel depth Y_c (m)	Floodplain depth Y_f (m)	Discharge Q (L/Sec)
0.077	0.016	4.30
0.0896	0.0286	5.94
0.106	0.0450	8.024
0.1161	0.0551	9.20
0.1266	0.0656	10.505
0.1341	0.0731	11.414
0.1431	0.0821	12.925
0.1488	0.0878	14.115
0.1573	0.0963	15.16
0.1689	0.1079	16.157
0.1769	0.1159	18.20
0.1841	0.1231	19.259
0.1929	0.1319	21.227
0.2013	0.1403	23.1608

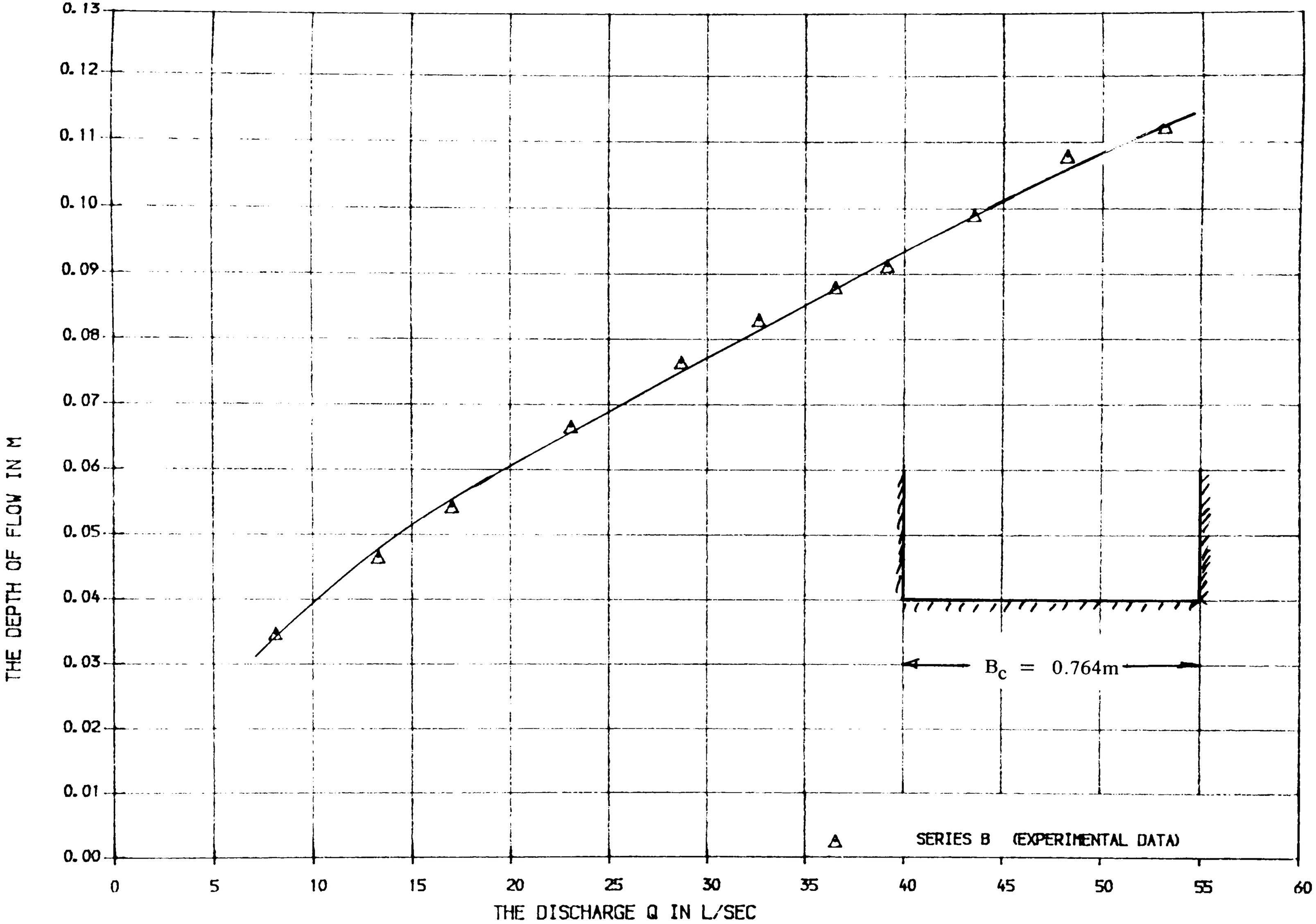

FIG (4.1) THE EXPERIMENTAL STAGE_ DISCHARGE RELATIONSHIP FOR THE BED MATERIAL USED FOR THE SMOOTH FLOODPLAIN.

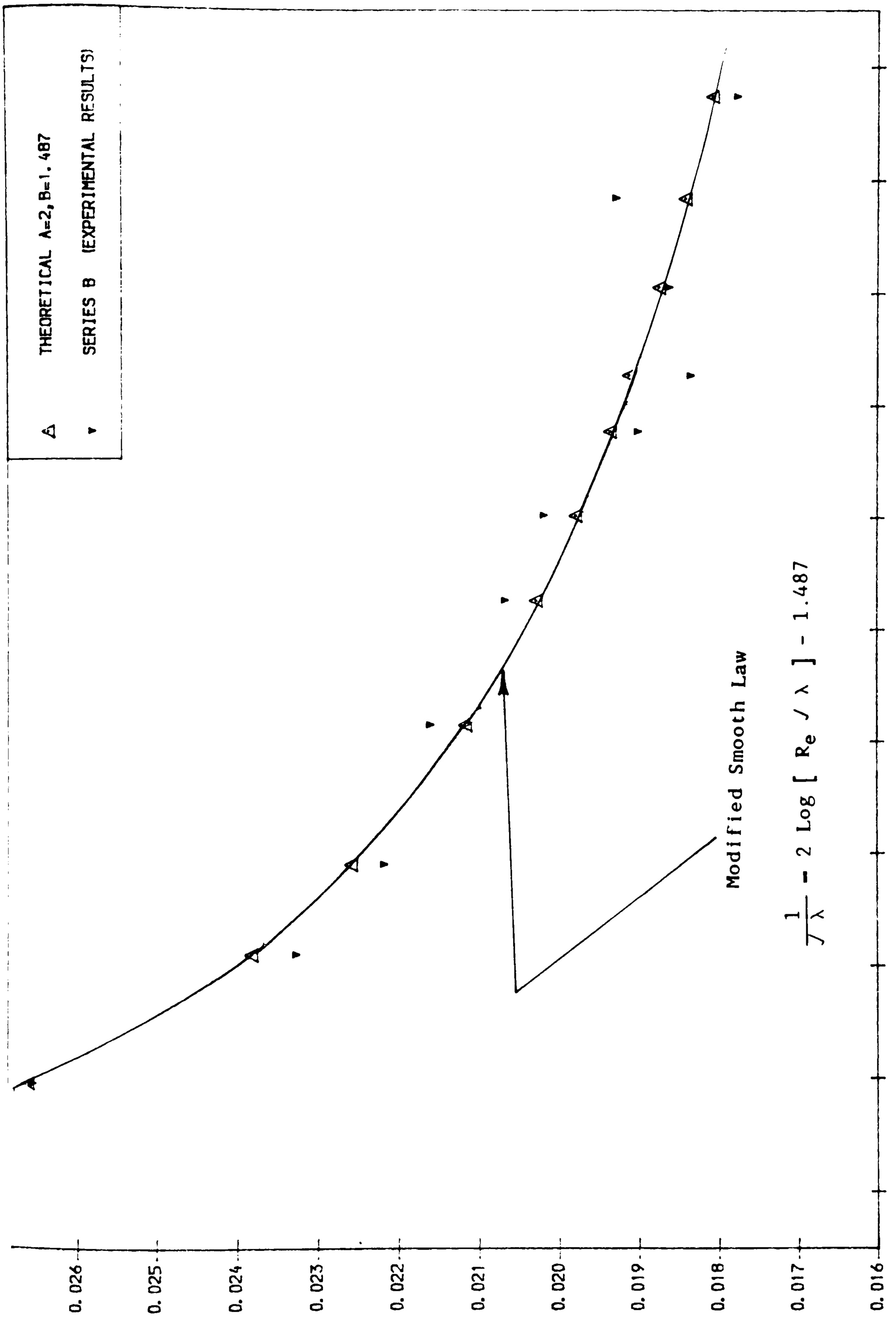

FIG (4.2) THE RELATIONSHIP BETWEEN THE REYNOLDS' NO. AND THE FRICTION FACTOR FOR BED MATERIAL USED FOR THE SMOOTH FLOODPLAIN.

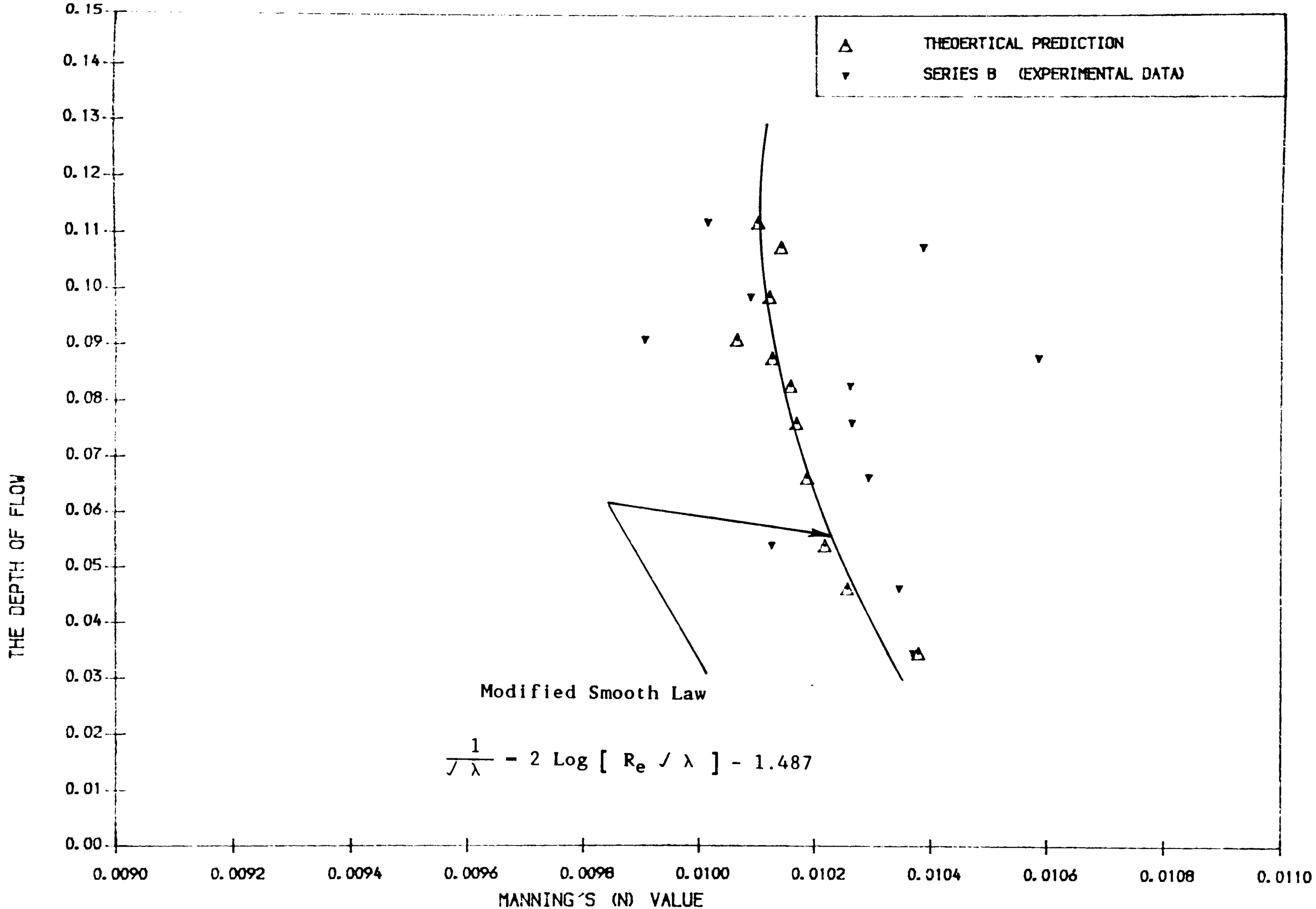

FIG (4.3) THE RELATIONSHIP BETWEEN MANNING'S (N) AND THE DEPTH OF FLOW FOR MATERIAL USED FOR SMOOTH FLOODPLAIN.

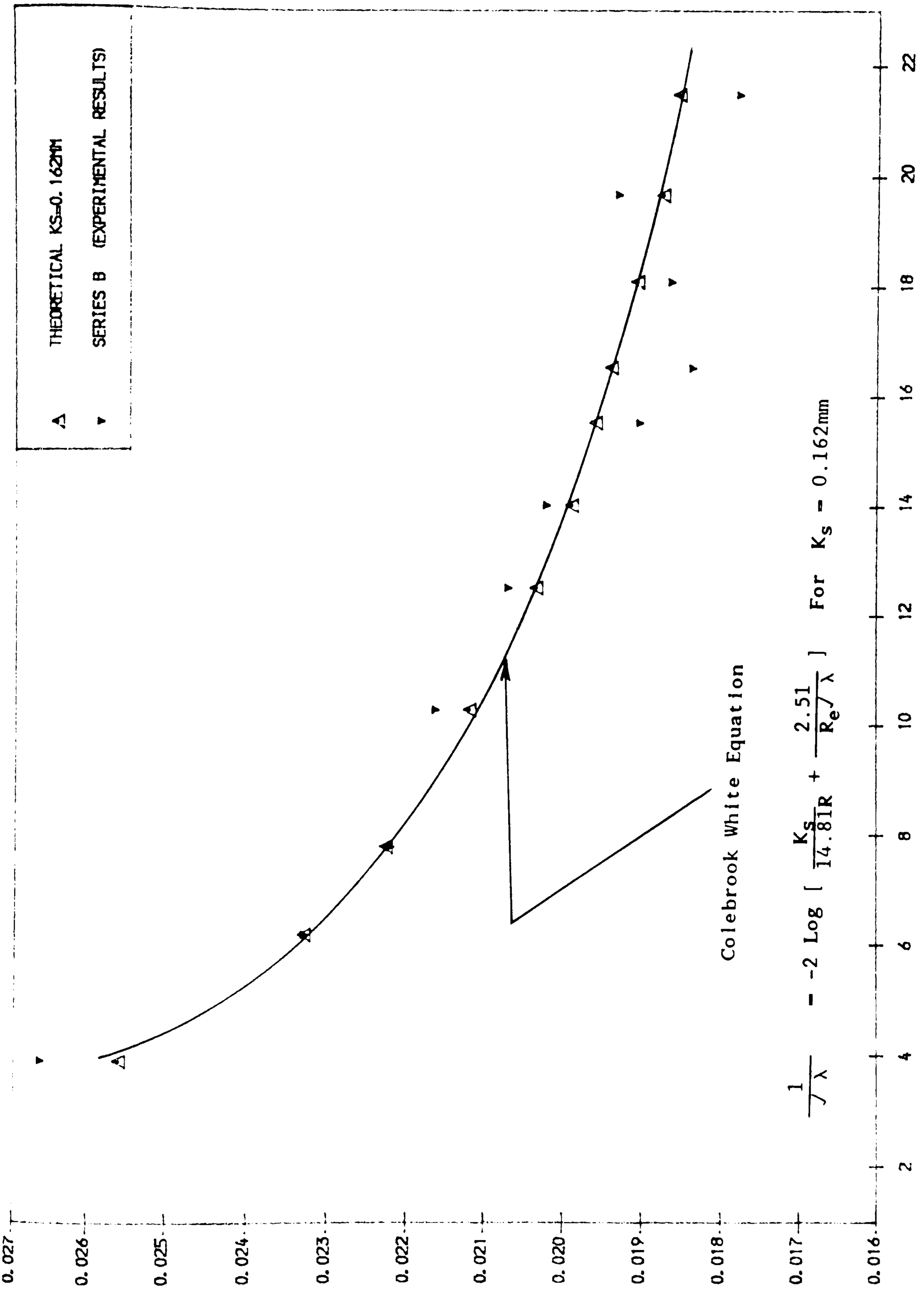

FIG (4.4) THE RELATIONSHIP BETWEEN THE REYNOLDS' NO. AND FRICTION FACTOR FOR BED MATERIAL USED FOR SMOOTH FLOODPLAIN.

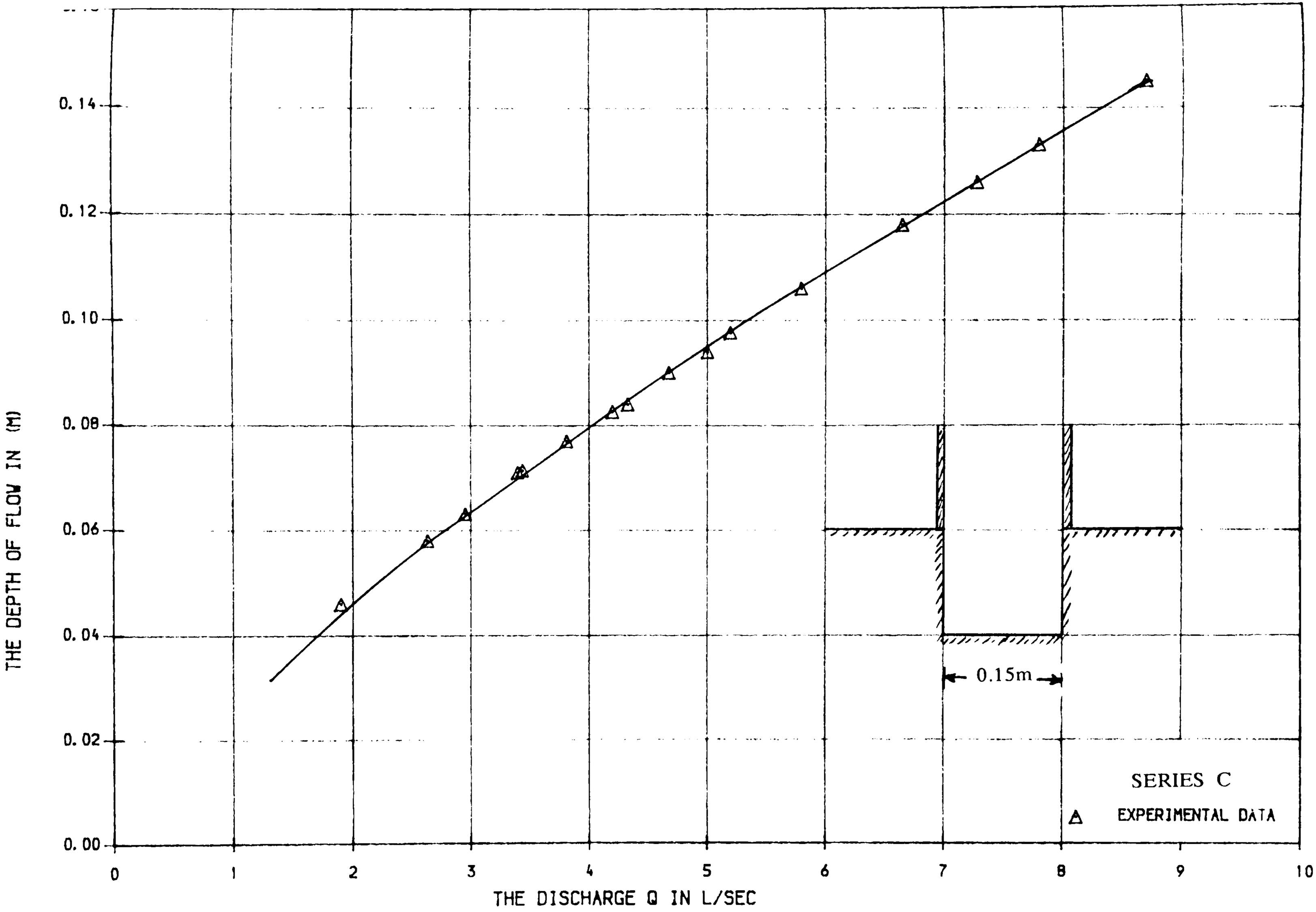

FIG (4.5) THE STAGE_ DISCHARGE RELATIONSHIP FOR THE SKEWED MAIN CHANNEL ISOLATED FROM FLOODPLAIN (SMOOTH CASE)

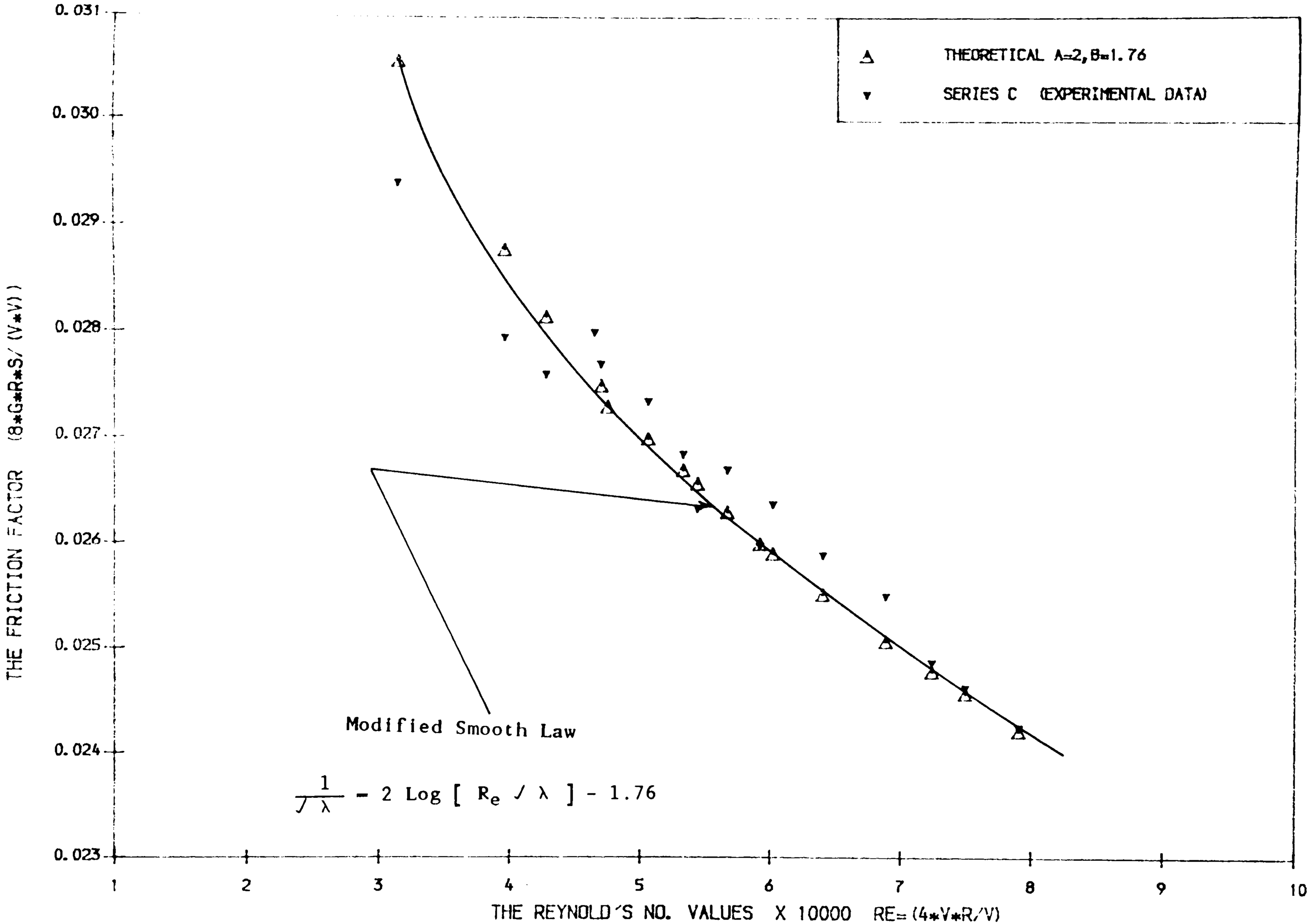

FIG (4.6) THE RELATIONSHIP BETWEEN THE REYNOLD'S NO. (RE) AND THE FRICTION FACTOR FOR SKEWED MAIN CHANNEL ISOLATED FROM FLOOD PLAIN .

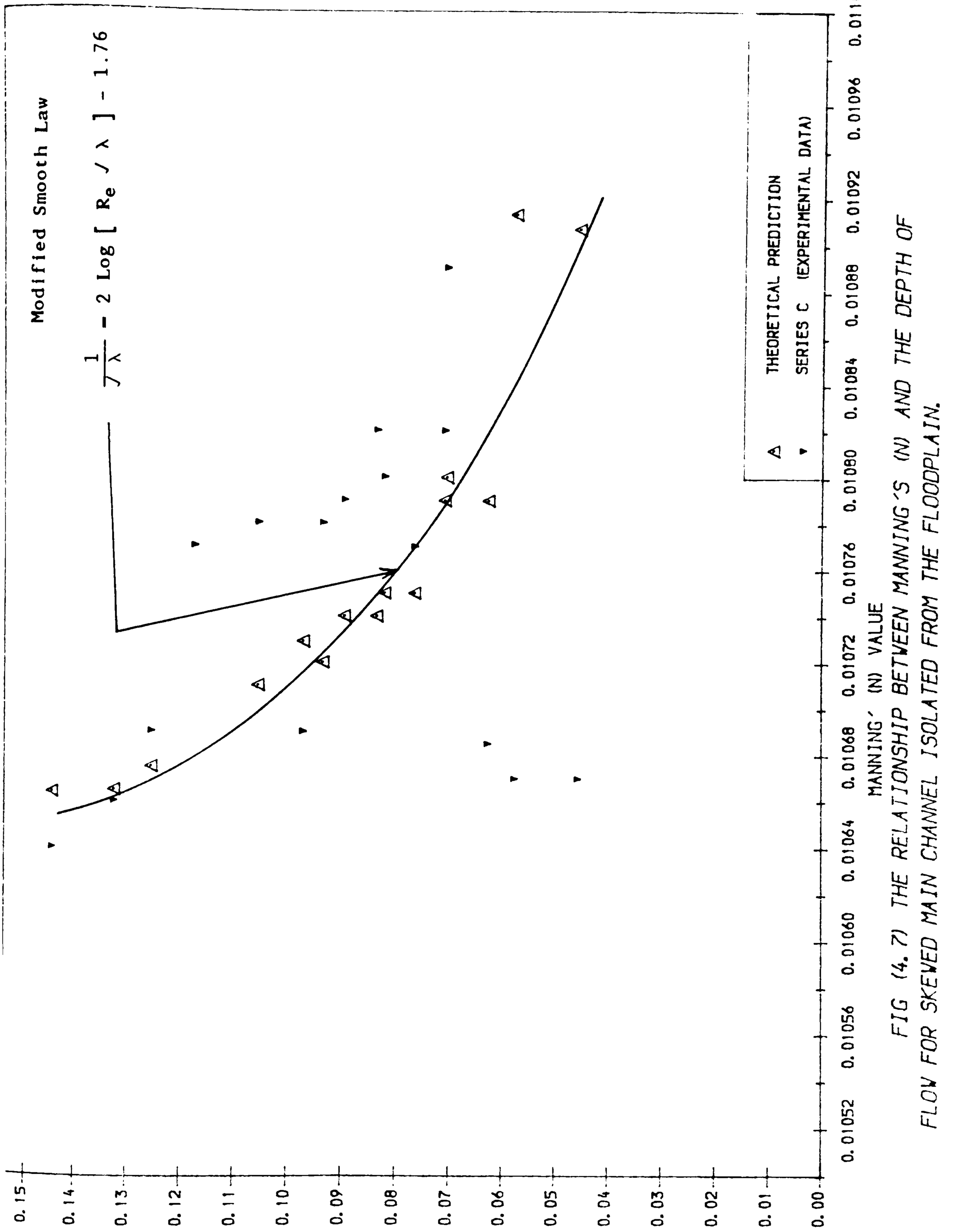

FIG (4.7) THE RELATIONSHIP BETWEEN MANNING'S (N) AND THE FLOW FOR SKEWED MAIN CHANNEL ISOLATED FROM THE FLOODPLAIN.

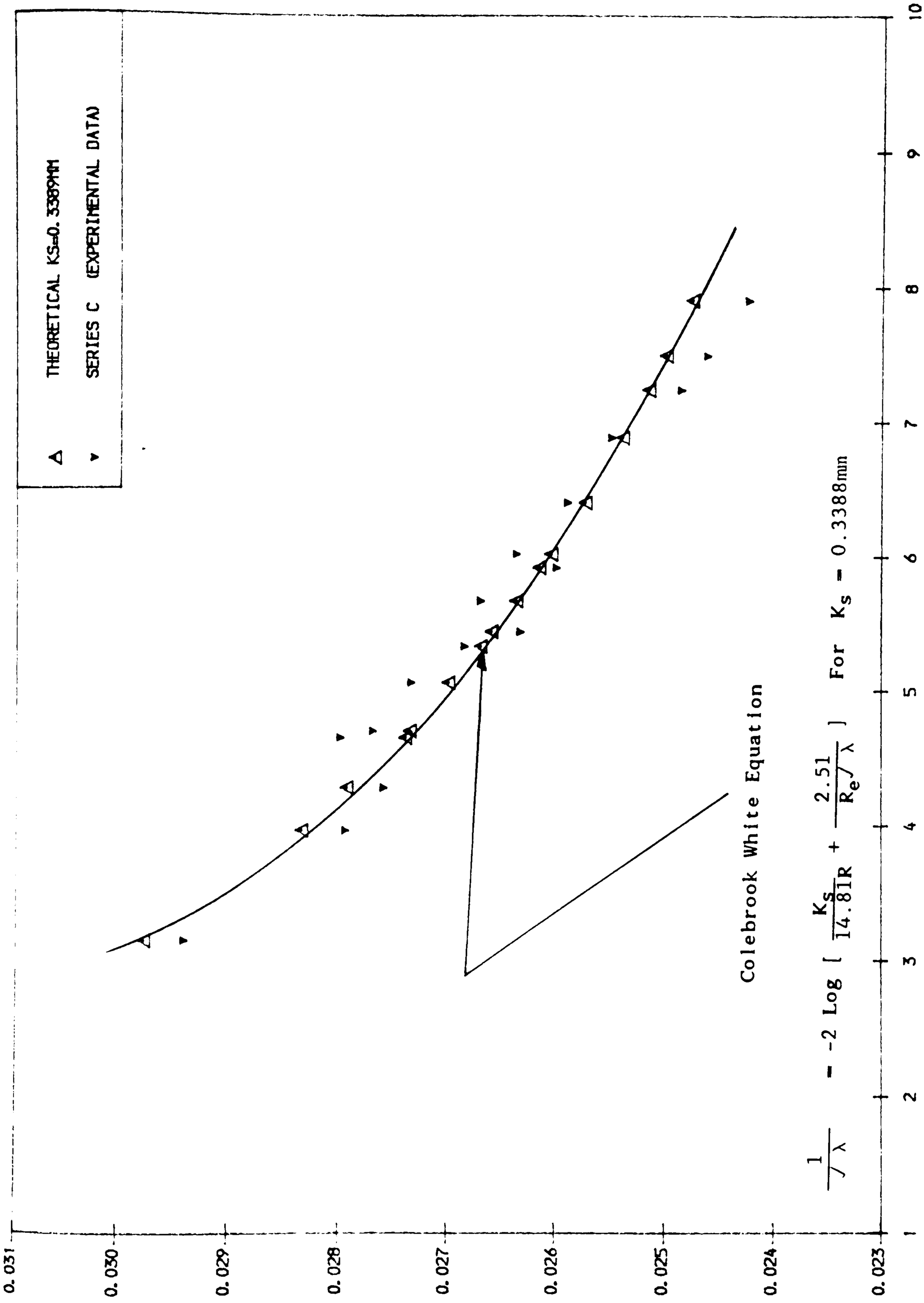

FIG (4.8) THE RELATIONSHIP BETWEEN THE

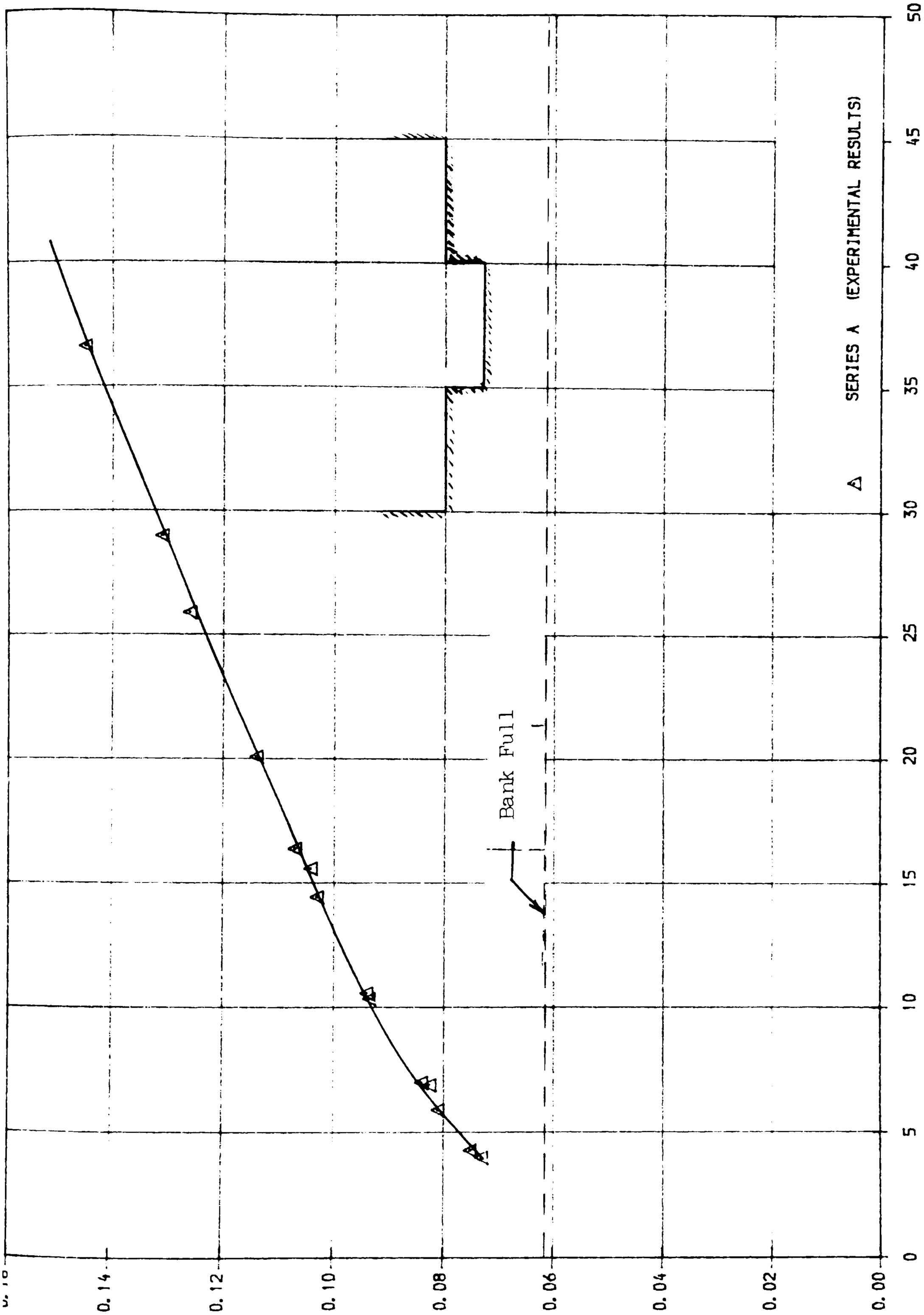

FIG (4.9) THE RELATIONSHIP OF THE EXPERIMENTAL STAGE_ DISCHARGE FOR THE SKEWED CHANNEL WITH OVERBANK FLOW .

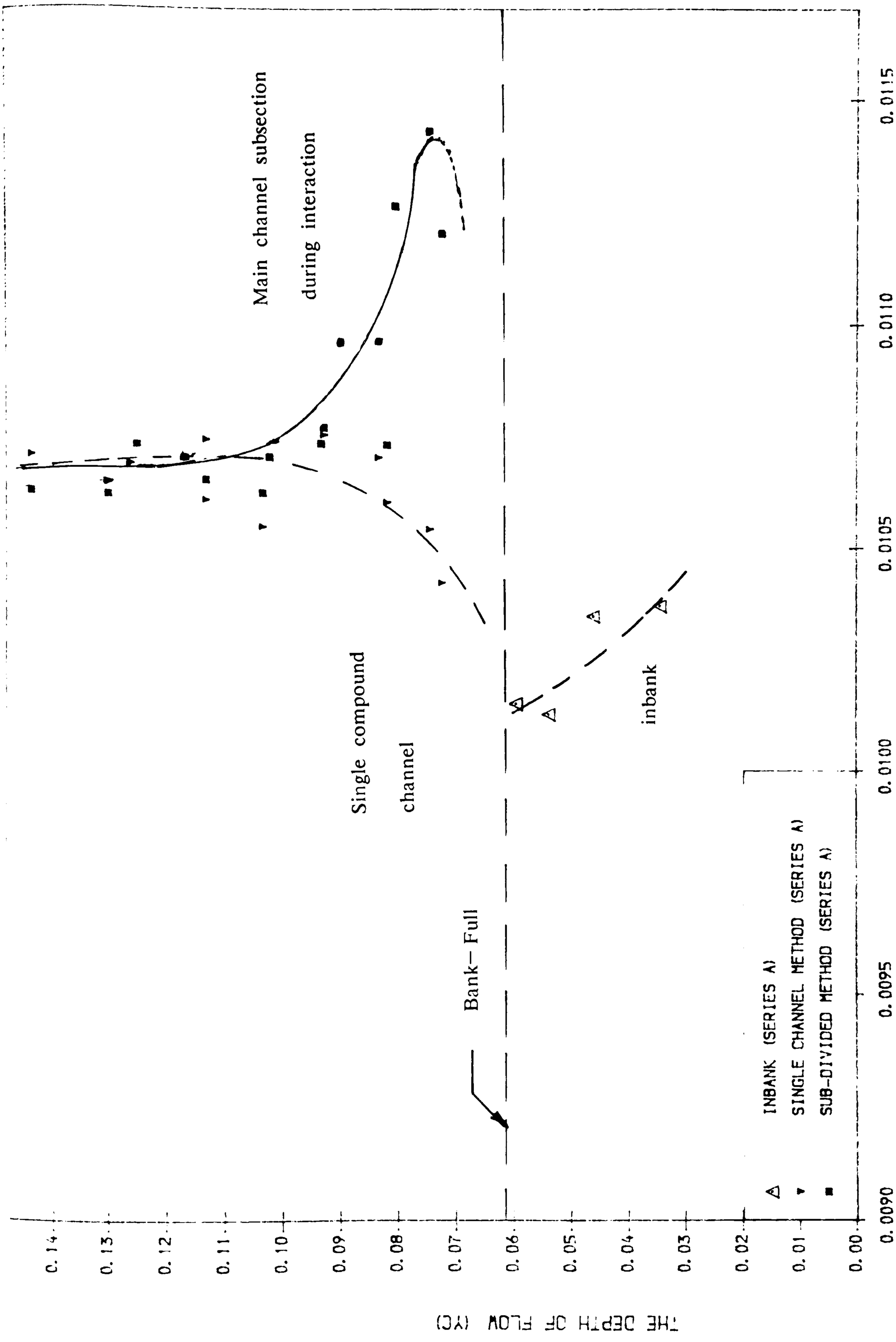

FIG 14.10 THE RELATIONSHIP BETWEEN MANNING'S (N) VALUES WITH DEPTH OF FLOW (YC).

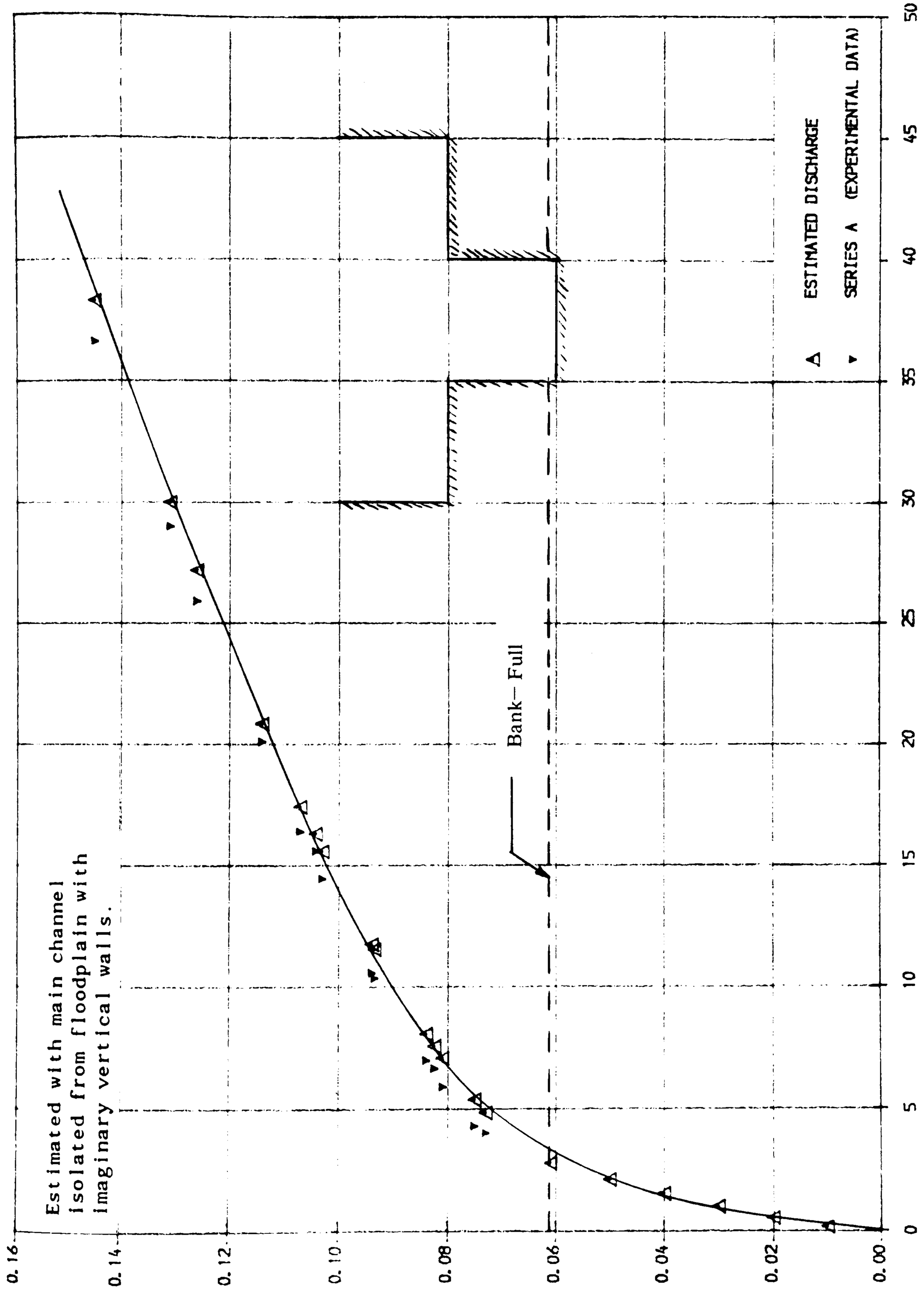

FIG (4.11) THE RELATIONSHIP BETWEEN THE ESTIMATED STAGE_DISCHARGE AND THE EXPERIMENTAL RESULTS FOR THE SKEWED CHANNEL WITH OVERBANKFLOW.

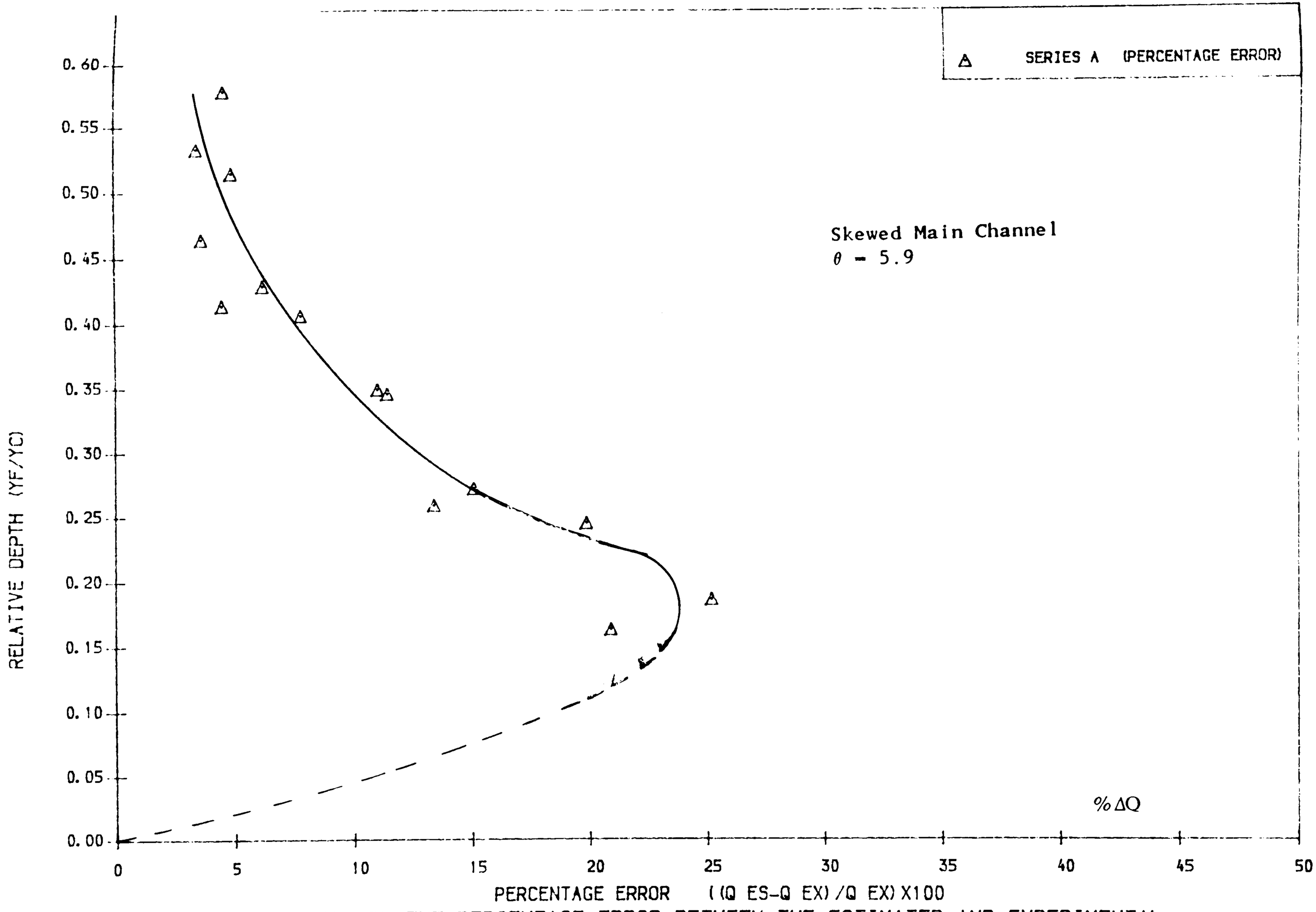

FIG (4.12) THE PERCENTAGE ERROR BETWEEN THE ESTIMATED AND EXPERIMENTAL DISCHARGE WITH THE RELATIVE DEPTH

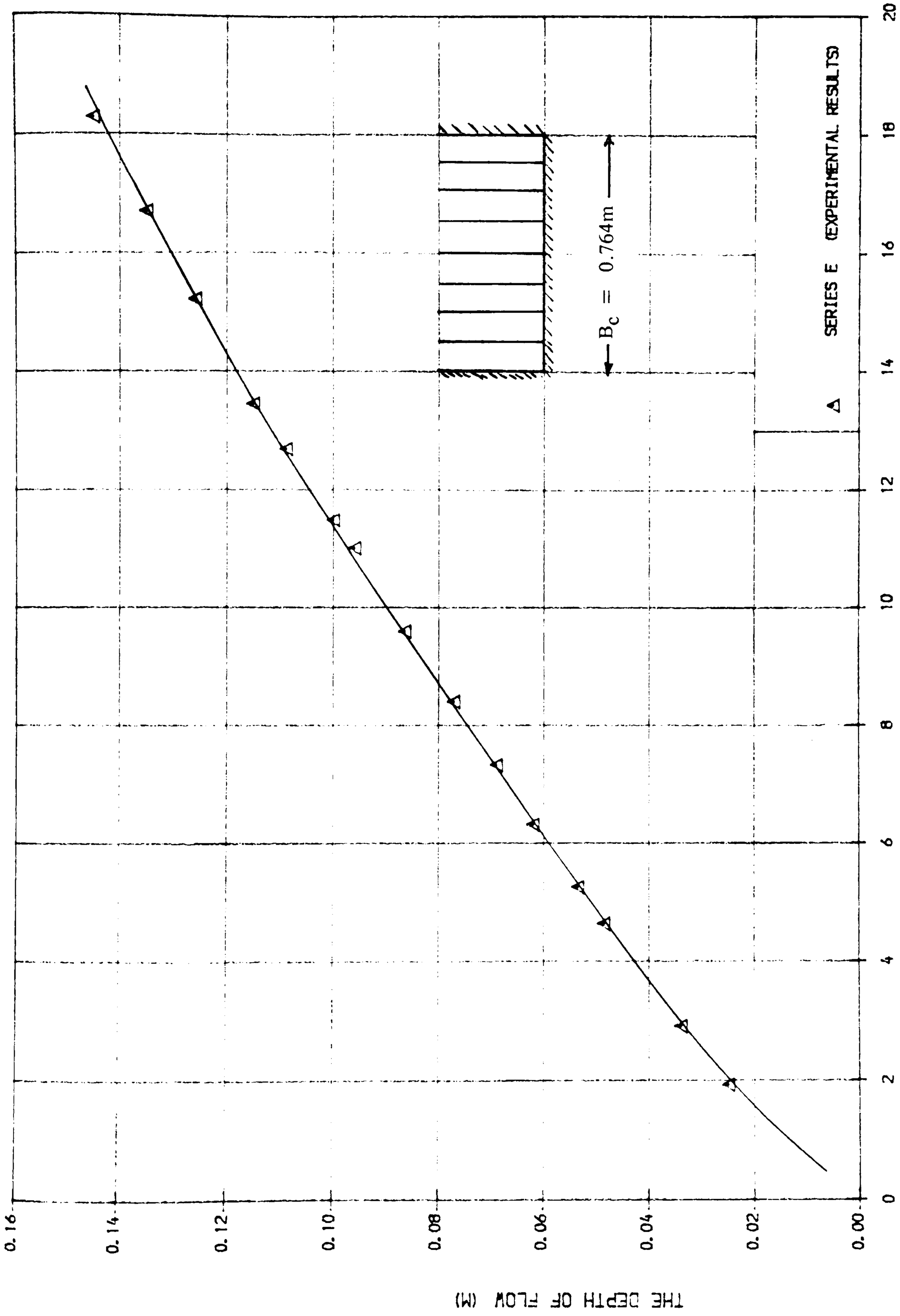

FIG (4. 13) THE EXPERIMENTAL STAGE_DISCHARGE RELATIONSHIP FOR THE ROUGH FLOODPLAIN MATERIAL USED FOR THE ROUGH FLOODPLAIN (10MM DIAM. DOWELS).

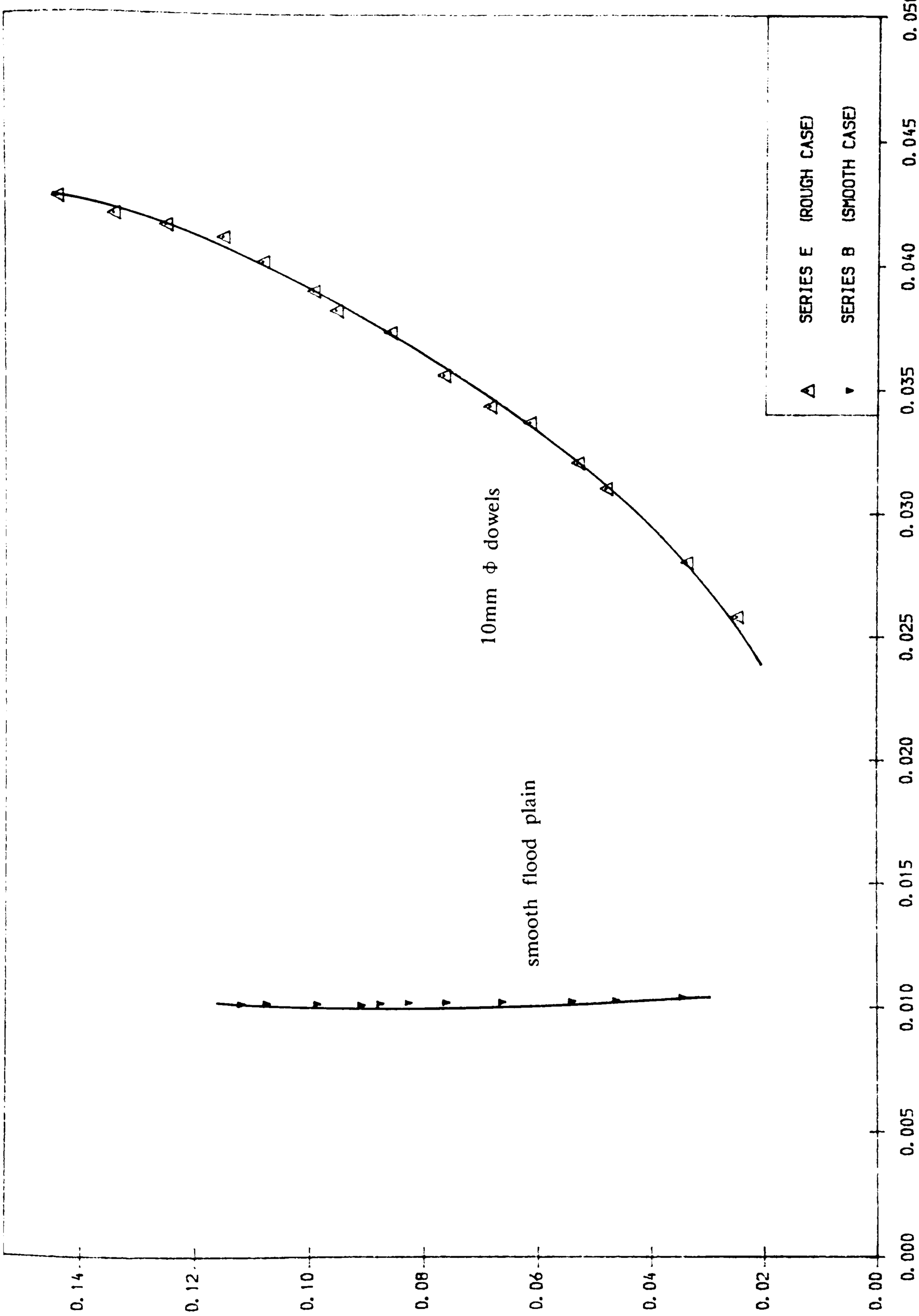

FIG (4.14) THE RELATIONSHIP BETWEEN EXPERIMENTAL MANNINGS OF FLOW FOR THE ROUGH AND SMOOTH FLOOD PLAIN.

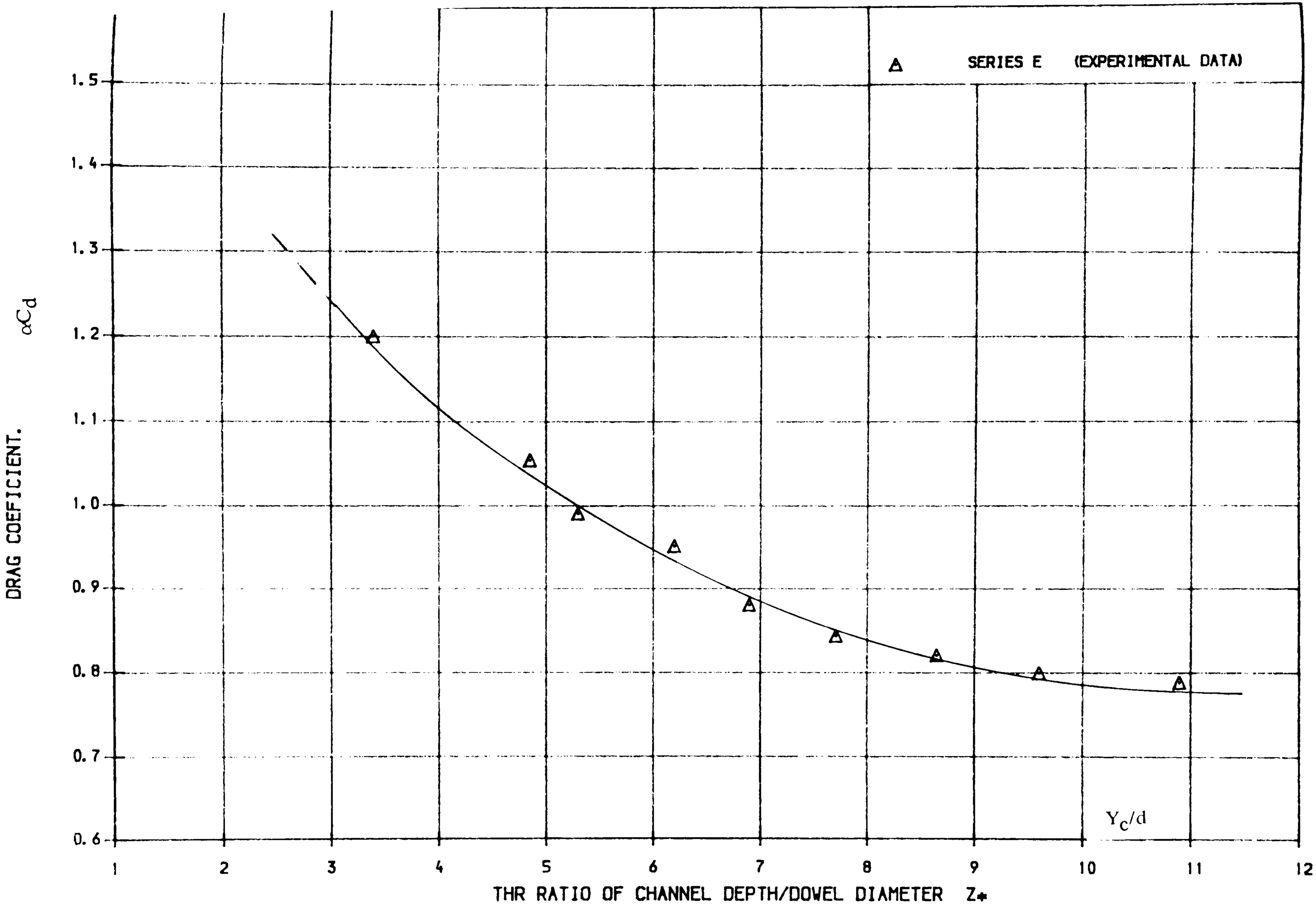

FIG (4.15) THE RELATIONSHIP BETWEEN THE (Z) AND DRAG COEFICIENT FOR VERTICAL RODS.*

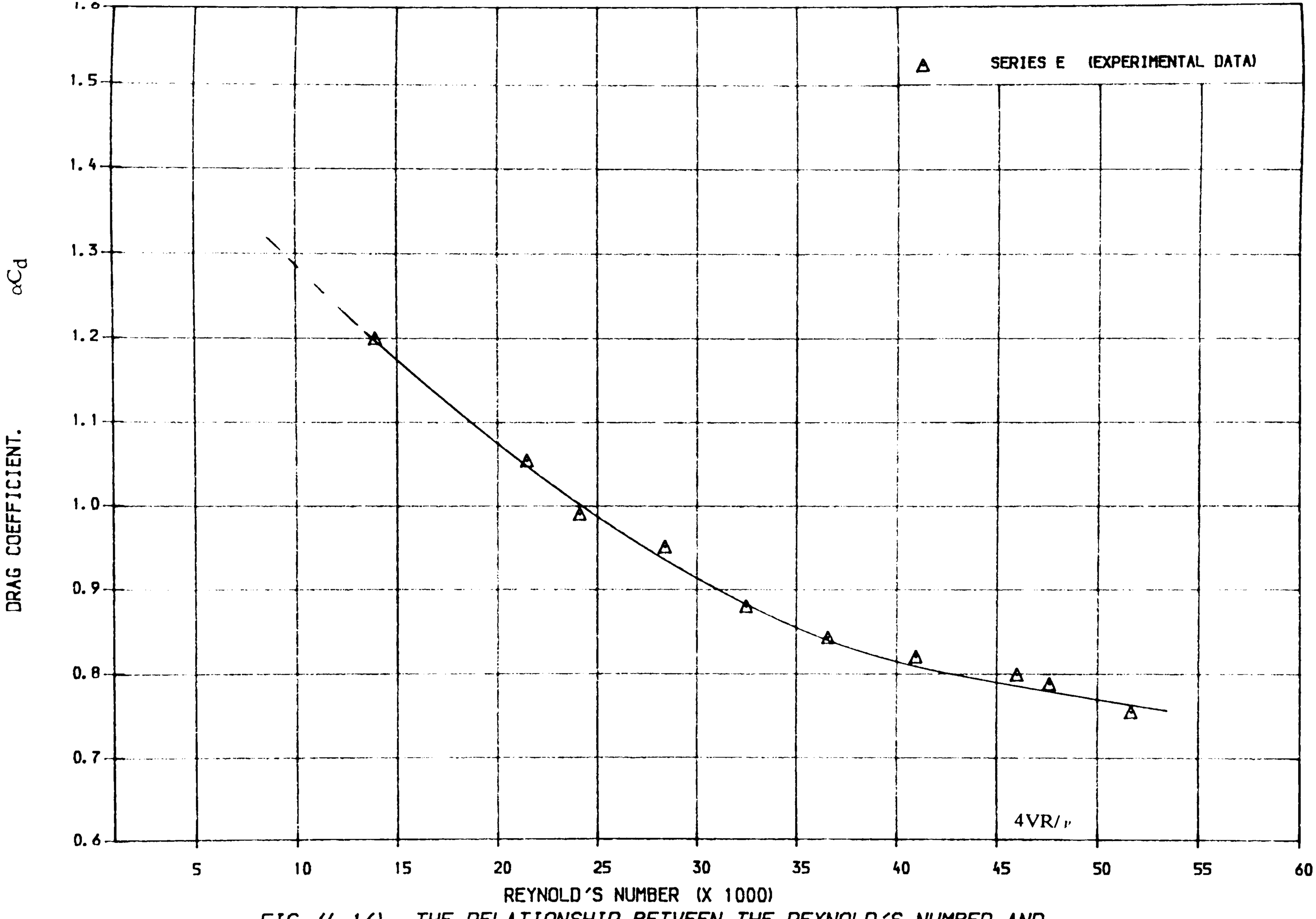

FIG (4.16) THE RELATIONSHIP BETWEEN THE REYNOLD'S NUMBER AND COEFICIENT FOR VERTICAL RODS.

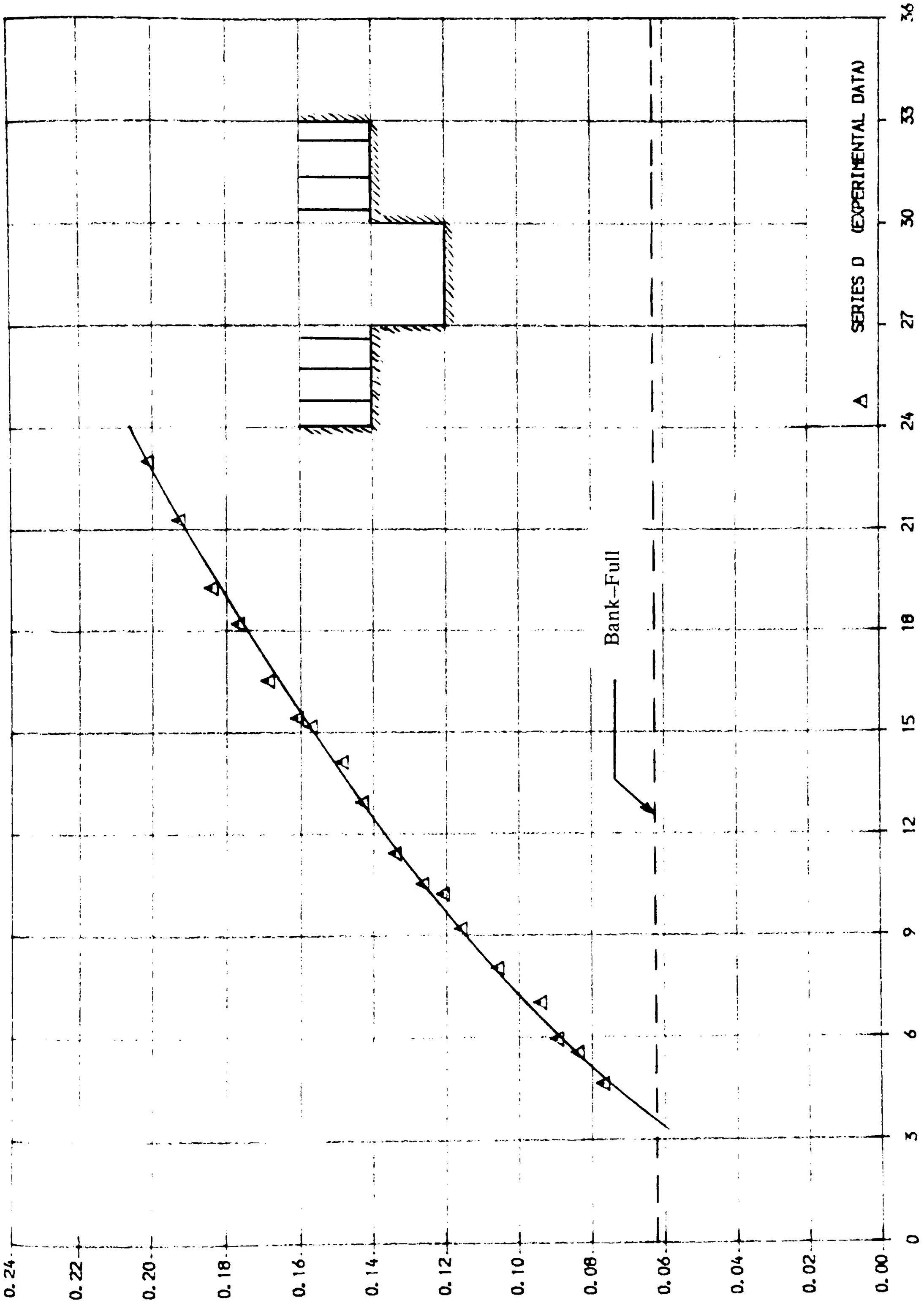

FIG (4.17) THE EXPERIMENTAL STAGE_DISCHARGE RELATIONSHIP FOR THE SKEWED CHANNEL WITH ROUGH FLOODPLAIN.

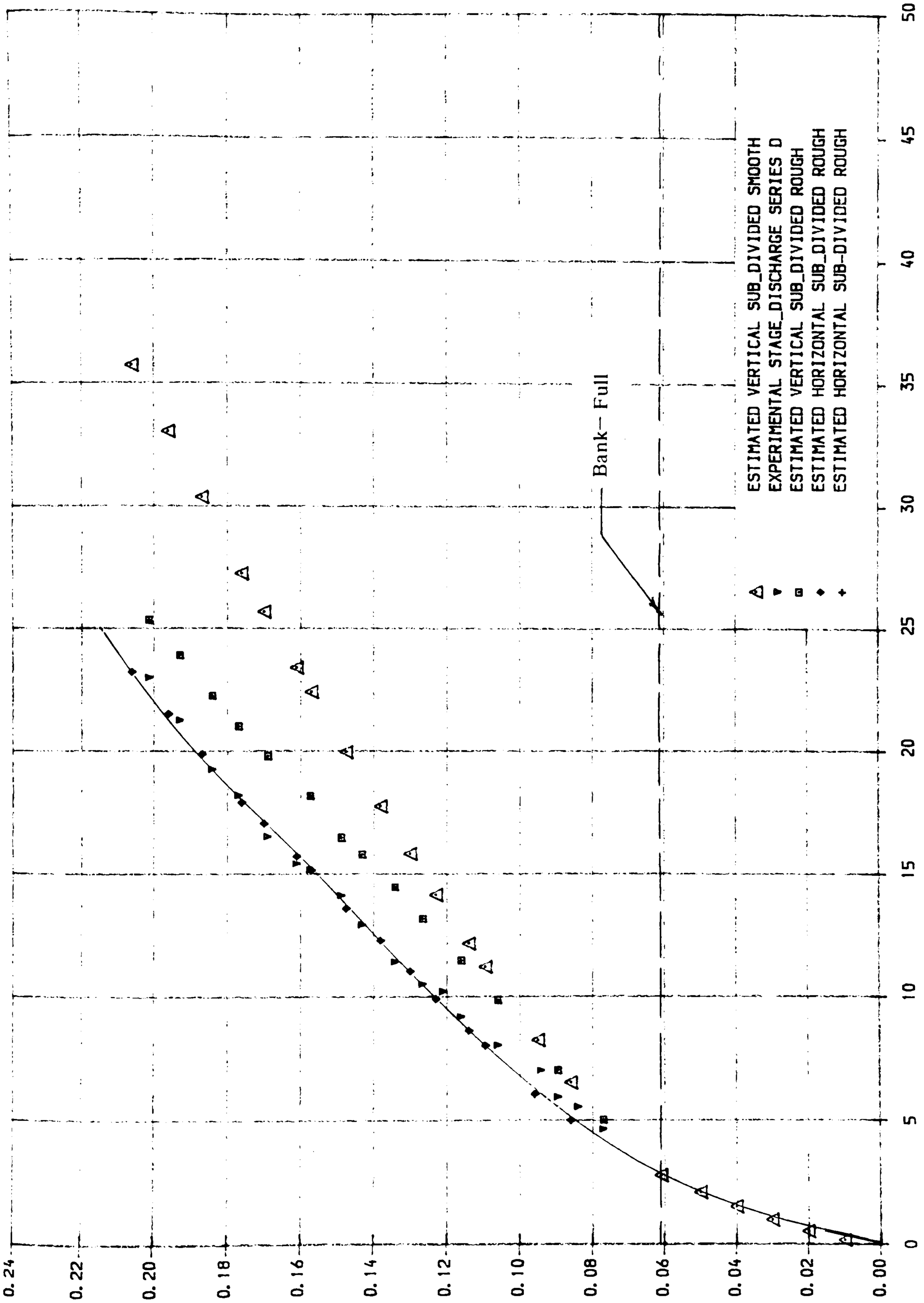

FIG(4. 18) THE ESTIMATED STAGE_DISCHARGE CURVES COMPARED WITH EXPERIMENTAL RESULTS FOR THE SKEWED MAIN CHANNEL WITH ROUGH FLOODPLAIN

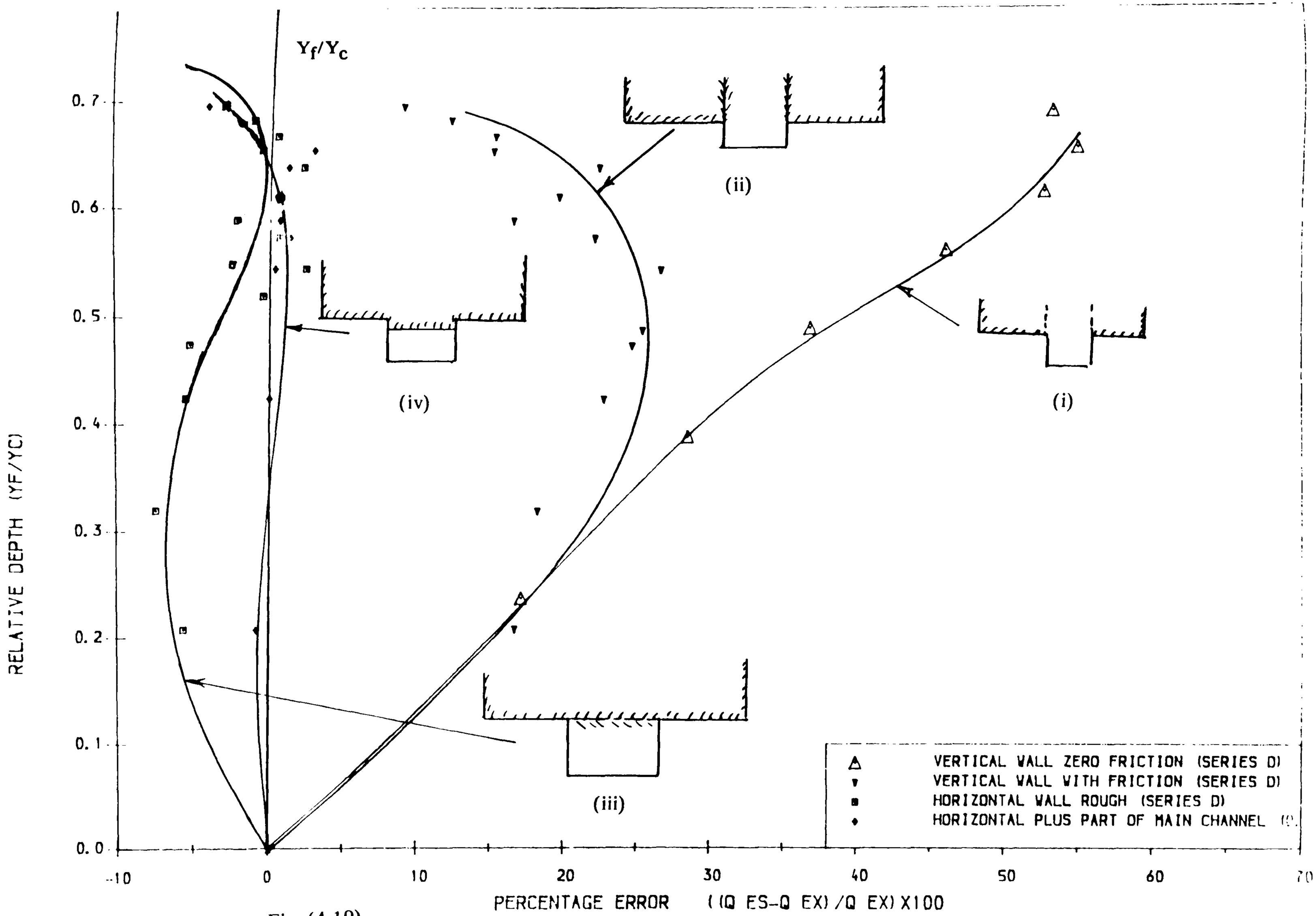

Fig (4.19) *THE PERCENTAGE ERROR BETWEEN THE ESTIMATED AND EXPERIMENTAL DISCHARGE WITH THE RELATIVE DEPTH FOR SKEWED CHANNEL WITH ROUGH FLOODPLAIN*

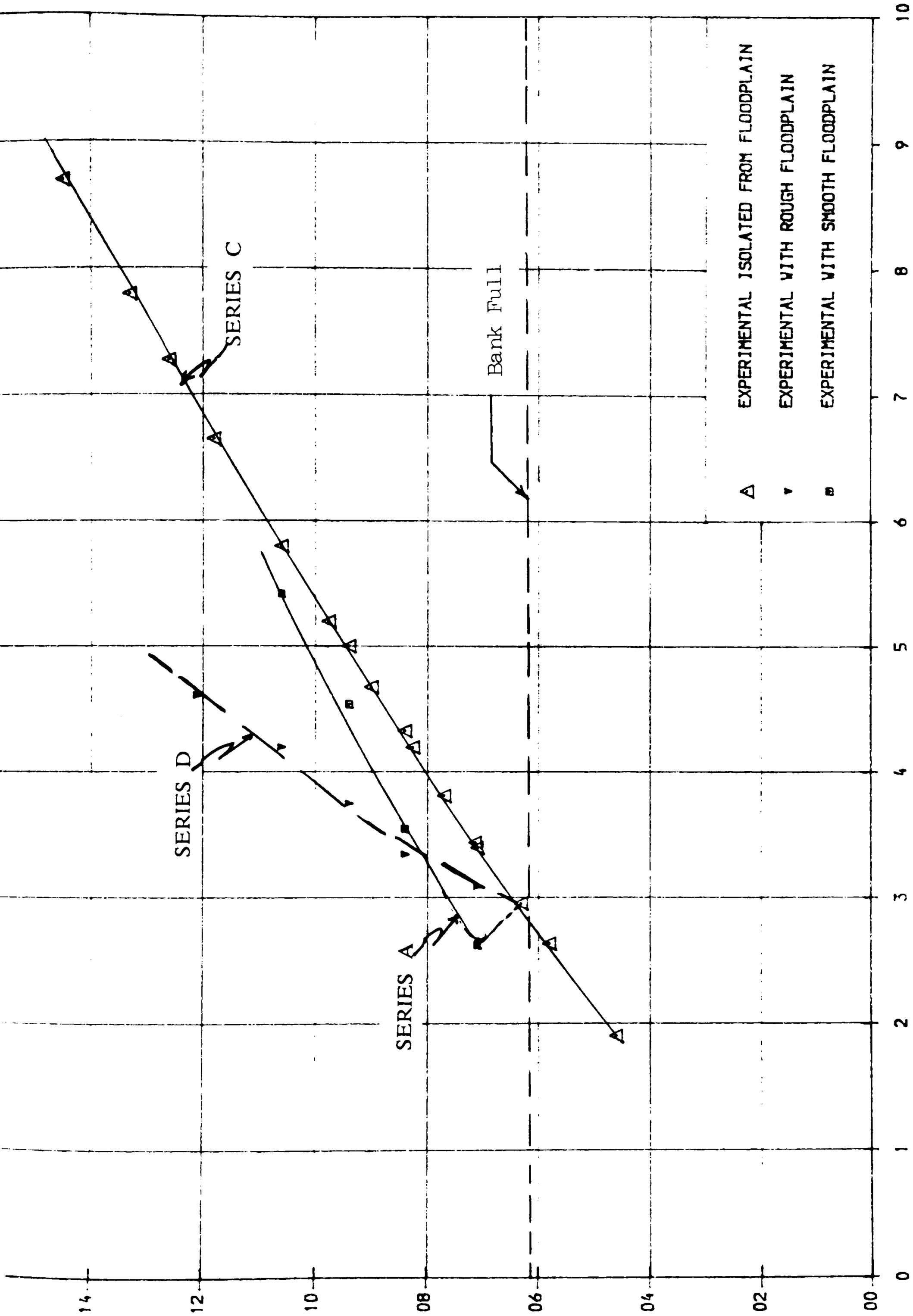

FIG (4.20) STAGE_ DISCHARGE RELATIONSHIPS FOR THE SKEWED MAIN CHANNEL ALONE.

CHAPTER 5

VELOCITY DATA FOR A SKEWED TWO-STAGE CHANNEL.

5.1 INTRODUCTION

5.2 THE PURPOSE OF THE VELOCITY MEASUREMENTS.

5.3 EXPERIMENTAL PROCEDURE.

5.4 EXPERIMENTAL RESULTS FOR SERIES A WITH SMOOTH FLOOD PLAIN

5.4.1 General Observations on Fig (5.1) to Fig (5.18).

5.4.2 General Observations on Transverse Velocities.

5.4.3 Observations on Flow Development Along the Flume Length.

5.4.4 The Effect of Increasing Relative Depth.

5.5 EXPERIMENTAL RESULTS FOR SERIES D WITH ROUGH FLOODPLAIN.

5.5.1 General Observation on Figures 5.19 to 5.33.

5.5.2 General Observation on Transverse Velocities (SERIES E)

5.5.3 Observations on Flow Development along the Flume Length.

5.6 VELOCITY DATA FOR THE SKEWED MAIN CHANNEL ALONE ISOLATED FROM FLOOD PLAIN FLOWS.

5.7 CONCLUSIONS.

CHAPTER 5

VELOCITY DATA FOR A SKEWED TWO–STAGE CHANNEL.

5.1 INTRODUCTION

Chapter 5 reports on the velocity measurements carried out in the skewed channel/floodplain flume. The purpose of the detailed velocity measurements was primarily to establish the mechanisms of flow in a compound section when the main channel is skewed in the direction of the flood plain. Other reasons for the velocity measurements, was to provide data for two–dimensional numerical models such as that produced by Wark (1988); to provide accurate values of the discharge carried within each sub–section of the compound flow, and to provide estimates of momentum transfer from one sub–section to the other.

This chapter provides information on two components of mean velocity, namely, the longitudinal velocity in the x–direction, and the transverse component, normal to the main channel walls, in the z–direction. The experimental procedure has been outlined in chapter 3, with longitudinal velocity components measured by a Pitot static tube connected to an ultra–low head pressure transducer. Transverse components of velocity were determined by the angular measurement transducer linked with a micro computer, measuring the angle of the maximum velocity filament θ. Knowing the longitudinal velocity component and the angle θ, then a transverse velocity component could be calculated. This procedure has been adopted by the Series B SERC flume programme at Wallingford as being the least expensive and least time consuming method.

Chapter 5 reports on three series of tests which were carried out to obtain the velocity profiles through skewed main channel with flood plain. The first set was SERIES A, carried out to investigate the velocity distribution for a skewed main channel with smooth flood plain. Six experiments were conducted in this series. The second set of experiments was SERIES D, carried out to investigate skewed main channel with rough flood plain area. Five experiments were conducted in this set. Finally, the third set of experiments was SERIES C,

carried out to investigate the velocity distribution for the skewed main channel isolated from the flood plain area. Four experiments were conducted in this set to obtain the velocity profiles.

Another feature of the velocity data, concerns the development of longitudinal and transverse velocities along the length of the flume. To achieve this purpose, velocity measurements were taken at three cross sections along the flume length. The symmetrical section (or section 1) was set at 4.5 m downstream from the entrance of the main flume, asymmetrical section (or section 2) set at 5.5m downstream from flume entrance, and finally asymmetrical section (or section 3) was set at 6.5m downstream from the flume entrance. The point velocity and angular measurements were measured at grid points for these cross sections as shown in Fig (3.21).

5.2 THE PURPOSE OF THE VELOCITY MEASUREMENTS

There are several reasons for producing an accurate data set of 2− dimensional velocity components, such as produced within this thesis. The reasons are listed below in no particular order of priority.

(1) For testing and calibration of two− dimensional numerical river models. This is an area of recent sudden expansion of interest especially in the field of rivers and estuaries. In terms of compound channel shapes, 2− D modelling has been attempted with some success by Samuels (1988) and Rodi and Keller (1988). This process is being continued by Wark using a finite element scheme.

1− D modelling of compound sections has been attempted successfully by Wark (1988), but the computational model is not applicable to skewed or meandering compound sections. The 1− D dynamic equation is for steady, uniform flow and is given by the expansion;

$$B\,\lambda\,\frac{u^2}{8h} + g\,\frac{dh}{dx} = \frac{d}{dy}\left(\epsilon_h\,\frac{du}{dy}\right) \qquad (5.1)$$

where u is the depth–averaged velocity, h the flow depth, y the lateral direction, λ the friction factor, ϵ_h the lateral turbulent eddy viscosity, and B an areal factor for transverse slopes.

Equation 5.1 is not applicable to skewed channel/flood plain systems for three reasons:–

(a) It excludes the convective term u du/dx, which is not a good assumption for skewed flows were the flood plain flow decelerated on "crossing over" the main channel flow area. This is demonstrated clearly in chapter 6.

(b) It excludes the term v du/dy, assuming zero transverse velocity components, which is not the case for skewed channels.

(c) It excludes horizontal turbulent shear and includes only lateral co–flowing shear in the term ϵ_h. Horizontal shear occurs where the flood plain flow shears over the skewed main channel flow beneath.

To this end, a skewed flow system can be modelled much better with a 2–D model, thus requiring velocity measurements in 2 directions simultaneously, at any point in the flow.

(2) Velocity measurements are useful in determining the conveyance in each sub–section of a skewed compound cross section. The velocity components are integrated over each sub–sectional area to obtain the discharge distribution. This information has great practical usefulness as it will allow a critical comparison with current methods of discharge assessment.

These include division line methods already discussed in chapter 4, where imaginary vertical, diagonal or horizontal lines are used to sub–divide the cross–section, and where the discharge is computed in each sub–section and then summed. Discharge assessment methods also include correction factor methods such as the Radojkovic indices (1975) which provide correction factors for the main channel (Φ_c) and flood plains (Φ_f) to give better estimates of the total compound section flow.

In a sense detailed velocity measurements with depth can be plotted on semi–logarithmic paper to determine an estimate of the boundary shear stress, even though the boundary shear stress has not been measured by Preston tube. Detailed estimates of boundary shear will thus allow force balances to be carried out at each sub–section for the cross–section, and will give estimates of the apparent shear force. This approach has not been used in this thesis.

(3) Perhaps the most important rational for velocity measurements in this thesis, is simply to obtain a physical appreciation of flow mechanisms in the compound skewed situation. The following areas will be investigated:–

(A) Flow development in the longitudinal x direction

– the development of longitudinal velocity on the right (narrowing) flood plain, the left (widening) floodplain, and also along the main skewed channel.

– the development of transverse velocities (secondary currents) along the main skewed channel.

– development of the position of the maximum velocity filament in the longitudinal direction.

– development of the widths of the shear layers formed at the main channel/flood plain junctions.

(B) Flow characteristics at a given cross section. This will include investigation into:–

– the relative longitudinal velocity magnitudes in each sub–section of the flow
– the position of the maximum velocity filament (longitudinal)
– the width of the lateral shear layers.
– the steepness of the lateral shear layers. (this is a measure of the lateral turbulent shear stress, as $\tau \alpha (du/dy)^2$.

– the distribution and magnitude of the transverse velocity components. u_y. This is an important exercise and it will determine in Chapter 7 if secondary flows in the main channel are driven directly by flood plain flow "crossing over".

– the steepness of the horizontal shear layers. (This is a measure of the horizontal turbulent shear stress as $\tau \propto (du/dz)^2$

(C) Flow development with increasing flow depth.

This area will simply investigate the influence of increasing the relative depth of flow (Y_f/Y_c) on the position and magnitude of longitudinal velocities as well as the variation of transverse recirculation velocities with increasing relative flow depth.

(D) Flow characteristics with increasing floodplain roughness.

All the flow characterstics noted above in (A)(B) and (C) will be investigated for both a smooth boundary flood plain as well as a flood plain covered in vertical roughening rods. The difference in flow behaviour between smooth and rough flood plain cases will be investigated in detail.

5.3 EXPERIMENTAL PROCEDURE

With six relative depths tested in Series A, five relative depths tested in Series E, four relative depths in Series C, and with three cross sections tested in each run, then a total of 45 cross–sections were investigated for SERIES A, SERIES E and SERIES C. The experimental procedure adopted for each test has been described in Chapter 3. A Pitot static tube was placed into the flow at known positions through out the cross sectional area of the channel and flood plain flow to give a velocity transverse U(y, z) as shown in Fig (3.1).

After obtaining all the transverse velocity measurements in the y– z cross–section, the Pitot static tube was moved by instrument carriage to the next cross section downstream. The point velocity measurements were recorded and stored on Pc computer. Then the Pitot static tube was removed and replaced by the angular measurement device to measure the direction of the maximum velocity filament of stream flow at the same position of Pitot static tube reading. The same procedures were used to record and store the angular measurement readings. A brief explanation of these tests is now given.

1. After each test run all of the results were entered and stored on the mainframe computer.

2. A computer program was written which would give a visualisation of the flow distribution for skewed main channel with flood plain interaction. It displays the results in three forms:

a) contours of the longitudinal velocity for both the skewed main channel and flood plain area over a complete cross–section of the flow.

b) the longitudinal depth– average velocity profiles across the channel/flood plain section in plan view.

c) the transverse recirculating velocity components normal to skewed main channel, at various vertical sections across the main channel width.

3. Another computer program was written to integrate the point velocities to find the overall discharge. This was checked against the overall discharge obtained from the orifice plate readings.

5.4 EXPERIMENTAL RESULTS FOR SERIES A WITH SMOOTH FLOOD PLAIN.

Six relative depths of flow were tested in detail for longitudinal and transverse velocities. These ranged from $Y_f/Y_c = 0.15$ to $Y_f/Y_c = 0.4$ covering a large part of the range for two– stage channels. The results are presented graphically in Fig (5.1) to Fig (5.18), inclusive, representing three cross– sections along the flume length, and the six relative depths tested. In each case the results are presented in the form of longitudinal velocity contours over the cross section, depth– averaged longitudinal velocity in plan– view, as well as transverse velocity components in the main channel only. The graphs are presented in groups of three, each group representing one relative depth but at three different positions along the flume length.

5.4.1 General Observations on Fig (5.1) to Fig (5.18).

Observation of the contours of longitudinal velocity reveals the maximum velocity filament to be either at the left wall of the skewed main channel or, at higher relative depths, on the left side flood plain (the flood plain which is becoming wider in the downstream section). Both these observations are true, even at the point of symmetry, which is half– way along the flume and has equal

flood plain widths on either side of the skewed main channel. This observation has also been confirmed by Elliot (1990) and is remarkable in the sense that it indicates substantial momentum transfer from the narrowing right side flood plain to the widening left side flood plain. Alternatively, it might indicate momentum transfer from the main channel alone to the left– side flood plain.

– Observation of the longitudinal depth averaged velocities reveals that in almost every case the mean velocity on the right side flood plain is substantially less than the left side flood plain, despite the fact that both flood plains have identical boundary material. This phenomena is not so much the case for very high relative depths around $Y_f/Y_c = 0.4$. Again this denotes right to left momentum transfer.

– The lateral shear layers are almost non– existent on the right side flood plains but very substantial on the left side flood plain. This is seen clearly in Fig (5.2), Fig (5.3), Fig (5.4), etc on the graph showing longitudinal depth– averaged velocity. The right side shear layer is usually contained within the main channel and often does not protrude onto the flood plain at all.
The steepness of the right– side turbulent shear layer implies large lateral turbulent in that region but not necessarily on the right side flood plain. On the left side flood plain the shear layer is very wide, and certainly much wider than expected for such flows.

The crudest estimates of shear layer width by Samuels (1985) reveals a width of;

$$W = 5.7\ (gHS/\lambda)^{1/4}\ \epsilon^{1/2} \qquad (5.2)$$

where ϵ is the turbulent eddy viscosity most crudely represented by

$$\epsilon \approx 0.16\ U_* H \qquad (5.3)$$

where U_* is the shear velocity $\surd gHS$. Estimates from Equation (5.2) above

reveal the left side shear layer to be wider than expected, but the right side shear layer to be much narrower than expected.

– Of course, the presence of ANY shear layers on the depth–averaged velocity graph shows that lateral shear between main channel and floodplain exists, and is apparent in these results up to a depth of 84mm which is a relative depth just under 0.3. For straight/parallel compound sections, lateral shear layers are apparent to greater relative depths around 0.4 to 0.5. This means that co–flowing shear, in the classical sense, is still evident in skewed meandering channels, although probably diminished in intensity. Momentum transfer seems most marked between the main channel and left flood plain.

– For large relative flow depths the mean velocity in the main channel can be less than the adjacent flood plains, implying the main channel is having a retarding effect on the flood plains rather than the other way round.

The points above can be summarised by the depth–averaged velocity sketch below for skewed compound sections.

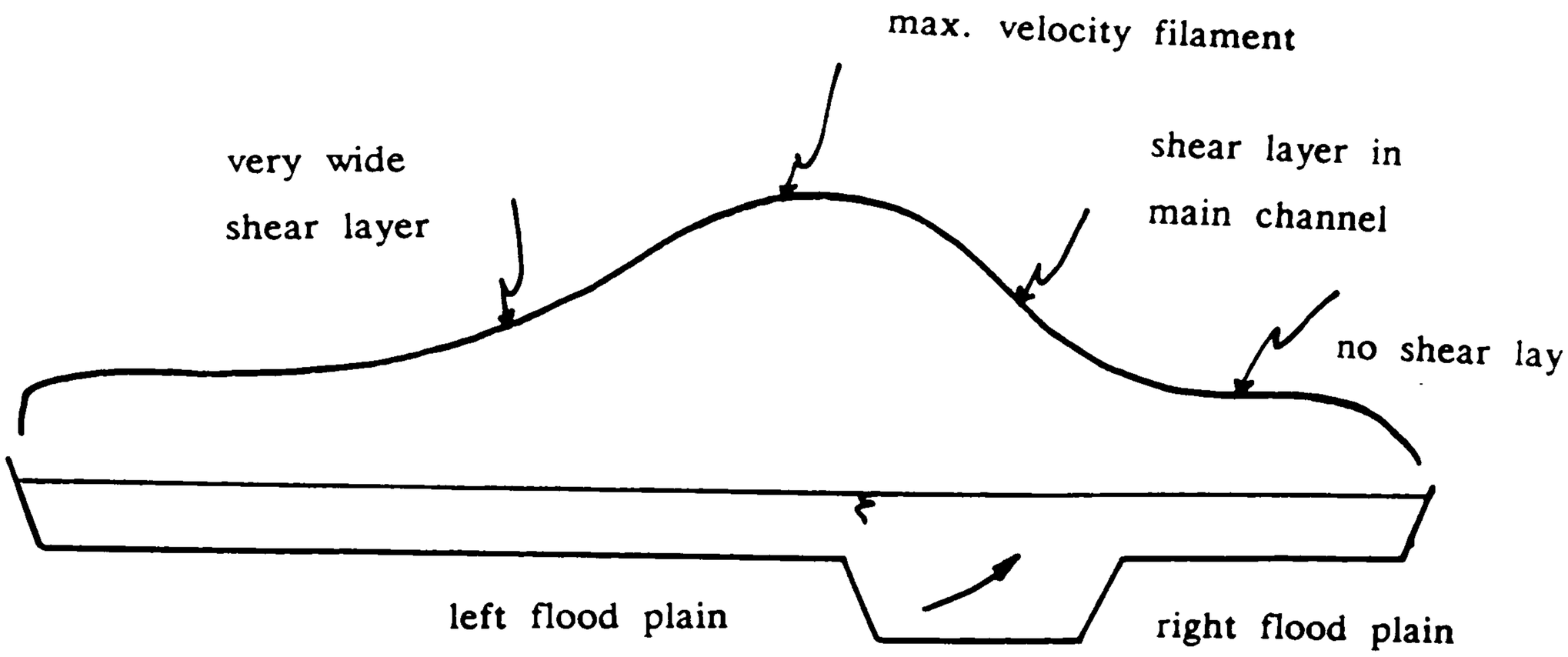

Depth averaged velocity

5.4.2 General Observations on Transverse Velocities.

By making the point measurements of flow angle as well as of longitudinal velocity in the main channel at three sections along the channel geometry, it is possible to construct a detailed picture of the transverse velocity components. The lower half of Fig (5.1) to Fig (5.18) represents the transverse velocity components normal to skewed main channel, showing quite clearly a large recirculation region.

It is interesting that all of the recirculation identified appears to rotate in one direction, that is anti–clockwise in the direction of the flow and in the same direction as might be suggested for flood plain flow passing over the top of the skewed main channel below. In the absence of any upstream bend of any consequence it might be concluded that this recirculation is primarily due to flood plain flow shearing over the main channel, although an element of secondary circulation will be present for a straight channel with overbank flow in any case.

– The recirculation appears to have the form of a single cell.

Only four vertical sections were measured within the main channel, thus not being detailed enough to pick up smaller cells of circulation. The single cell idea, however, is consistent with the aspect ratio of the main channel, which is only 2.5. Most of the literature on secondary cells driven by the step–down in a channel bed, suggest circulation lengths of the order of 6 times bank–full depth which is significantly greater than the Glasgow flume. This is sketched below for a very wide main channel.

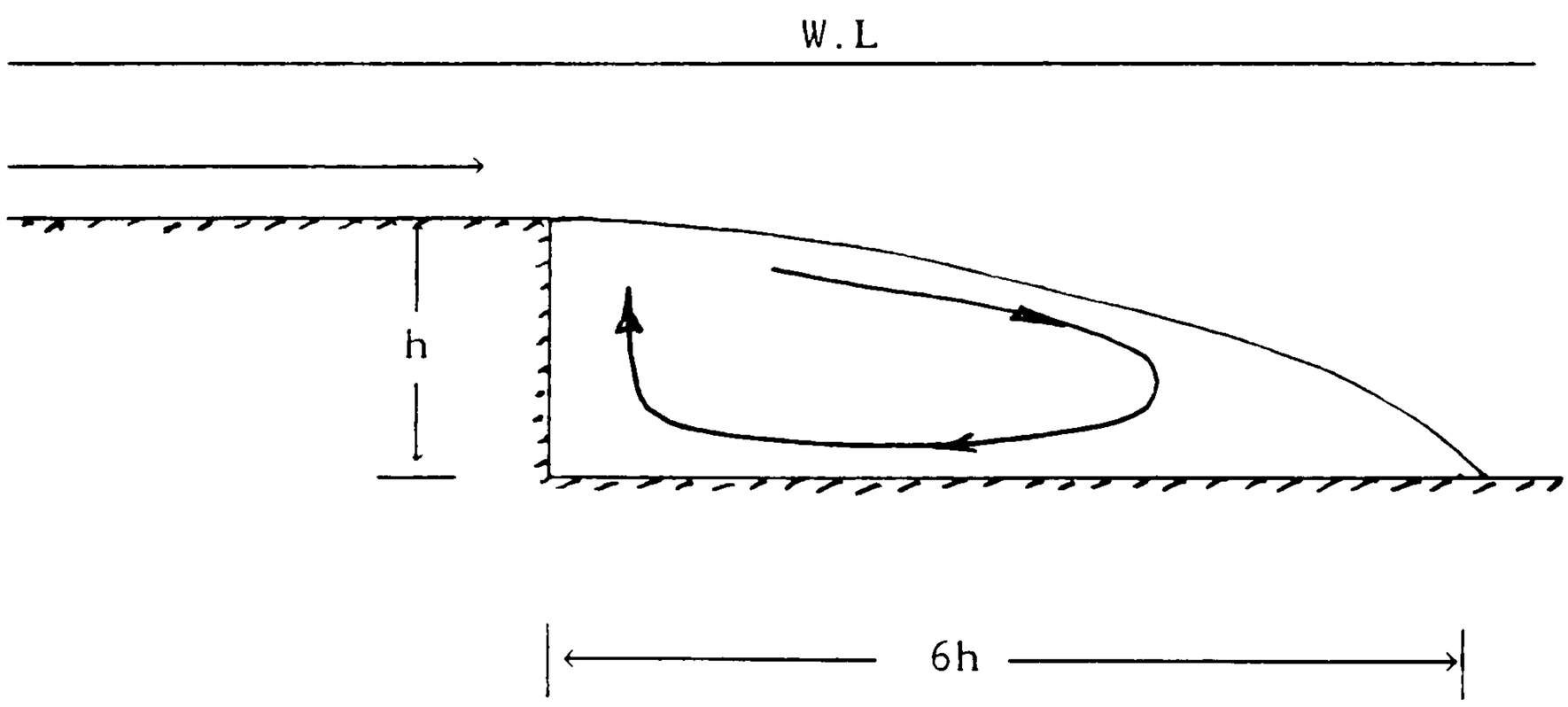

– It should be noted at this stage that the upper part of the transverse velocity graphs, above bank full level, simply represents the component of flow normal to the main channel walls and will register a strong value even if the streamlines are simply moving straight down the flume as sketched below.

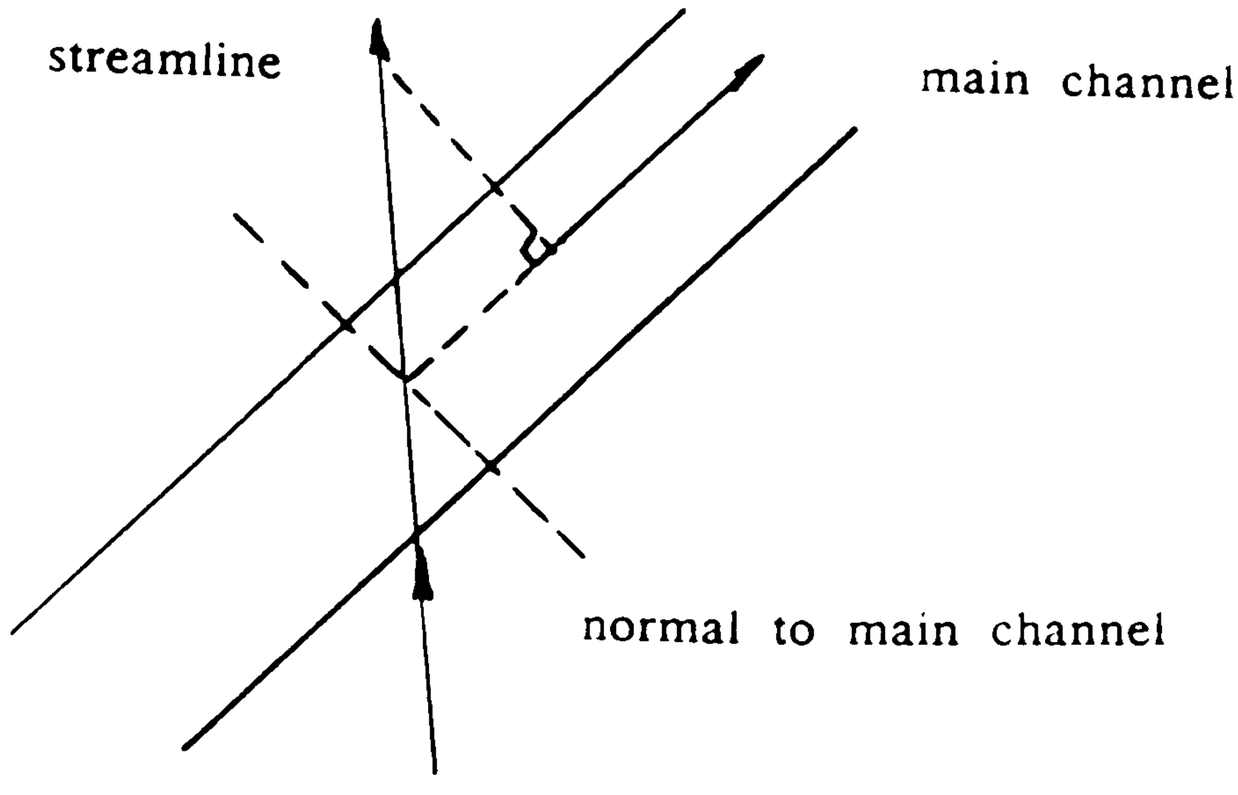

From the sketch above, the component xy will be registered as the transverse velocity above full– bank level.

– Our main interest concerns the recirculation region below bank– full level. Confining our attention meantime to the positive values of recirculation in the lower half of the main channel acting "backwards" towards the oncoming flood plain flow direction.

Fig (5.1) to Fig (5.3) indicate a maximum backward recirculation around 0.01m/sec, when compared with a main channel longitudinal velocity of around 0.25m/sec gives a ratio of 4% for the secondary cells in a skewed main channel when the angle of skew is only 5.843^0.
Fig (5.4) to Fig (5.6) similarly give a ratio of 4% relative to the longitudinal velocity component in the main channel.

This process is continued right on to Fig (5.16) to Fig (5.18) respesenting a large relative depth, but still producing substantial secondary currents with the ratio of backward recirculating velocity to longitudinal component velocity around $3 \longrightarrow 4\%$.

These values will be analysed further in chapter 7, but it can be noted that ratios of 4% are much higher than weak secondary currents in straight channels, and about the same value as secondary currents in a gentle river bend.

– The next fundamental question concerning floodplain flow passing over the skewed main channel asks the question, "Does all the flood plain flow approaching the main channel pass over it to emerge on the left side flood plain, or does some of it get drawn into the recirculating region and become transferred along the main channel?" The question can also be put in the form, "Is the driven recirculation in the main channel a constant helical flux or is fluid added to it and taken away from it?". The answer to these questions will not be clear until after further analysis in Chapter 7 but it is of interest to speculate that if fluid was transferred from the flood plain flow down into the main channel, then the main channel flow rate would increase in the downstream direction, which is not occurring (see section 5.4.3). Also if some of the flow from the right flood plain was not reaching the left flood plain (but being diverted down the main channel) why is the left flood plain velocity higher than that of the right?

– Above bank–full level the streamlines have a tendency to deviate towards the direction of the main channel flow, as shown in sketch below. This deviation is due to the main channel flow passing underneath. The value of θ is fixed at 5.843^0 in these experiments. Φ is the designated angle of deviation. Analysis of the transverse components of flow reveal the deviation angle to be around 1.5^0 to 2.0^0 for the lowest tested relative depth of $Y_f/Y_c = 0.15$, whereas this value of Φ tends towards zero for the largest relative depth in Fig (5.16) to Fig (5.18).

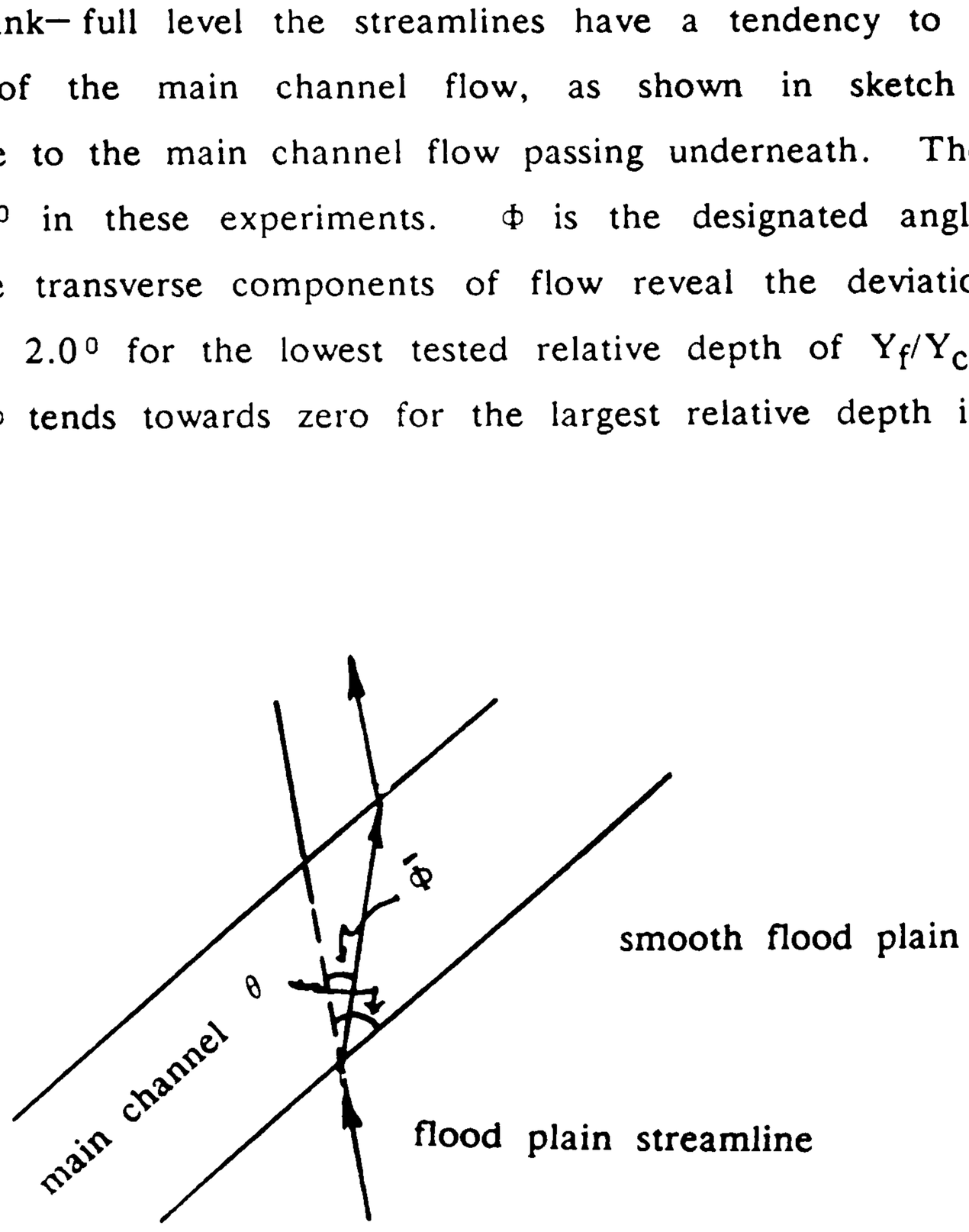

5.4.3 Observations on Flow Development Along the Flume Length.

As stated already, Fig (5.1) to Fig (5.18) are presented in groups of three, representing section 1 at the point of symmetry in the flume and sections 2 and 3, one and two metres downstream from that point respectively.

– The first observation concerning the maximum velocity filament on the velocity contour graphs is that at lower relative flow depths the maximum filament remains in a constant position around the left wall of the skewed main channel, and moves in the downstream direction. This means that it moves to the right, relative to the outer flume walls, or in other words it is dominated by the main channel flow. For larger relative depths, the maximum velocity filament moves approximately to the centre of the compound flume section implying that the influence of the main channel becomes negligible and the compound skew becomes dominated by flow above bank full level.

– Moving in the downstream direction from section 1 to section 3, the mean velocity on the right side flood plain decreases. This is true particularly for lower relative depths of flow, but not so much in evidence for the two highest relative depths tested. From the application of Bernoullis equation along a streamtube, a reduction in velocity should be accompanied by a rise in water level. Changes in water level were not observed sufficiently accurately in this experiment to comment in detail, but certainly a small increase in water level on the right flood plain would provide the additional driving head to transfer flow from right to left in the flume generally.
A reduction in right flood plain velocity implies a mass transfer of fluid from the right flood plain to the main channel.

– Moving in the downstream direction from section 1 to section 3, the mean velocity in the skewed main channel remains approximately constant, although sometimes decreasing slightly downstream. This means that any mass transfer from the right flood plain may have some effect in the main channel, but substantially must causing lateral shear transfer to the left flood plain.

– Moving in the downstream direction the mean velocity on the left flood plain tends to remain approximately constant. This is explained in the context of widening shear layers (which would tend to increase the mean velocity) and a

widening left flood plain width (which would tend to decrease the mean velocity).

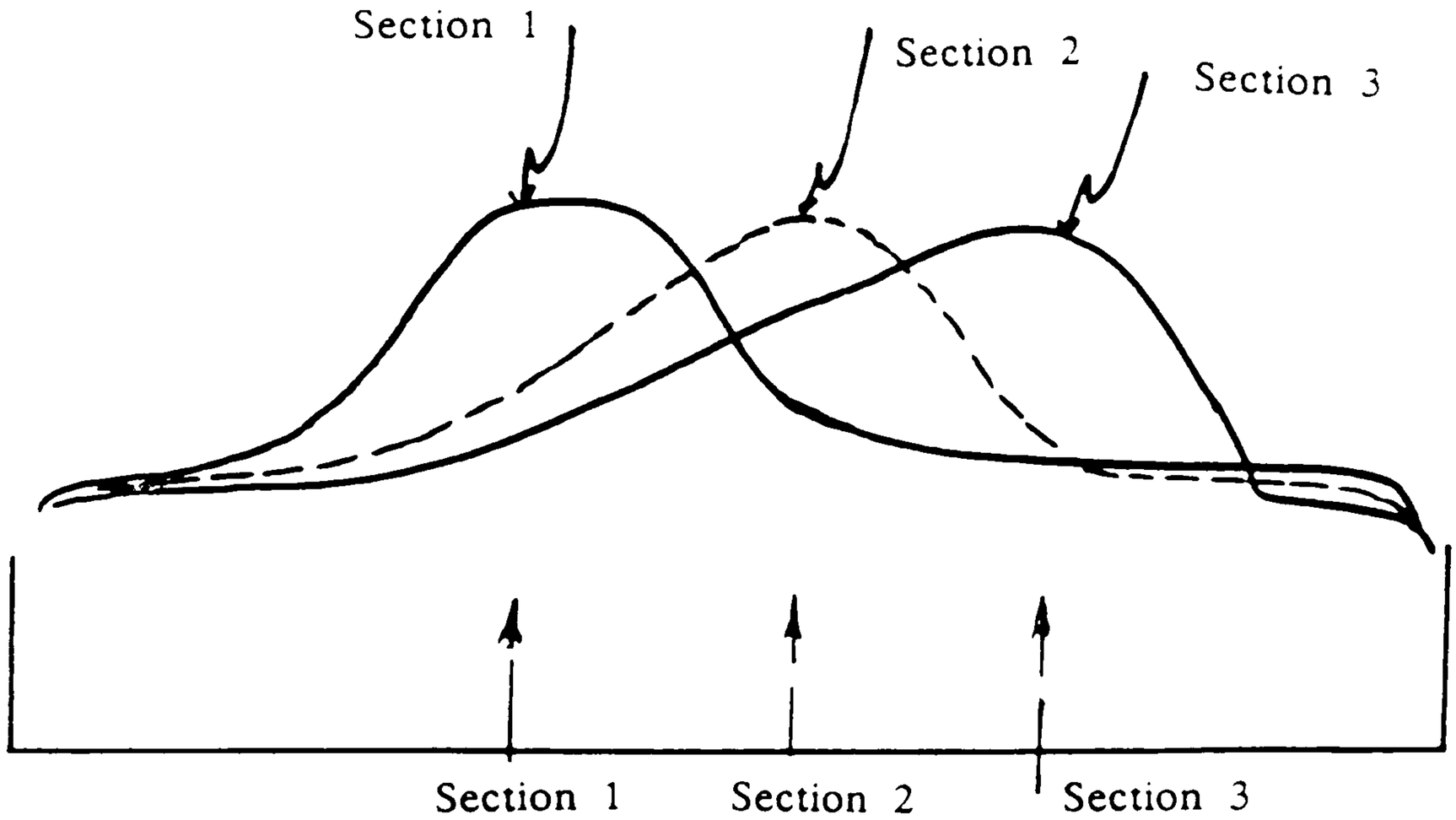

A summary of the effect of downstream movement on the depth averaged velocity is sketched above. The velocity peaks are relatively constant in position relative to the left wall of the skewed main channel and are very constant in terms of magnitude. The shear layer widths are increasing on the left flood plain in the downstream direction. The velocities on the right flood plain are lower compared with the left flood plain and are also decreasing in the downstream direction. Shear layers do not penetrate onto the right flood plain.

– Moving in the downstream direction from section 1 towards section 3, the transverse recirculating velocity components decrease in magnitude.

This can be seen by comparing Fig (5.1) to Fig (5.3). Why do these secondary cells decrease in the downstream direction? The main reason seems to be that the velocity on the right flood plain is decreasing, which in turn produces smaller cross–over velocities and smaller driven recirculation. This phenomenon is not so much in evidence at higher relative depths where the right side flood plain velocity is not decreasing in the x–direction.

5.4.4 The Effect of Increasing Relative Depth.

– An increase in flow depth reduces the difference between the velocity in the main channel and the adjacent flood plains to zero, or even negative in Fig (5.16) to Fig (5.18).

– An increase in flow depth moves the maximum longitudinal velocity filament from the centre of the skewed main channel to the centre of the flume. At section 3, for instance, this represents a left– ward movement.

– At higher relative depths the flow begins to behave as a single channel with less and less effect from the skewed main channel.

– At higher relative depths, the angle of deviation of streamlines passing over the skewed main channel tends towards zero. (0^0). i.e. the streamlines pass straight over the skewed main channel.

– Higher relative depths of flow continue to produce large recirculations in the skewed main channel with ratios of transverse to longitudinal velocities still around 3% to 4%.

5.5 EXPERIMENTAL RESULTS FOR SERIES D WITH ROUGH FLOOD PLAIN.

The vertical dowel rods used for flood plain roughening have been described in detail in Chapter 3 and 4. They are 10mm diameter, placed vertically at 100mm centres both laterally and longitudinally, and have a Manning's 'n' value which increases with flood depth in the range of 0.02 to 0.04.

Five relative flow depths have been tested in detail from a relative depth of 0.14 (Y_f/Y_c) to a relative depth of 0.5 covering the full range of two– stage channel behaviour. Relative flow depths less than 0.14 would have produced very shallow flows on the flood plain, leading possibly to laminar flow in that region. The format presentation of the results is as before, with contours of longitudinal

velocity over the cross–section, a plan view of the depth averaged velocity as well as data on the transverse velocity in the main channel. Graphs are presented in groups of three corresponding to the three cross–sections along the flume length. The total data presentation for Series D is contained within Fig (5.19) to Fig (5.33).

5.5.1 General observations on Fig (5.19) to Fig (5.33).

– In every case the maximum velocity filament is contained within the skewed main channel usually between the centre of the main channel and the left side wall. This is also true for the highest relative depth of 0.5, and is a function of high flood plain roughness which becomes relatively rougher with increasing flood plain depth. This is in contrast to the smooth flood plain case where the maximum velocity filament moves into the left (widening) flood plain.

– There is a wide discrepancy between velocities in the skewed main channel and the flood plains on either side. The ratio between main channel velocity and flood plain velocity is of the order of 2 to 3, again reflecting the differences in boundary roughness. This is even true at the highest relative depth of 0.5 (Fig (5.31) to Fig (5.33)) implying that lateral shear will be significant at such high relative depths in a skewed channel, in fact more so than the smooth flood plain case.

– Velocities on the right (narrowing) flood plain tend to be slightly less than those on the left (widening) flood plain. This is most obvious at section 3, but the effect is not nearly as significant as the smooth flood plain case, implying less lateral transfer from right to left. The actual values of velocity are obscured at times by cross–sectional measurements falling right behind dowel rods, which causes a small local wake, and significant undulations in the measured flood plain velocities.

– There is usually no shear layer extending onto the right flood plain. The right shear layer is usually contained within the main channel section. There is a more significant shear layer on the left flood plain, which extends some

distance onto the left flood plain, but not as far as the smooth flood plain case in Series A. The extent of lateral shear layer width is inhibited by additional roughness. This is also predicted by Samuels (1985) Equation (5.2), which produces smaller values of shear layer width (W) for larger values of friction factor λ.

– The combination of slightly higher velocities on the left flood plain compared with the right, as well as wider shear layers on the left compared with the right, shows some lateral momentum transfer with a net direction from right to left.

– Most significantly, the presence of such large velocity gradients between main channel and flood plain at all values of relative depth, implies large lateral shear (co– flowing shear) in the classical compound cross– section mould. Lateral shear is likely to be more prominent than horizontal shear in the rough flood plain case.

These points are summarised in the sketch below of the depth– averaged longitudinal velocity.

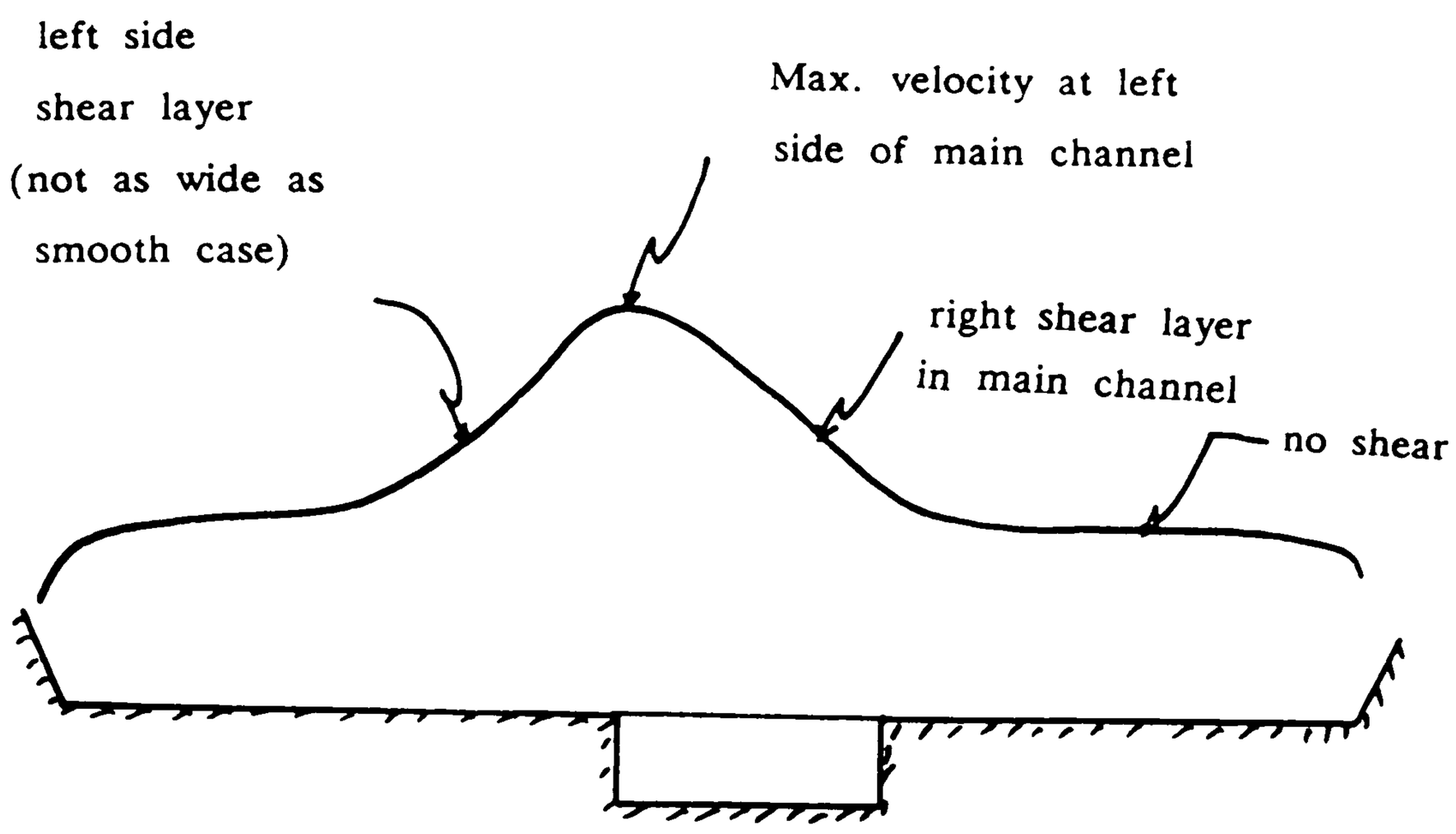

5.5.2 General Observation on Transverse Velocities (Series D)

Angular measurements were again carried out at four vertical sections in the main channel, thus producing estimates of the transverse velocity components normal to the skewed main channel. These are again shown in the lower half of Figures (5.19) to Fig (5.33).

– The secondary circulation measured is, as before, in one direction, namely anticlockwise. A single cell can be inferred which is rotating in the same sense as flood plain flow passing over the top of the main channel, again implying that the cell is being driven by this mechanism.

– Above bank full level, the transverse components are substantially less than the smooth flood plain case (section 5.4). This may be due to lower velocities on flood plain flow crossing over the main channel, thus producing lower transverse components. An analysis of the transverse components above bank full level reveals an element of acceleration by the faster moving main channel flow beneath. This will be discussed further in Chapter 7.

An examination of the deviation angle Φ was carried out for flood plain streamlines approaching the main channel cross over region. The mean deviation angle Φ for the rough flood plain case is of the order of 2.5^0 to 3.5^0, which when considering that the skew angle is only 5.843^0 represents a large percentage deviation. The deviation angle does not reduce at higher relative depths of flow indicating that for rough flood plains the streamlines follow the skewed main channel even at a relative depth of 0.5. This is in contrast to the smooth flood plain case where the deviation angle reduces to zero at higher relative depths.

– Below bank full level the circulation appears to take a form similar to the smooth case. The magnitudes of recirculation below bank full are very surprising, because in terms of absolute magnitude they are very similar to the smooth flood plain case where the crossing over velocity was much higher.
Backward recirculations reach maximum values in most cases (5 relative depths) of around 0.01 m/sec, which when related to the main channel longitudinal velocities of 0.25 to 0.3 m/sec, gives a ratio of transverse to longitudinal velocity of around 3% to 4% which is exactly the same range as the smooth flood plain case.

The difference, though, is that the driving flood plain velocity in the rough case is typically only half that of the smooth flood plain Series A tests, whereas the recirculating velocity magnitudes are broadly similar.

Is there a difference between recirculations in rough boundary flows to recirculations in smooth boundary flows? This question will be developed in Chapter 7.

5.5.3 Observations on Flow Development along the Flume Length.

– In moving downstream from section 1 to section 3, the maximum velocity filament tends to 'cling' to the inside of the left wall of the main channel and does not move left wards unto the left flood plain.

The magnitude of the maximum velocity remains approximately constant in the downstream direction.

– The left flood plain shear layer becomes wider in moving downstream from section 1 to section 3.

The right side shear layer continues to be contained within the width of the main channel at all sections and does not develop unto the right flood plain in the downstream direction.

– The mean velocity on the left flood plain tends to increase in the downstream direction. This is related to a widening shear layer on the left flood plain and indicative of momentum transfer from right to left.

– The mean velocity on the right flood plain appears to increase between section 1 and section 2, followed by a decrease from section 2 to 3. This often gives a zero net change in mean velocity from section 1 to 3. This process will be developed further in Chapter 7.

– The mean velocity in the main channel shows small decreases in the downstream direction between section 1 to 3. This decrease is usually within the range of experimental error and is perhaps not significant. On the other hand

the mean velocity is increasing on the left flood plain, so it may be indicative of momentum transfer from the main channel to left flood plain.

– The recirculating transverse velocities in the main channel remain approximately constant in magnitude in moving downstream from section 1 to section 3. This is in comparison to the smooth flood plain case where the secondary cells decreased in strength moving downstream. This phenomenon may be closely related to the velocity on the right flood plain, which remains approximately constant from section 1 to 3 in the rough flood plain case.

5.6 VELOCITY DATA FOR THE SKEWED MAIN CHANNEL ALONE ISOLATED FROM FLOOD PLAIN FLOWS.

Series C experimental test runs were set up to investigate the flow in the skewed main channel alone, when isolated from adjacent flood plains. This was achieved by the construction of small vertical walls at the main channel flood plain junction, the walls being of the same material as the part of the main channel below bankfull level.

The purpose of this set of experiments was as follow:–

(i) To obtain an expression for the friction factor λ for the main channel alone. This has been discussed in Chapter 4.

(ii) to obtain a relationship between stage and discharge for the main channel alone. This then becomes a benchmark to compare with the main channel behaviour when it is interacting with flood plains, either rough or smooth.

(iii) To investigate the magnitude and distribution of longitudinal velocity in the main channel alone, again acting as a benchmark with interacting cases.

(iv) Most importantly, the Series C tests were carried out to investigate the magnitude of transverse secondary currents in the main channel when there is no flood plain flow passing over the top. This will provide answers to the magnitude of residual secondary currents generated by a very slight bend at the

upstream end of the skew, or simply secondary currents generated naturally in a straight channel by non uniform shear distribution.

Fig (5.34) to Fig (5.45) presents the longitudinal and transverse velocity values for the three cross sections along the flume, and for four values of the flow depth in the channel up to 120mm. The upper two graphs on the figures represent values of longitudinal and depth average velocities through the channel cross sections. The lower half of these figures represent the transverse velocity components in the main channel generated by skewed main channel. Only longitudinal and transverse velocities will be discussed in this section.

Contours of velocity over the cross section and depth averaged velocities are shown in the upper half of the Fig (5.34) to Fig (5.45). These figures show reasonable symmetry of the velocity contours about the centre line of the main channel. Any deviations are within the order of magnitude of experimental error.

Comparing the main channel mean velocities with those of the main channel alone in Series A with the smooth flood plain, it is clear from Fig (5.10) to Fig (5.18), that high relative depths of flow produce very similar main channel velocities during interaction as compared with non– interaction. For lower relative depths of flow, the interacting case produces lower mean velocities in the main channel as would be expected.

An analysis of the recirculating transverse velocities reveals maximum values of recirculating velocity around 0.002 to 0.003 m/sec. The horizontal velocity scale is greatly expanded compared with Fig (5.1) to Fig (5.33). In view of longitudinal velocity components between 0.3 to 0.4 m/sec, this means that the ratio of transverse to longitudinal is around 1/2% to 1% which is the normal for straight channels. Not only is it the norm, but it is also a small fraction of the 4% to 5% maxima found for the main channel during interaction, proving that flood plain flows passing over the top of the skewed main channel are responsible for strong circulations in the interacting case.

5.7 CONCLUSIONS

The main conclusions of this chapter can be summarised as follows:–

(i) Flow behaviour in a compound skewed channel reveals flow patterns that are much more complex than the straight parallel compound case. This complexity involves asymmetric velocity profiles and secondary currents derived from horizontal shear.

(ii) The maximum longitudinal velocity filament tends to follow the left wall of the main channel, and at higher relative depths moves onto the flood plain as if moving towards the centre–line of the flume. This is the case for the smooth flood plains. For the rough flood plain case the maximum velocity filament follows the line of the main channel, again near the left side wall, but does not go onto the left flood plain at higher relative depths.

(iii) As a general rule there are no lateral shear layers extending onto the right flood plain. The right shear layer is contained within the main channel. The left side shear layers extend a considerable distance onto the left flood plain, certainly further than predicted by conventional formulae. The left shear layer tends to become wider in the downstream direction. This implies large lateral momentum transfer from main channel to left flood plain and no lateral momentum transfer from main channel to right flood plain.

(iv) The mean velocity on the right flood plain shows slight decreases in the downstream direction, and sometimes shows increases on the left flood plain moving in the same direction. This is particularly true for the rough flood plain case. The mean velocity in the main channel sub section remains reasonably constant in the downstream direction, but does show very slight decreases in the smooth flood plain case in moving from section 1 to section 3. As a general rule the mean velocity on the left flood plain is greater than on the right flood plain.

(v) Flood plain flow streamlines have a tendency to deviate in the same direction as the main channel, when they approach the main channel region.

For the smooth flood plain case the mean deviation angle is of the order of 1.5° to 2.0° at the lowest flood plain depth tested. $Y_f/Y_c = 0.15$. The deviation angle tends towards zero for high relative flow depths.

For the rough flood plain case, the mean deviation angle is of the order of 2.5° to 3.5°, irrespective of the relative depth of flow.

(vi) Flood plain flow passing over the skewed main channel produces secondary recirculations with maximum ratios of transverse to longitudinal velocity around 4%. This ratio is true for both rough and smooth flood plains. The 4% ratio is also much greater than secondary currents in the skewed main channel when isolated from adjacent flood plains, where the ratio is of the order of 1/2% to 1%. The secondary circulation occupies one main cell (at this aspect ratio), rotates in the same sense as the crossing over flood plain flow, and the strength of these secondary cells reduces in the downstream direction.

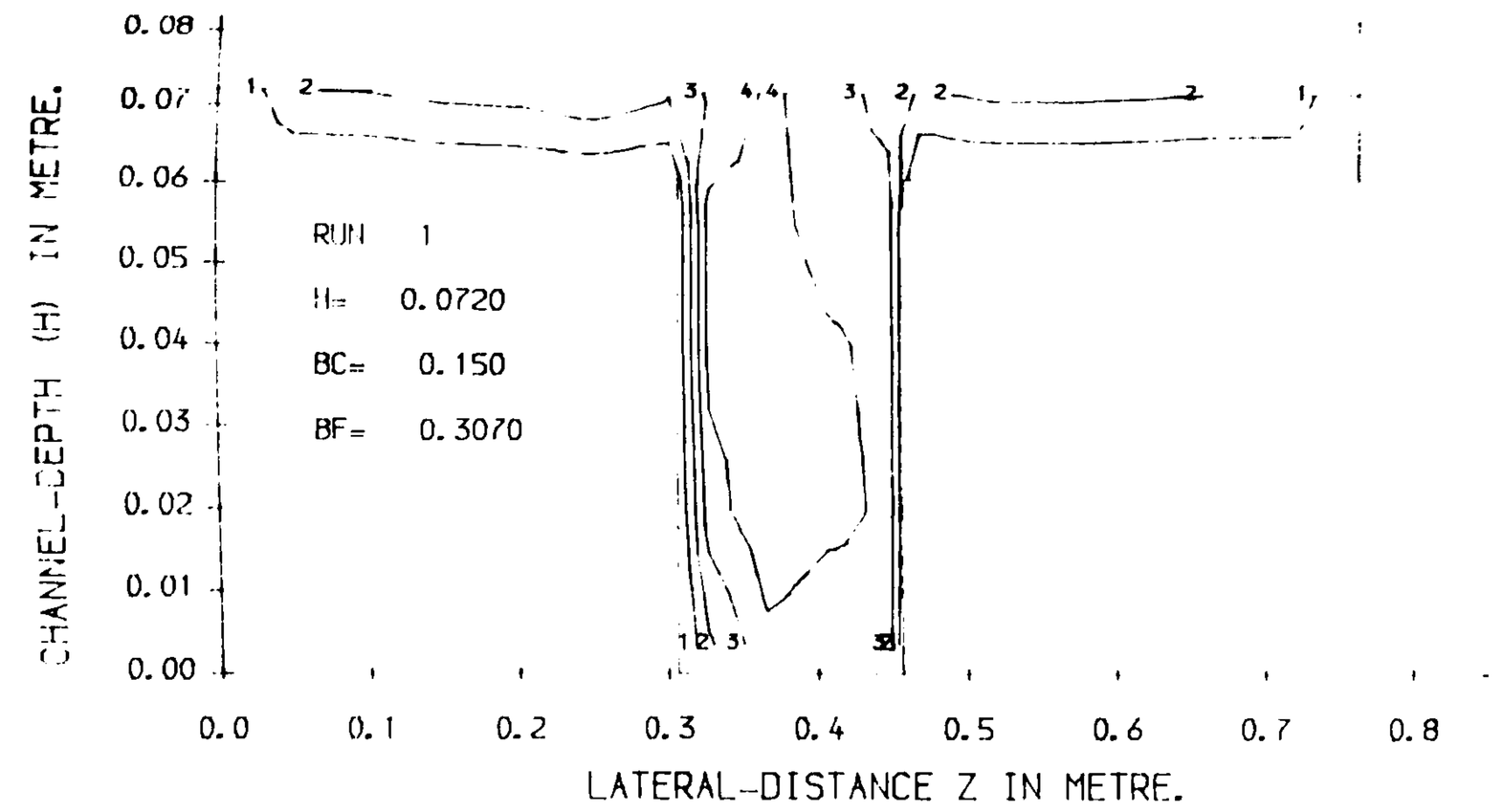

LONGITUDINAL VELOCITY CONTOURS IN CROSS SECTION. 1

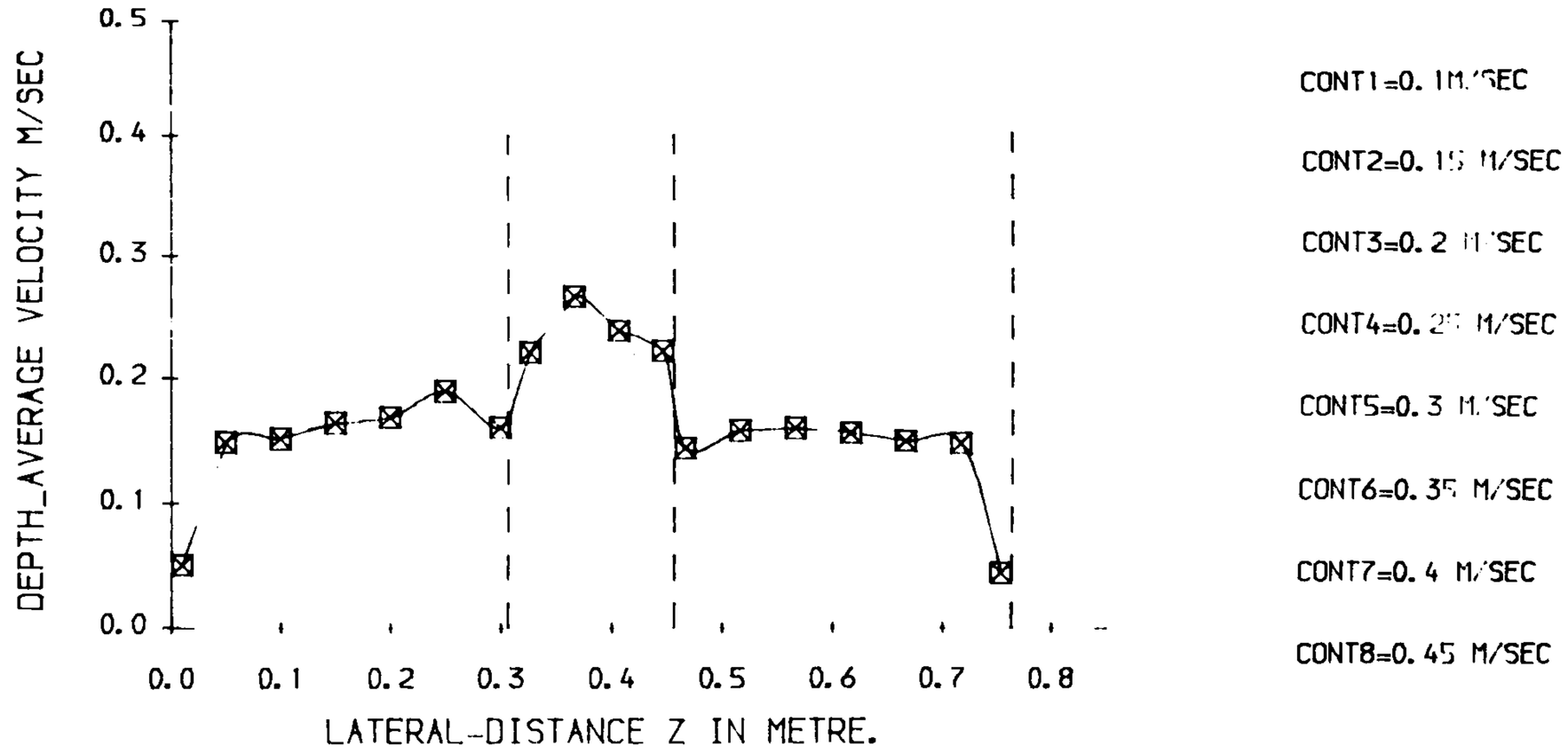

LONGITUDINAL DEPTH_AVERAGE VELOCITY PROFILE IN PLAN.

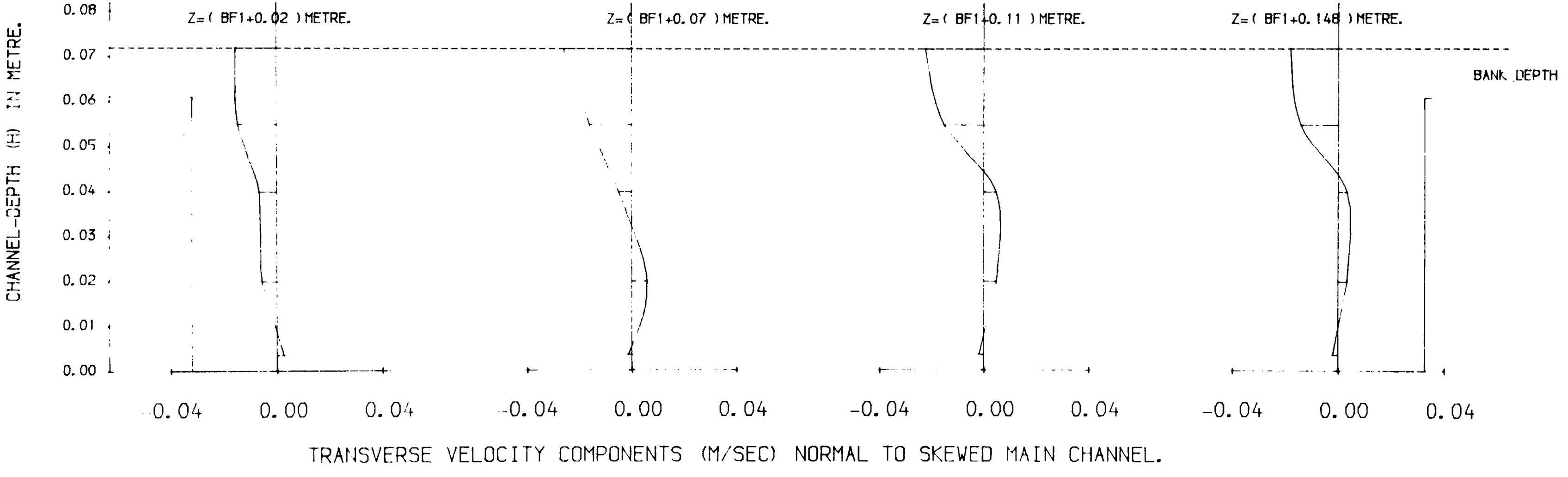

FIG(5.1) LONGITUDINAL & TRANSVERSE VELOCITY COMPONENTS IN SKEWED CHANNEL WITH SMOOTH FLOODPLAIN

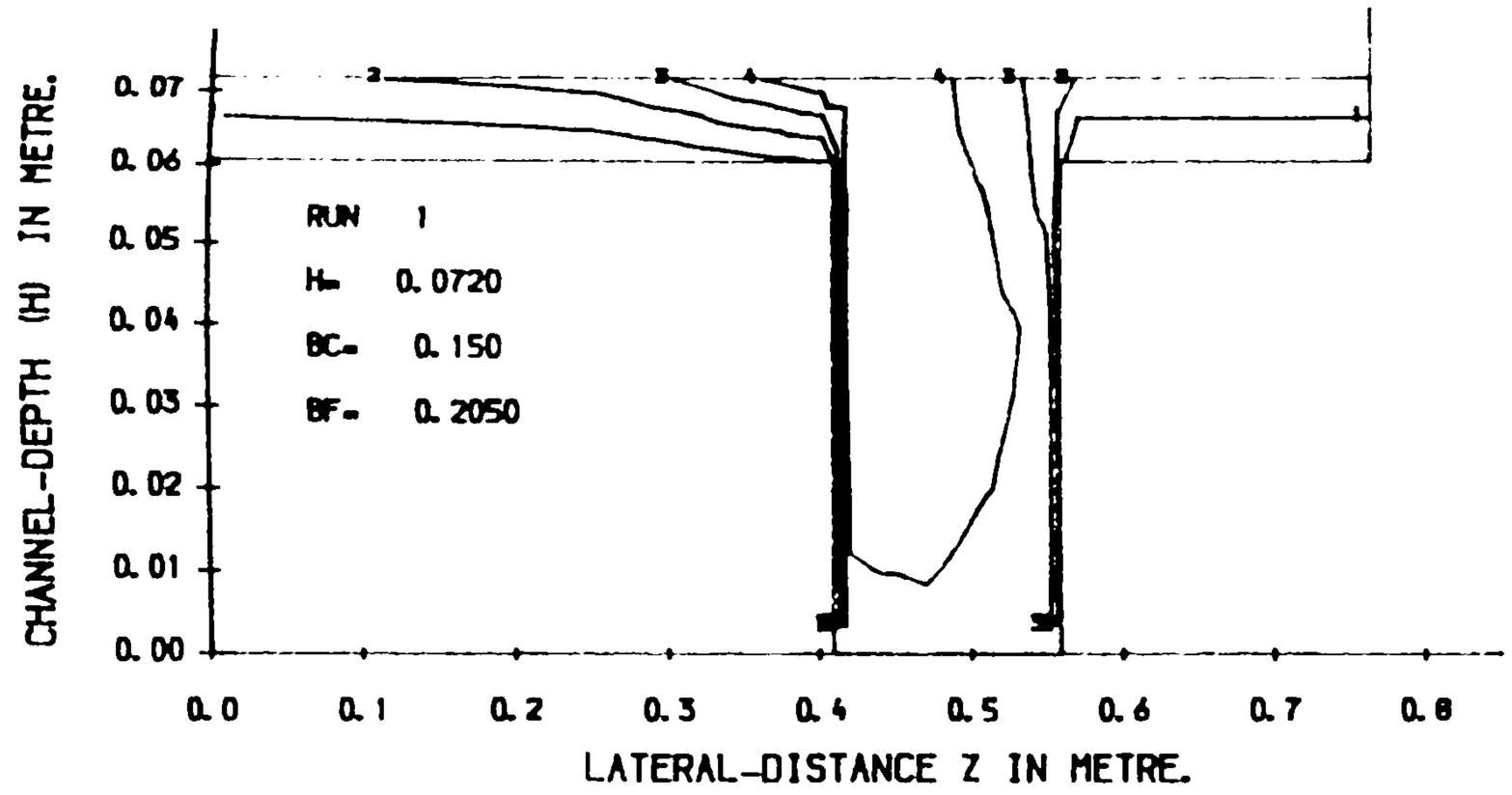

LONGITUDINAL VELOCITY CONTOURS IN CROSS SECTION.2

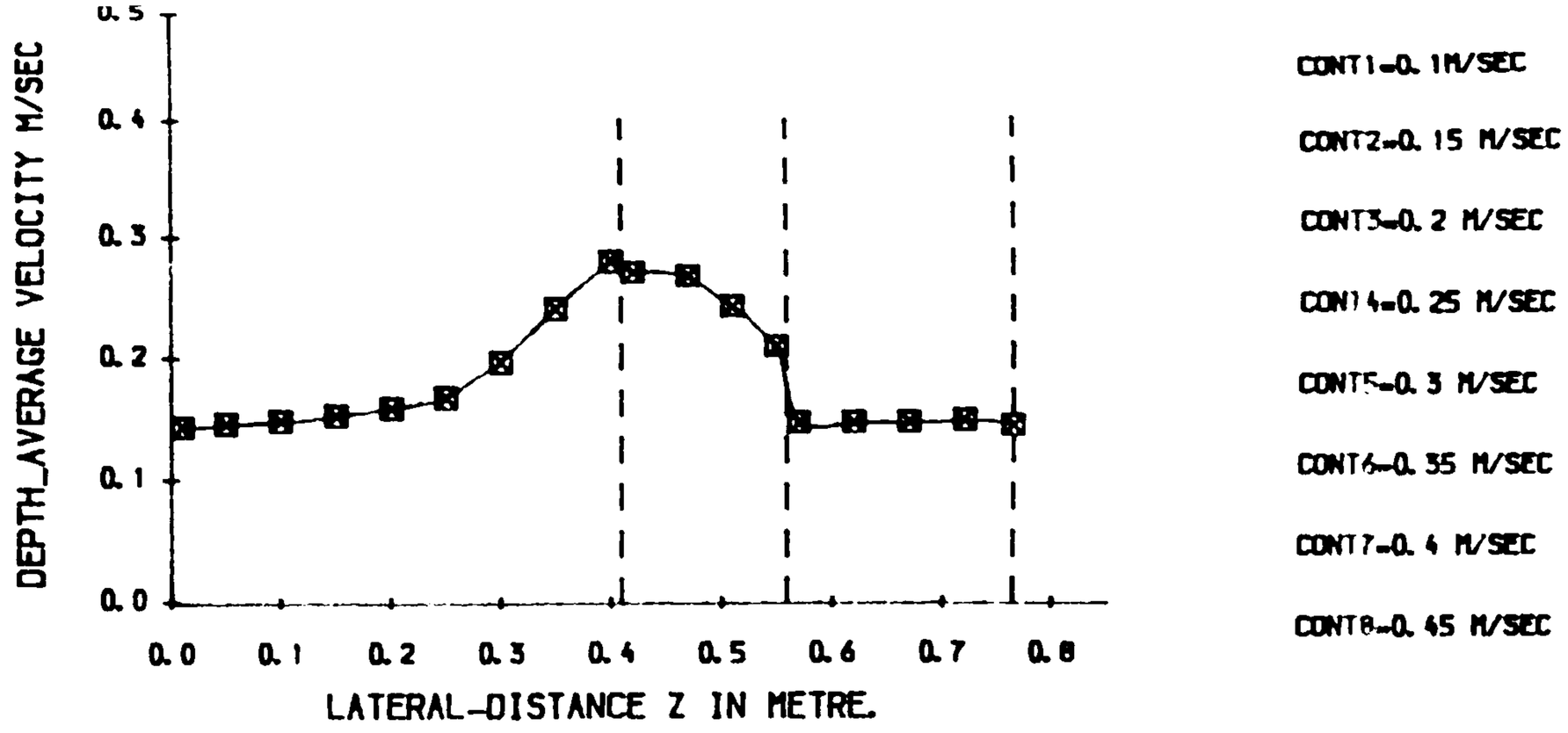

LONGITUDINAL DEPTH_AVERAGE VELOCITY PROFILE IN PLAN.

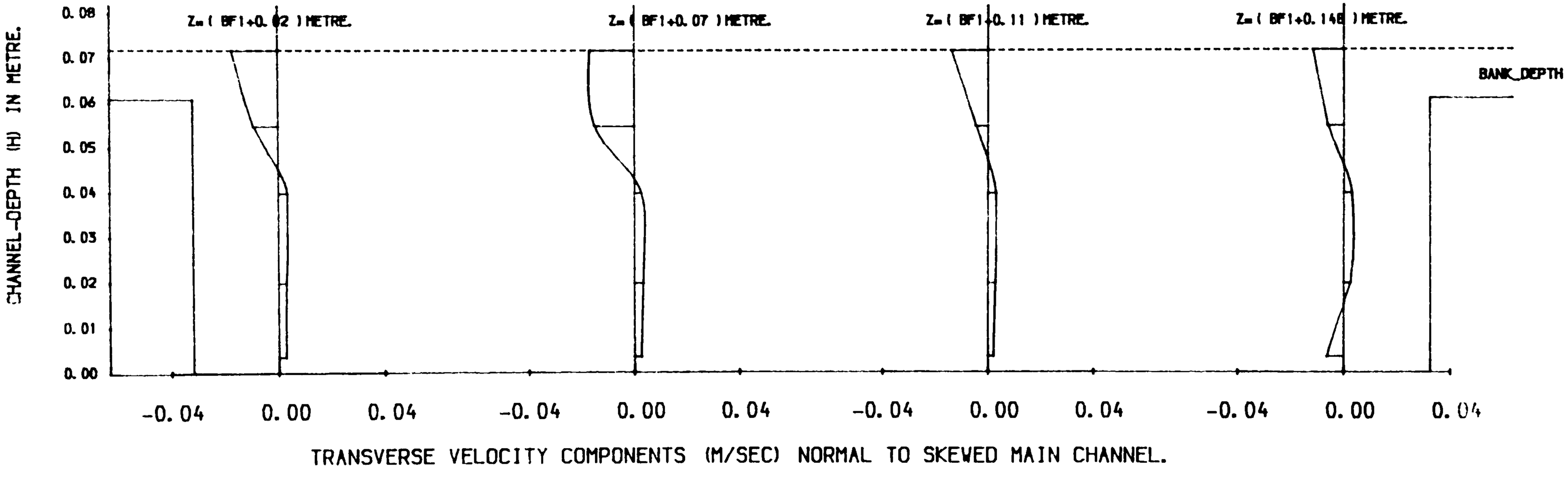

FIG(5.2) LONGITUDINAL & TRANSVERSE VELOCITY COMPONENTS IN SKEWED CHANNEL WITH SMOOTH FLOODPLAIN

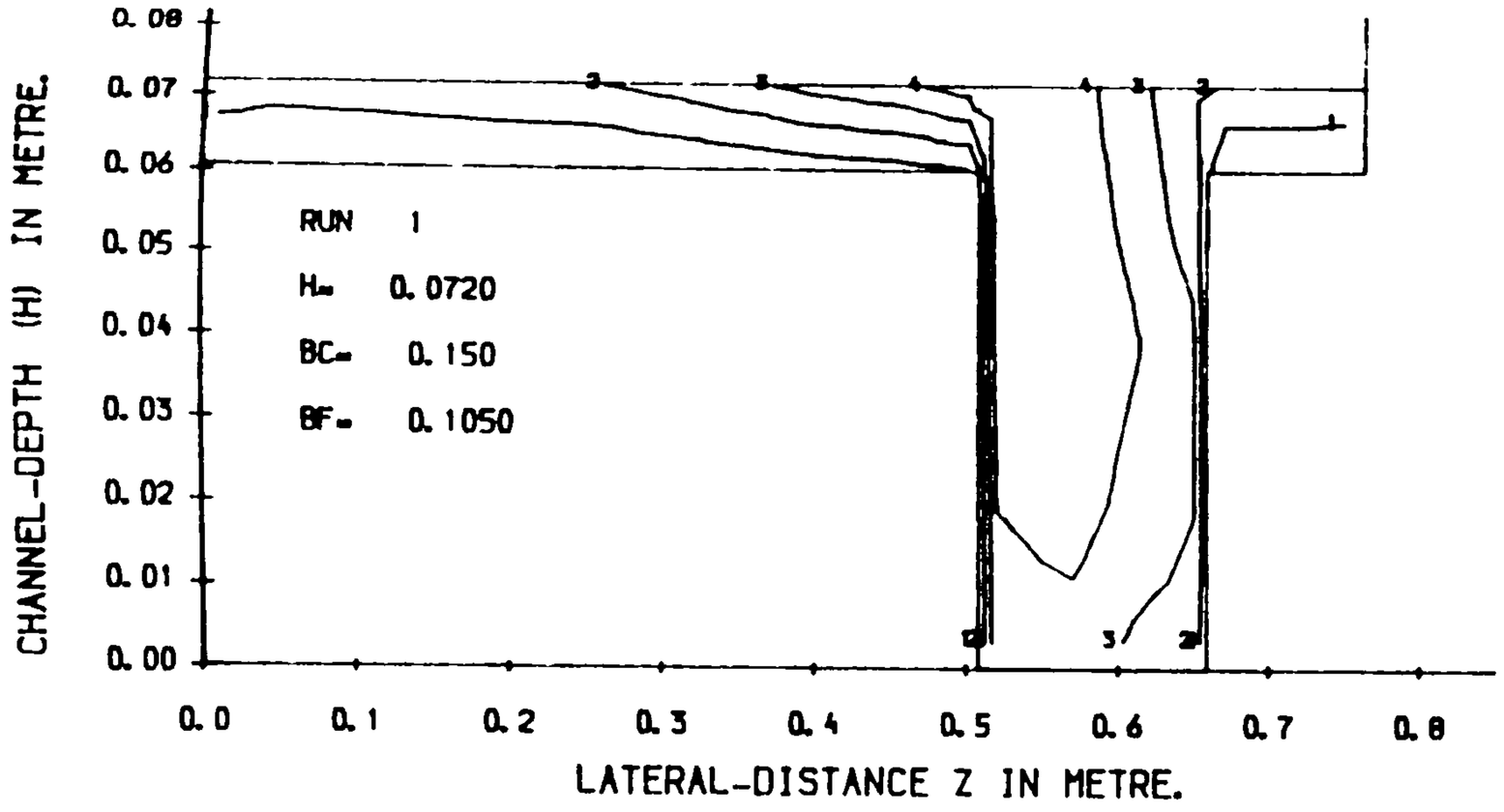

LONGITUDINAL VELOCITY CONTOURS IN CROSS SECTION. 3

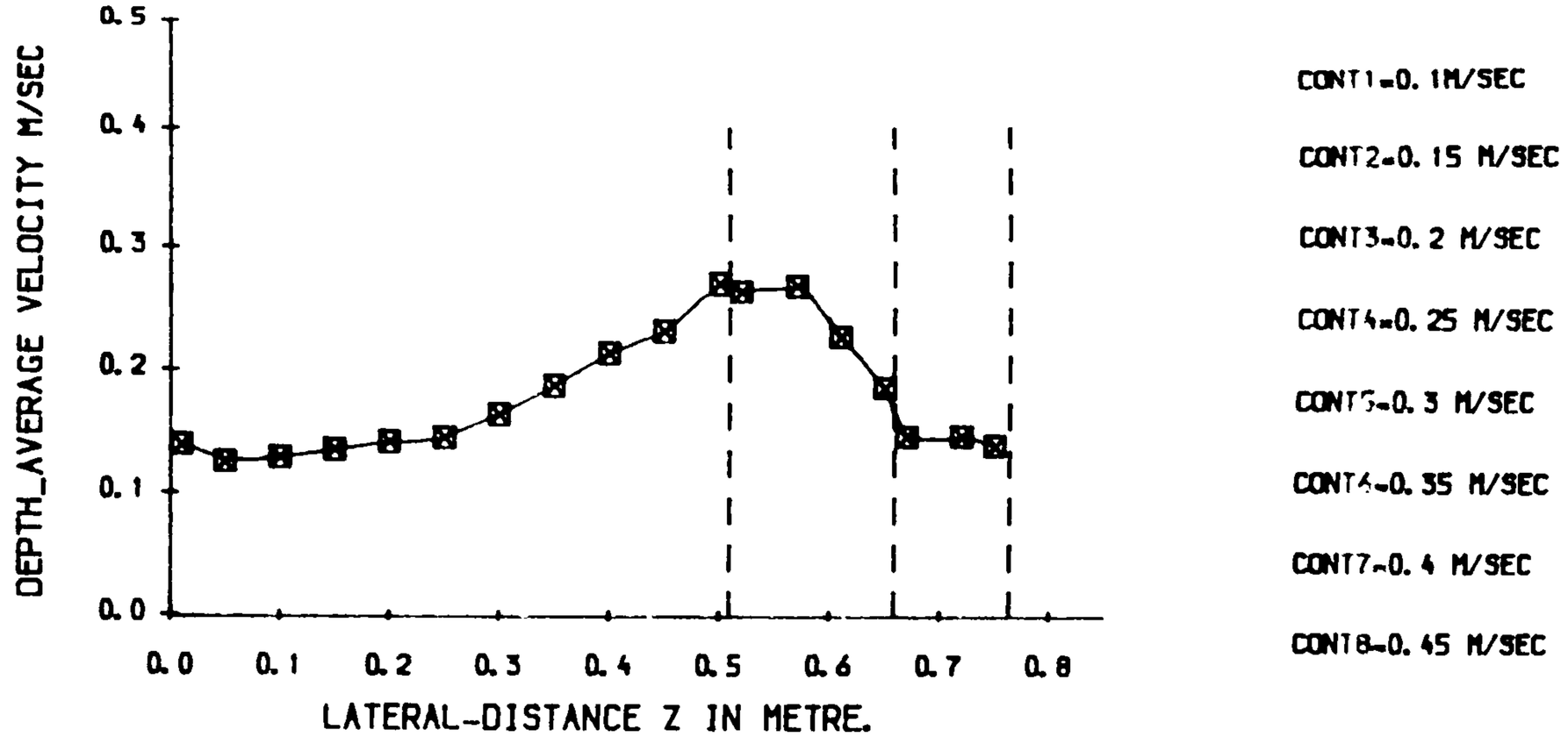

LONGITUDINAL DEPTH_AVERAGE VELOCITY PROFILE IN PLAN.

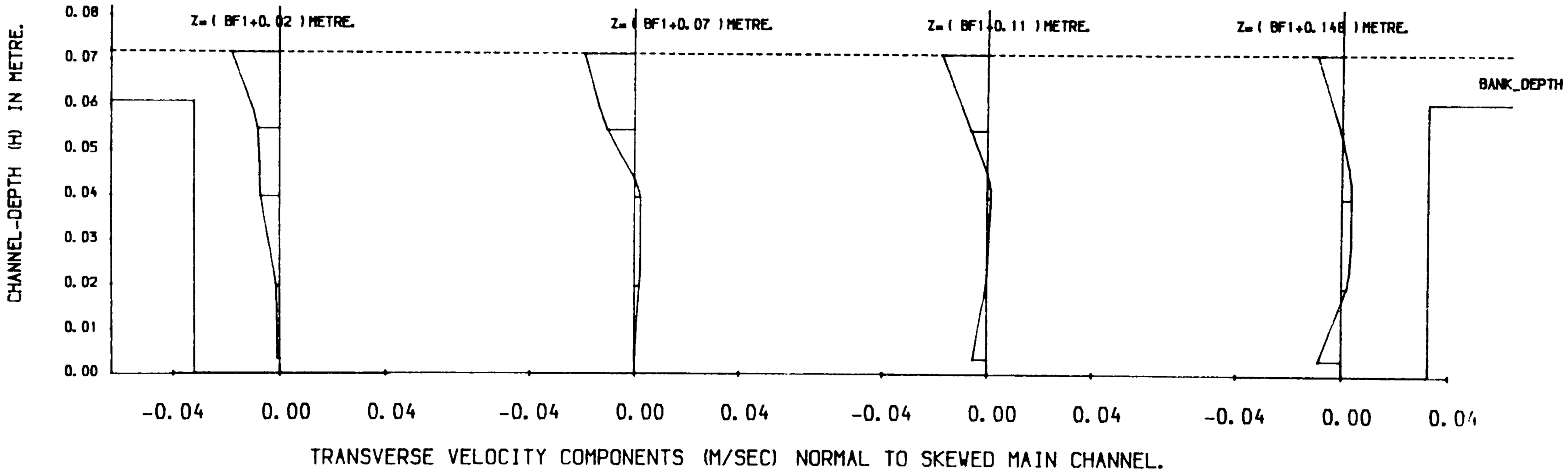

FIG(5.3) LONGITUDINAL & TRANSVERSE VELOCITY COMPONENTS IN SKEWED CHANNEL WITH SMOOTH FLOODPLAIN

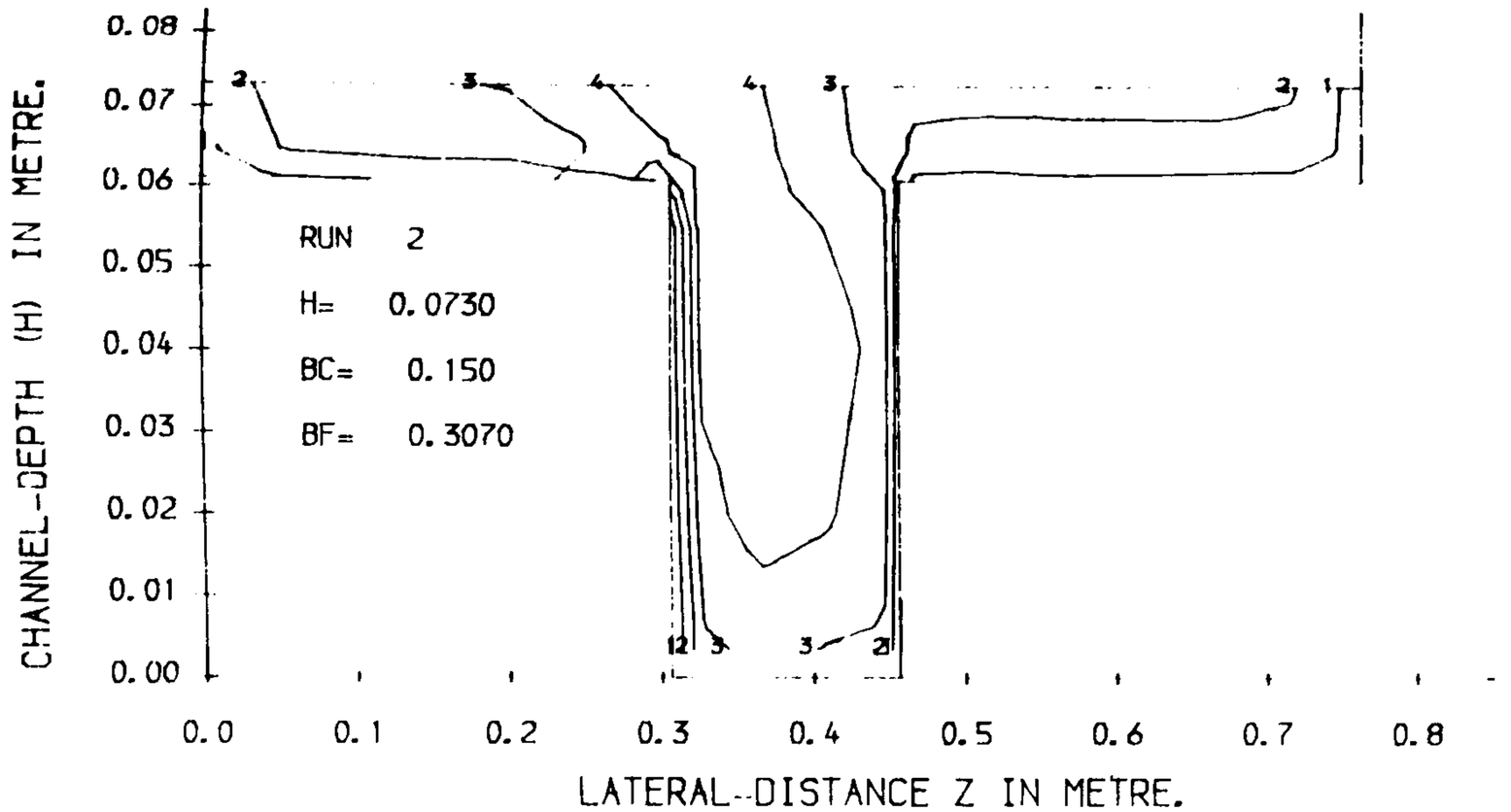

LONGITUDINAL VELOCITY CONTOURS IN CROSS SECTION. 1

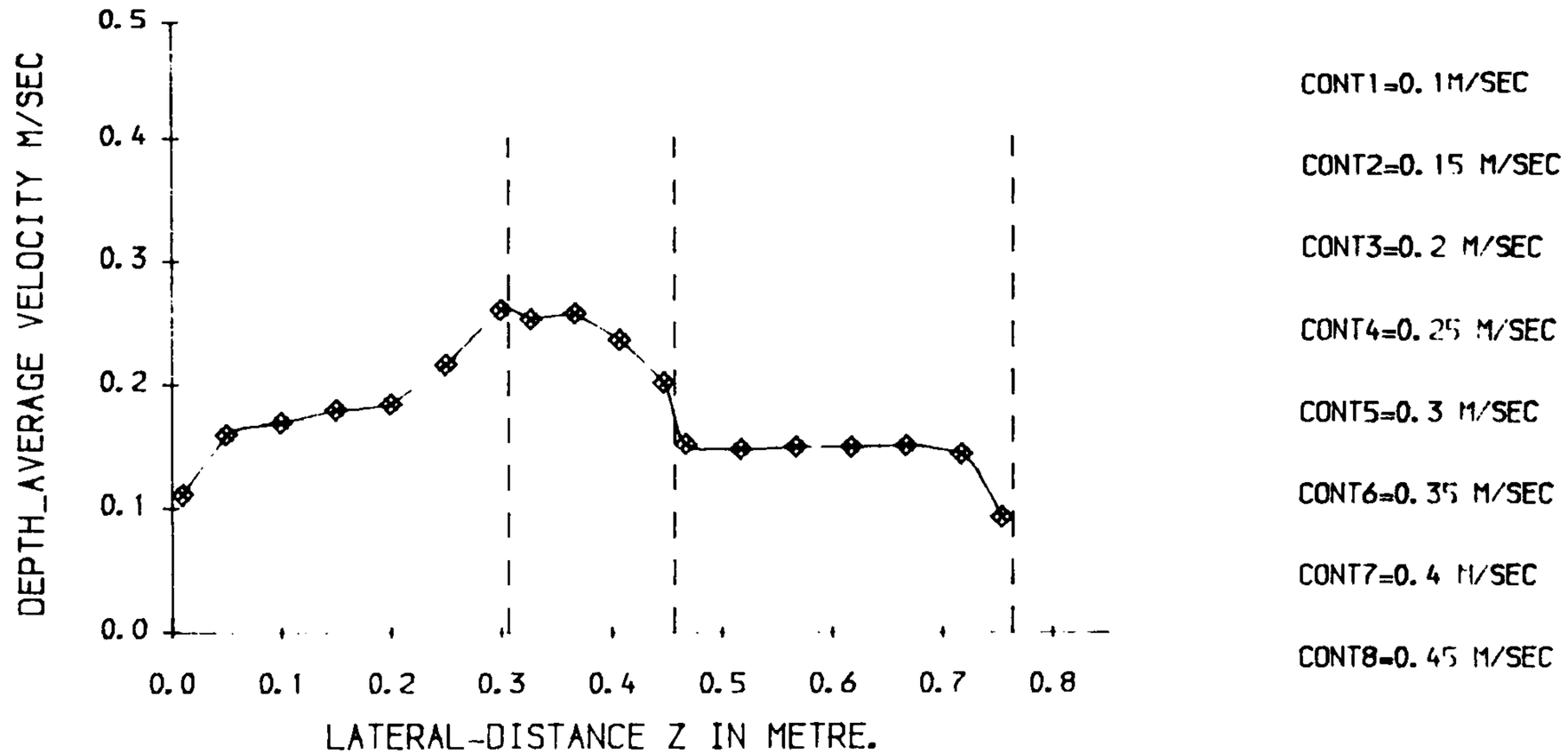

LONGITUDINAL DEPTH_AVERAGE VELOCITY PROFILE IN PLAN.

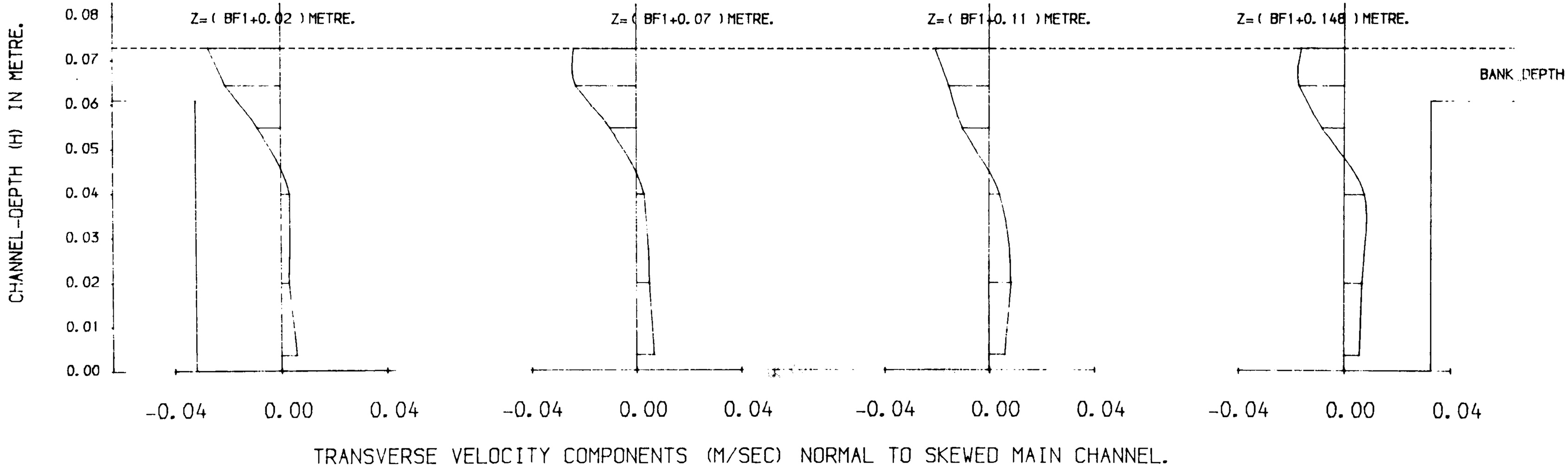

FIG(5.4) LONGITUDINAL & TRANSVERSE VELOCITY COMPONENTS IN SKEWED CHANNEL WITH SMOOTH FLOODPLAIN

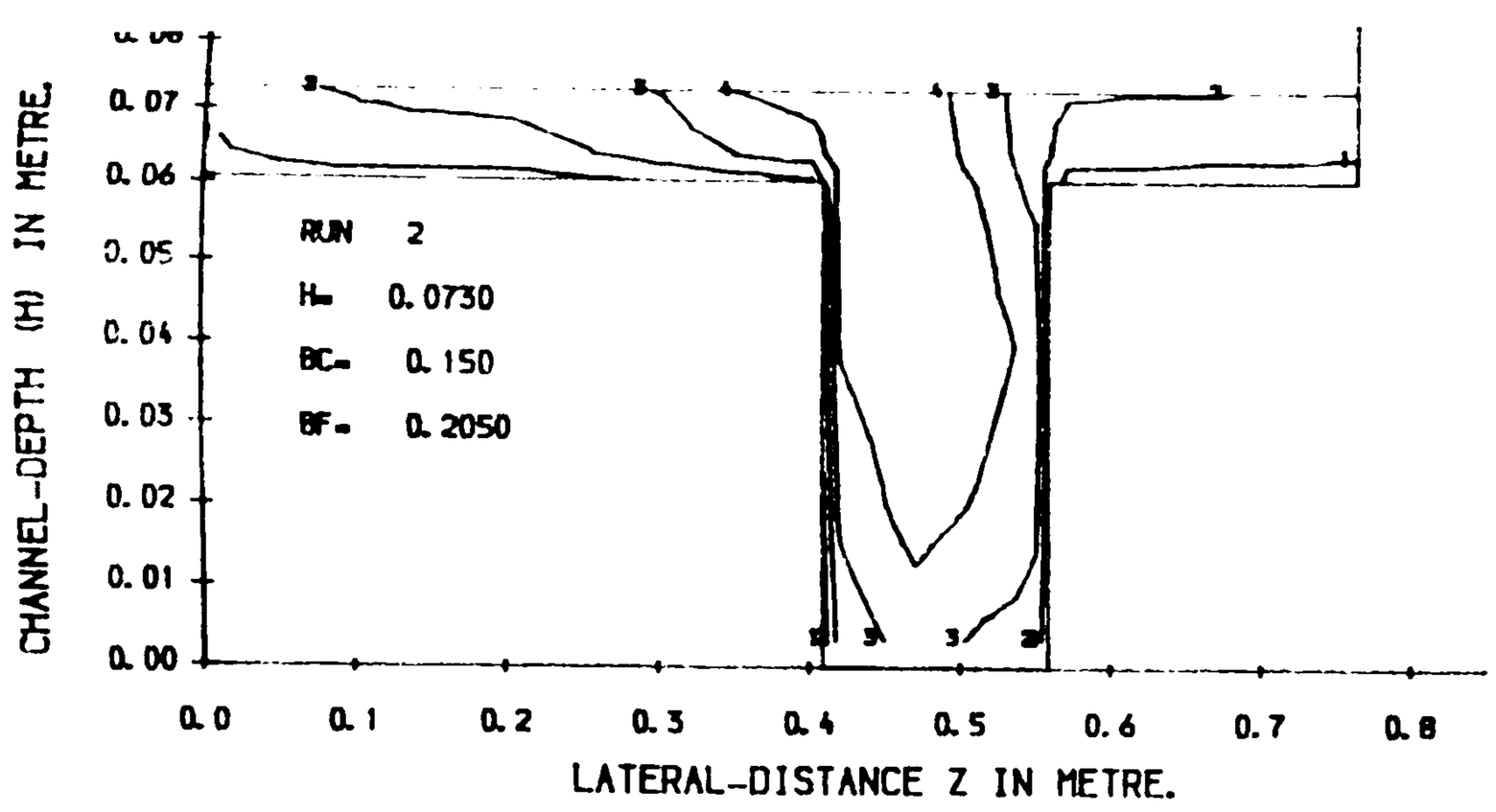

LONGITUDINAL VELOCITY CONTOURS IN CROSS SECTION. 2

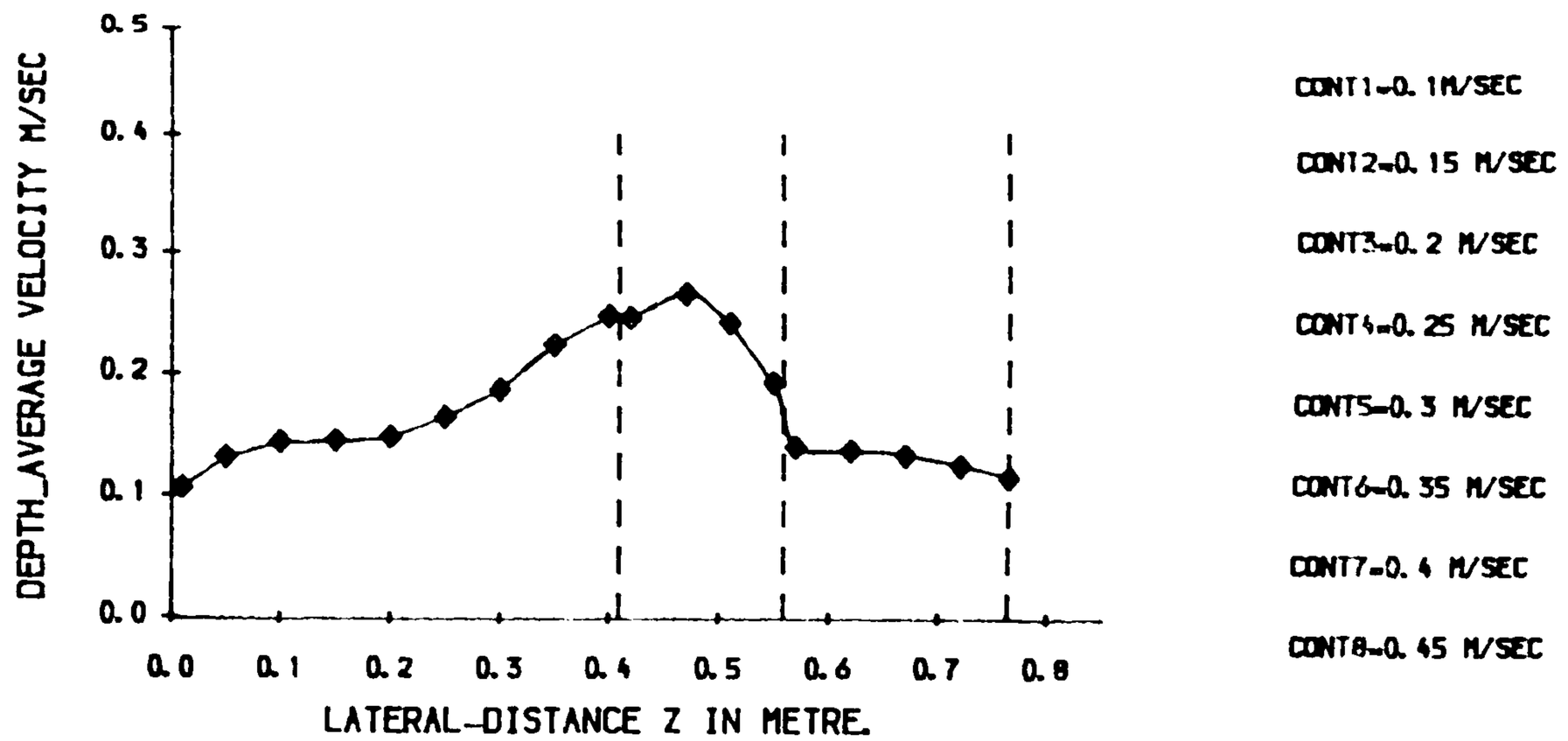

LONGITUDINAL DEPTH_AVERAGE VELOCITY PROFILE IN PLAN.

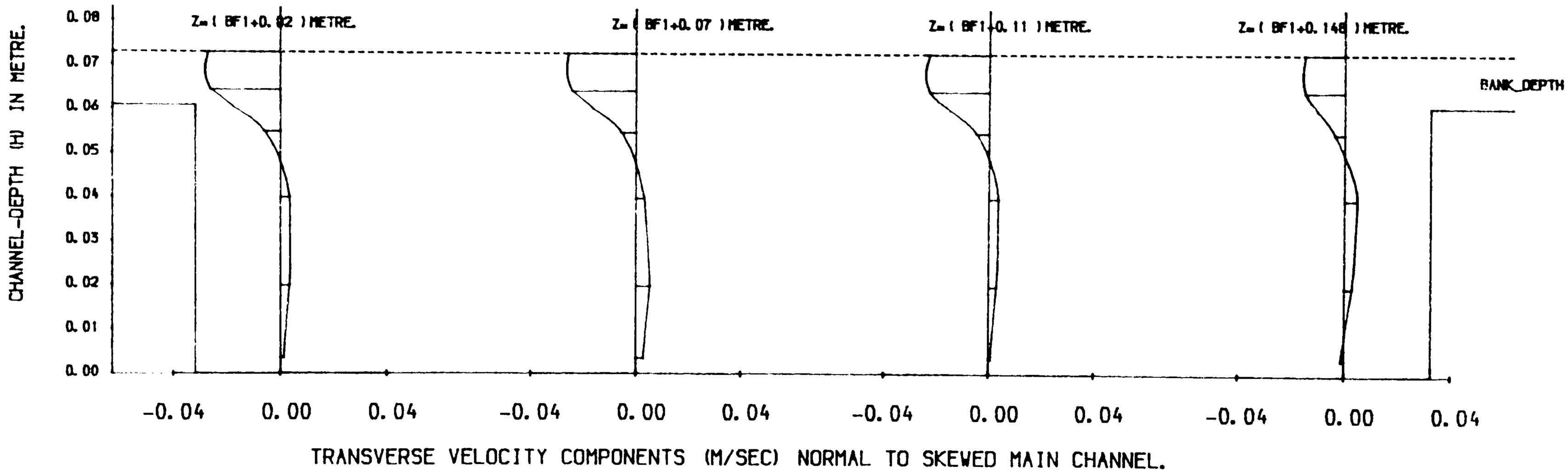

FIG(5.5) LONGITUDINAL & TRANSVERSE VELOCITY COMPONENTS IN SKEWED CHANNEL WITH SMOOTH FLOODPLAIN

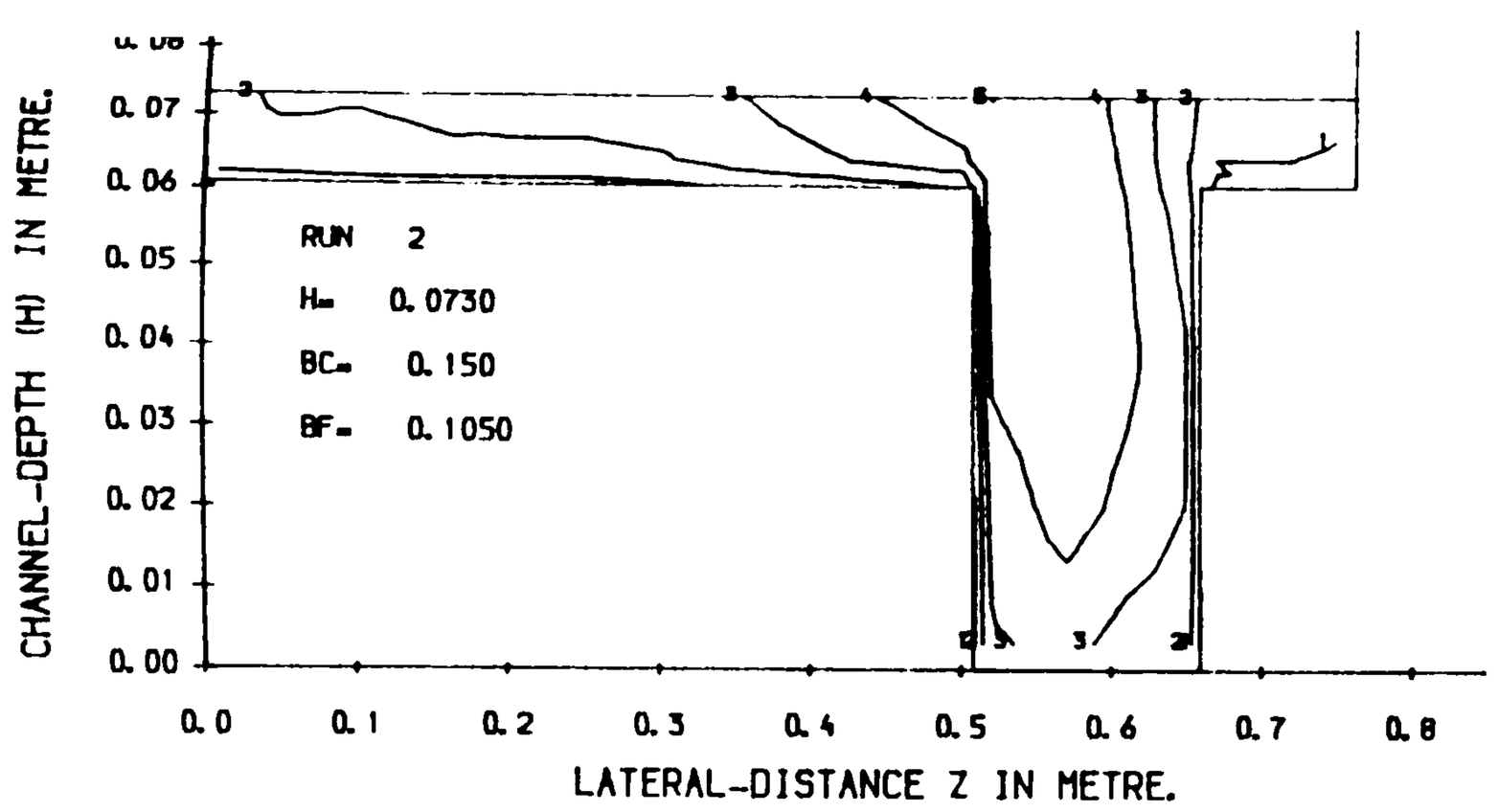

LONGITUDINAL VELOCITY CONTOURS IN CROSS SECTION. 3

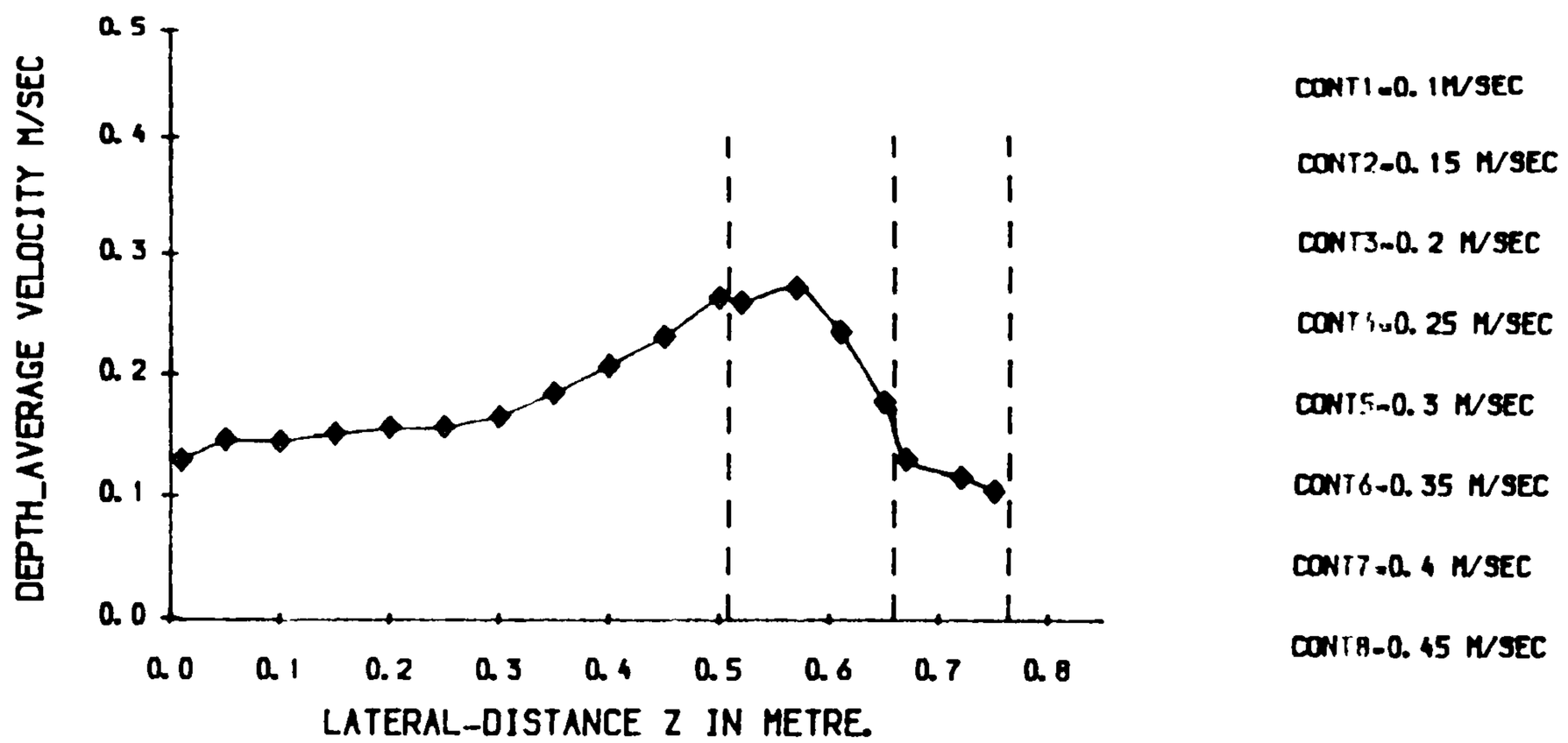

LONGITUDINAL DEPTH_AVERAGE VELOCITY PROFILE IN PLAN.

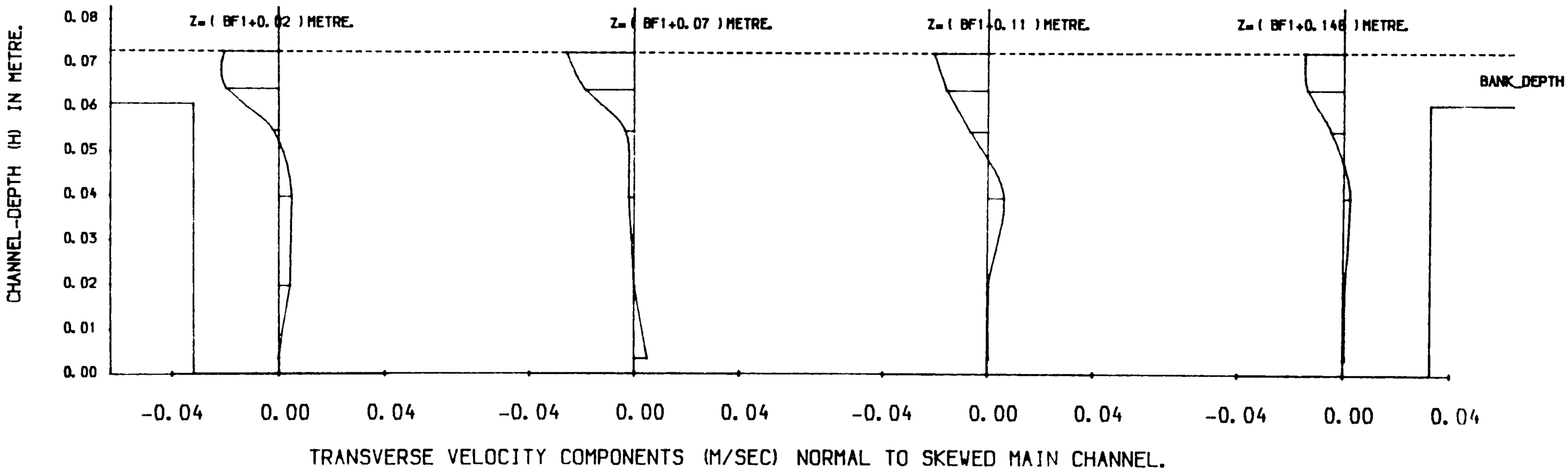

FIG (5.6) LONGITUDINAL & TRANSVERSE VELOCITY COMPONENTS IN SKEWED CHANNEL WITH SMOOTH FLOODPLAIN

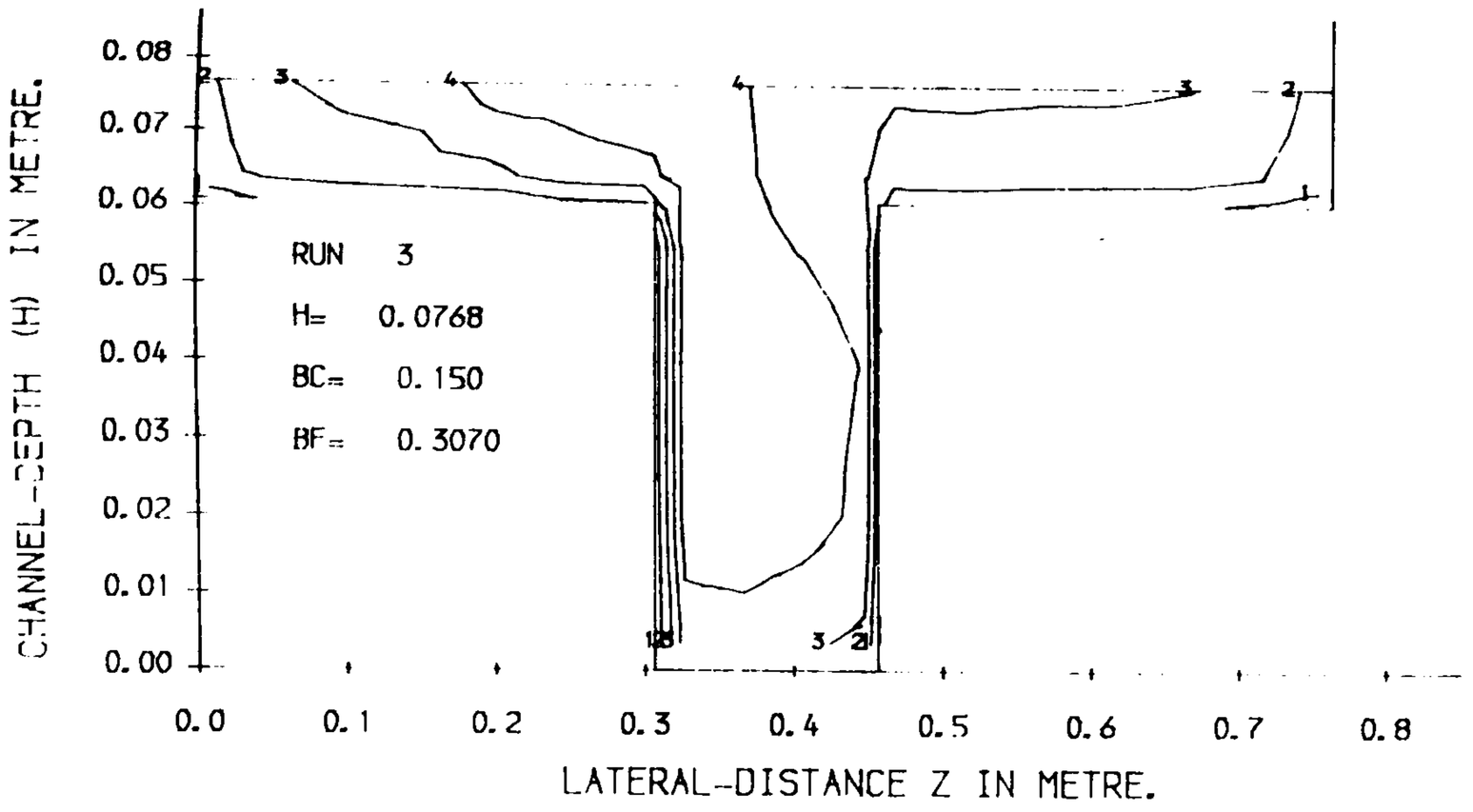

LONGITUDINAL VELOCITY CONTOURS IN CROSS SECTION. 1

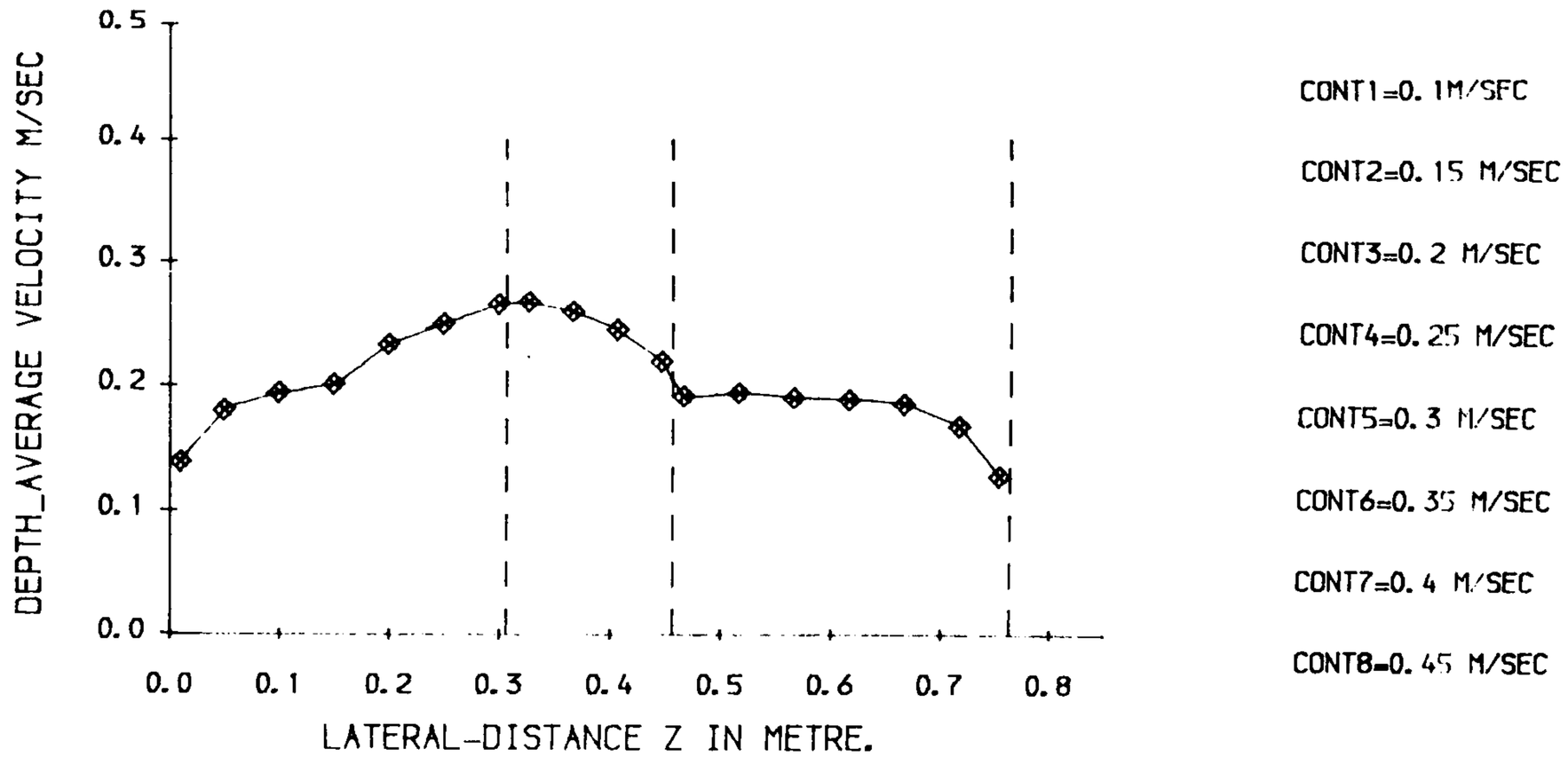

LONGITUDINAL DEPTH_AVERAGE VELOCITY PROFILE IN PLAN.

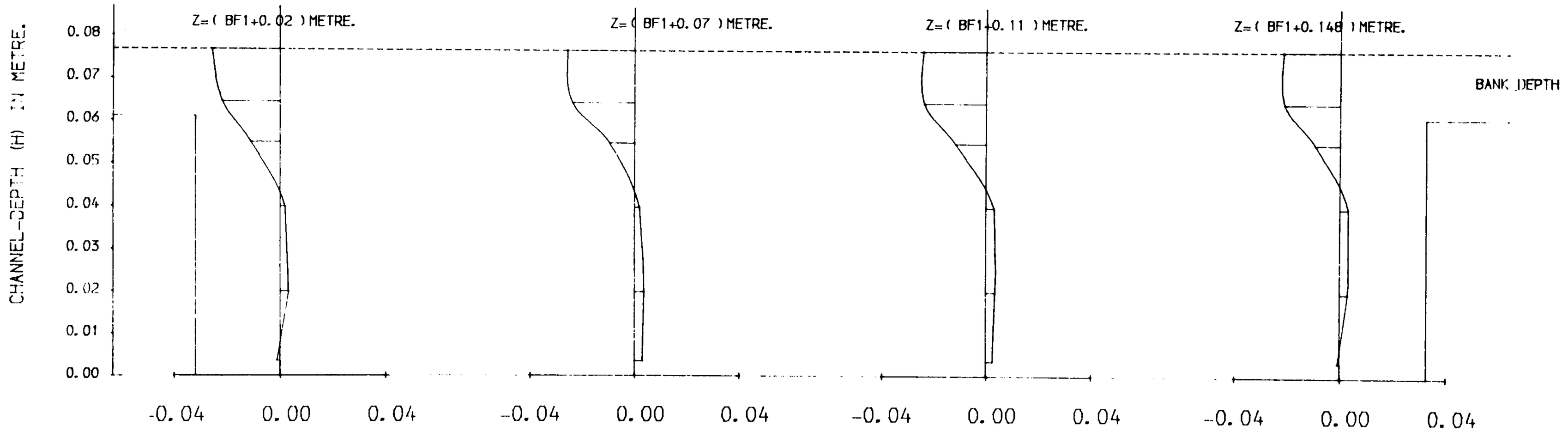

FIG(5.7) LONGITUDINAL & TRANSVERSE VELOCITY COMPONENTS IN SKEWED CHANNEL WITH SMOOTH FLOODPLAIN

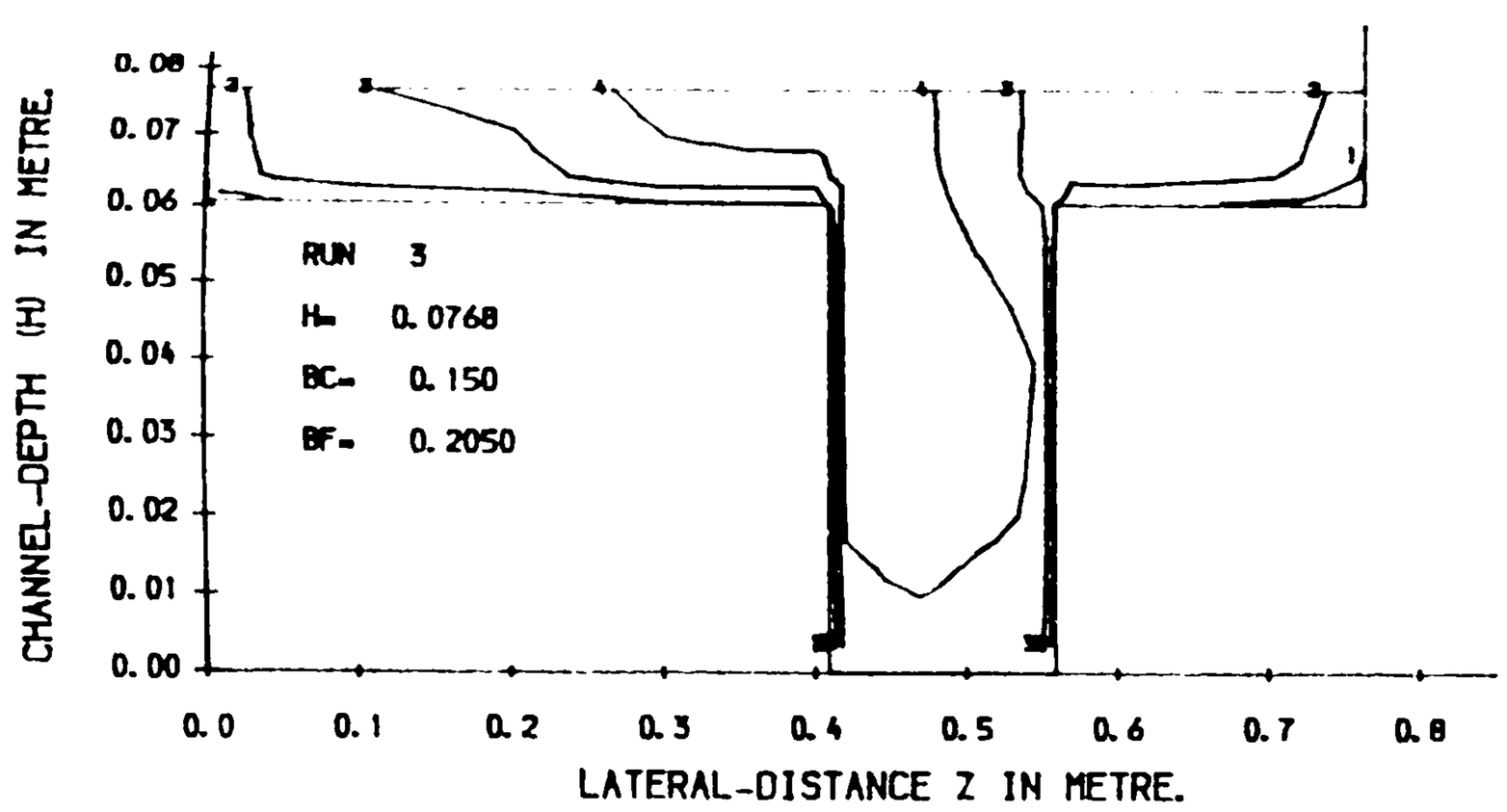

LONGITUDINAL VELOCITY CONTOURS IN CROSS SECTION. 2

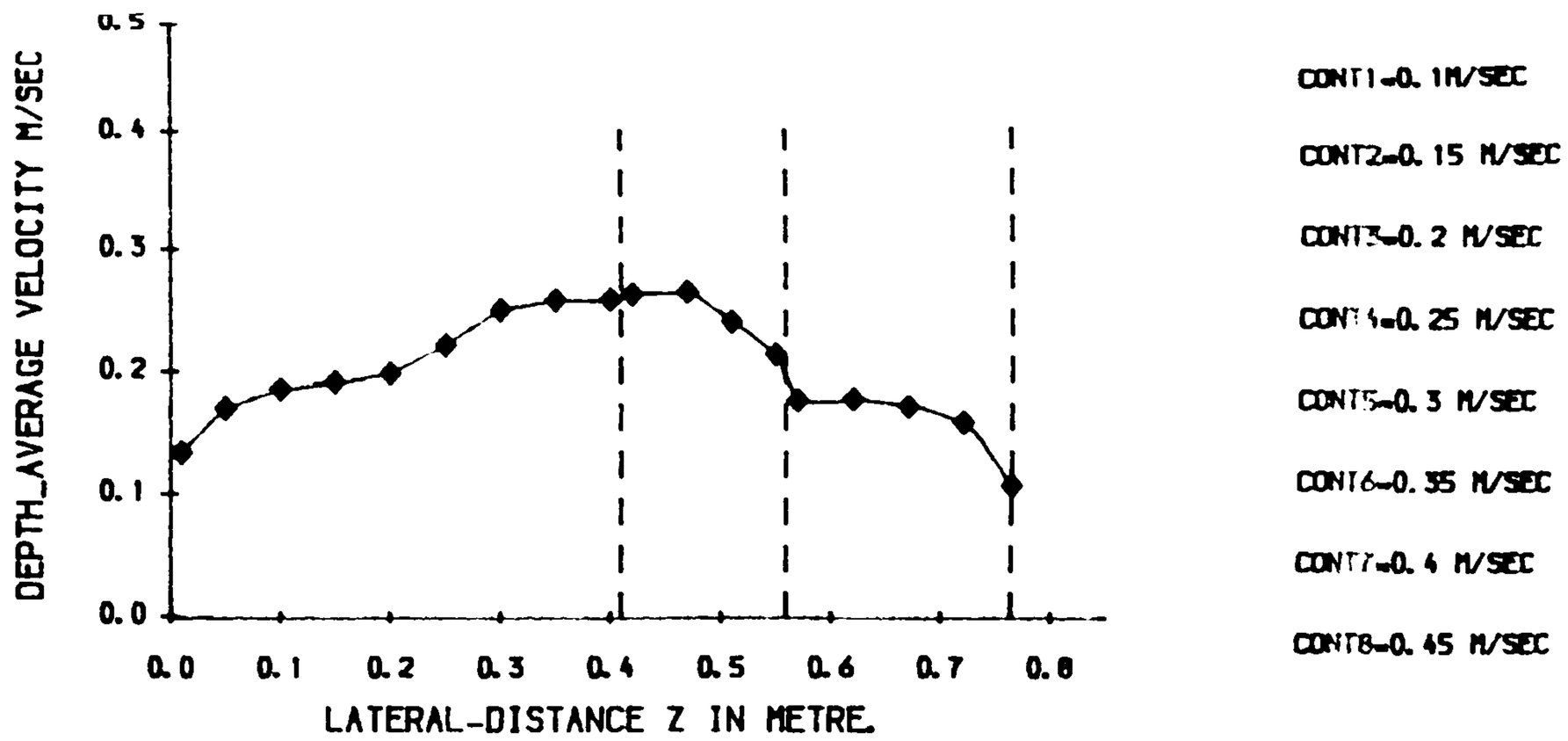

LONGITUDINAL DEPTH_AVERAGE VELOCITY PROFILE IN PLAN.

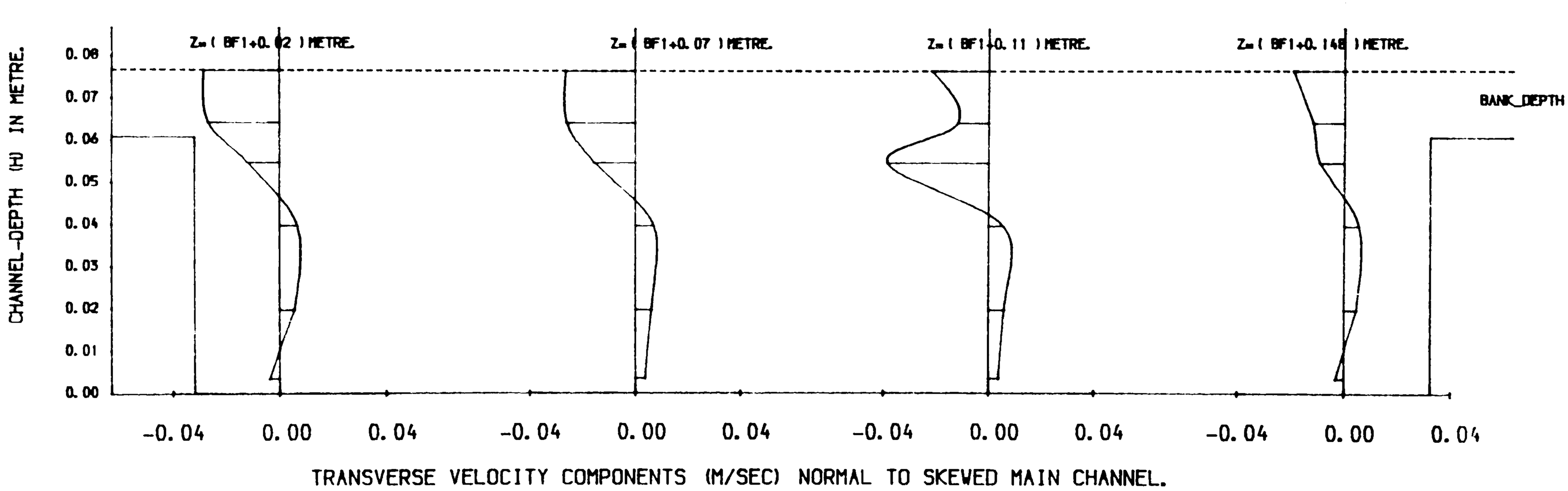

FIG(5.8) LONGITUDINAL & TRANSVERSE VELOCITY COMPONENTS IN SKEWED CHANNEL WITH SMOOTH FLOODPLAIN

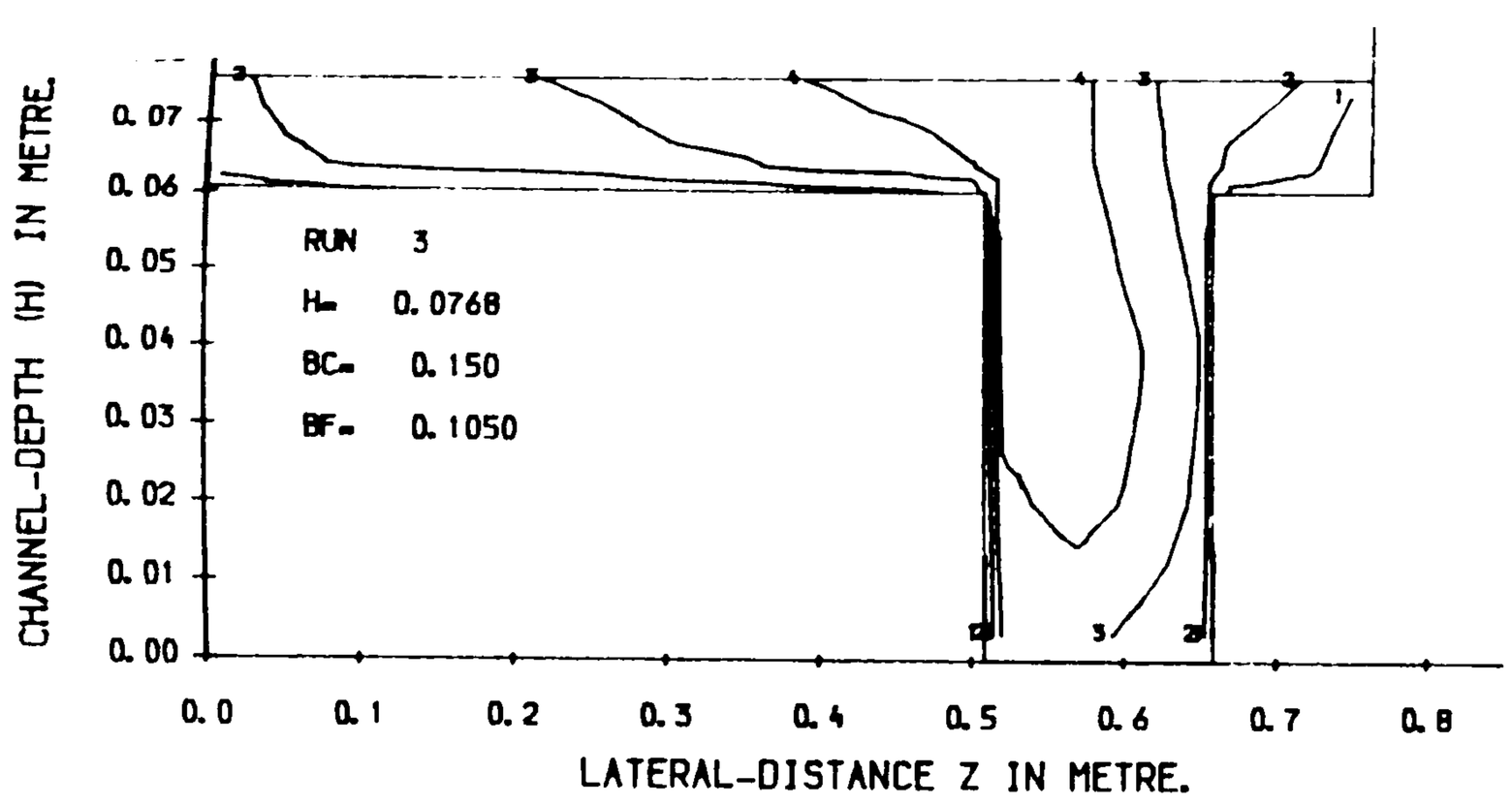

LONGITUDINAL VELOCITY CONTOURS IN CROSS SECTION. 3

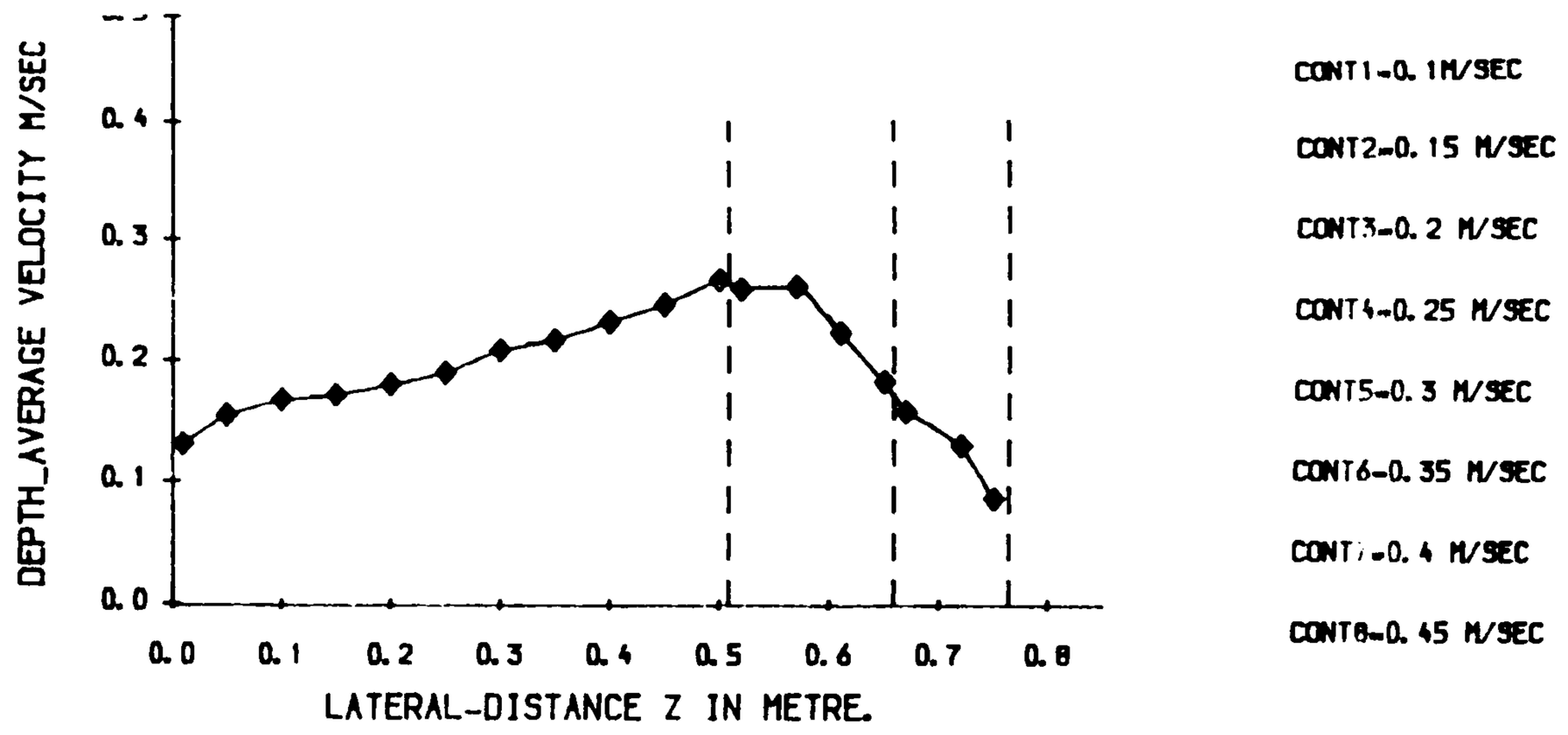

LONGITUDINAL DEPTH_AVERAGE VELOCITY PROFILE IN PLAN.

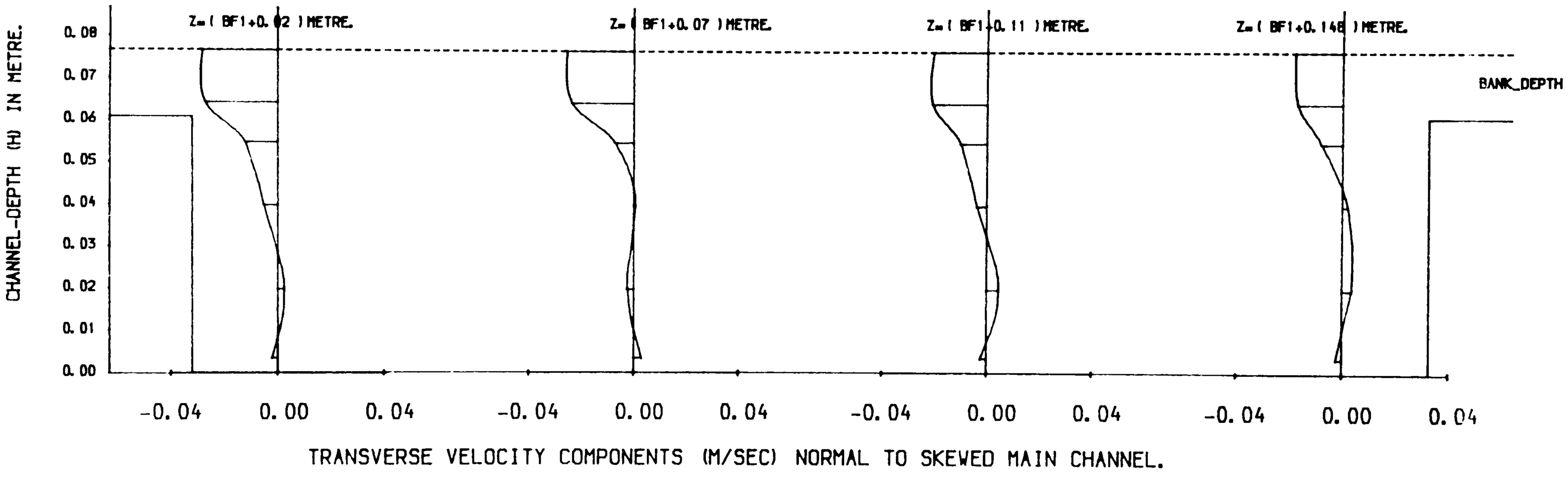

FIG(5.9) LONGITUDINAL & TRANSVERSE VELOCITY COMPONENTS IN SKEWED CHANNEL WITH SMOOTH FLOODPLAIN

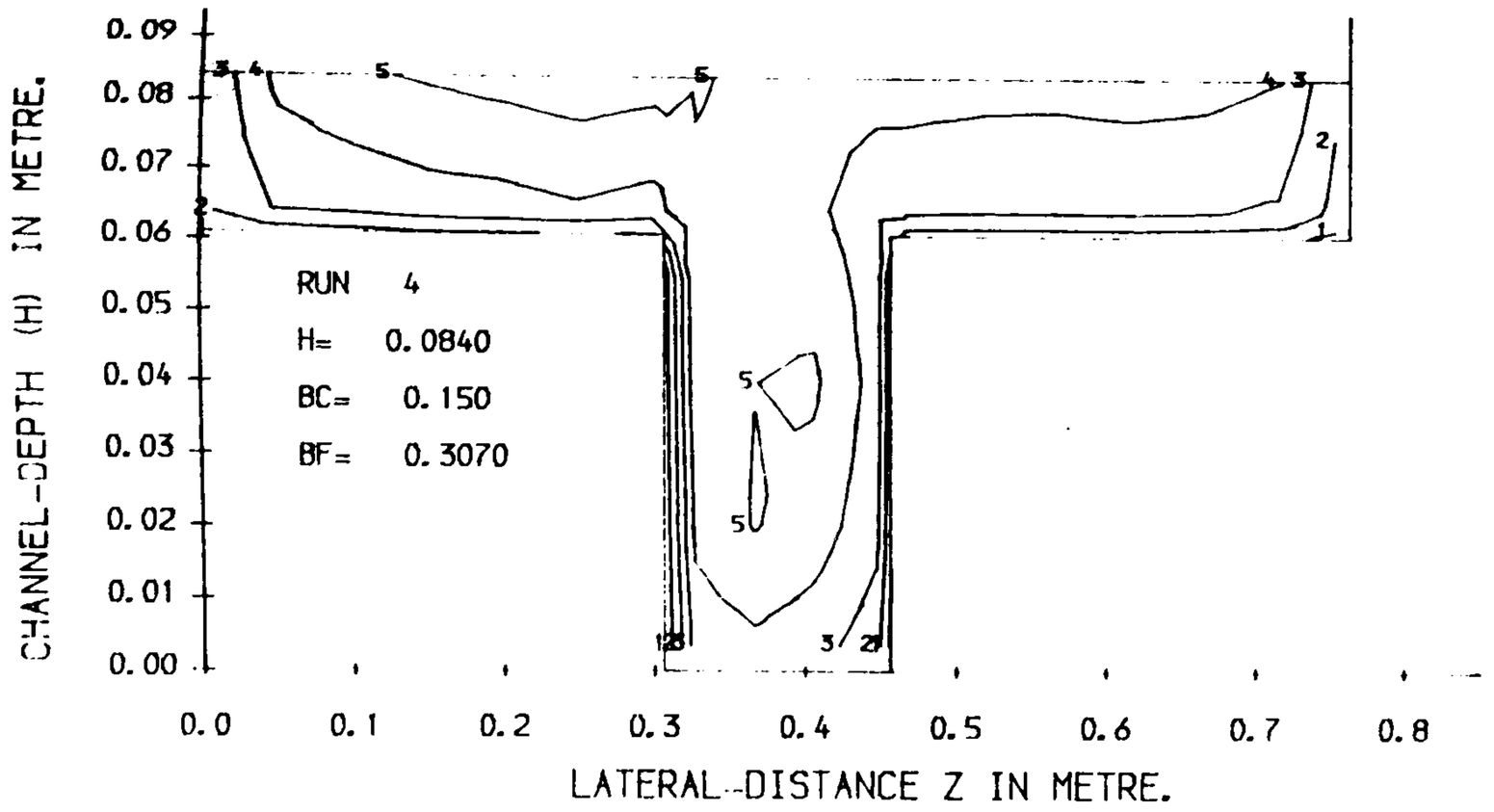

LONGITUDINAL VELOCITY CONTOURS IN CROSS SECTION. 1

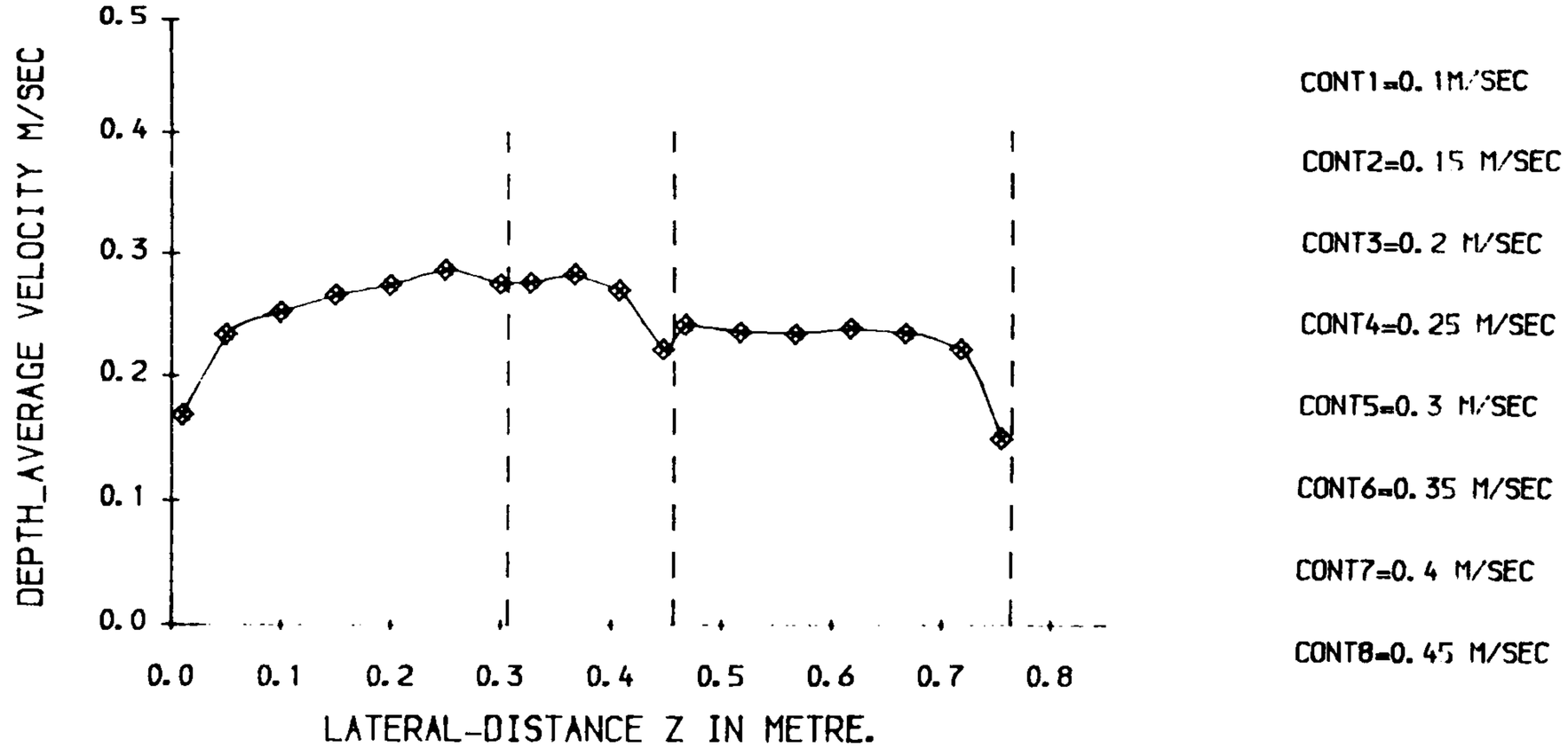

LONGITUDINAL DEPTH_AVERAGE VELOCITY PROFILE IN PLAN.

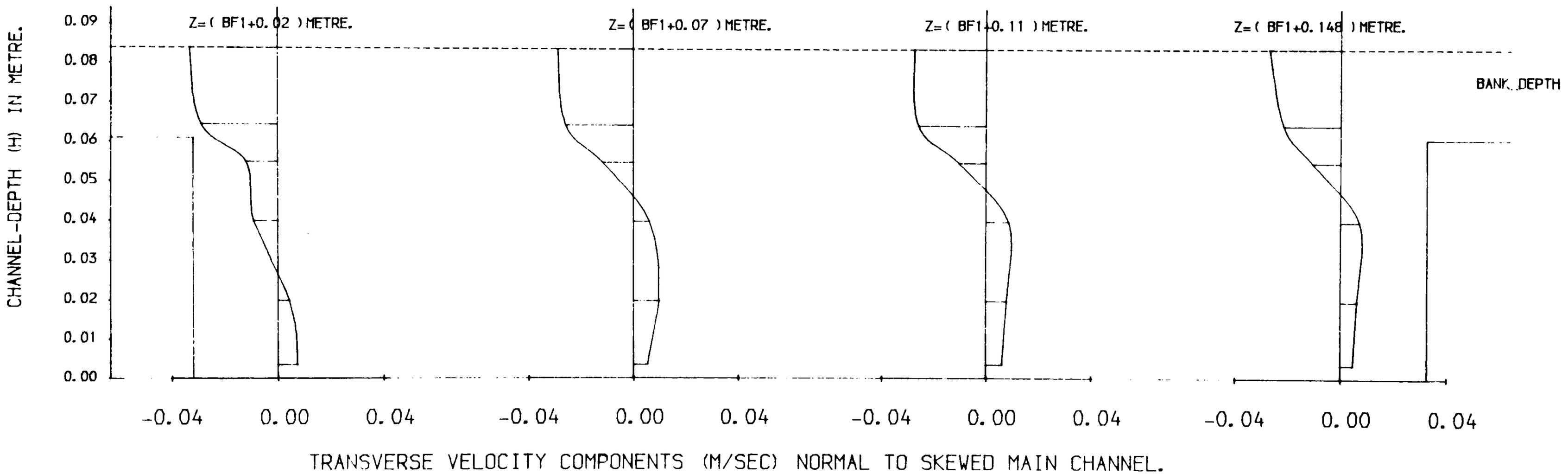

FIG (5. 10) LONGITUDINAL & TRANSVERSE VELOCITY COMPONENTS IN SKEWED CHANNEL WITH SMOOTH FLOODPLAIN

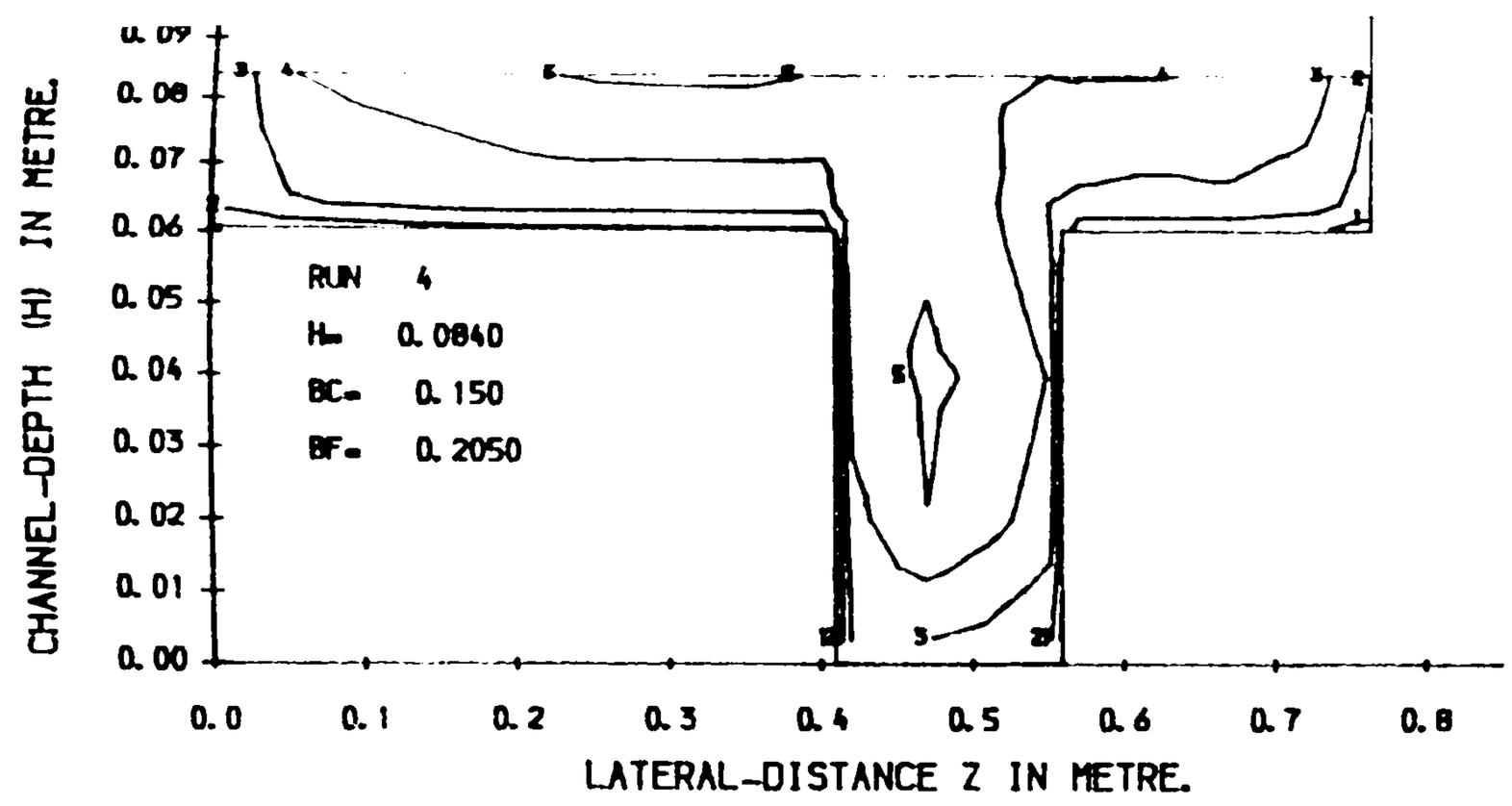

LONGITUDINAL VELOCITY CONTOURS IN CROSS SECTION. 2

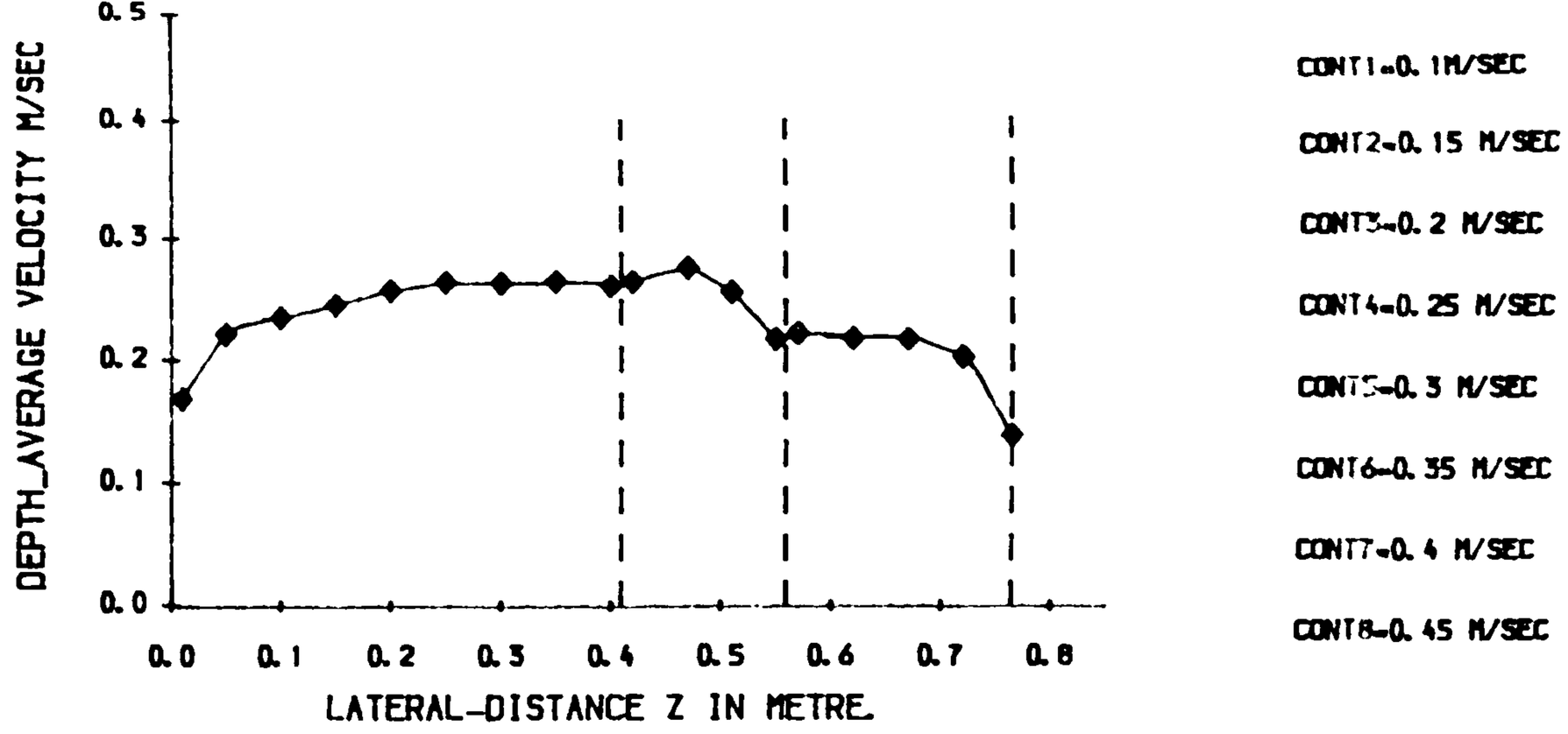

LONGITUDINAL DEPTH_AVERAGE VELOCITY PROFILE IN PLAN.

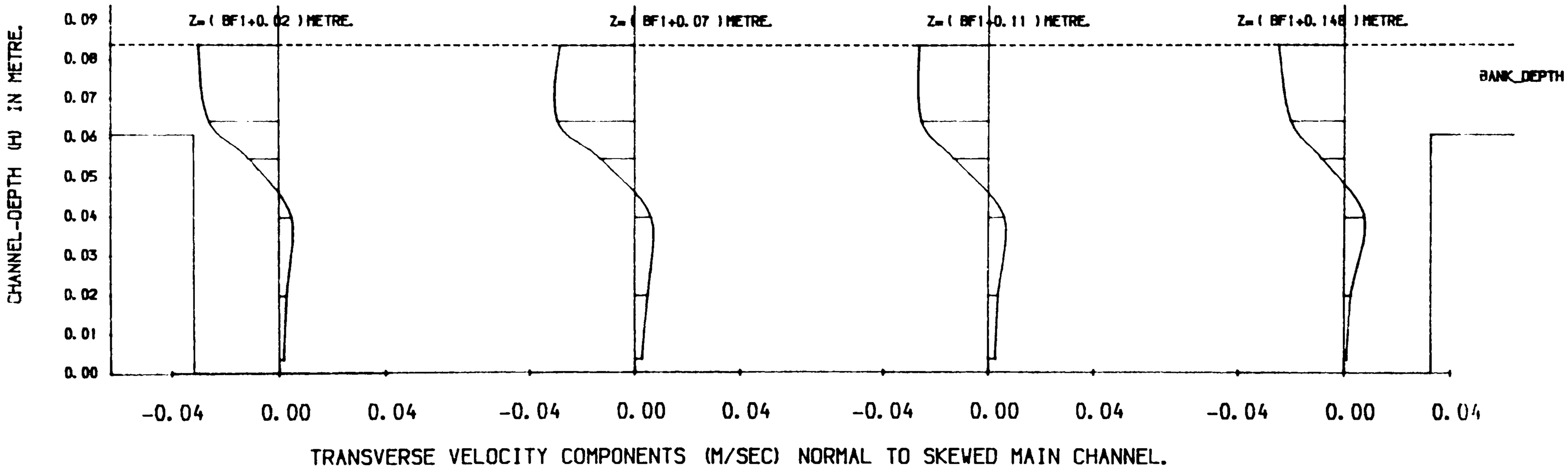

FIG (5. 11) LONGITUDINAL & TRANSVERSE VELOCITY COMPONENTS IN SKEWED CHANNEL WITH SMOOTH FLOODPLAIN

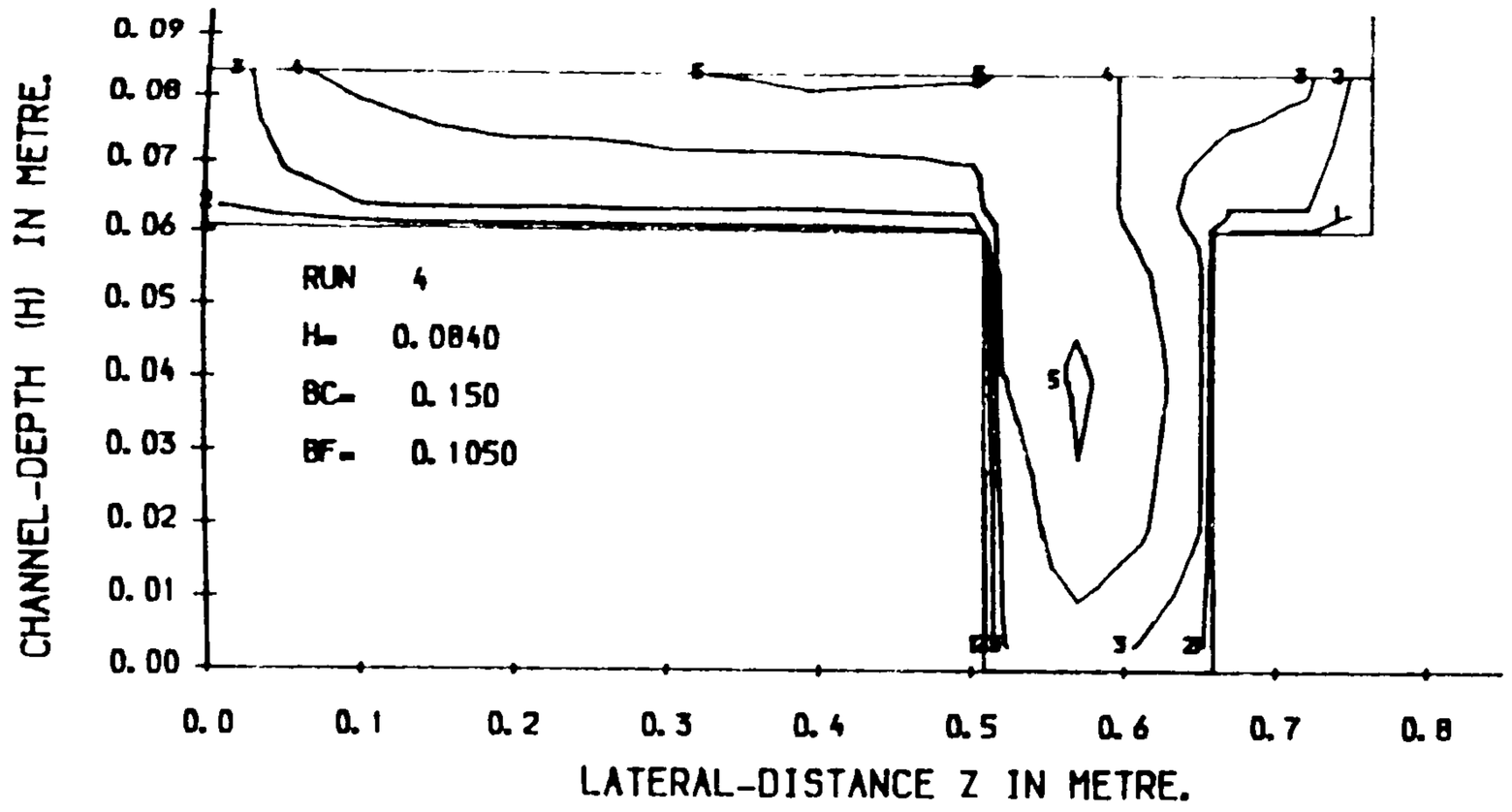

LONGITUDINAL VELOCITY CONTOURS IN CROSS SECTION. 3

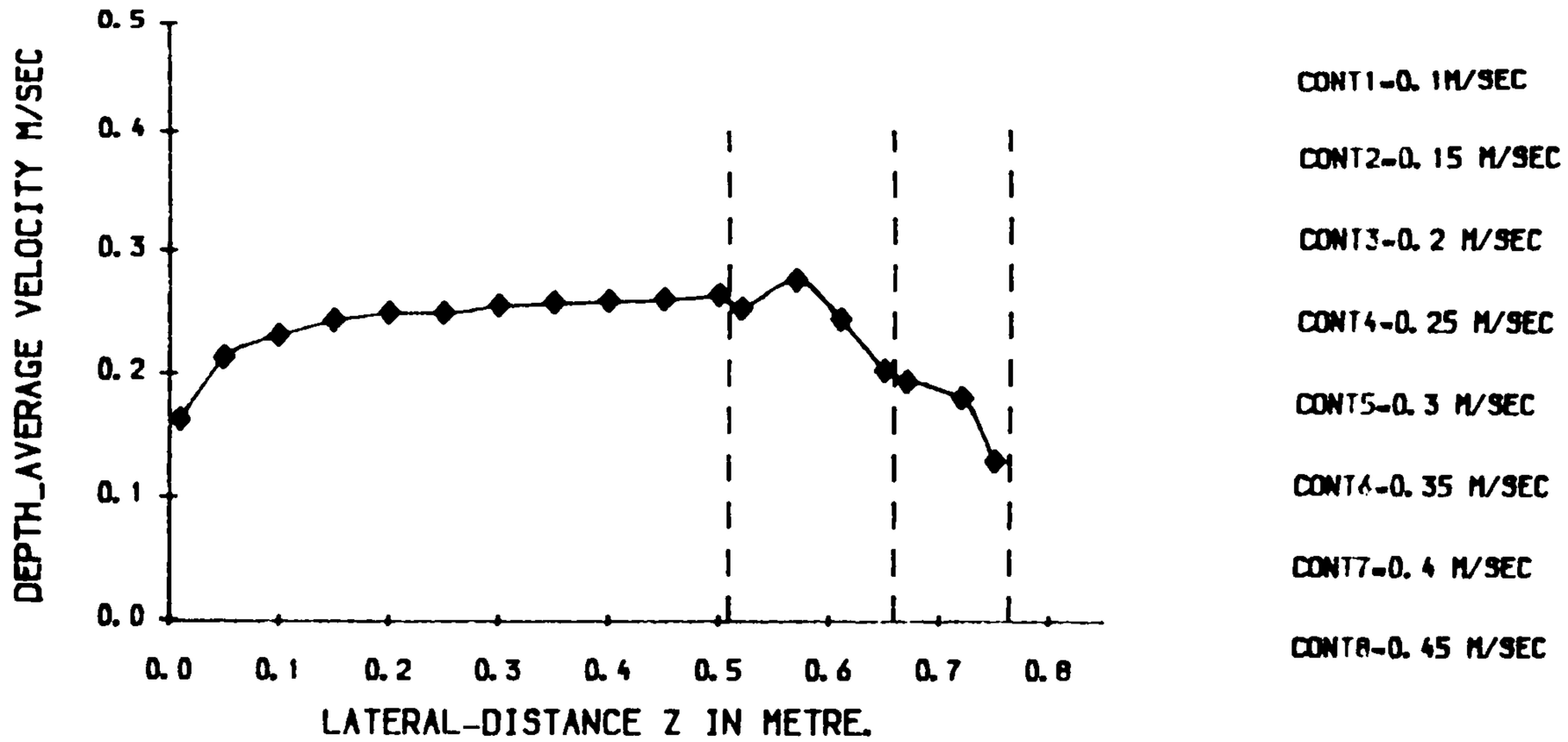

LONGITUDINAL DEPTH_AVERAGE VELOCITY PROFILE IN PLAN.

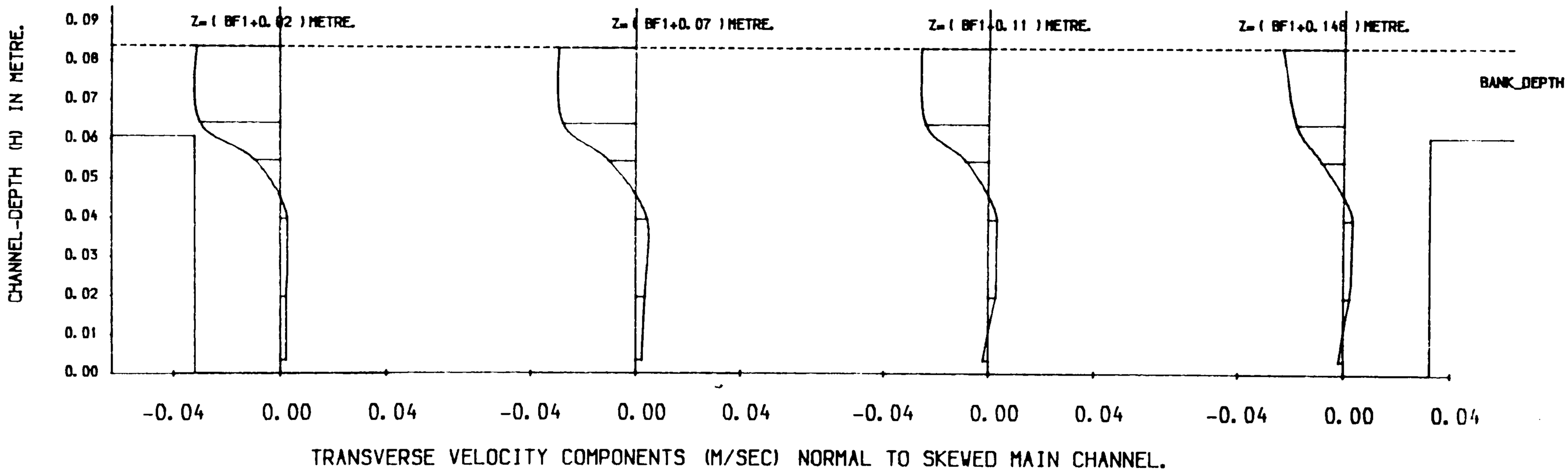

FIG (5. 12) LONGITUDINAL & TRANSVERSE VELOCITY COMPONENTS IN SKEWED CHANNEL WITH SMOOTH FLOODPLAIN

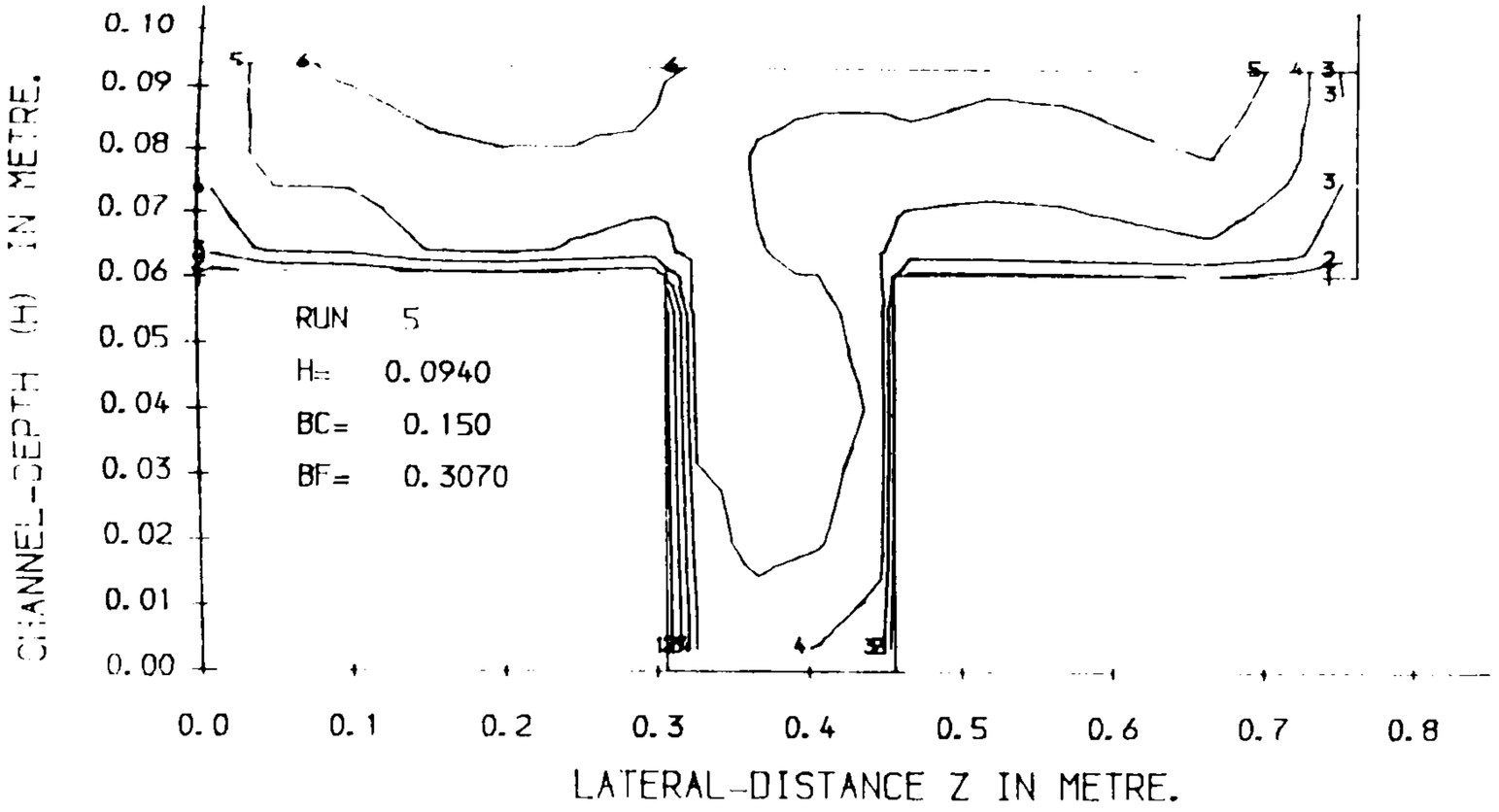

LONGITUDINAL VELOCITY CONTOURS IN CROSS SECTION. 1

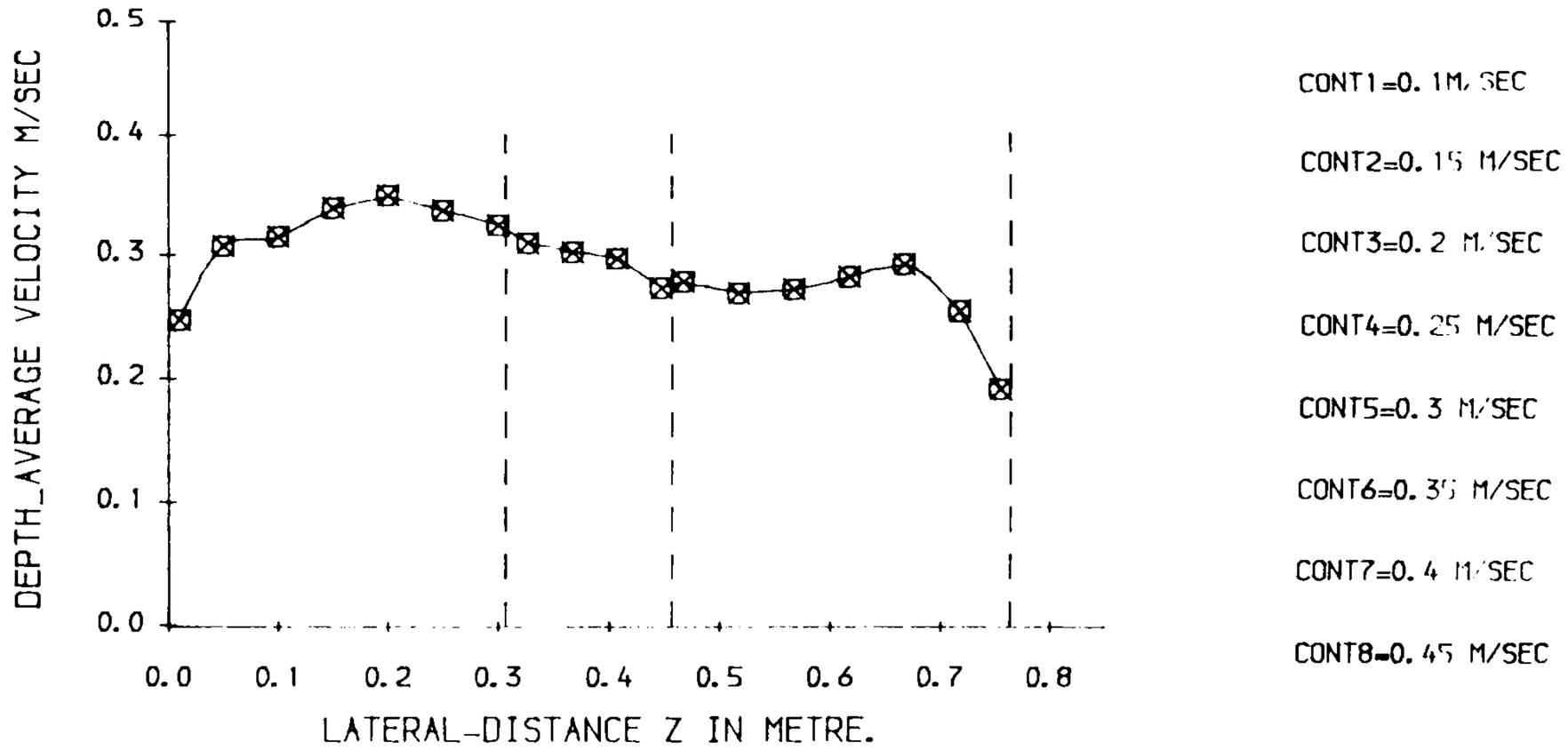

LONGITUDINAL DEPTH_AVERAGE VELOCITY PROFILE IN PLAN.

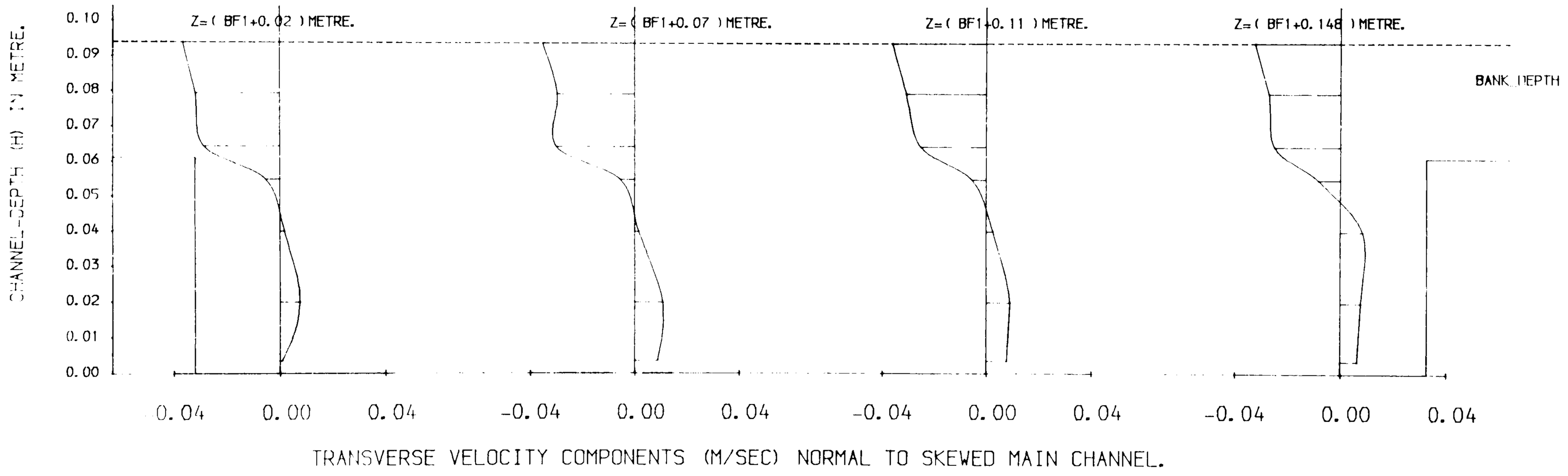

FIG (5. 13) LONGITUDINAL & TRANSVERSE VELOCITY COMPONENTS IN SKEWED CHANNEL WITH SMOOTH FLOODPLAIN

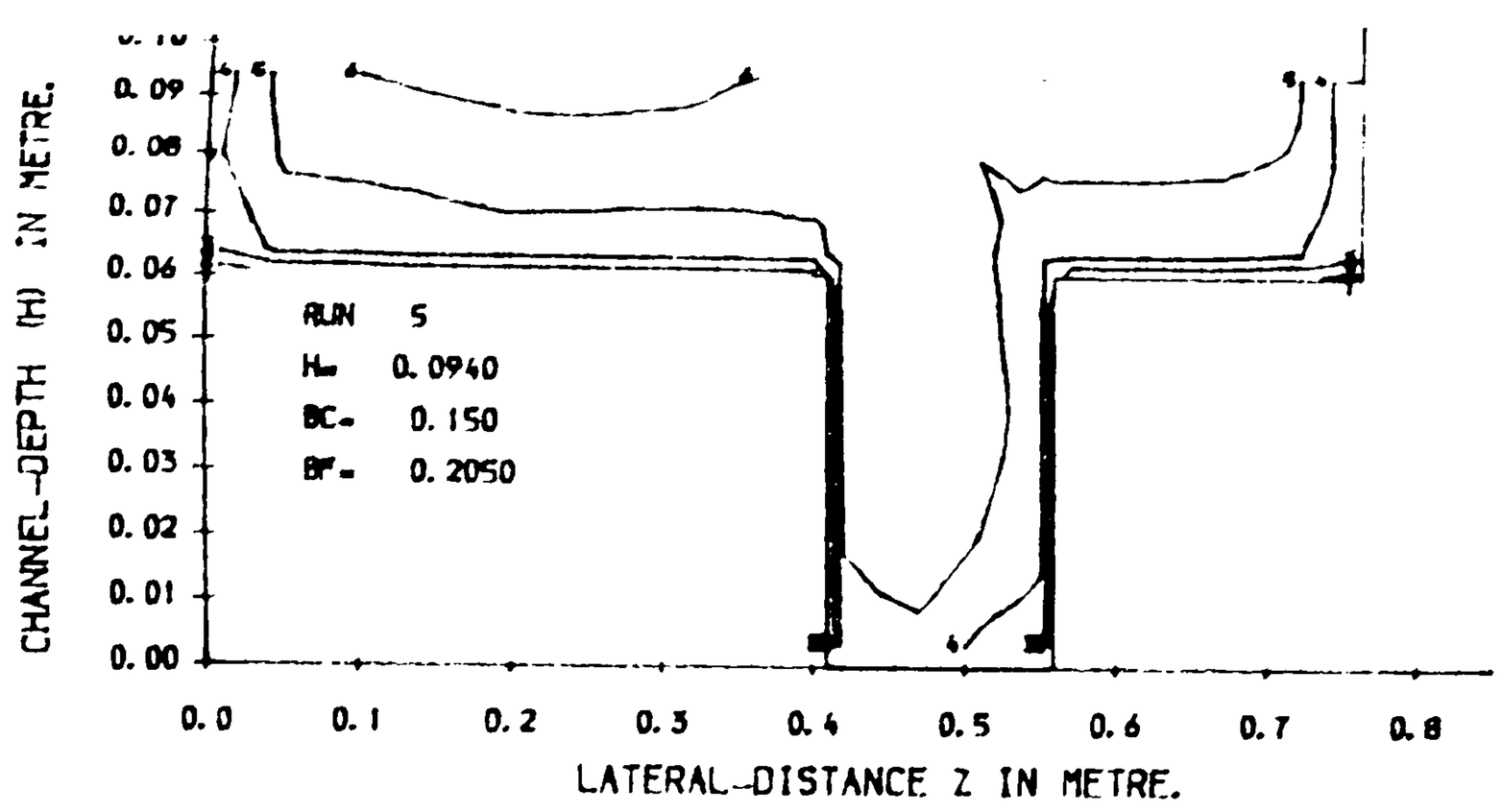

LONGITUDINAL VELOCITY CONTOURS IN CROSS SECTION. 2

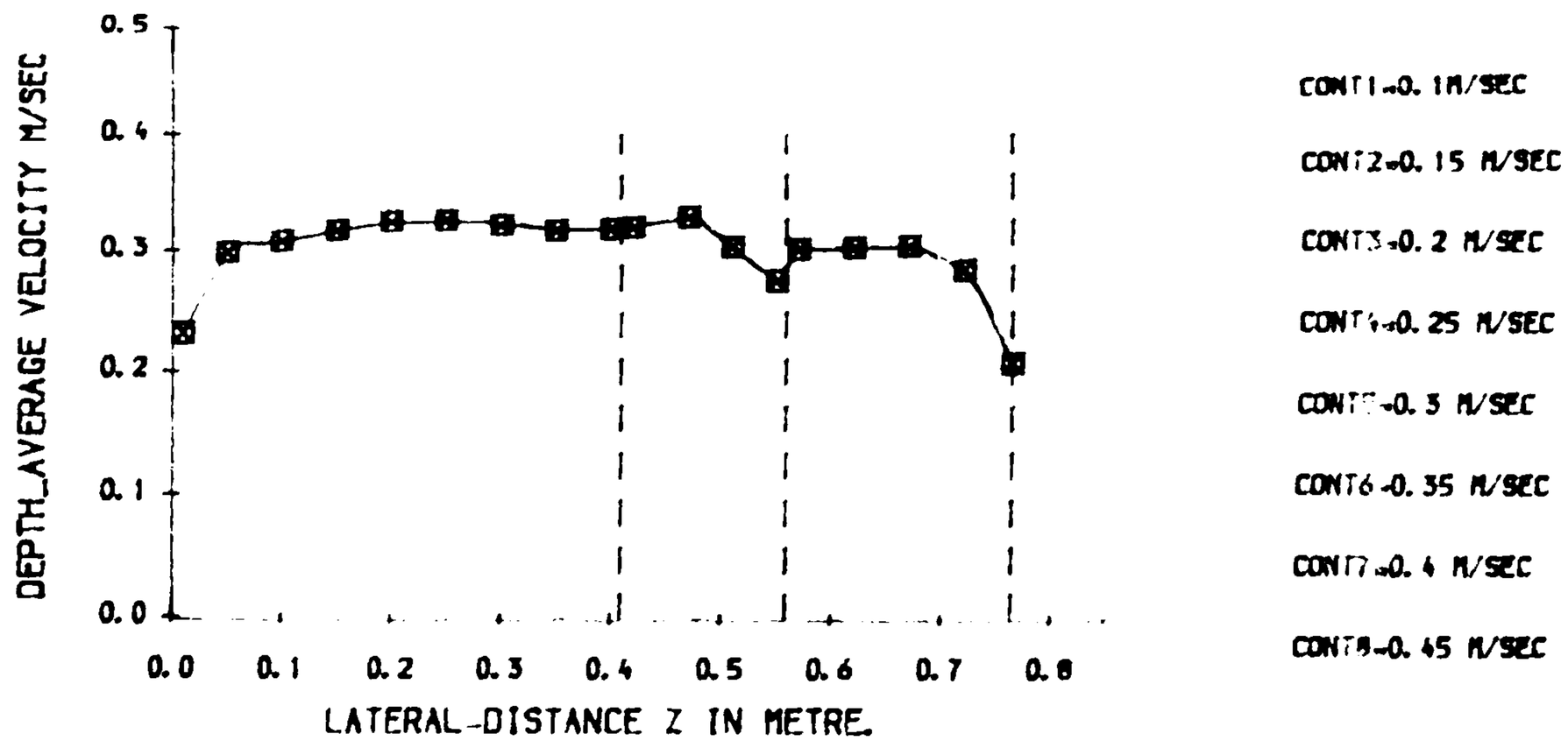

LONGITUDINAL DEPTH_AVERAGE VELOCITY PROFILE IN PLAN.

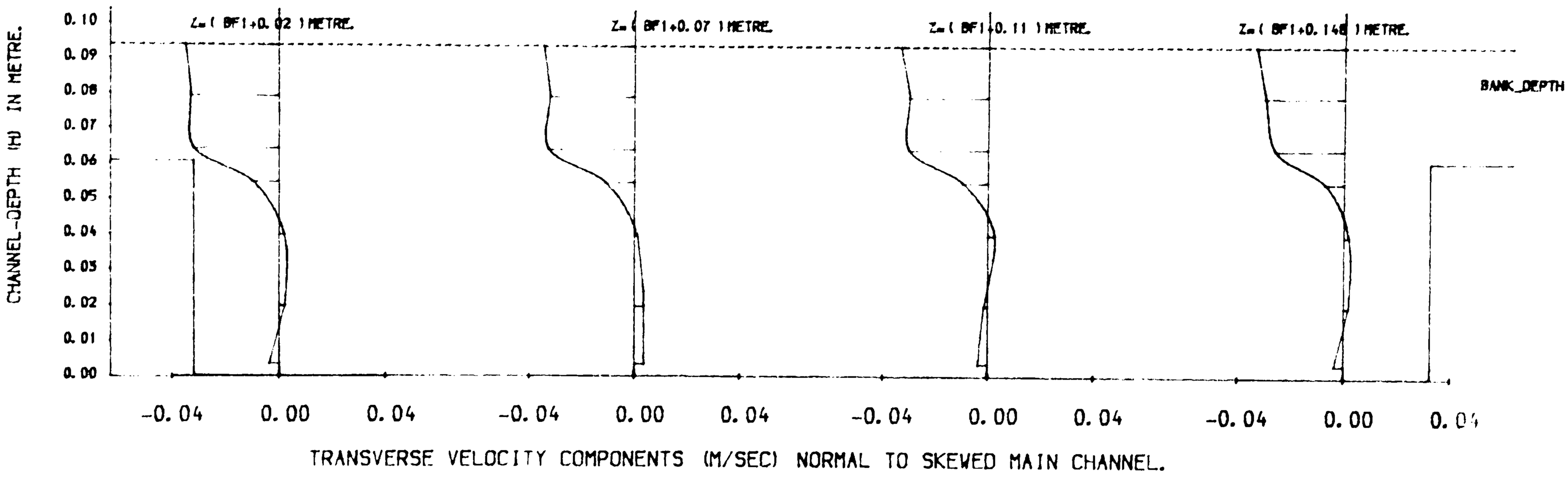

FIG (5. 14) LONGITUDINAL & TRANSVERSE VELOCITY COMPONENTS IN SKEWED CHANNEL WITH SMOOTH FLOODPLAIN

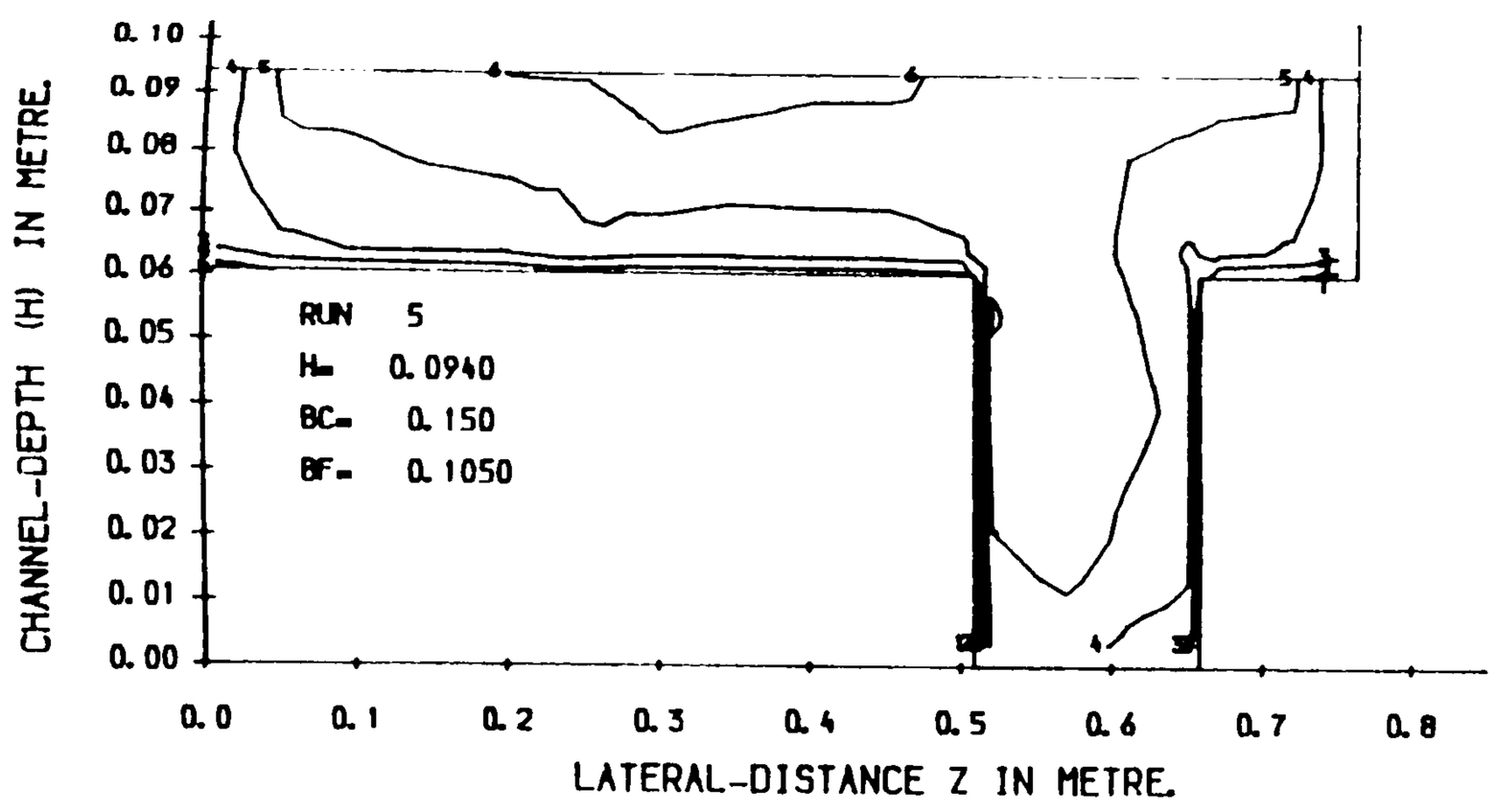

LONGITUDINAL VELOCITY CONTOURS IN CROSS SECTION. 3

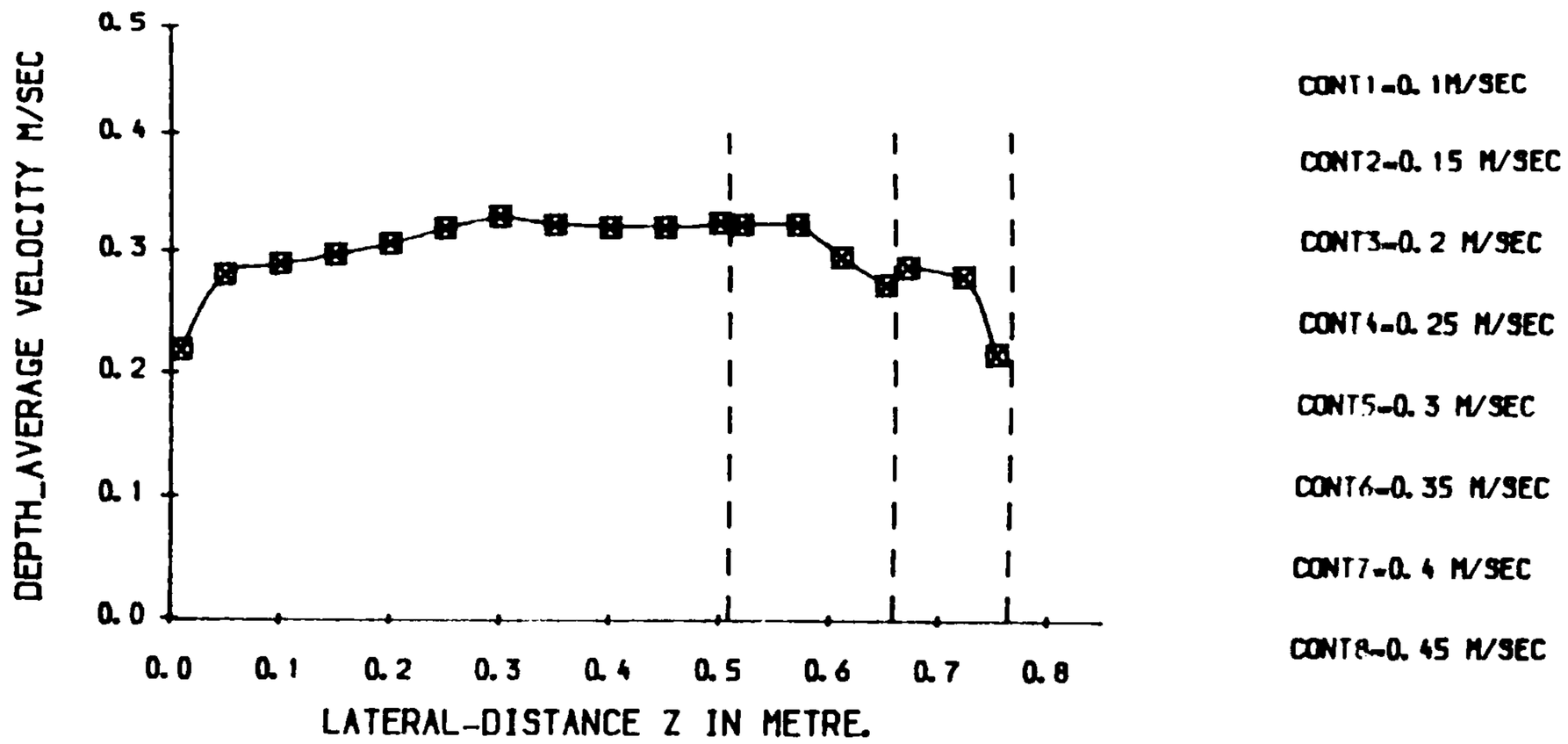

LONGITUDINAL DEPTH_AVERAGE VELOCITY PROFILE IN PLAN.

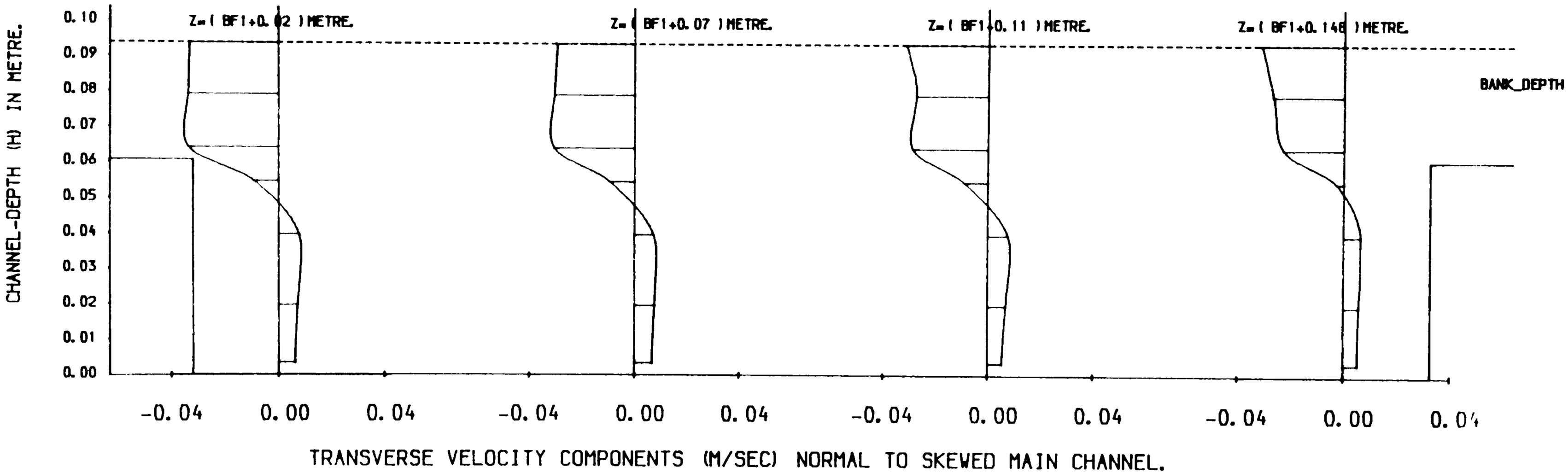

FIG (5.15) LONGITUDINAL & TRANSVERSE VELOCITY COMPONENTS IN SKEWED CHANNEL WITH SMOOTH FLOODPLAIN

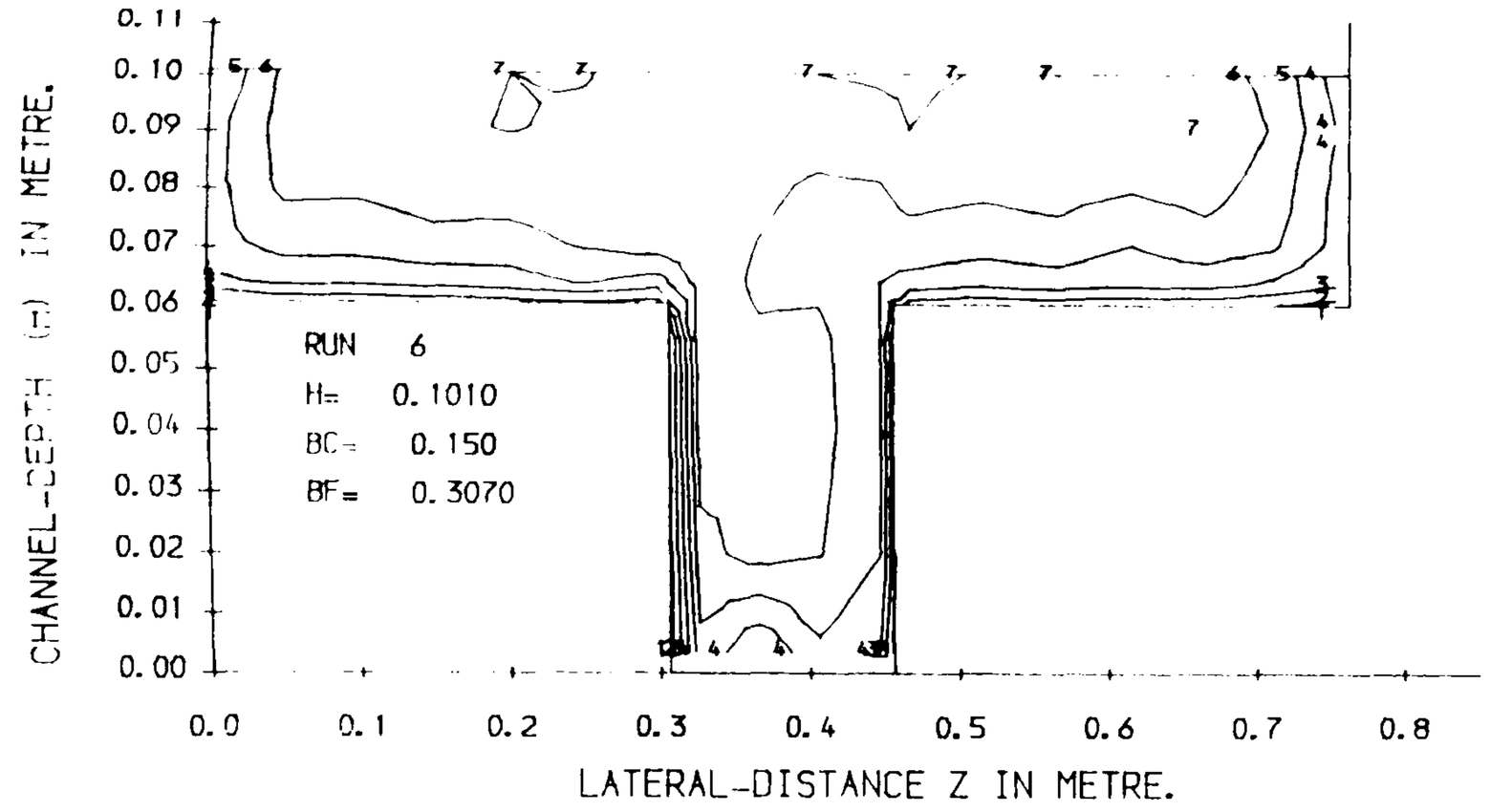

LONGITUDINAL VELOCITY CONTOURS IN CROSS SECTION. 1

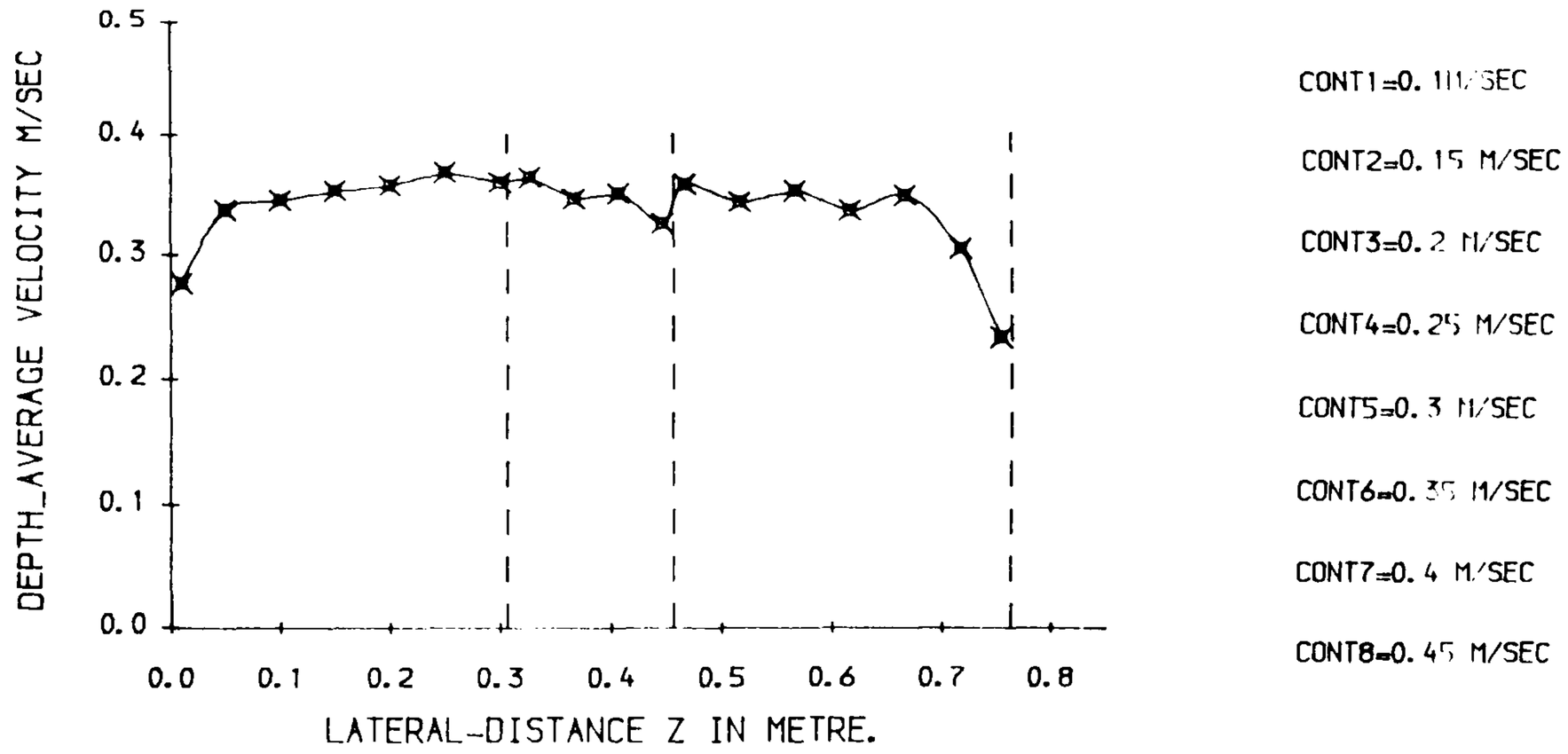

LONGITUDINAL DEPTH_AVERAGE VELOCITY PROFILE IN PLAN.

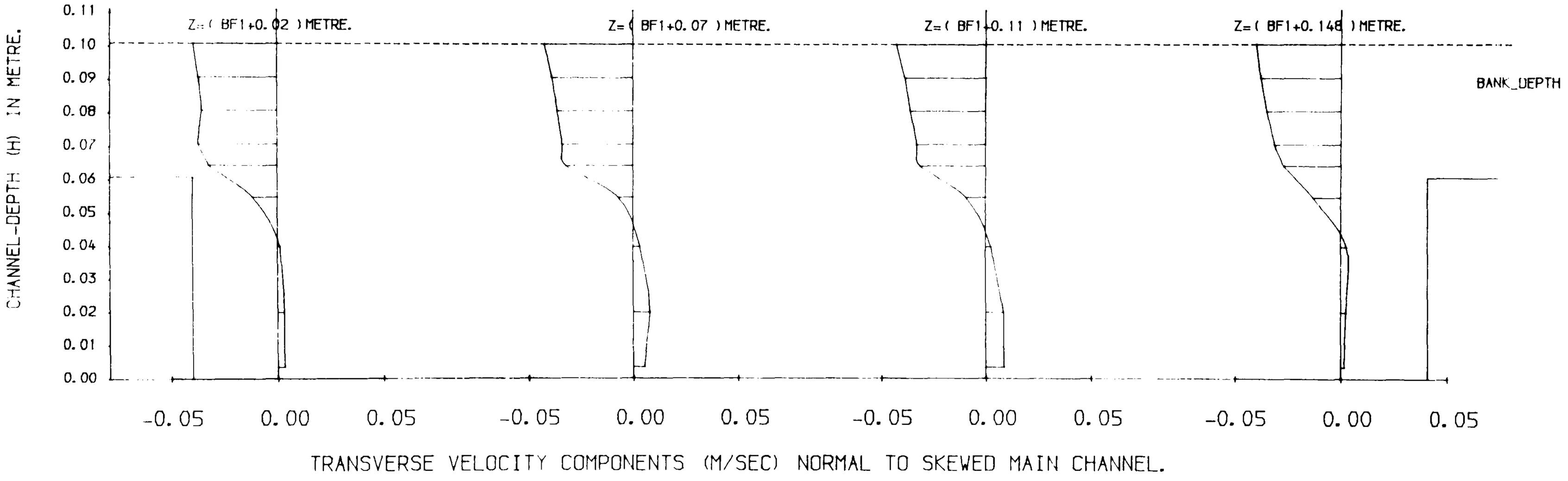

FIG(5.16) LONGITUDINAL & TRANSVERSE VELOCITY COMPONENTS IN SKEWED CHANNEL WITH SMOOTH FLOODPLAIN

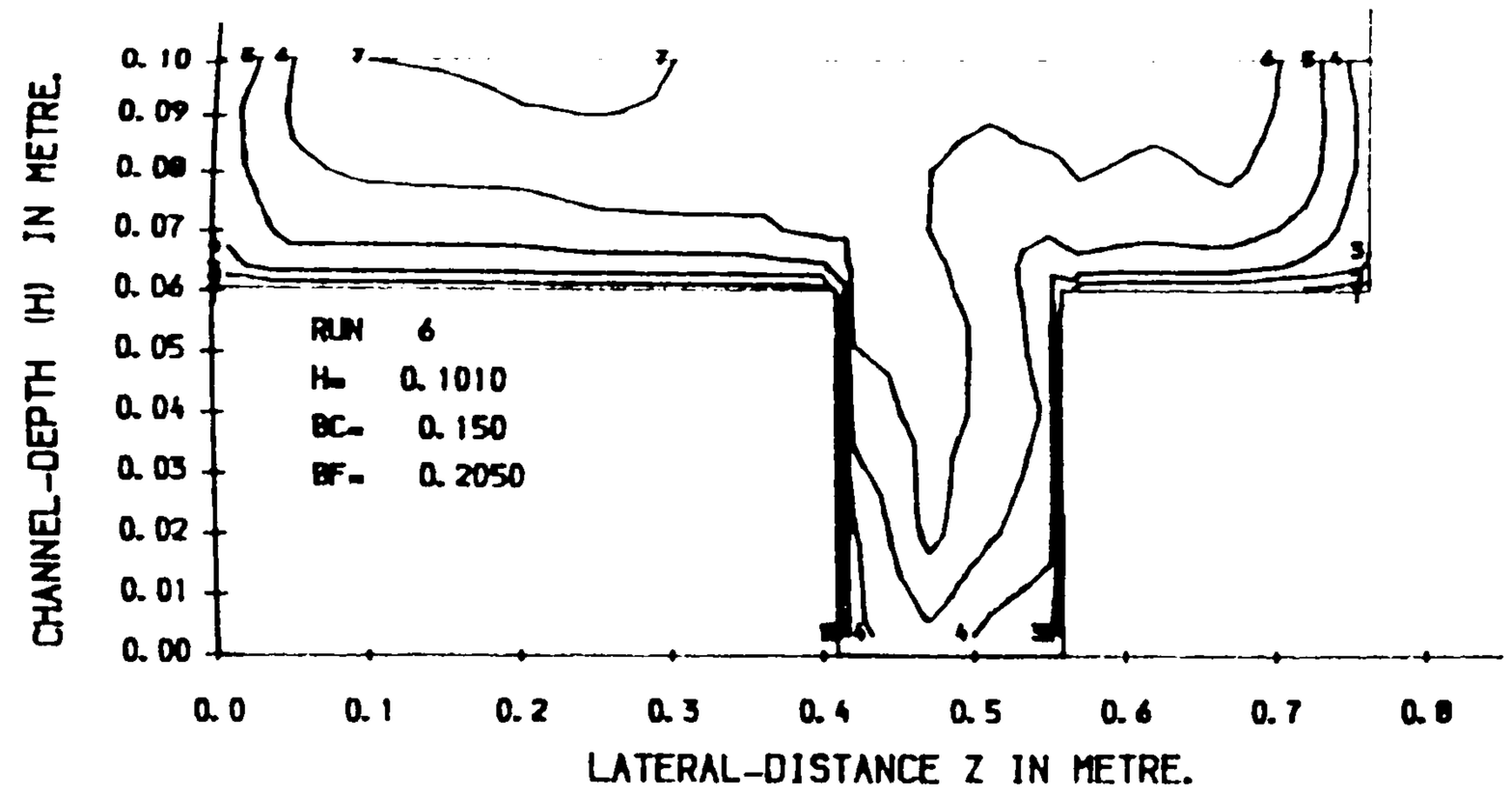

LONGITUDINAL VELOCITY CONTOURS IN CROSS SECTION. 2

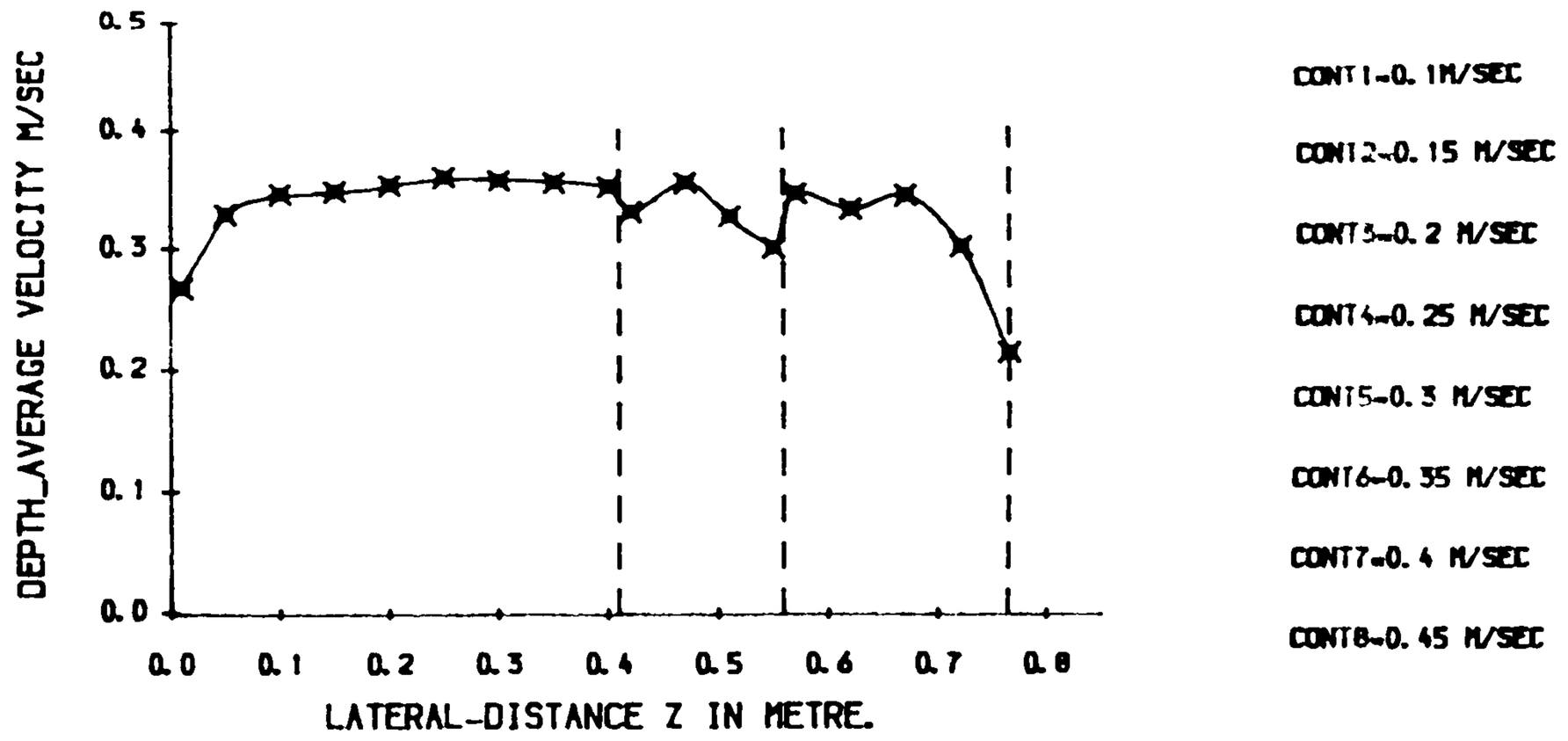

LONGITUDINAL DEPTH_AVERAGE VELOCITY PROFILE IN PLAN.

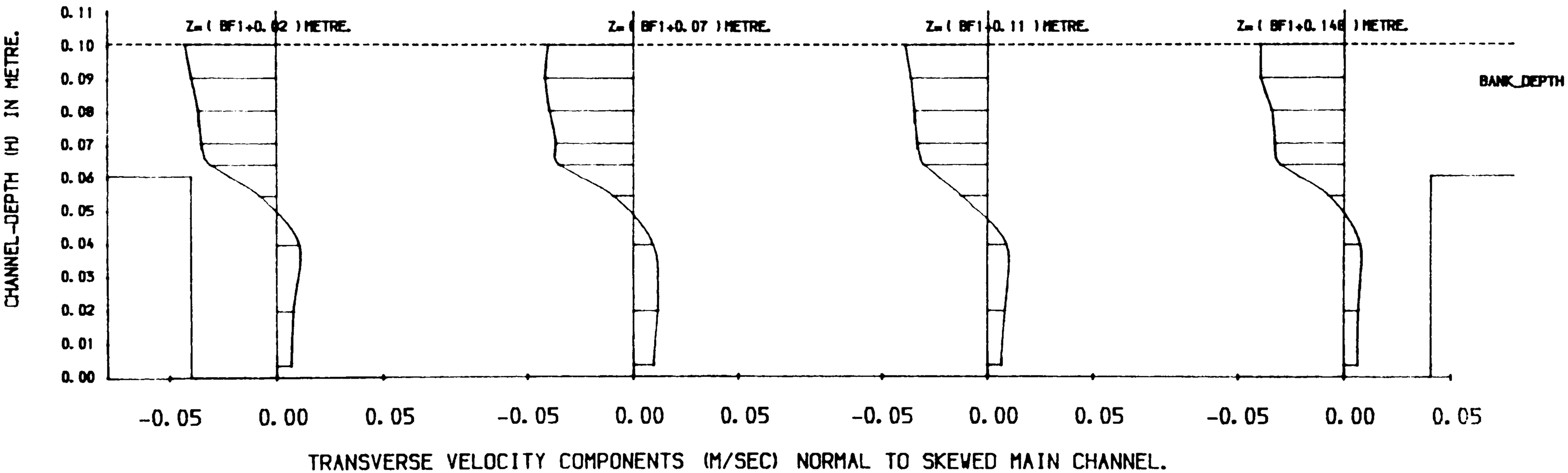

FIG (5. 17) LONGITUDINAL & TRANSVERSE VELOCITY COMPONENTS IN SKEWED CHANNEL WITH SMOOTH FLOODPLAIN

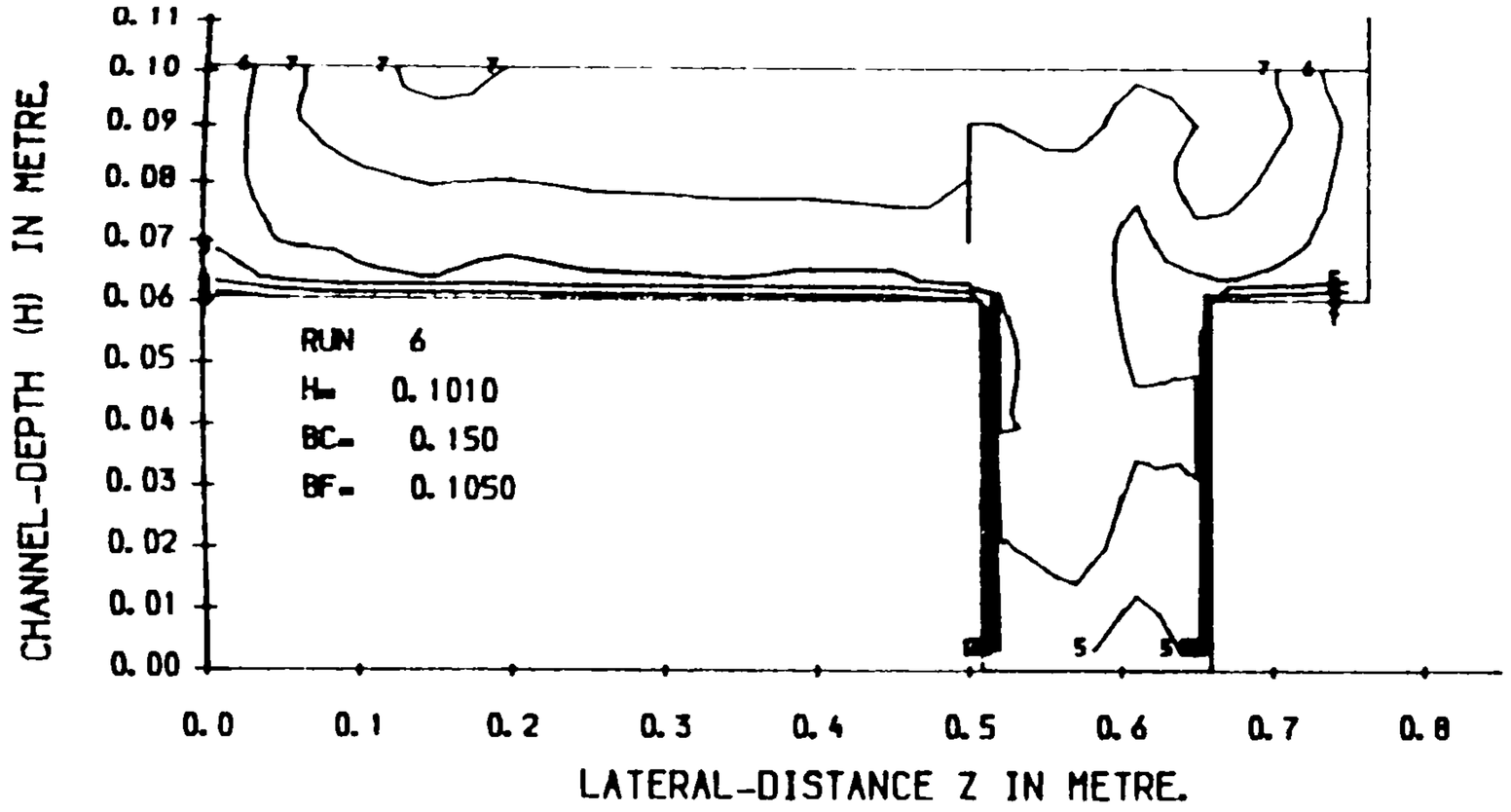

LONGITUDINAL VELOCITY CONTOURS IN CROSS SECTION. 3

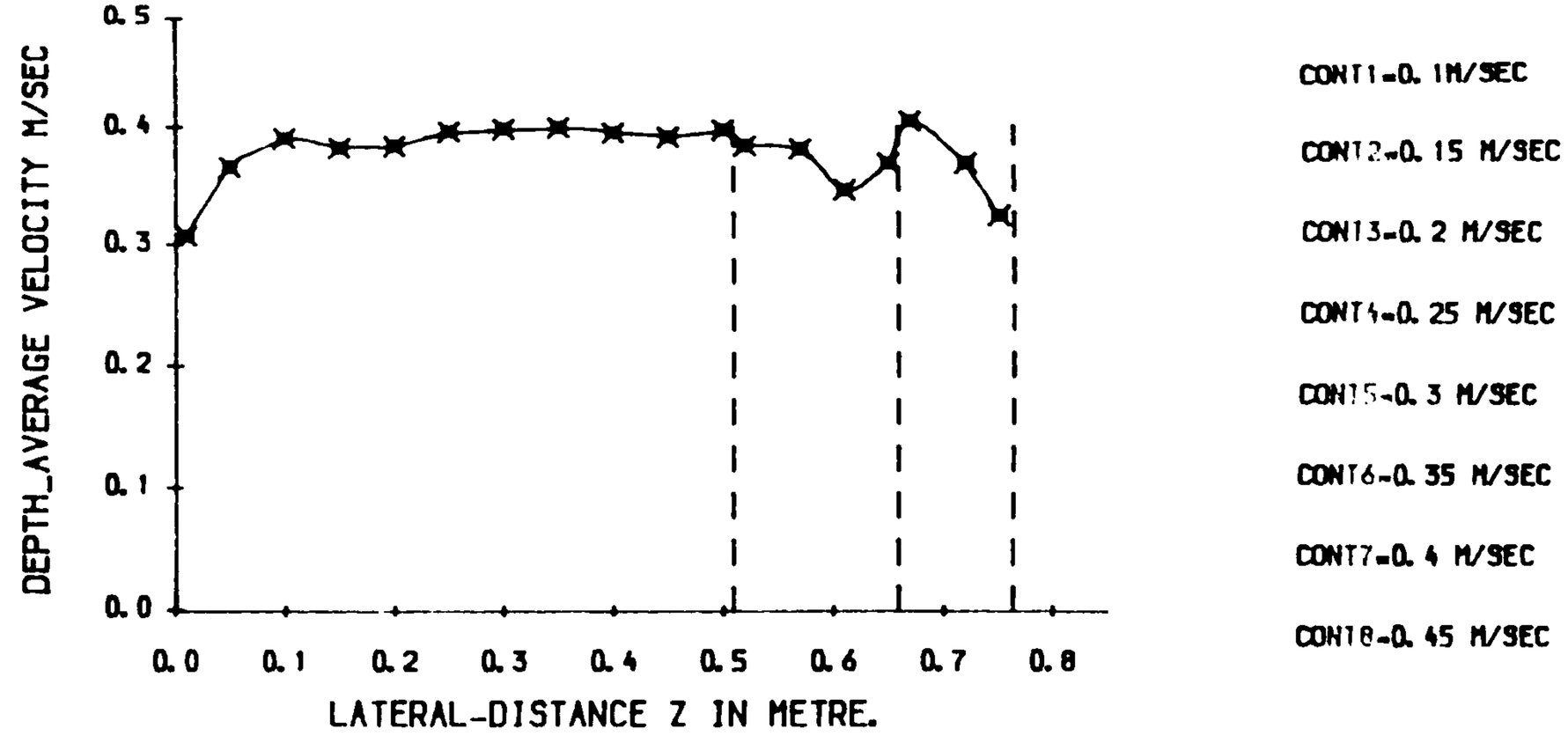

LONGITUDINAL DEPTH_AVERAGE VELOCITY PROFILE IN PLAN.

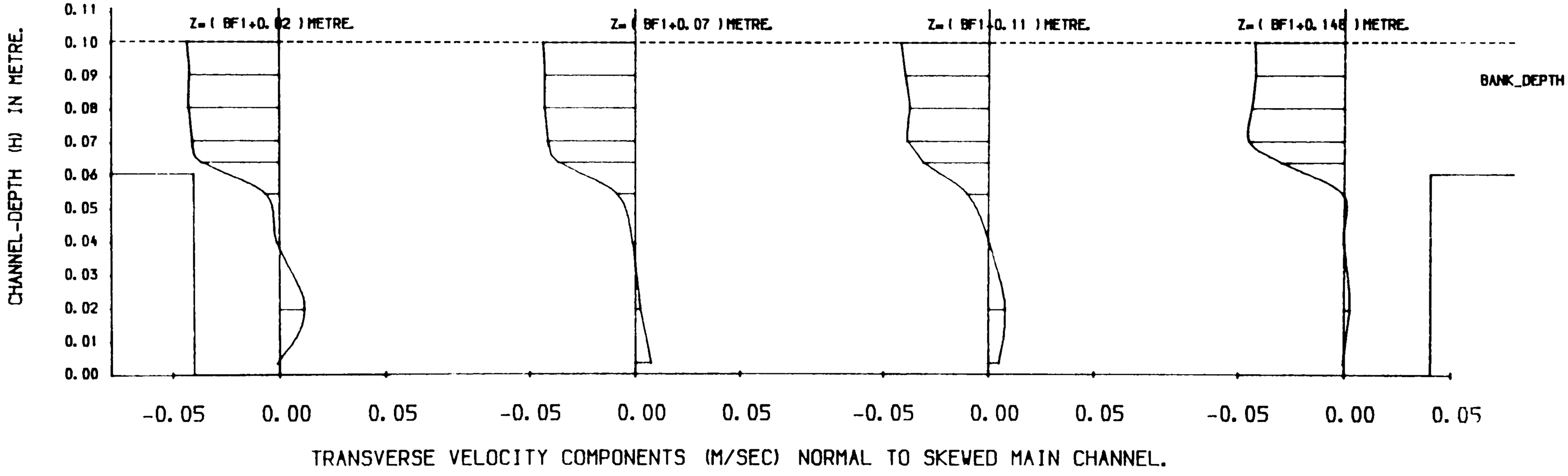

FIG (5.18) LONGITUDINAL & TRANSVERSE VELOCITY COMPONENTS IN SKEWED CHANNEL WITH SMOOTH FLOODPLAIN

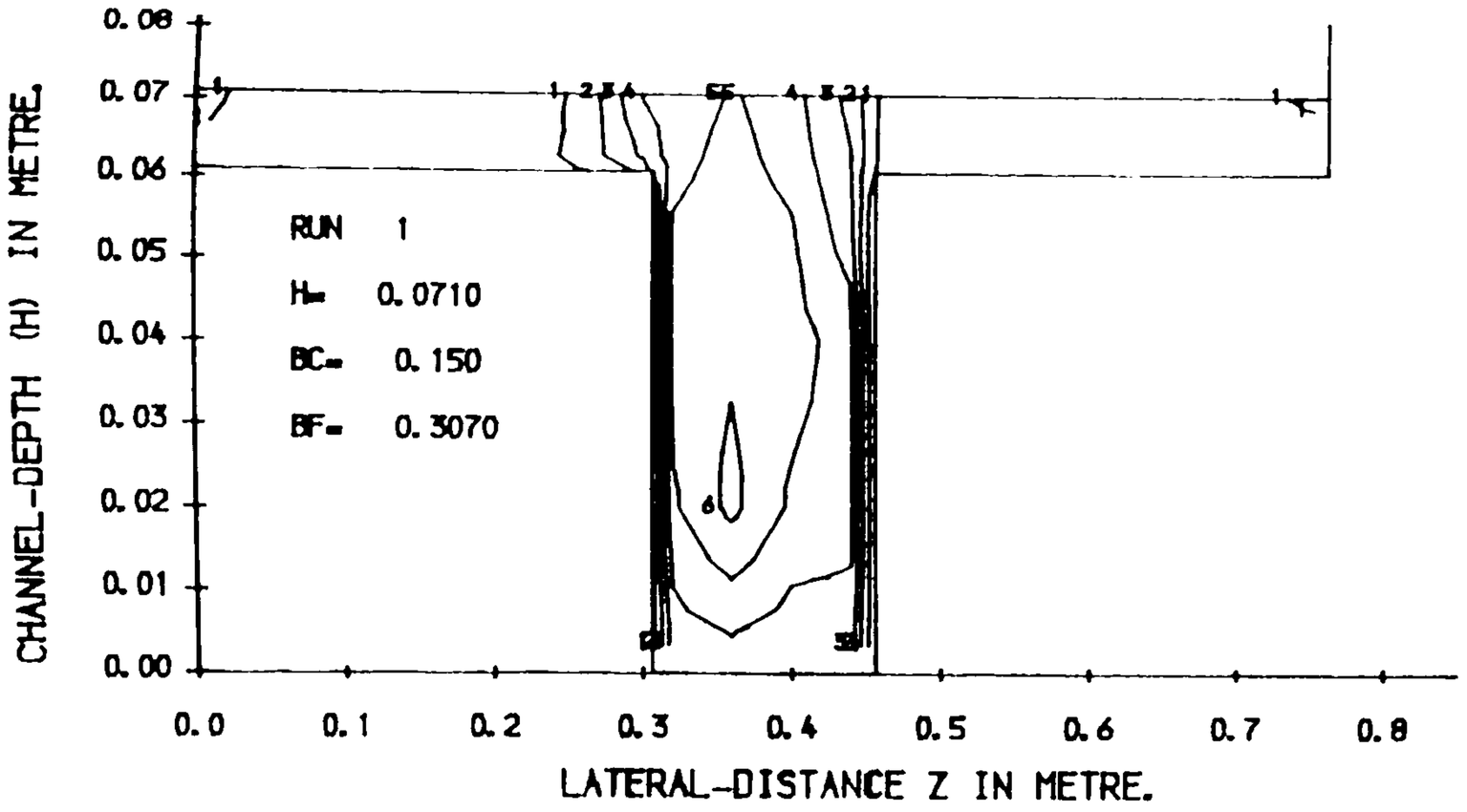

LONGITUDINAL VELOCITY CONTOURS IN CROSS SECTION. 1

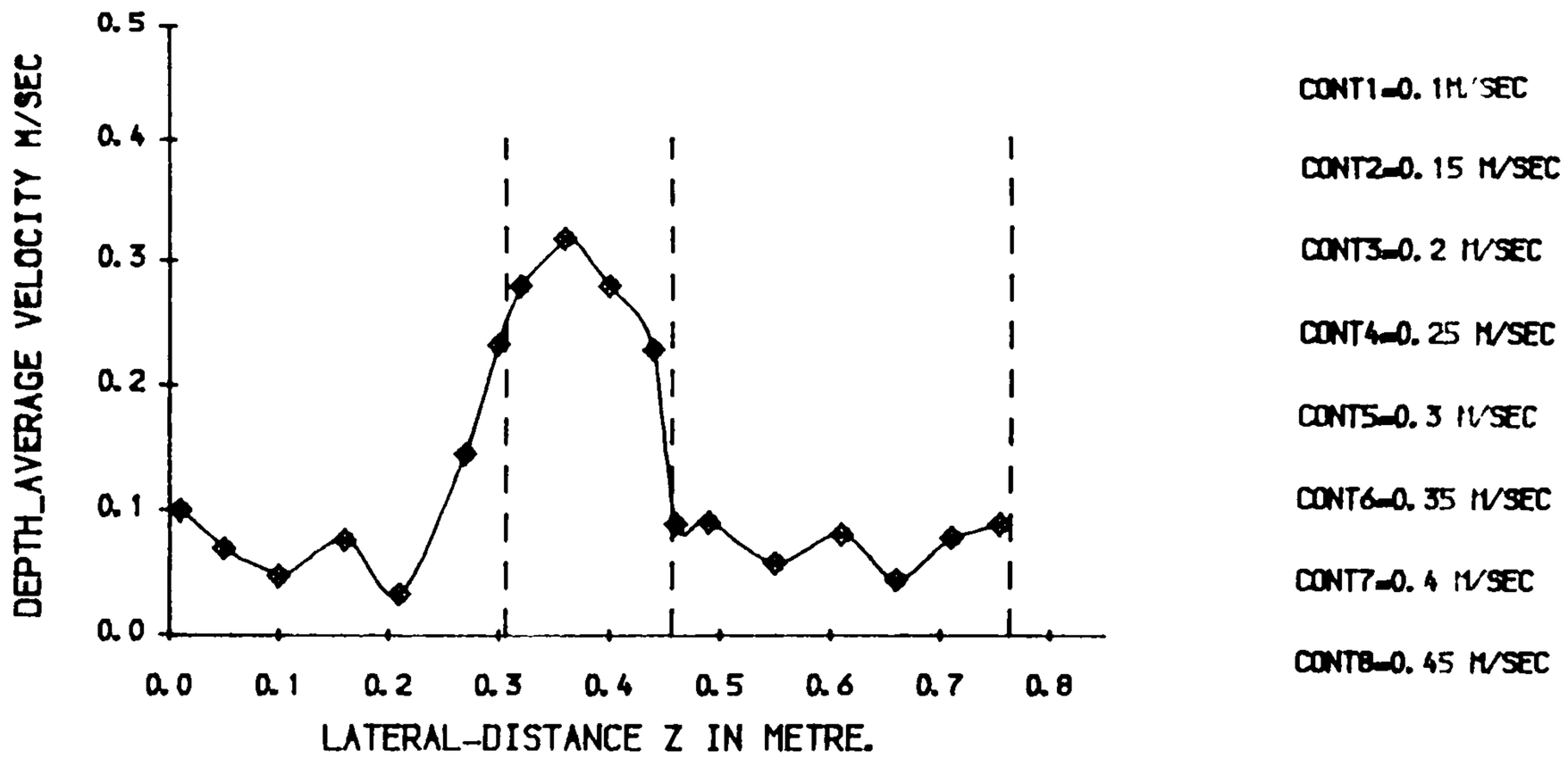

LONGITUDINAL DEPTH_AVERAGE VELOCITY PROFILE IN PLAN.

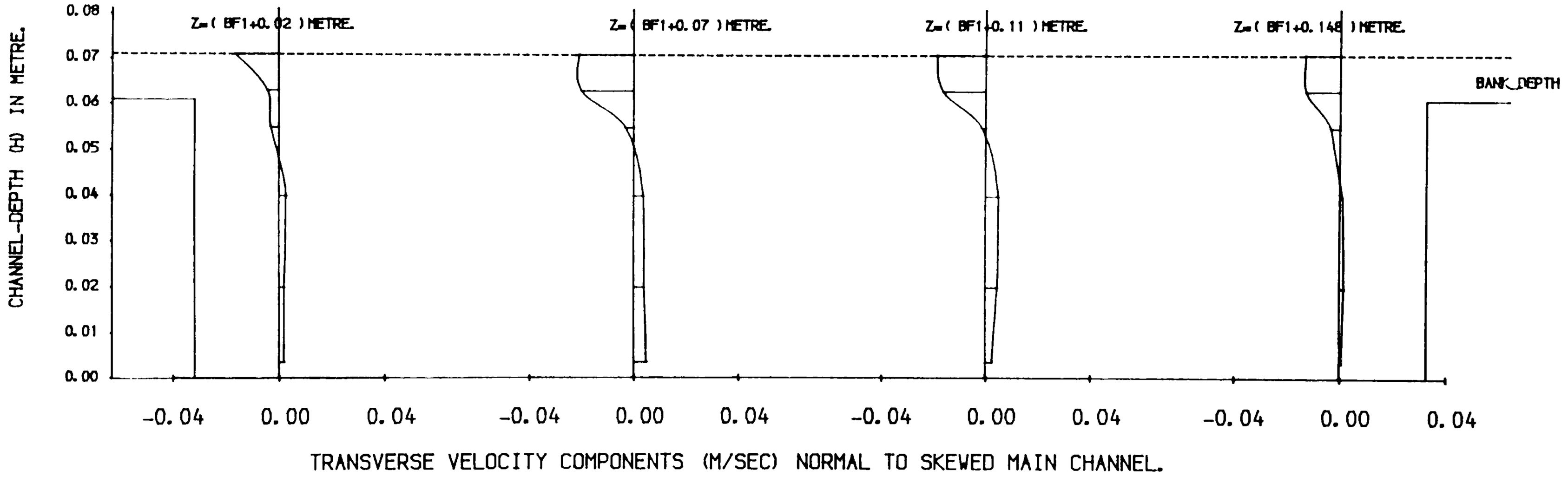

FIG(5.19) LONGITUDINAL & TRANSVERSE VELOCITY COMPONENTS IN SKEWED CHANNEL WITH ROUGH FLOODPLAIN

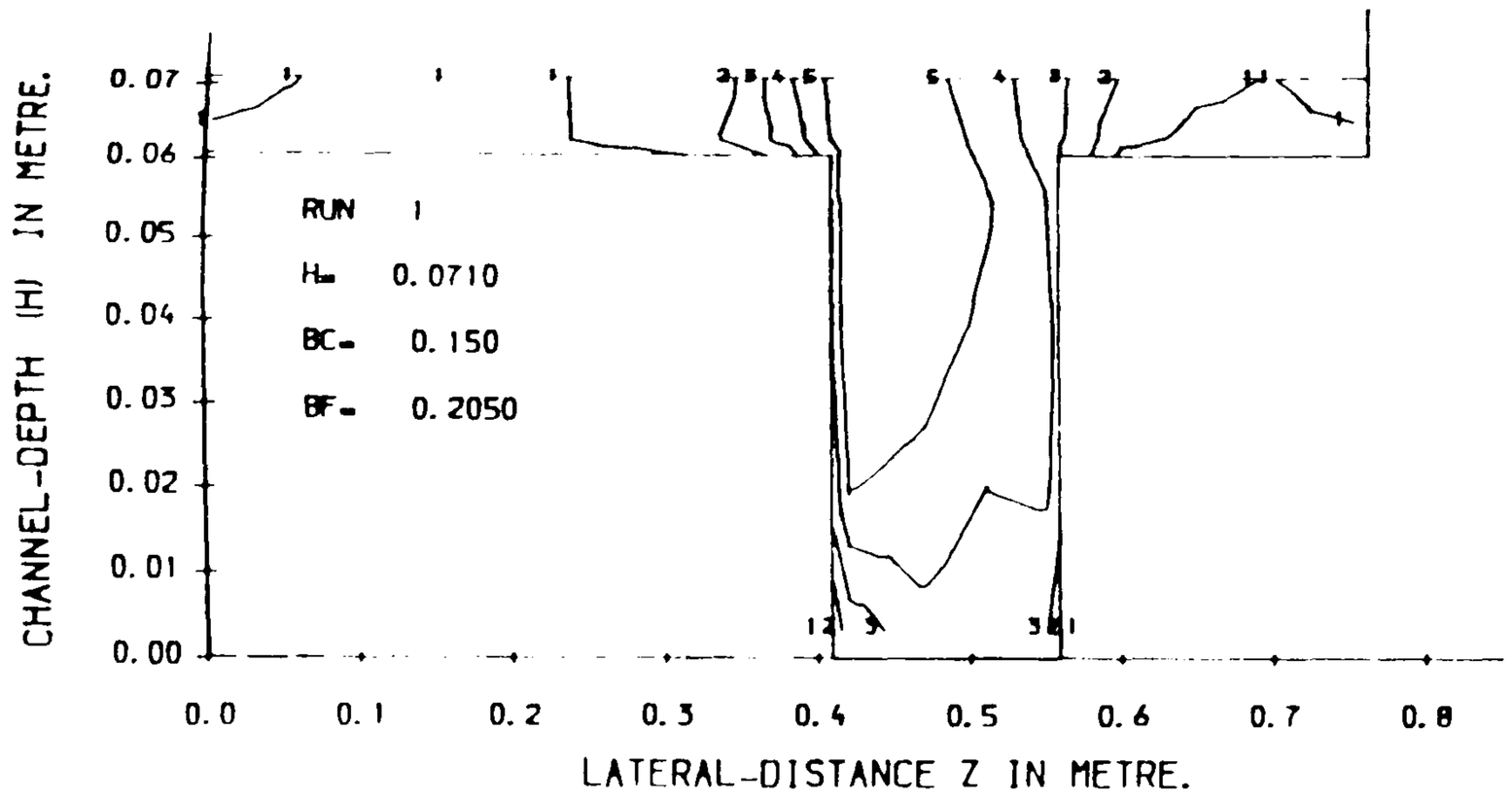

LONGITUDINAL VELOCITY CONTOURS IN CROSS SECTION. 2

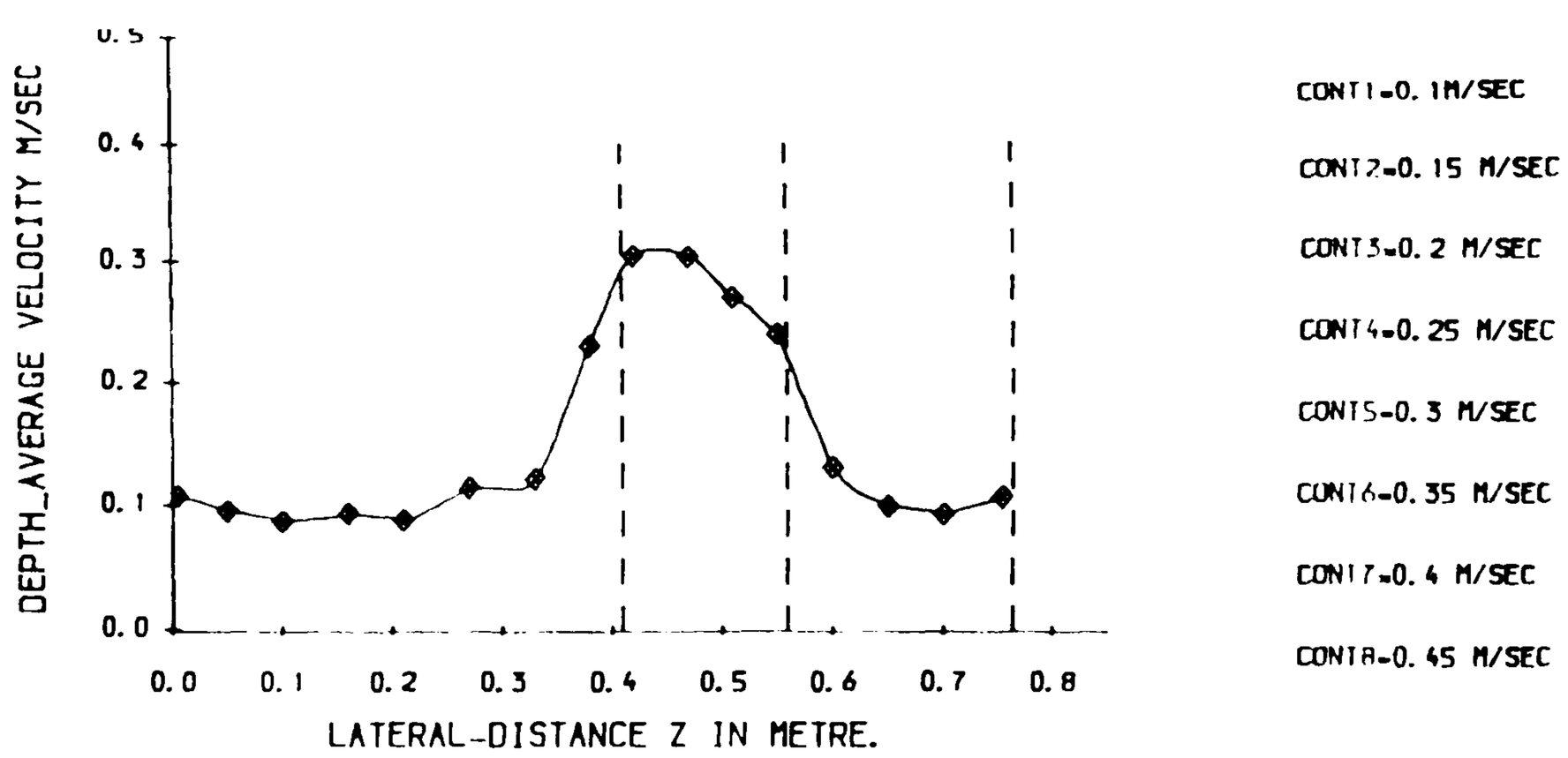

LONGITUDINAL DEPTH_AVERAGE VELOCITY PROFILE IN PLAN.

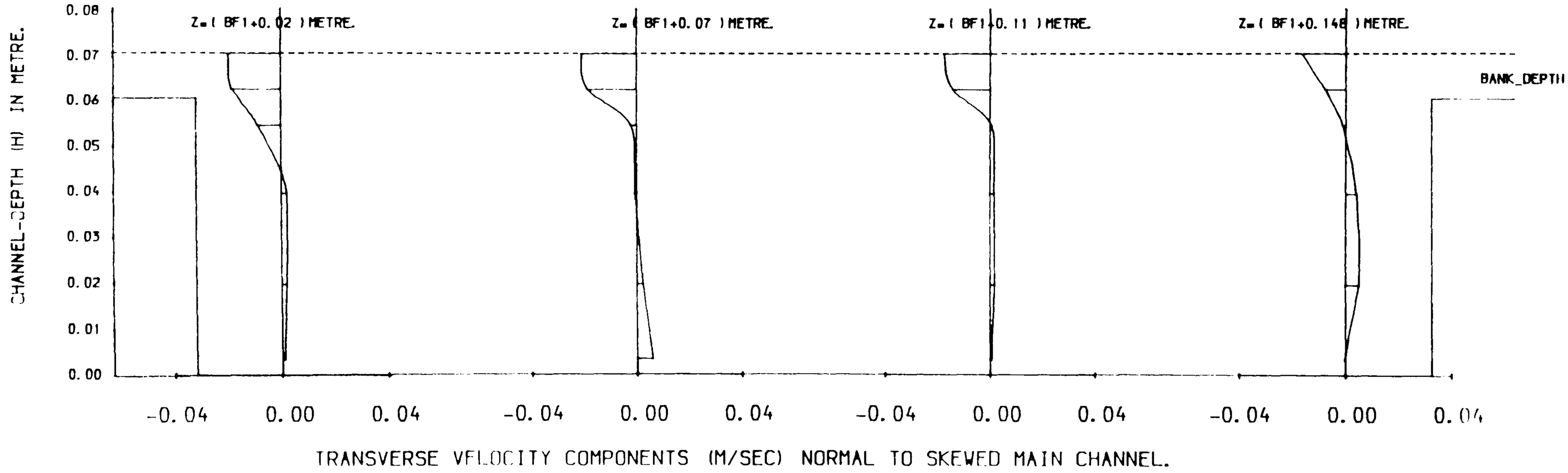

FIG (5.20) LONGITUDINAL & TRANSVERSE VELOCITY COMPONENTS IN SKEWED CHANNEL WITH ROUGH FLOODPLAIN

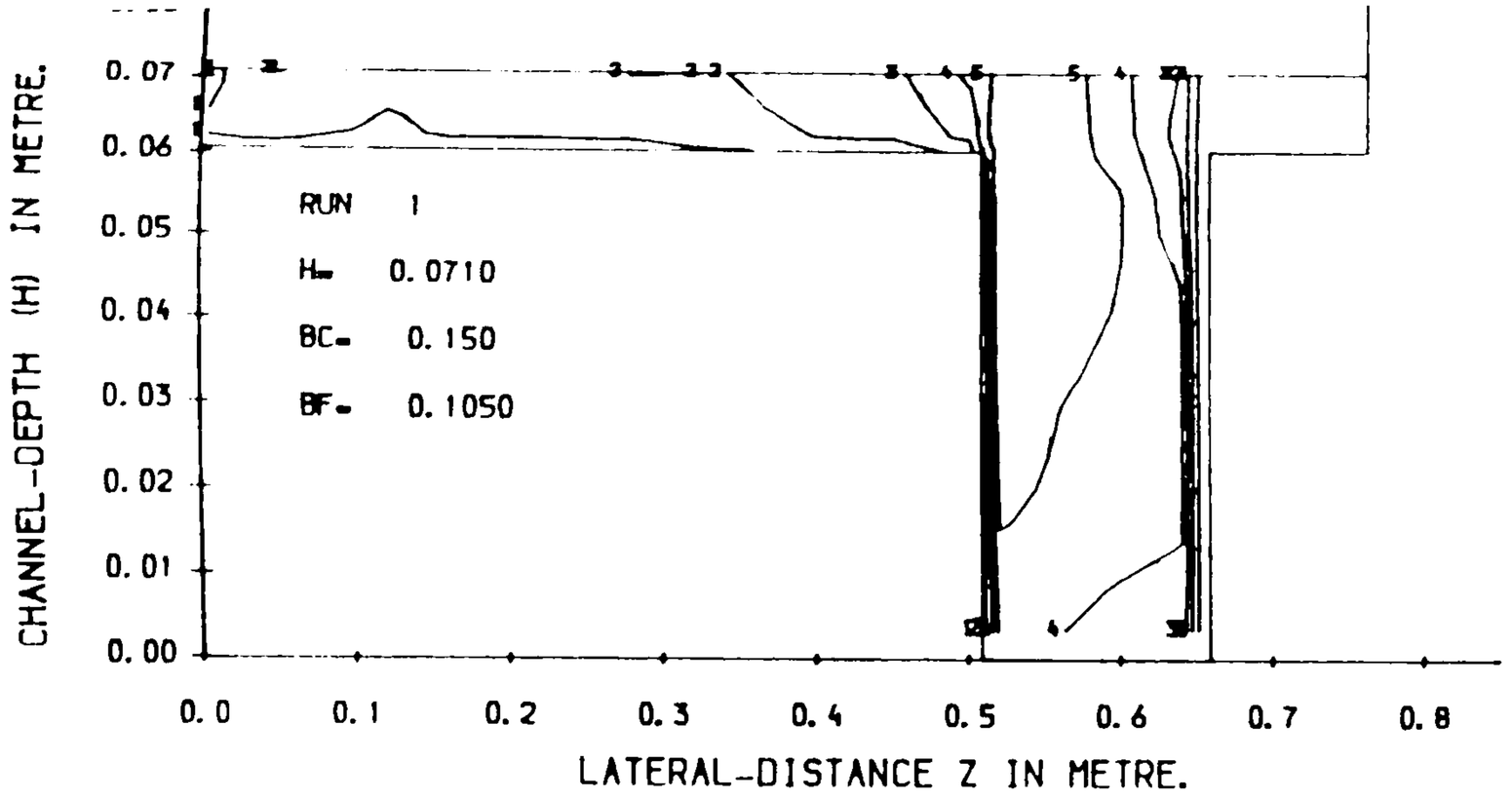

LONGITUDINAL VELOCITY CONTOURS IN CROSS SECTION. 3

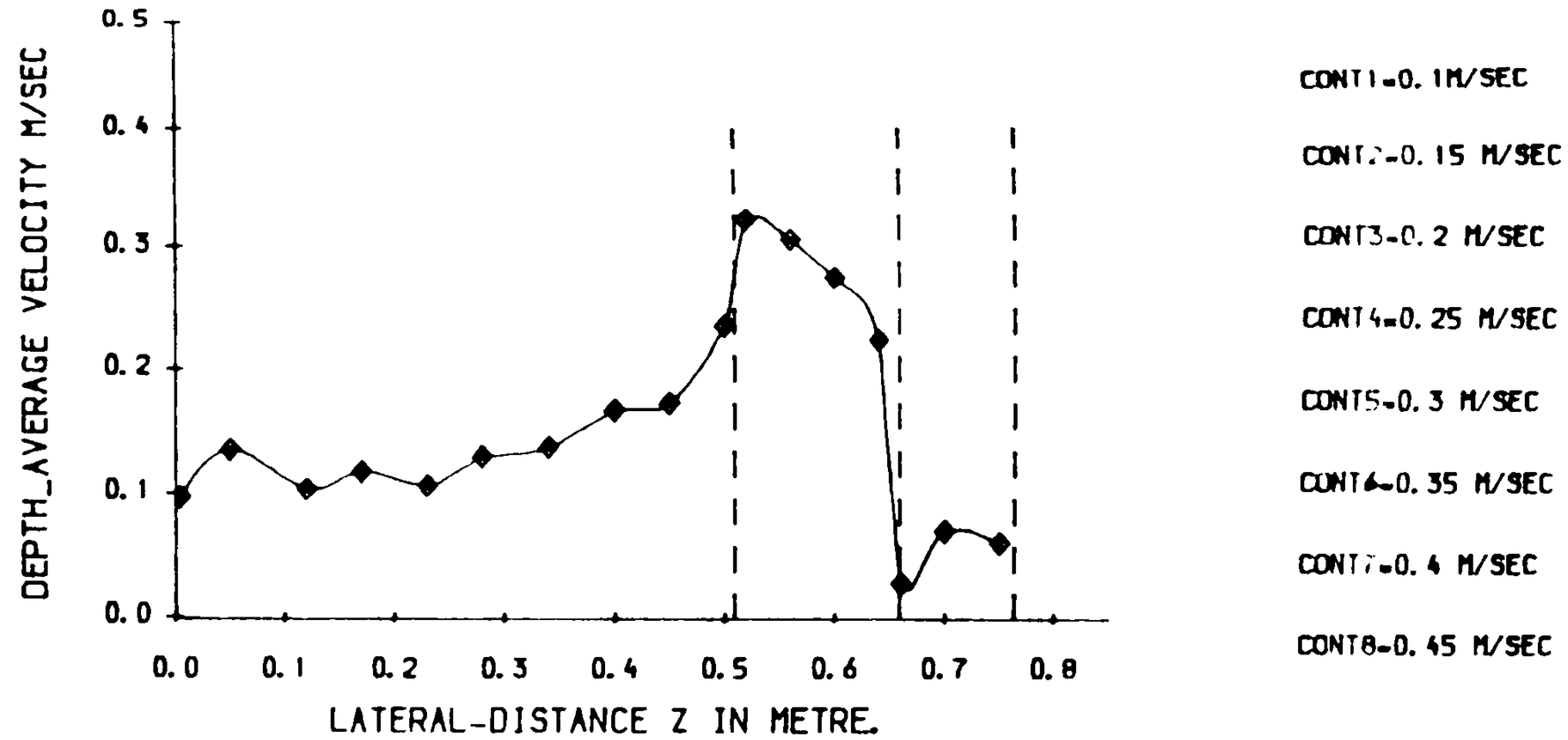

LONGITUDINAL DEPTH_AVERAGE VELOCITY PROFILE IN PLAN.

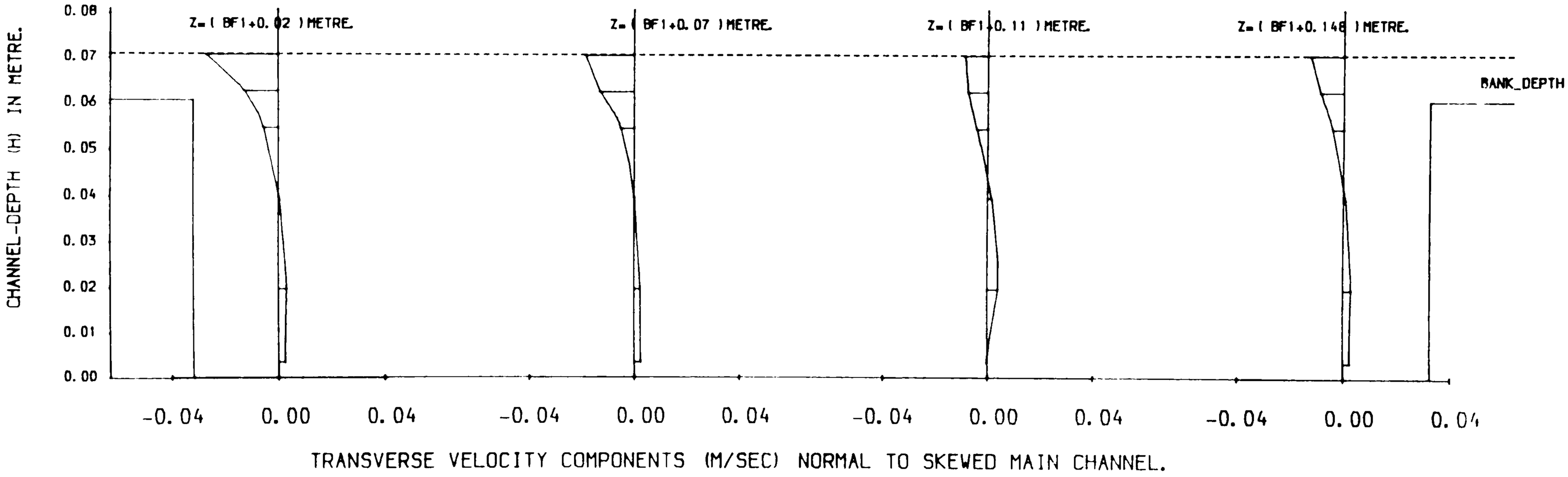

FIG (5.21) LONGITUDINAL & TRANSVERSE VELOCITY COMPONENTS IN SKEWED CHANNEL WITH ROUGH FLOODPLAIN

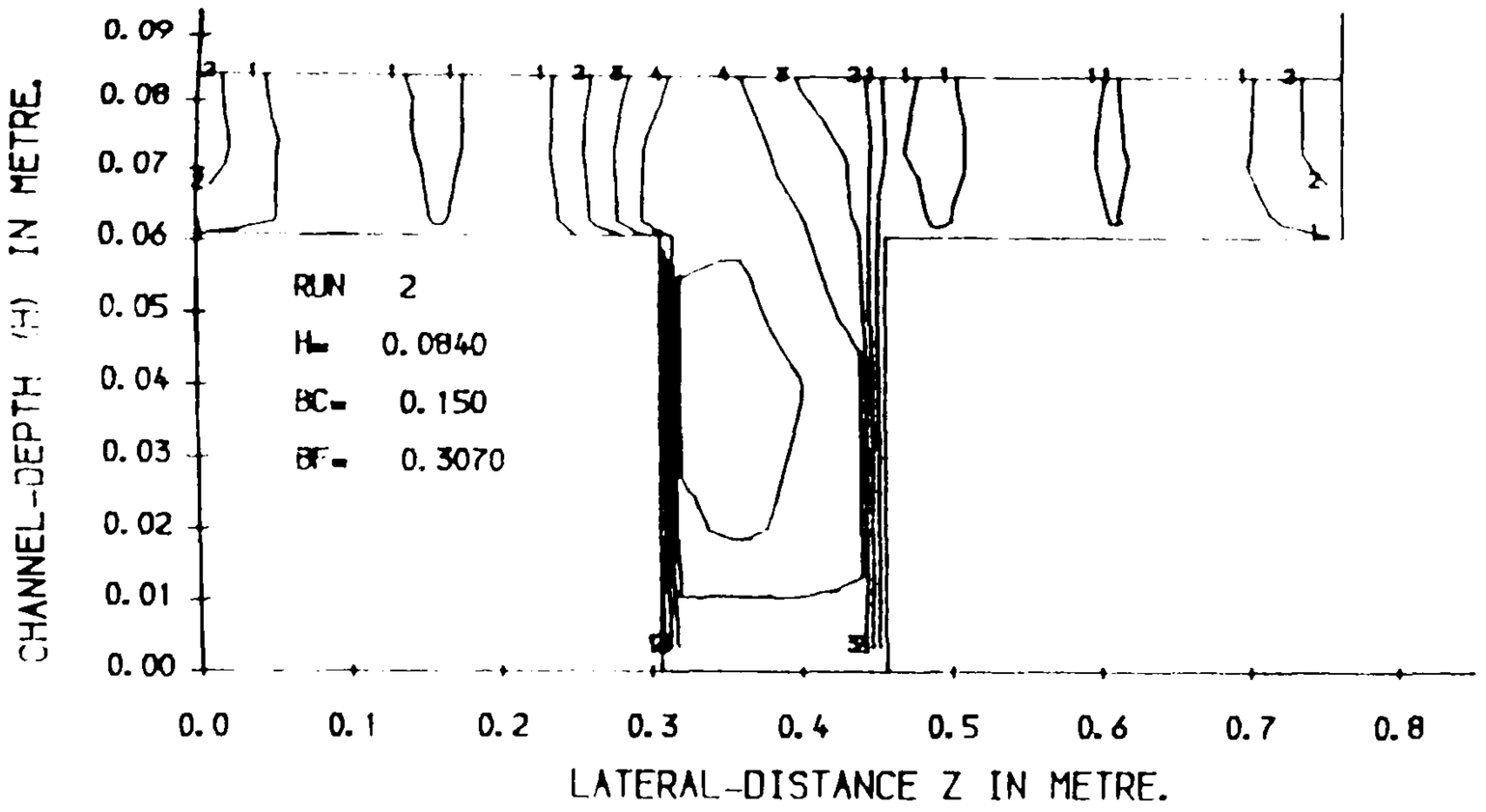

LONGITUDINAL VELOCITY CONTOURS IN CROSS SECTION. 1

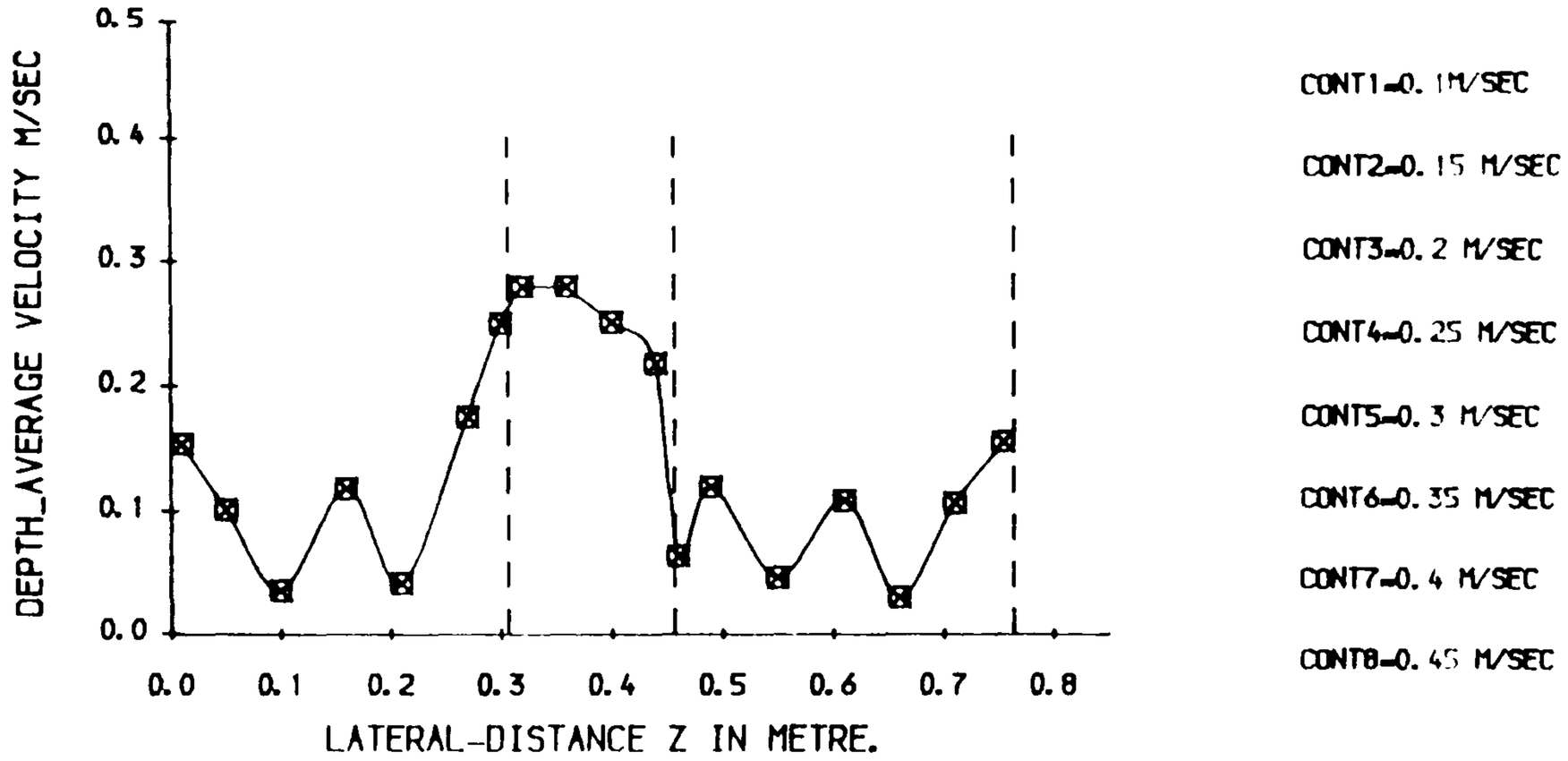

LONGITUDINAL DEPTH_AVERAGE VELOCITY PROFILE IN PLAN.

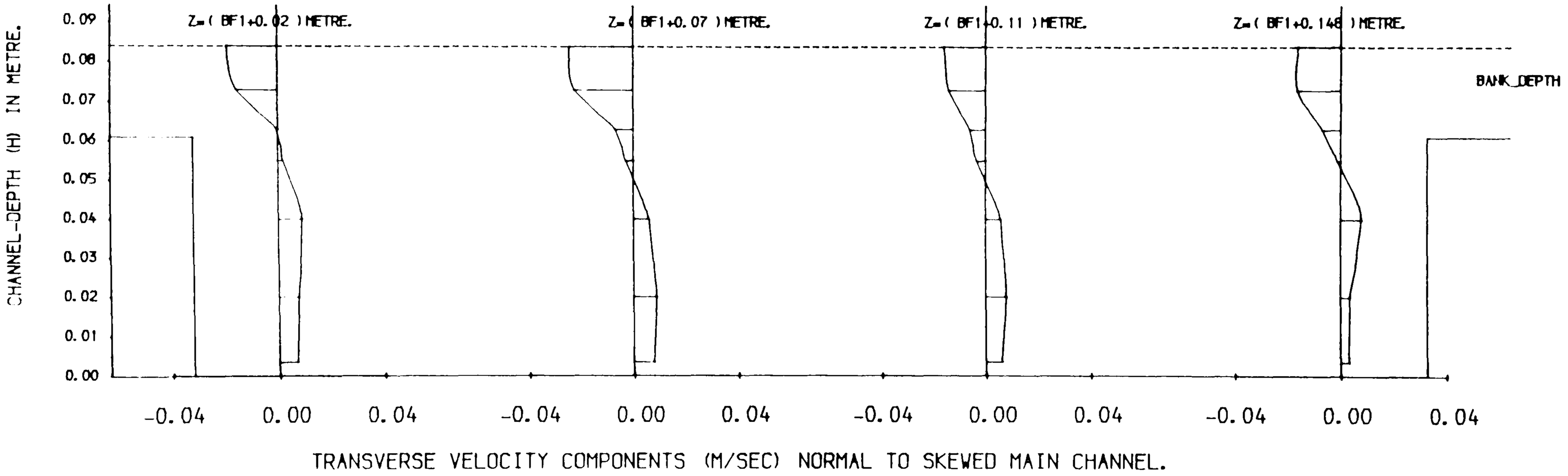

FIG (5.22) LONGITUDINAL & TRANSVERSE VELOCITY COMPONENTS IN SKEWED CHANNEL WITH ROUGH FLOODPLAIN

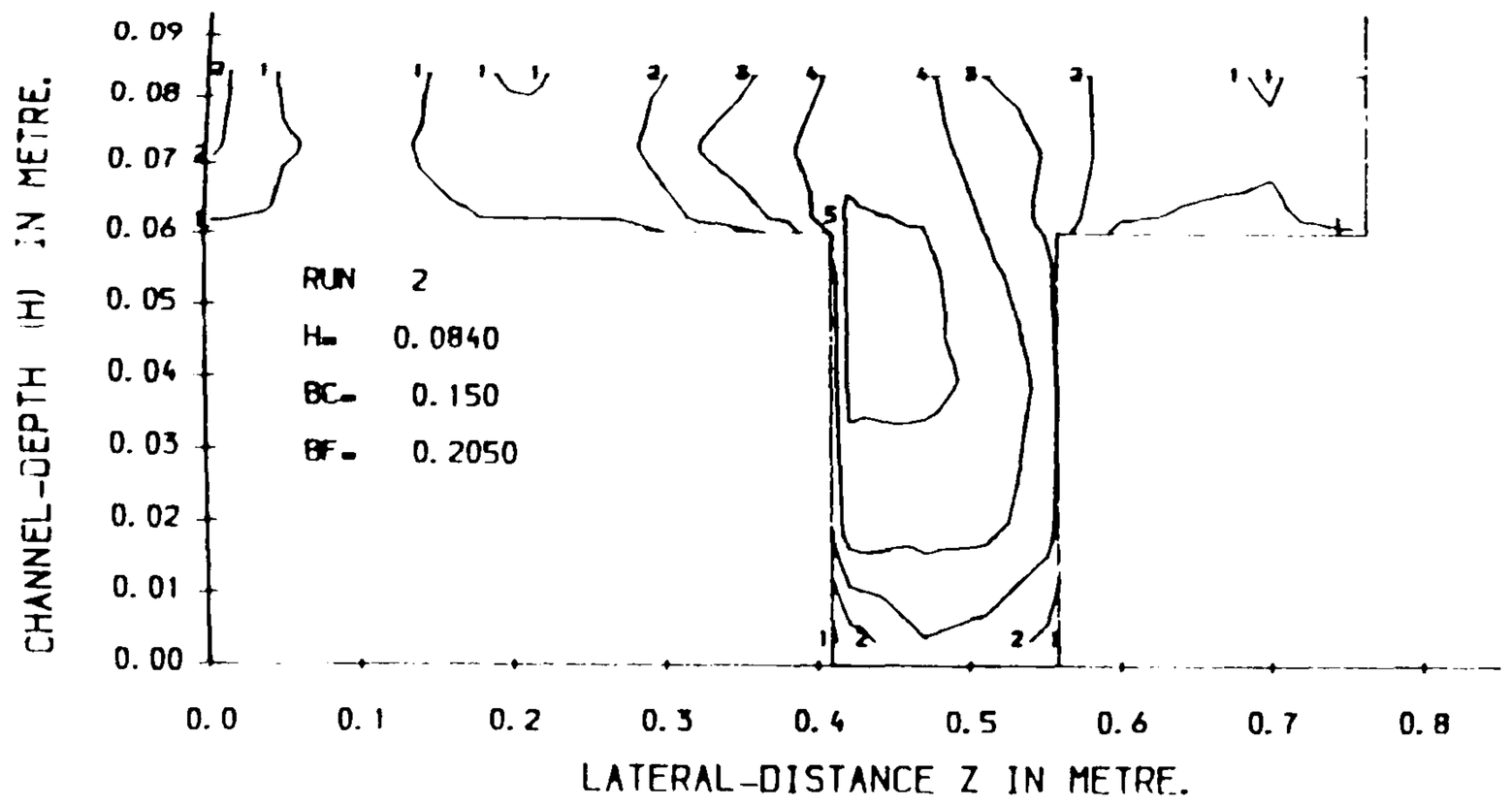

LONGITUDINAL VELOCITY CONTOURS IN CROSS SECTION. 2

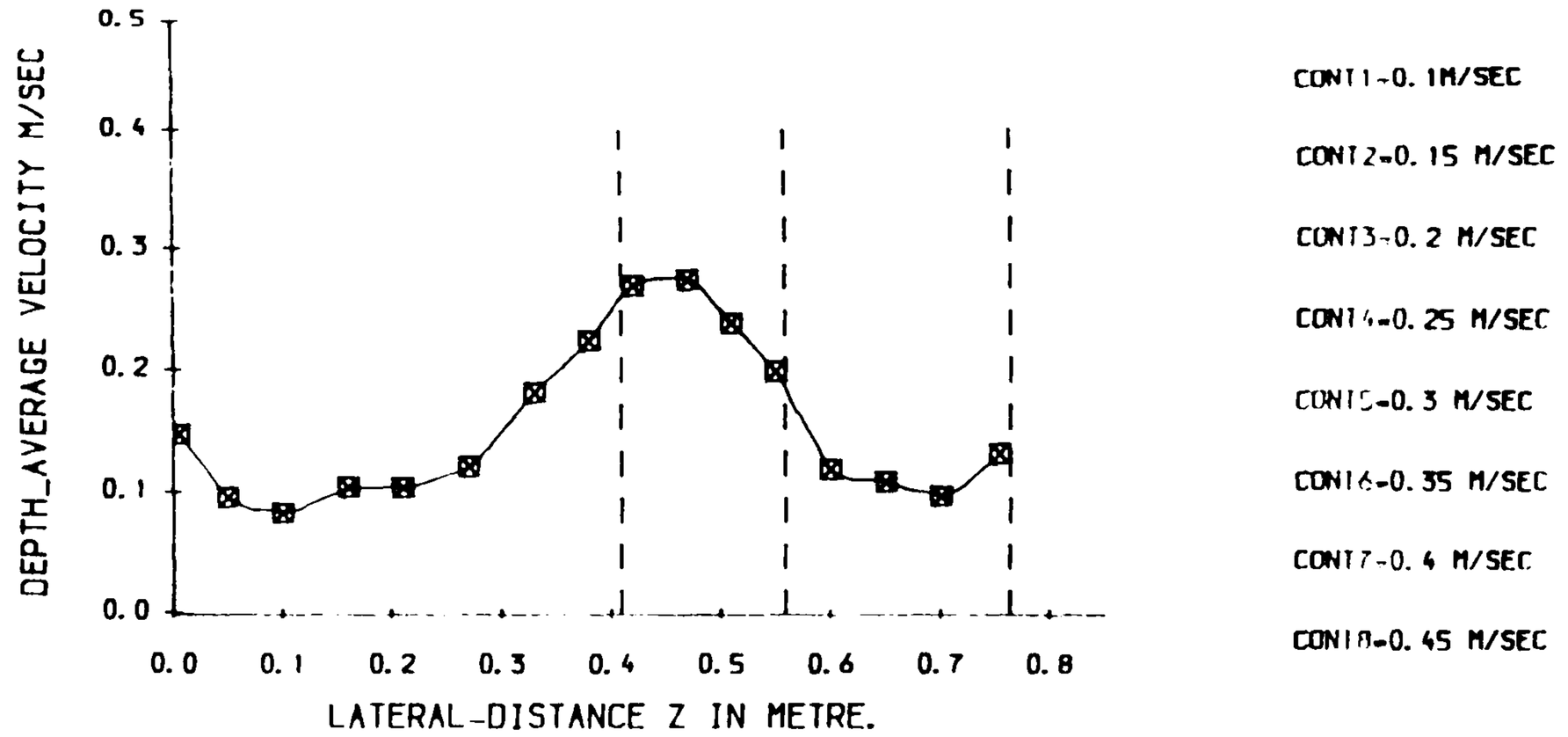

LONGITUDINAL DEPTH_AVERAGE VELOCITY PROFILE IN PLAN.

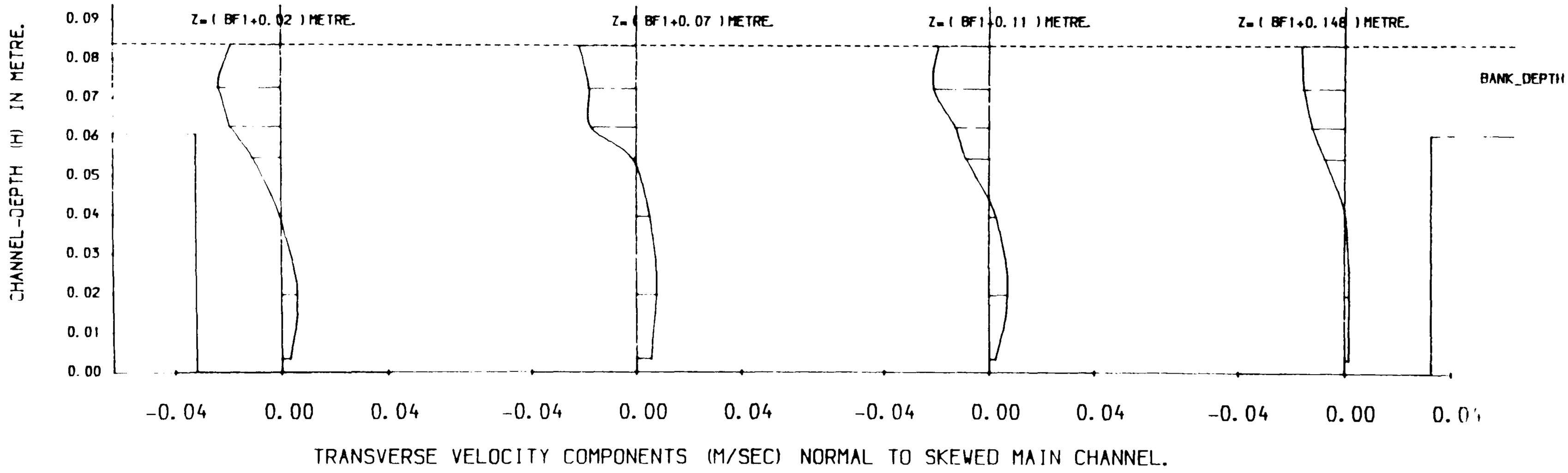

FIG (5.23) LONGITUDINAL & TRANSVERSE VELOCITY COMPONENTS IN SKEWED CHANNEL WITH ROUGH FLOODPLAIN

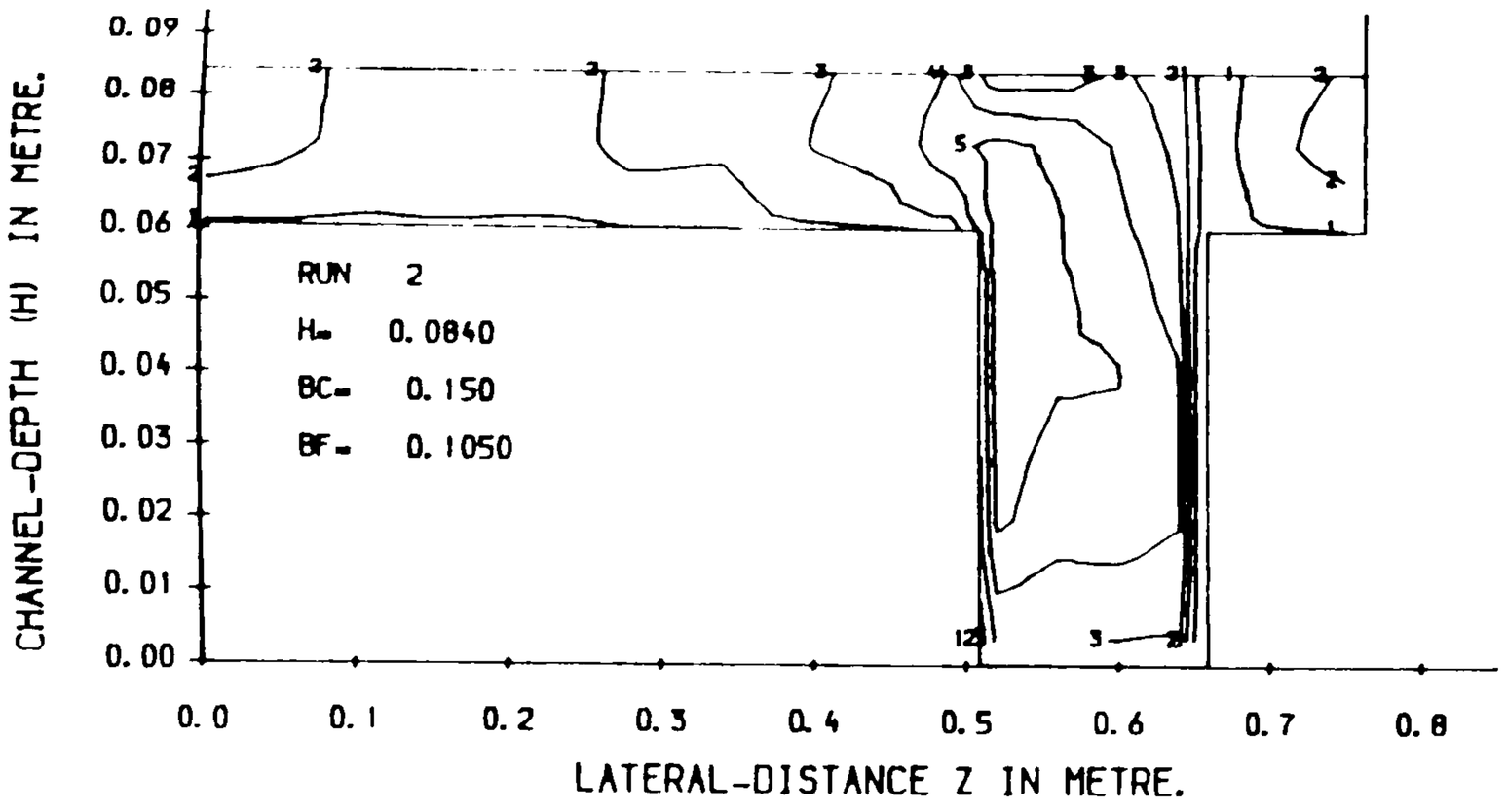

LONGITUDINAL VELOCITY CONTOURS IN CROSS SECTION. 3

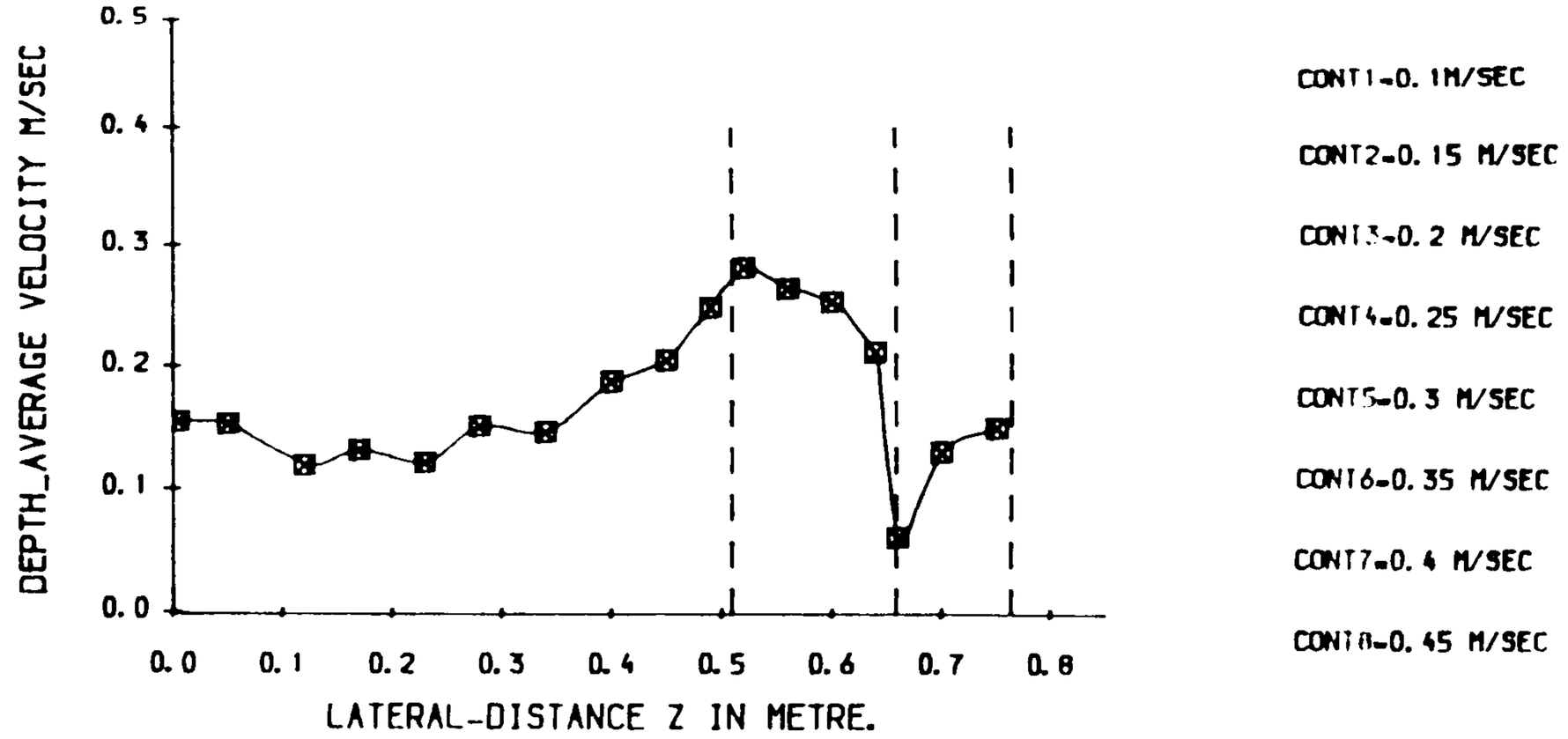

LONGITUDINAL DEPTH_AVERAGE VELOCITY PROFILE IN PLAN.

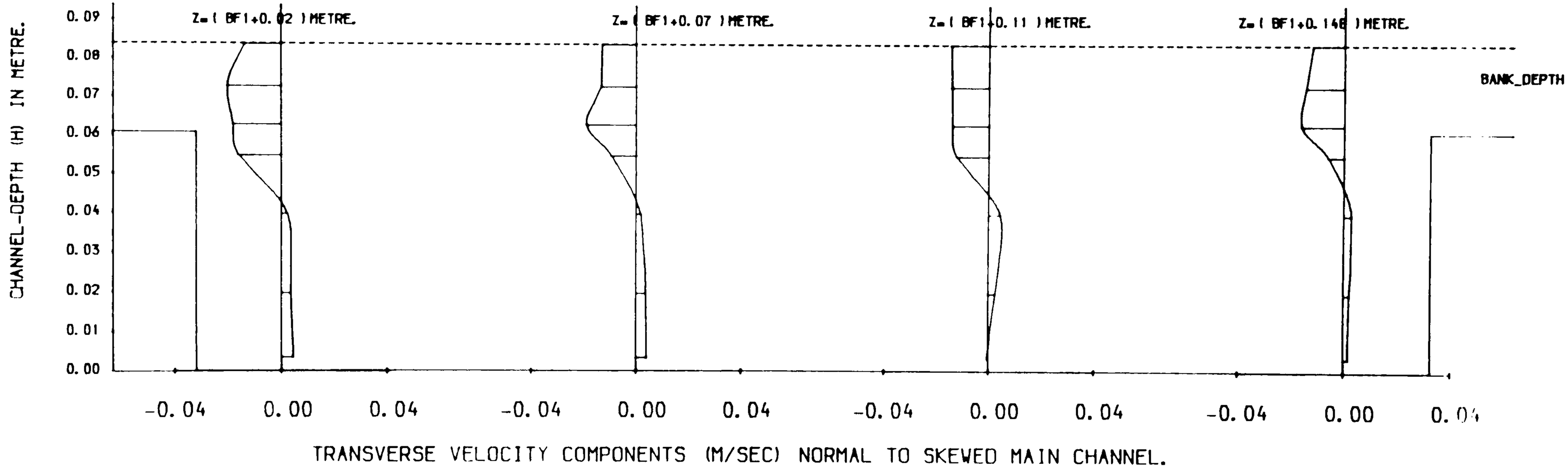

FIG (5.24) LONGITUDINAL & TRANSVERSE VELOCITY COMPONENTS IN SKEWED CHANNEL WITH ROUGH FLOODPLAIN

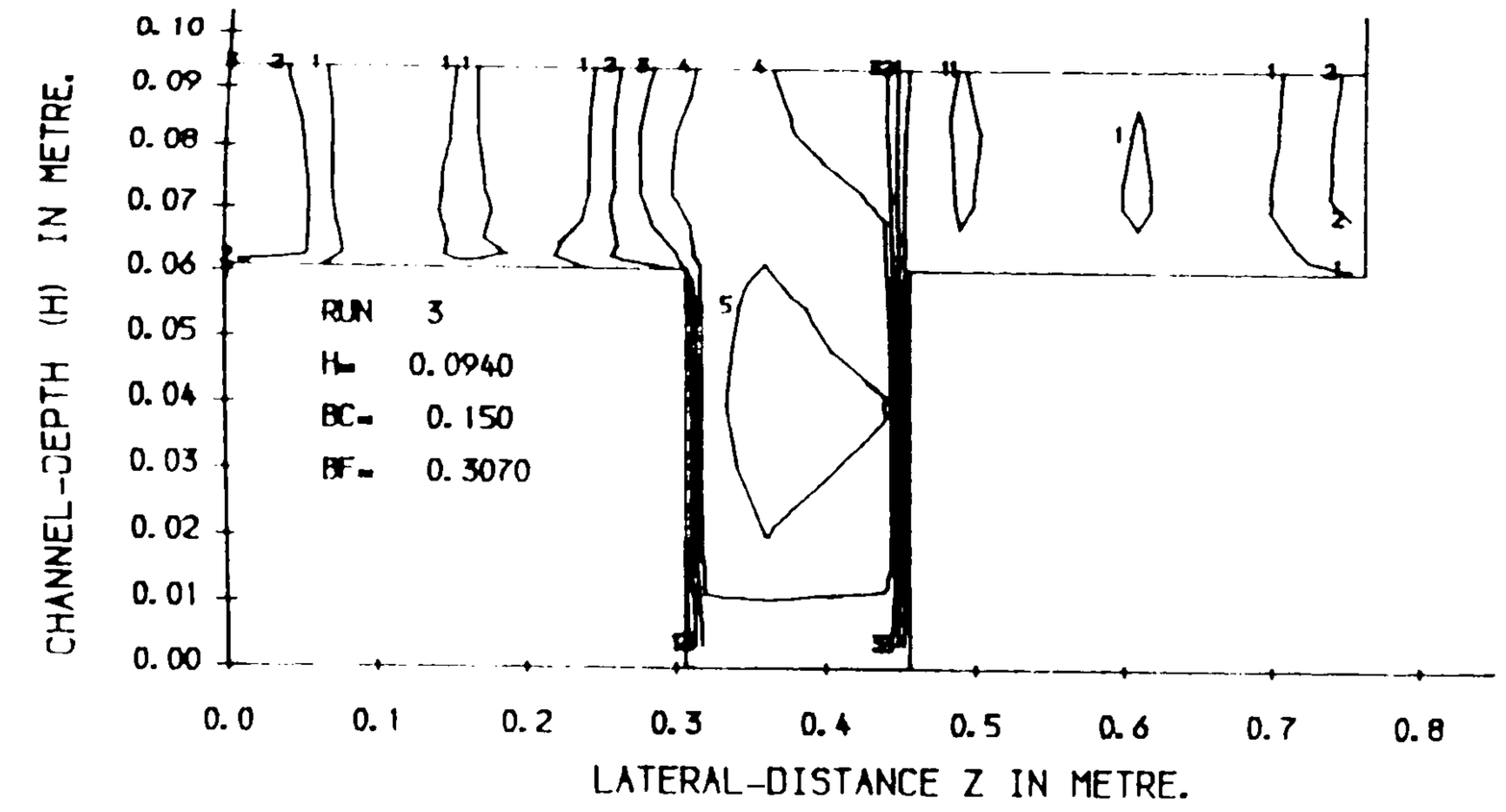

LONGITUDINAL VELOCITY CONTOURS IN CROSS SECTION. 1

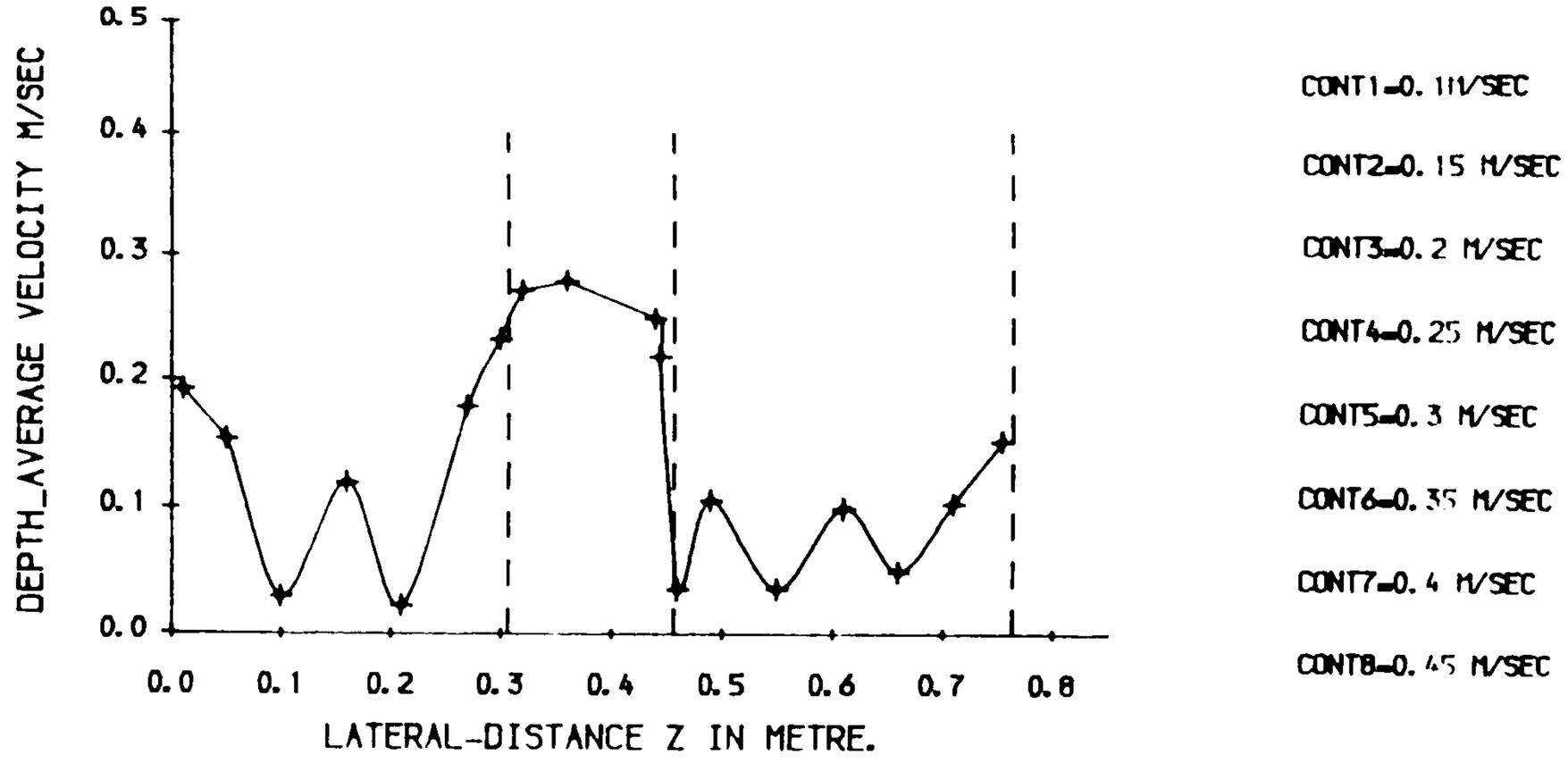

LONGITUDINAL DEPTH_AVERAGE VELOCITY PROFILE IN PLAN.

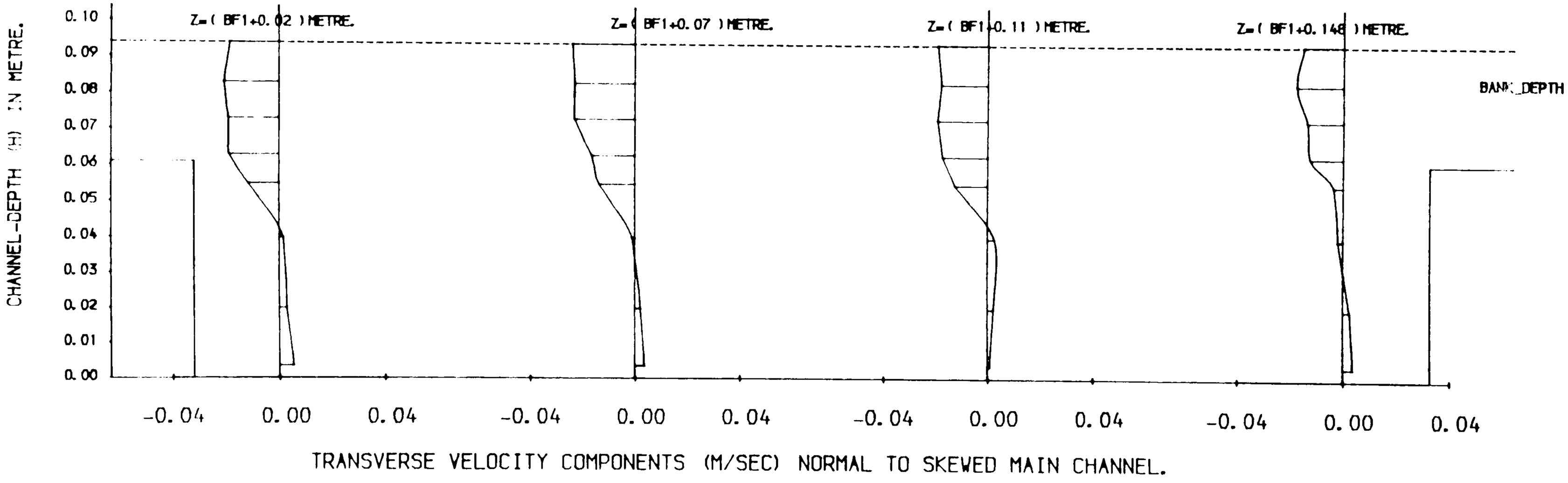

FIG (5.25) LONGITUDINAL & TRANSVERSE VELOCITY COMPONENTS IN SKEWED CHANNEL WITH ROUGH FLOODPLAIN

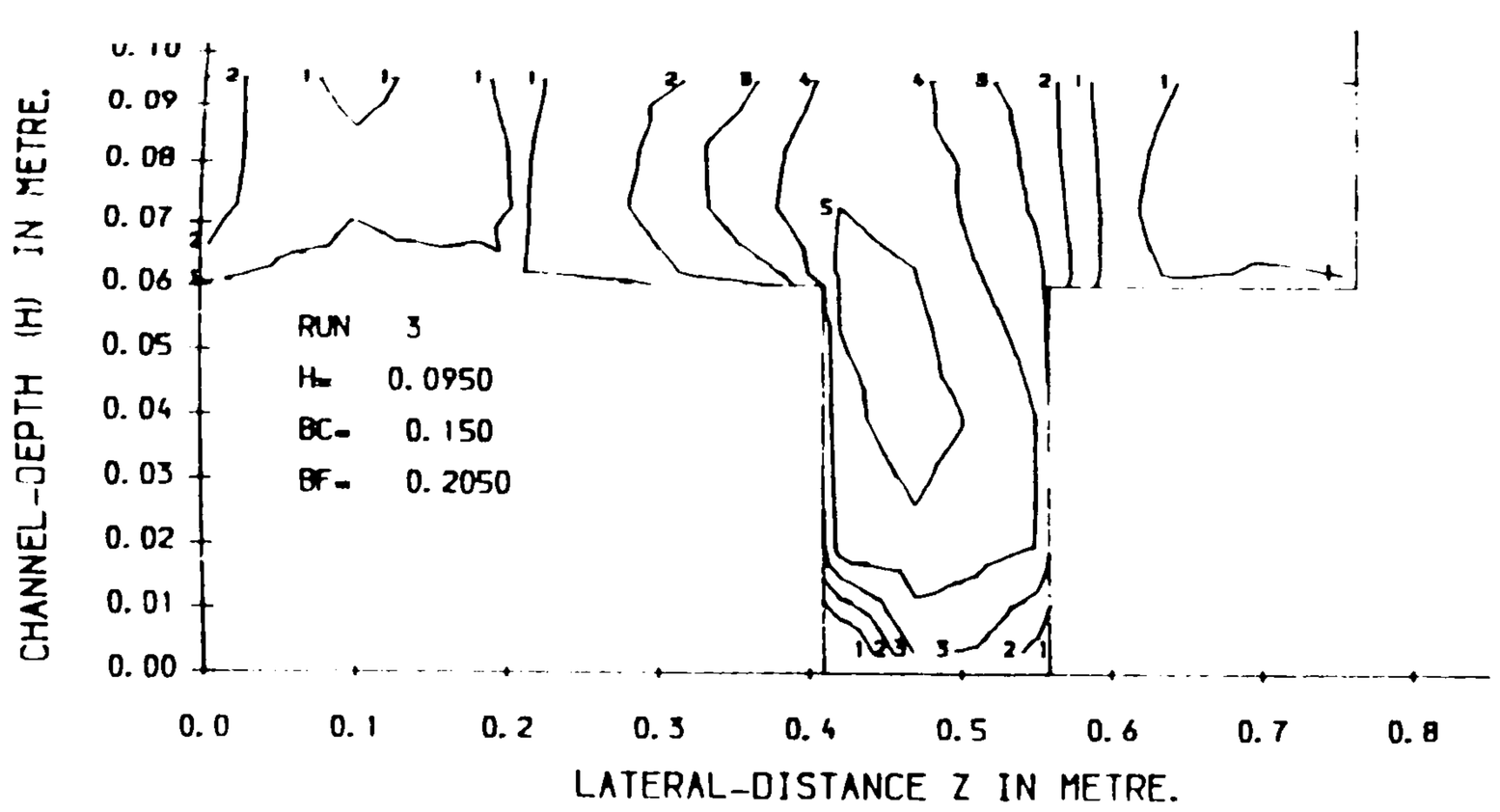

LONGITUDINAL VELOCITY CONTOURS IN CROSS SECTION. 2

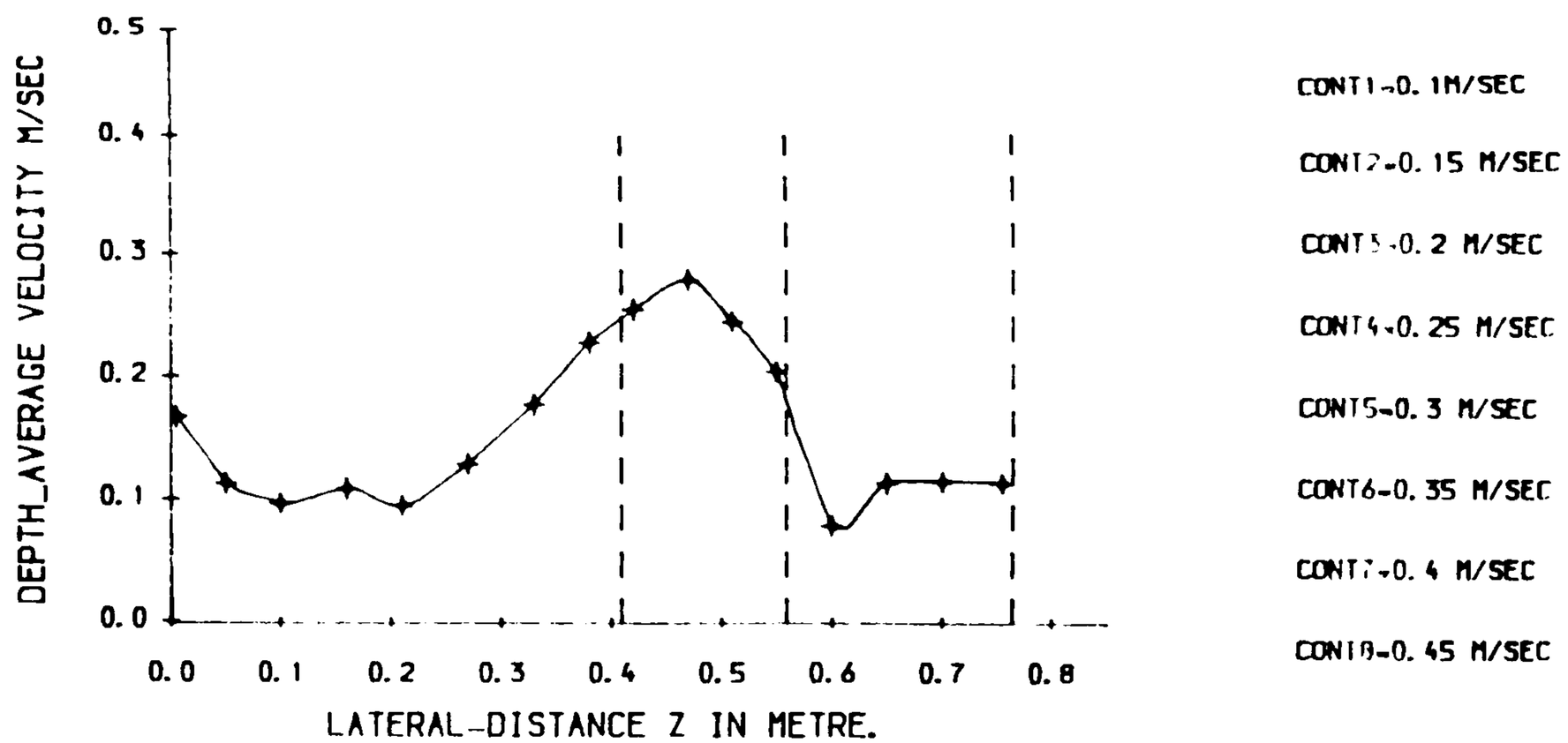

LONGITUDINAL DEPTH_AVERAGE VELOCITY PROFILE IN PLAN.

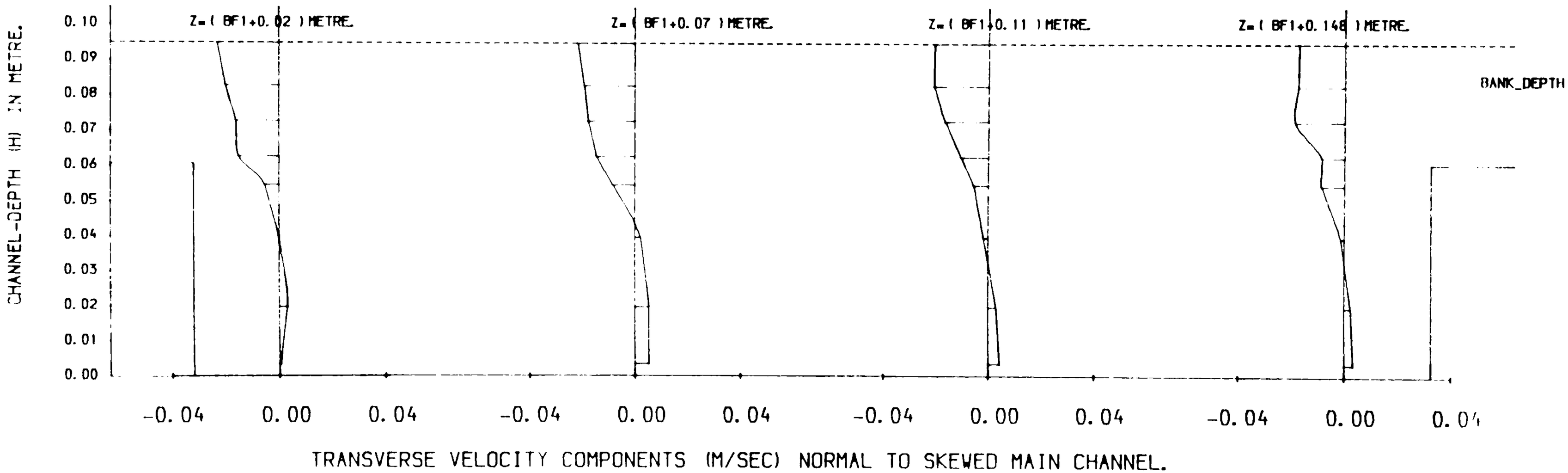

FIG (5.26) LONGITUDINAL & TRANSVERSE VELOCITY COMPONENTS IN SKEWED CHANNEL WITH ROUGH FLOODPLAIN

PAGE NUMBERING AS ORIGINAL

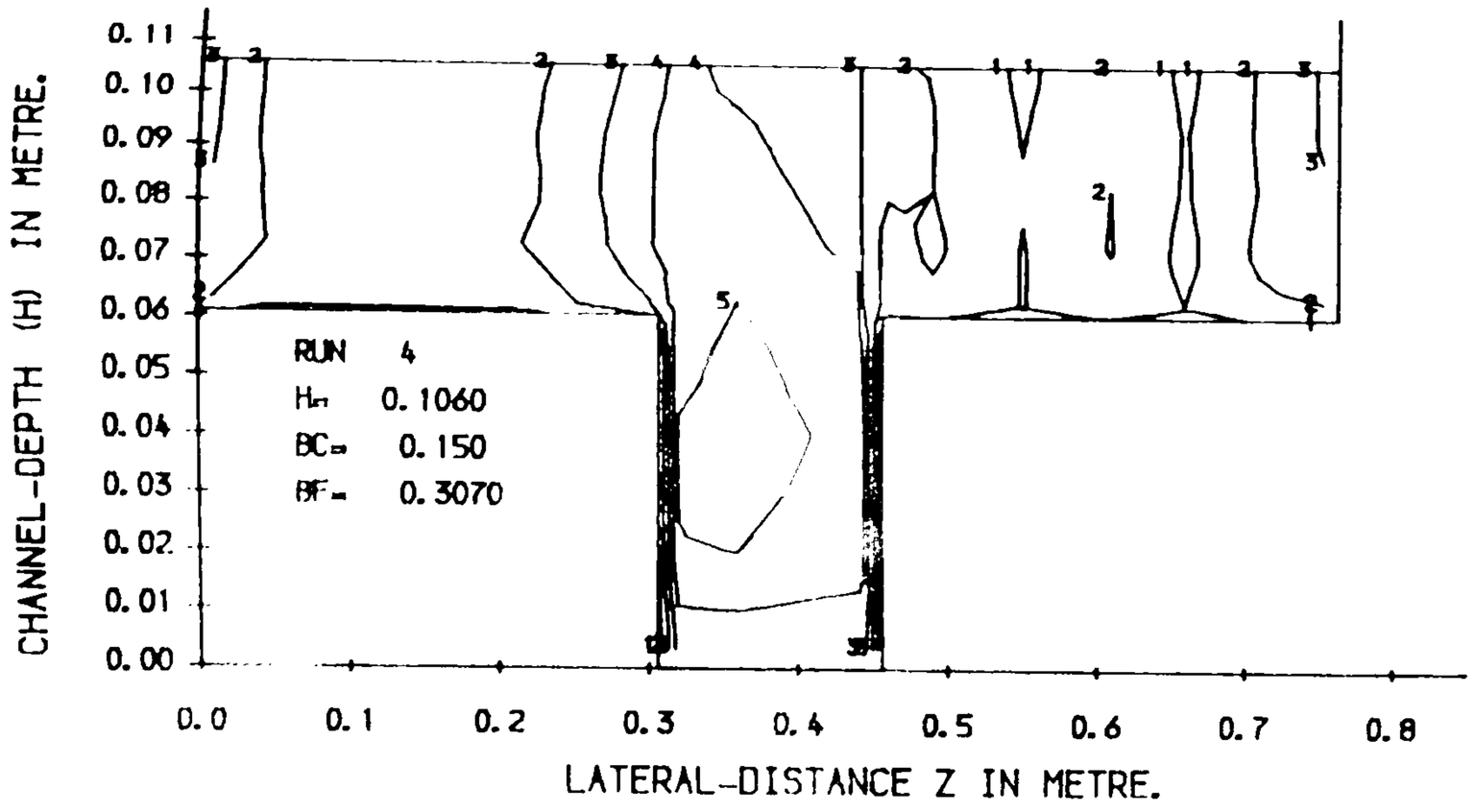

LONGITUDINAL VELOCITY CONTOURS IN CROSS SECTION. 1

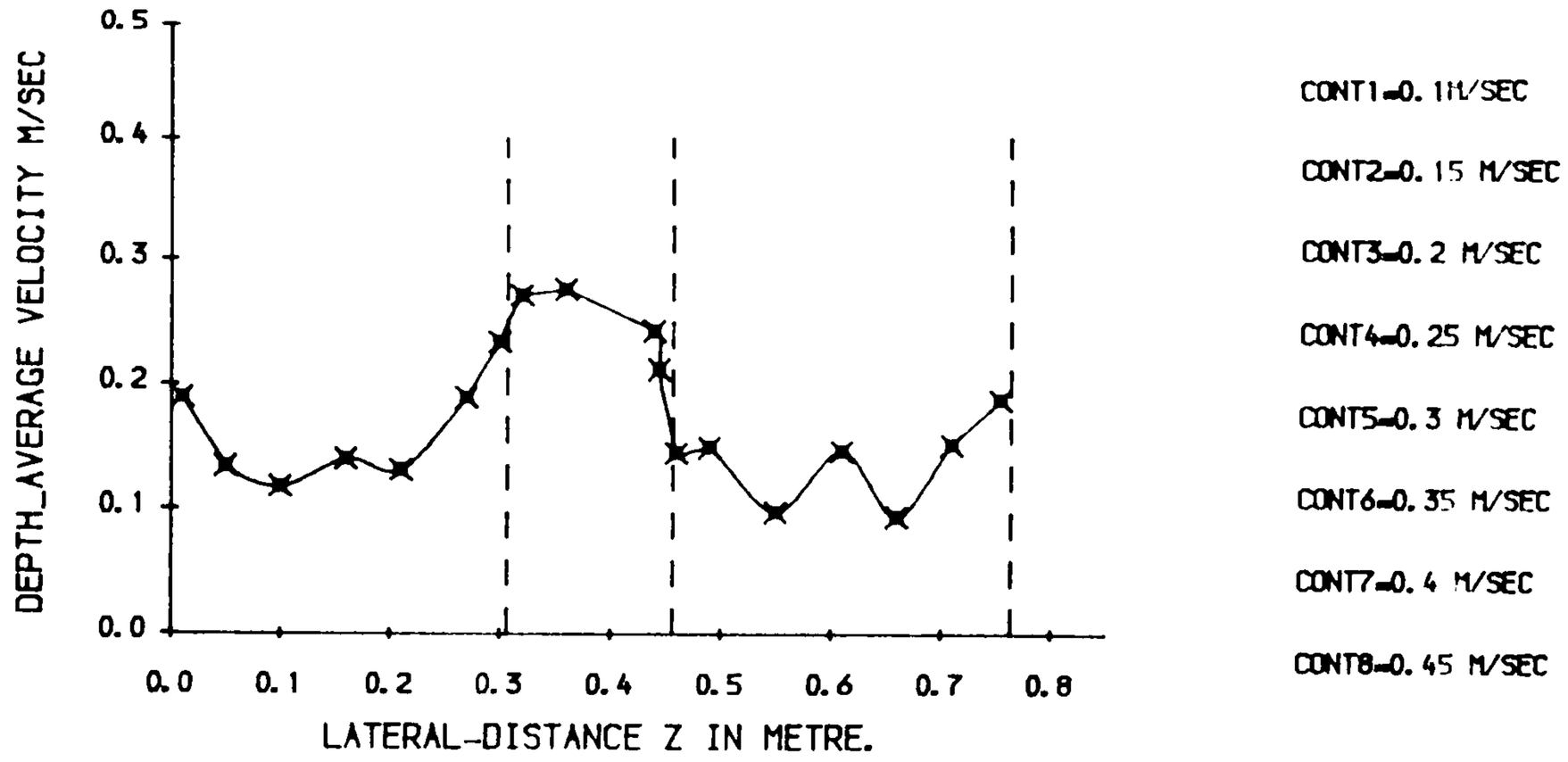

LONGITUDINAL DEPTH_AVERAGE VELOCITY PROFILE IN PLAN.

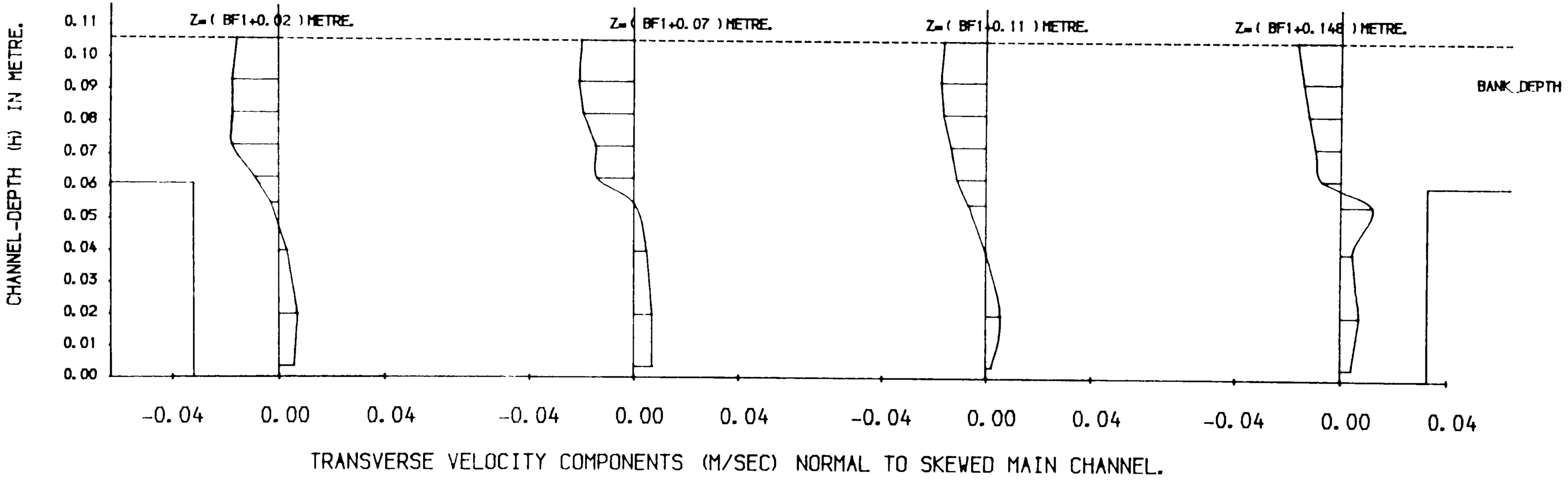

FIG (5.28) LONGITUDINAL & TRANSVERSE VELOCITY COMPONENTS IN SKEWED CHANNEL WITH ROUGH FLOODPLAIN

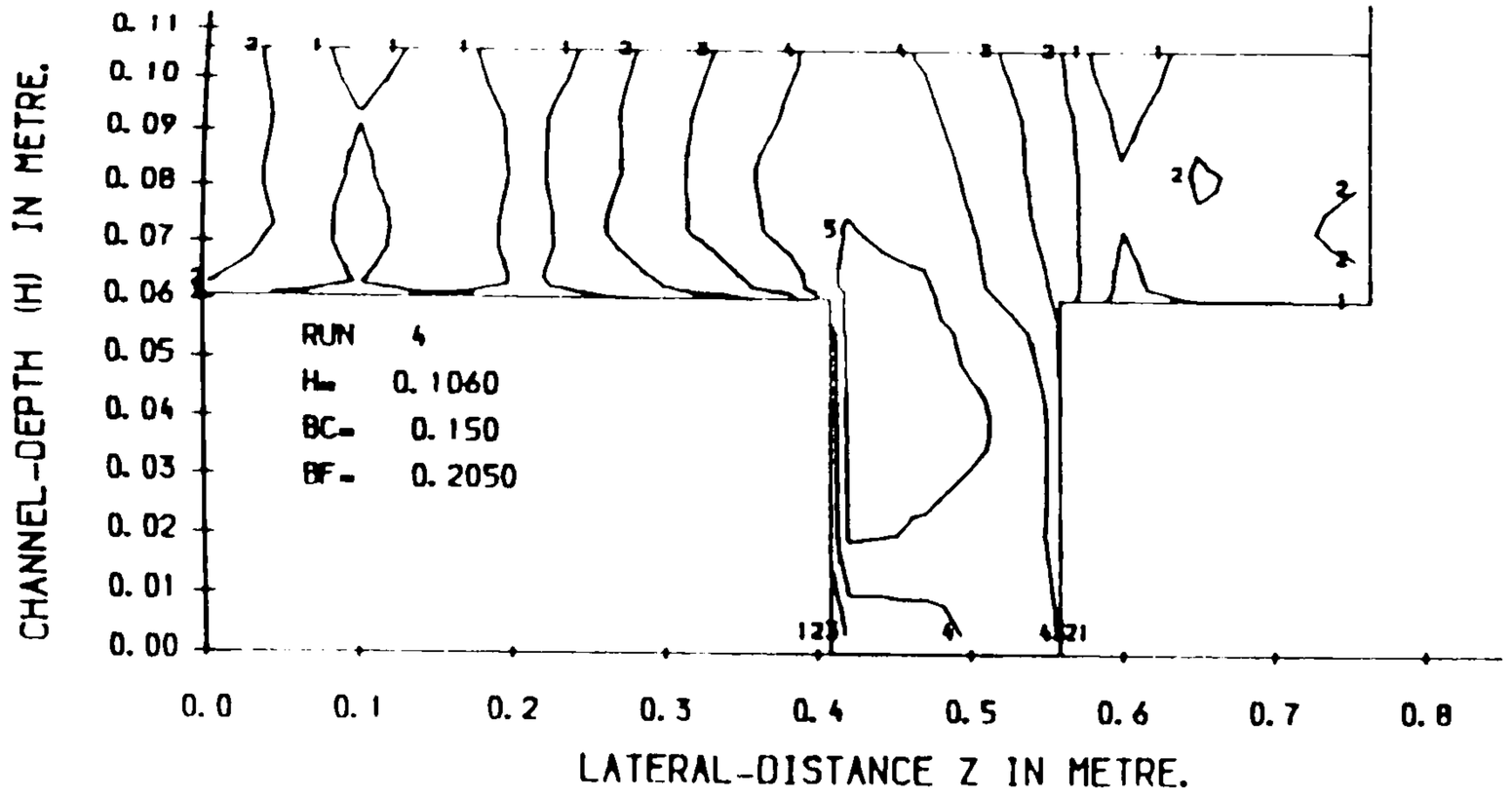

LONGITUDINAL VELOCITY CONTOURS IN CROSS SECTION. 2

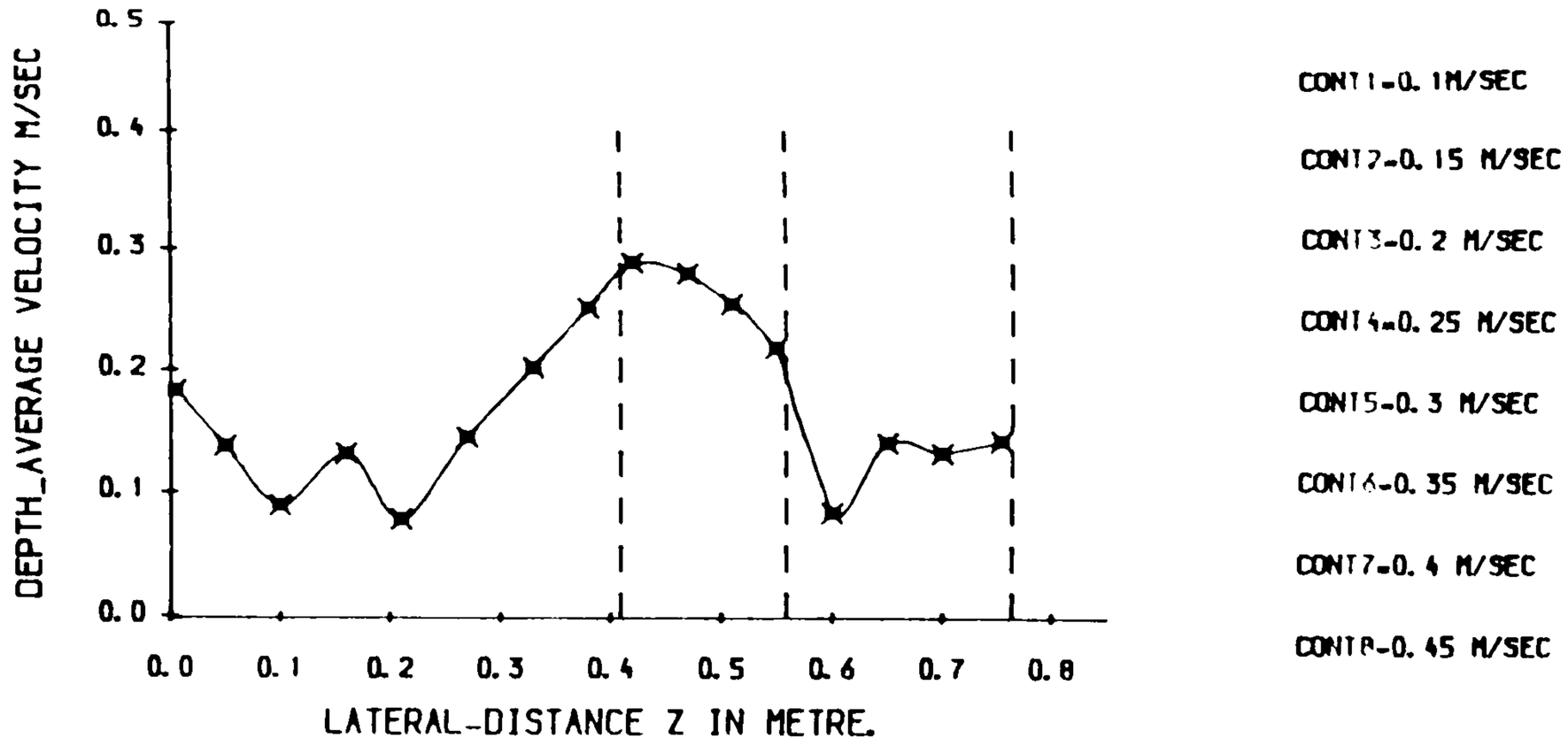

LONGITUDINAL DEPTH_AVERAGE VELOCITY PROFILE IN PLAN.

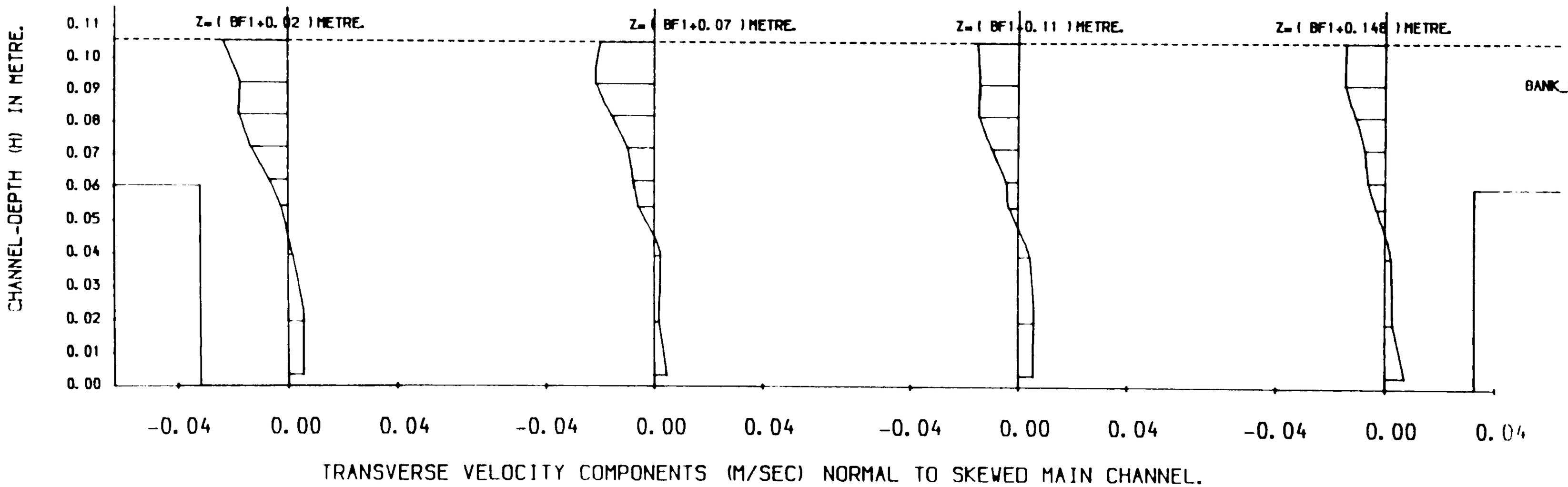

FIG (5.29) LONGITUDINAL & TRANSVERSE VELOCITY COMPONENTS IN SKEWED CHANNEL WITH ROUGH FLOODPLAIN

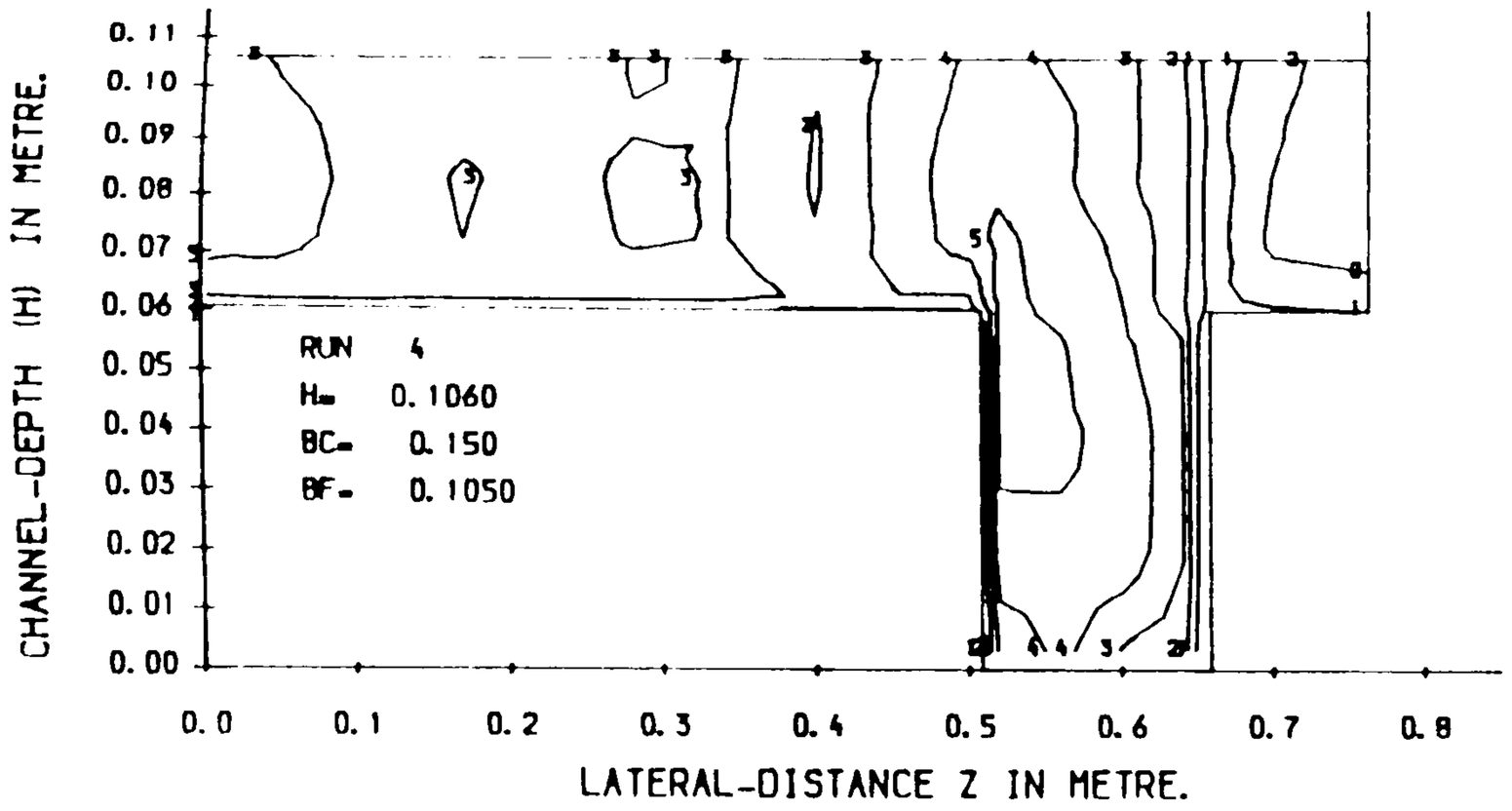

LONGITUDINAL VELOCITY CONTOURS IN CROSS SECTION. 3

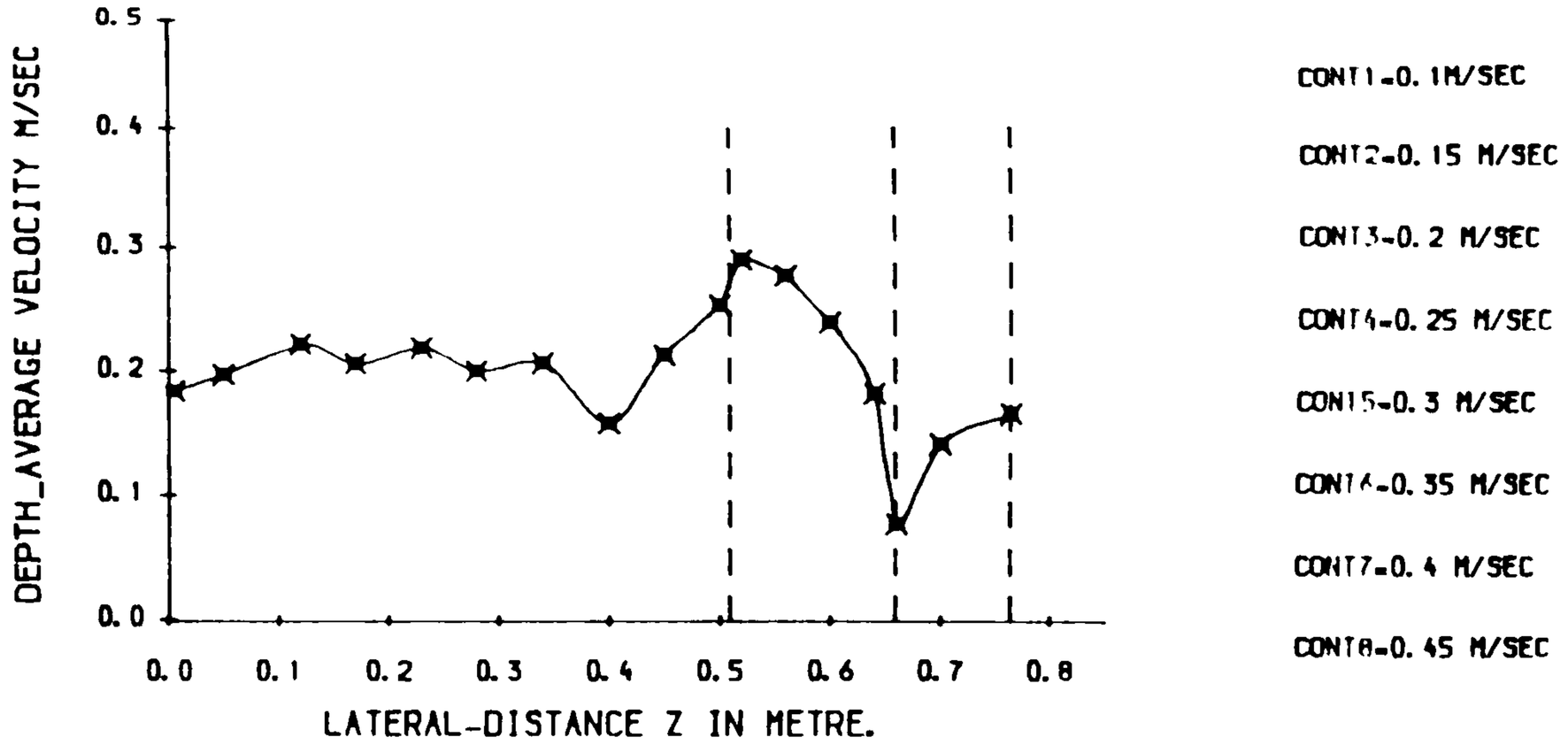

LONGITUDINAL DEPTH_AVERAGE VELOCITY PROFILE IN PLAN.

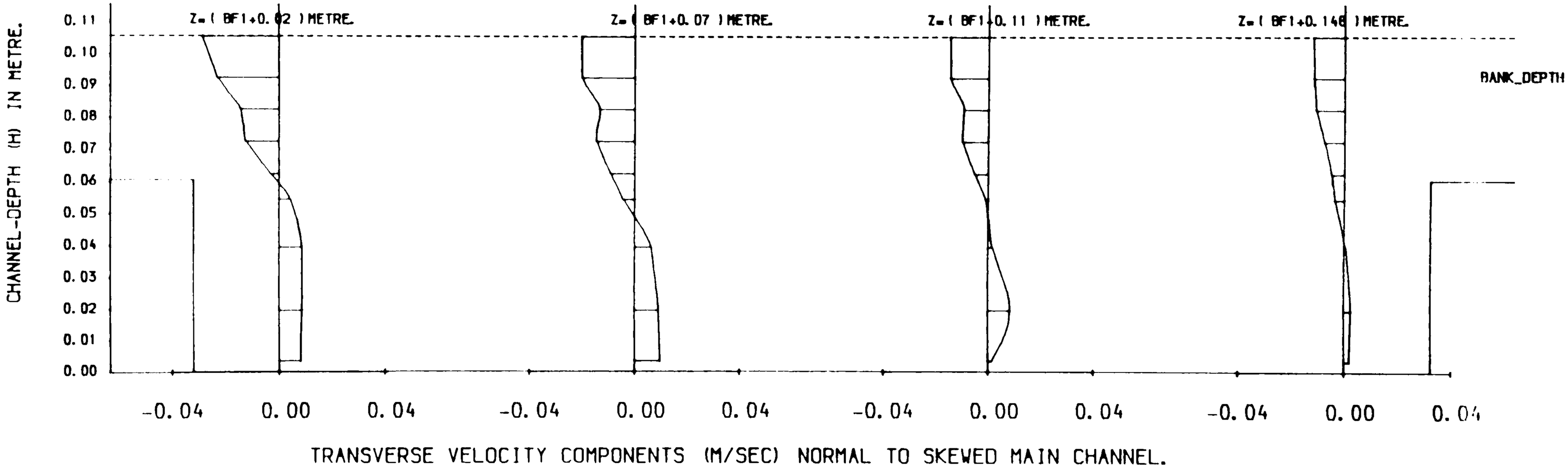

FIG (5. 30) LONGITUDINAL & TRANSVERSE VELOCITY COMPONENTS IN SKEWED CHANNEL WITH ROUGH FLOODPLAIN

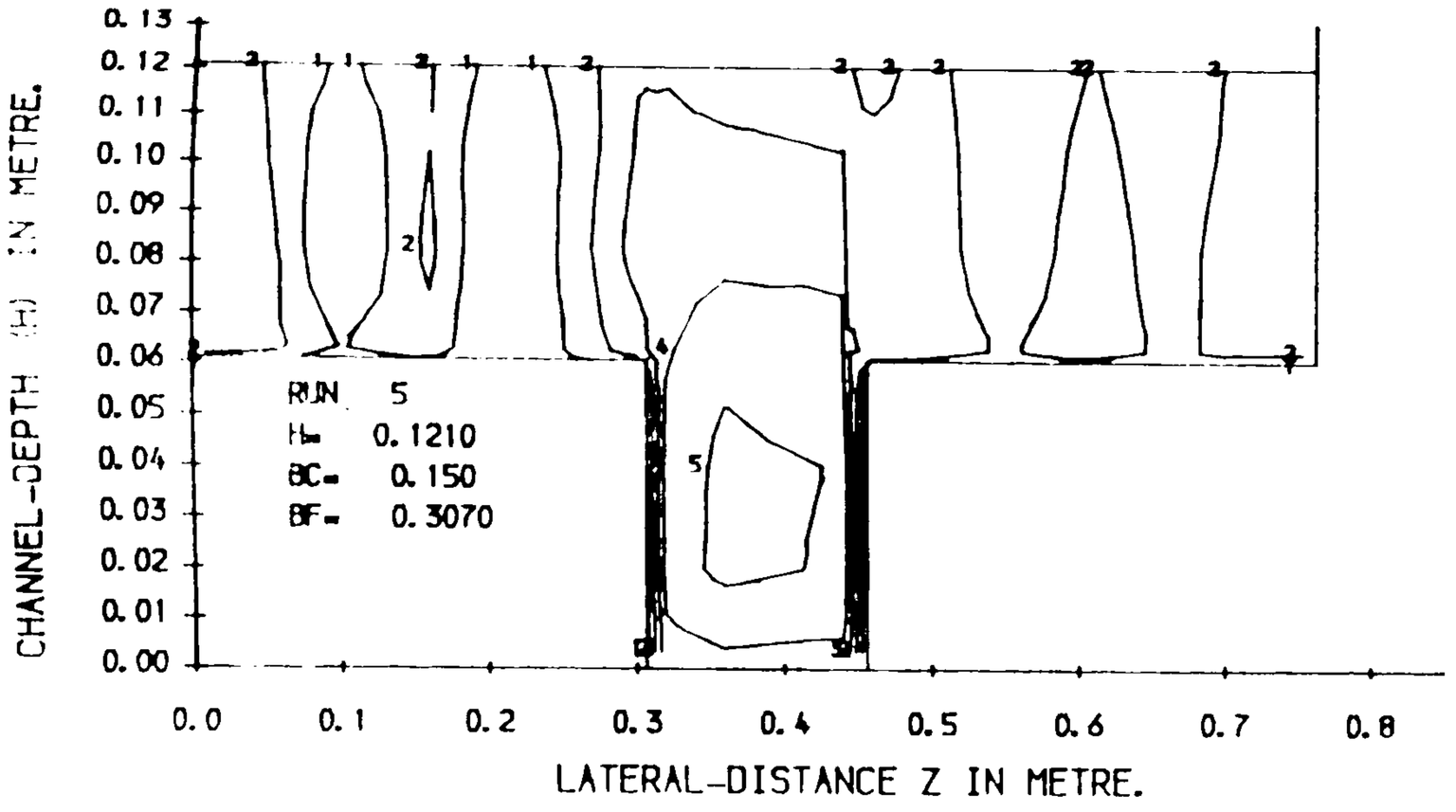

LONGITUDINAL VELOCITY CONTOURS IN CROSS SECTION. 1

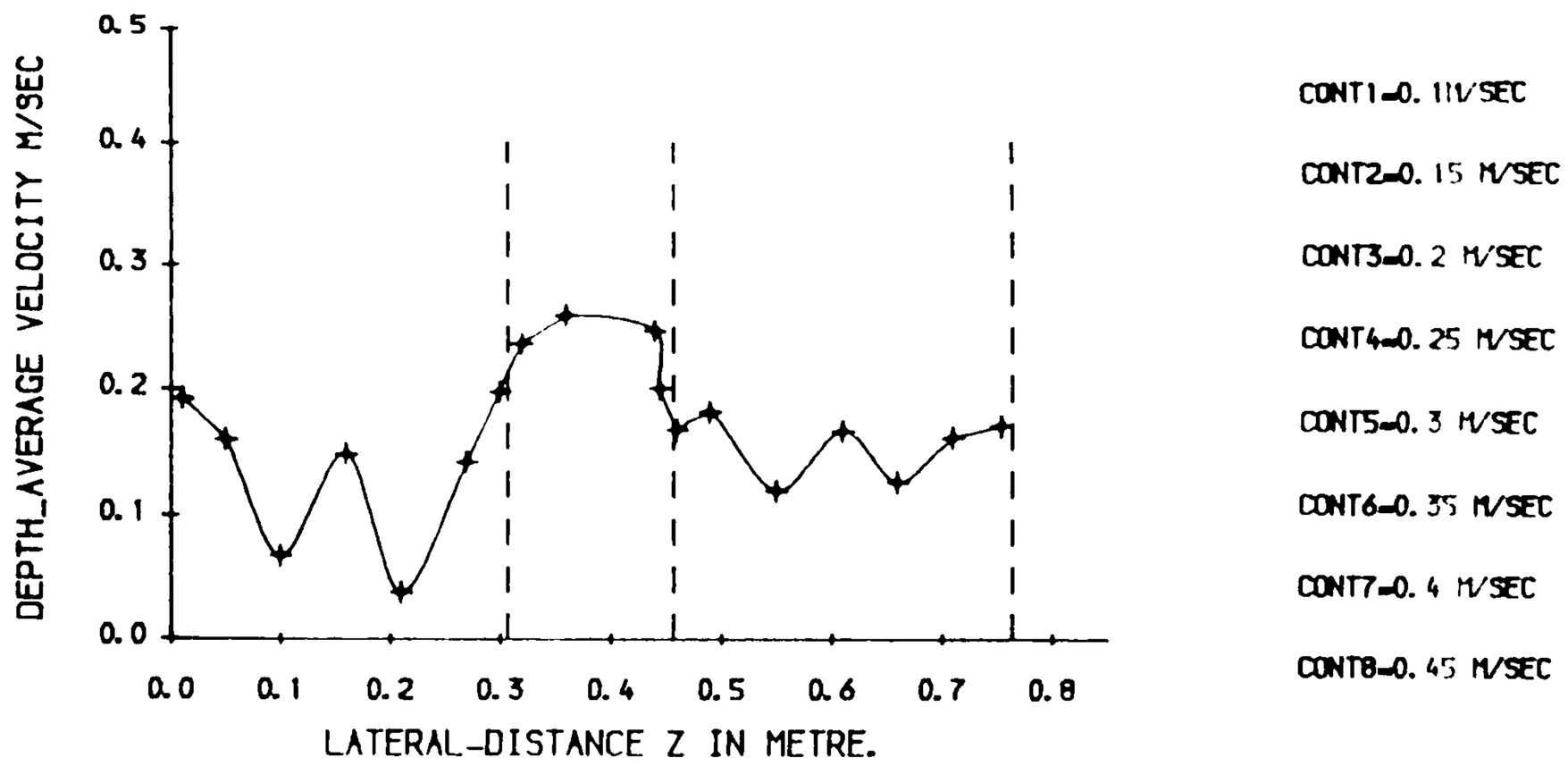

LONGITUDINAL DEPTH_AVERAGE VELOCITY PROFILE IN PLAN.

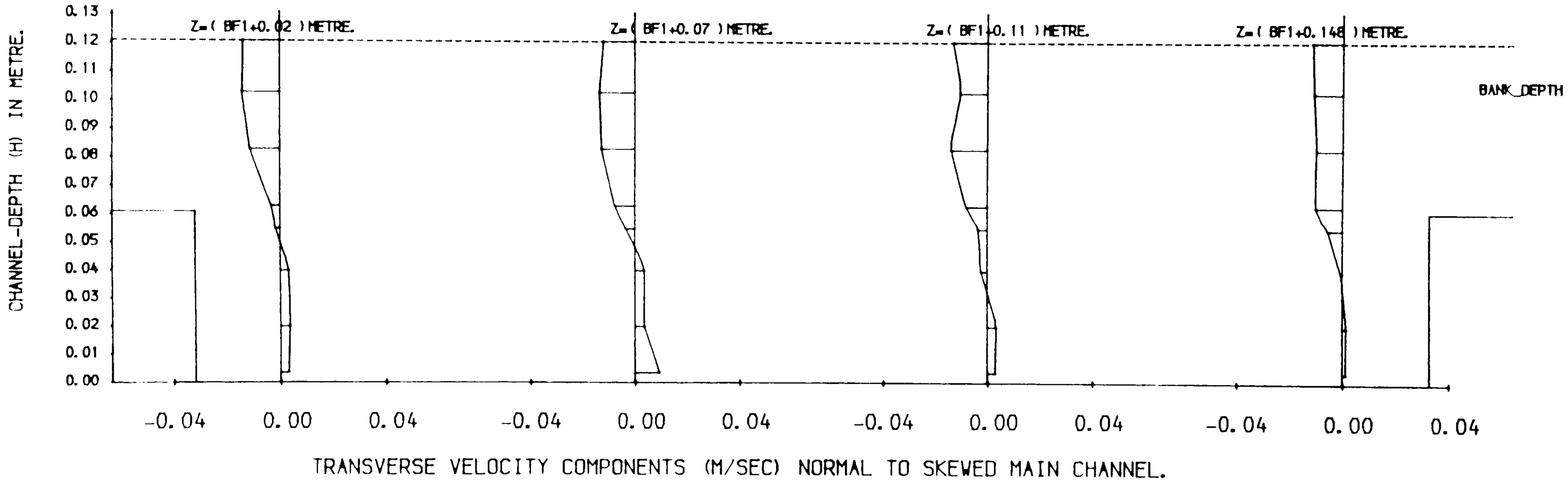

FIG (5.31) LONGITUDINAL & TRANSVERSE VELOCITY COMPONENTS IN SKEWED CHANNEL WITH ROUGH FLOODPLAIN

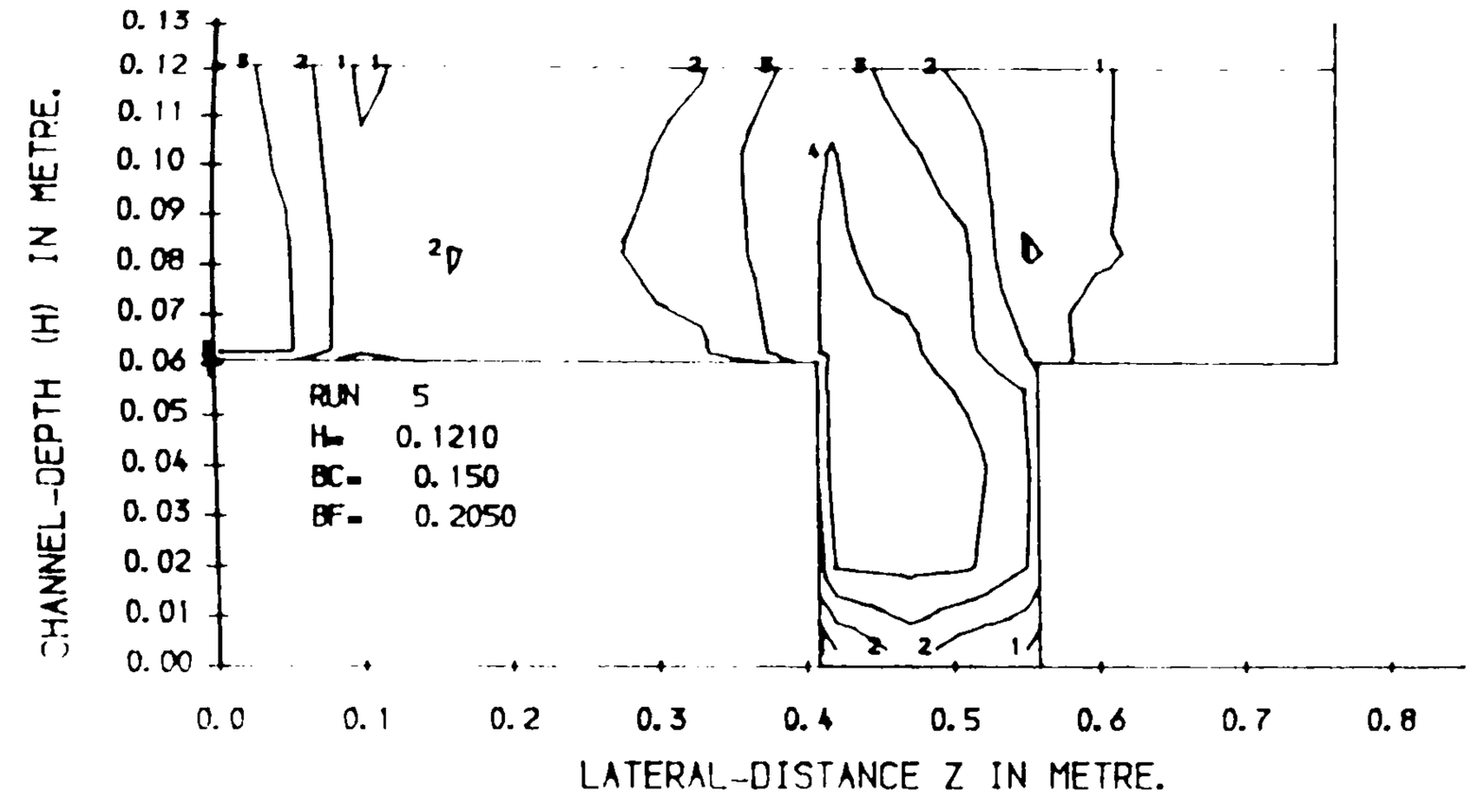

LONGITUDINAL VELOCITY CONTOURS IN CROSS SECTION. 2

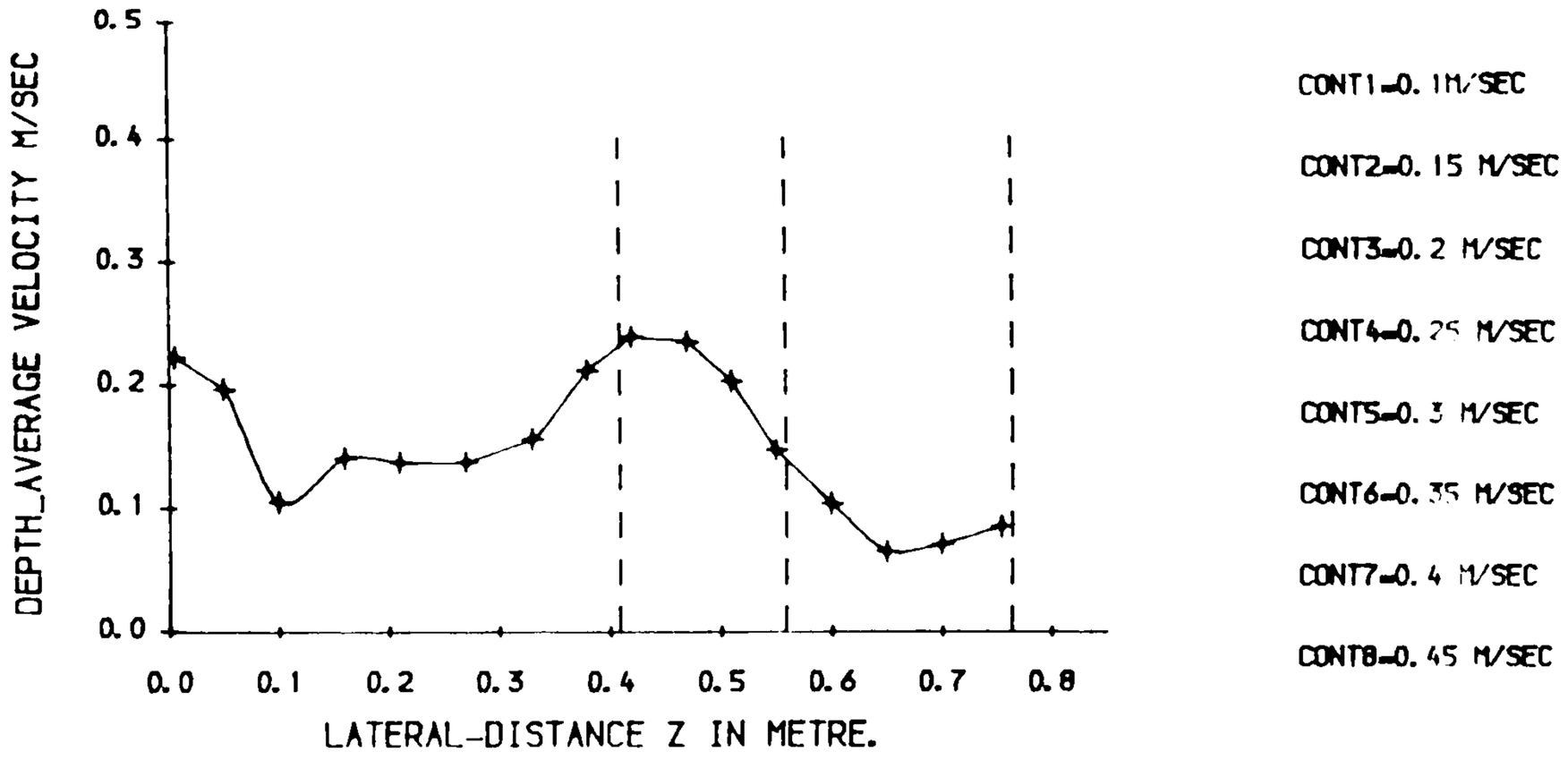

LONGITUDINAL DEPTH_AVERAGE VELOCITY PROFILE IN PLAN.

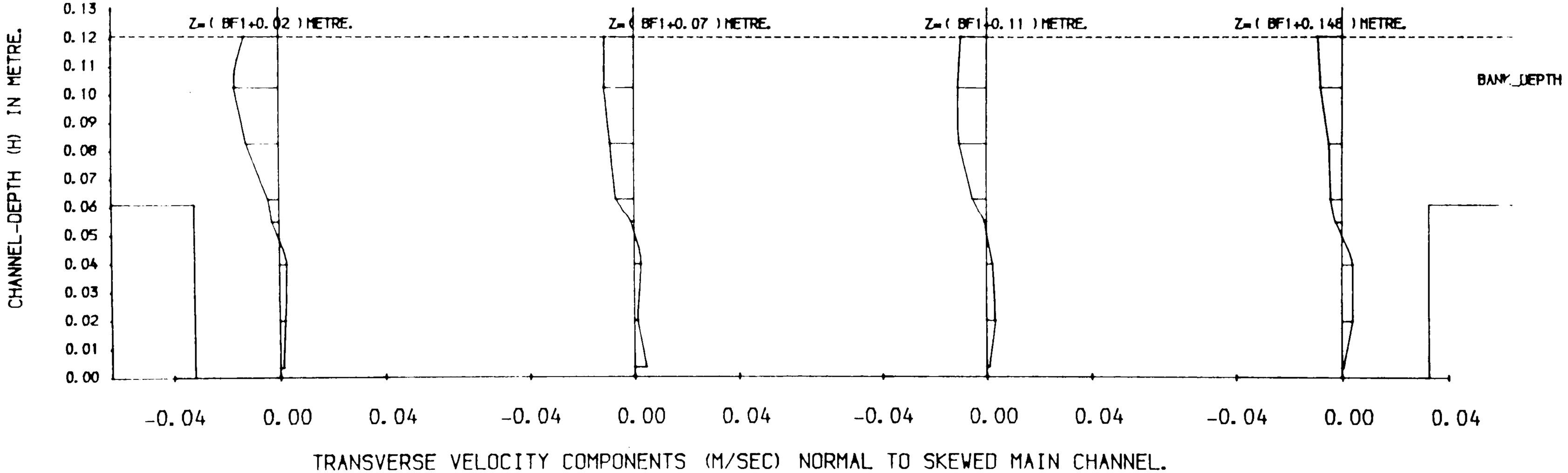

FIG (5.32) LONGITUDINAL & TRANSVERSE VELOCITY COMPONENTS IN SKEWED CHANNEL WITH ROUGH FLOODPLAIN

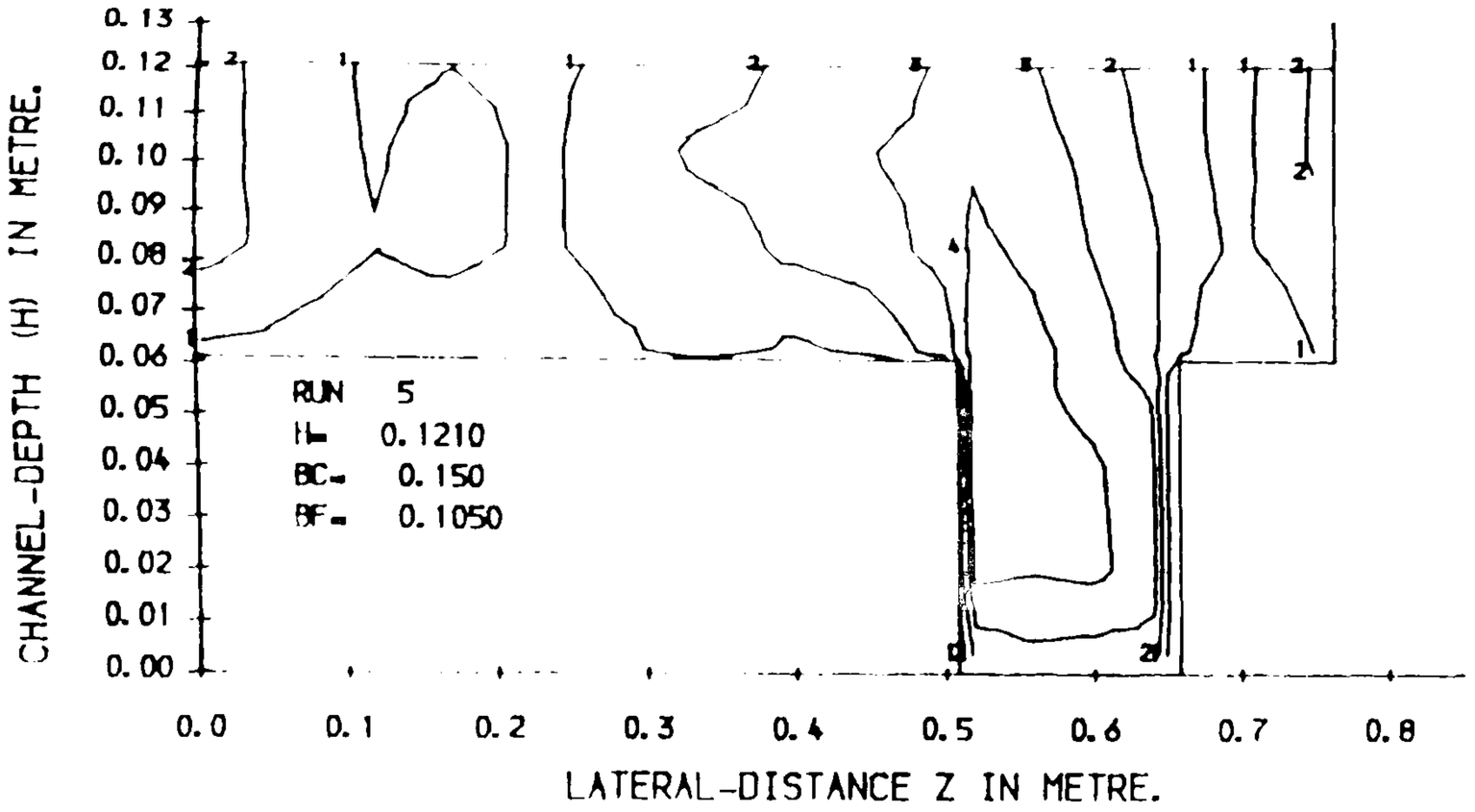

LONGITUDINAL VELOCITY CONTOURS IN CROSS SECTION. 3

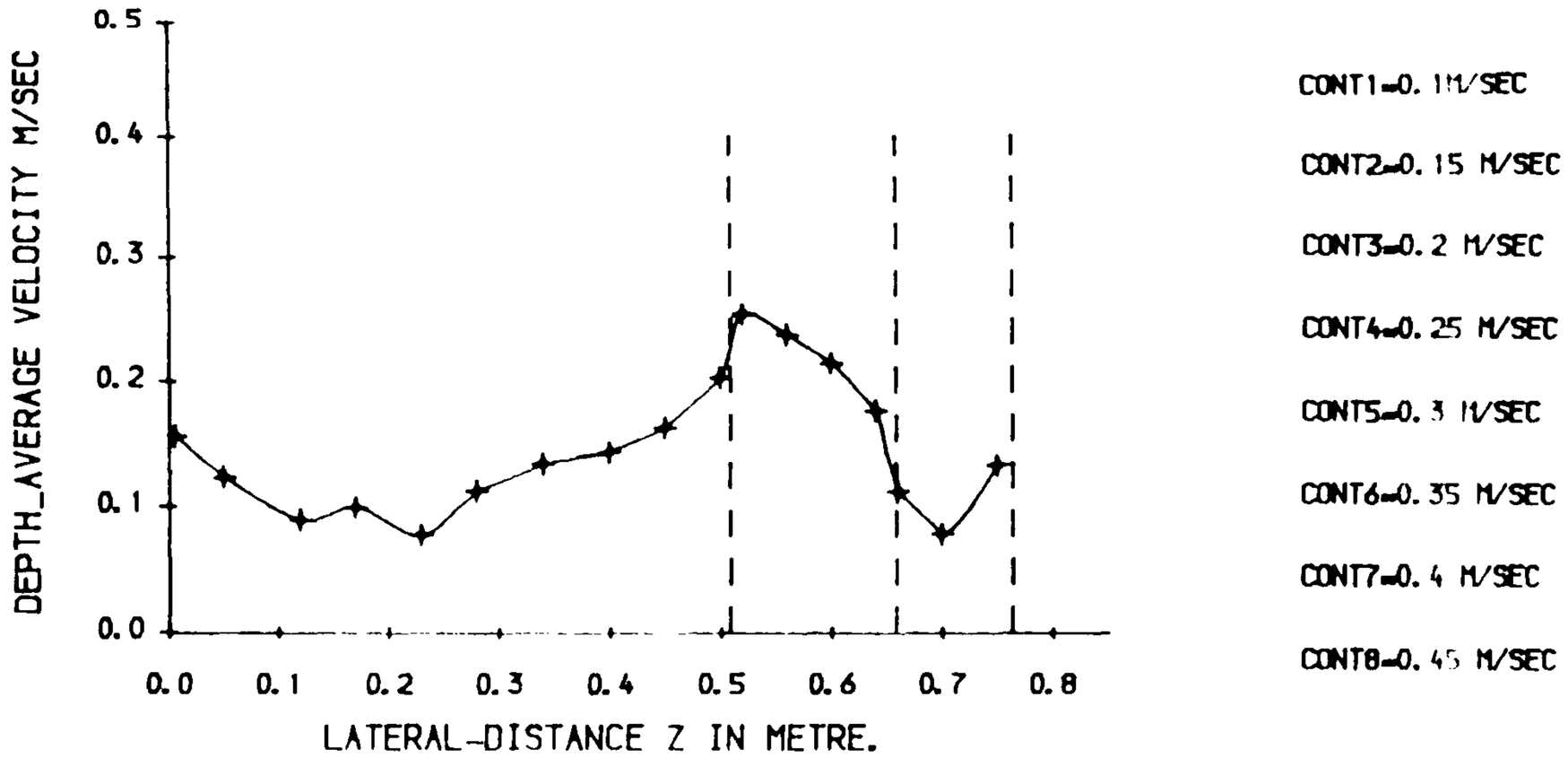

LONGITUDINAL DEPTH_AVERAGE VELOCITY PROFILE IN PLAN.

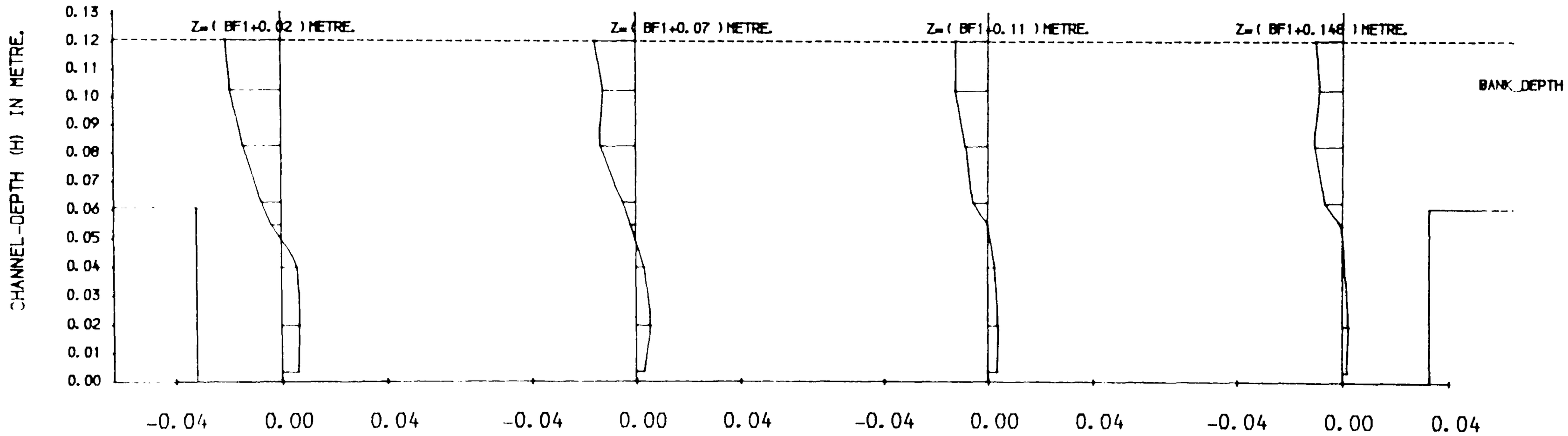

FIG (5.33) LONGITUDINAL & TRANSVERSE VELOCITY COMPONENTS IN SKEWED CHANNEL WITH ROUGH FLOODPLAIN

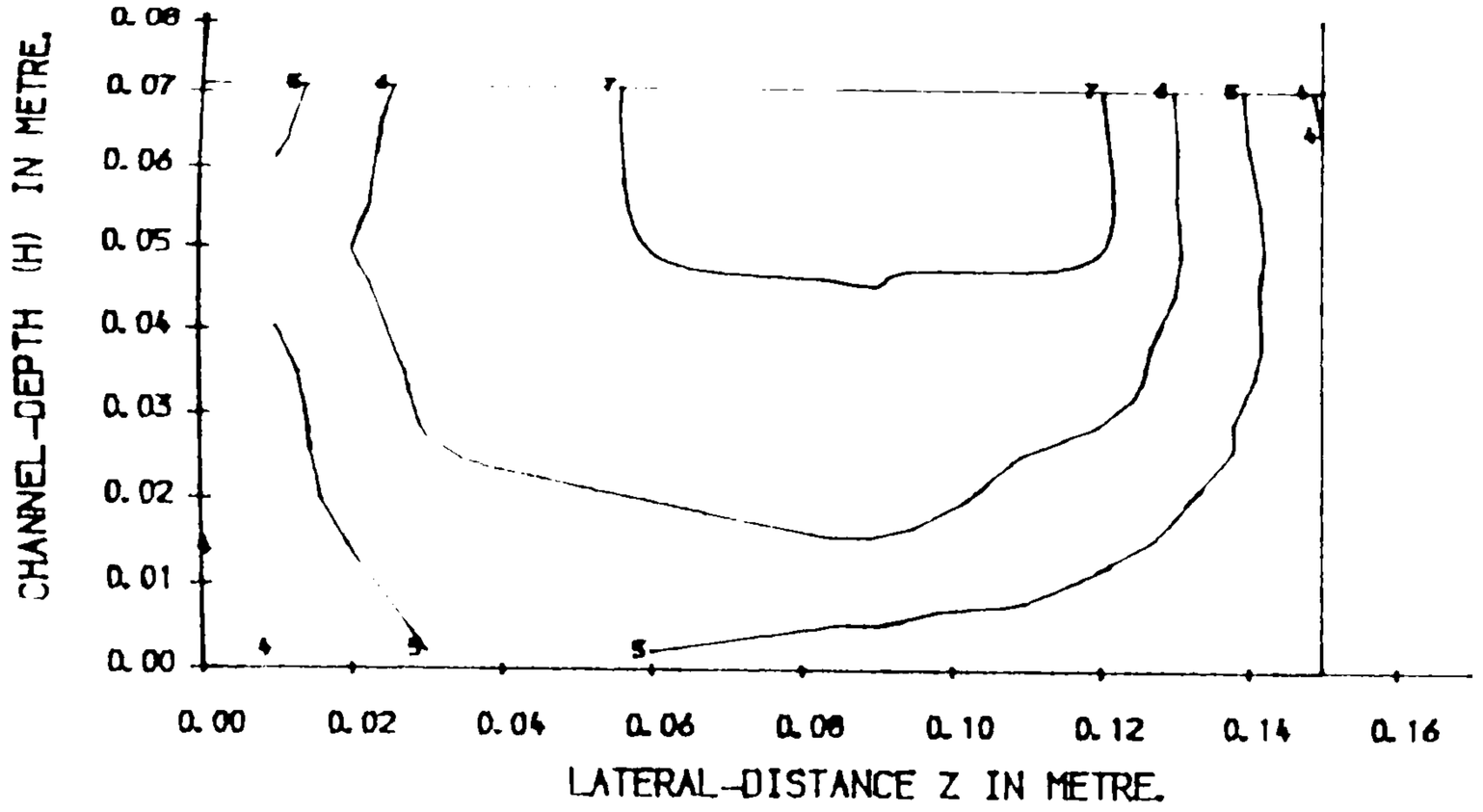

LONGITUDINAL VELOCITY CONTOURS IN CROSS SECTION. 1

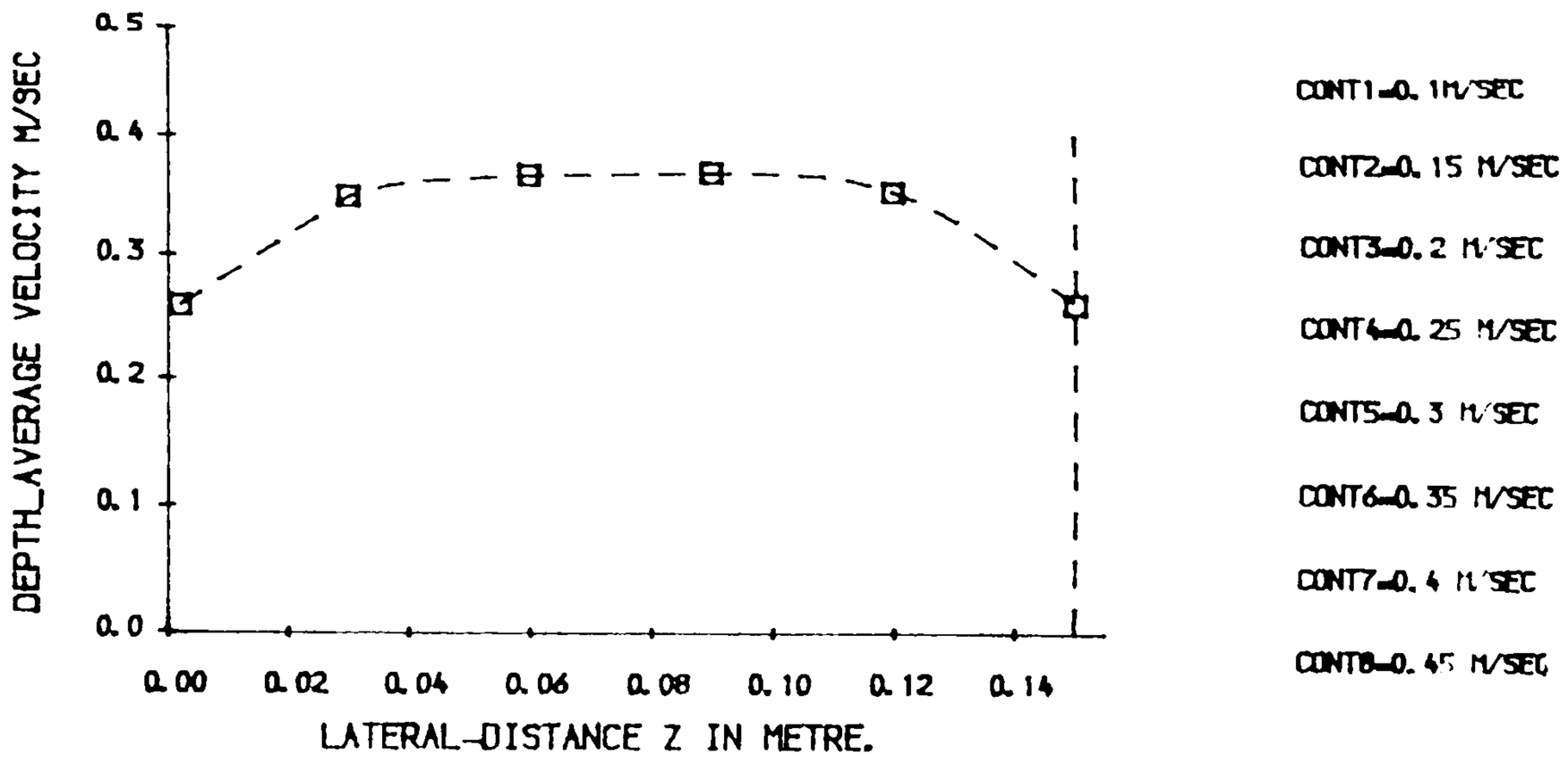

LONGITUDINAL DEPTH_AVERAGE VELOCITY PROFILE IN PLAN.

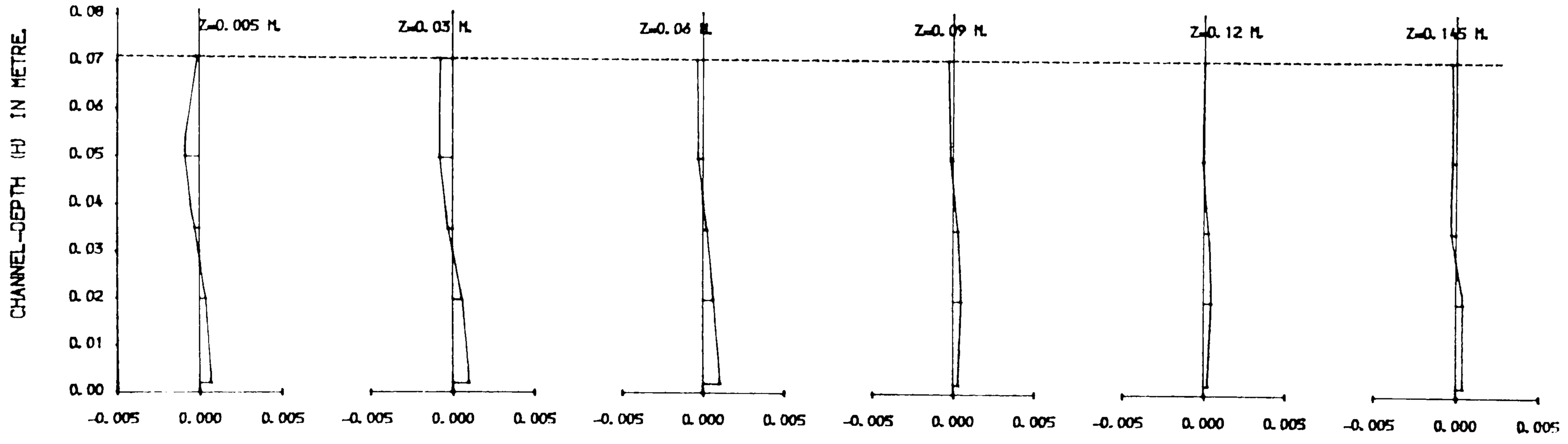

TRANSVERSE VELOCITY COMPONENTS (M/SEC) NORMAL TO SKEWED MAIN CHANNEL.

FIG (5.34) LONGITUDINAL & TRANSVERSE VELOCITY COMPONENTS IN THE SKEWED CHANNEL ISOLATED FROM THE FLOODPLAIN ZONE.

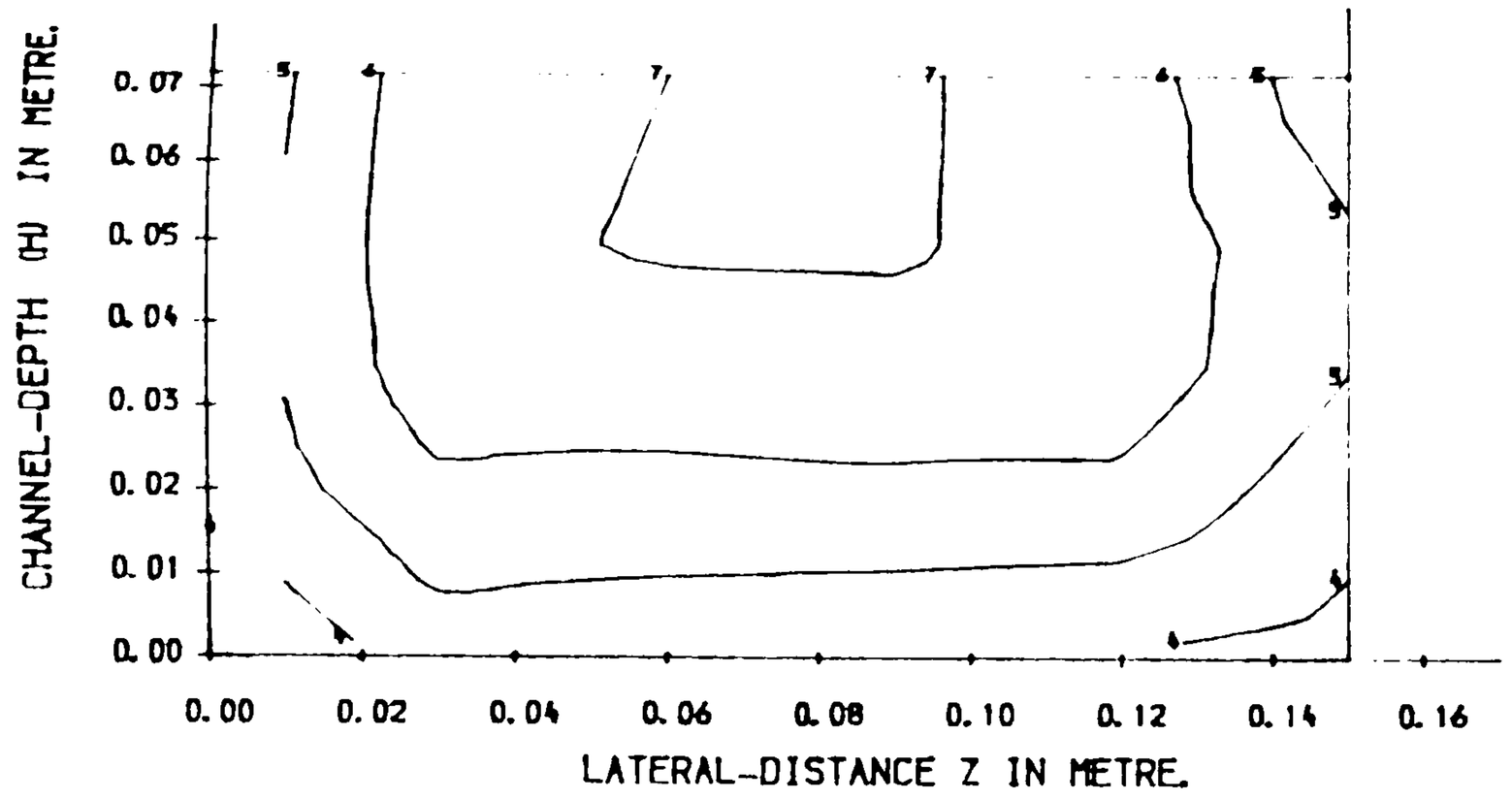

LONGITUDINAL VELOCITY CONTOURS IN CROSS SECTION. 2

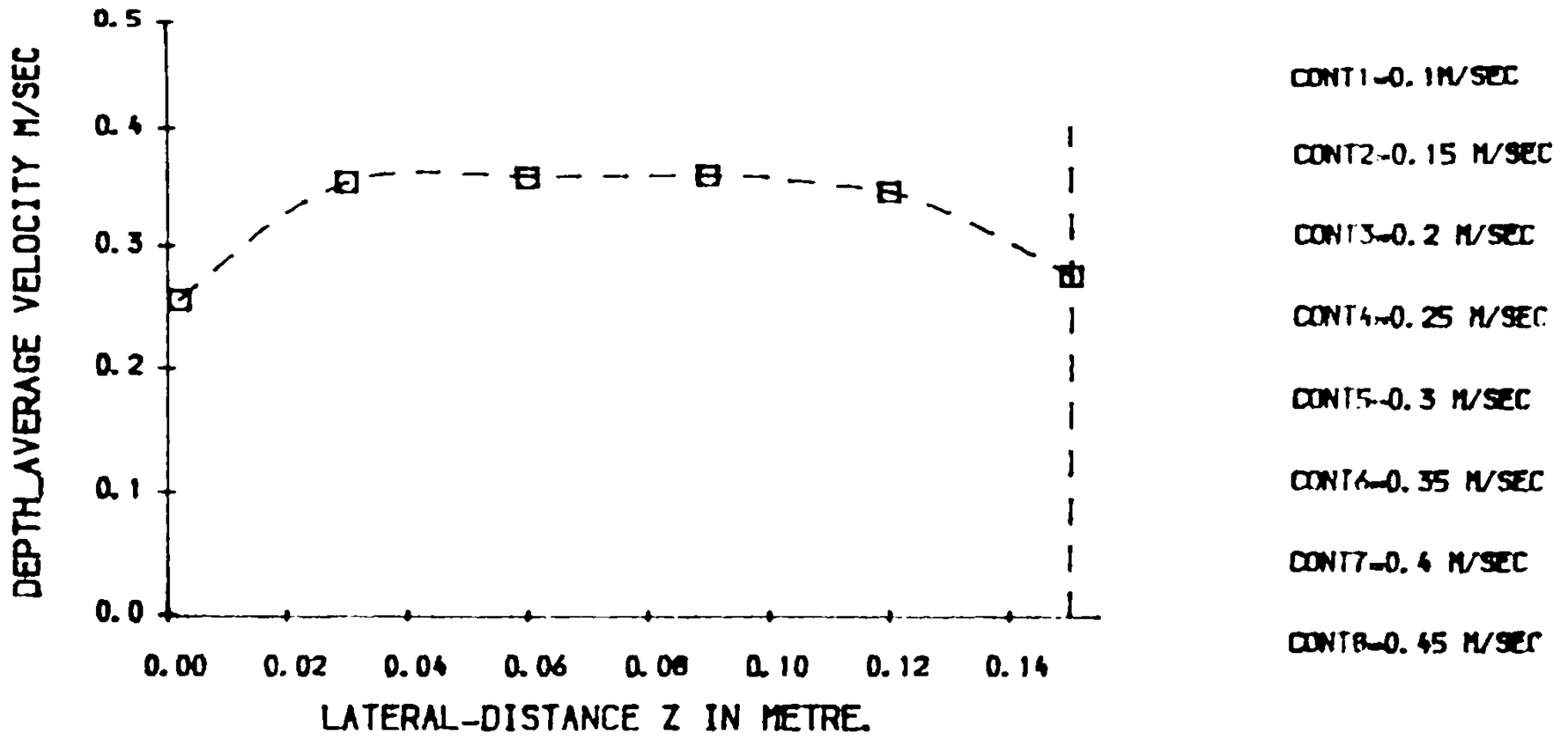

LONGITUDINAL DEPTH_AVERAGE VELOCITY PROFILE IN PLAN.

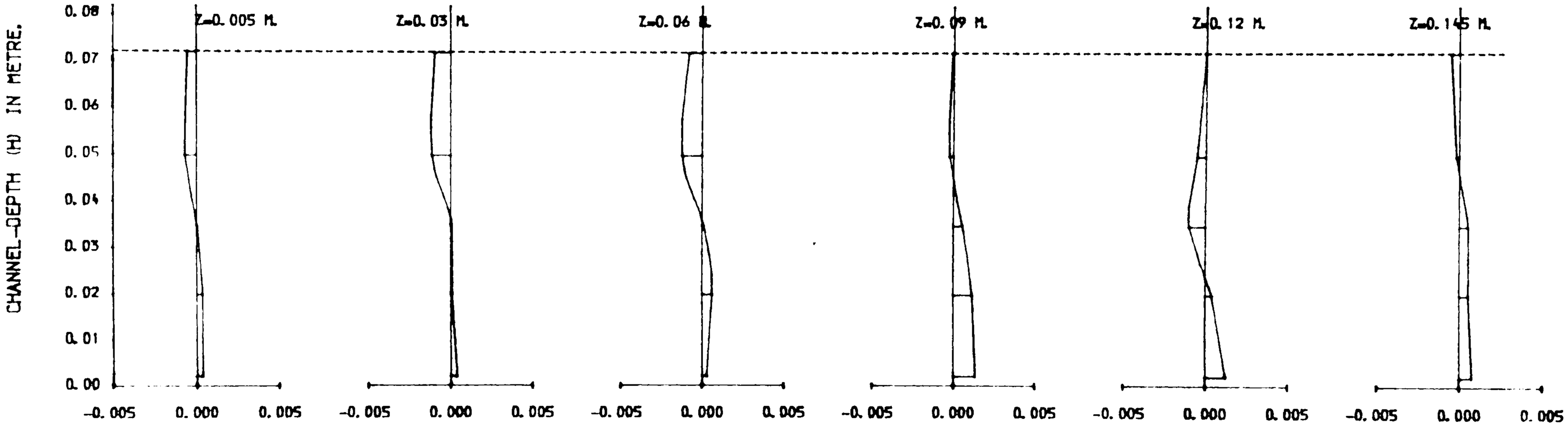

TRANSVERSE VELOCITY COMPONENTS (M/SEC) NORMAL TO SKEWED MAIN CHANNEL.

FIG (5. 35) LONGITUDINAL & TRANSVERSE VELOCITY COMPONENTS IN THE SKEWED CHANNEL ISOLATED FROM THE FLOODPLAIN ZONE.

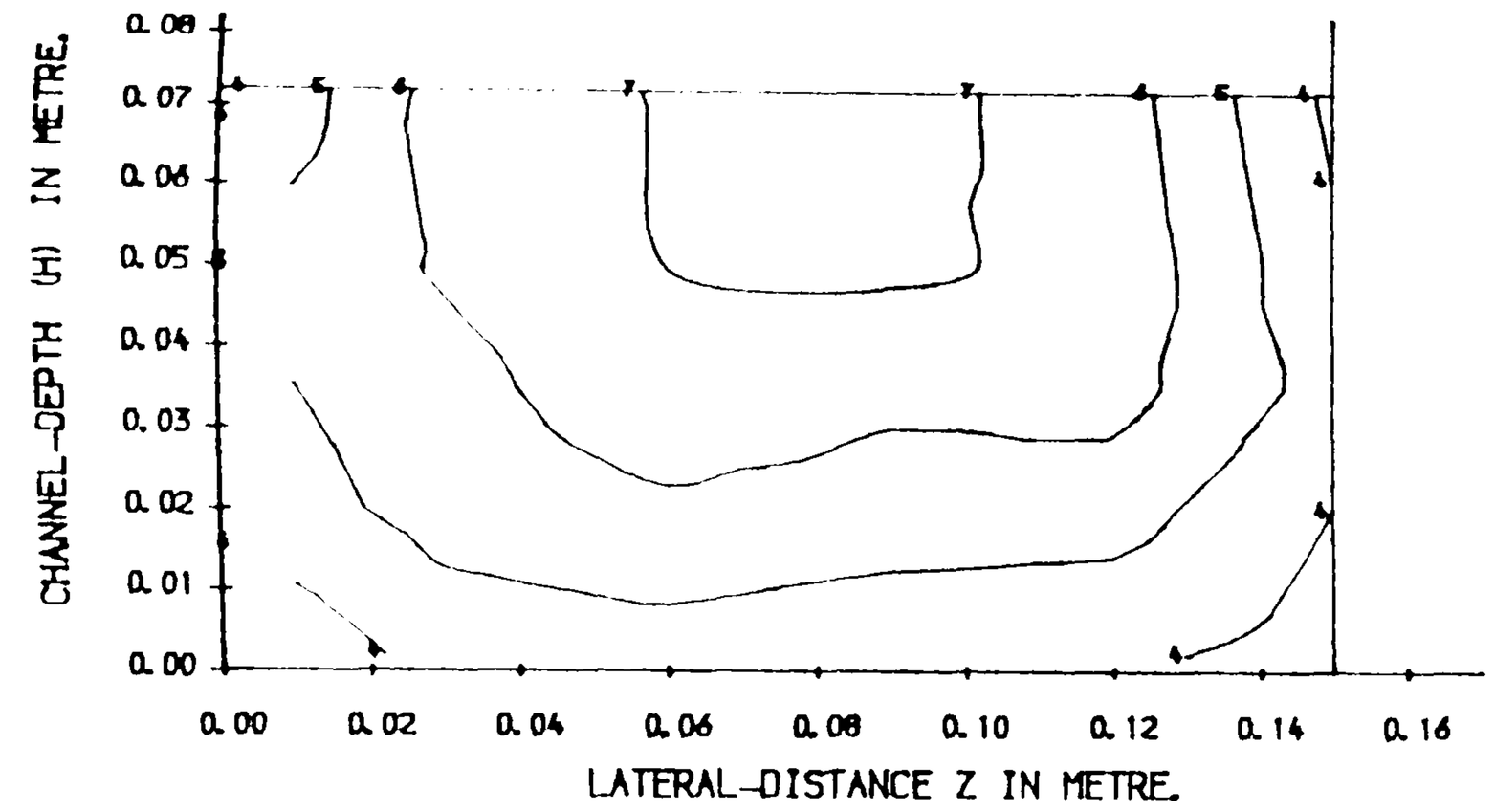

LONGITUDINAL VELOCITY CONTOURS IN CROSS SECTION 3

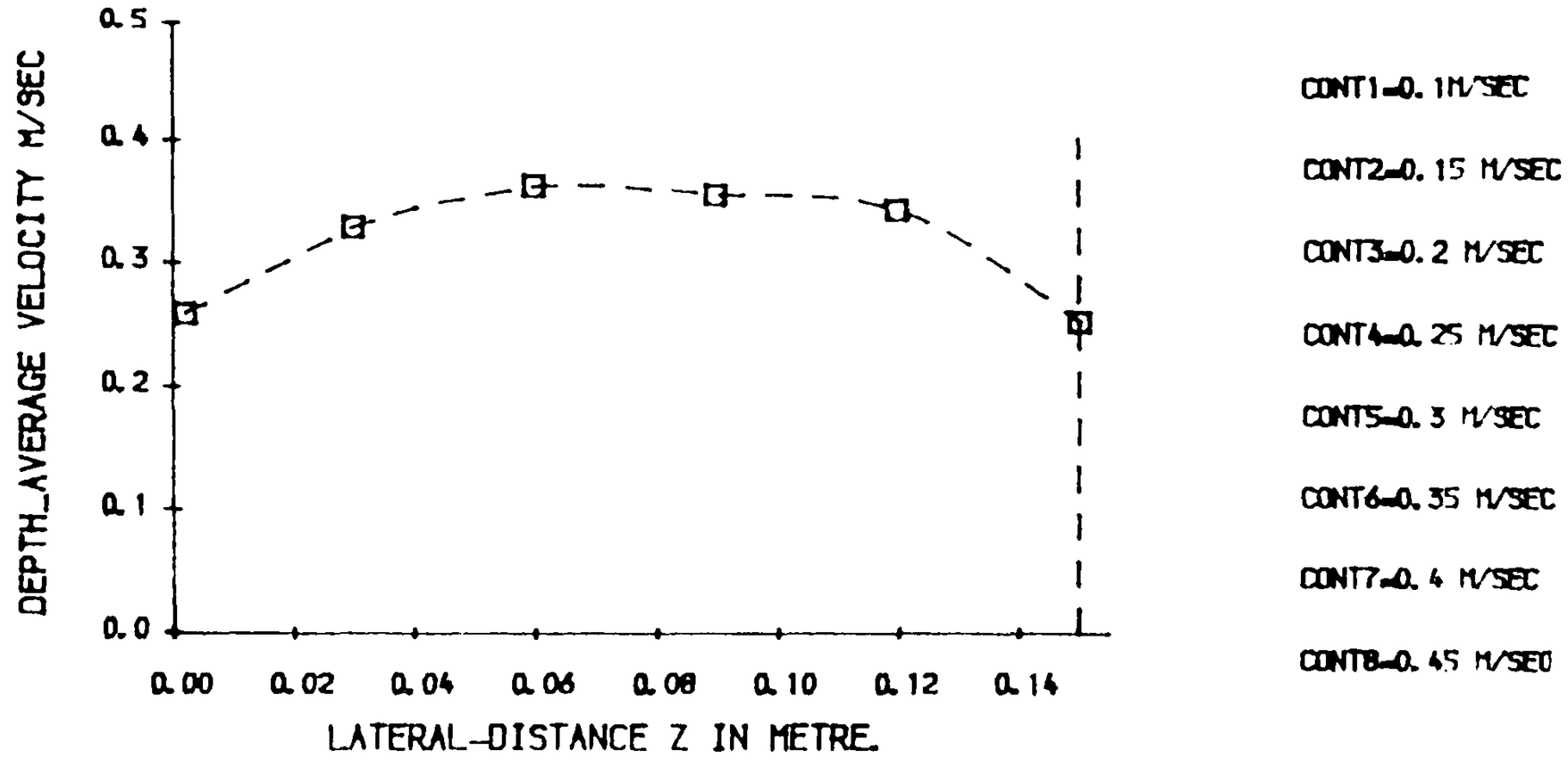

LONGITUDINAL DEPTH-AVERAGE VELOCITY PROFILE IN PLAN.

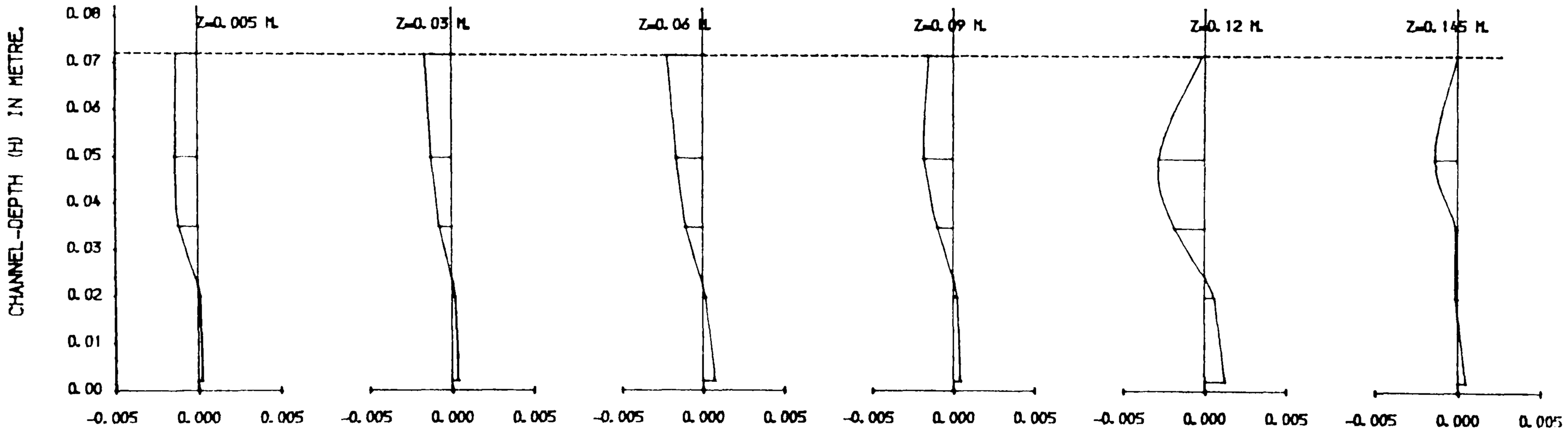

TRANSVERSE VELOCITY COMPONENTS (M/SEC) NORMAL TO SKEWED MAIN CHANNEL.

FIG (5.36) LONGITUDINAL & TRANSVERSE VELOCITY COMPONENTS IN THE SKEWED CHANNEL ISOLATED FROM THE FLOODPLAIN ZONE.

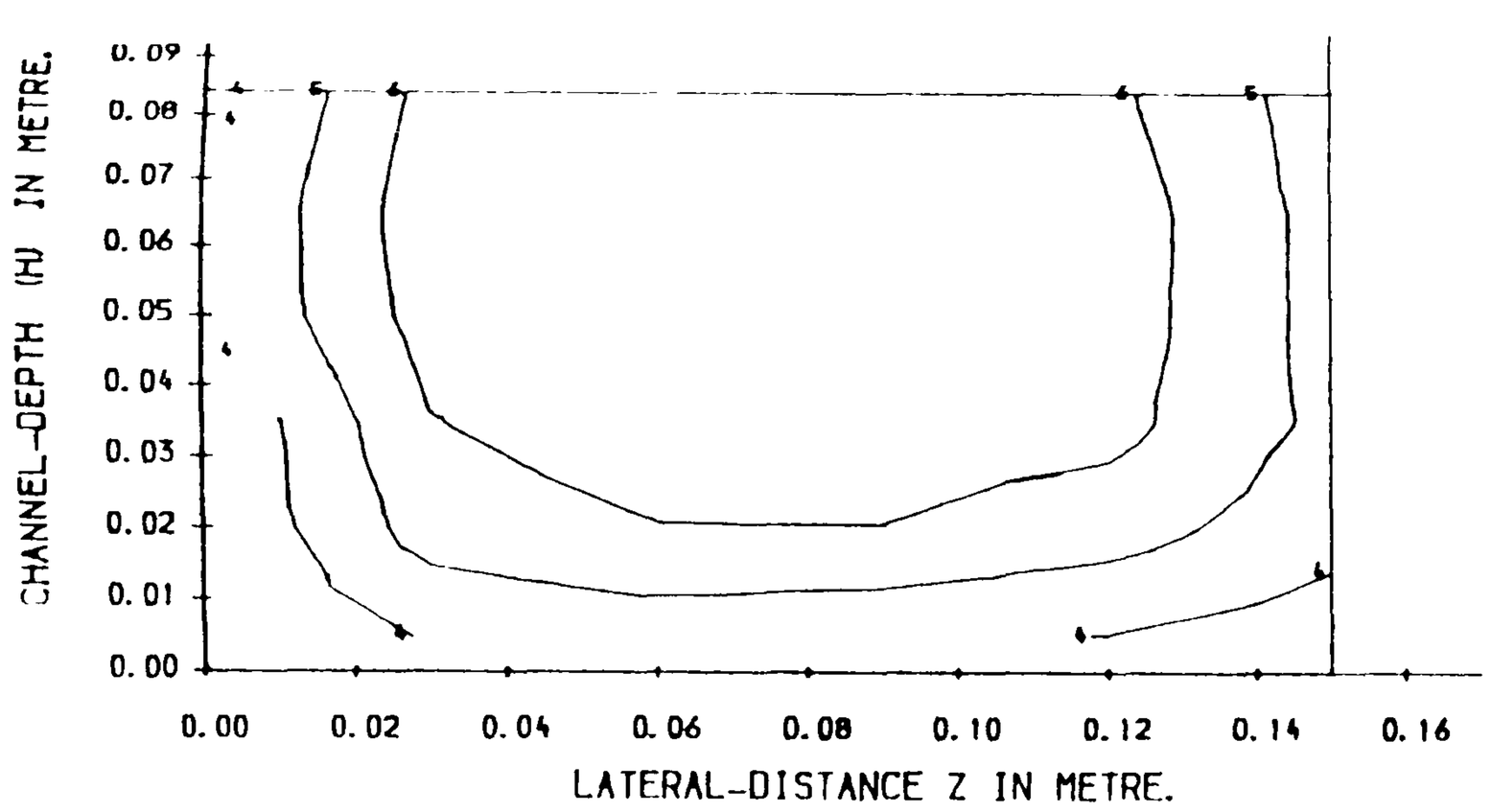

LONGITUDINAL VELOCITY CONTOURS IN CROSS SECTION. 1

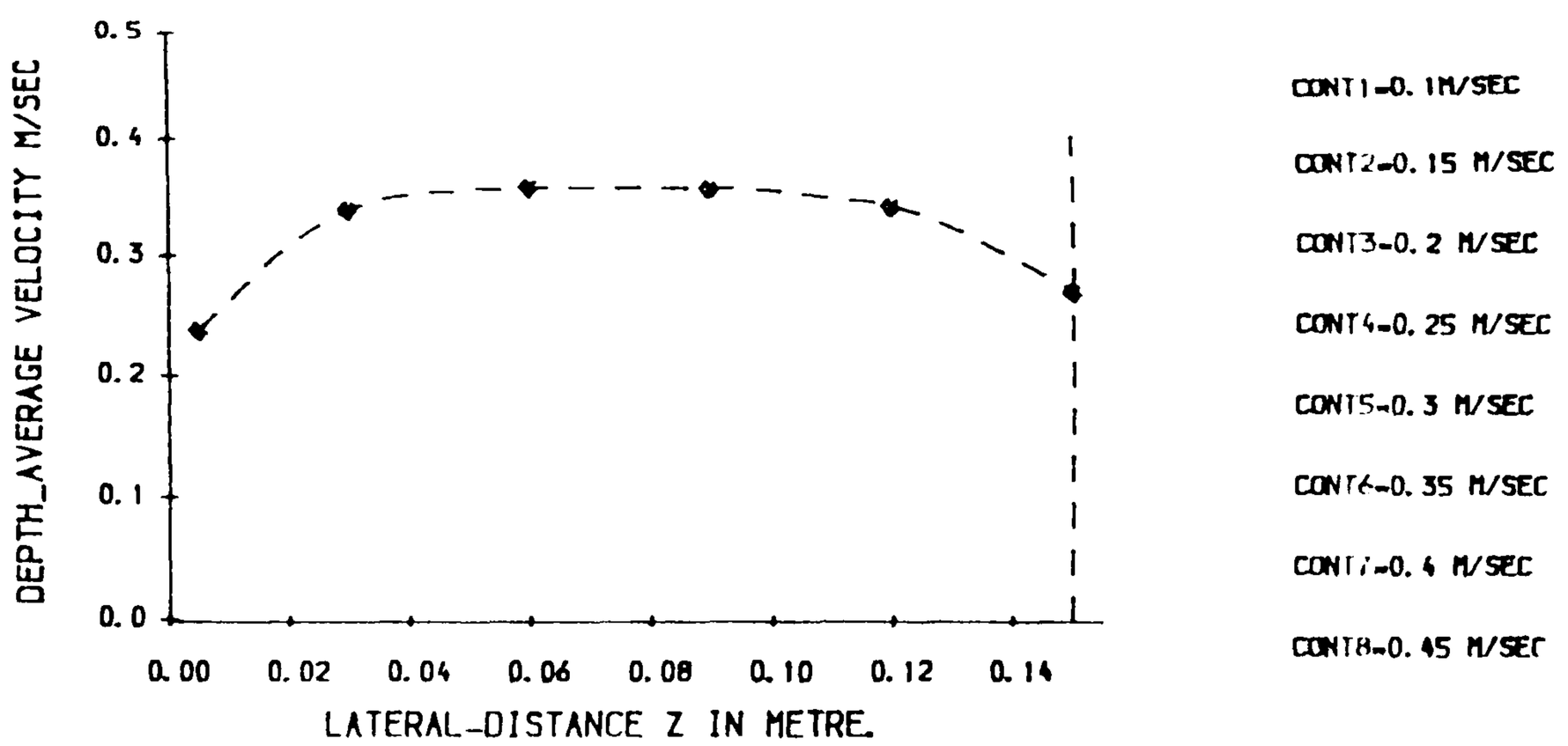

LONGITUDINAL DEPTH_AVERAGE VELOCITY PROFILE IN PLAN.

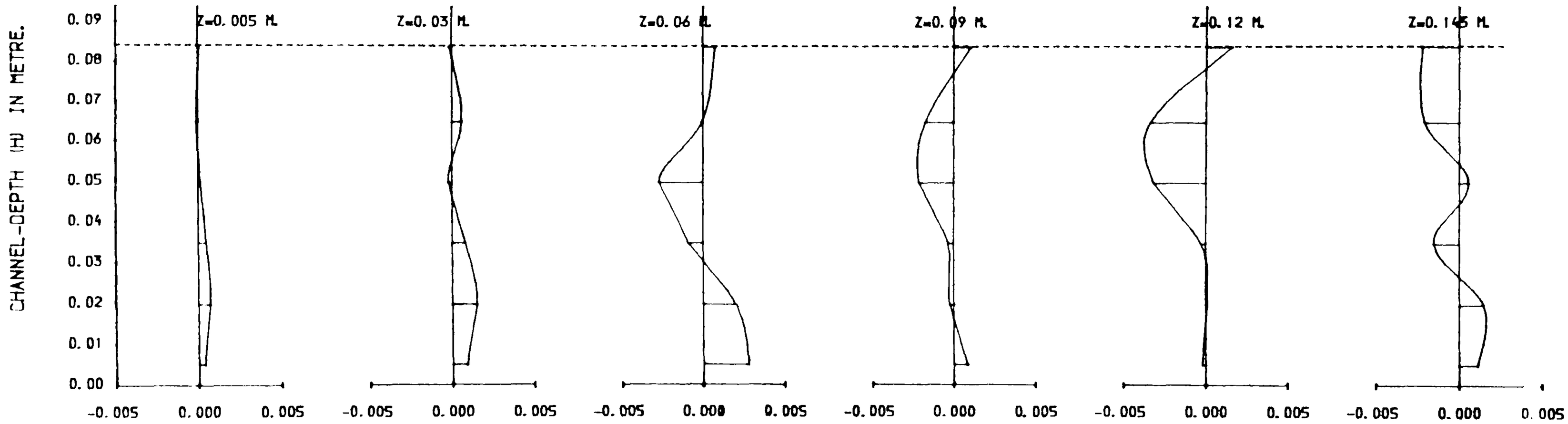

TRANSVERSE VELOCITY COMPONENTS (M/SEC) NORMAL TO SKEWED MAIN CHANNEL.

FIG (5.37) LONGITUDINAL & TRANSVERSE VELOCITY COMPONENTS IN THE SKEWED CHANNEL ISOLATED FROM THE FLOODPLAIN ZONE.

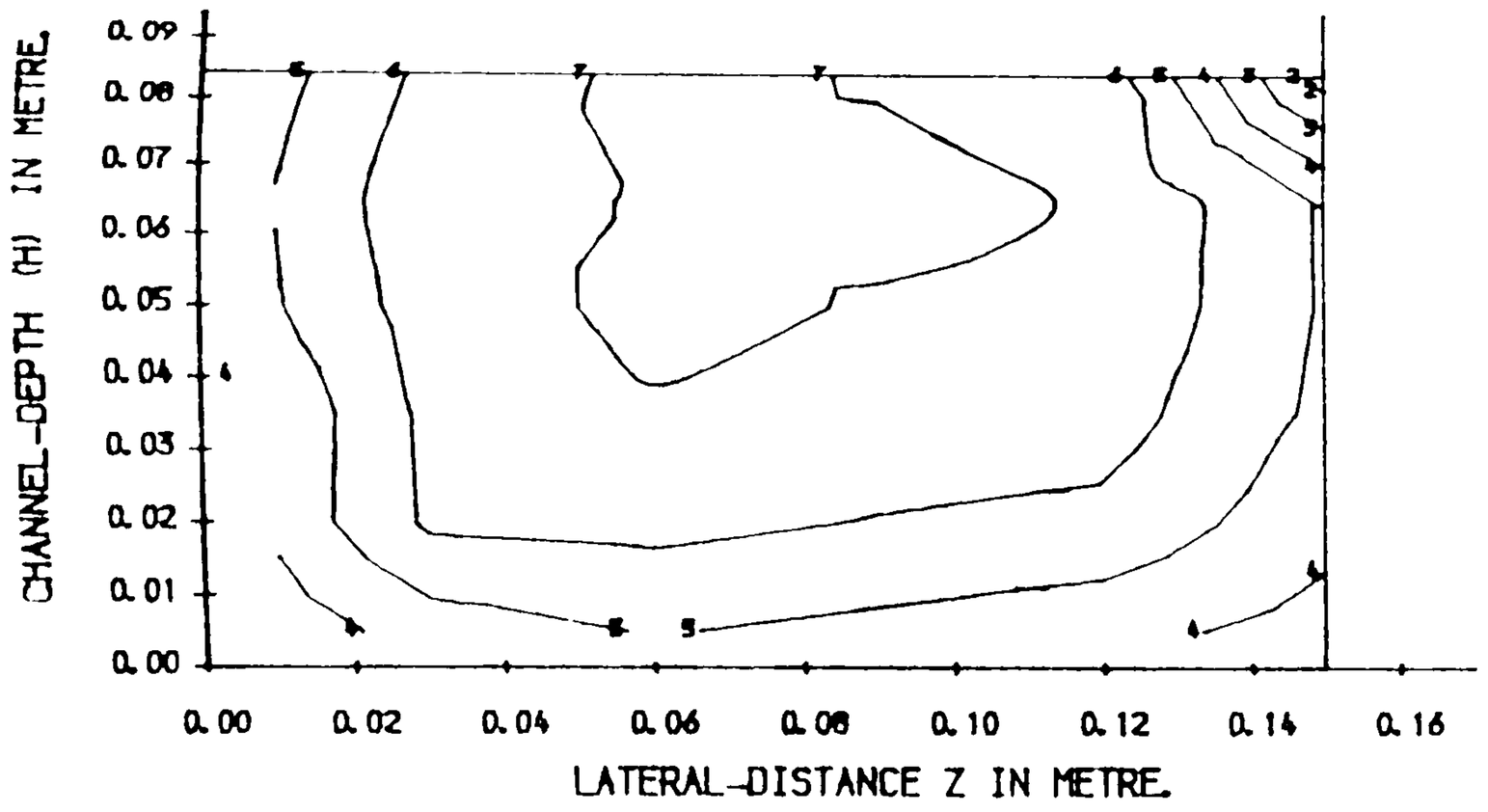

LONGITUDINAL VELOCITY CONTOURS IN CROSS SECTION. 2

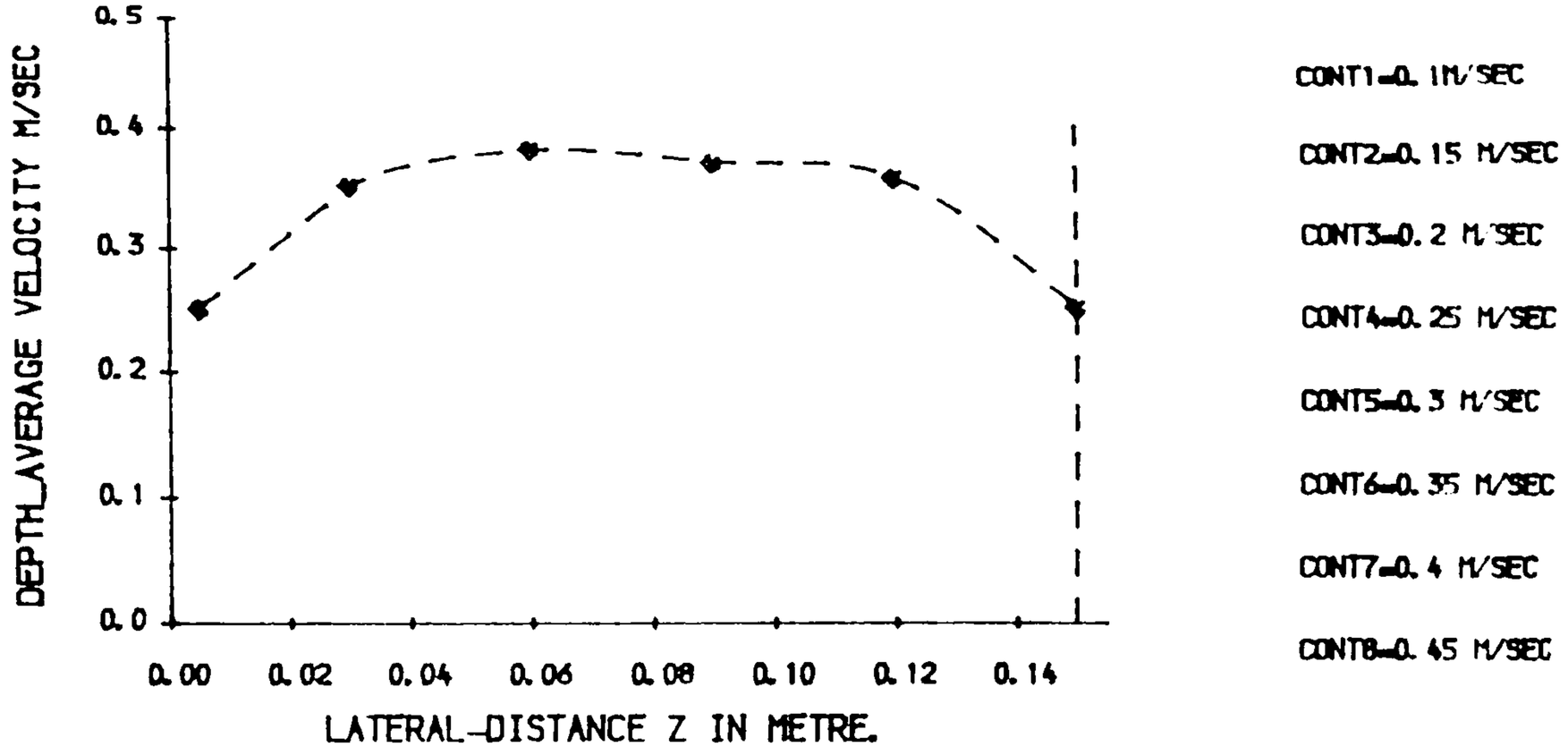

LONGITUDINAL DEPTH_AVERAGE VELOCITY PROFILE IN PLAN.

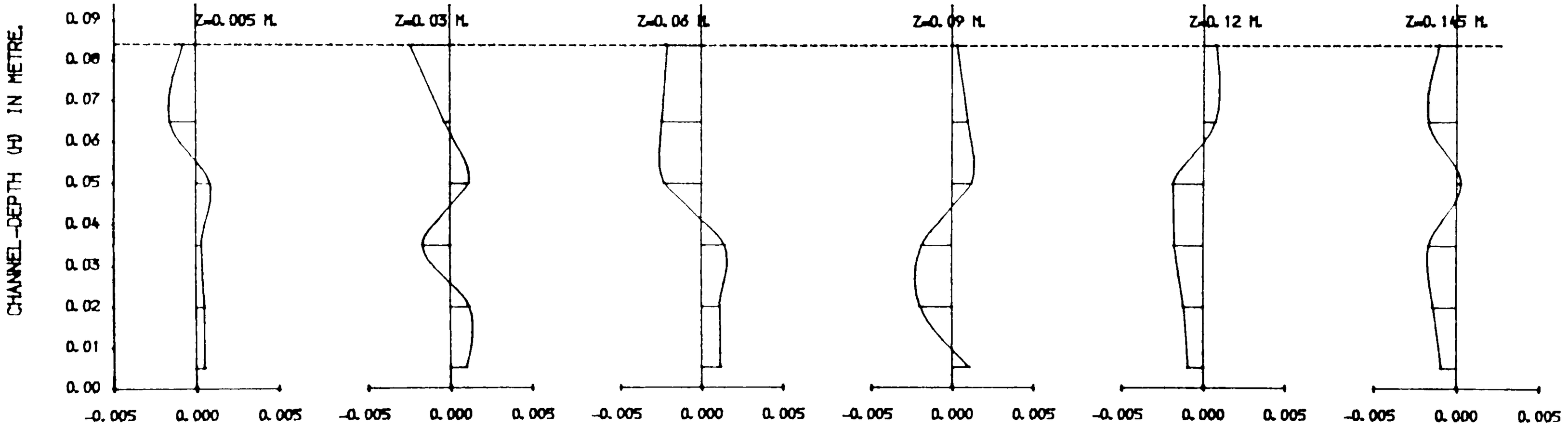

TRANSVERSE VELOCITY COMPONENTS (M/SEC) NORMAL TO SKEWED MAIN CHANNEL.

FIG (5.38) LONGITUDINAL & TRANSVERSE VELOCITY COMPONENTS IN THE SKEWED CHANNEL ISOLATED FROM THE FLOODPLAIN ZONE.

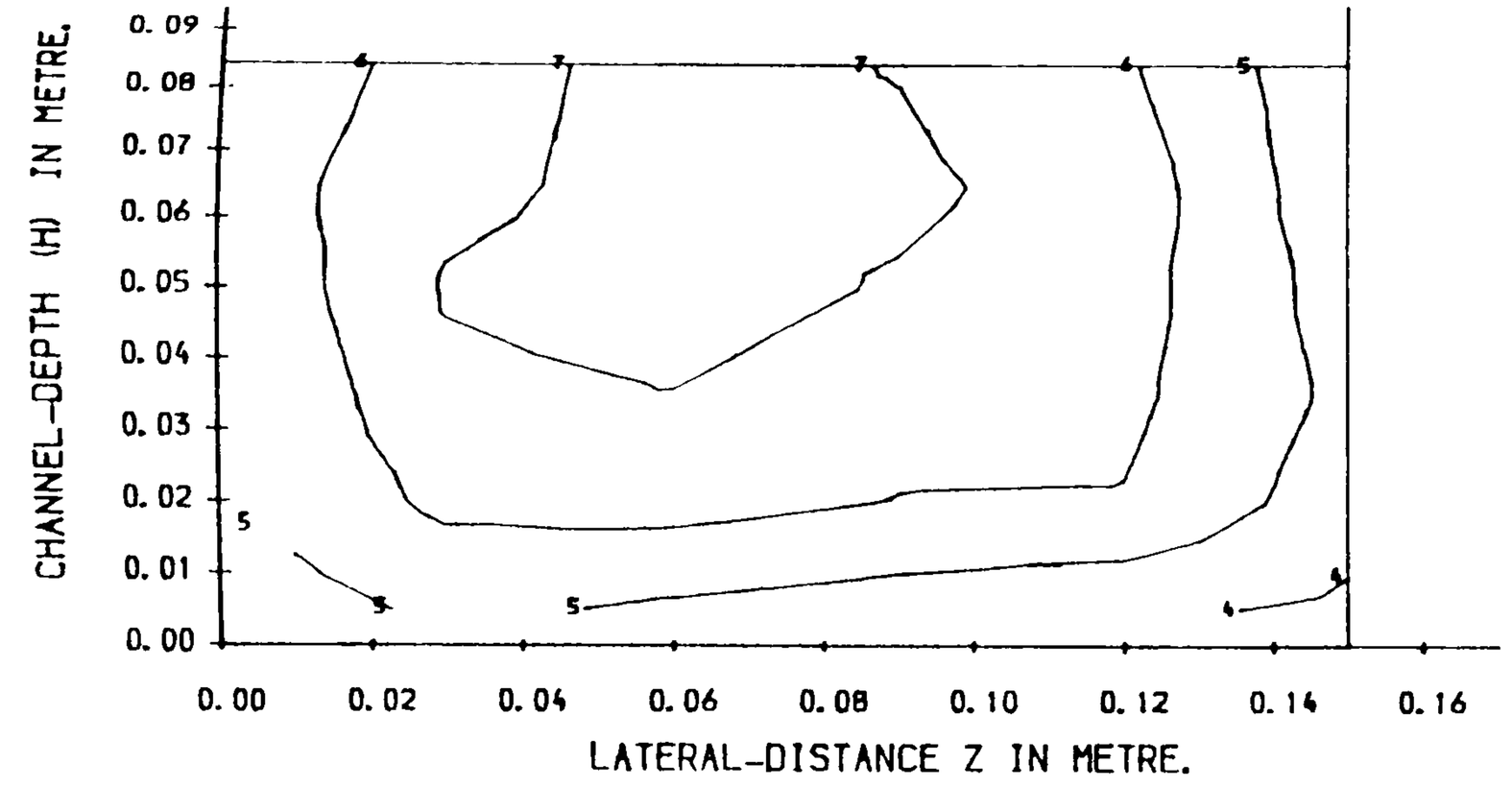

LONGITUDINAL VELOCITY CONTOURS IN CROSS SECTION. 3

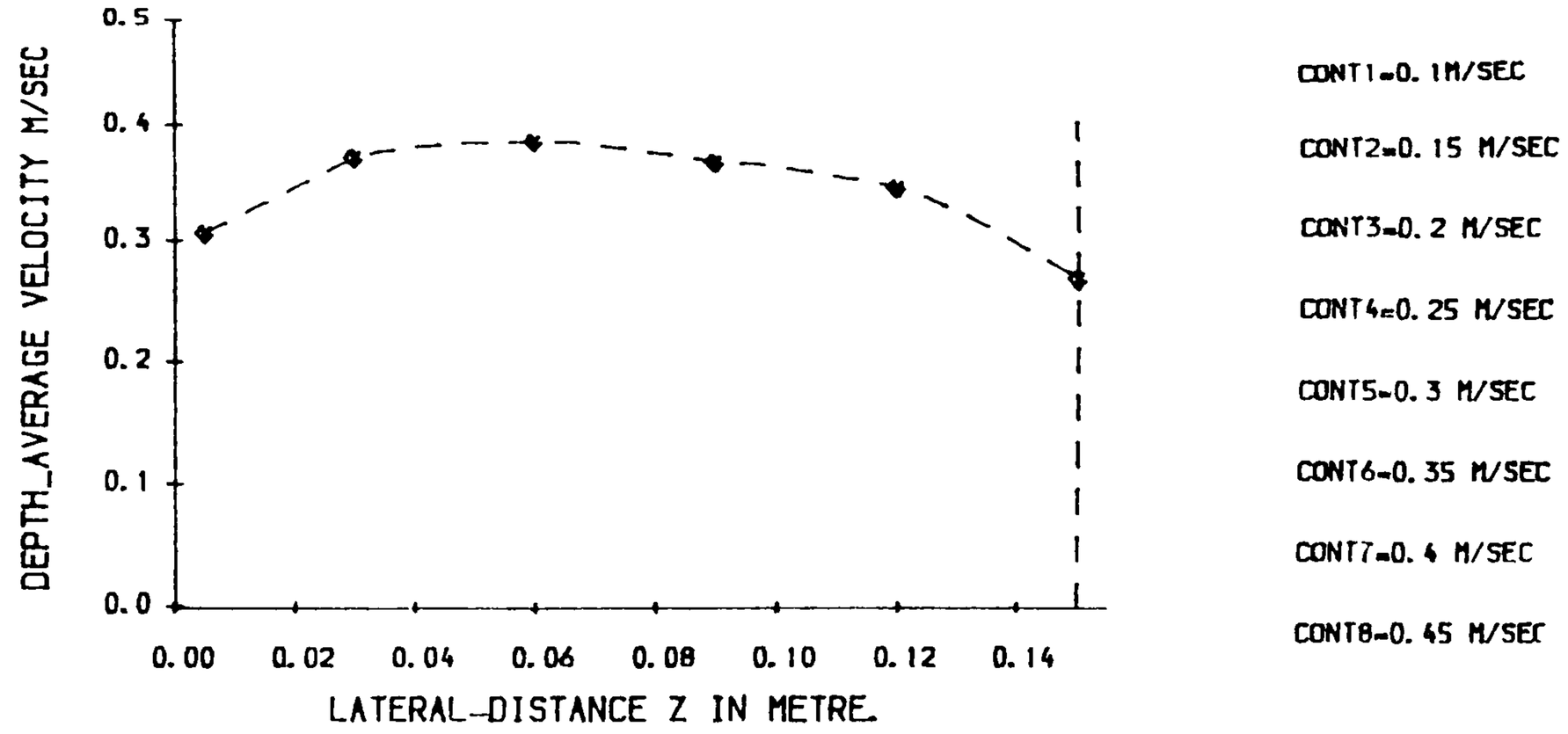

LONGITUDINAL DEPTH_AVERAGE VELOCITY PROFILE IN PLAN.

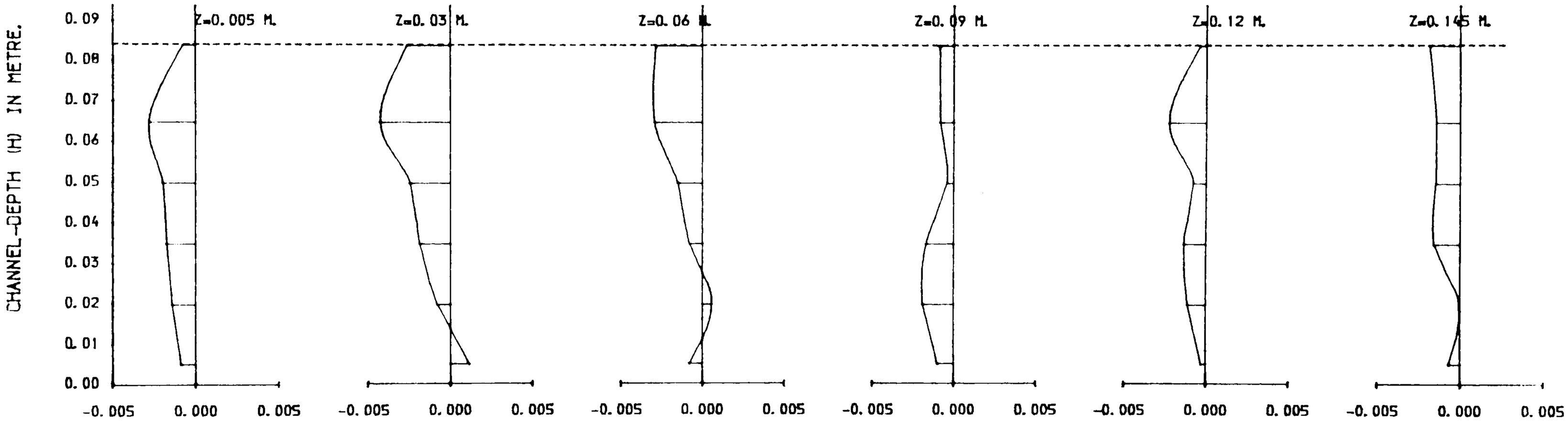

FIG (5.39) LONGITUDINAL & TRANSVERSE VELOCITY COMPONENTS IN THE SKEWED CHANNEL ISOLATED FROM THE FLOODPLAIN ZONE.

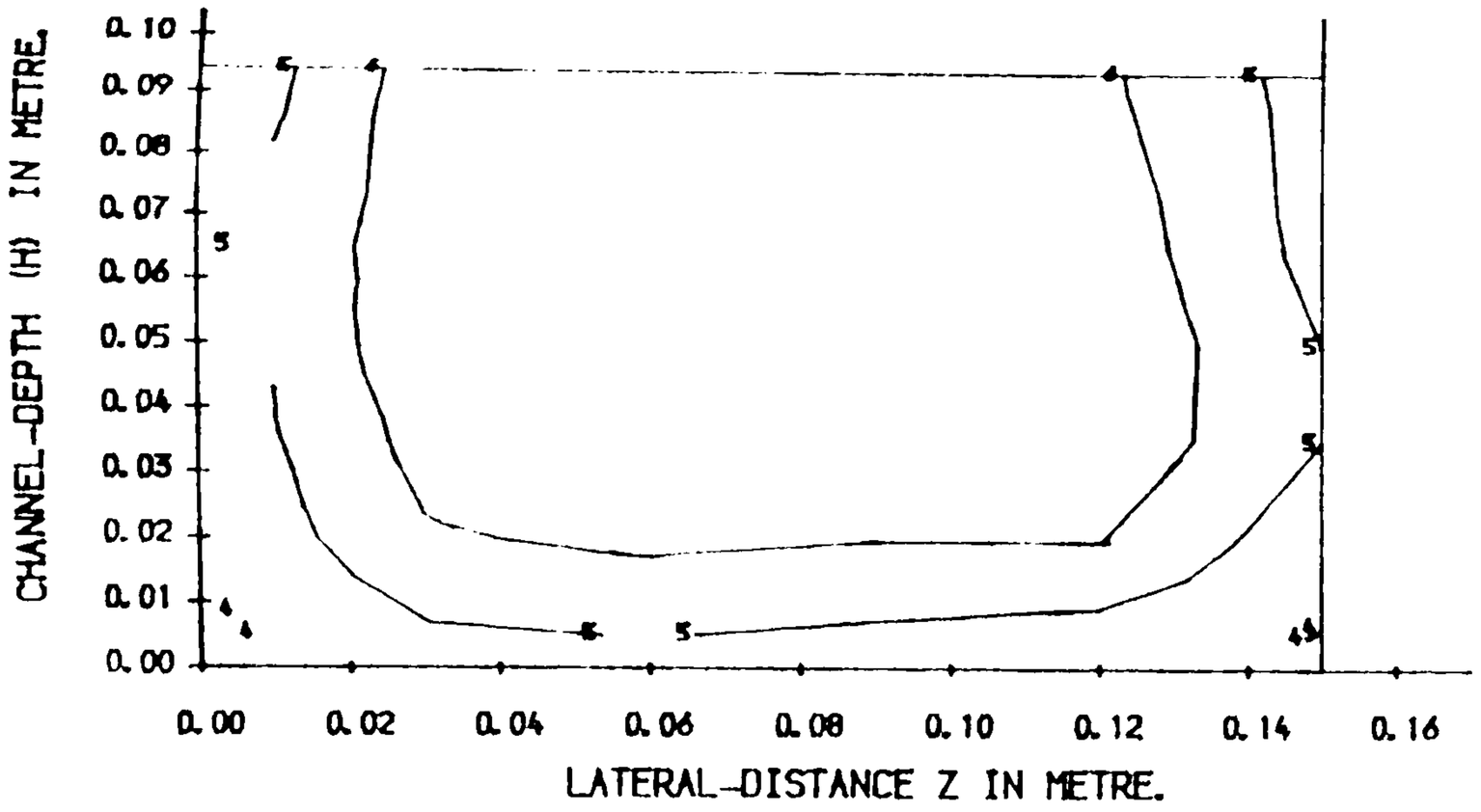

LONGITUDINAL VELOCITY CONTOURS IN CROSS SECTION. 1

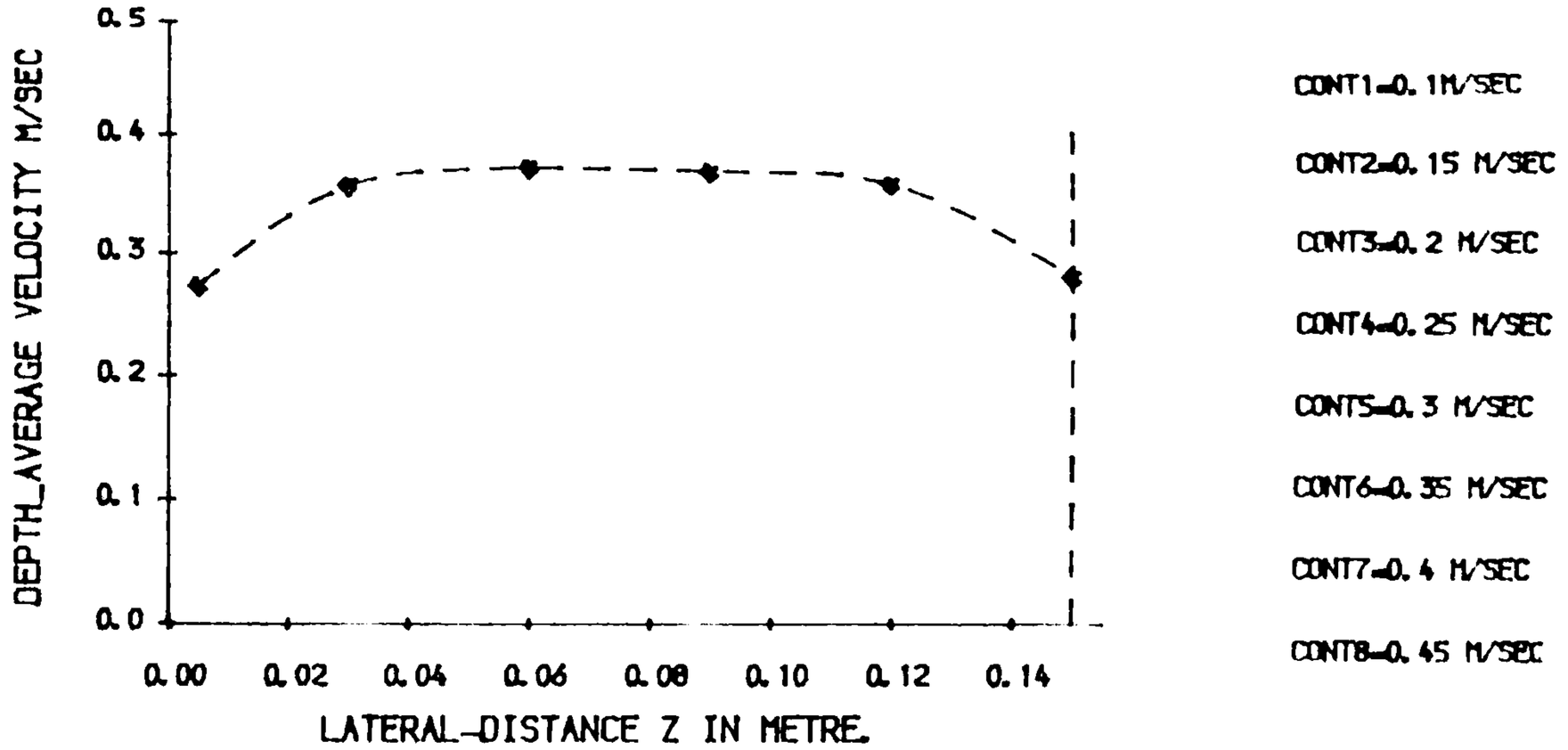

LONGITUDINAL DEPTH_AVERAGE VELOCITY PROFILE IN PLAN.

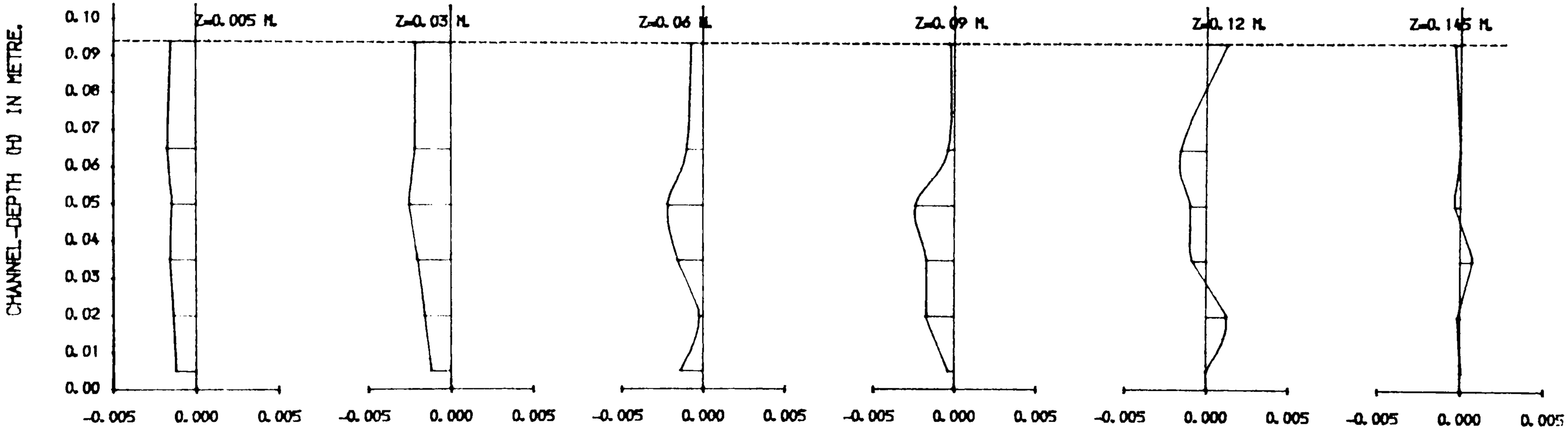

TRANSVERSE VELOCITY COMPONENTS (M/SEC) NORMAL TO SKEWED MAIN CHANNEL.

FIG (5.10) LONGITUDINAL & TRANSVERSE VELOCITY COMPONENTS IN THE SKEWED CHANNEL ISOLATED FROM THE FLOODPLAIN ZONE.

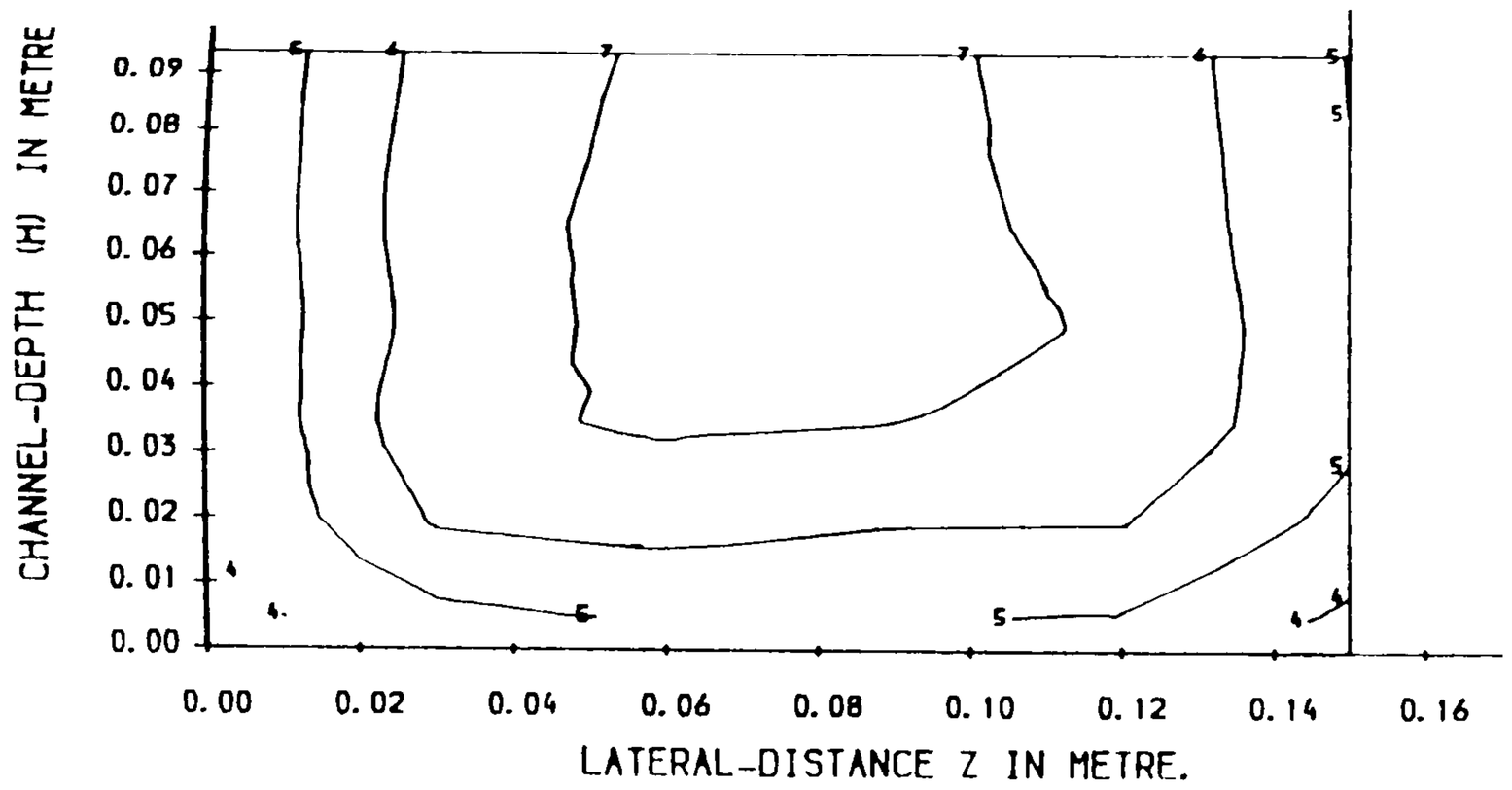

LONGITUDINAL VELOCITY CONTOURS IN CROSS SECTION. 2

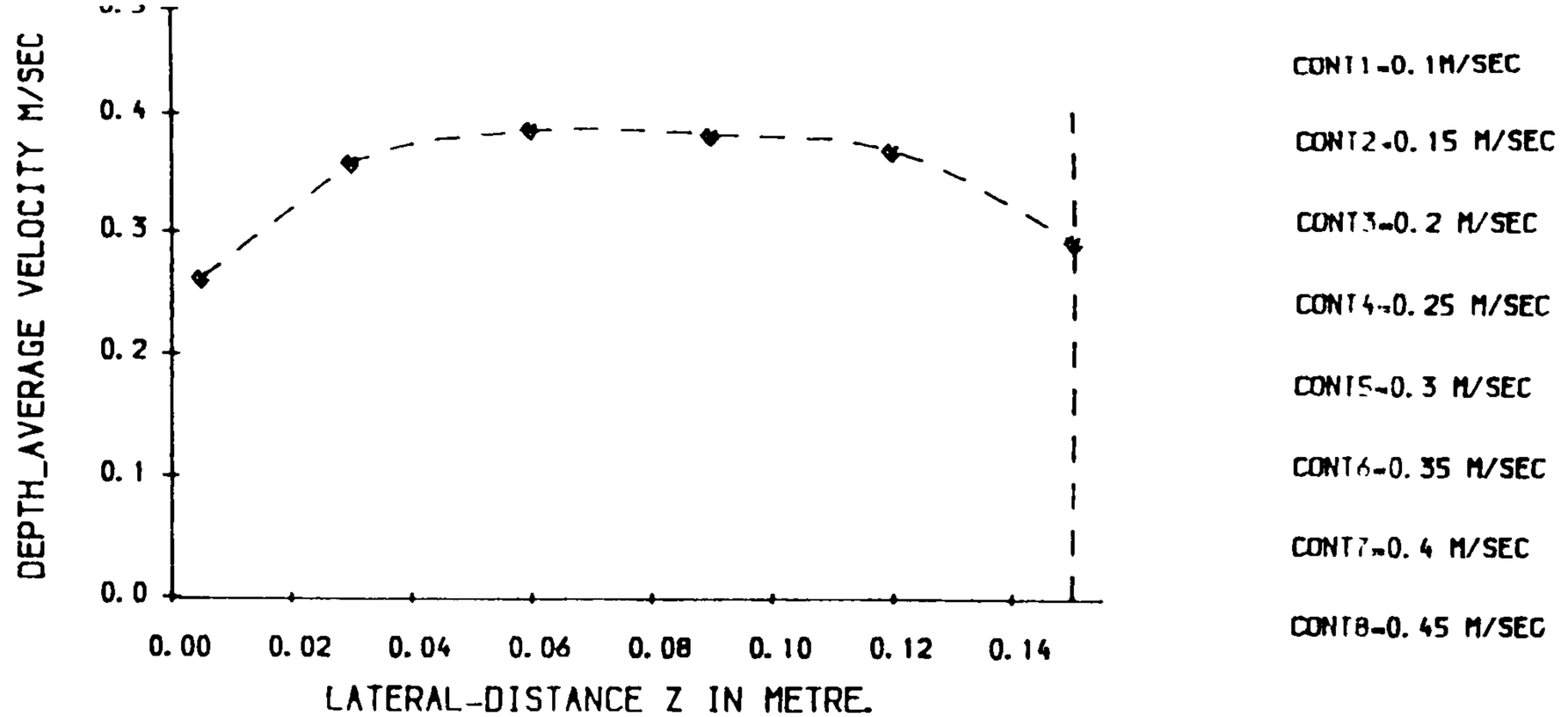

LONGITUDINAL DEPTH_AVERAGE VELOCITY PROFILE IN PLAN.

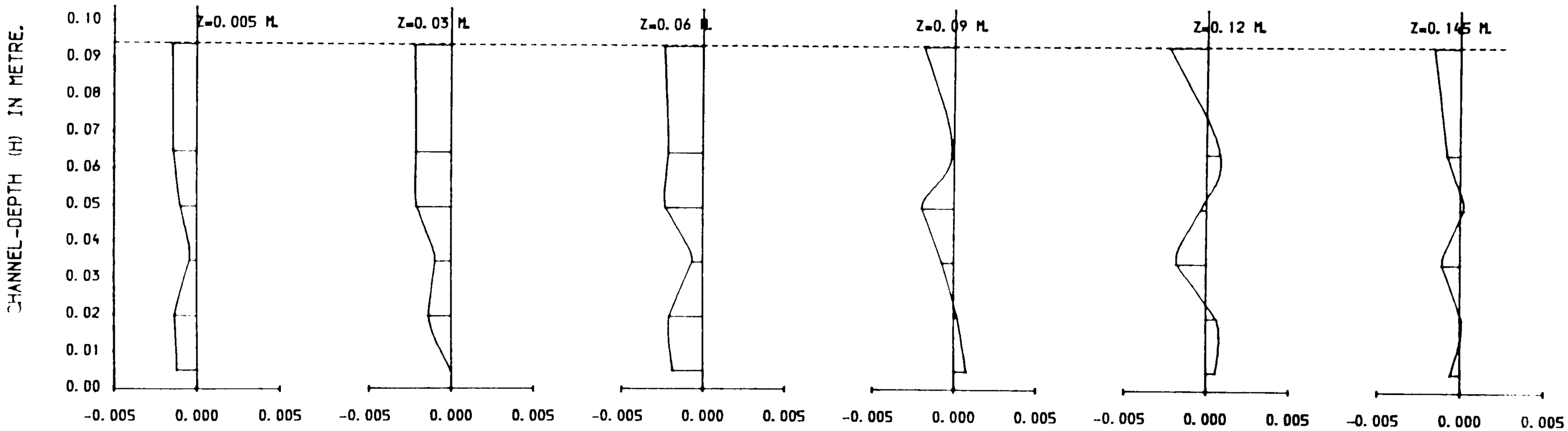

FIG (5. 4) LONGITUDINAL & TRANSVERSE VELOCITY COMPONENTS IN THE SKEWED CHANNEL ISOLATED FROM THE FLOODPLAIN ZONE.

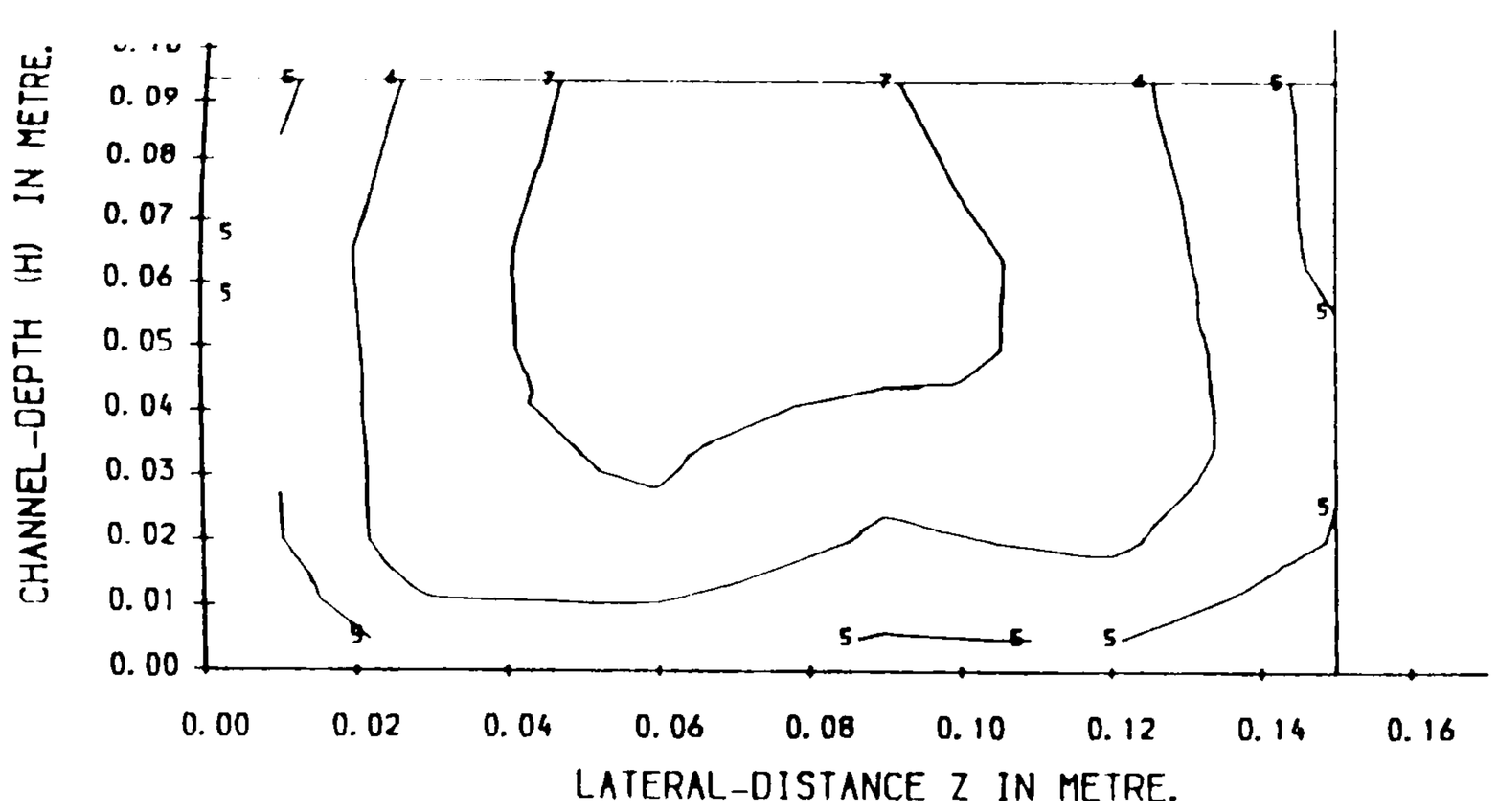

LONGITUDINAL VELOCITY CONTOURS IN CROSS SECTION. 3

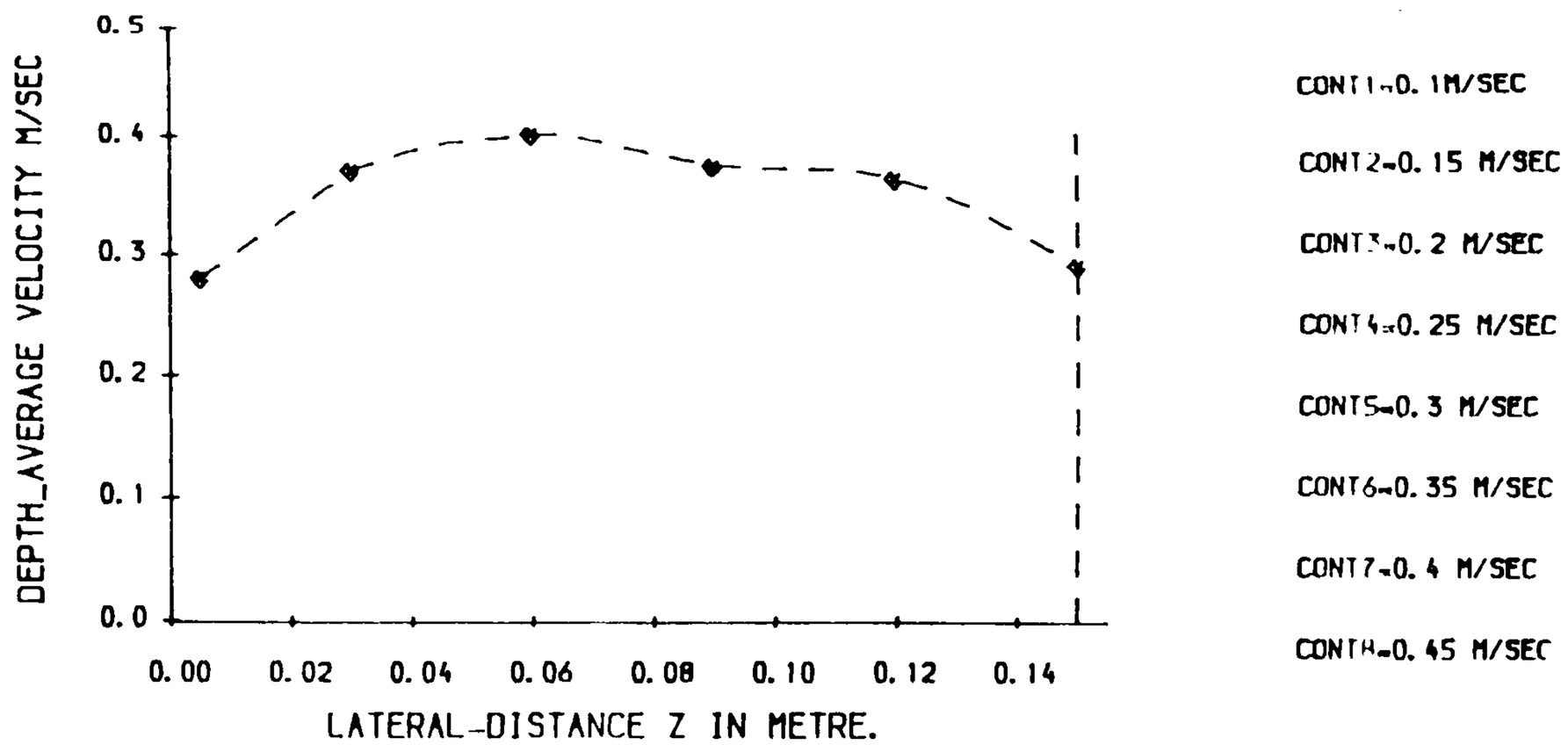

LONGITUDINAL DEPTH_AVERAGE VELOCITY PROFILE IN PLAN.

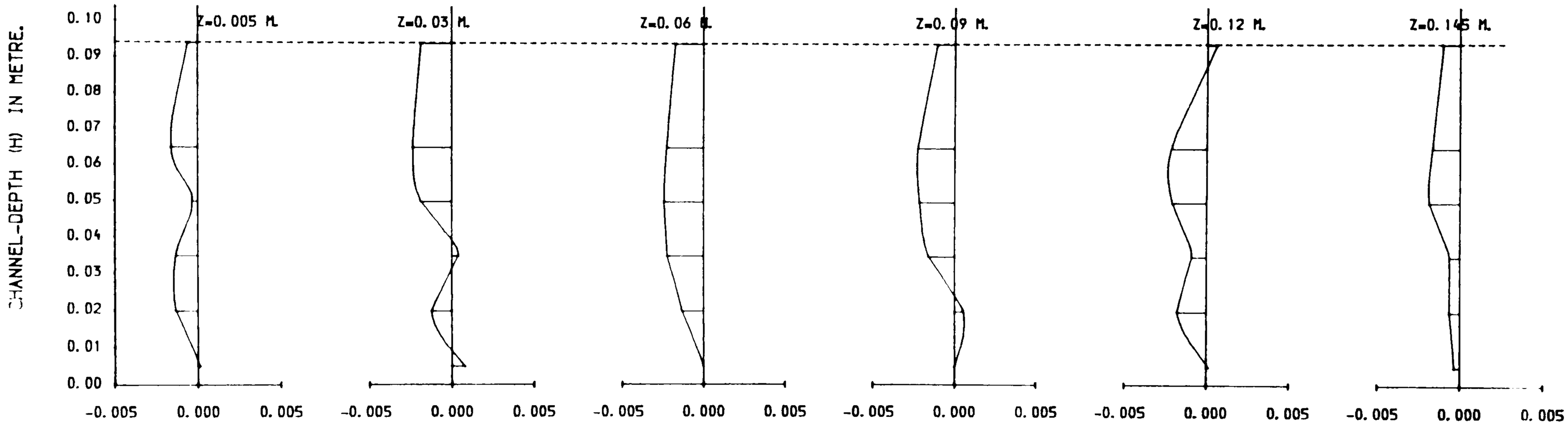

FIG (5.42) LONGITUDINAL & TRANSVERSE VELOCITY COMPONENTS IN THE SKEWED CHANNEL ISOLATED FROM THE FLOODPLAIN ZONE.

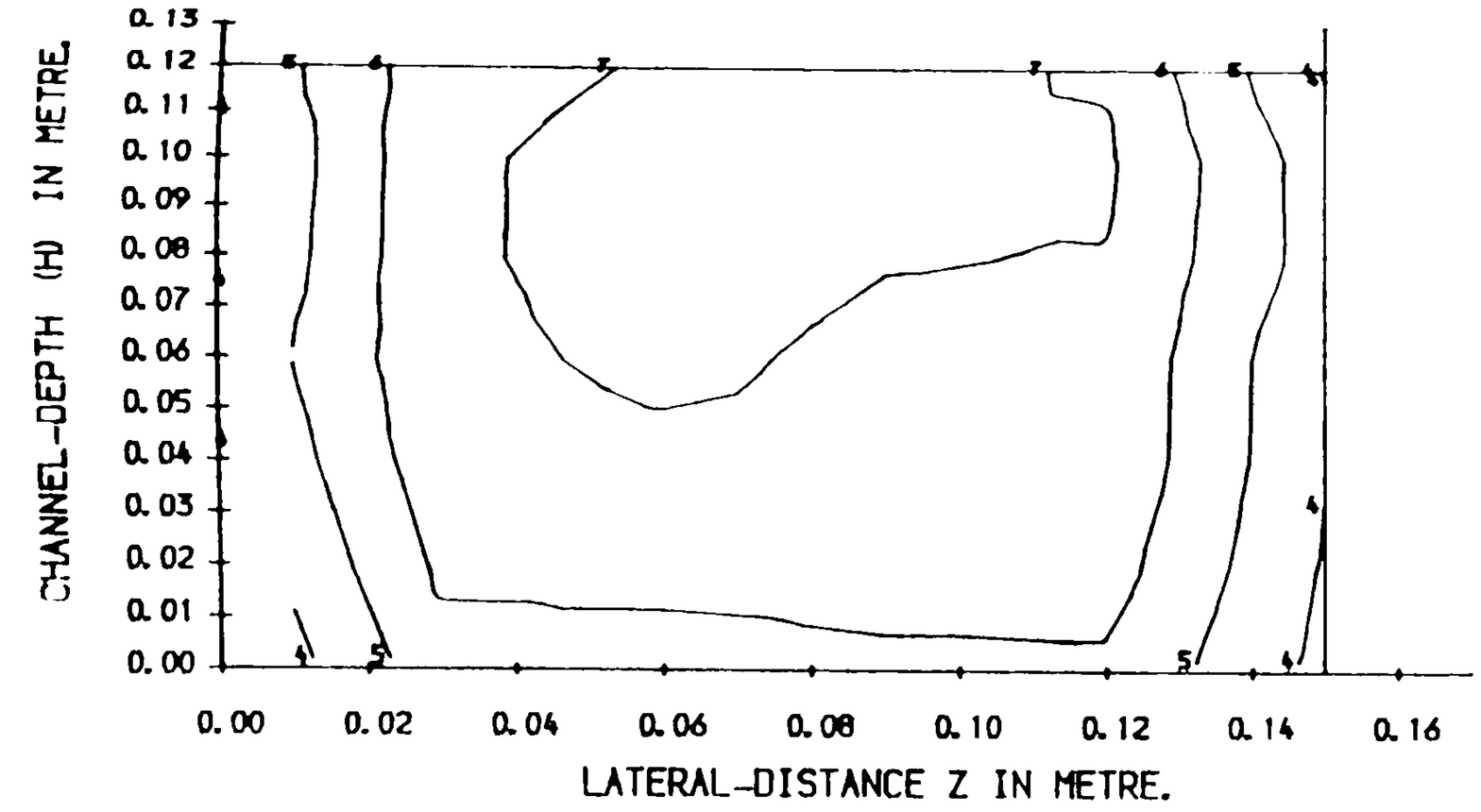

LONGITUDINAL VELOCITY CONTOURS IN CROSS SECTION. 1

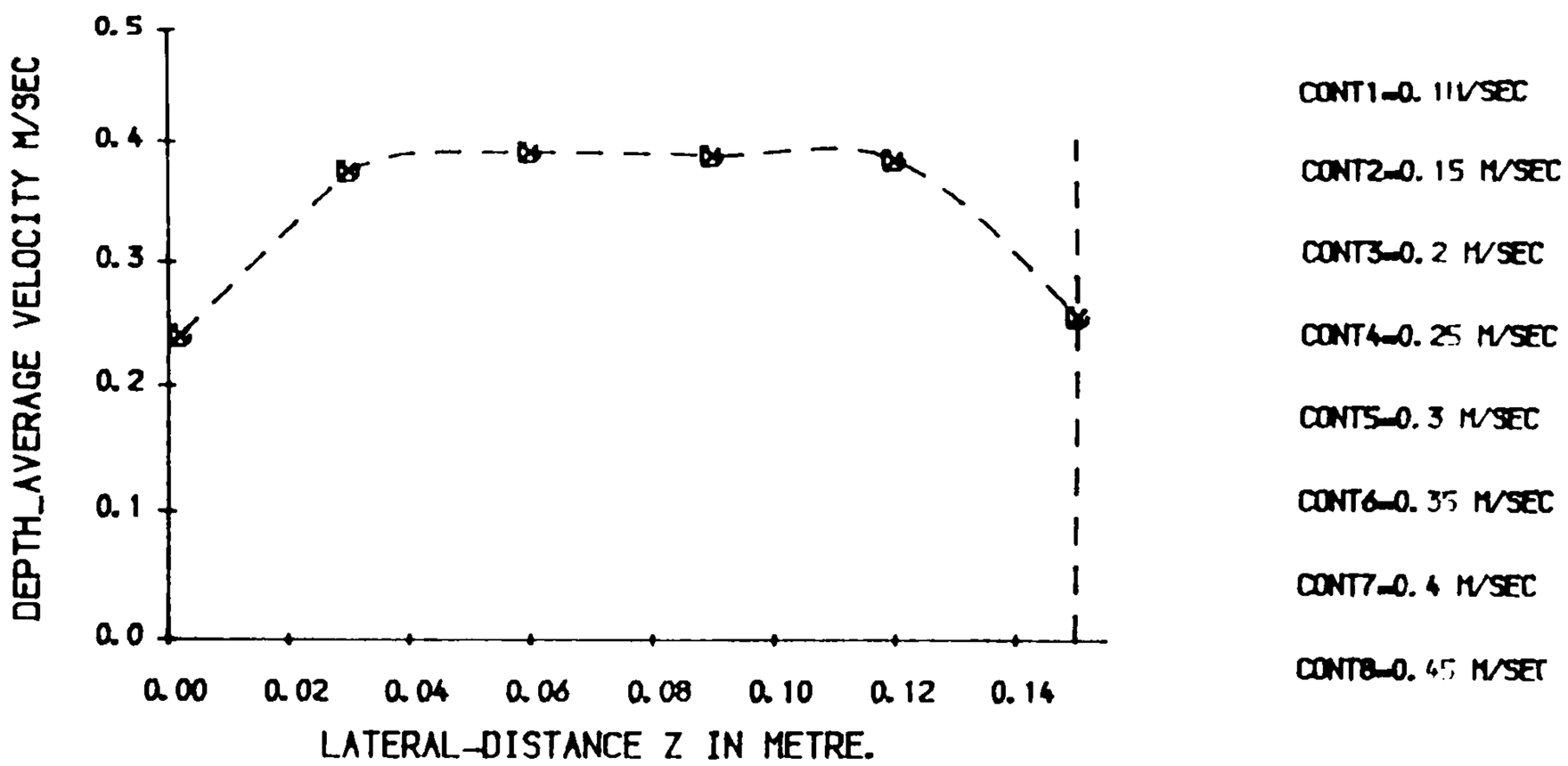

LONGITUDINAL DEPTH_AVERAGE VELOCITY PROFILE IN PLAN.

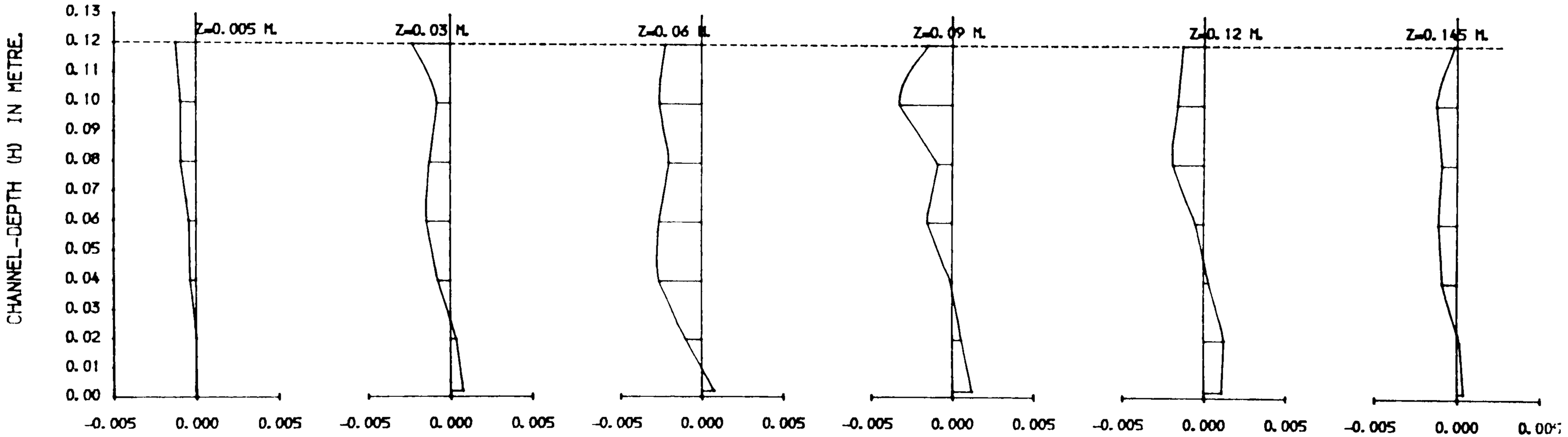

TRANSVERSE VELOCITY COMPONENTS (M/SEC) NORMAL TO SKEWED MAIN CHANNEL.

FIG (5. 43) LONGITUDINAL & TRANSVERSE VELOCITY COMPONENTS IN THE SKEWED CHANNEL ISOLATED FROM THE FLOODPLAIN ZONE.

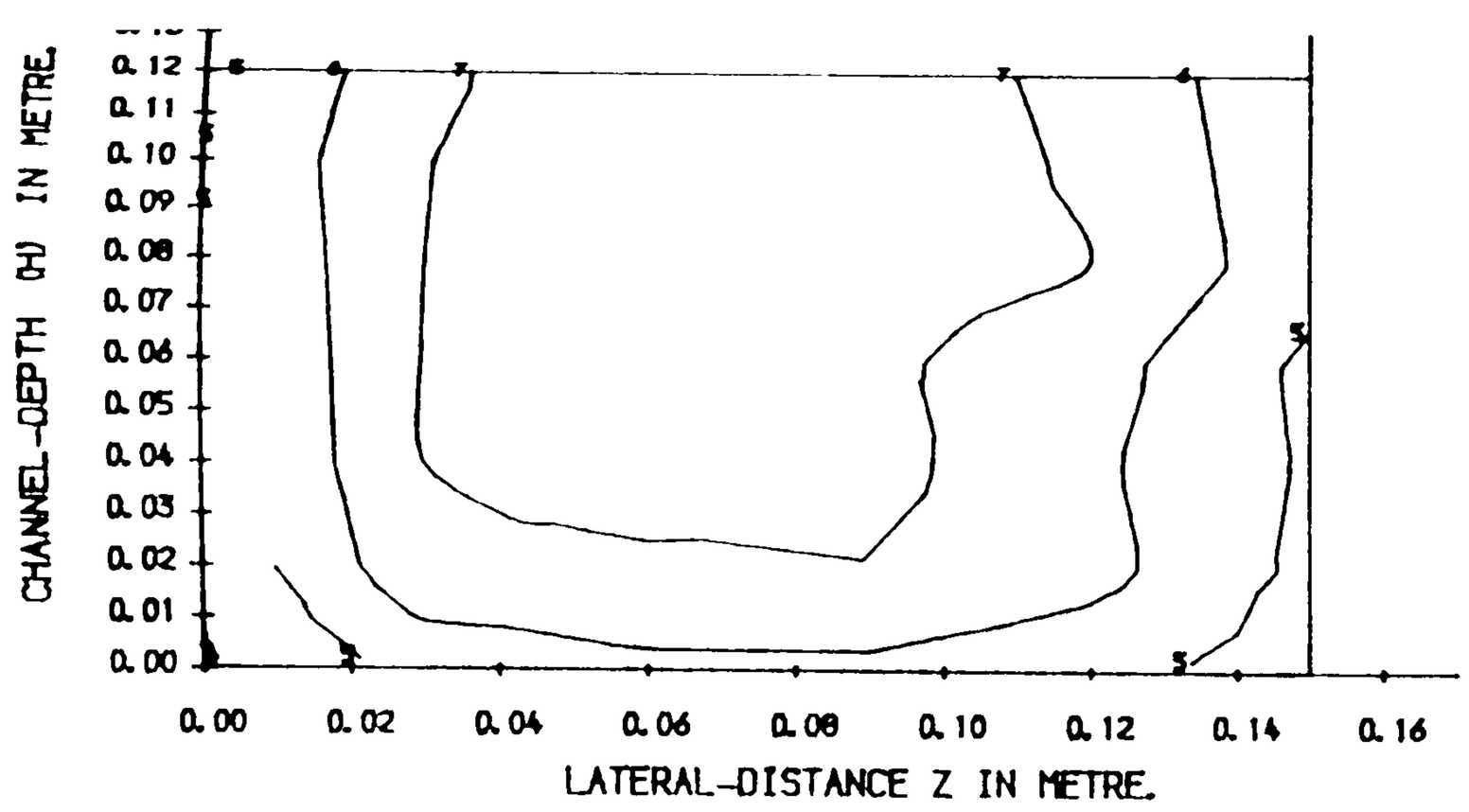

LONGITUDINAL VELOCITY CONTOURS IN CROSS SECTION. 2

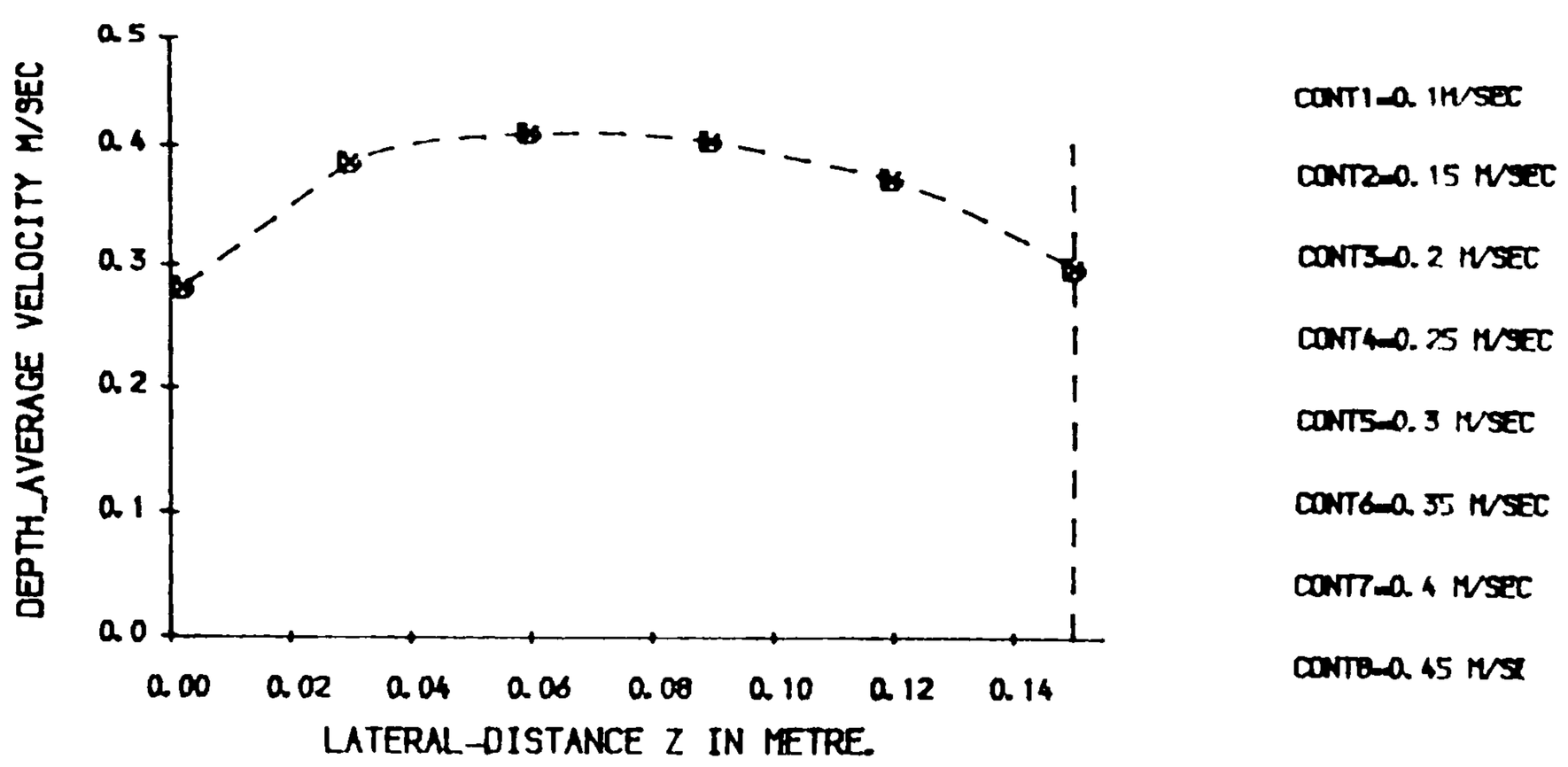

LONGITUDINAL DEPTH_AVERAGE VELOCITY PROFILE IN PLAN.

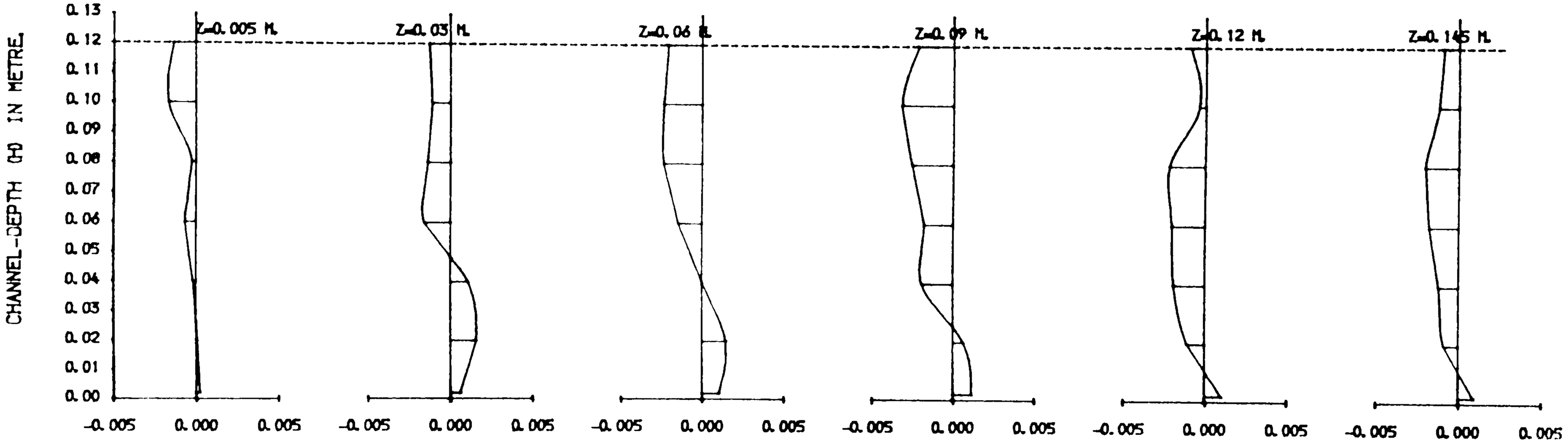

TRANSVERSE VELOCITY COMPONENTS (M/SEC) NORMAL TO SKEWED MAIN CHANNEL.

FIG(5.41) LONGITUDINAL & TRANSVERSE VELOCITY COMPONENTS IN THE SKEWED CHANNEL ISOLATED FROM THE FLOODPLAIN ZONE.

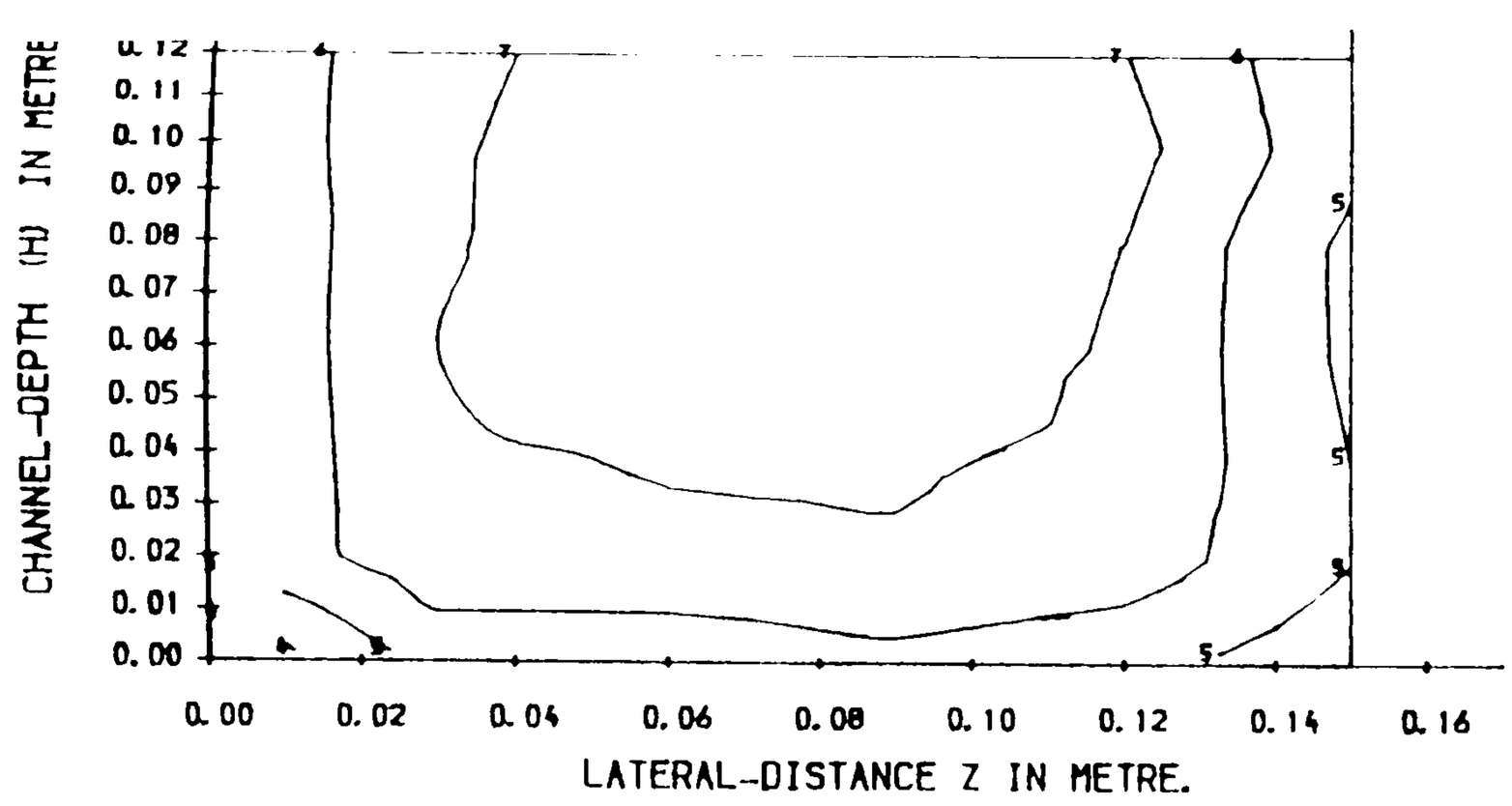

LONGITUDINAL VELOCITY CONTOURS IN CROSS SECTION. 3

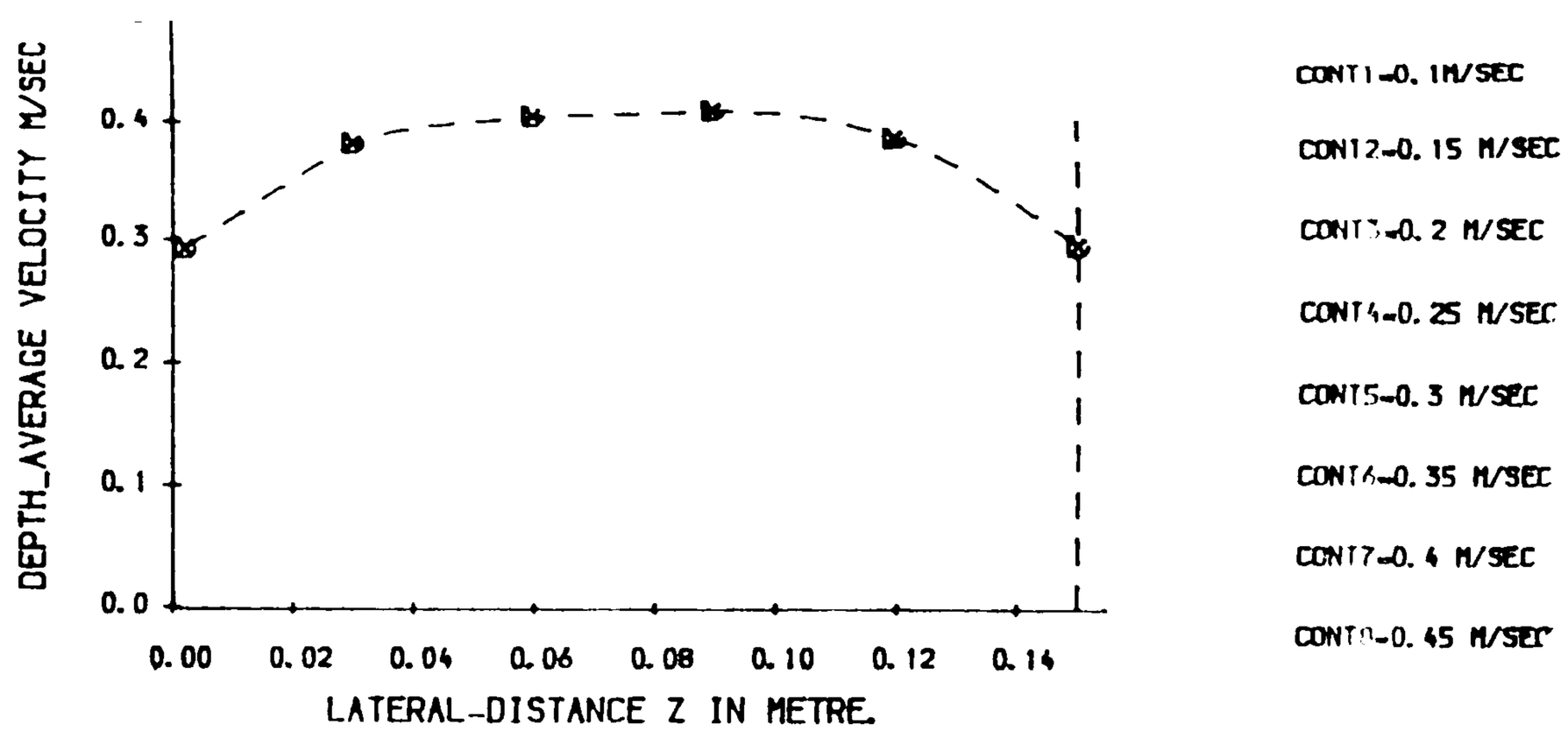

LONGITUDINAL DEPTH_AVERAGE VELOCITY PROFILE IN PLAN.

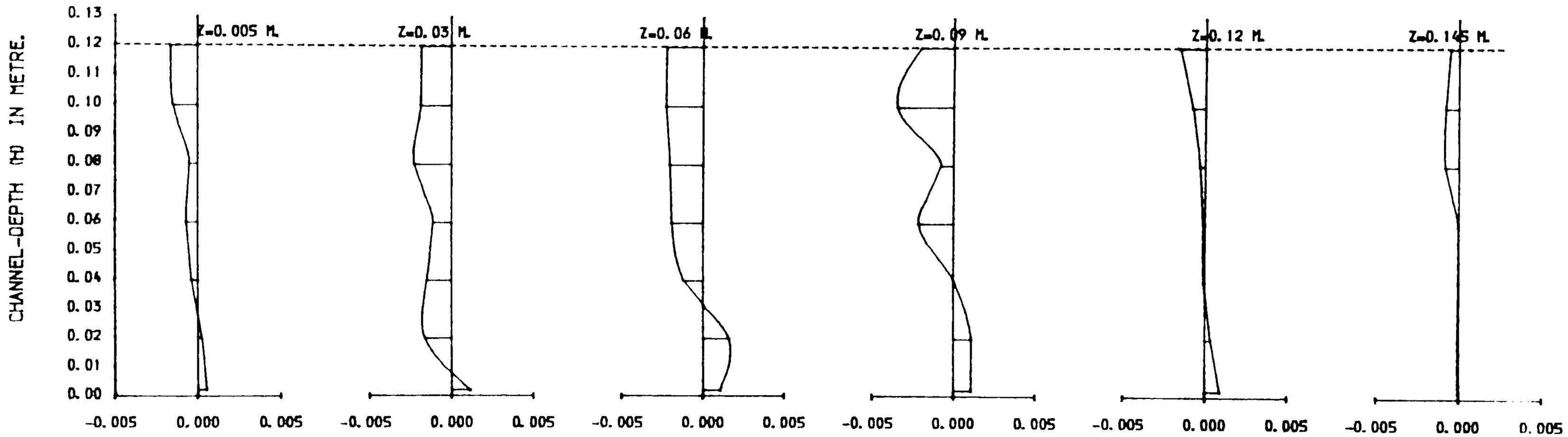

TRANSVERSE VELOCITY COMPONENTS (M/SEC) NORMAL TO SKEWED MAIN CHANNEL.

FIG (5.45) LONGITUDINAL & TRANSVERSE VELOCITY COMPONENTS IN THE SKEWED CHANNEL ISOLATED FROM THE FLOODPLAIN ZONE.

CHAPTER 6

EXPERIMENTAL INVESTIGATION OF FLOW OVER A SLOT IN THE CHANNEL BED

6.1 INTRODUCTION

6.2 CALIBRATION OF THE ARMFIELD FLUME WITH CHANNEL BED OF CONCRETE BLOCKS

6.3 THE SERIES F EXPERIMENTAL RESULTS

6.3.1 Introduction

6.3.2 Water Surface Profile Measurements

6.3.3 The Energy Line Profile

6.3.4 Approximate Analysis of Expansion Loss Coefficients

6.3.5 Approximate Analysis of Contraction Loss Coefficients

6.3.6 Total Energy Losses at a Slot in the Channel Bed.

6.4 VELOCITY PROFILES IN THE SLOT REGION

6.4.1 The Experimental Results

6.4.2 A Universal Velocity Profile

6.5 CONCLUSIONS

CHAPTER 6

EXPERIMENTAL INVESTIGATION OF FLOW OVER A SLOT IN THE CHANNEL BED

6.1 INTRODUCTION

Chapter 6 reports the results of a separation series of experiments carried out in a separate flume (Armfield S−5). These are SERIES F experiments as described in Chapter 3, Section 5, and refer to the flow characteristics along a straight perspex flume with a slot of varying widths cut in the base of the flume.

This is a simplification and idealisation of flood plain flow passing over the skewed main channel beneath, as sketched below.

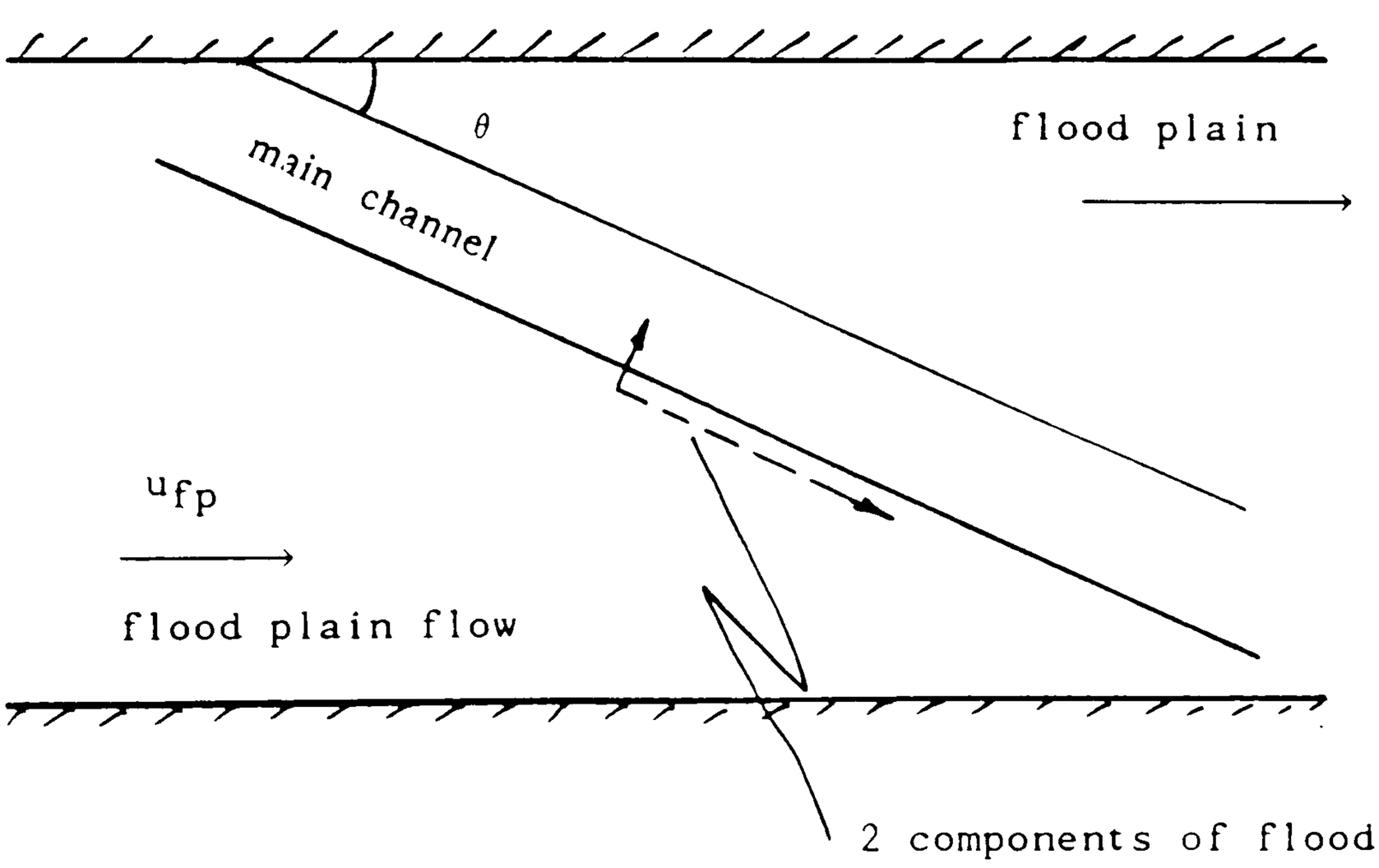

The flood plain flow can be separated into two components as it approaches the main channel. One component is longitudinal with the main channel direction and the other component can be considered to pass− over the main

channel at right angles. This component ($u_{fp} \sin\theta$) will thus experience a sudden expansion following by a sudden contraction and may also be responsible for driving a circulation in the main channel, as discussed in Chapter 5.

The Series F tests attempt to simulate certain aspects of this cross–over component of flow. There is one important difference between the Series F slot tests and cross–over flow. It stems from the fact that cross over flow may be partly drawn down into the main channel flow and hence be partly transported off in the main channel direction. This does not occur in the slot tests with all flood plain flow crossing over directly (with no deviation) to the opposite flood plain. These phenomena are sketched below.

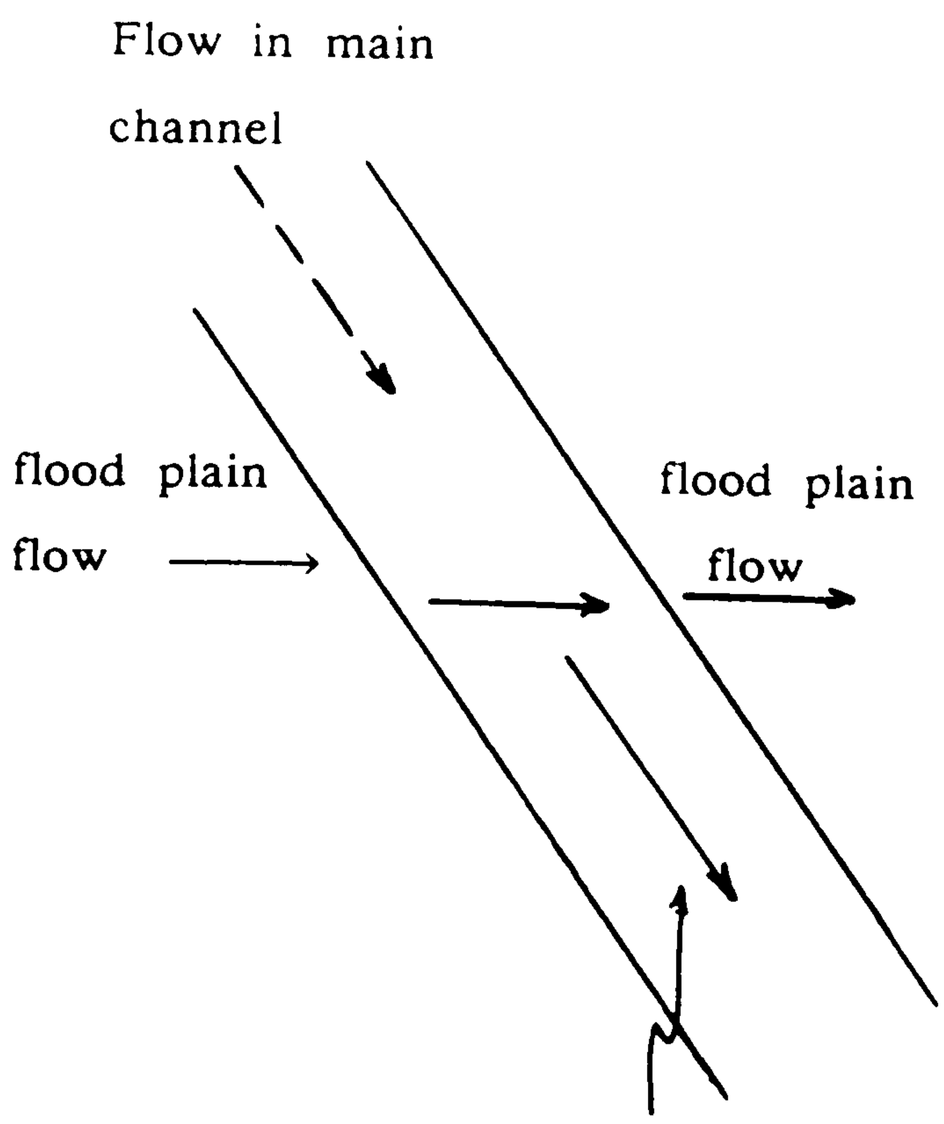

flood plain flow can be drawn into main channel flow

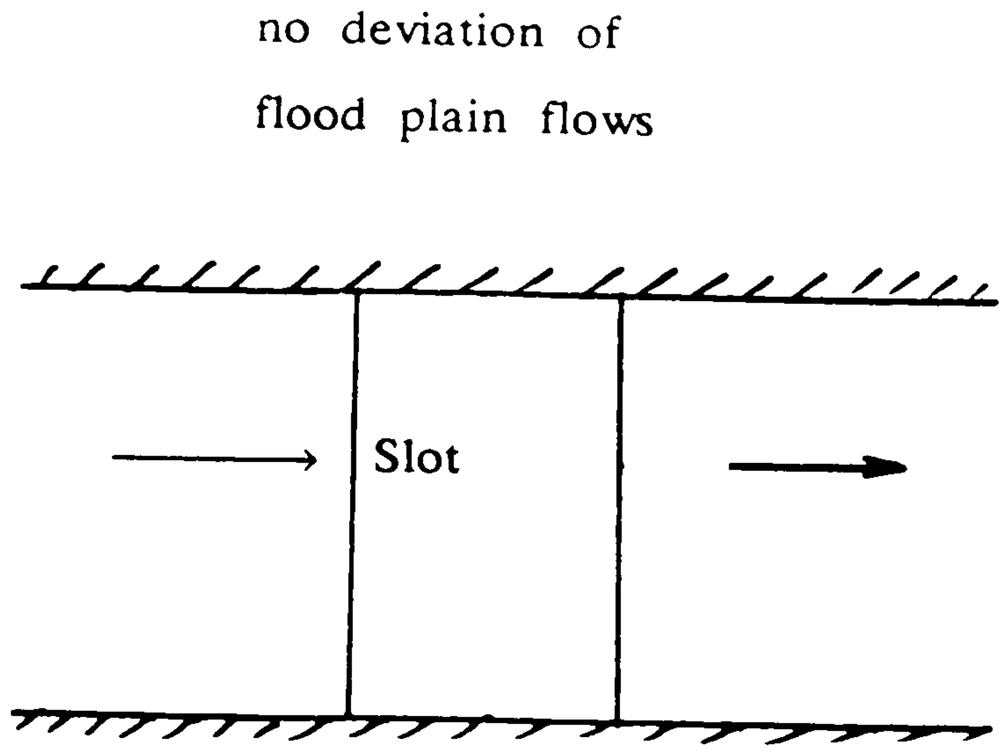

Plan view of Series F slot tests

Despite fundamental differences between the two types of flow, it was agreed that the slot tests might provide some valuable information about cross–over flows in general, which might be combined with results already described in Chapter 4 and 5 to produce a clearer picture of the flow mechanisms involved. The following information was sought from the Series F tests.

(i) Exactly how much energy is lost at the flow expansion region of the slot, and how much is lost at the flow contraction region where the flow re–enters the downstream flood plain. Can this energy loss be related to channel/flood plain flows?

(ii) What is the effect of the slot on the free surface water profile? The flow decelerates in the expansion region and accelerates in the contraction region. Does this result in an increase and subsequent decrease in water surface level, and if so, is it similar to the skewed main channel/flood plain case.

(iii) What is the effect of varying the slot width to bankfull depth ratio? B_S/h_S.

(iv) What is the length of the recirculation zone in the flow expansion region of the slot? How does this translate to the skewed channel/flood plain results?

(v) What are the values of the recirculation velocities in the slot expansion region. Are the values comparable to recirculation velocities in the skewed main channel, for comparable flood plain incoming velocities?

(vi) Is it possible to produce a theoretical relationship for the velocity distribution throughout the slot expansion region?

6.2 STAGE–DISCHARGE AND RESISTANCE TO FLOW FOR THE ARMFIELD FLUME WITH NO SLOT IN THE CHANNEL BED

The Series F slot tests were conducted in an Armfield S–5 flume of length 5m, width 80mm and depth 300mm. The flume was set at a constant slope of 0.001 and the channel bed was lined with concrete blocks which were removed in sequence to provide the slot in the channel bed. The initial set of tests in this section were carried out with no slot in the channel bed, with concrete blocks extending the full length of the flume.

This initial arrangement produced smooth perspex walls to the flume, but a relatively rough concrete base. It was important to obtain the equivalent

roughness of the whole flow cross–section, and also the roughness coefficients for both perspex and concrete parts of the boundary.

First, it was decided to carry out tests to establish the stage–discharge curve for the Armfield flume with concrete blocks on the flume bed. For each test the bed slope remained fixed at 0.001. A discharge was chosen and the tail–gate was altered many times by trial and error to make sure the water surface slope was parallel to bed slope. This was done by measuring the flow depth at different cross sections until uniform flow conditions were reached. The flow depth and discharge were then recorded. The discharge was then varied and new uniform flow conditions set up. This procedure was carried out repeatedly to obtain fifteen results. These results are shown in Fig (6.1). The minimum discharge recorded was 0.1605 L/Sec at 0.017m depth and maximum discharge was 2.5 L/Sec at depth of 0.116m. Manning's equation was used to calculate the equivalent roughness coefficient as follow:

$$Q = \frac{1}{n_e} R^{2/3} S^{1/2} A \qquad (6.1)$$

where Q is the discharge, R is the hydraulic radius, A is the cross section area, S longitudinal slope and n_e Manning's coefficient value.

The results for the equivalent Manning's values are shown in Fig (6.2) showing an almost linear decrease in Manning's n value for the flume as the flow depth increases. This is a reflection of the decreasing influence of the rough concrete block base with increasing depth. It is clear from Fig (6.2) that the Manning's 'n' value for the concrete base is likely to be around 0.014 whilst for the perspex walls, the value will lie in the region of 0.01 to 0.011.

The Darcy–Weisbach equation was also used to determine the equivalent friction factor,

$$\lambda_e = \frac{8gRS}{V^2} \qquad (6.2)$$

where λ_e is the equivalent friction factor for the composite cross–section.

It was decided to subdivide the equivalent friction factor into its two components using the equation

$$\lambda_e P = \lambda_b B + 2 \lambda_w Y_c \qquad (6.3)$$

where

λ_e is the equivalent friction factor value.

λ_b is the friction factor values for the bed material.

λ_w is the friction factor values for the walls material.

P is the wetted parameter in (m).

B is the width of Armfield flume and was 0.08m.

Y_c is the water depth in (m).

The solution of Equation (6.3) was made possible by a knowledge of the friction factor λ_w for the smooth perspex walls. This had been investigated in a previous experiment and found to have the form,

$$\frac{1}{\surd \lambda_w} = 2.0 \text{ Log } (R_e \surd \lambda_w) - 1.5 \qquad (6.4)$$

where R_e is Reynold's Number of the flow ($4VR/\nu$) and Equation (6.4) is a quasi– smooth friction law.

The next step was to solve Equation (6.3) for values of friction factor for the channel bed only (λ_b). The values of λ_b were then used to obtain the value of k_s, the equivalent sand grain roughness, for the concrete bed material. The average value of k_s was determined from the Colebrook– White Equation,

$$\frac{1}{\surd \lambda} = -2.0 \text{ Log } \left(\frac{k_s}{14.8\ R} + \frac{2.51}{R_e \surd \lambda} \right) \qquad (6.5)$$

This yielded a mean value of k_s for the concrete blocks of 2.75mm.

The final result is shown in Fig (6.3) which is a plot of the experimental

equivalent friction factor λ_b plotted against the Reynolds Number R_e. This is compared with the theoretical value composed of λ_b calculated from Equation(6.5) with k_s= 2.75mm, as well as λ_w calculated from Equation (6.4).

6.3 THE SERIES F EXPERIMENTAL RESULTS

6.3.1 Introduction

Having calibrated the 5m long Armfield flume it was decided to commence experimental work with a slot in the channel bed. This was achieved by removing a concrete block to give a step of height h_s= 53.0mm set up 2.0m downstream from the flume entrance. Extensive studies investigated four width to depth ratios of the slot, to test the flow mechanism in a range of sudden expansion and contraction flows.

The first set of experiments examine the slot width/depth ratio B_s/h_s= 20, the second set of data was B_s/h_s= 10, the third set of data was B_s/h_s= 5, and the final set of experiment was a ratio of B_s/h_s= 2 (where B_s was the width of slot and h_s the height of the step).
This covers the ratio of aspect ratios normally found in natural rivers and also in scale models.

The flow depths (and relative flow depths) associated with each aspect ratio are shown in Table (6.1) to Table (6.4). To obtain reasonably accurate results it was decided not to use flood plain flow depths lower than 20mm. This produced minimum relative depths of the order of 0.3 and maximum relative depths of the order of 0.5. This covers only the upper range of two–stage channel behaviour, but never the less it was felt that the limited range of relative depths would still produce clear pointers for cross over flow mechanisms. The values of Y_c noted are the maximum values of the flow within the deeper slot section.

Time did not permit a detailed investigation of very rough flood plain cross–over mechanisms similar to Series D and E work, with vertical roughening bars.

Nor did time permit a detailed investigation of relative depths less than 0.28. This would have involved construction of much deeper concrete blocks to give a step height of, say, 150mm, in which case the minimum relative flow depth might have been 20/170 ≐ 0.12. A definition sketch of all the parameters used in this chapter is given in Fig (6.4).

6.3.2 Water Surface Profile Measurements

The water surface profile was measured first by adjusting the tail–gate to establish uniform flow. Manual pointer gauges along the flume centreline were used to measure the water depths along the longitudinal direction of the flume. These readings were based on a constant datum. The results of the water depth are shown as the dotted line in Fig (6.5) to Fig (6.24).

The accurate water surface profile was measured at seventeen cross sections along the flume, in the first set of experiments ($B_s/h_s = 20$). These measurements are shown in Fig (6.5) to Fig (6.10). More than twenty cross sections were used to measure the water level for the second set of experiments ($B_s/h_s = 10$), and are shown clearly in Fig (6.11) to Fig (6.15). Figs (6.16) to (6.20) show the water surface profile for the third set of the experiments ($B_s/h_s = 5$). The water surface was measured in the final set of the experiments $B_s/h_s = 2$ and is shown clearly in Fig (6.21) to Fig (6.24).

It is clear from these figures that when the flow enters the slot region, the water surface profile rises in the downstream direction giving an adverse water surface gradient. The maximum water level is reached normally just at the downstream end of the slot at the point of the flow entry back onto the flood plain. We can define the rise in water level Δh by the expression

$$\Delta h = Yc - (Y_f + h_s) \qquad (6.6)$$

where

Y_c is the maximum water depth in the slot region

Y_f is the water depth upstream of the slot

h_s is the step height

Thus Δh is the water level rise relative to a horizontal fixed datum. The results show for example that the Y_c value was 76.9 mm in table (6.1) and the Y_f value was 22.3mm for the same set, and if the slot depth was 53.0mm, then the maximum value of Δh was 1.6mm. This gives an adverse surface slope of approximately 0.016. The maximum value of Δh was found from Table (6.2), Y_c= 76.8mm, Y_f= 22.5mm, and the value of Δh was 1.3mm. This gives a water surface slope of 0.025. The maximum values of Δh for set three and four are found to be 1.0mm and 0.7mm respectively, giving adverse water surface slopes of the order of 0.004 and 0.0067 respectively. This mean that although the absolute value of Δh reduces as the slot width B_s/h_s reduces, the water surface gradient increases substantially.

The other major point from Figs (6.5) to (6.24) is that for each value of B_s/h_s the values of Δh, (the water level increase across the slot) decreases as the value of relative depth increases.

A clearer picture of rise in water level can be obtained from the application of the force– momentum as well as the continuity equation for the simplified case of a horizontal channel or at least a channel where body weight of the fluid is cancelled by bed friction. This is sketched below.

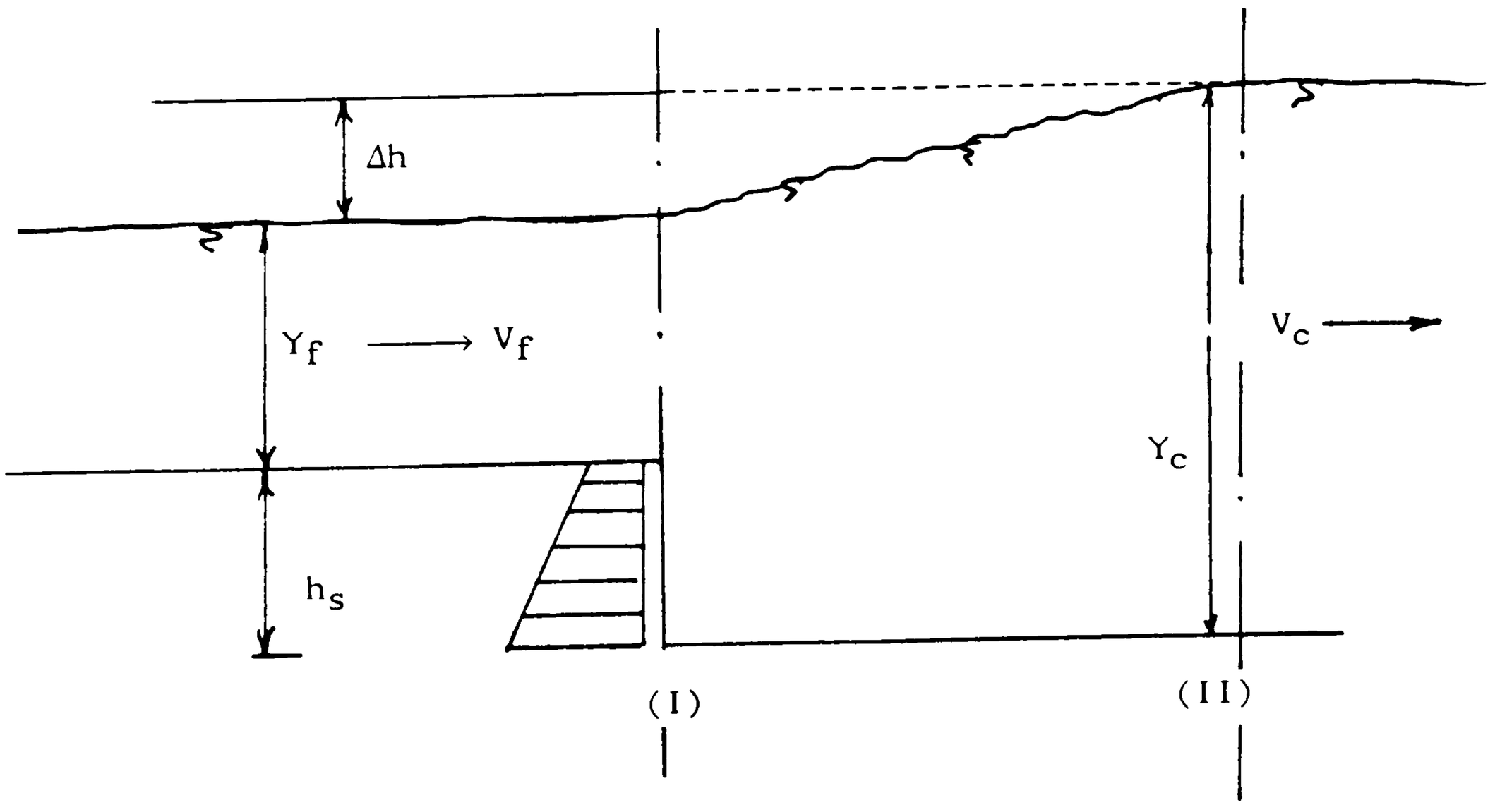

Application of the force– momentum equation between the start and end of the expansion region, gives, per unit width,

$$0.5\rho g Y_c^2 - 0.5\rho g(Y_f + h_s)^2 = \rho q(\beta_1 V_f - \beta_2 V_c) \qquad (6.7)$$

where

β_1 is the momentum correction factor at section 1

β_2 is the momentum correction factor at section 2

$$\beta = \int_0^y v^2 \, dy \; / \; V^2 \, Y \qquad (6.8)$$

The continuity equation is simply stated as

$$V_f \, Y_f = V_c \, Y_c \qquad (6.9)$$

Referring to the sketch above where $Y_c = Y_f + h_s + \Delta h$ we obtain

$$0.5\rho g[(Y_f+h_s)^2 + 2(Y_f+h_s)\Delta h + \Delta h^2] - 0.5\rho g(Y_f+h_s)^2 = \rho g V_f(\beta_1 - \beta_2 \, V_c/V_f) \qquad (6.10)$$

Then dividing by $\rho g Y_f^2$ and substituting $q = V_f Y_f$ we obtain

$$\left(\frac{\Delta h}{Y_f}\right)^2 + 2\left(\frac{\Delta h}{Y_f}\right)\left(1 + \frac{h_s}{Y_f}\right) = 2F_r^2 \left(\beta_1 - \beta_2 \frac{V_c}{V_f}\right) \qquad (6.11)$$

Substituting from the continuity Equation (6.9) and assuming as an approximation that $\beta_1 = \beta_2 =$ unity, then

$$\left(\frac{\Delta h}{Y_f}\right)^2 + 2\left(\frac{\Delta h}{Y_f}\right)\left(1 + \frac{h_s}{Y_f}\right) = 2F_r^2 \left[\frac{h_s/Y_f + \Delta h/Y_f}{1 + h_s/Y_f + \Delta h/Y_f}\right]$$

---------- (6.12)

giving a general equation predicting the rise in water level due to a sudden expansion or slot in the channel bed. This is plotted in Fig (6.25) for a range of subcritical Froude Numbers on the flood plain and for a range of values of Y_f/h_s from 0.1 to 1.0. Experimental values of the water level rise $\Delta h/h_s$ are also plotted on Fig (6.25) showing reasonable agreement with the theoretical estimates. It is clear from **Fig (6.25)** that Equation 6.12 gives reasonable agreement with experimental results, as the values of Y_f/h_s tested varied between approximately 0.4 and 1.0, and this corresponds to the theoretical curves between 0.2 and 1.0.

6.3.3 The Energy Line Profile

The computed energy line profile is also shown in Figs (6.5) to (6.24) for the range of aspect ratios of the slot and for the range of relative depths already noted in Table (6.1) to (6.4). The energy line was computed from the expression

$$E.L = W.L + \alpha V^2/2g \qquad (6.13)$$

where

E.L is the energy level

W.L is the measured water level

V is the average velocity for any cross section

α is the energy coefficient at each cross section

The energy coefficient calculation was made possible by the measurement of velocity by miniature propellor meter as discussed in Chapter 3, Section 3.5. The point velocity was measured in detail at each cross–section along the flume length at various depths into the flow and at various locations across the channel width. A computation of the energy coefficient α is then possible from,

$$\alpha = \frac{\int v^3 \, dA}{V^3 \, A} = \frac{\sum v^3 \, \Delta A}{V^3 \, A} \qquad (6.14)$$

where

v is the point velocity in m/sec.

dA is the sub– divided area that v acts over

A is the total area of cross section.

This coefficient is applied to the term $V^2/2g$ and added to the measured water levels, already discussed in section 6.3.2.

The results of the energy line profiles reveal the following points from Figures 6.5 to 6.24.

(i) The slope of the energy line is not uniform as the flow passes the slot in the channel bed. A sudden loss of energy is experienced in the sudden expansion region. This is followed by a levelling–off of the energy line and followed again by a sudden drop in the energy line at the contraction region. This is sketched below for a slot of large aspect ratio.

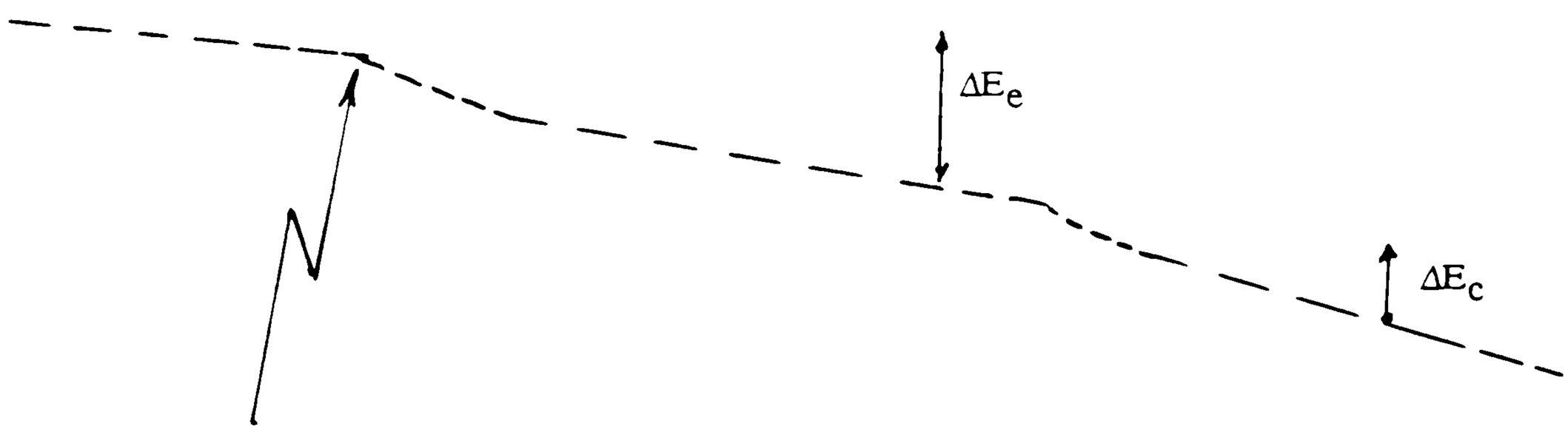

slope of energy line passing
a slot in the channel bed

(ii) The marked changed in the energy line slope sketched above allowed a sub– division of the total slot energy loss into expansion losses ΔE_e and contraction ΔE_c.

(iii) An analysis of the results showed that both the expansion and contraction losses increased as the aspect ratio (B_s/h_s) of the slot increased. This will be discussed in more detail in later sections. It is clear however that wide aspect ratio slots allow the full jet expansion to occur which tends to maximise the energy losses. Velocity measurements (section 6.4) show that the expansion region is of the order of 5 ⟶ 7 x step height (ie. 5 ⟶ $7h_s$).

(iv) Figures 6.5 to 6.24 also reveal that the magnitude of both the expansion and the contraction losses decreases as the relative flow depth (Y_f/Y_c) increases. This seems logical in the sense that the ultimate case is no step or a relative depth of unity, which should give zero expansion and contraction loss.

(v) Later analysis reveals that the expansion energy losses vary almost linearly with distance from the start of the expansion. When the distance reaches about $7h_s$, the expansion losses thereafter increase only very slightly. This shows that the expansion losses coincide with eddy formation in the expanding shear layer region.

6.3.4 Approximate Analysis of Expansion Energy Loss Coefficient

In the sudden expansion region a turbulent shear layer is set up, forming a recirculation region in the manner of a bounded expanding jet. Energy is lost due to the formation of vortices and eddies and turbulence which are produced in the expansion region and dissipated in this region as well as further downstream.

The most approximate energy balance is given in the sketch below for a horizontal channel with zero bed friction.

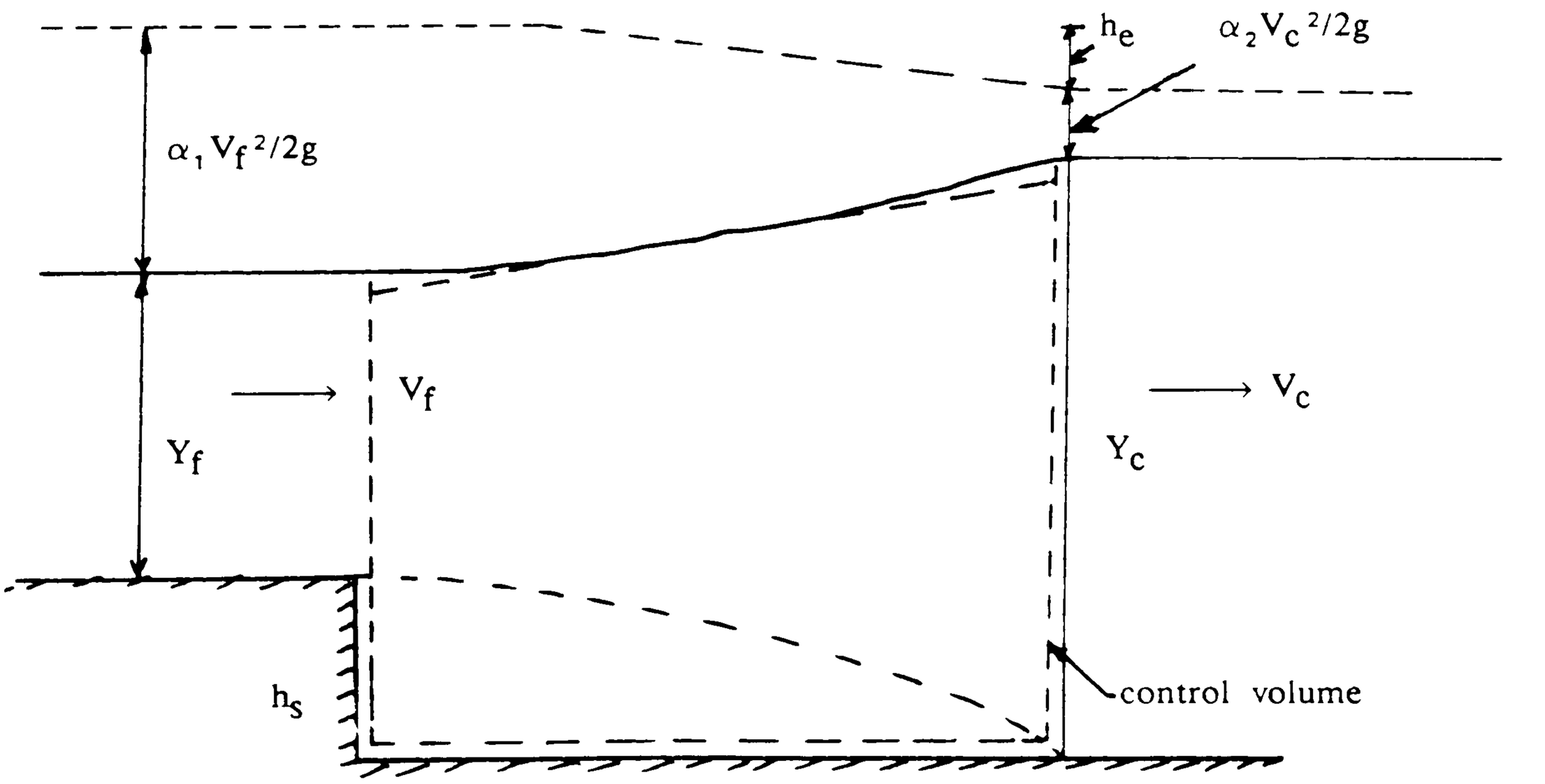

For zero bed friction and zero body weight

$$h_s + Y_f + \alpha_1 V_f^2/2g = Y_c + \alpha_2 V_c^2/2g + h_e \qquad (6.15)$$

where h_e is the total energy loss in the expansion region

Thus

$$h_e = \alpha_1 V_f^2/2g - \alpha_2 V_c^2/2g - [\, Y_c - (Y_f + h_s)] \qquad (6.16)$$

From the force momentum equation applied over the control volume shown as the dashed volume above

$$0.5\ \rho g Y_c^2 - 0.5\ \rho g (Y_f + h_s)^2 = \rho q (V_f - V_c) \qquad (6.17)$$

giving

$$[Y_c - (Y_f + h_s)][Y_c + (Y_f + h_s)] = 2q/g\ (V_f - V_c) \qquad (6.18)$$

Assuming $Y_c + (Y_f + h_s) \triangleq 2Y_c$, and $q = V_c Y_c$

$$[Y_c - (Y_f + h_s)] = 2V_c/2g\ (V_f - V_c) \qquad (6.19)$$

which when substituted back into the energy equation with

$\alpha_1 = \alpha_2 =$ unity, becomes,

$$h_e = V_f^2/2g - V_c^2/2g - 2V_c V_f/2g + 2V_c^2/2g$$

$$h_e = (V_f - V_c)^2/2g \qquad (6.20)$$

$$h_e = V_f^2/2g\ (1 - V_c/V_f)^2 \qquad (6.21)$$

or

$$h_e = (1 - Y_f/Y_c)^2 V_f^2/2g \qquad (6.22)$$

where

h_e is the total expansion loss over the control volume

Y_f is the flow depth upstream of the slot (or flood plain depth)

Y_c is the maximum flow depth in the slot

V_c is the mean upstream flow velocity.

Equation (6.22) can be rewritten

$$h_e = k_e V_f^2/2g \qquad (6.23)$$

where k_e is the expansion loss coefficient. Thus the theoretical expansion loss coefficient is given by

$$k_e = (1 - Y_f/Y_c)^2 \qquad (6.24)$$

As already mentioned the experimental values of the expansion loss coefficient were obtained from the experimental expansion losses. This was done for a range of relative depths and a range of slot width to depth ratios B_s/h_s.

A plot of the experimental expansion loss coefficients against the theoretical loss coefficient is shown in Fig (6.26). A perfect correlation between the two is shown by the solid line. It is clear from Fig (6.26) that the loss coefficient varies considerably with the slot width to depth ratio. A slot aspect ratio of 20 gives losses well in excess of the theoretical value, whereas a slot width to depth ratio of 2 gives much lower losses than the theoretical value. This seems particularly the case at larger relative flow depths, of the order of $Y_f/Y_c \geq 0.5$, and $(1 - Y_f/Y_c)^2 \approx 0.25$. The reason for this phenomena is not difficult to see. At large slot width/depth ratios the full expansion occurs, plus further turbulent dissipation downstream of the expansion region for a narrow slot width/depth around 2, the expansion region does not have room to develop and hence will only produce a fraction of the turbulence possible.

It is clear that the variation of relative depth also has significant effect on the experimental value of the expansion energy loss coefficient. This is shown

plotted in Fig (6.27) over the range of relative depths tested and for the four values of aspect ratio. Fig (6.27) shows that large relative depths produce low expansion loss coefficients (compared with theoretical) whereas, smaller relative depths produce large energy loss coefficients relative to the theoretical estimate.

The reason for this is not immediately clear, but it may be a Reynolds Number effect or alternatively it may be due to large deviations of the energy correction factor α, away from unity (which was assumed) as the relative depth decreases.

6.3.5 Approximate Analysis of Contraction Energy Loss Coefficients.

The loss of energy in a sudden contraction of streamlines is usually considered to exist only in the streamline expansion following the contraction. This is sketched below in the case of flow re-entering a flood plain.

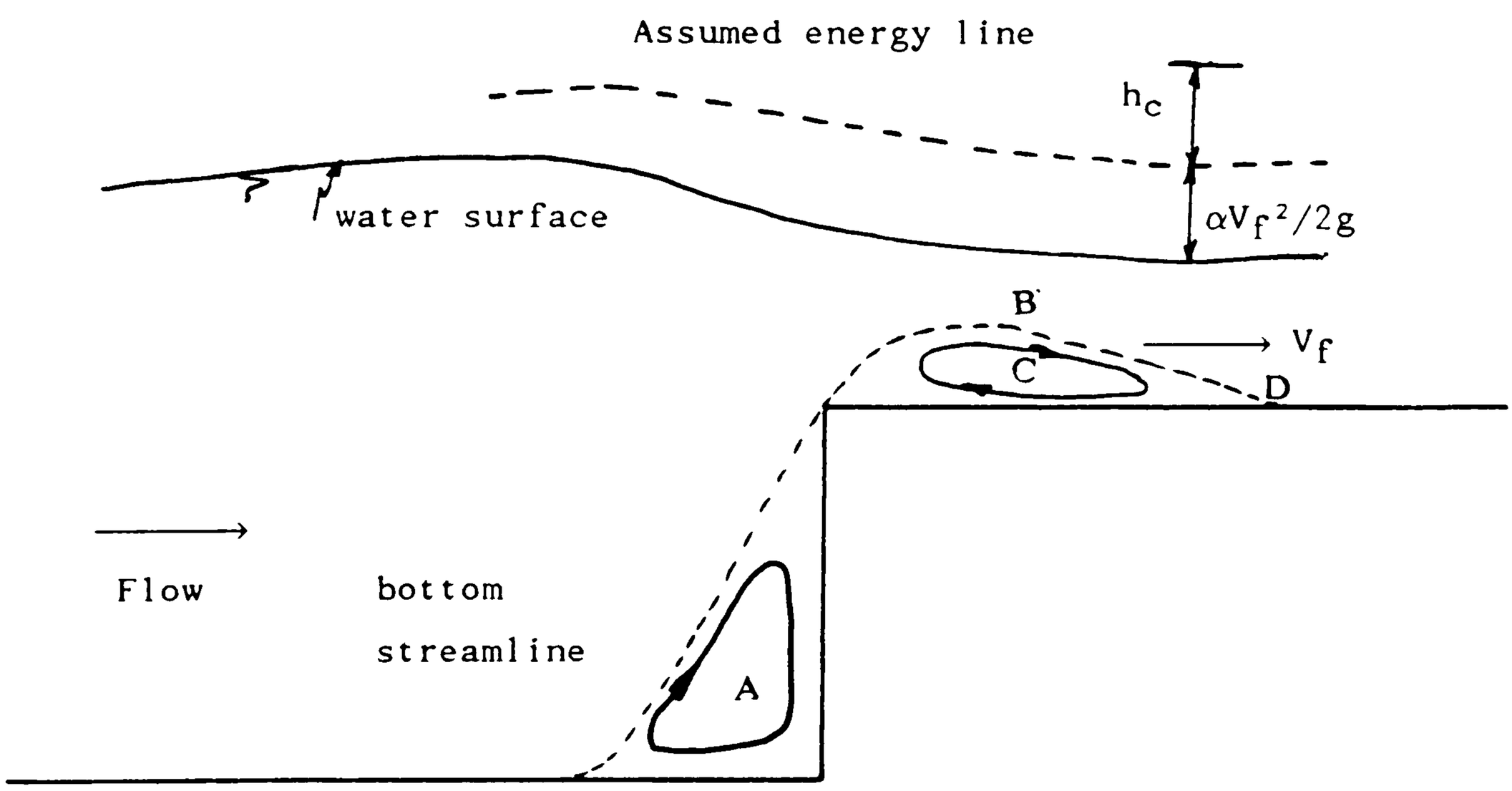

The bottom streamline is assumed to separate some distance upstream of the step causing a separation bubble A, which is a recirculation zone assumed to have

zero energy loss. This is because contracting flows have much less energy loss than expanding flows. On entering the flood plain the bottom streamline forms a further recirculation zone C, and a vena contracta at B. Up until point B, all the energy losses are assumed to be small.

After the vena contracta at B, the flow expands producing significant energy loss h_c along the shear layer BD, as shown in the sketch above.

Thus the contraction loss is really an expansion loss, and can be given by the same type of relationship at Equation (6.20). The expansion loss can be given by

$$h_c = (1 - Y_B/Y_f)^2 \, V_B^2/2g \qquad (6.25)$$

$$h_c = (1 - Y_B/Y_f)^2 \, V_f^2/2g \, (Y_f/Y_B)^2 \qquad (6.26)$$

as $Y_f \, V_f = Y_B \, V_B$

giving

$$h_c = (Y_f/Y_B - 1)^2 \, V_f^2/2g \qquad (6.27)$$

or

$$h_c = C_L \, V_f^2/2g \qquad (6.28)$$

where

h_c is the total energy loss in the contraction.

C_L is the contraction loss coefficient.

V_f is the mean velocity downstream.

From Equation (6.27) the value of Y_f/Y_B is then simply dependent on the

value of relative depths Y_f/Y_c as well as the coefficient of contraction C_L. Yen and Yen (1983) published a Table of the contraction loss coefficient C_L for relative depths (Y_f/Y_c). This is shown on Figure (6.28), representing theoretical values of C_L.

The experimental values of the contraction loss (h_c) were determined from the slope of the energy line for the range of relative depths tested, and the range of slot widths to depths B_s/h_s from 2 $\longrightarrow$ 20. The comparison between the theoretical and experimental contraction loss coefficients is shown in Fig (6.29). A perfect correlation is indicated by the solid line. Fig (6.29) clearly reveals that the slot aspect ratio is also an important parameter in the contraction loss coefficient C_L. Small slot widths B_s/h_s of 2, for instance, produce contraction loss coefficients much less than the theoretical value, whereas a slot width of $B_s/h_s = 20$, produces a loss coefficient in excess of the theoretical value.

The reason for this is connected with the fact that narrow slots do not allow proper expansion to proceed within the slot which means that the bottom streamline is not coming from the base of the slot but from a point much further up in the flow, as sketched below. In effect, narrowing the slot width has the same effect as increasing the relative depth Y_f/Y_c.

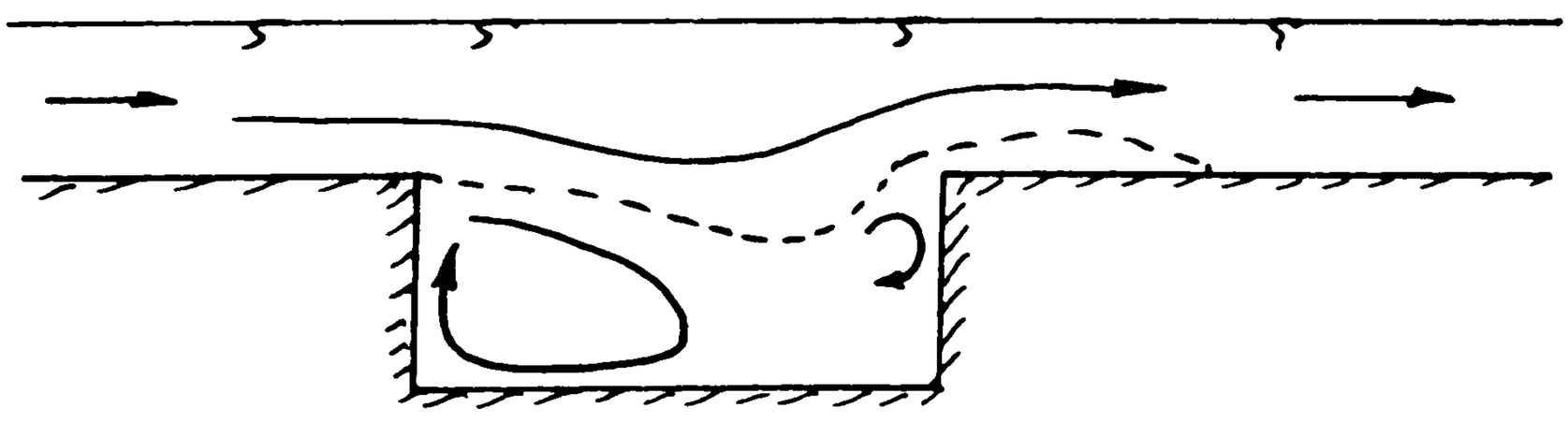

Small B_s/h_s ratio

6.3.6 Combined Expansion and Contraction Losses

One of the main sources of interest in the Series F slot tests is the total energy due to flow passing over the slot. It has been pointed out that this is not directly comparable to flood plain flow passing over a skewed main channel below, but it does have many similarities.

The total loss coefficient is a cumulative value from the expansion and contraction losses added together. The theoretical value for instance would have the form,

$$h_T = [(1 - Y_f/Y_c)^2 + C_L] V_f^2/2g \qquad (6.29)$$

although it has become clear in sections 6.3.4 and 6.3.5 that such a theoretical estimate is not particularly accurate.

The experimental expansion, contraction and total loss coefficients have been determined from the experimental data and are shown in Table (6.5). Table 6.5 contains all the experimental data for the four values of slot width to depth ratio $B_s/h_s = 2 \longrightarrow 20$ as well as the data for all values of relative depth tested.

The experimental results are also shown plotted in Fig (6.30) with the experimental total energy loss coefficient plotted against the relative depth of flow, for a range of slot width to depth ratios.
Fig (6.30) shows that the total head loss coefficient decreases with increasing relative flow depth. The total loss coefficient increases with increasing slot width/depth ratio.

It was decided to carry out a further analysis at least to incorporate the effect of B_s/h_s in Equation (6.29) above. This will be presented in Chapter 7.

6.4 VELOCITY PROFILES IN THE SLOT REGION.

6.4.1 The Experimental Results

Point velocities have been measured in detail throughout the slot region, the purpose being mainly to compare recirculations in a slot with those in a skewed main channel with flood plain flow passing over the top.

The velocity was measured using a miniature propellor meter as described in Chapter 3. Measurements were made at approximately 20mm intervals with depth and 20mm intervals across the channel width. The velocity measurements were averaged across the channel width and presented in Figures 6.31 to 6.50.

Figures (6.31) to (6.36) give the results for the widest slot of $B_s/h_s = 20$, where $h_s = 53.0$mm. The results are given at eight vertical sections along the slot with the distances from the start of the slot given at the top of each figure. These distances are 0.03m, 0.06m, 0.15m, 0.3m, 0.7m , 0.88m, 0.9m and 0.98m from the start of the slot.

Figs (6.37) to (6.41) give the results for $B_s/h_s = 10$ for a range of relative depths. In this case the width–averaged velocities are at 0.02m, 0.05m, 0.13m, 0.26m, 0.35m, 0.42m and 0.48m from the start of the slot.

Figs (6.42) to (6.46) show the results for slot width $B_s/h_s = 5$, this time with width–averaged velocities at 0.02m, 0.05m, 0.08, 0.14m, 0.22m and 0.24m from the start of the slot.

Figs (6.47) to (6.50) give the results of the shortest slot $B_s/h_s = 2$, for four relative flow depths, and at distances 0.02m, 0.04m, 0.08m and 0.1m from the start of the slot.

It should be noted that in all cases the graphs are drawn with uniform spacing between each vertical section, for clarity. The actual distances are as noted on each figure.

The following observations can be made:–

– The width–averaged velocity profiles show the classical shear layer type expansion with a recirculation region, followed downstream with more uniform velocity profiles containing no recirculation regions.

– The recirculation region extends to 0.3m ⟶ 0.4m from the start of the slot. This represents a non–dimensional recirculation length L_r/h_s of 5.5 to 7.0.

– The results of the two smaller slot lengths $B_s/h_s = 5$ and 2, reveal that the recirculation region is never fully extended to the base of the slot. This means that both these slots contain recirculations over the full length of the slot, with no area of more uniform velocity distribution for $B_s/h_s = 2$ for instance a typical shear layer and recirculation is as sketched below. The shear layer does not reach the channel base when $B_s/h_s = 2$ or 5 but does when $B_s/h_s = 10$ or 20.

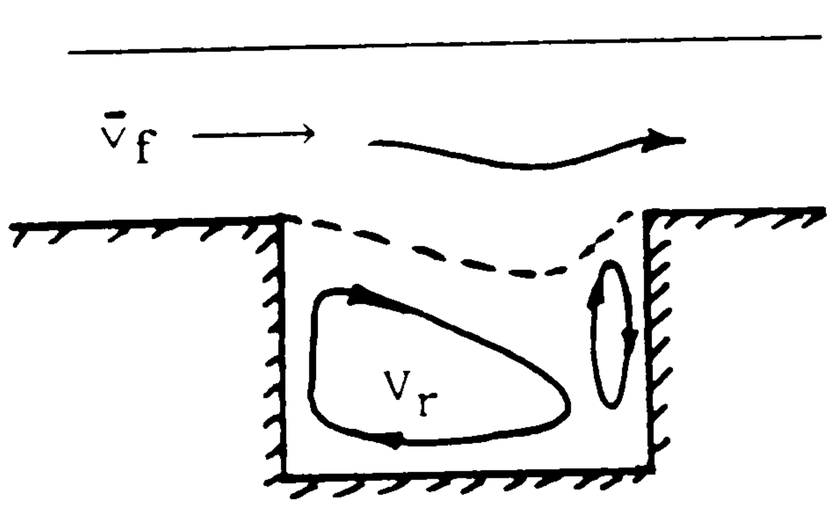

small aspect ratio

$B_s/h_s = 2$ or 5

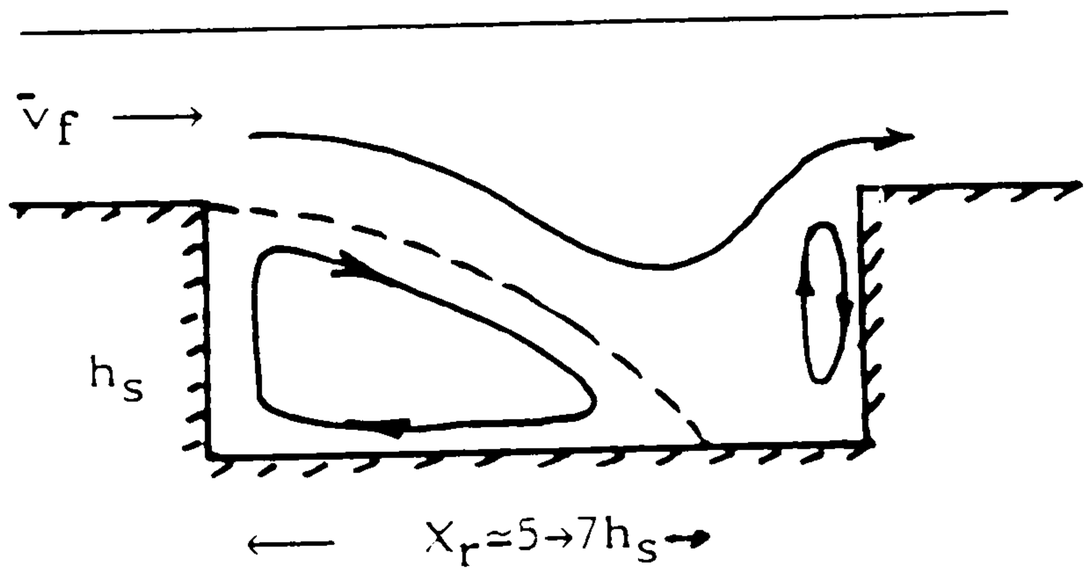

large aspect ratio

$B_s/h_s = 10$ or 20

– It was decided to investigate the magnitude of the recirculating velocities in the recirculation region for all slot widths and relative depths. This is characterised, for the sake of brevity, as the maximum recirculation velocity, V_{rmax}, found at any given relative flow depth or slot dimension. The results are given in Table (6.6) showing the relative flow depth, the maximum

recirculating velocity V_{rmax}, the mean velocity upstream of the slot U_f, and most importantly the ratio V_{rmax}/U_f.

It is clear from Table (6.6) that the ratio of maximum recirculation velocity to mean upstream velocity is usually between 0.1 and 0.3. The smallest recirculation velocities appear in the widest slot $B_s/h_s = 20$, whilst the maximum recirculations occur at a slot dimension $B_s/h_s = 5$. The ratio of V_{rmax}/U_f is around 0.26 for $B_s/h_s = 5$, whereas it is only around 0.14 for $B_s/h_s = 20$. The narrowest slot width, $B_s/h_s = 2$, gives a ratio around 0.21. The magnitudes of the recirculations will be discussed in detail in Chapter 7.

6.4.2 A Universal Velocity Profile

Figures 6.51 and 6.52 represent an attempt to produce a universal velocity profile for the recirculating expansion region for all relative depths and for all vertical sections along the slot expansion region. A definition sketch of each parameter is given overleaf:–

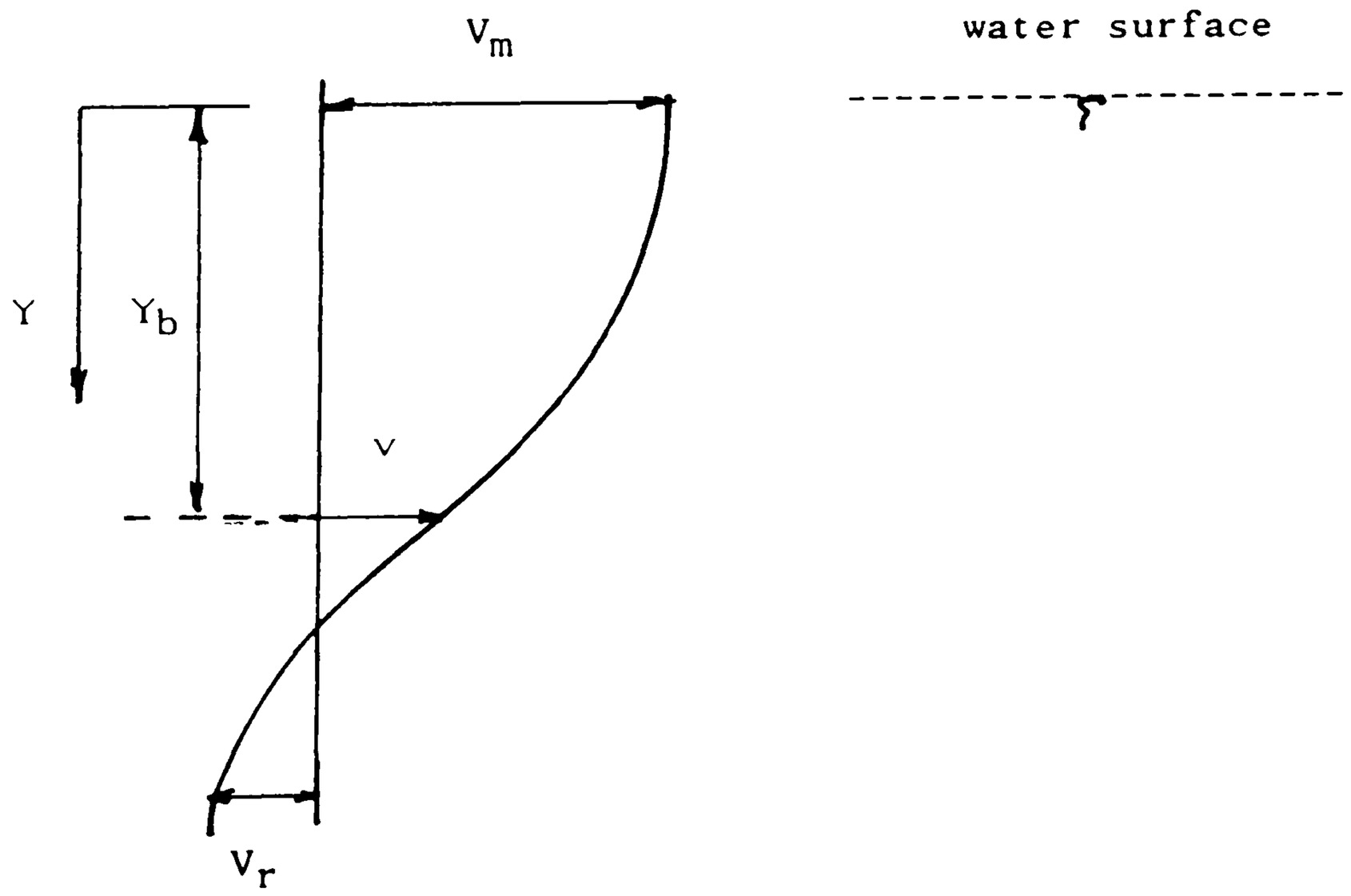

where

v is any velocity

V_m is the maximum velocity

V_r is the maximum recirculation velocity (− ve)

Y is the depth from the free surface

Y_b is the normalising depth when the velocity $v = (V_m + V_r)/2$

As a first attempt at a universal profile, the method of Lean and Weare (1979) was adopted initially. Lean and Weares work concerned the recirculation in an open channel flow downstream of an obstruction. They proposed two methods of estimating the turbulent shear stress in the recirculation region, depending on the relative importance of the boundary friction. Large boundary friction is simulated by the eddy viscosity model $\epsilon = 0.16 v_* Y$. Small boundary friction is simulated best by $\epsilon = 0.01 |\Delta v| \delta$, thus concentrating on turbulence generated purely in the recirculating shear layer.

Lean and Weare produced an expression for the universal velocity profiles downstream in the recirculation region, in the form,

$$\frac{v}{V_m} = \frac{1}{2}\left[1 + \operatorname{erf}\left\{\frac{Y}{x}\left(\frac{R}{2}\right)^{1/2}\right\}\right] \qquad (6.30)$$

where x is the distance downstream from the obstruction and (erf) is the error function, given in standard text books. The value of R is approximately 288.

Many attempts were made to relate the form of Equation (6.30) to the velocity data in these experiments, over a range of relative depths and slot width/depth ratios. Despite various trials for the value of R, and despite incorporating V_r in the left side of Equation (6.30), no successful correlation was obtained.

As a second approach the method of Rajaratnam (1976) was used. In this approach, the universal profile, at all relative depths and all distances along the recirculation zone, is assumed to have a gaussian form from the point of maximum velocity V_m to the point of minimum velocity V_r. The point of minimum velocity is at V_r which is a negative value. This mean that any correlation cannot be based simply on the ratio v/V_m but needs a "shift" of axis by the value V_r.

According to Rajaratnam (1976) the most convenient normalising velocity form is $(v - V_r)$, where V_r is essentially the maximum recirculating velocity at any vertical section.

Similarly, the flow depth parameter also requires to be normalised. This is usually achieved by defining Y_b as the depth of flow measured down from the free surface where the velocity is exactly half–way between V_m and V_r. For jet type flows in an infinite medium, $V_r = 0$ and Y_b is the depth at $V_m/2$. In this case Y_b is defined at $u = (V_m + V_r)/2$.

Finally, for a recirculating type flow the most appropriate correlation is of the form,

$$\frac{v - V_r}{V_m - V_r} = (1 + t)e^{-t} \qquad (6.31)$$

The result in Fig (6.51) is for the recirculation zone in the widest slot $B_s/h_s = 20$, at all relative depths and distances along the expansion region. The comparison with a previous experiment test by Etheridge and Kemp (1978) is very satisfactory. There is considerable spread in the data, but it should be remembered that it covers a wide range of conditions.

The results in Fig (6.52) are for expansion region in the slot $B_s/h_s = 10$ for a range of relative depths and positions along the length of the expansion region. Again there is spread in the data, and again a good correlation with the work of Etheridge and Kemp (1978).

The best fit value for A from Equation (6.31) above and for both slot widths is,

$$t = 1.67 \left(Y_c/Y_b \right)^{2.5} \qquad (6.32)$$

This was achieved after numerous trial and error attempts at correlation. Thus the final expression for the velocity in a slot in the channel bed is given by

$$\frac{v - V_r}{V_m - V_r} = (1 + t)e^{-1.67(Y/Y_b)^{2.5}} \qquad (6.33)$$

where

$$t = 1.67 \left(Y_c/Y_b\right)^{2.5}$$

The solution of this equation is only possible when the value of the maximum free surface velocity V_m is known, when the value of the maximum recirculating velocity is known, V_r, and when the normalising depth Y_b is known. Methods for determining these parameters will be presented in Chapter 7.

6.5 CONCLUSIONS

(1) Flow passing over a slot in the channel bed produces a horizontal shear layer associated energy loss, a recirculation region of maximum length $7h_s$, as well as a rise in the free surface water level Δh.

(2) The rise in free water surface can be predicted reasonably accurately by the application of the force–momentum equation combined with the continuity equation. The maximum rise in water level Δh was 1.7mm giving a non–dimensional rise of $\Delta h/h_s = 0.05$. The rise in free water surface level decreases with decreasing slot width/depth ratio.

(3) Energy losses through the slot in the channel bed comprise of both expansion and contraction losses. The total energy loss coefficient increases with increasing slot width/depth ratio. The energy loss coefficient increases with decreasing relative flow depth (Y_f/Y_c).

The total energy loss can be predicted from conventional expansion and contraction loss theory, with a correction factor for the width/depth ratio of the slot, B_s/h_s.

(4) Velocity measurements through the slot show a large recirculation, of non–dimensionalised length, $L_r/h_s = 5.5$ to 7. Maximum recirculation velocities, non–dimensionalised by the mean upstream velocity V_f, gave values of V_{rmax}/U_f

between 0.14 and 0.26 depending on the slot width/depth ratio. The patterns of recirculation are different for small B_s/h_s ratios compared with larger B_s/h_s ratios.

(5) The velocity at any point in the recirculation region can be expressed in the form,

$$\frac{v - V_r}{V_m - V_r} = (1 + t)e^{-t} \qquad (6.34)$$

where

$$t = 1.67 \left(Y_c/Y_b \right)^{2.5}$$

Table (6.1) $B_s/h_s=20$

Y_f/Y_c	0.29	0.369	0.377	0.4556	0.4827	0.508
Y_f mm	22.3	31.80	32.80	45.20	50.20	55.40
Y_c mm	76.9	86.2	87.0	99.20	104.0	109.0

Table (6.2) $B_s/h_s=10$

Y_f/Y_c	0.293	0.382	0.41	0.4716	0.5046
Y_f mm	22.5	33.10	37.4	47.40	54.20
Y_c mm	76.80	86.70	91.2	100.5	107.40

Table (6.3) $B_s/h_s=5$

Y_f/Y_c	0.28	0.3134	0.366	0.412	0.4707
Y_f mm	21.0	24.6	31.0	37.5	47.5
Y_c mm	75.0	78.5	84.7	91.0	100.9

Table (6.4) $B_s/hs=2$

Y_f/Y_c	0.296	0.373	0.4288	0.4763
Y_f mm	22.60	31.80	40.1	48.40
Y_c mm	76.40	85.30	93.50	101.6

Table (6.1) to Table (6.4) Represent flow depths for SERIES F slot tests

Y_f is the depth of flow upstream the slot

Y_c is the maximum depth of flow in the slot

Table (6.5) The Experimental Results For the Expansion, Contraction, and Total Losses (Width Depth Ratio B_c/H_s = 20 , 10, 5, 2)

	Y_f/Y_c	K_e (mm)	K_c (mm)	K_t (mm)
B_S/h_S = 20	0.29	0.6055	0.42389	1.0294
	0.369	0.4254	0.400	0.8254
	0.377	0.405	0.385	0.790
	0.4556	0.3257	0.3613	0.687
	0.4827	0.25	0.3253	0.5753
	0.508	0.2689	0.24968	0.5186
B_S/h_S = 10	0.293	0.454	0.454	0.908
	0.376	0.3188	0.368	0.687
	0.410	0.2503	0.345	0.5953
	0.465	0.2432	0.28376	0.52696
	0.5009	0.235	0.2433	0.4783
B_S/h_S = 5	0.28	0.49	0.32	0.81
	0.3134	0.472	0.258	0.730
	0.366	0.385	0.255	0.64
	0.412	0.305	0.305	0.610
	0.4707	0.276	0.324	0.60
B_S/h_S = 2	0.296	0.1869	0.336	0.5229
	0.373	0.279	0.2786	0.5576
	0.4288	0.296	0.2547	0.5507
	0.476	0.109	0.15217	0.2611

k_e is expansion loss coefficient, k_c is the contraction loss coefficient, and kt total energy loss coefficient.

Table (6.6) Maximum Recirculation Velocities in Slot Tests.

	Y_c (m)	Y_f (m)	Y_f/Y_c	Vr_{max}	U_f	Vr_{max}/U_f
B_s/h_s = 20	0.0769	0.0223	0.290	0.025	0.19	0.131
	0.0862	0.0318	0.369	0.027	0.207	0.130
	0.087	0.0328	0.377	0.030	0.163	0.180
	0.0992	0.0452	0.4556	0.030	0.1863	0.161
	0.104	0.0502	0.48269	0.020	0.1953	0.102
	0.109	0.0554	0.508	0.025	0.228	0.109
B_s/h_s = 10	0.0768	0.0225	0.293	0.026	0.1825	0.140
	0.0867	0.0331	0.382	0.022	0.209	0.1050
	0.0912	0.0374	0.410	0.0350	0.2305	0.1518
	0.1005	0.0474	0.4716	0.030	0.21966	0.1360
	0.1074	0.0542	0.5046	0.0570	0.262	0.210
B_s/h_s = 5	0.075	0.0210	0.28	0.0320	0.1605	0.1990
	0.0785	0.0246	0.3134	0.057	0.178	0.320
	0.0847	0.0310	0.366	0.055	0.182	0.30
	0.091	0.0375	0.412	0.045	0.210	0.218
	0.1009	0.0475	0.4707	0.060	0.2173	0.276
B_s/h_s = 2	0.0764	0.0226	0.296	0.042	0.160	0.26
	0.0853	0.0318	0.373	0.022	0.152	0.144
	0.0935	0.0401	0.4288	0.036	0.181	0.199
	0.1016	0.0484	0.4763	0.046	0.1983	0.23

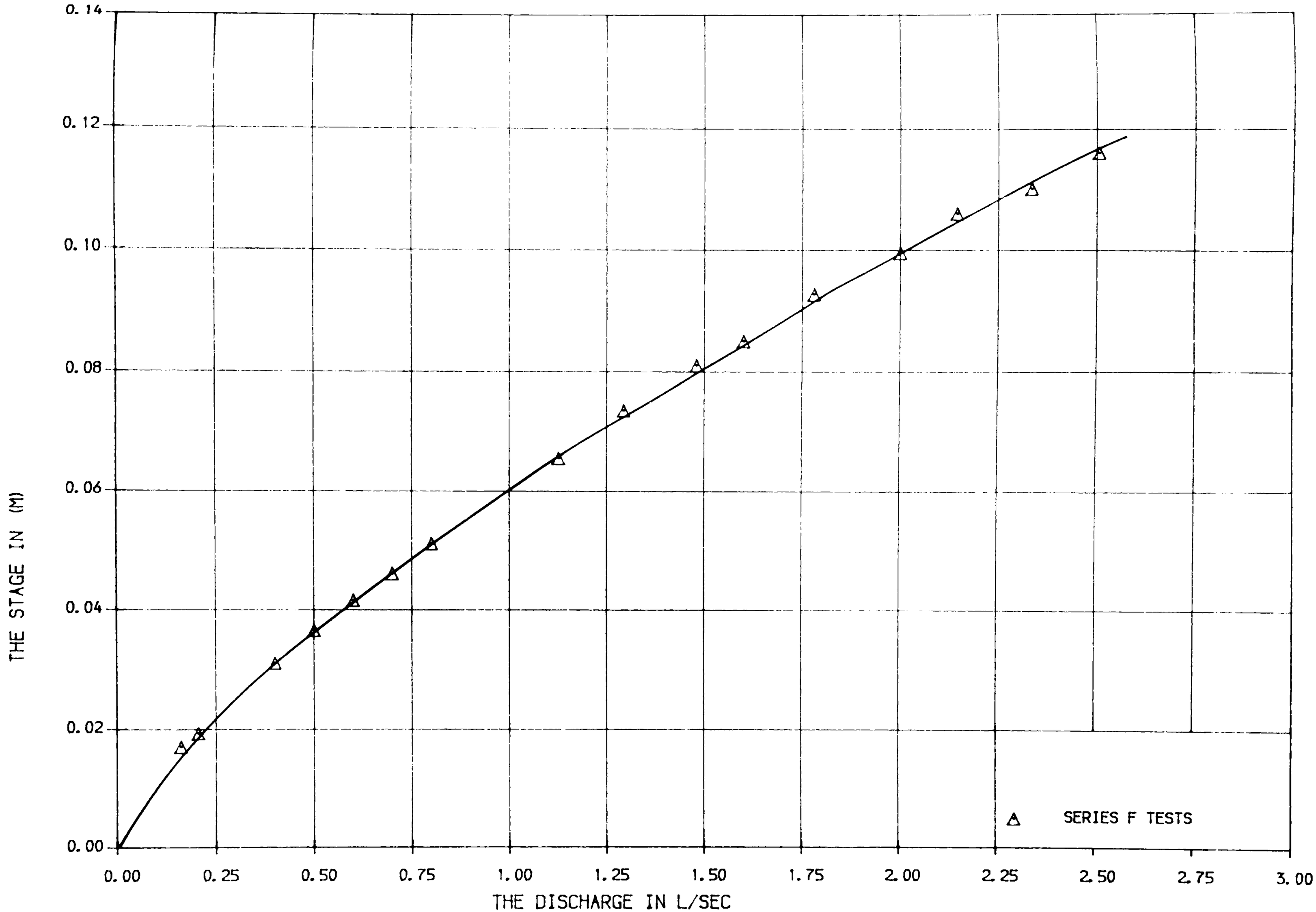

FIG (6.1) THE STAGE-DISCHARGE RELATIONSHIP FOR THE ARMFIELD FLUME WITH CONCRETE BED AND PERSPEX WALLS.

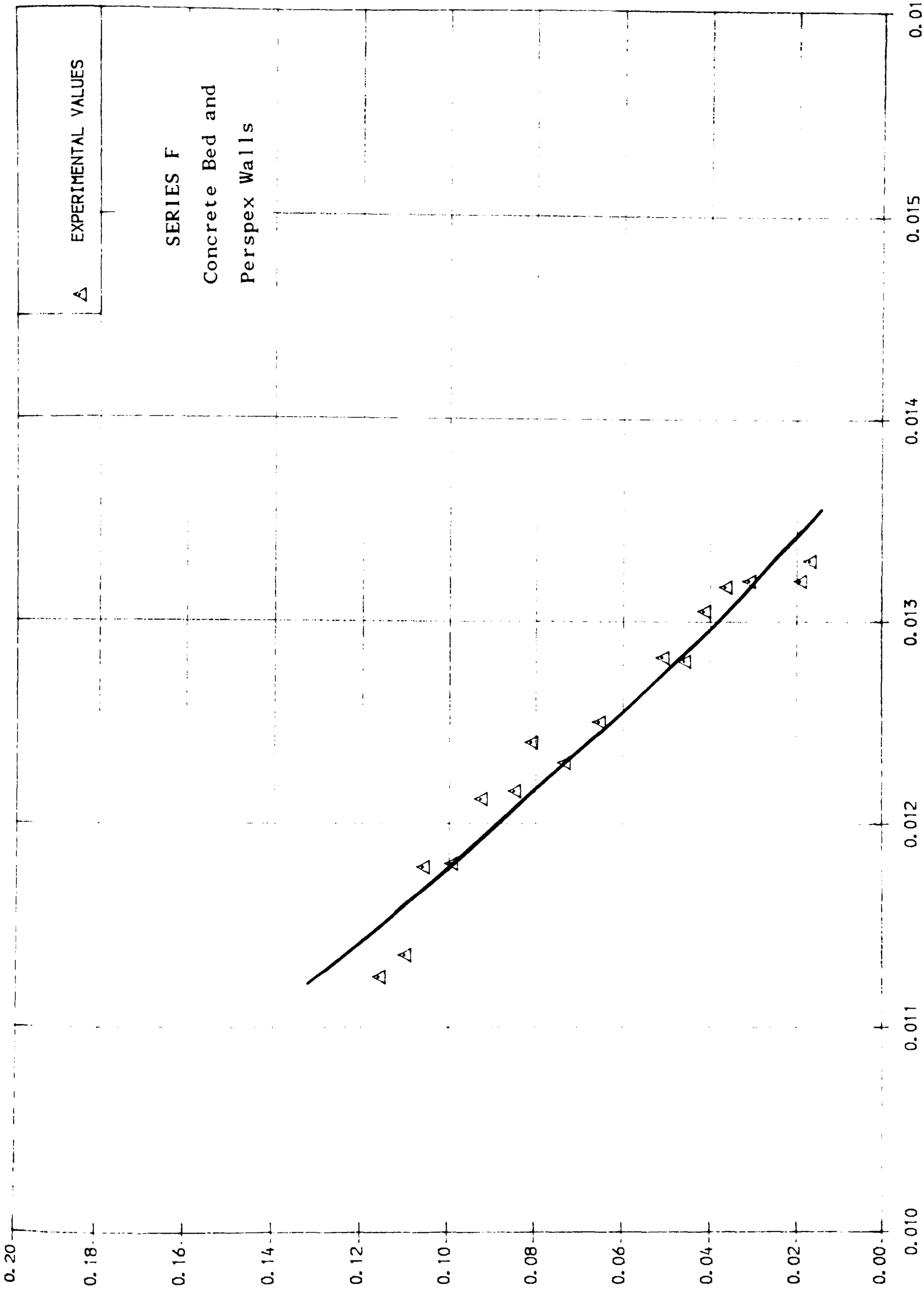

FIG (6.2) THE RELATIONSHIP BETWEEN MANNING'S (N) AND THE DEPTH OF FLOW FOR ARMFIELD FLUME.

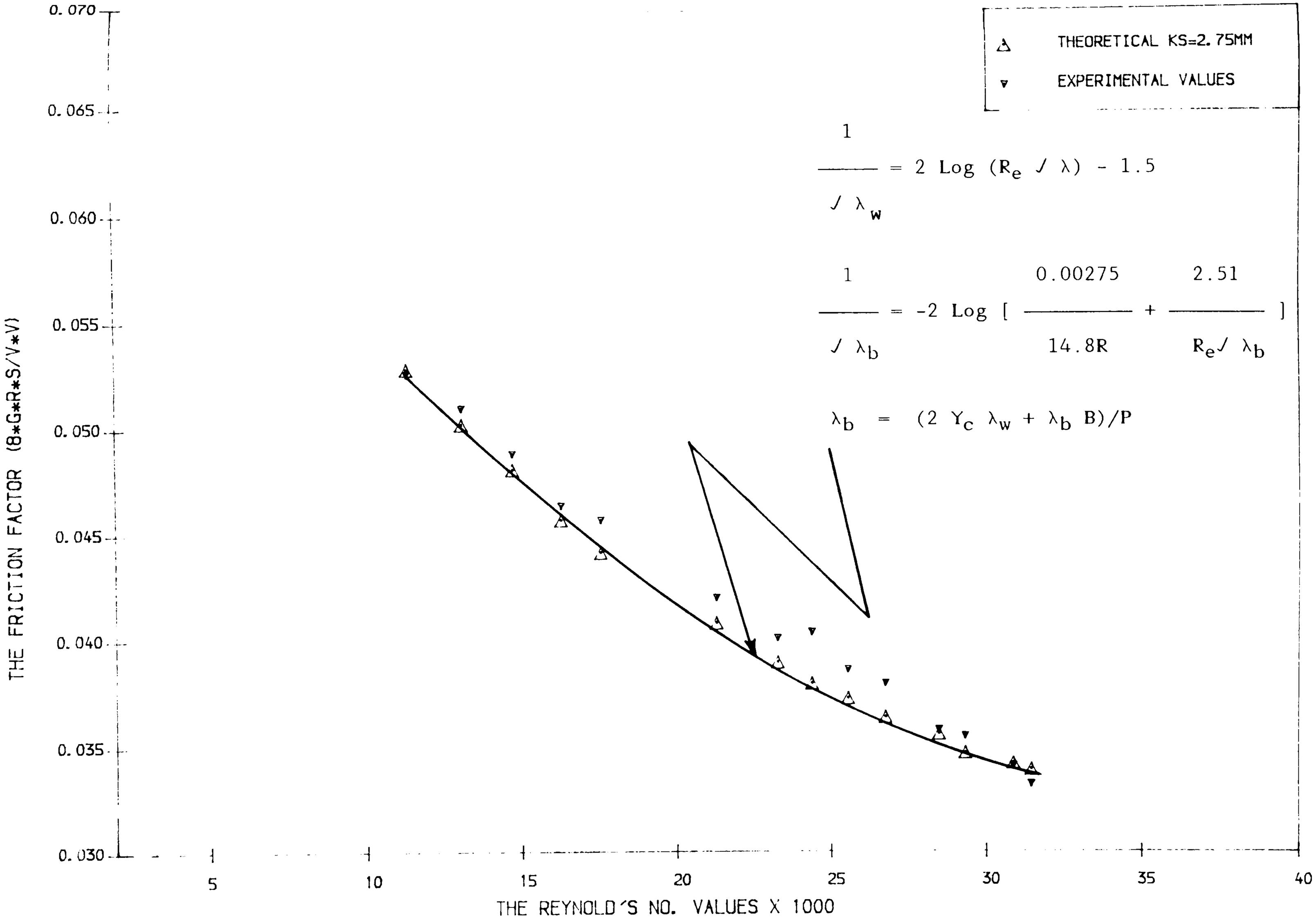

FIG (6.3) THE RELATIONSHIP BETWEEN THE REYNOLD'S NO. AND FRICTION FACTOR FOR BED MATERIAL USED FOR ARMFIELD FLUME.

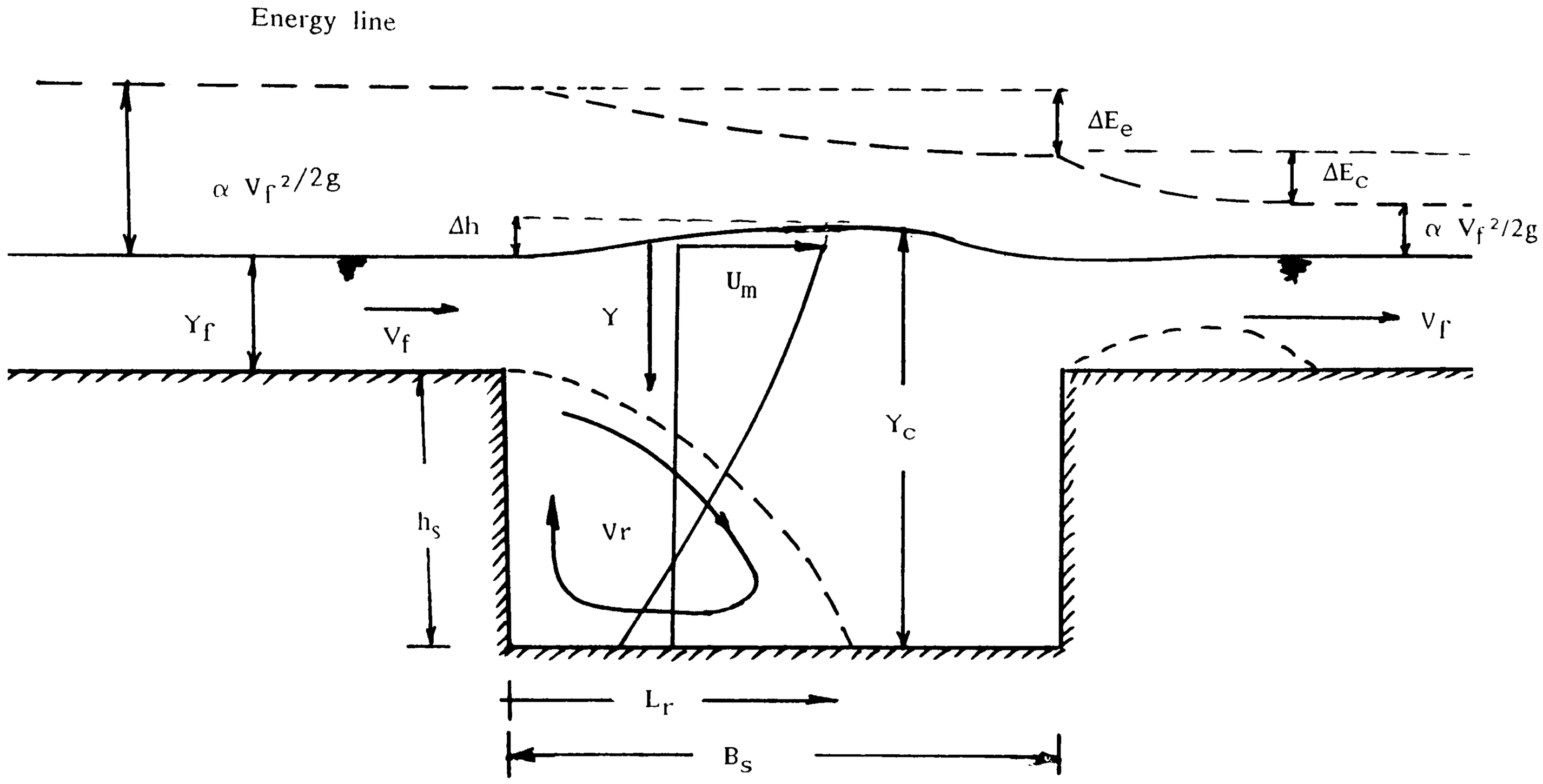

Fig (6.4) The Expansion and Contraction Flow Pheneomena.

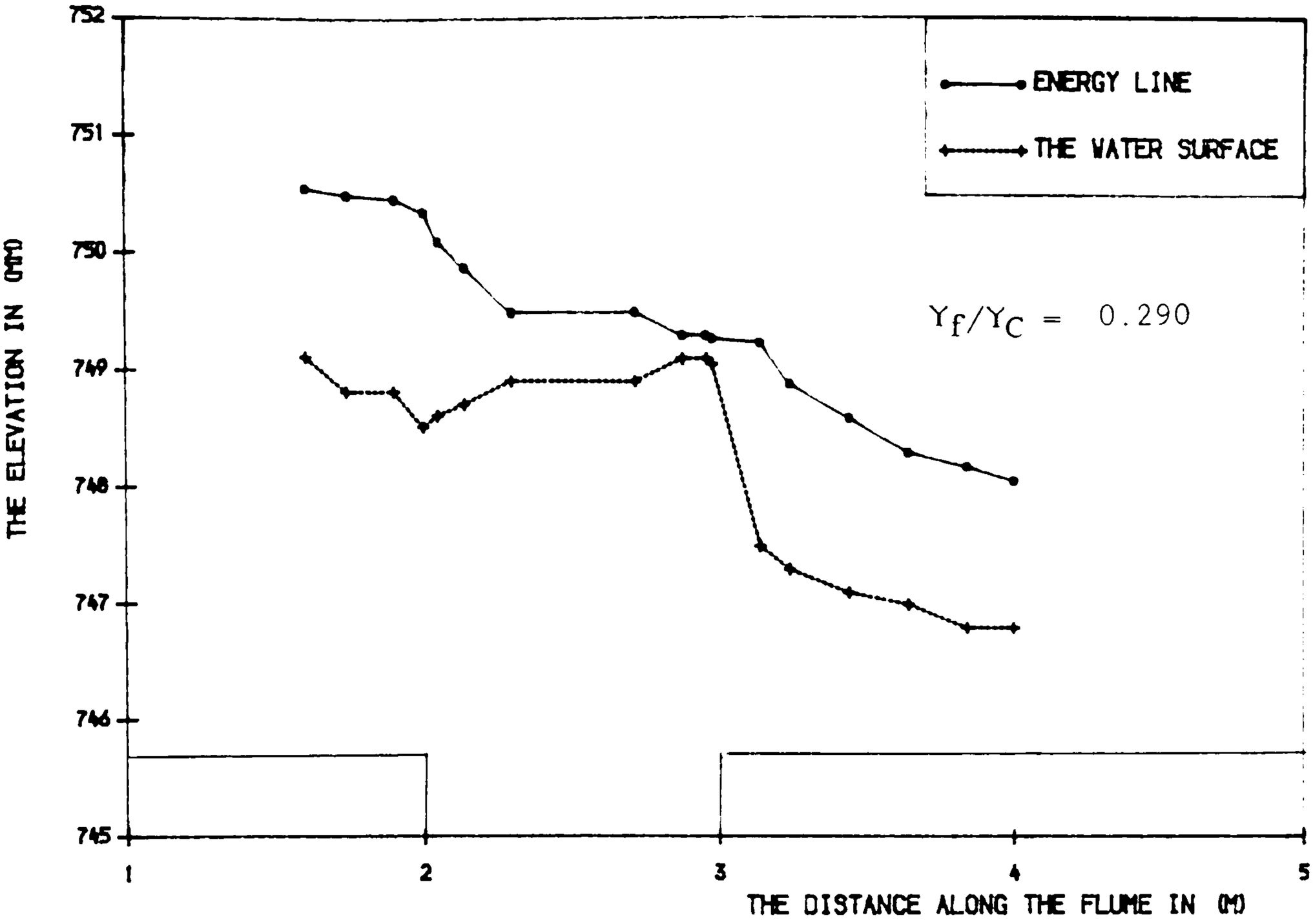

FIG (6.5) THE ENERGY LINE AND THE WATER-LEVEL IN (MM) ALONG THE FLUME WITH THE SLOT (Bs/hs=20).

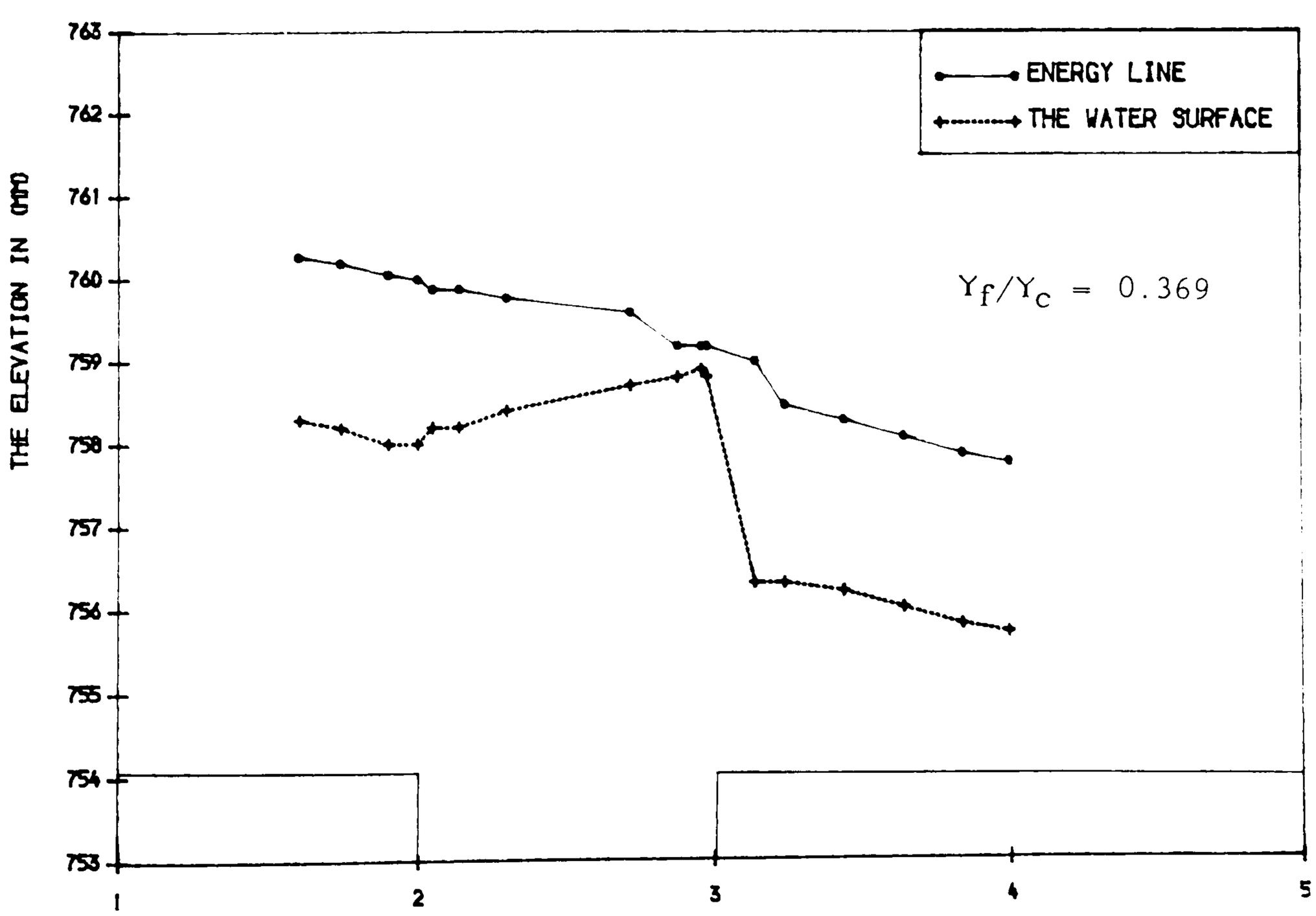

FIG (6.6) THE ENERGY LINE AND THE WATER-SURFACE IN (MM) ALONG THE FLUME WITH THE SLOT (Bs/hs=20).

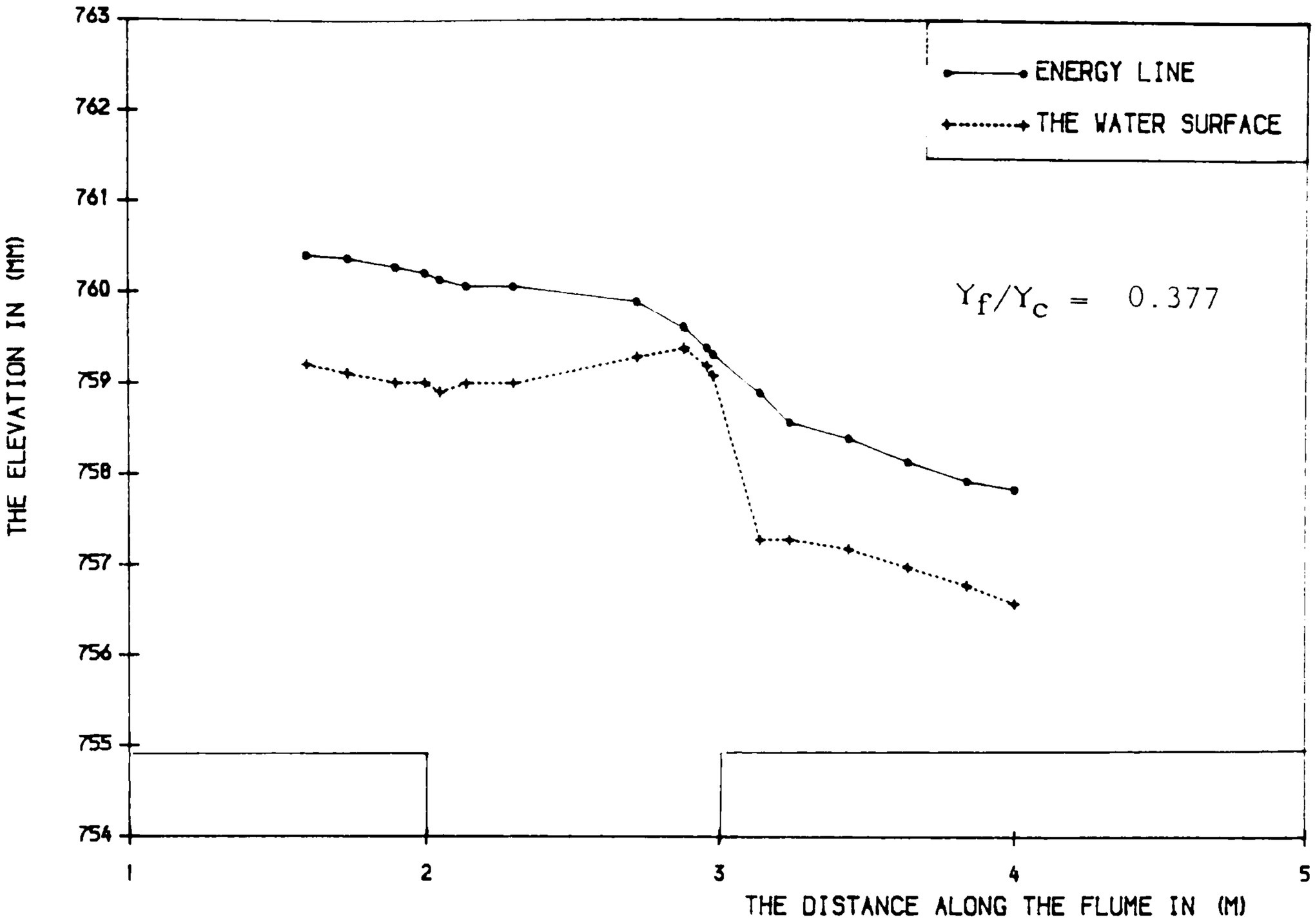

FIG(6.7) THE ENERGY LINE AND THE WATER-LEVEL IN (MM) ALONG THE FLUME WITH THE SLOT (Bs/hs=20).

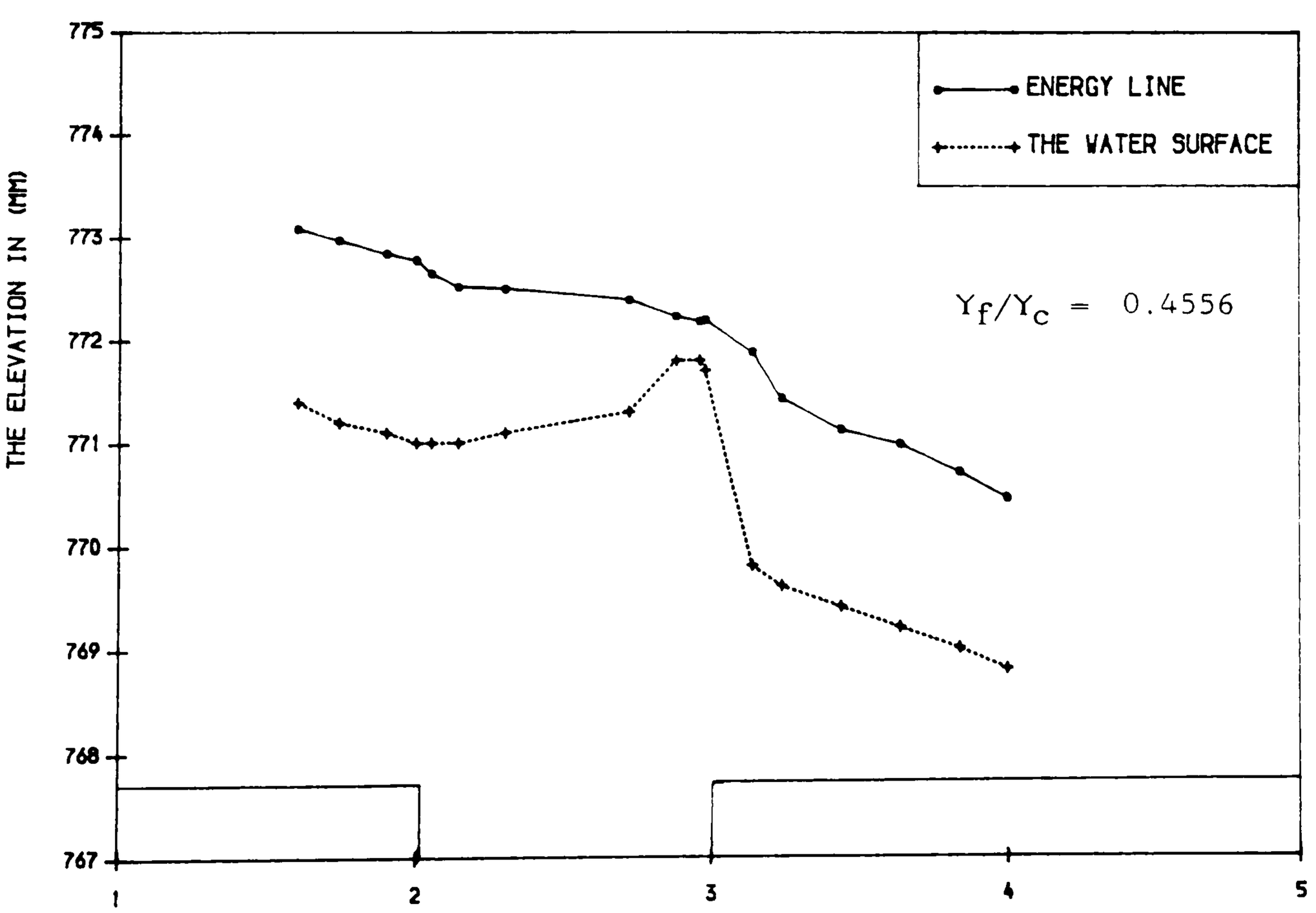

FIG(6.8) THE ENERGY LINE AND THE WATER-LEVEL IN (MM) ALONG THE FLUME WITH THE SLOT (Bs/hs=20).

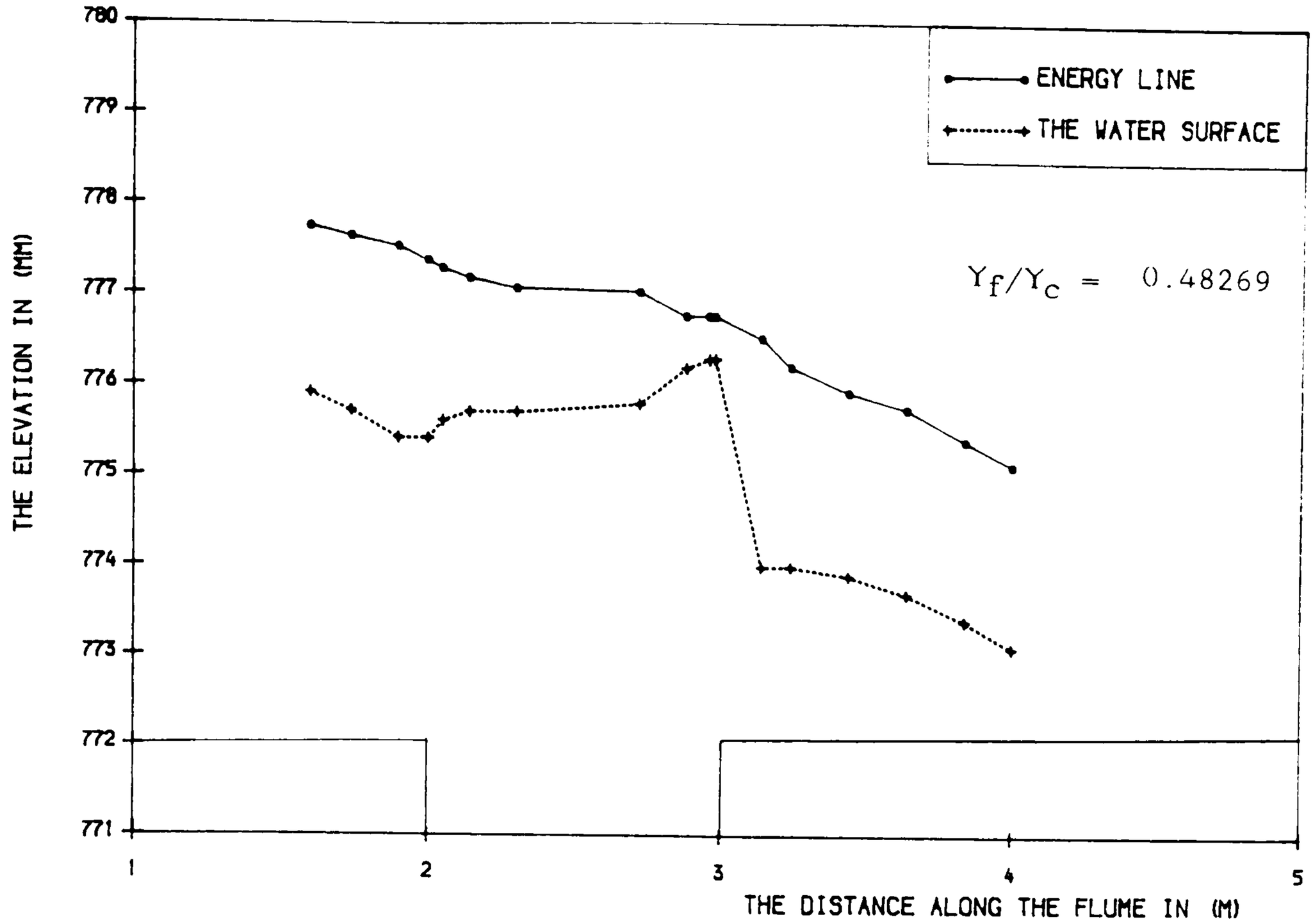

FIG(6.9) THE ENERGY LINE AND THE WATER-LEVEL IN (MM) ALONG THE FLUME WITH THE SLOT (Bs/hs=20).

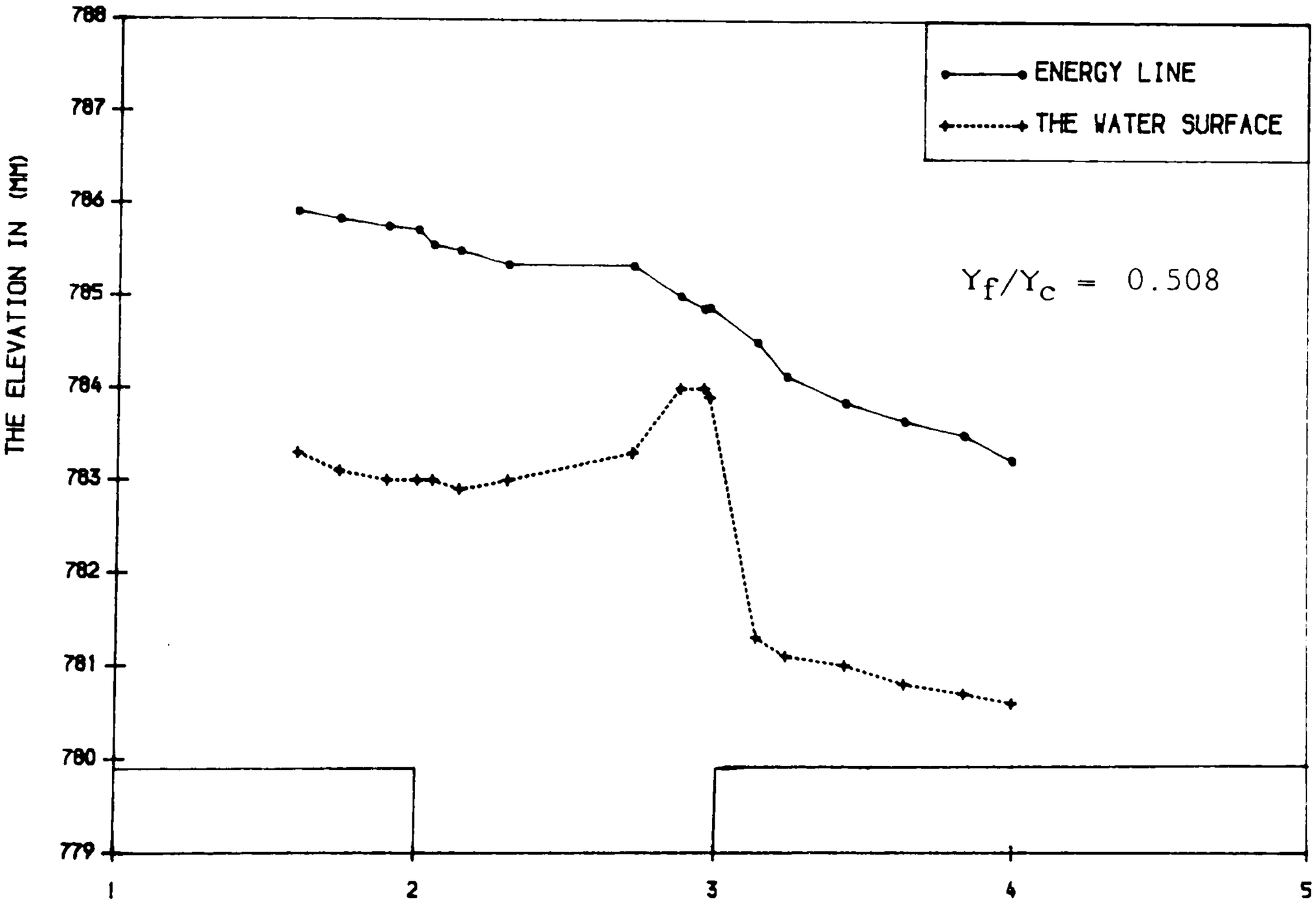

FIG(6.10) THE ENERGY LINE AND THE WATER-LEVEL IN (MM) ALONG THE FLUME WITH THE SLOT (Bs/hs=20).

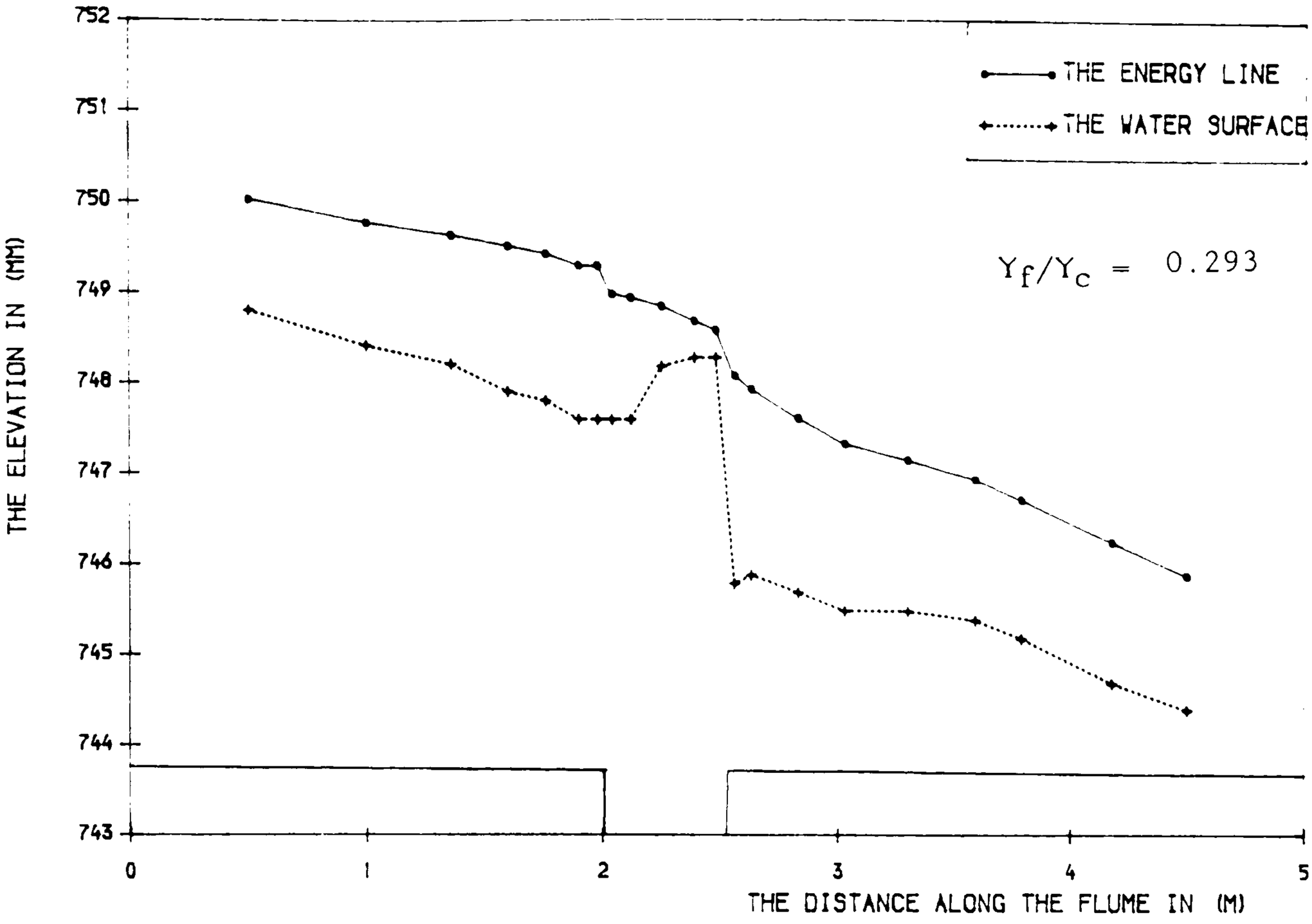

FIG(6.11) THE ENERGY LINE AND THE WATER-LEVEL IN (MM) ALONG THE FLUME WITH THE SLOT (Bs/hs=10).

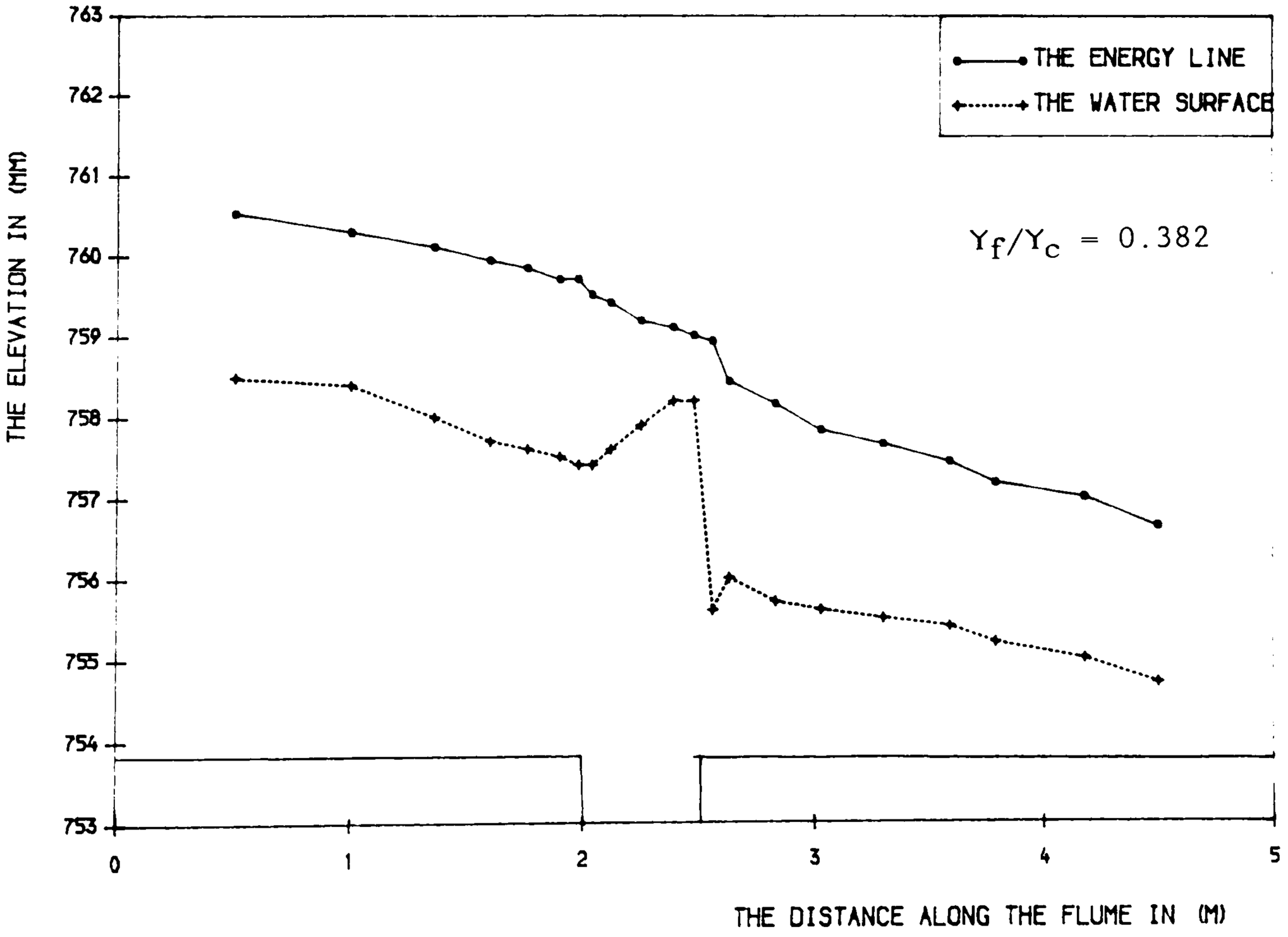

FIG(6.12) THE ENERGY LINE AND THE WATER-LEVEL IN (MM) ALONG THE FLUME WITH THE SLOT (Bs/hs=10).

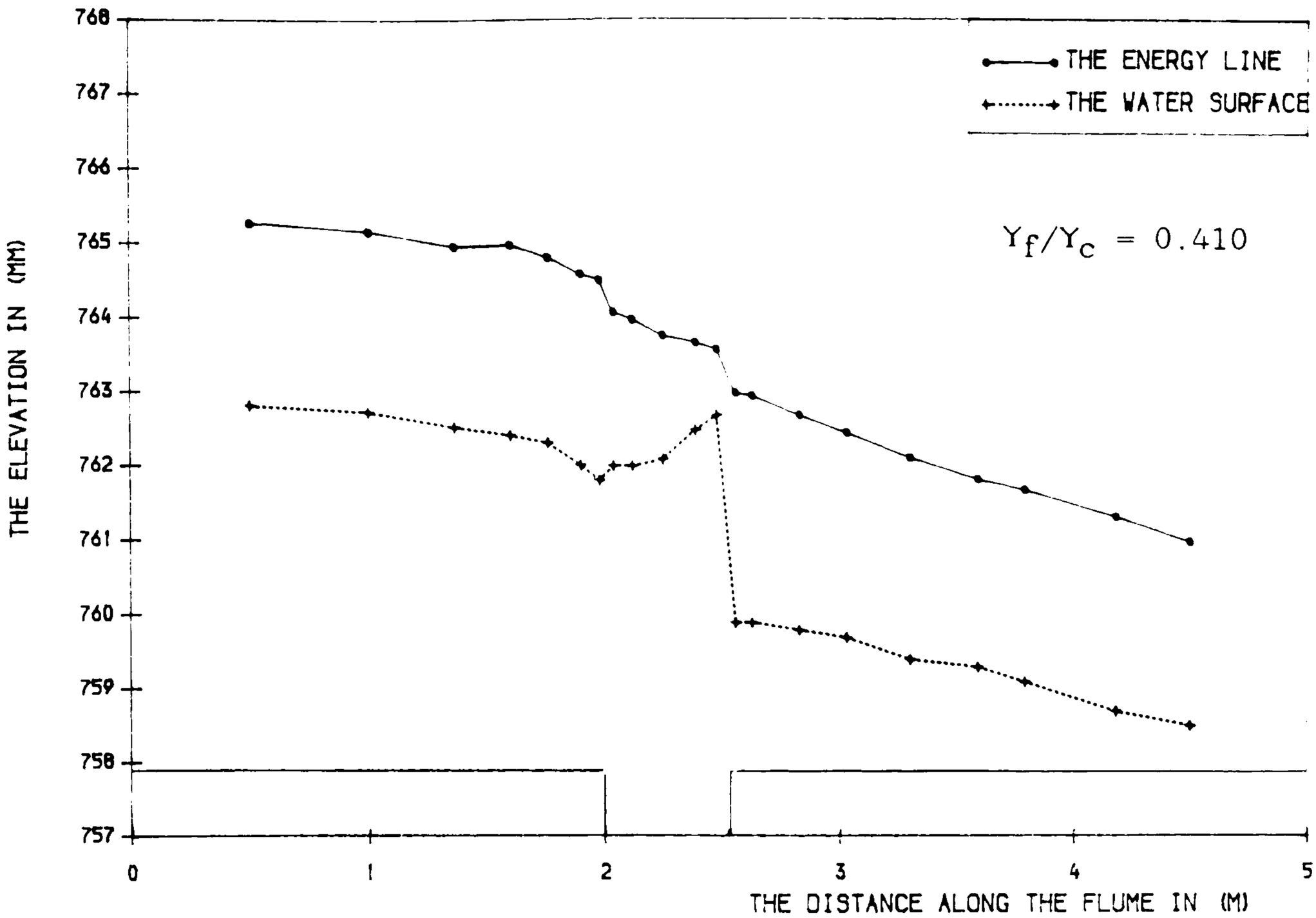

FIG(6. 13) THE ENERGY LINE AND THE WATER-LEVEL IN (MM) ALONG THE FLUME WITH THE SLOT (Bs/hs=10).

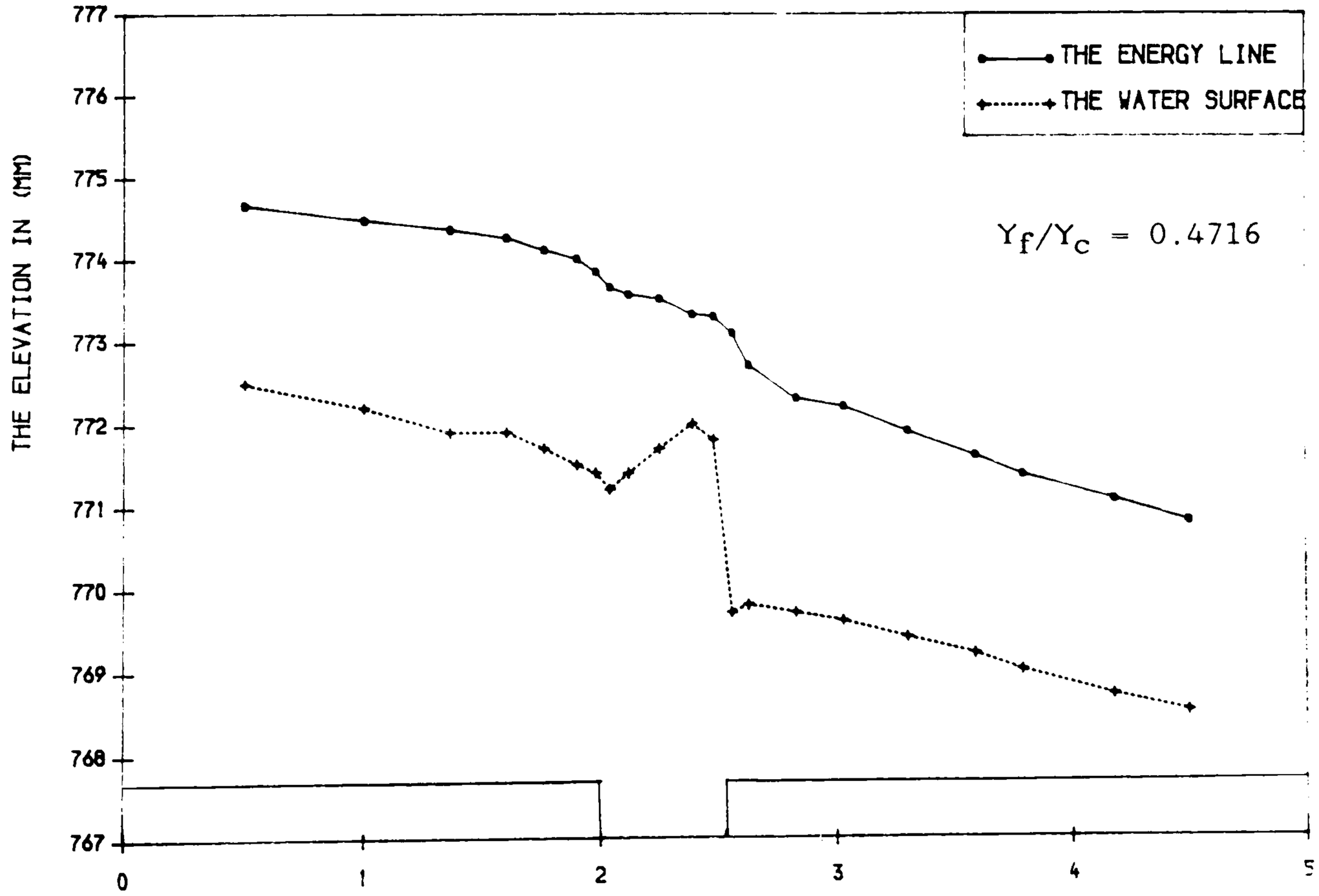

FIG(6. 14) THE ENERGY LINE AND THE WATER-LEVEL IN (MM) ALONG THE FLUME WITH THE SLOT (Bs/hs=10).

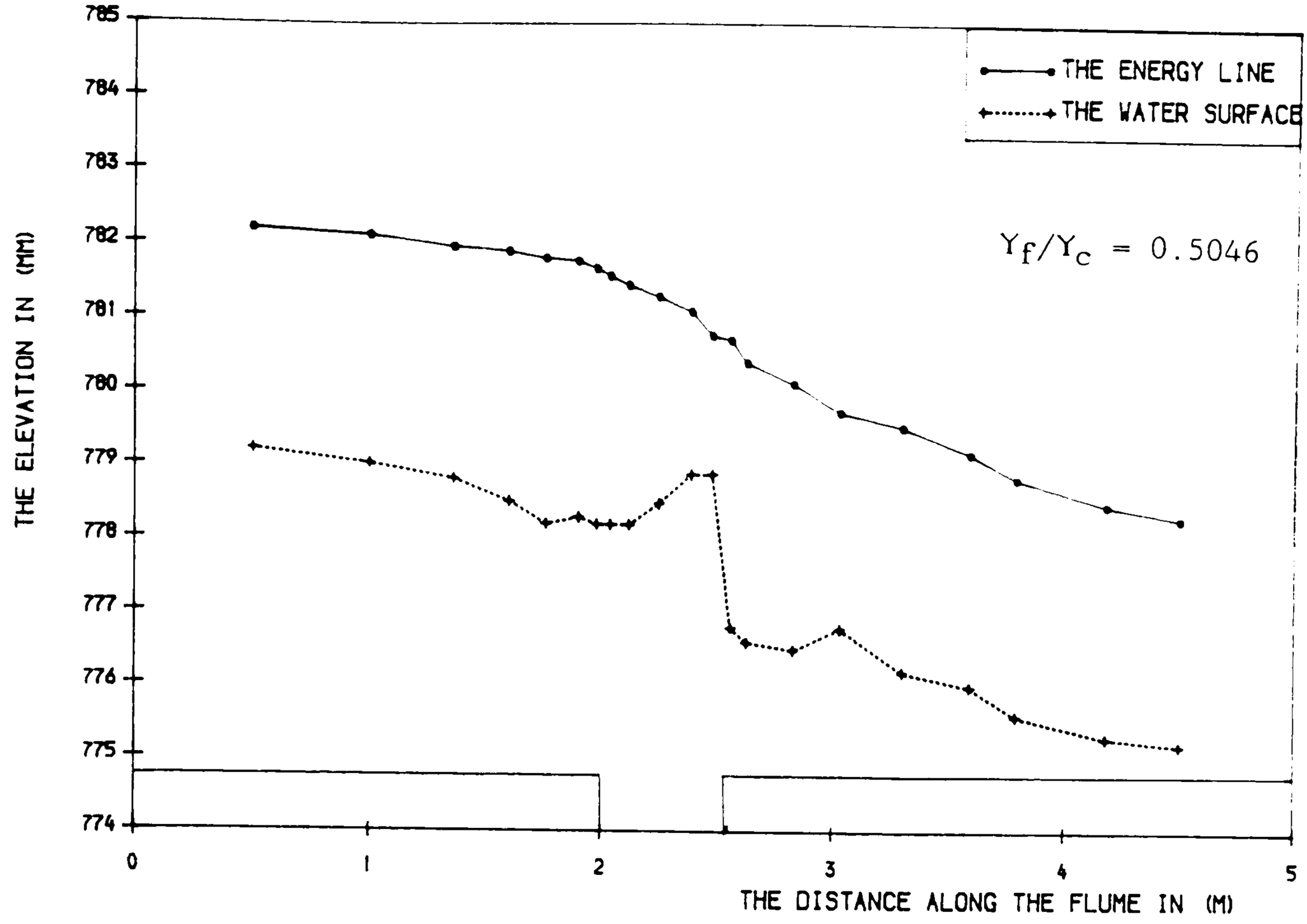

FIG(6.15) THE ENERGY LINE AND THE WATER-LEVEL IN (MM) ALONG THE FLUME WITH THE SLOT (Bs/hs=10).

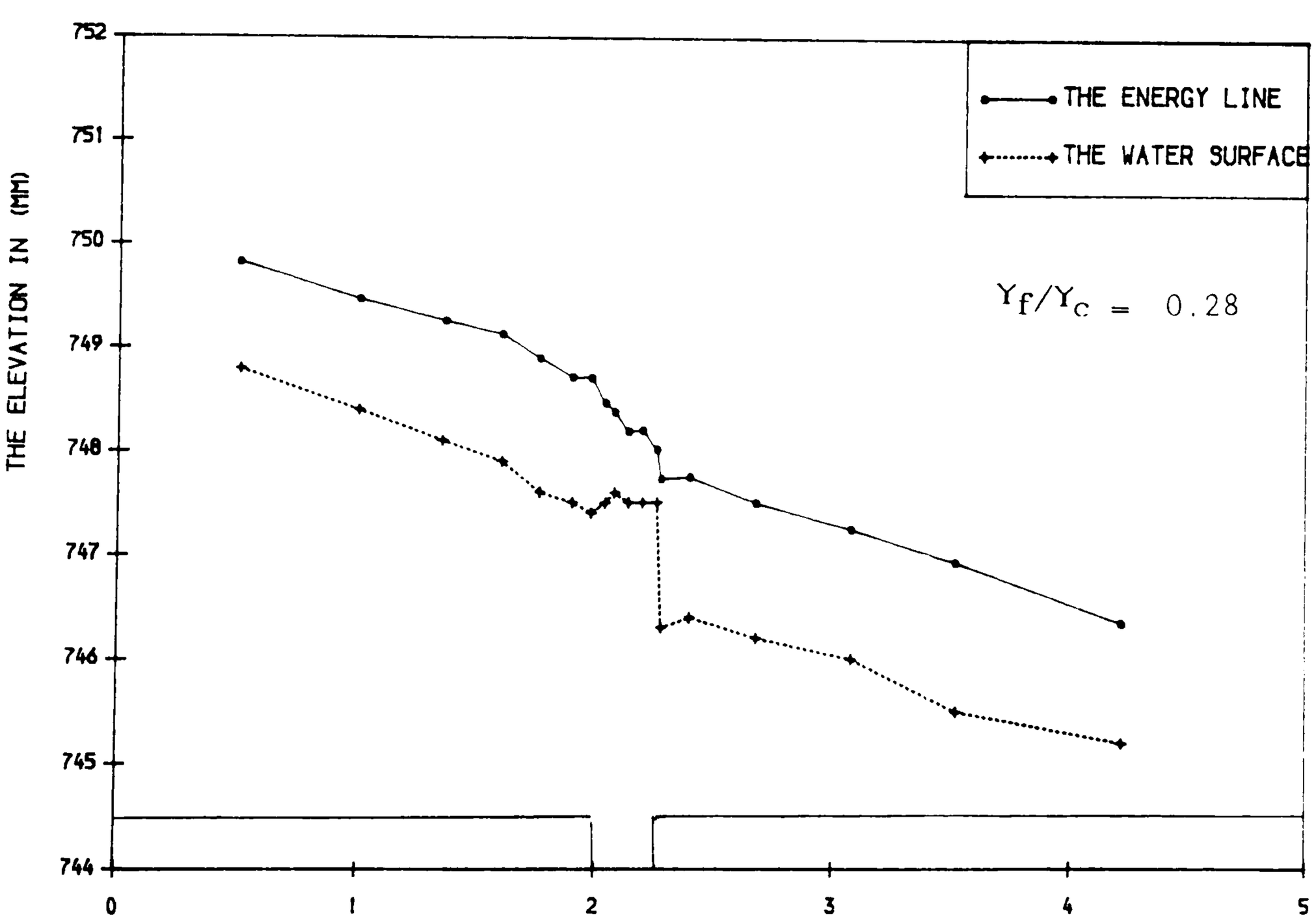

FIG(6.16) THE ENERGY LINE AND THE WATER-LEVEL IN (MM) ALONG THE FLUME WITH THE SLOT (Bs/hs=5).

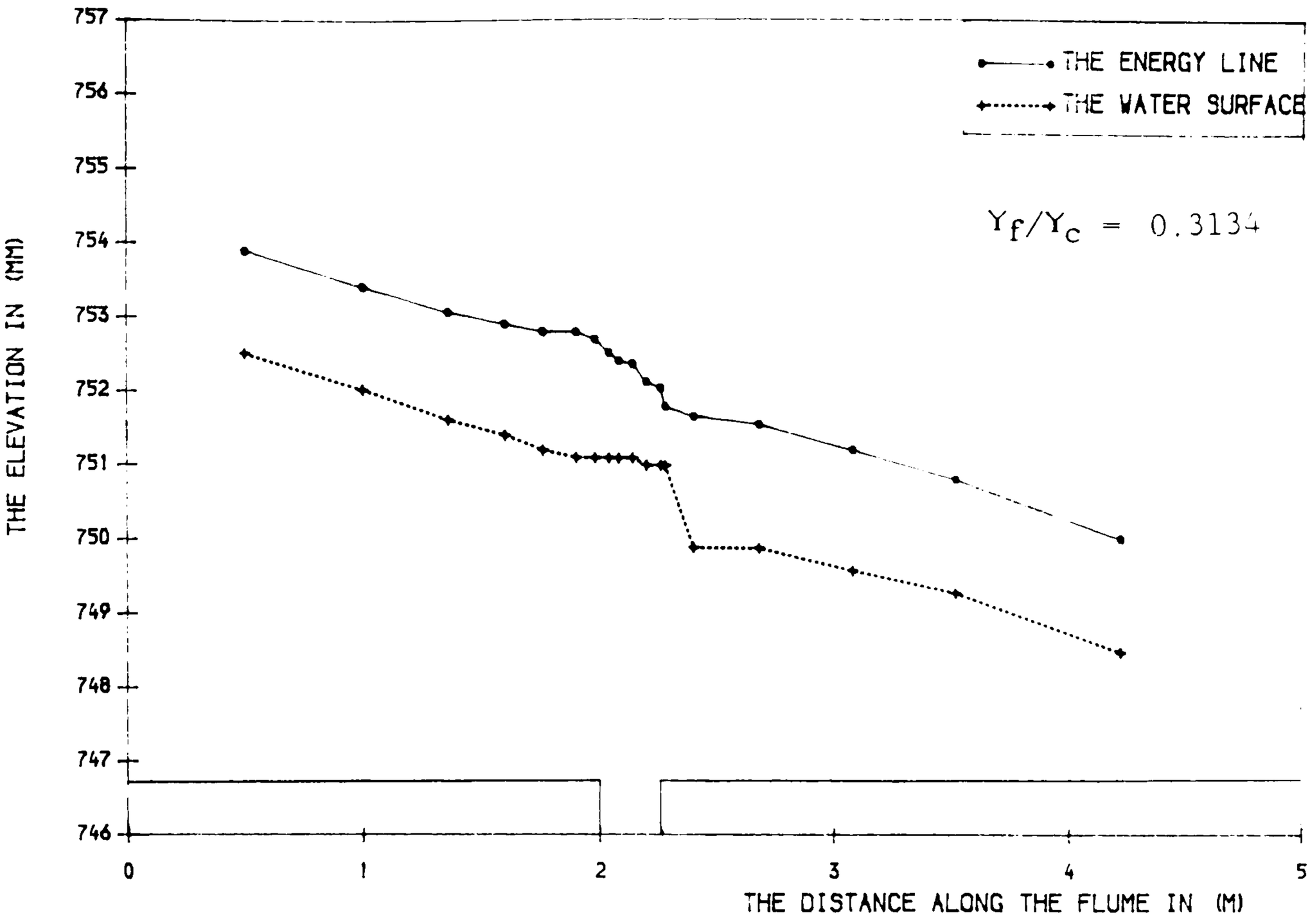

FIG(6.17) THE ENERGY LINE AND THE WATER-LEVEL IN (MM) ALONG THE FLUME WITH THE SLOT (Bs/hs=5).

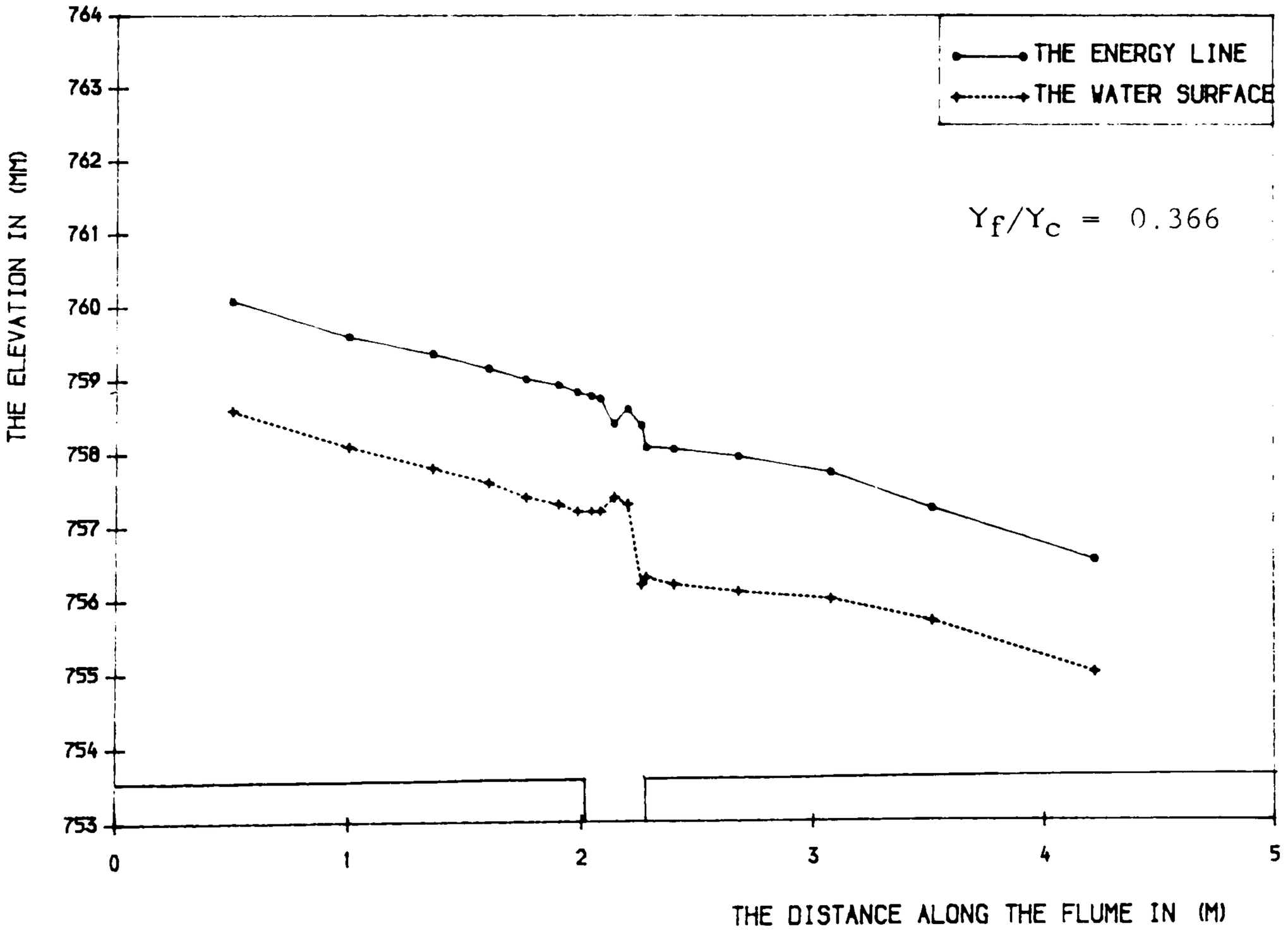

FIG(6.18) THE ENERGY LINE AND THE WATER-LEVEL IN (MM) ALONG THE FLUME WITH THE SLOT (Bs/hs=5).

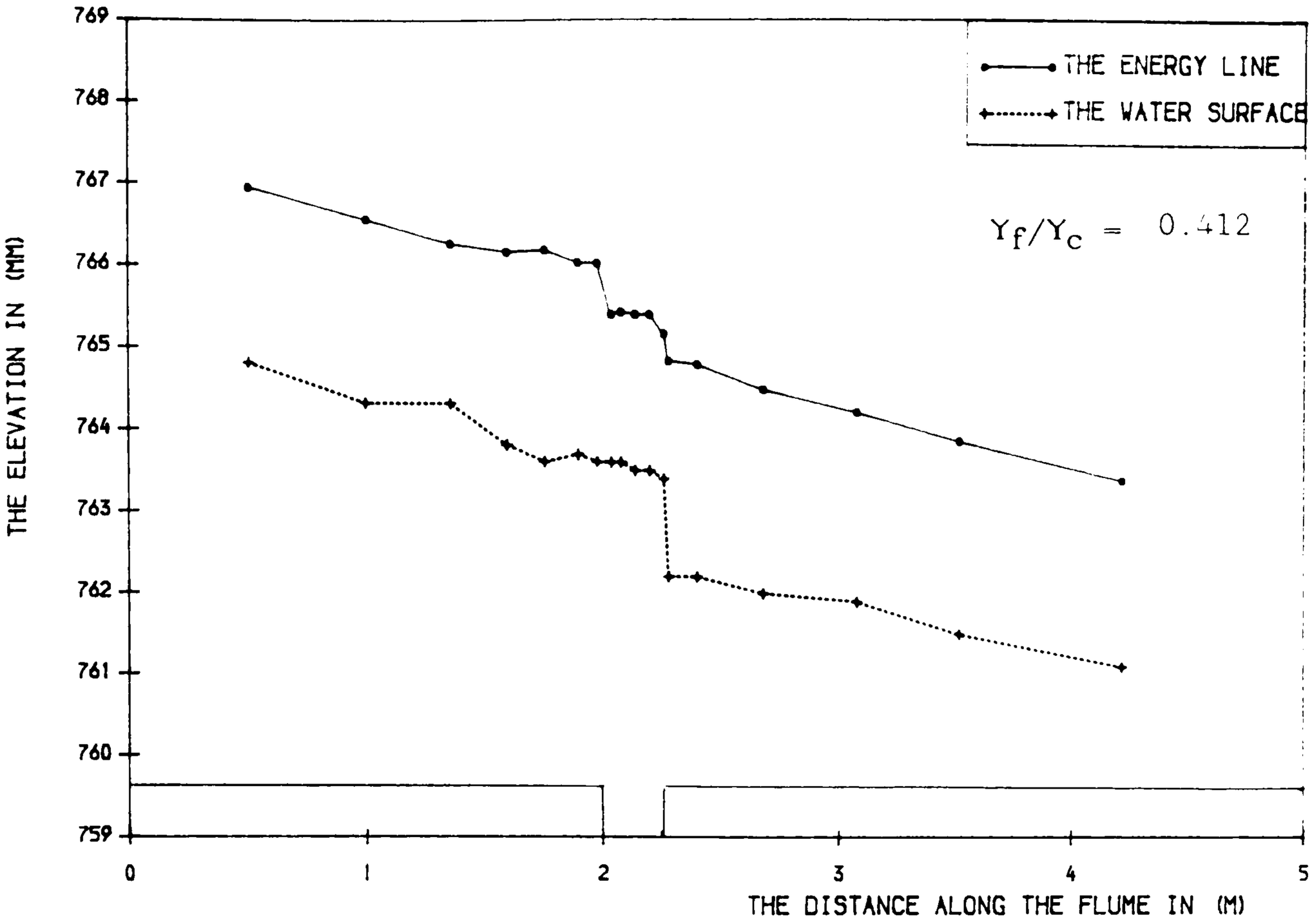

FIG(6.19) THE ENERGY LINE AND THE WATER-LEVEL IN (MM) ALONG THE FLUME WITH THE SLOT (Bs/hs=5).

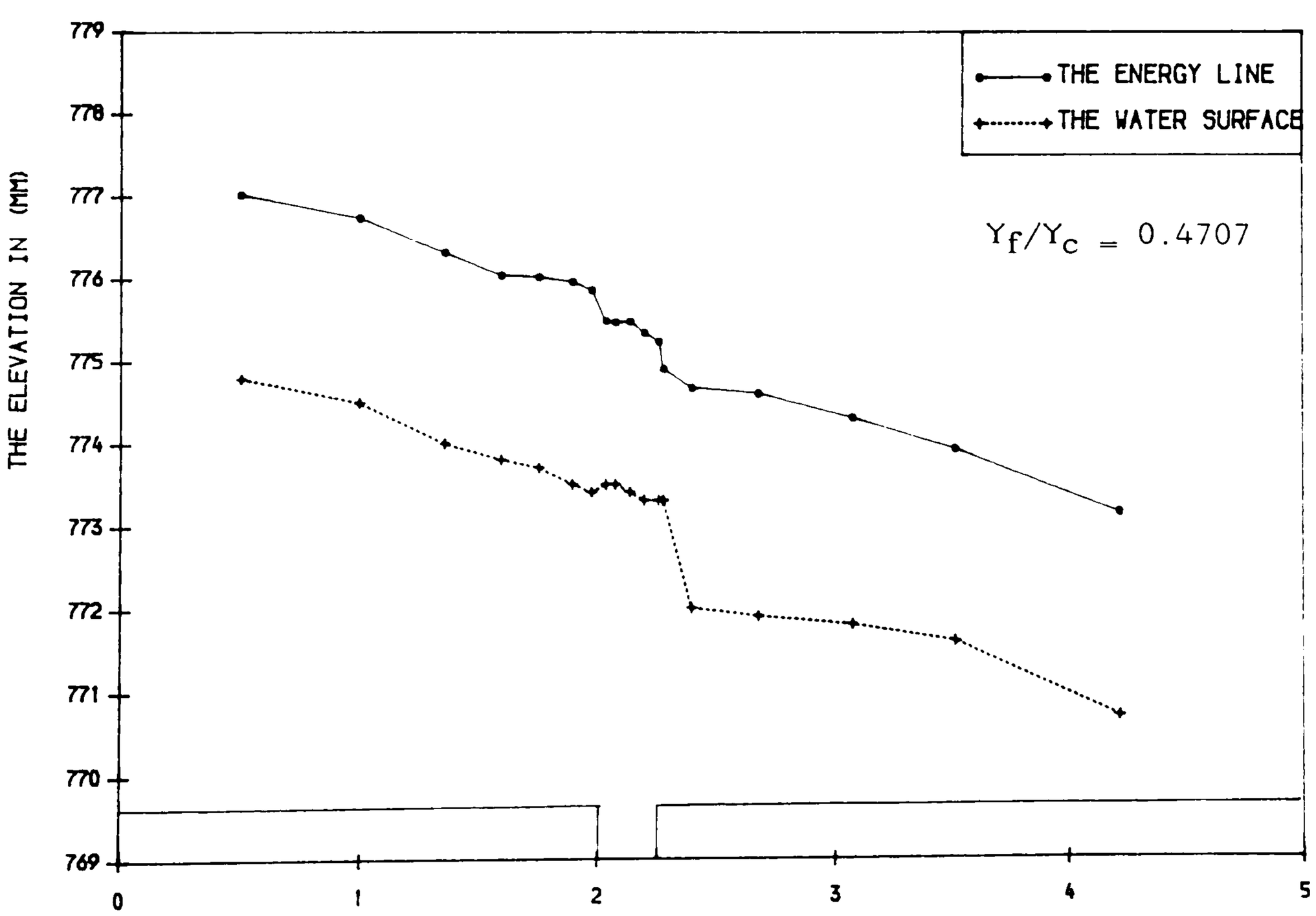

FIG(6.20) THE ENERGY LINE AND THE WATER-LEVEL IN (MM) ALONG THE FLUME WITH THE SLOT (Bs/hs=5).

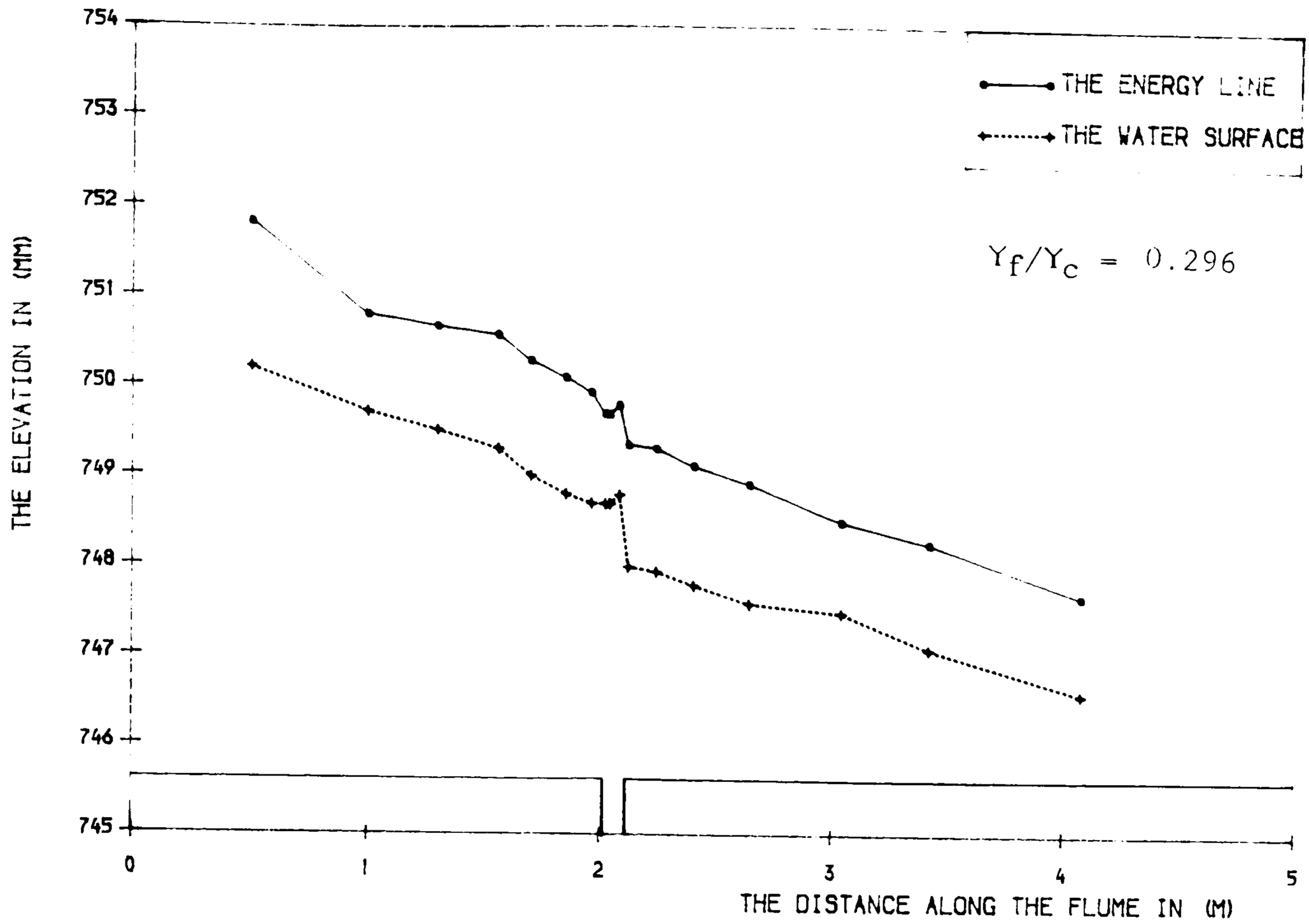

FIG (6.21) THE ENERGY LINE AND THE WATER-LEVEL IN (MM) ALONG THE FLUME WITH THE SLOT (Bs/hs=2).

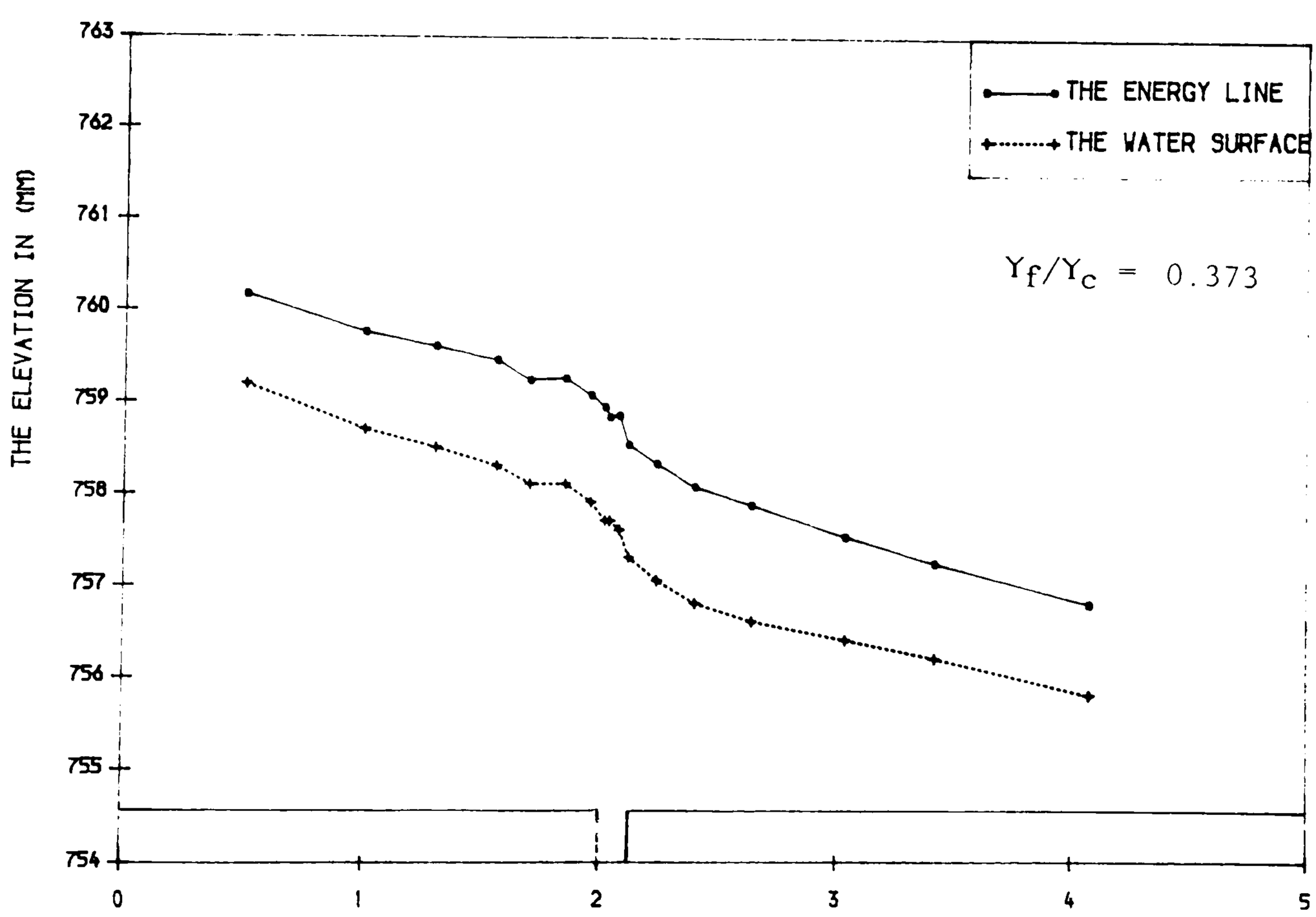

FIG (6.22) THE ENERGY LINE AND THE WATER-LEVEL IN (MM) ALONG THE FLUME WITH THE SLOT (Bs/hs=2).

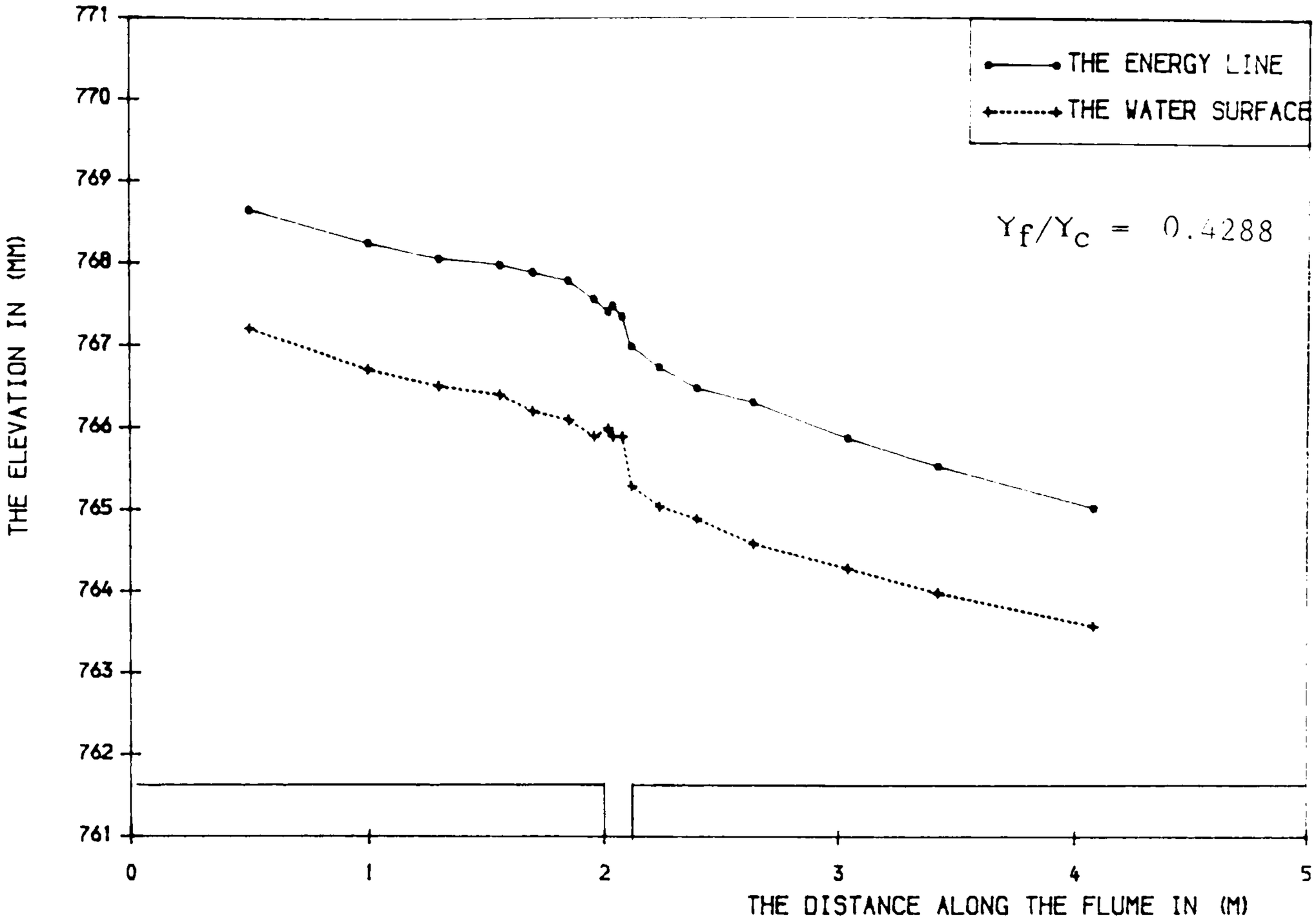

FIG (6.23) THE ENERGY LINE AND THE WATER-LEVEL IN (MM) ALONG THE FLUME WITH THE SLOT (Bs/hs=2).

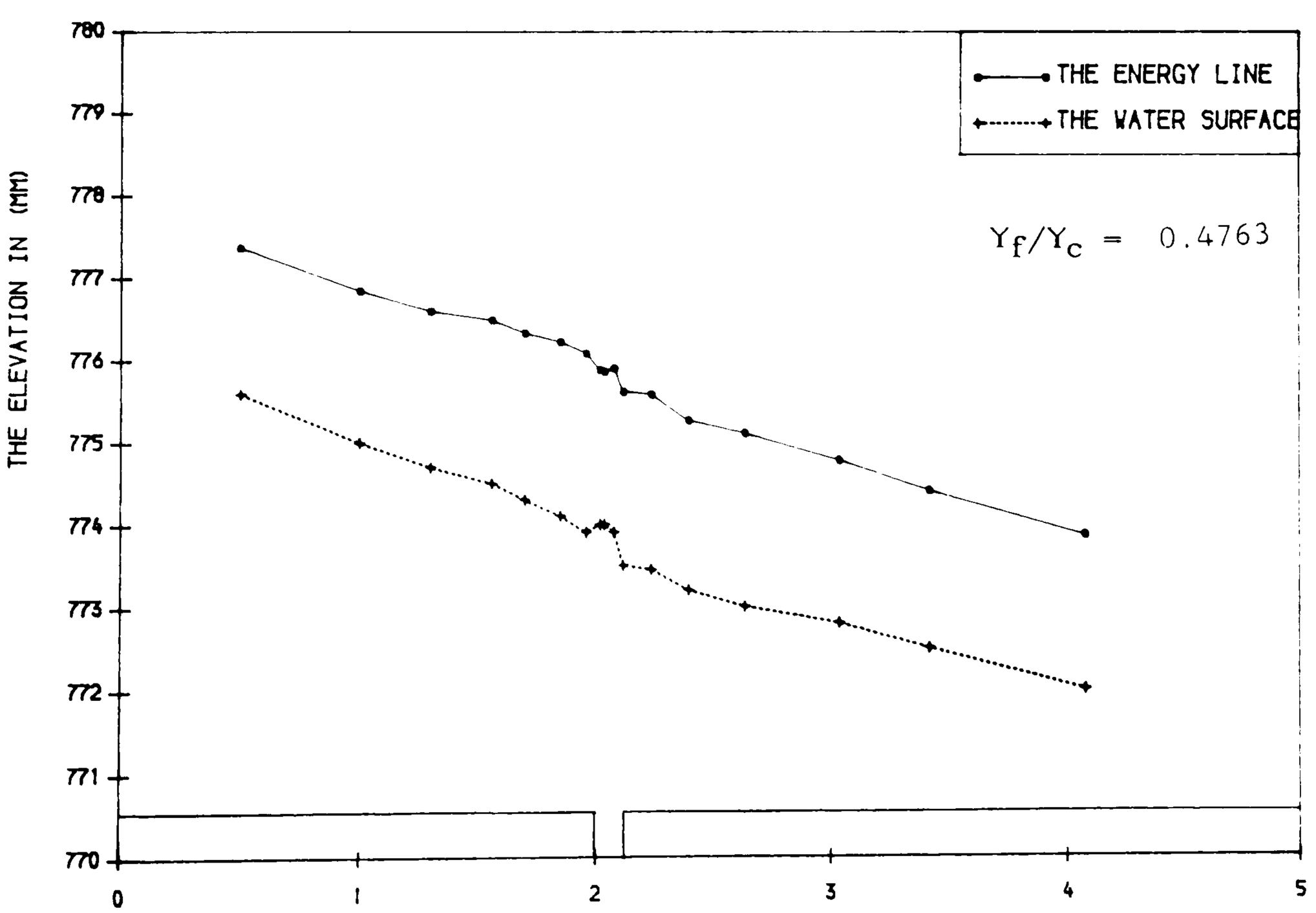

FIG (6.24) THE ENERGY LINE AND THE WATER-LEVEL IN (MM) ALONG THE FLUME WITH THE SLOT (Bs/hs=2).

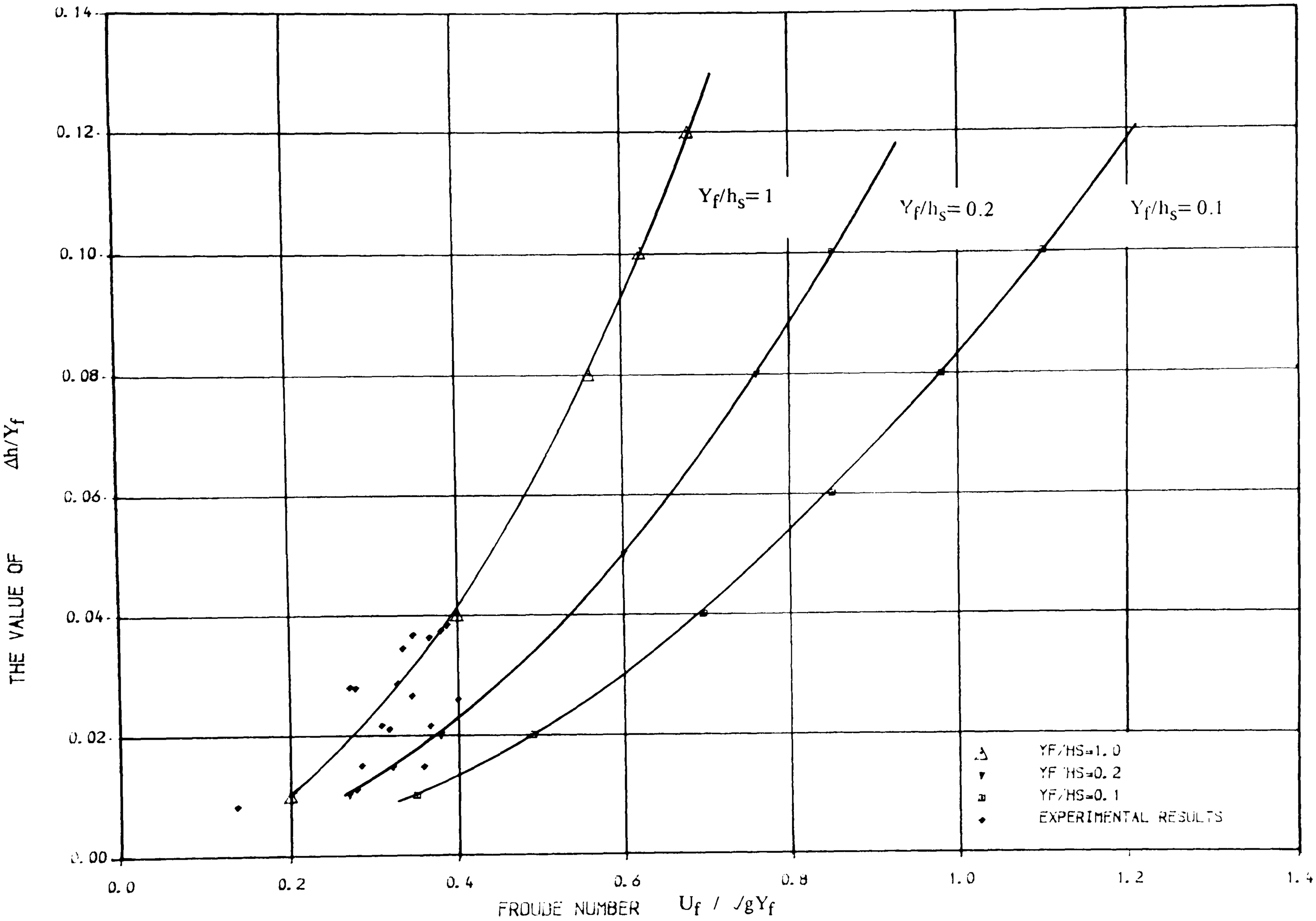

FIG (6.25) THE RELATIONSHIP BETWEEN FROUDE NUMBER ON FLOOD PLAIN AND

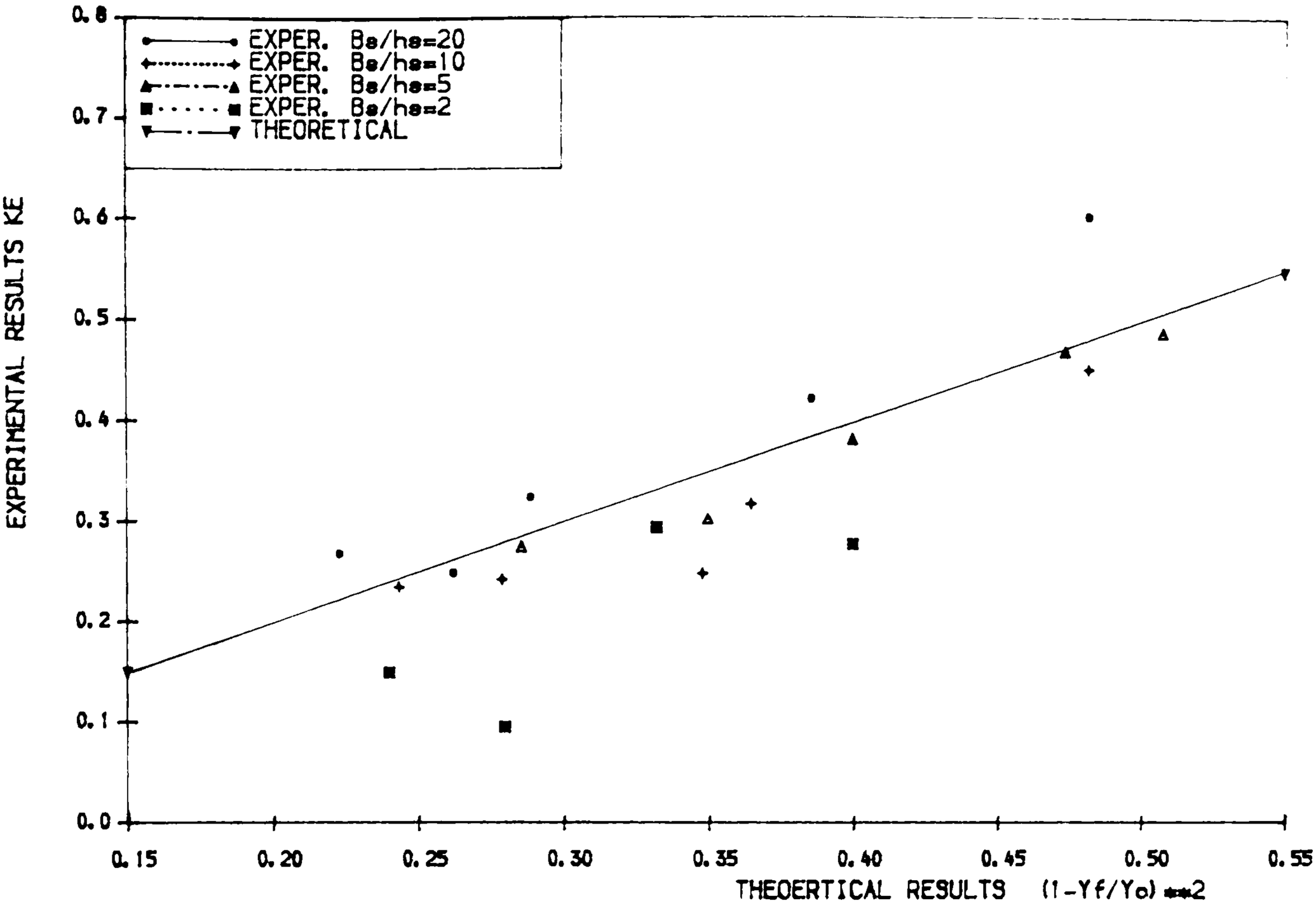

FIG(6.26) THE RELATIONSHIP OF THE EXPANSION LOSS BETWEEN THE EXPERIMENTAL AND THEORETICAL RESULTS.

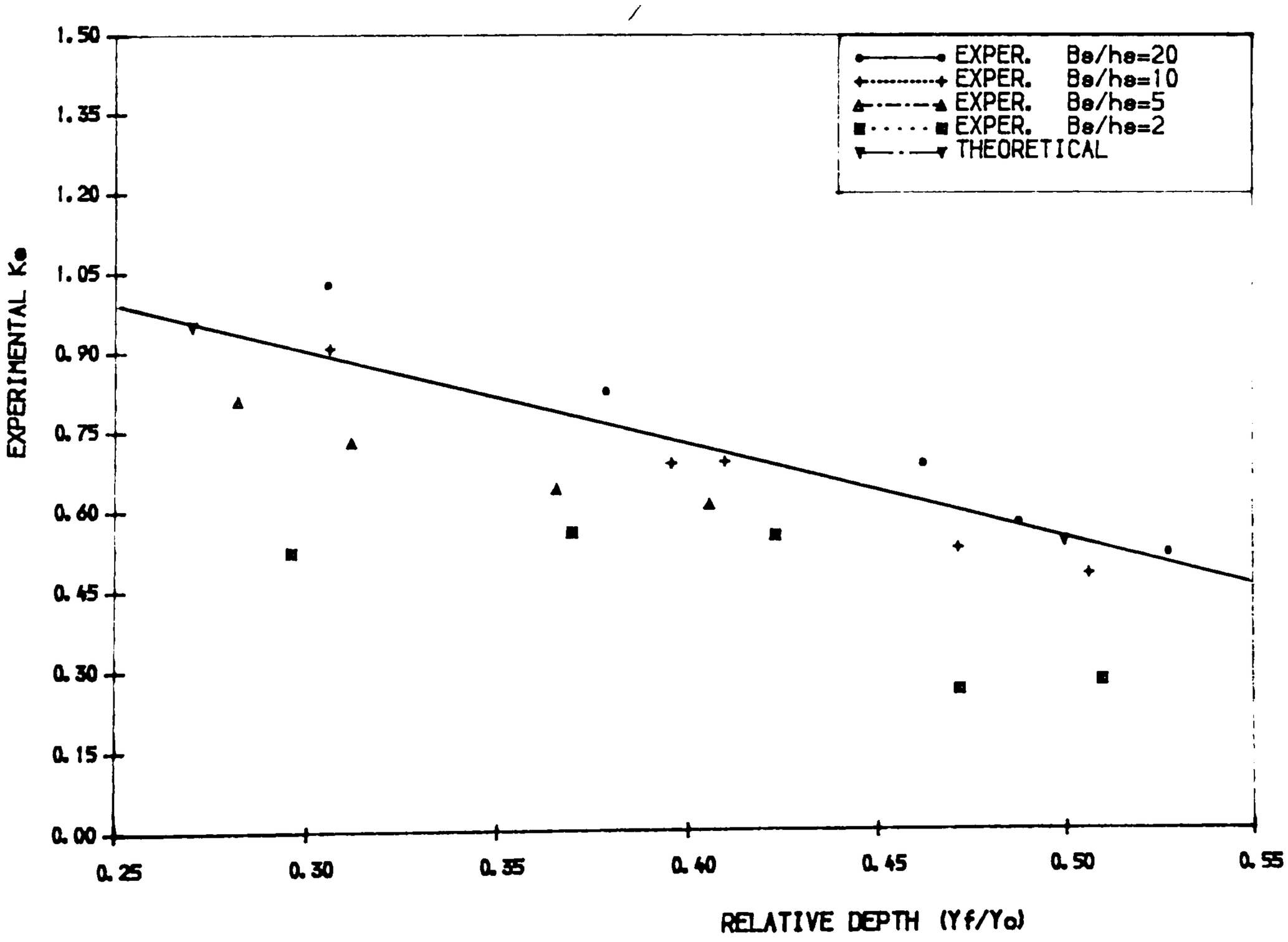

FIG(6.27) THE TOTAL ENERGY LOSS OVER A SLOT.

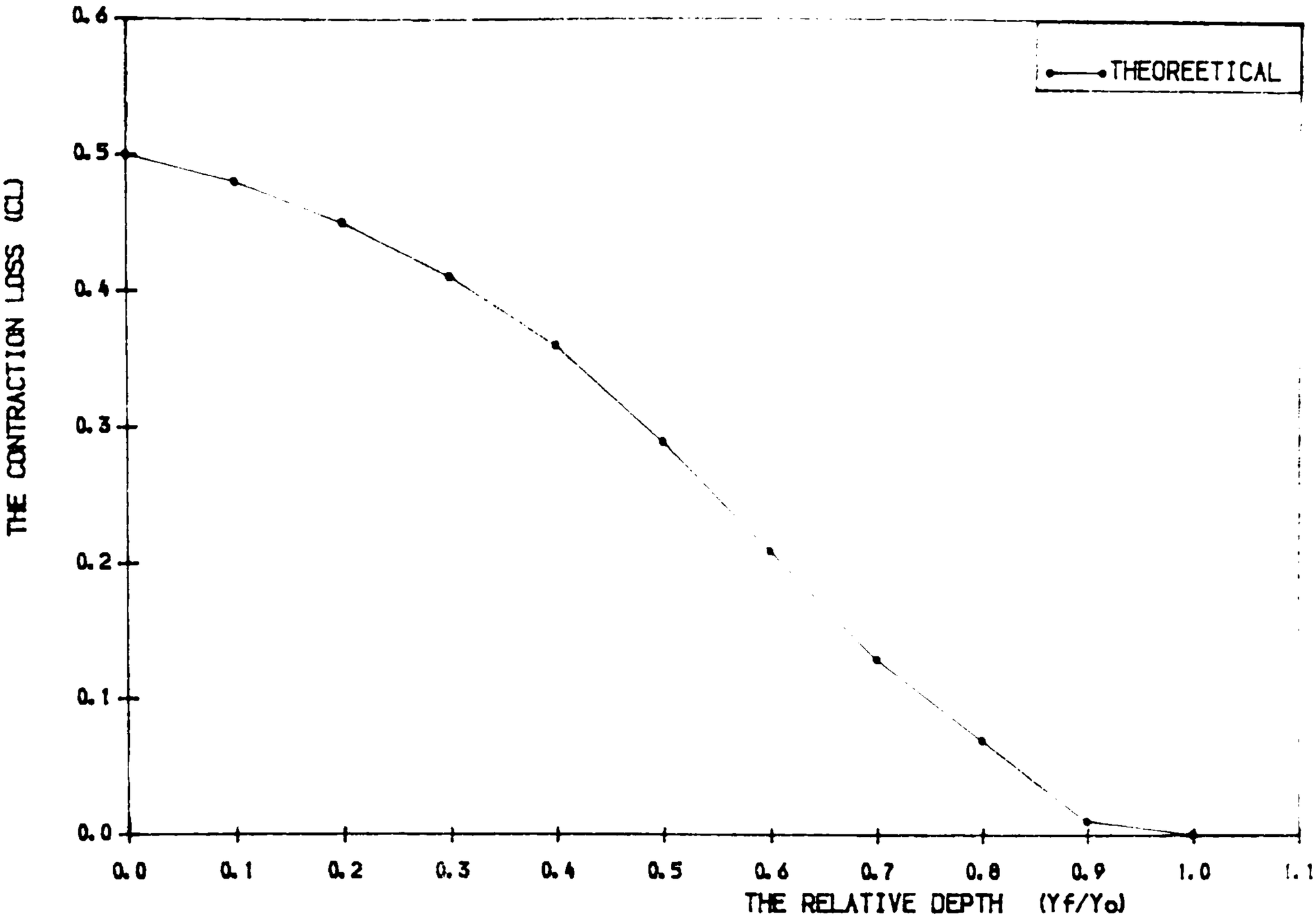

FIG(6.28) THE RELATIONSHIP BETWEEN THE CONTRACTION LOSS AND RELATIVE DEPTH (Yf/Yc)

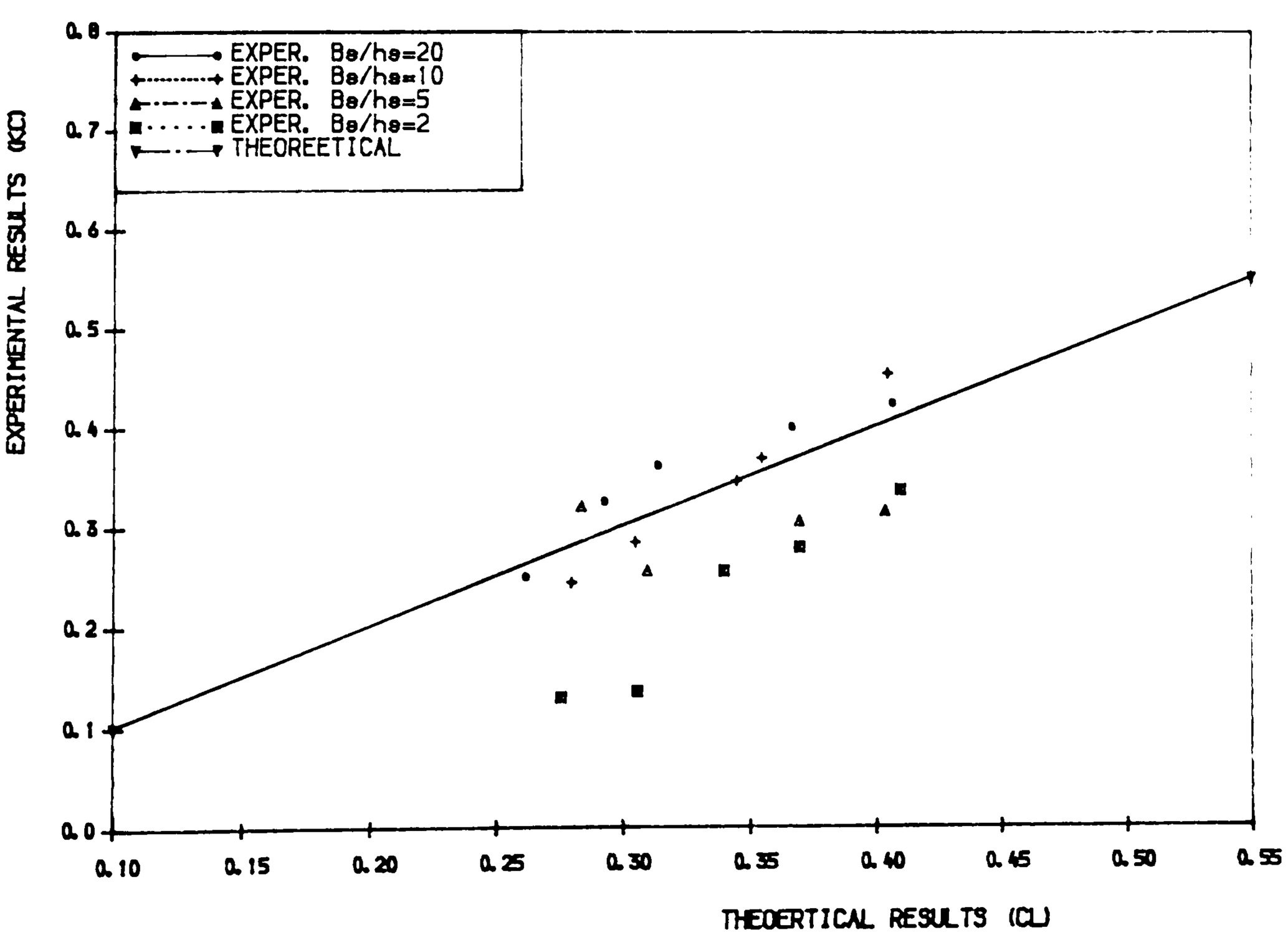

FIG(6.29) THE RELATIONSHIP OF THE CONTRACTION LOSS BETWEEN THE EXPERIMENTAL AND THEOERTICAL RESULTS.

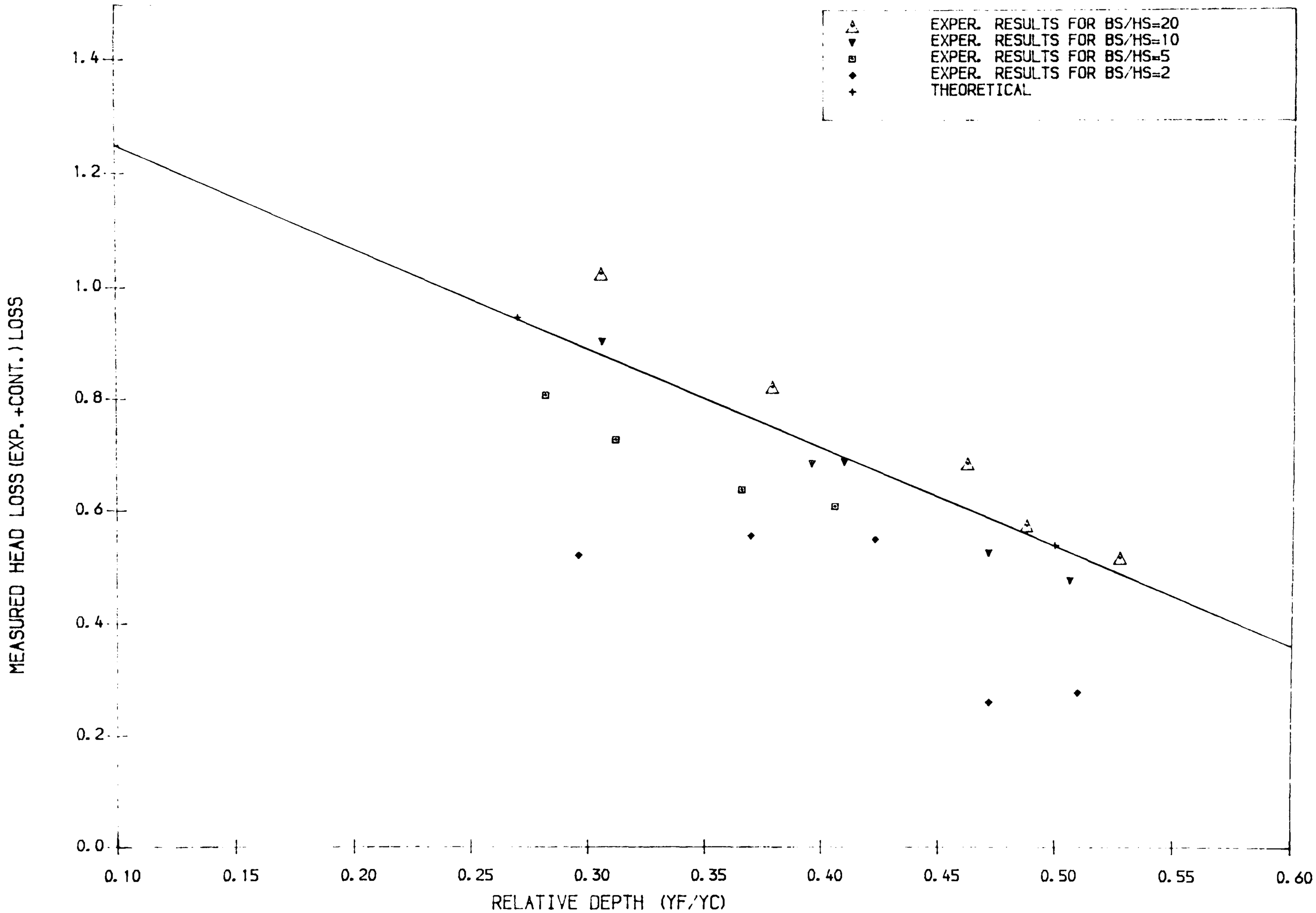

FIG (6.30) TOTAL ENERGY LOSS FOR FLOW OVER A SLOT.

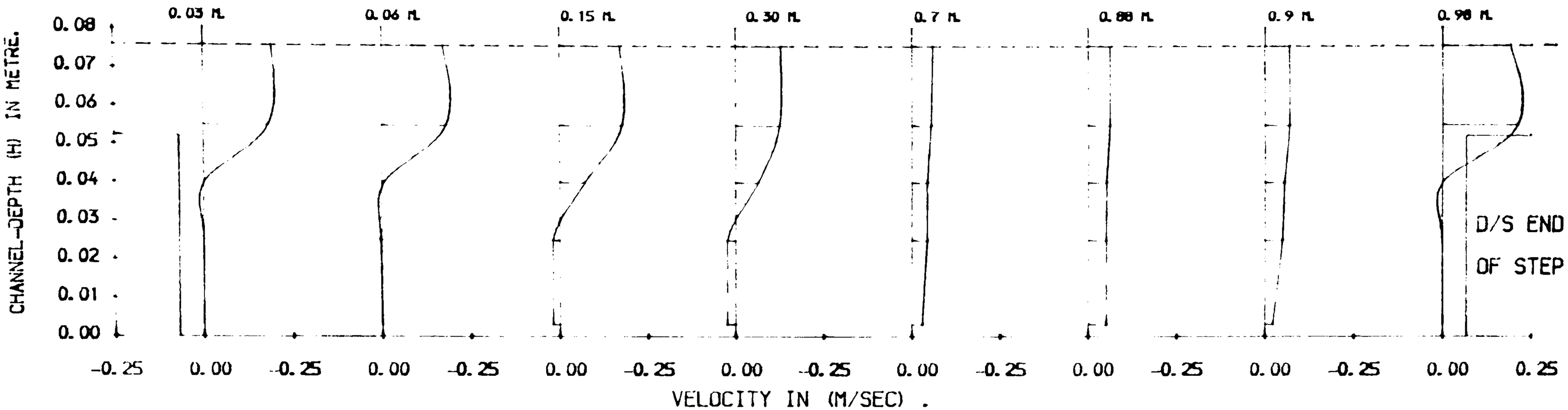

FIG(6.31) THE VELOCITY PROFILE THROUGH THE SLOT (Bs/hs=20)

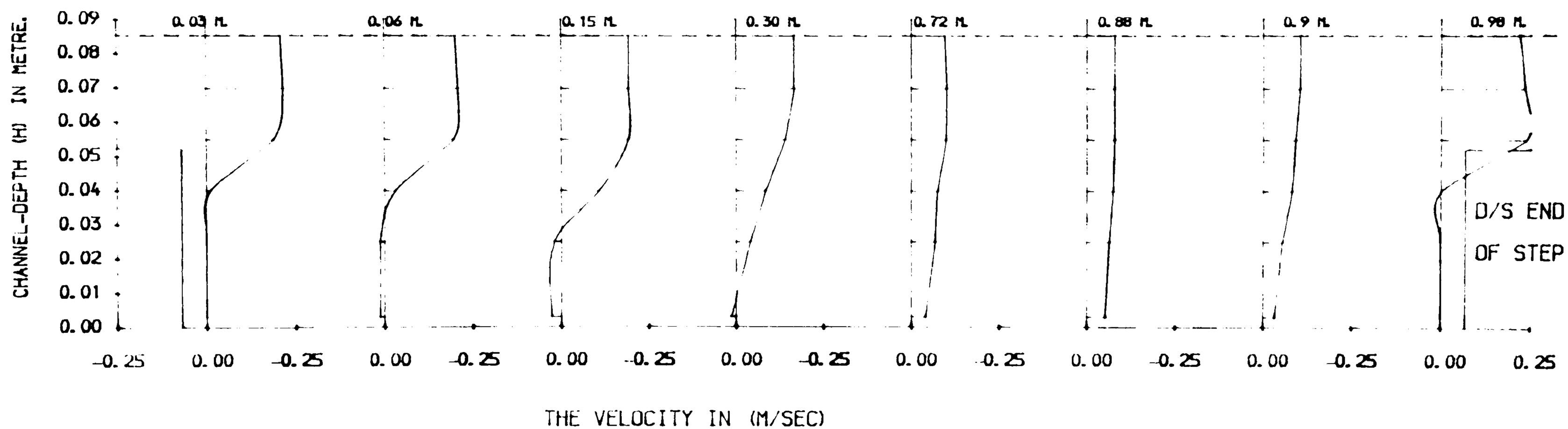

FIG(6.32) THE VELOCITY PROFILE THROUGH THE SLOT (Bs/hs=20)

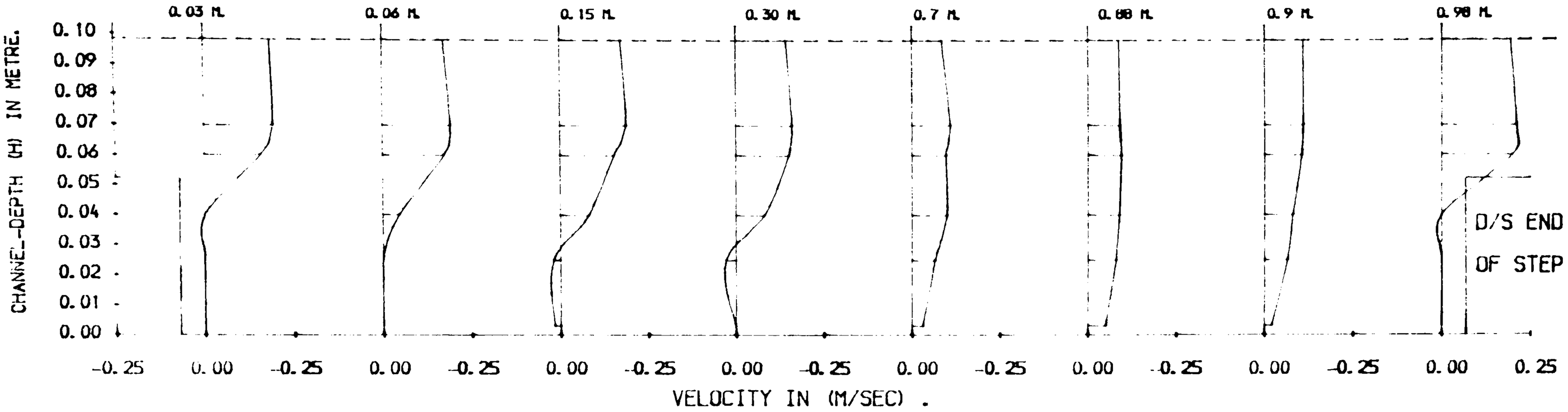

FIG (6.33) THE VELOCITY PROFILE THROUGH THE SLOT (Bs/hs=20)

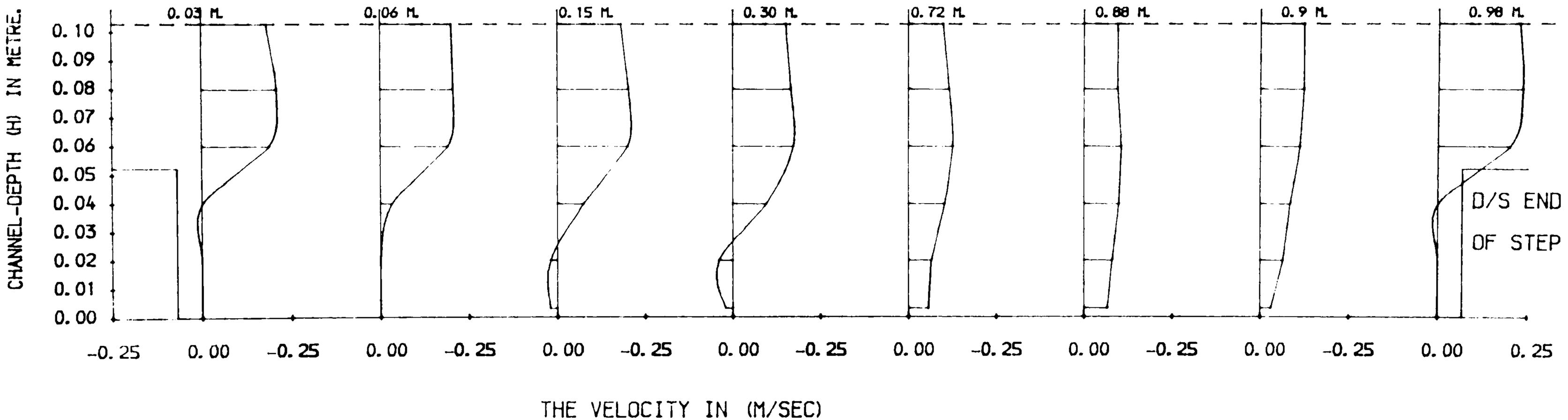

FIG (6.34) THE VELOCITY PROFILE THROUGH THE SLOT (Bs/hs=20)

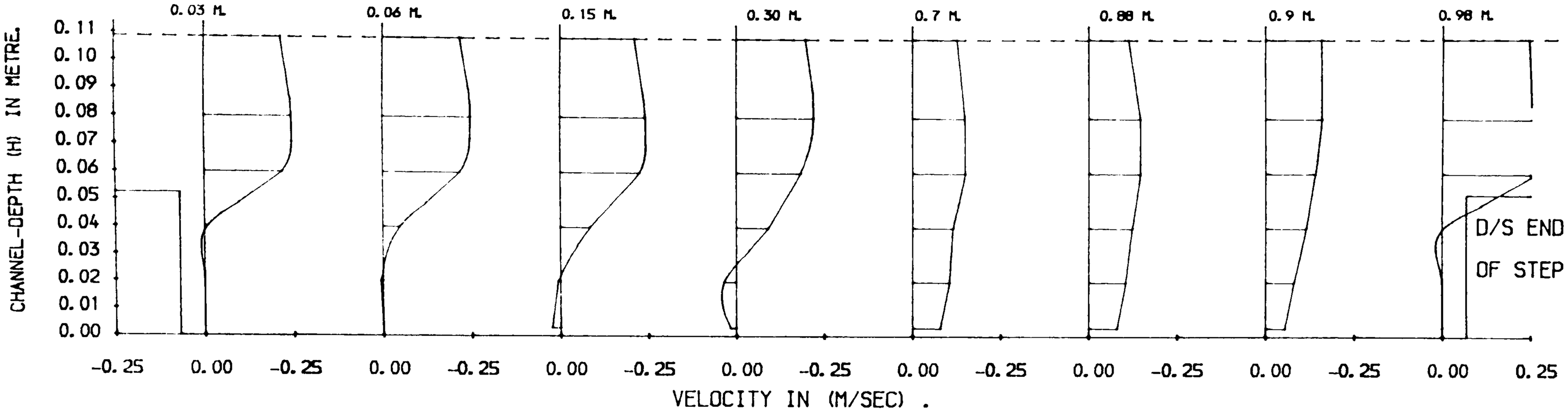

FIG(6.35) THE VELOCITY PROFILE THROUGH THE SLOT (Bs/hs=20)

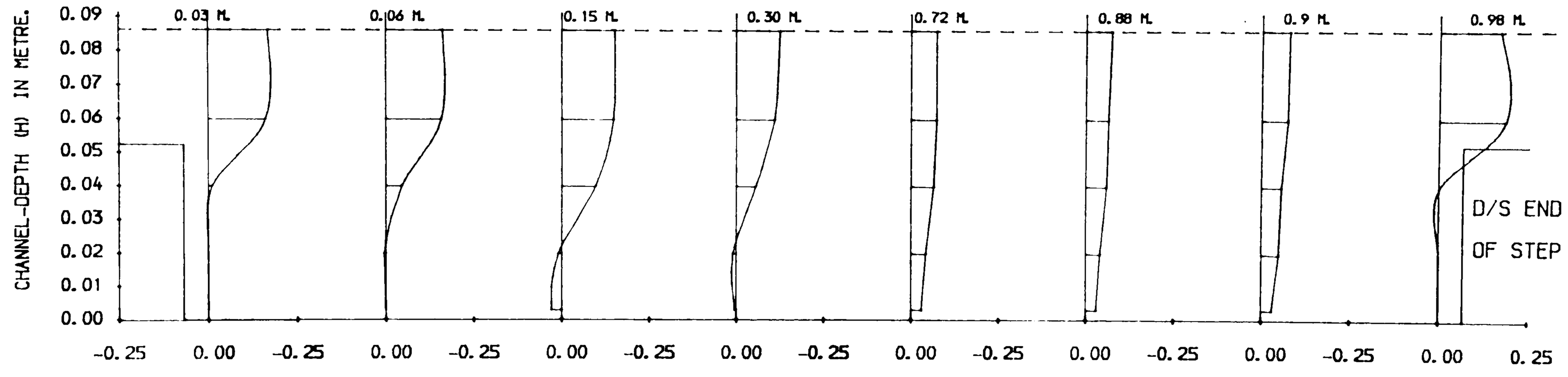

FIG(6.36) THE VELOCITY PROFILE THROUGH THE SLOT (Bs/hs=20)

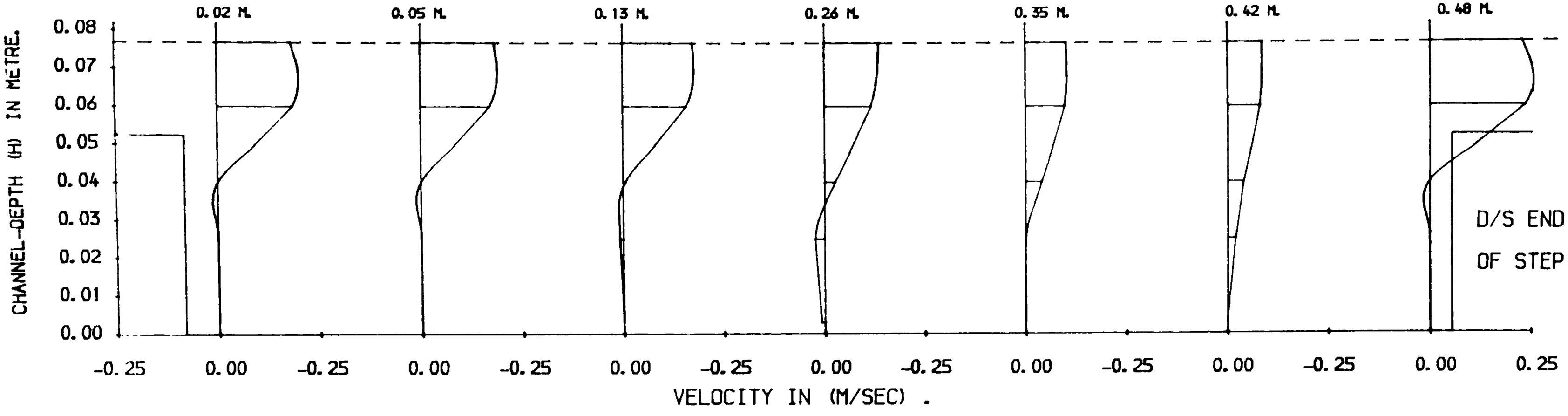

FIG (6.37) THE VELOCITY PROFILE THROUGH THE SLOT (B_s/h_s = 10)

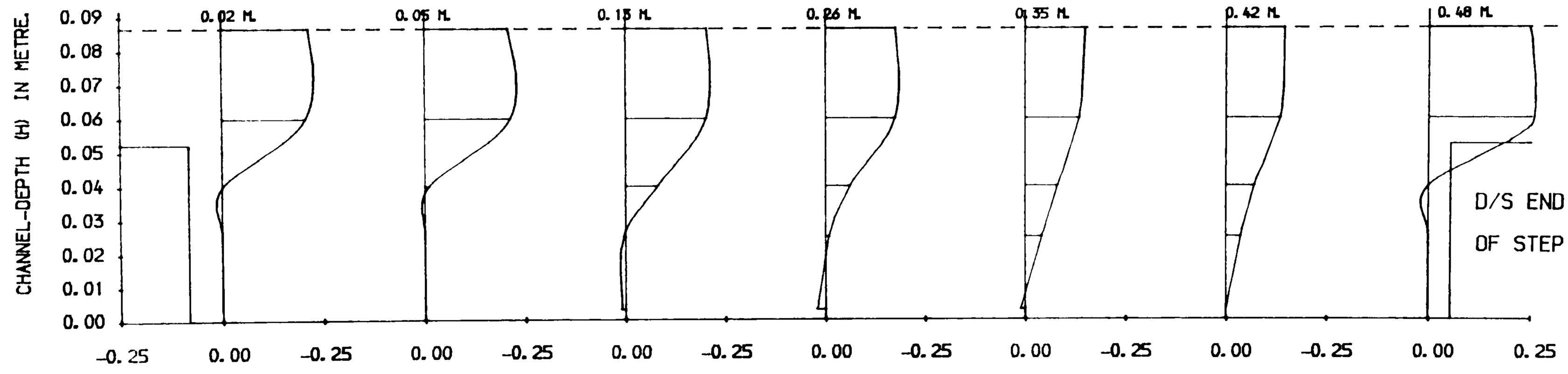

FIG (6.38) THE VELOCITY PROFILE THROUGH THE SLOT (B_s/h_s = 10)

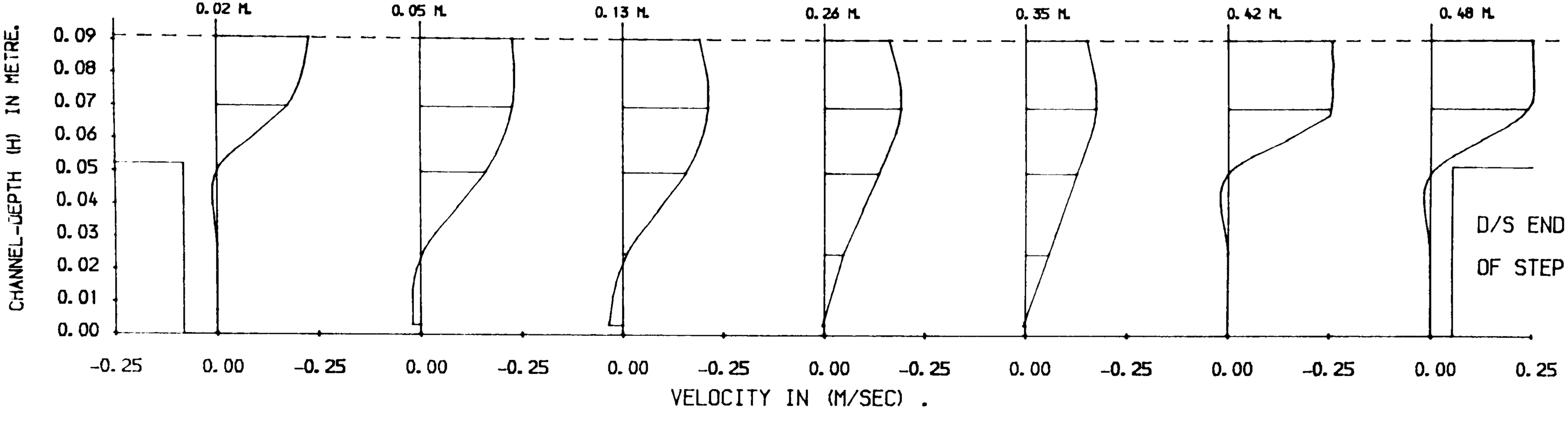

FIG (6.39) THE VELOCITY PROFILE THROUGH THE SLOT (B_s/h_s = 10)

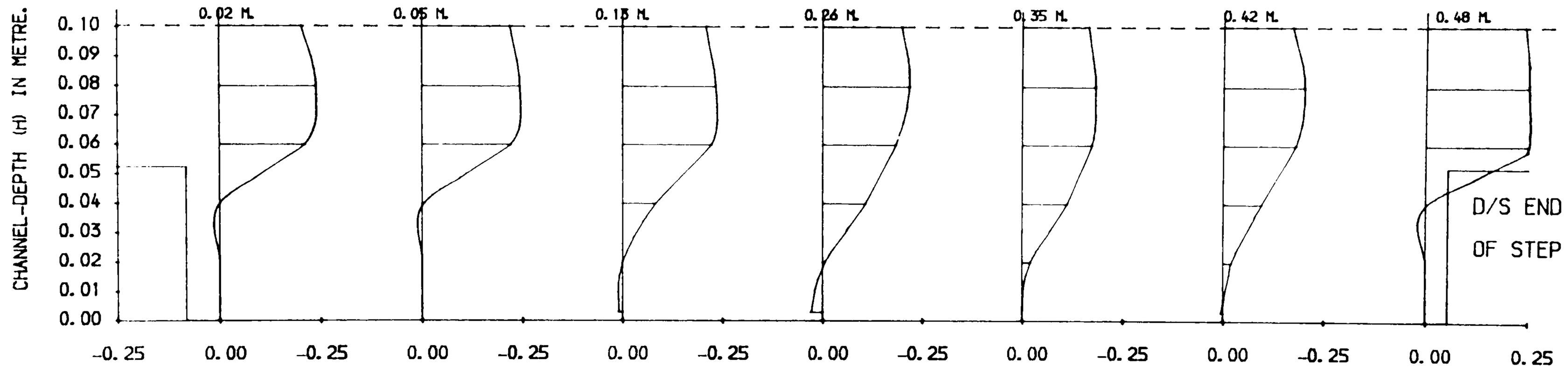

FIG (6.40) THE VELOCITY PROFILE THROUGH THE SLOT (B_s/h_s = 10)

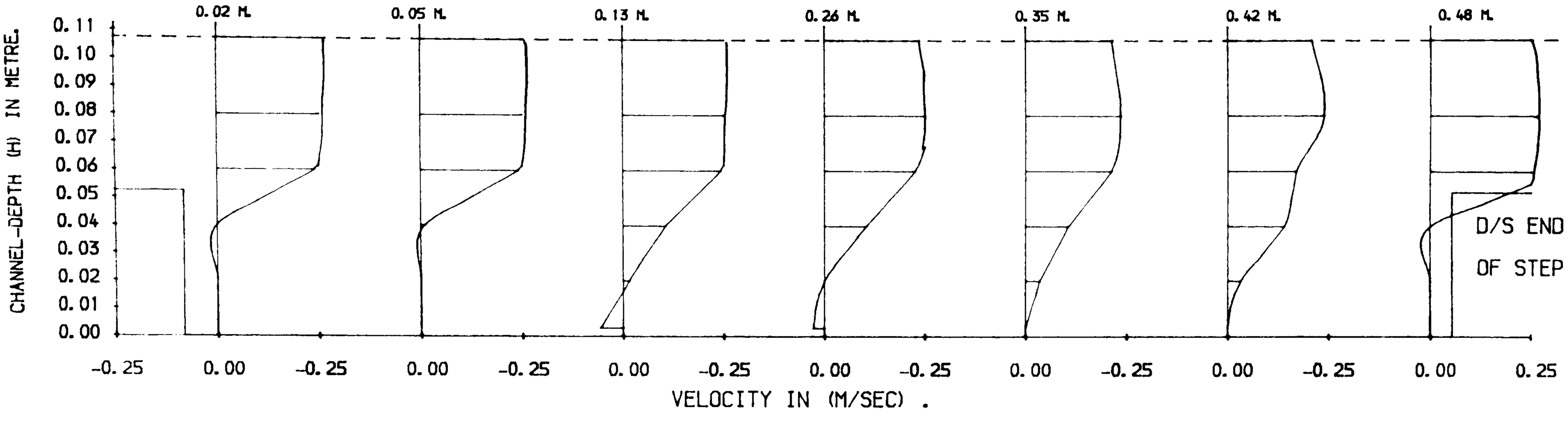

FIG (6.41) THE VELOCITY PROFILE THROUGH THE SLOT (B_s/h_s = 10)

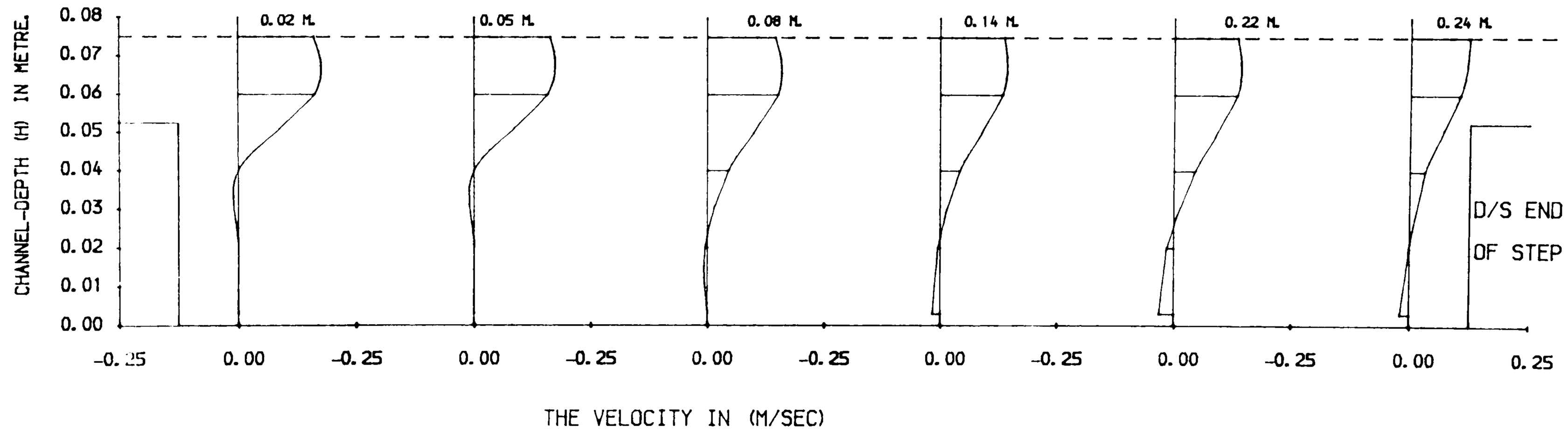

FIG (6.42) THE VELOCITY PROFILE THROUGH THE SLOT (B_s/h_s = 5)

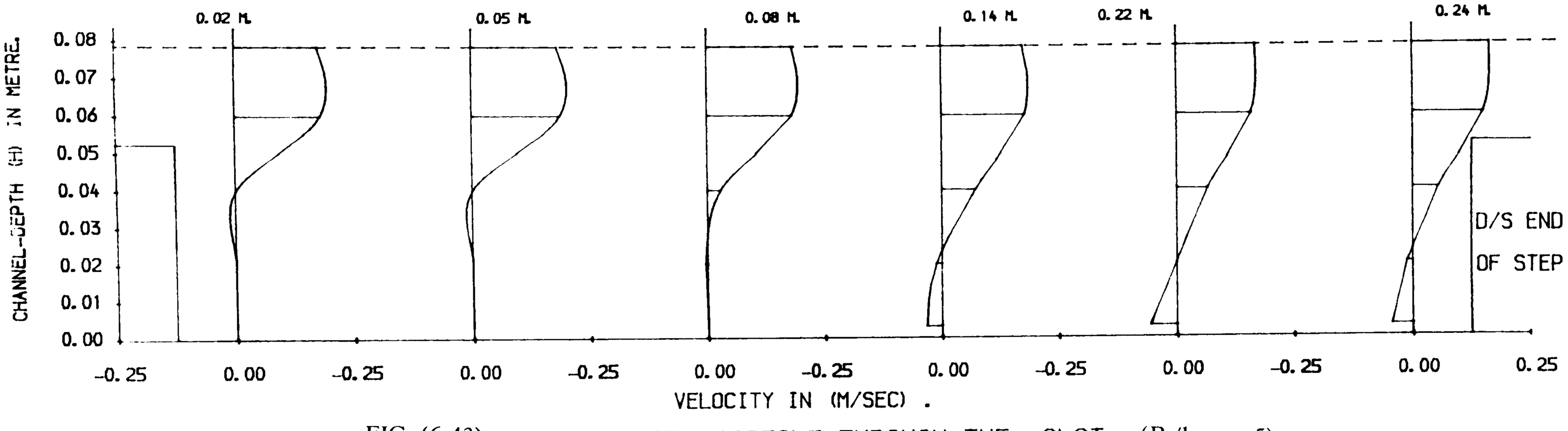

FIG (6.43) THE VELOCITY PROFILE THROUGH THE SLOT (B_s/h_s = 5)

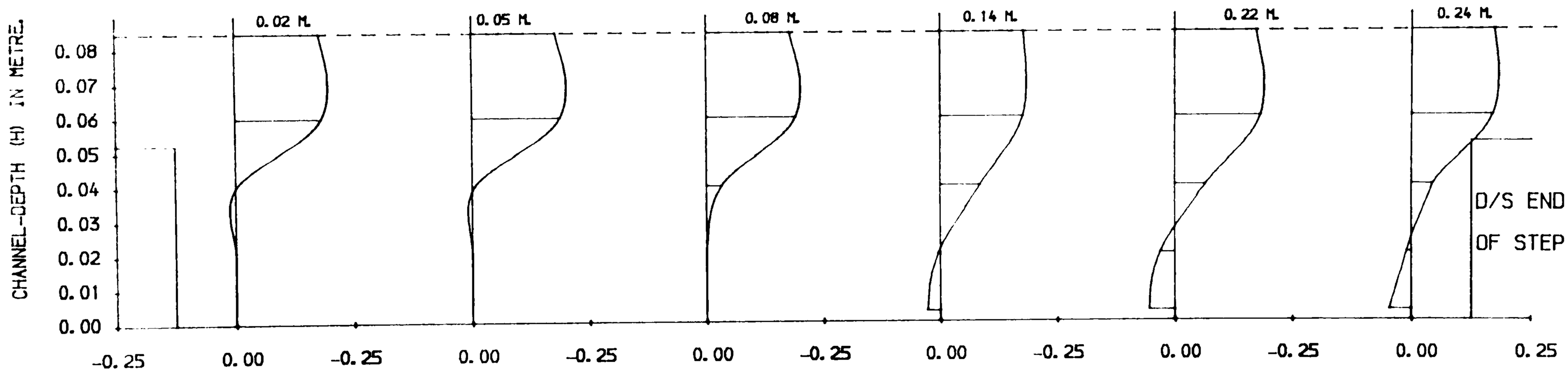

FIG (6.44) THE VELOCITY PROFILE THROUGH THE SLOT (B_s/h_s = 5)

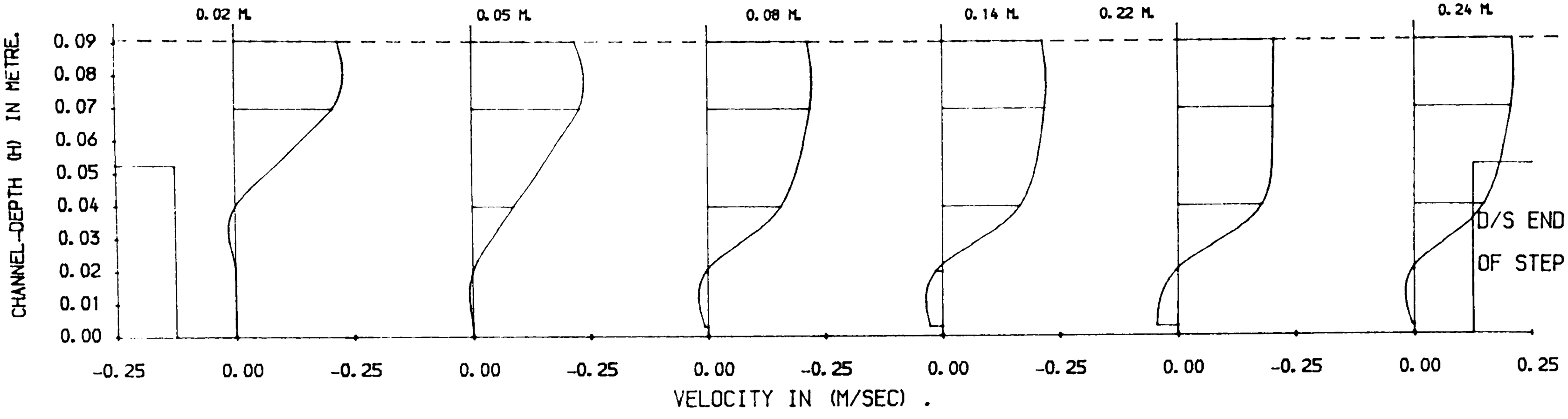

FIG (6.45) THE VELOCITY PROFILE THROUGH THE SLOT (B_s/h_s = 5)

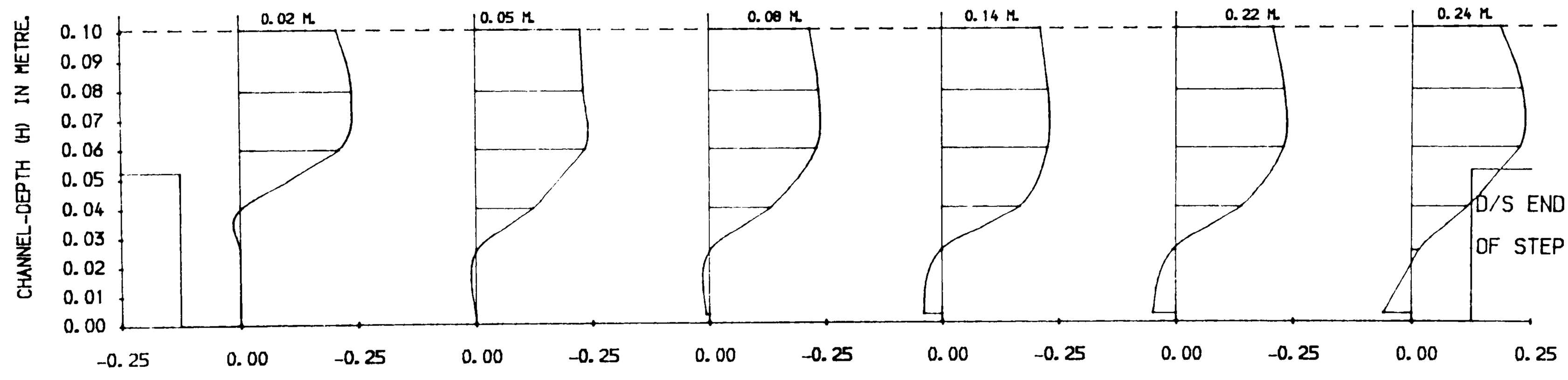

FIG (6.46) THE VELOCITY PROFILE THROUGH THE SLOT (B_s/h_s = 5)

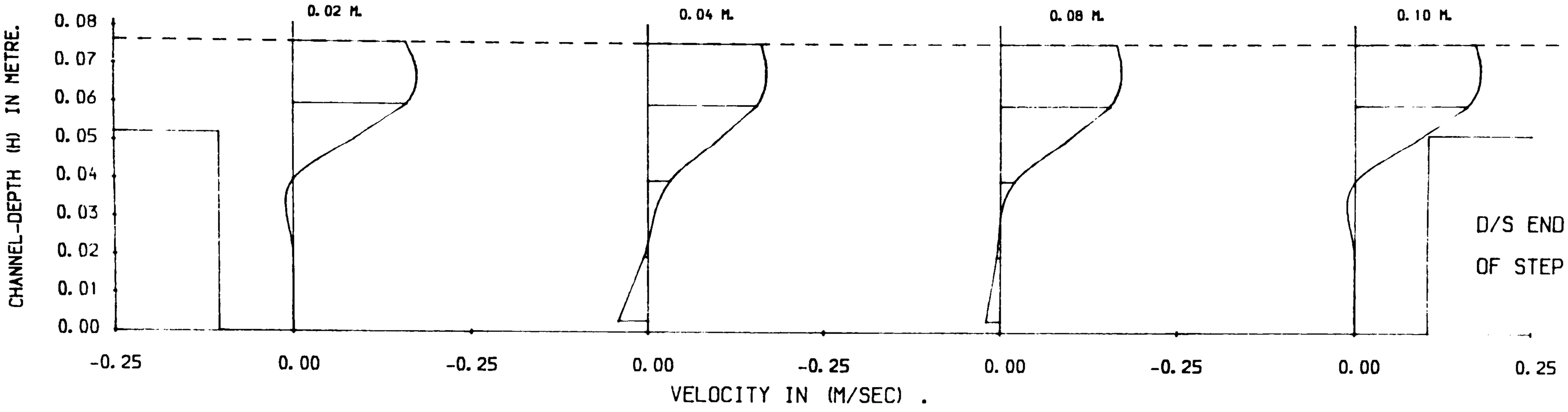

FIG (6.47) THE VELOCITY PROFILE THROUGH THE SLOT $(B_s/h_s = 2)$

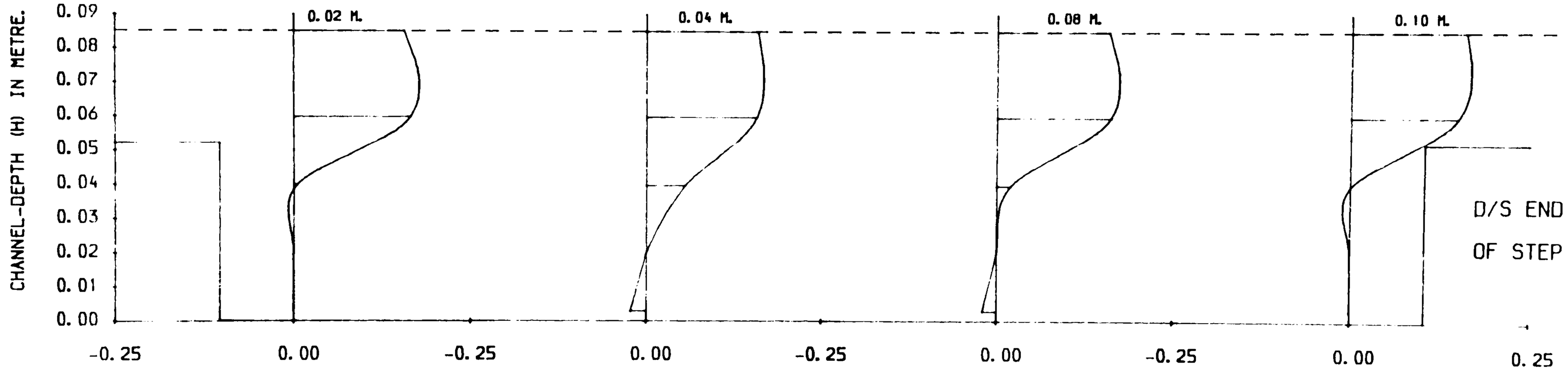

FIG (6.48) THE VELOCITY PROFILE THROUGH THE SLOT $(B_s/h_s = 2)$

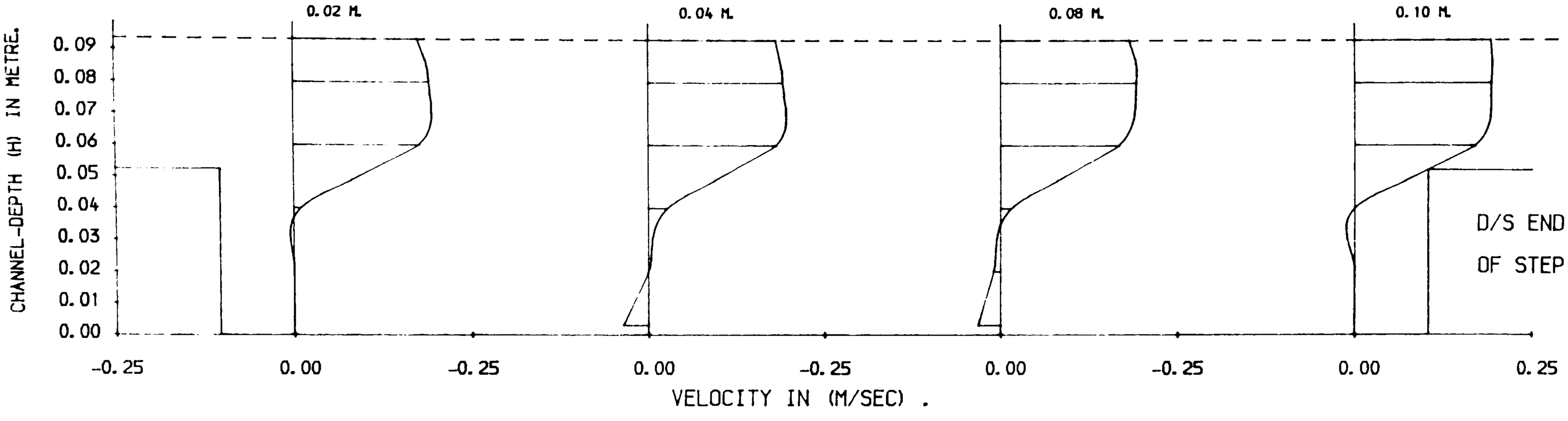

FIG (6.49) THE VELOCITY PROFILE THROUGH THE SLOT ($B_s/h_s = 2$)

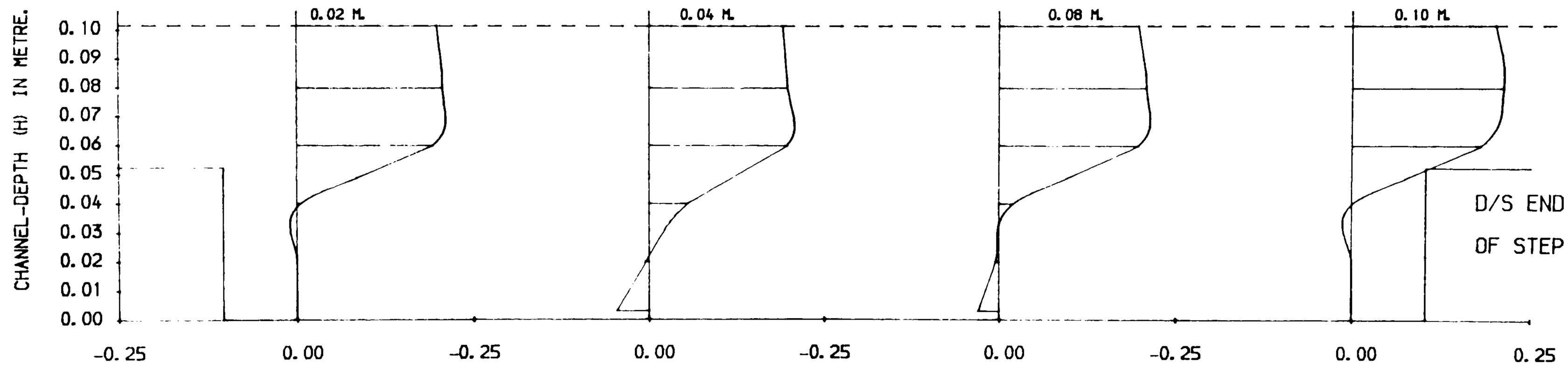

FIG (6.50) THE VELOCITY PROFILE THROUGH THE SLOT ($Bs/h_s = 2$)

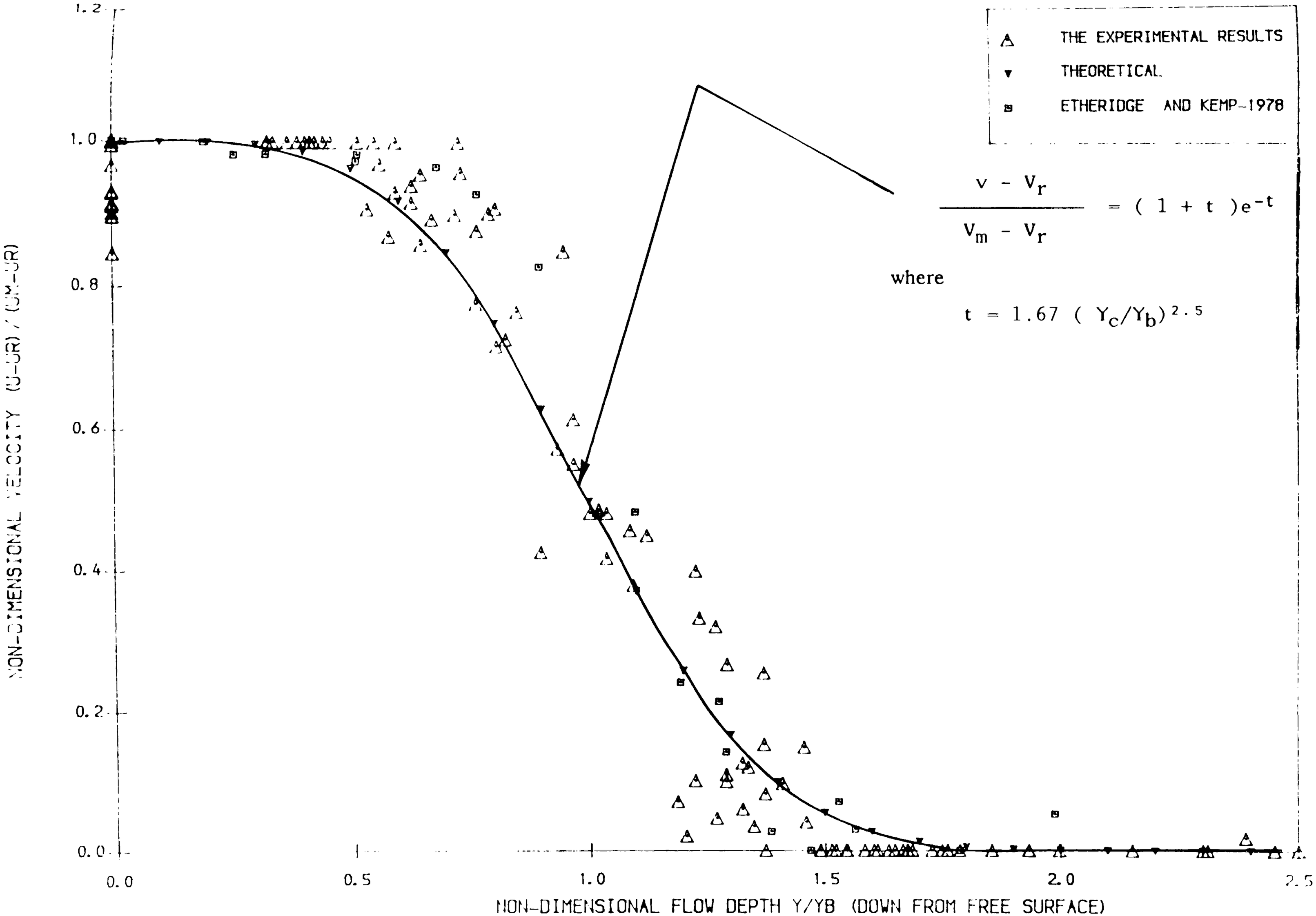

FIG (6.51) UNIVERSAL VELOCITY PROFILE IN THE SUDDEN EXPANSION REGION (BS/HS=10)

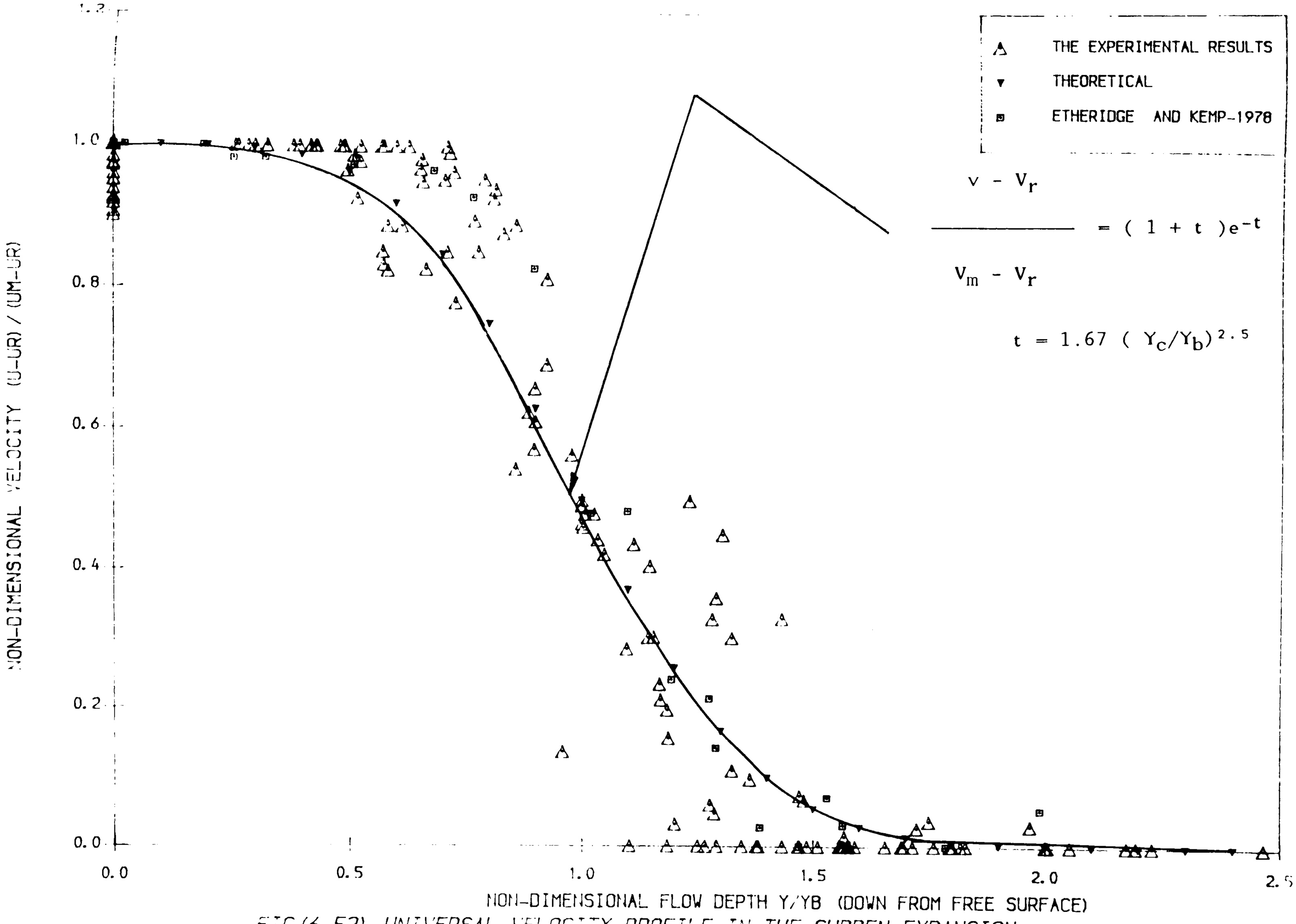

FIG (6.52) UNIVERSAL VELOCITY PROFILE IN THE SUDDEN EXPANSION REGION (BS/HS=2.0)

CHAPTER 7

ASPECTS OF THE FLOE BEHAVIOUR OF SKEWED TWO-STAGE CHANNELS

7.1 INTRODUCTION

7.2 DISCHARGE ASSESSMENT IN SKEWED TWO-STAGE CHANNELS WITH SMOOTH BOUNDARIES

7.2.1 Background

7.2.2 Errors in Discharge Assessment in the Skewed Channel

7.2.3 A Broader Picture of Discharge Assessment Errors.

7.3 DISCHARGE ASSESSEMENT IN SKEWED TWO STAGE CHANNELS WITH ROUGH FLOOD PLAIN

7.4 FLOW RESISTANCE FUNCTIONS FOR SKEWED TWO-STAGE CHANNELS

7.5 DEVIATION OF FLOOD PLAIN STREAMLINES DOWN INTO SKEWED MAIN CHANNEL

7.6 BIFRUCATION OF FLOOD PLAIN STREAMLINE DOWN INTO SKEWED MAIN CHANNEL

7.7 TRANSVERSE RECIRCULATION FLOW PATTERNS WITHIN THE MAIN CHANNEL.

7.7.1 Introduction

7.7.2 Experimental Evidence

7.7.3 Theoretical Background to Recirculations at a Channel Step

7.7.4 Conclusions on Circulating Flows in The Skewed Main Channel

7.8 DEPTH–AVERAGED LONGITUDINAL VELOCITIES IN A SKEWED TWO–STAGE CHANNEL

7.8.1 Depth Averaged Velocity Profile

7.8.2 Maximum Velocity Filament

7.8.3 Width of Lateral Shear Layers

7.8.4 Variations in Velocity in Each Sub–Sections of the Flow in the Downstream Direction

7.9 APPLICATIONS TO THE DESIGN OF TWO–STAGE CHANNELS

7.10 LONG TERM BEHAVIOUR OF TWO–STAGE CHANNELS

CHAPTER 7

ASPECTS OF THE FLOW BEHAVIOUR OF SKEWED TWO–STAGE CHANNELS

7.1 INTRODUCTION

Chapter 7 investigates ten ideas or points of interest in the flow behaviour of skewed two–stage channels, based primarily on experimental evidence presented in chapters 4 to 6, as well as background evidence from meandering and other skewed channel studies carried out elsewhere.

The ten points of interest are outlined below, and are in most cases, new observations which will be helpfull in the design of two–stage channels and in predicting the long term behaviour of the two–stage channels. The ten points of interest will also be of benefit in assessing the validity of two–dimensional numerical models with their many inherent assumtions.

It will be of interest to note that the data set presented in chapter 5 of this thesis is at present being used to compare the effectiveness of finite element models with finite different models for the two–dimensional case.

(i) Discharge assessment in skewed two–stage channels with smooth flood plain roughness. The question posed in this section concern whether the stage–discharge relationship can be predicted with reasonable accuracy for a skewed geometry. This question may put in an alternative form as to whether the lateral shear, as well as horizontal shear, can be combined with frictional shear to provide an accurate assessment of the overall energy loss.

(ii) Discharge assessment in skewed two–stage channels with rough flood plain roughness. This concerns an analysis of the series D tests where the flood plain roughness was two to four times greater than the main channel roughness. The analysis in this section deals with the stage–discharge prediction for the rough flood plain case. Is lateral turbulent shear still important is horizontal turbulent shear still important, or is the whole flow regime dominated by flood plain roughness, including the main channel flow with its smooth boundary?

(iii) Flow resistance functions. A classical method of representing resistance to flow is given by the friction factor– Reynolds Number diagram ($\lambda - R_e$). This section reveals how skewed compound channels fit into the $\lambda - R_e$ diagram and how this compared with straight– parallel compound channels as well as meandering channels.

(iv) Deviation of streamlines as the flood plain flow passes over the main channel below. Detailed measurements of streamline direction were carried out using an angular measurement transducer. This enabled estimates of the mean deviation angle of the flood plain streamlines as they passed over the skewed main channel. This section reveals the influence of increasing flood plain flow depth on the deviation angle of streamlines. It investigates the influence of the flood plain roughness of streamline deviation and discusses the implication for two– stage channel behaviour.

(v) Bifrucation of flood plain streamlines down into the skewed main channel. Dye tests reveal that streamlines near the right flood plain floor get dragged down into the main channel spiral, moving off in the direction of the skew rather than crossing over directly to the opposite flood plain. This section deals with the mechanism, and the implications of this type of flow behaviour.

(vi) Recirculating transverse velocity components in the skewed main channel. This section will deal with the magnitude of the swirl velocities in the skewed main channel and will offer evidence that the swirl is caused by flood plain flow shearing over the main channel flow. It will compare recirculating velocities with those of the slot tests. It will compare recirculating velocities between the smooth and rough flood plain cases, and will offer a theoretical explanation for the difference between the rough and the smooth cases.

(vii) The depth– averaged longitudinal velocity in skewed compound channels. This section investigates the specific characterstics of the depth– averaged velocity profiles both for the smooth and rough flood plain cases. This includes a comparsion of the flood plain velocities on the left (expanding) flood plain compared with the right (contracting) flood plain. It includes an investigation of the position of the maximum velocity filament as well as the width of the lateral shear layers on the left and right floodplains. The purpose of this section is to highlight differences in behaviour compared with a straight/parallel compound

channel and to provide pointers to the long term behaviour of two–stage channels.

(viii) Varations in flow development along the flume. The results in this thesis were taken at three different cross–sections along the length of the flume. The purpose of this was to provide some ideas on flow development along the channel length. This includes variations in velocity on the left and right flood plains as well as the main channel, as we move downstream. It also includes variations in shear layer width and position of the maximum velocity filament as we move downstream. Variations in transverse velocity components are also noted.

(ix) Application of the results to the design of two–stage channel.
The results and ideas expressed in parts (i) to (viii) above are brought together to offer guidance and advice on the design of two–stage channels.

(x) Application of the results to the long–term behaviour patterns of two–stage channels. A two–stage channel is designed by cutting out side berms and hence allowing more flow and flood events to use the side berms. Most sediment is transported during floods so are the side berms simply going to silt–up with time?' Is deposition going to be uneven on the side berms developing a kind of braided two–stage channel?

7.2 DISCHARGE ASSESSMENT IN SKEWED TWO–STAGE CHANNELS WITH SMOOTH BOUNDARIES

7.2.1 Background

The conventional text book method of discharge assessment in the compound cross section is to place imaginary walls vertically at the main channel/flood plain junction. The discharge in each sub–section of the flow is then estimated from a knowledge of the boundary roughness of each sub–section (Mannings 'n' value) using Mannings equation with the total discharge being the sum of the parts. The immaginary walls are considered to have zero friction.

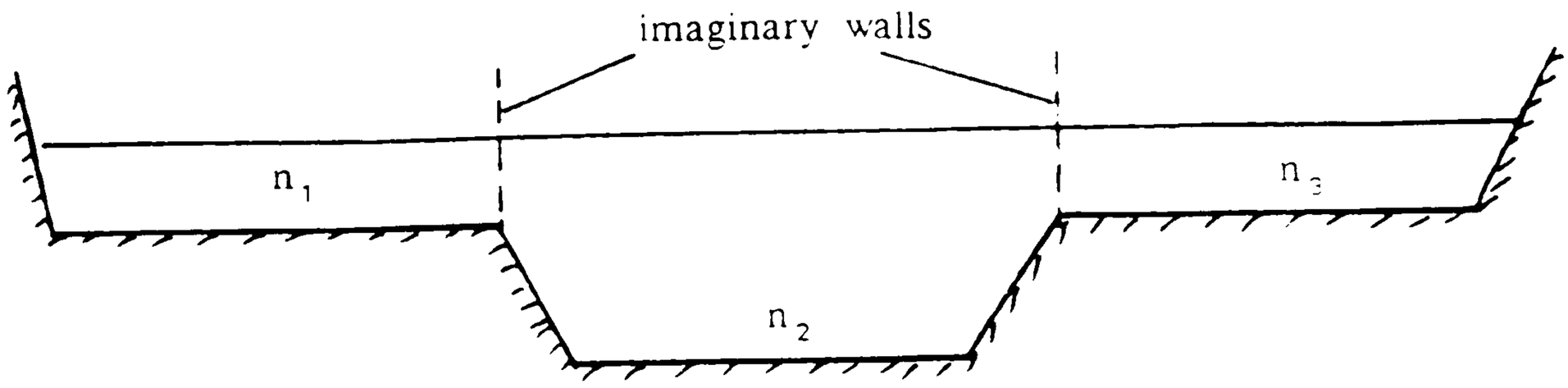

This method involves error in the estimated discharge primarily because it ignores lateral shear between faster moving sections and lower moving sections. This lateral turbulent shear transfers momentum usually to the flood plain and errors in discharge assessment can be up to 25% for the simplest case of a straight/parrallel flood plain.

The problem of inclusion of lateral shear has now been overcome for the case of a straight and parrallel channel and flood plain where the flow is all in the longitudinal direction, there is no curvature in the flow and cross–over flows do not exist.

For steady uniform flow, the simplest equation is given by Wark et al (1988) in the form.

$$gDS_{xf} = \frac{B\lambda q|q|}{8D^2} + [\ \nu_t dq/dy\ ] = 0 \qquad (7.1)$$

where

$B = (1 + S^2_x + S^2_y)^{1/2}$ a factor relating stress on an inclined plane to stress on horizontal plane.

S_x, S_y are longitudinal and lateral channel bed slopes.

λ is the Darcy friction factor.

q is the longitudinal flow per unit width.

D is the flow depth.

ν_t is the lateral eddy viscosity, given in its simplest form for the case of turbulence dominated by bed friction as

$$\nu_t = \lambda\ u_*\ D \qquad (7.2)$$

where

λ is the non− dimensional lateral eddy viscosity.

u_* is the shear velocity $(\tau_0/\rho)^{1/2}$.

Wark has solved Equation (7.1) by an iterative method using Newtons method, with an initial seed solution putting $\nu_t = 0$ in Equation (7.1) and with a boundary condition of $q = 0$ at solid boundaries. Convergence is usually achieved within five iterations.

Equation (7.1) has been applied by Wark (1990) to seven U.K rivers with overbank flow, to the SERIES A data from the SERC flume at Wallingford, and also to smaller scale model studies such as that of Kiely (1989). The method has been very successful in cases that are primarily straight/parallel channel/floodplain systems.

What happens if there is a skew in the main channel relative to the flood plain is sketch below?

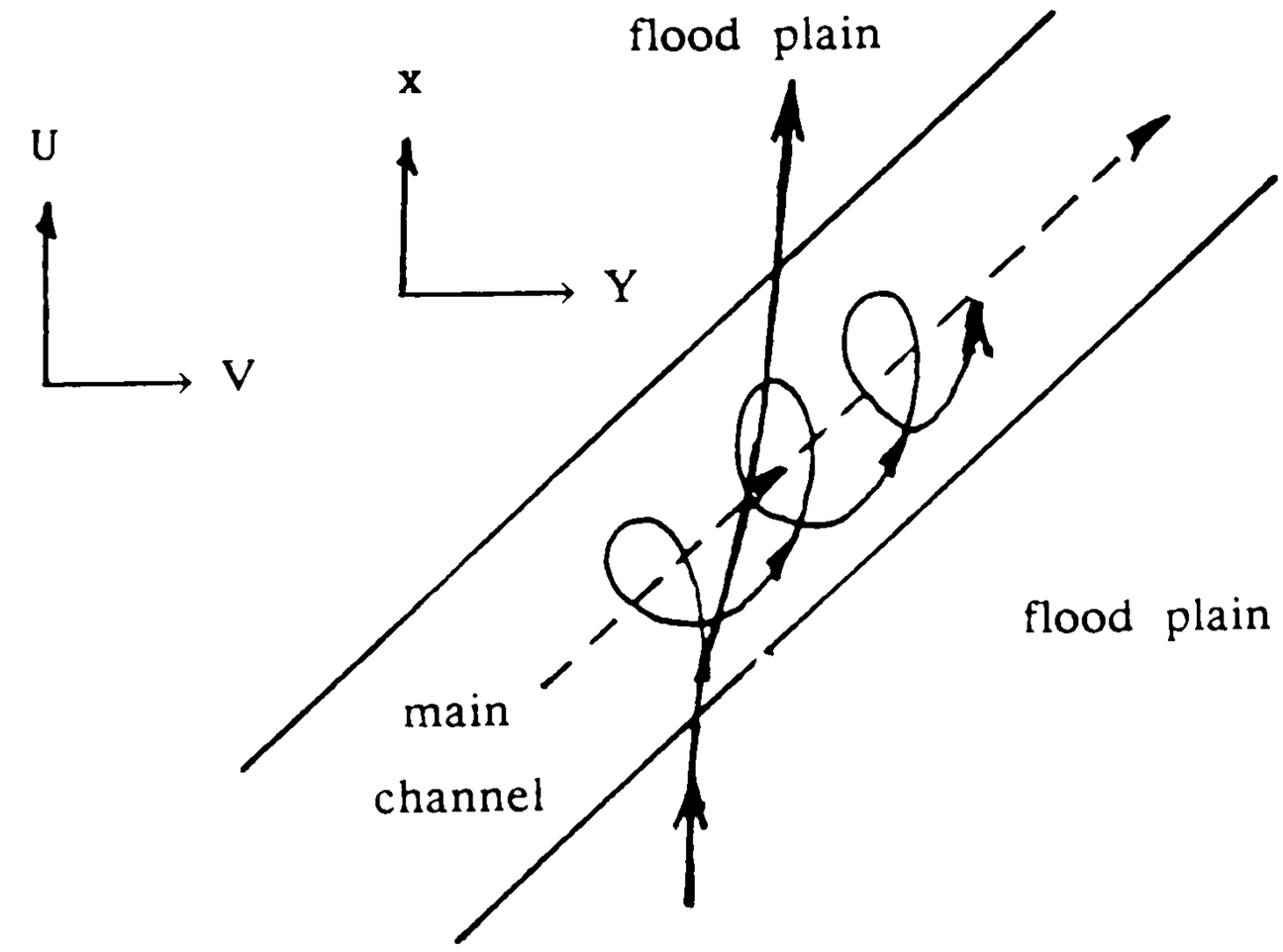

Equation 7.1 is no longer applicable in skewed flows for the following reasons.

(i) Large sections of the flow now have large lateral components of velocity V, so that the term vdu/dy for instance is not zero as in Equation 7.1.

(ii) Flood plain flow passing over the main channel will have an element of

convective deceleration and acceleration so that the term u du/dx is not zero as in Equation (7.1).

(iii) Equation 7.1 produces an estimate of the depth averaged velocity across the width of the main channel and flood plain. This means that the model is unable to pick–up horizontal shear where the flood plain flow passes over the main channel because everything is depth averaged. This means that lateral shear is included in equation (7.1) but horizontal shear is not.

(iv) Chapter 5 has revealed that strong secondary cells are generated in the skewed main channel, driven by flood plain flow crossing over the skew. These are not included of course in Equation (7.1), not unless the secondary cells are assumed to act laterally only, then they can be simulated by additional lateral turbulent shear. This is not satisfactory in skewed channels.

This means that it is only possible to carry out discharge assessment in skewed compound channels by solving the full two–dimensional equations as in section (7.2.1), an area now being investigated by Wark, at University of Glasgow.

Thus for the purposes of this thesis, analysis will be confined to the errors involved in discharge assessment in skewed compound channels. The definition of discharge error will be:

$$\Delta Q = (Q_{estimate} - Q_{actual}) / Q_{actual} \qquad (7.3)$$

where

$Q_{estimate}$ is based on an accurate knowledge of Mannings n at each depth of flow in each sub–section of the flow.

Q_{actual} is the measured total discharge (experimentally).

7.2.2 Error in Discharge Assessment in Series A Skewed Tests

The SERIES A tests in this work involved a skewed main channel at angle 5.843°, a longitudinal bed slope of 0.001, a main channel width 0.15m, bank–full depth of 0.061m, and total flood plain width of 0.614m as described in chapters 3 and 5. The boundaries of both the main channel and flood plain were smooth, with friction factors quoted in detail in chapter 4.

It was decided to use the imaginary vertical wall sub–division method to determine the errors involved in discharge assessment in skewed channels. The result for the Glasgow flume is shown in Fig (7.1) with percentage error plotted against relative depths around 0.15, the error increases to 25%.

By coincidence the dimensions of the Glasgow flume with $n \approx 0.01$, bed slope $S_0 = 0.001$ and flood plain/ main channel width B/b of 4.1, were in effect, a scale model of tests carried out on the SERC flume for the straight parallel case with $n \approx 0.01$, $S_0 = 0.001$ and $B/b = 4.2$.
The comparison is also shown in Fig (7.1) revealing that errors in discharge assessment are greater in skewed sections.

The reason for this is clear. This straight case omits lateral shear, whereas the skewed case omits lateral shear, as well as horizontal shear and strong secondary currents driven by cross–over flows.

At this point it was thought that errors due to energy loss from horizontal shear and driving secondary currents might be corrected by simply using energy loss values obtained from slot tests in chapter 6. That is, if there is a direct analogy between flow over a slot in a channel bed with flow over a skew in a compound section, then the cross–over energy losses from one situation might be used to simulate the losses in the other situation. Flow in the slot does form an expansion region of high turbulent shear as well as driving a strong recirculation cell. This to some extent seems to be the case in the skewed channel as well. It was decided to look for more direct evidence of this in results already obtained. Fig (7.2a) shows the transverse components of velocity in the skewed main channel with cross over flow from right to left. This is for the smooth boundary case $n \approx 0.01$ to 0.011, $S_0 = 0.001$ and with skewed main channel aspect ratio of 2.46. This compared in Fig (7.2b) with transverse components from the slot

tests (chapter 6) for the same bed slope, approximately the same values of Mannings 'n', but this time the nearest aspect ratio tested in the slot tests being 2, which is a slightly lower value than the skewed main channel. The values of relative depth are approximately 0.35 in both cases.

Allowing for the fact that transverse flows in the skewed channel are shown from right to left, and in the slot tests from the left to the right, the pattern of recirculation is very similar at most vertical slices especially the middle two shown. A large recirculation is evident which occipies the whole area. This is a fuction of the small aspect ratio in both cases of 2.46 for the skew and 2 for the slot.

The one major difference between Fig (7.2a) and (7.2b) is the relative magnitudes of the recirculating velocity when normalised to the normal upstream velocity. This ratio is almost twice as large (V_r/U_f Sinθ) in the skew compared with the slot test.

Further evidence of similarity of flows in a skew and a slot is shown in Fig(7.3a) and Fig (7.3b). Fig (7.3b) shows transverse velocity components in the cross–over region of the meandering SERIES B SERC flume at Wallingford, where the cross–over angle is 60^0, the boundaries are smooth, $S_0 = 0.001$ on the flood plain the aspect ratio of the main channel is 8 and the relative depth is 0.25. This is compared in Fig (7.3a) with a slot test from chapter 6 where the boundaries are again smooth, the bed slope again 0.001 and the aspect ratio is 10.

One thing is clear. Both cases exhibit a recirculation region which extends about six bank–full depths in the transverse direction. The magnitude of the recirculating velocities (when normalised with the upstream flood plain velocity) is about twice as great in the meandering cross over compared with the slot. The maximum value of V_r/U_{fp} is around 0.3 in the skewed cross–over, compared with a maximum value of V_r/U_{fp} of 0.15 in the slot.

Thus it can be stated initially that transverse velocity components in a skewed compound channel have a similar pattern to flow over a slot, the magnitudes of the recirculating velocities are not identical.

Assuming that significant similarity exists in transverse velocity components in the skewed main channel and flow through a slot, it was decided to apply the slot total energy loss to the skewed channel data. This was done by applying the total energy loss through the slot shown in Fig (6.30) to the skew, varying the loss coefficient at each relative flow depth.

Thus the estimated discharge was determined again by sub–dividing the compound section with imaginary walls, but this time adding a horizontal shear loss due to flow through the slot. The resulting percentage errors in discharge assessment are shown in Fig (7.4). In this case the percentage errors are greatly reduced, becoming zero for relative flow depths above 0.4.

The SERC flume straight/parallel case is also shown for comparison revealing similar errors to the skewed case with slot losses accounted for. Theoretically both graphs should be in error only because of lateral shear, and this appears to be borne out in Fig (7.4), with the skewed channel apparently giving smaller lateral shear than the straight/parallel case. Thus is to be expected even for small skew angles of 5.8^0.

At this stage it was thought appropriate to compare the errors in discharge assessment in the Glasgow skewed flume with the errors in three different angles of skew tested in the SERC flume by Elliot (1990).
The result is shown in Fig (7.5) with errors determined simply from bed friction losses, with no account made for slot losses. It is clear from Fig (7.5) that the Glasgow results fit broadly in the middle of the SERC data with skew angle 2.1^0 to 9^0. There also appears a peak in errors at relative depth around 0.15 to 0.2. Most significantly the errors increase with increasing skew angle.

The explanation for this is most likely to be that secondary cells in the skewed main channel are driven by the cross–over flood plain flow. As the angle of the skew increases then so do the magnitude of the NORMAL component of flood plain flow, $U_f \mathrm{Sin}\,\theta$. This means that the magnitude of the secondary velocity V_r in the skewed main channel will increase also with increasing skew angle, simply because the ratio $U_r/U_f \mathrm{Sin}\,\theta$ will be reasonably constant. This will be demonstrated later.

Now according to Chang (1984), the energy loss in a secondary cell is

proportional to the secondary velocity squared (V^2_r) for a given boundary friction value. Thus energy losses at various skew angles will be proportional to V^2_r and hence $U^2_f \, Sin\theta$. Therefore for a given flood plain velocity U_f, the energy loses in the secondary cells will vary in the ratio 1 : 6 : 20 as the skew angle changes from 2^0 to 5^0 to 9^0.

This significant increase and secondary cell energy loss and is reflected in the discharge errors shown in Fig (7.5). However it should be remembered that the increase in the skew angle from 2^0 to 9^0, also produces a DECRESE in lateral turbulent shear which at present is unquantifiable for a skewed compound channel. Thus losses which increase with skew angle in the form of secondary cell, produce a decrease in lateral shear, the two not exactly cancelling each other out.

7.2.3 A Broader Picture of Discharge Assessment Errors.

Fig (7.6) reveals the pattern of errors in discharge assessment for the imaginary vertical wall case, for straight/parallel, skewed and meandering systems. The first conclusion is that sinuous compound flows produce greater flow resistance than either skewed or straight/parallel systems.

A guide to **Fig (7.6)** is to produce simple subdivisions of the energy loss mechanism in each case.

(i) Straight/parallel omits lateral shear only. Hence lateral shear can account for up to 20 – 25% of the errors in any discharge assessment.

(ii) Skewed compound flows omit both lateral shear and horizontal shear on **Fig (7.6)**. The difficulty is in assessing the contribution from each area. As the skew angle increases then the lateral shear component decreases. For a 90^0 skew angle, the lateral shear from the channel to flood plain is zero, whereas with a zero skew angle, we return to the straight parallel case where errors of discharge assessment can be up to 20 – 25%. For the skew angle tested in this work, $\theta = 5.843^0$, and for the range of skew angles tested in the SERIES A SERC flume study, from 2^0 to 9^0, a rough guide line reveals that the worst discharge

assessment errors occur at a relative depth around 0.15 and can reach a total of 25°. This is composed of approximately 5–10% horizontal shear and 15–20% lateral shear depending of the skew angle.

(iii) Meandering compound flows produce errors in discharge assessment as high as 35– 40% as shown in **Fig (7.6)**. In this case lateral shear, horizontal shear and bend losses are all ommitted. It is almost impossible to sub– divide these three areas in meandering compound flows because all three areas interact with each other. Cross over flows produce large secondary currents in the main channel which become transported to the next bend and may dominate bend behaviour. **Kiely (1989)** has shown that the bend itself will have a secondary cell driven in the opposite direction to the normal centrifugal force vectors for inbank flows. As well as this lateral shear will play a part near the bend apex and increasingly less part near the cross– over regions.

Initial calculations from the SERIES B SERC flume results indicate errors in discharge assessment up to 35– 40% for compound meandering flows. This translates into approximately 20% losses for bends, 10% for lateral shear and 10% for horizontal shear, depending on the sinuosity of the flow.

7.3 DISCHARGE ASSESSMENT IN SKEWED TWO– STAGE CHANNELS WITH A ROUGH FLOOD PLAIN.

The Series D tests consisted of the skewed smooth boundary as before, combined with a roughened flood plain as described in section 4.4. The skew angle θ is again 5.843°, with other features such as bed slope, dimensions of the skewed main channel and the flood plain width remaining as before.

The essential difference between Series A and D tests is flood plain roughness, which in this case has been achieved by means of 10mm diameter vertical rods, placed at 100mm centres both laterally and longitudinally on the flood plain. Chapter 4 outlines the effect of these roughening rods in producing free surface drag, internal vortex street drag and interaction effects with other rods. This results in a flood plain value of Mannings 'n' which lies in the region of 0.02 to 0.04 as shown in Fig (4.14). The vertical rod behaviour has

also been analysed in terms of an effective drag coefficient for rods, given by the expression.

$$F_{tot} = 4\alpha C_d(\beta_1 N_1 + \beta_2 N_2)dY_c/P + (\beta_1+\beta_2)\lambda_b/2 \qquad (7.4)$$

where

F_{tot} is the total drage force per unit length

β_1, β_2 are the blockage effect, i.e. square of area ratios for alternate rows, and equal

$$\beta_1 = (1 - n_1 Y_c d/A)^{-2}$$

$$\beta_2 = (1 - n_2 Y_c d/A)^{-2}$$

n_1, n_2 are number of rods of diameter (d) across channel/flood plain rows 1 and rows 2.

N_1, N_2 are the number of rods per unit length of main channel/flood plain.

A is the gross sectional area of zone under consideration

αC_d is the effective drag coefficient of rods, shown in Fig (4.15)

It is clear from Fig (7.7) that flood plain roughness produces a significant reduction in discharge, the reduction becoming more significant at greater flood plain depths. This is due to large increases in Mannings 'n' for flood plain roughness, as the depth increases.

It was decided to investigate discharge assessment in the skewed rough case by a range of sub–division methods. As each sub–division method was attempted, the errors between actual and estimated discharges were determined using Equation 7.3 as in the previous section.

This method of error analysis reveals the extent of the interaction which is ignored by considering only boundary friction.

(i) The first method is simply to use imaginary vertical walls placed at the main channel flood plain junction. The resulting error for the smooth case has been shown already in Fig (7.1). The resulting error for the rough case is shown in curve (a) in Fig (7.8). Here it is clear that an entirely different pattern of errors is involved compared to the smooth flood plain case.
From Fig (7.8a) it is clear that errors increase significantly with increasing depth despite the fact that accurate boundary roughness have been used at each depth. Therefore the interaction between main channel and flood plain gets larger at greater depths.

Also significantly at the lowest flood plain depths, the interaction effect goes towards zero which is the opposite trend of the smooth case. It appears from this that errors due to ignoring lateral turbulent shear are not nearly as significant as in the smooth case in Fig (7.1), but other interactions are more important.

(ii) The second method is to again use vertical walls at the channel/flood plain junctions, but this time to give the walls friction on both sides. The friction given to the vertical walls was calculated on the basis of flood plain roughness values. This method is shown as curve (b) in Fig (7.8)., revealing reduced errors in discharge, but still having a similar pattern to curve (a) where errors increase with depth, and also indicate smaller errors due to the classical lateral turbulent shear.

(iii) It was clear from an inspection of velocities in the skewed main channel, that velocities in that region were so low that it appeared that the main channel was behaving as if it had flood plain roughness rather than smooth roughness which was the case. It was decided therefore to introduce flood plain roughness into the main channel flow by the introduction of an imaginary horizontal wall drawn across the main channel at bank–full level, and with flood plain roughness on <u>both</u> the upper and lower sides of this sub–division.

The resulting error in discharge is as shown in Fig (7.8) curve (c), which produces much lower errors in discharge than the vertical wall cases, but over estimates the amount of roughness to be used on the horizontal sub–division. This is a form of horizontal shear which has been introduced which is significantly greater in magnitude than the horizontal shear loss determined from the slot tests in chapter 6.

(iv) A fourth method of sub–division produced almost zero errors in discharge assessment at all relative–depths. This is shown as curve (d) in Fig (7.8), and represents an imaginary horizontal wall, placed at a distance of one third of bankfull depth below bank full depth. ie. at 20mm below bankfull or 40mm above the main channel bed. The imaginary wall carries flood plain friction on its upper side only, but flood plain friction is also added to the main channel walls above this imaginary subdivision.

With errors in discharge effectively zero using this method, it is clear that the main interaction for the SERIES D tests is flood plain friction extending its influence into the main channel. This influence is extended right across the width of the main channel probably because of the small aspect ratio (2.5) of the main channel. The flood plain influence also extends down into the main channel, to a distance around 1/3 of bankfull below the bankfull level.

Thus it can be stated, and this is borne out by investigating velocities in the main channel in chapter 5, Figs (5.19) to (5.33) that the upper part of the main channel behaves as if it has flood plain roughness even though it has a smooth boundary. The main interaction between channel and flood plain is therefore the main channel behaviour dominated by flood plain roughness. This means that the classical lateral turbulent shear as well as the classical horizontal turbulent cross–over shear appear to be completely dominated by flood plain boundary roughness. This is an important conclusion.

Fig (7.9) shows the comparison of errors in discharge assessment for rough flood plain cases using the imaginary vertical wall method. The main comparison is with the data of Elliot and Sellin (1990) from the SERC flume. The SERC flume was at slope 0.001, main channel Mannings 'n' ≅0.01, main channel aspect ratio 10., flood plain roughness in the range n = 0.03 to 0.04 and flood plain/main channel width ratio of 3.7, with the skew angle equal 2.1^0 to 9^0.

The most important observation from Fig (7.9) is that the pattern of error in discharge assessment is very similar to the result of this work, even though the geometries are not identical.

A comparison is also given with rough flood plain tests carried out by Stein and Rouve (1988). The main channel of Stein and Rouve contained one

complete meander as sketched in Fig (2.17) and operated with flood plain roughness in the range n= 0.03 to 0.04, with the main channel roughness around n = 0.01. It is clear from Fig (7.9) that a similar mechanism is at work, simply because it gives a very similar pattern of discharge errors, due primarily to main channel behaviour dominated by flood plain roughness.

Fig (7.10) shows a comparison of method (iv) above (with a horizontal subdivision) applied to both the Glasgow, flume and the much larger aspect ratio SERC flume, again using the data of Elliot and Sellin. It is clear from Fig(7.10). That the horizontal sub– division method (with flood plain roughness extended along the imaginary wall) produces slightly too much roughness for the wide aspect case. This is to be exoected, but it does again confirm the relevance of horizontal sub– division for rough flood plain cases.

Finally it can be shown that horizontal shear, determined from the slot tests in chapter 6, due to the expansion and contraction losses is a small component in the case of the rough flood plain. Fig (7.11) shows the Glasgow skewed flume with rough flood plain errors in discharge using the vertical imaginary wall method. This is compared with the same method but allowing for expansion and contraction slot losses. It is clear from the comparison in Fig (7.11) that the incorporation of horizontal turbulent shear from expansion and contraction losses (Chapter 6) produces a very small alteration in discharge errors, implying that this component is small compared with the transmission of flood plain roughness effects into the main channel to retard to main channel flow. The latter appears to be the primary mechanism for very rough flood plain cases.

7.4 RESISTANCE TO FLOW FUNCTIONS

The variation of Darcy– Weisbach resistance coefficient with Reynolds Number for flood plain isolated from main channel (SERIES B) and skewed main channel isolated from flood plain area (SERIES C) was discussed in Section 4.3. Using the Colebrook White equation, an average value for Nikuradse's equivalent sand roughness (k_s) for the flood plain material as 0.162mm and 0.3389mm for the skewed main channel isolated from flood plain material as below:

$$\frac{1}{\sqrt{\lambda}} = -2.0 \text{ Log } \left[\frac{k_s}{14.81\ R} + \frac{2.51}{R_e \sqrt{\lambda}} \right] \qquad (7.5)$$

where

k_s = Nikuradse's equivalent sand roughness.

However, it was clear that such sand grain roughness did not exist in the Glasgow flume in reality, so it was decided instead to use a modified smooth law, when the boundary is smooth and the sand grain roughness can be considered zero, then the equation of circular pipes can be used with some modification for the constant B value as below.

$$\frac{1}{\sqrt{\lambda}} = A \text{ Log } [R_e \sqrt{\lambda}] - B \qquad (7.6)$$

where A and B are the experimental coefficient values depending on the type of material used.

From the experimental results the value of A remained approximately constant and the value of B was found to be 1.487 for the flood plain material isolated from skewed main channel, and 1.76 for skewed main channel isolated from flood plain area as below,

$$\frac{1}{\sqrt{\lambda}} = 2.0 \text{ Log } [R_e \sqrt{\lambda}] - 1.487 \qquad (7.7)$$

equation 7.7 was used for the smooth flood plain material

$$\frac{1}{\sqrt{\lambda}} = 2.0 \text{ Log } [R_e \sqrt{\lambda}] - 1.76 \qquad (7.8)$$

Equation 7.8 was used for skewed main channel isolated from flood plain.

Myers (1988) investigated the relationship between the Darcy– Weisbach friction factor and Reynolds Number for the case of inbank flows in the SERC flume at Wallingford. Again a modified smooth law was found to be applicable in the form

$$\frac{1}{\sqrt{\lambda}} = 2.17 \text{ Log } [R_e \sqrt{\lambda}] - 2.07 \qquad (7.9)$$

The question which arises is whether the modified smooth laws above can be applied to the smooth compound cross– section when both main channel and flood plain are smooth.

For a compound cross– section we will consider the cross– section to be a single channel where the friction factor λ is determined from

$$\lambda = 8g R_T S / V^2_t \qquad (7.10)$$

where

V_T is the average velocity of the compound section.

R_T is the total cross section hydraulic radius (A_T/P_T)

A_T is the total compound area

P_T is the total compound wetted perimeter.

and the Reynold Number computed from

$$R_e = 4 V_T R_T / \nu \qquad (7.11)$$

Fig (7.12) shows the resulting varations for the SERC flume data comparing the inbank flow relationship for the trapezoidal section described by Equation (7.9) above, the SERIES A SERC data for the straight/parallel case, and the SERIES B data for the meandering compound case.

It is clear from **Fig (7.12)** that compound flows do not obey conventional $\lambda - R_e$ relationship, given the wide varation in λ values over a short range of R_e.

For the straight/parallel case the values of friction factor tend towards the single channel curve only at high relative flow depths. For meandering compound case, the friction factors are considerably higher than the straight parallel case. This is a function of both lower Reynolds Numbers and greater resistance to flow due to bends and cross– overs.

At higher relative flow depths the $\lambda - R_e$ diagram for meandering compound flows, behaves almost identically to a roughened channel with a value of roughness k/4R in the region of 0.003.

The diagram of $\lambda - R_e$ relationships for skewed flumes is shown in **Fig (7.13)** both for the case of the Glasgow flume $\theta = 5.843^0$ and also the SERC flume with its skew angles from 2^0 to 9^0.

It is clear from the SERC data, that skew angles of 2^0 and 5^0 produce a $\lambda - R_e$ diagram which approaches that of a single channel at least for higher relative flow depths. However a skew angle of 9^0 produces a $\lambda - R_e$ diagram which bears no relationship to the smooth single channel curve, and in fact behaves more like the meandering case in **Fig (7.12)**, where the channel behaves as if it has considerable roughness even though the boundaries are smooth.

The Glasgow flume data on **Fig (7.13)** behaves similarly to the SERC data for a skew angle of 5^0, only at a much reduced Reynolds Number because of the much smaller channel dimensions. It is clear that the 5.843^0 angle of skew in the Glasgow flume produces a $\lambda - R_e$ relationship very close to the smooth single channel, at least at higher relative depths. The smooth channel curve shown in **Fig (7.13)** is for the flood plain given in Equation 7.7. The curve for the skewed main channel alone is given by Equation 7.8 and hence most of the compound data appears to lie between these two curves.

In conclusion, it is clear from **Figs (7.12) and (7.13)** that compound flows approximate to conventional $\lambda - R_e$ relationships only at larger relative depths. It is also clear that straight/parallel systems, as well as skew angles up to 6^0, approximate to the single channel curve at higher relative depths, but a skew of 9^0 and the meandering case approximate to $\lambda - R_e$ relationship with definite roughness values k/4R. In this case these are in the region of $k/4R \approx 0.0005$ for the 9^0 skew and $k/4R \approx 0.003$ for the meandering channel with sinuosity 1.33.

7.5 DEVIATION OF FLOOD PLAIN STREAMLINES PASSING OVER THE SKEWED MAIN CHANNEL

Introduction

One of the most robust features of compound skewed flows is the deviation of flood plain flows once they come in contact with the main channel flow. This is sketched diagramatically below in an idealised form

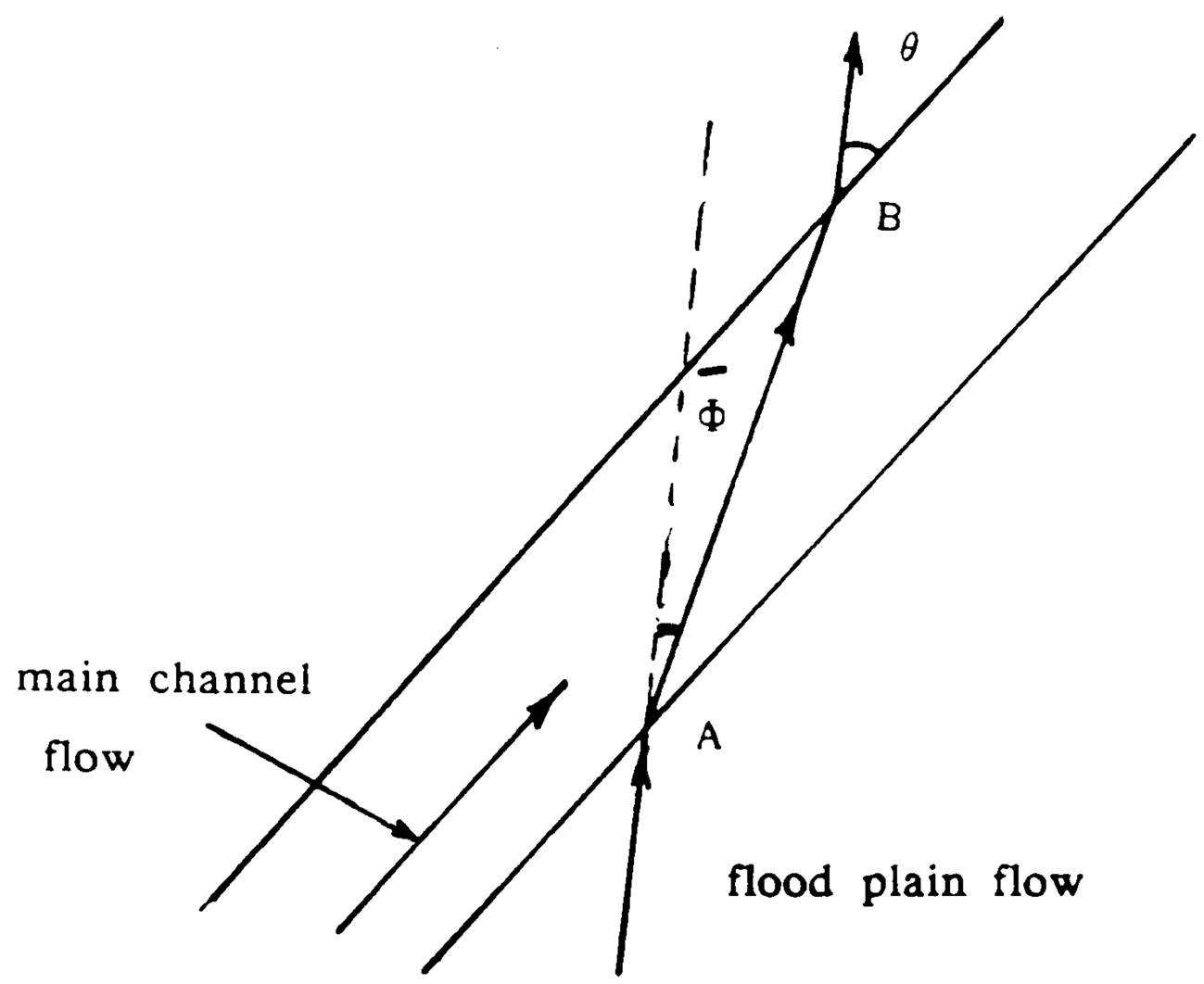

Flow from the flood plain is assumed to be longitudinal in direction and approaches the skewed main channel, making an angle θ with the skewed main channel. Flood plain streamlines passing over the skewed main channel are assumed to deviate by a mean angle Φ, eventually reaching the opposite flood plain where the flow returns to the longitudinal direction.

The angle Φ is assumed to be acting only above bankfull level and is an average value, averaged over the width of the skewed main channel and also averaged over the depth above bankfull level. Thus it is an area–average deviation angle in the main channel above bank–full level.

The angle Φ is a crude representation of reality, in the sense that it can vary enormously over the depth above bankfull. Dye tests reveal that streamlines close to the flood plain bed can deviate down into the main channel flow giving $\Phi = \theta$. Alternatively, streamlines near the surface can show very little deviation

giving $\Phi \rightarrow 0$. It follows therefore that the ratio Φ / θ is always less or equal to one, and greater or equal to 0.

It is clear from the sketch above that large main channel velocities and low flood plain velocities will produce considerable deviation angles. This means that the main channel flow below acts to change the direction of the flood plain flow with turbulent shear being the mechanism to cause deviation. This turbulent shear might be considered to be acting on a horizontal plane (around bank full level) and must have components acting longitudinally along the main channel direction as well as components acting normally to the main channel walls. This means that the slot tests in Chapter 6 cannot hope to represent all the horizontal turbulent shear, as it will describe only the components normal to the main channel walls. It is argued therefore that any application of the slot test results in Chapter 6 to the skewed channel data, must incorporate at least the total length of the streamline crossing over the main channel, given by the length AB in the sketch above. In the Glasgow flume the minimum distance AB is around 1.47m giving a minimum aspect ratio along the length AB of 25.

An alternative way of viewing the sketch above is for the case of a high flood plain velocity crossing over a low main channel velocity below. This is most likely to occur for smooth flood plains at high relative depths of flow. In this case it could be argued that the flood plain flow is able to deviate the main channel streamlines despite the fact that below bank full the main channel streamlines are confined by the walls. A study of Fig (5.1)to (5.33) reveals that this is very much the case, as maximum velocity contours become shifted more and more towards the left main channel wall, eventually "spilling out" onto the left floodplain.

Results of Deviation Angles, Φ.

It has been described in Section 3.3.5 how the angular fin transducer was used to measure streamline angles at all points within the main channel. The measured angles were then combined with longitudinal velocity components to determine the transverse velocity components at cross sections along the length of the flume. In this case the angular fin measurements were also used to determine the mean deviation angle Φ at any given cross section by averaging

values of Φ across the channel width, and depth above bank full level.

The results were normalised in the form Φ/θ and plotted against relative depth. The result for the SMOOTH flood plain case is shown on Fig (7.14). The result for the smooth flood plain case is significant in that it reveals an almost zero deviation of streamlines for relative depths higher than 0.3 approximately. This means that if the flood plain flow is crossing "straight– over" the skewed main channel then there is ZERO lateral shear above this bank full level. This has already been borne out in Fig (7.4) concerning errors in discharge assessment, which also reveals little or no lateral shear above Y_f/Y_c of 0.3, especially after horizontal shear losses have been included.

Alternatively for relative depths below 0.3, the angle of streamline deviation increases remarkably so that at a relative depth around 0.15, the deviation angle Φ is almost half the skew angle θ (5.843^0). This is shown clearly in Fig (7.14) and reveals that lateral turbulent shear will increase rapidly as relative depths go below 0.2 even in a skewed situation. Fig (7.14) does not show significant variation in Φ between the three measurement sections along the flume length.

The angles of streamline deviation for the rough flood plain case are shown in Fig (7.15), again plotted against relative depth and again at all three cross– sections along the flume length. The pattern of deviation is significantly different compared with the smooth flood plain case in the sense that large deviation angles are obtained even a high relative flow depths. (It should be remembered that vertical rods produce greater roughness as the depth increases) The result shows that for this flood plain roughness, the deviation angles are mostly within the range of 40% to 50% of the total skew angle θ.

This means that in effect, a rough flood plain almost acts like a physical barrier preventing crossing over flow reaching the opposite flood plain. As water flow will want to take the route of least resistance, this type of flow phenomena is not surprising.

The implications of these results are significant in the design of two– stage channels.

7.6 BIFRUCATION OF FLOOD PLAIN STREAMLINES INTO MAIN CHANNEL

One of the most significant findings of this research work concerned the fact that flood plain flow could enter the main channel flow and be transported off in the direction of the skewed main channel. This was confirmed by dye tests, and the idea is sketched below.

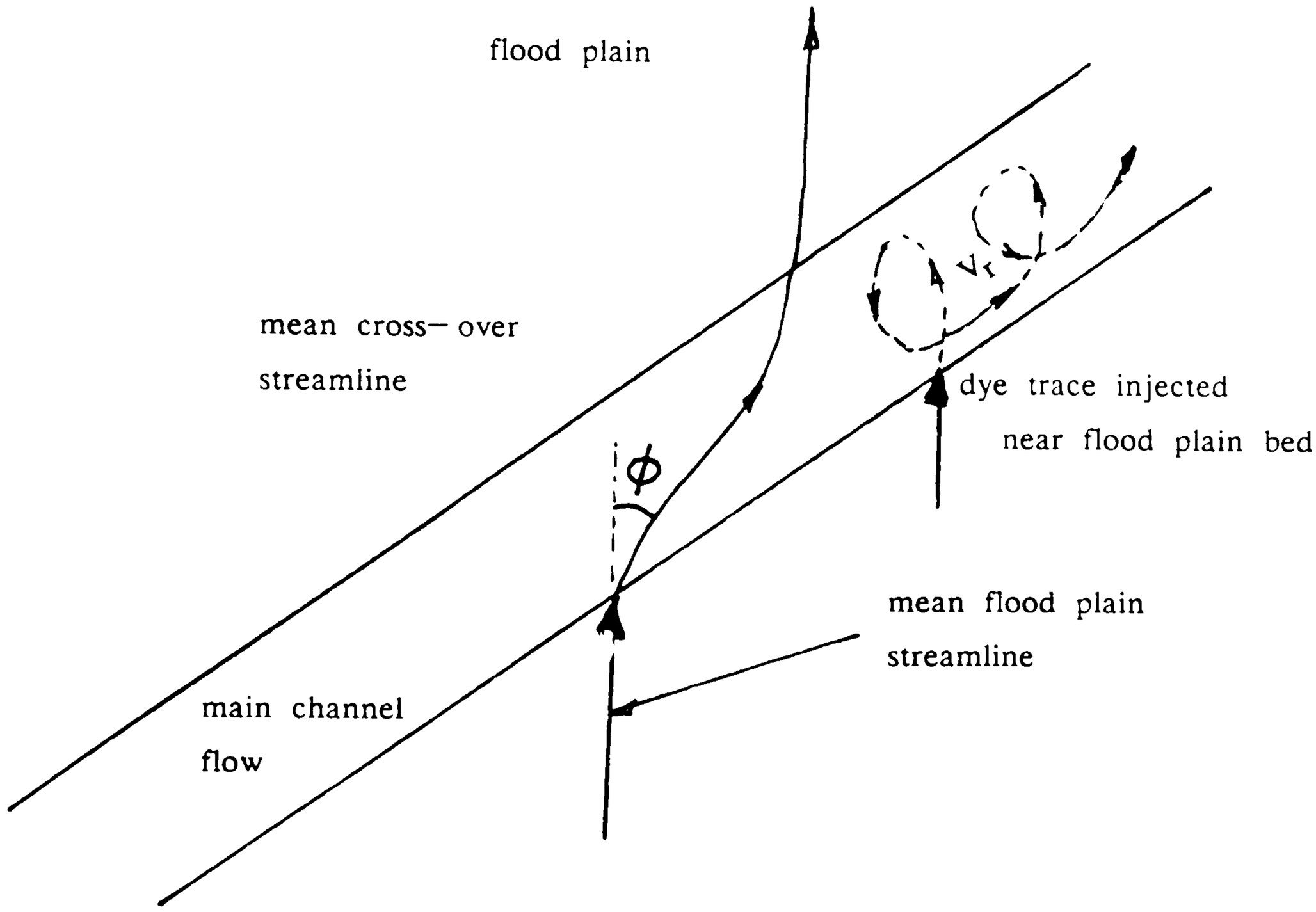

The finding can be summarised as follows:–

The mean flood plain streamline passes over the skewed main channel at angle Φ, entering the left flood plain at some distance downstream. A dye injection at the flood plain bed (shown as a dotted line in the sketch above) reveals that streamlines in that area can be entrained into the large circulation in the main channel and be transported off in the circulation in the same direction as the skew. This means

(i) That flood plain flow can bifrucate, (or split in two) with lowest layers

joining the main channel flow with the remainder crossing over to the opposite flood plain.

(ii) The horizontal shear model from the slot tests (Chapter 6) is not exactly applicable as not all the flow is crossing over to the opposite flood plain.

(iii) The recirculation velocities (V_r) in the main channel are not only caused by flood plain flow shearing over the main channel, but also can be added to, by flow entrained from the flood plain.

(iv) The amount added to u_r from flood plain flow will depend to some extent on the angle Φ. Large values of Φ are likely to entrain more flood plain fluid down into the main channel. Small values of Φ represent streamlines crossing straight over the main channel, thus adding less entrained flow to the main channel recirculation, but still developing horizontal shear secondary circulation.

(v) This means that the magnitudes of the recirculating velocities in the main channel depend on two criteria. (a) how much flow is entrained into the swirl and (b) how much horizontal shear is available to generate a swirl or recirculation.

(vi) If the phenomenon of adding to the main channel flow from the lower flood plain layers, occurred over the full skewed length then the main channel flow would increase in energy and mean velocity, as we move in the downstream direction. This is not the case. Fig (7.16) and (7.17) will reveal that the main channel velocity remains approximately constant in the downstream direction, and in some cases decreases in the downstream direction.

(vii) This means that a process of SUBSTITUTION must be occurring, where flow added to the main channel directly from one flood plain by entrainment into the large secondary current, must produce a comparable removal of fluid from the main channel to the left flood plain. This is a necessary condition for no net increase in flow along the skewed main channel in the downstream direction.

(viii) For the case when the mean velocity in the main channel is decreasing slightly in the downsream direction, and the magnitude of the

recirculating swirl is also decreasing slightly in the downstream direction, then more flow must be Lost out of the swirl to the left flood plain than is GAINED into the swirl from the right flood plain.

7.7 TRANSVERSE RECIRCULATION FLOW PATTERNS IN THE SKEWED MAIN CHANNEL.

7.7.1 Introduction

It is clear from Chapter 5 that the transverse recirculation patterns which occur within the skewed main channel are caused by floodplain flow passing over the skew. The main evidence for this is the comparison of the skewed main channel secondary currents with and without floodplain flows. Series C tests, for instance, which have been described in Section 5.6, consist of walls built up along the banks of the skewed main channel thus preventing overbank flow. The recirculating patterns produce transverse velocity components of the order of 1% ? of the longitudinal velocity. When these walls are removed and compound overbank flow occurs, as in Series A and D tests, then the ratio of the transverse to the longitudinal velocity components rises to 5%, indicating very clearly, additional recirculation due to cross–over flow.

The question therefore in this thesis is not whether cross–over flow causes secondary currents, but more, what is the exact mechanism whereby it causes secondary currents? Ervine and Ellis (1987) have already speculated an analogy with flow over a slot where a static recirculation is driven by a horizontal shear mechanism as sketched below

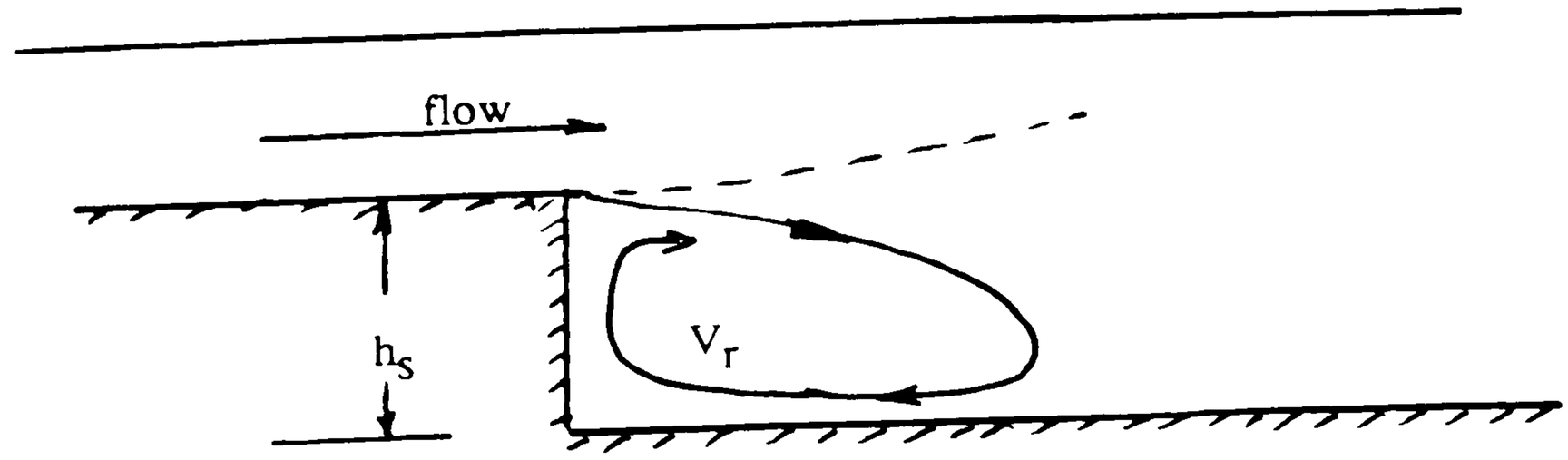

One of the purposes of carrying out the slot tests experiments in Chapter 6. was to measure the magnitude and flow patterns of the driven recirculation, and to compare it with the magnitude and pattern of the recirculation in the skewed main channel. A close comparison of the two would confirm the horizontal shear layer type analogy.

Sections 7.5 and 7.6 of this Chapter have already confirmed that an exact analogy with flow over a slot is not possible. First, the streamlines passing over the skewed main channel deviate to a considerable degree (Φ), ending up in some cases almost parallel to the main channel flow. Secondly and perhaps more significantly, dye tests reveal that flow from the floodplain can bifrucate down into the main channel spiral and move off in the main channel direction, rather than crossing over the skew to the opposite floodplain. This is a complete departure compared to the slot tets in Chapter 6, where streamlines are forced to cross to the opposite floodplain. The skewed channel phenomenon is sketched below

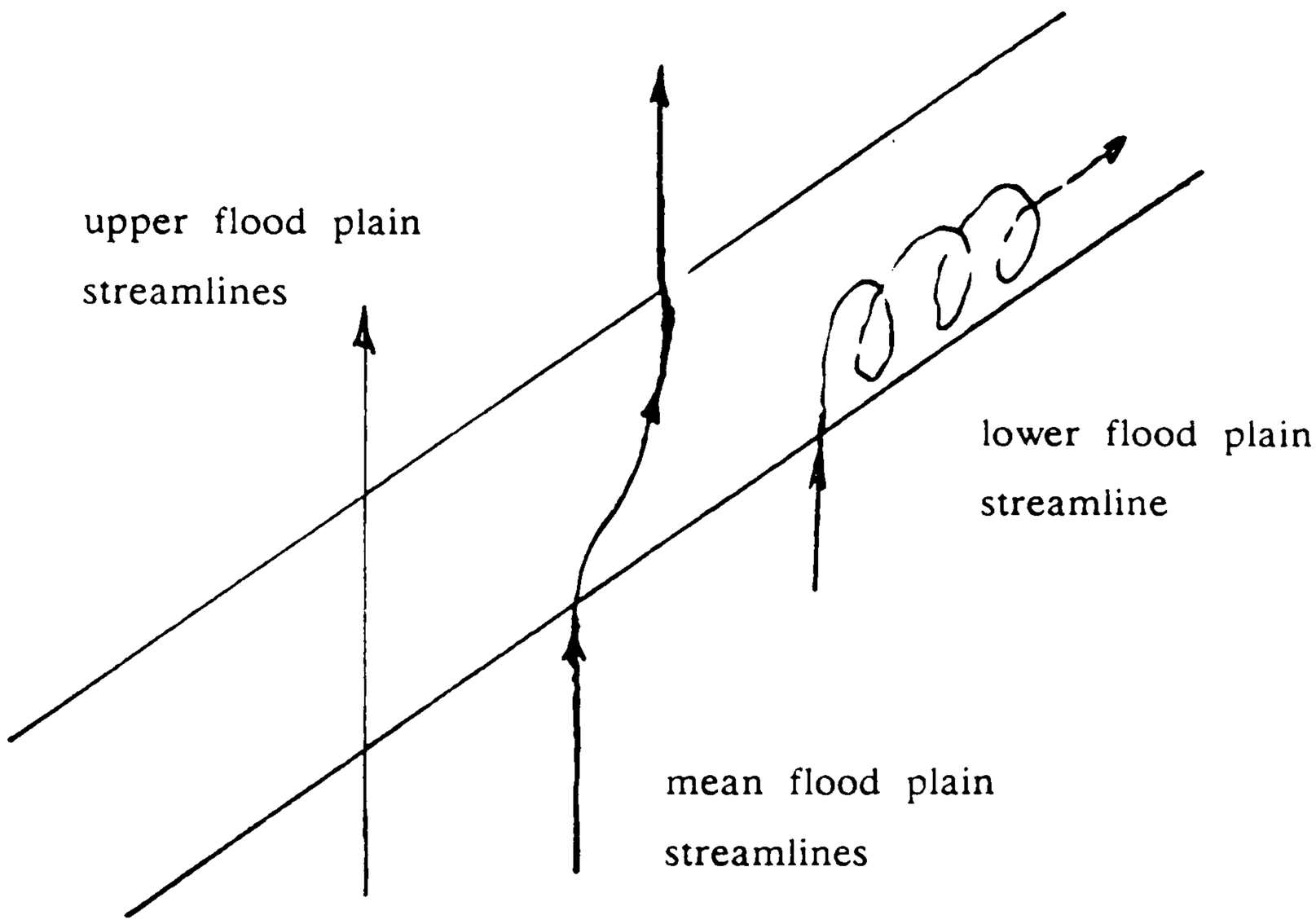

A third aspect of this section will concentrate on the influence of boundary roughness on transverse velocity components within the main skew. It has already become clear in Sections 7.2 and 7.3 that for the rough flood plain case, the velocities in the main channel are substantially reduced, often down to levels as if the main channel contained floodplain roughness as well. What effect does this have on recirculating components within the main channel?

It is clear that rougher flood plains produce greater deviation angles of streamlines. Does this mean lower recirculations because of less direct cross–over flows, or does it mean more recirculations because of extra floodplain flow diverted down into the main channel?.

7.7.2 Experimental Values of Recirculation Within the Skew.

Figs (5.1) to (5.33) show the transverse velocity components within the skewed main channel. For both the rough and smooth floodplain cases, the main channel width remained at 0.15m with a bank full depth of 0.061m. This gave a constant aspect ratio of 2.5 for all tests in the skewed flume. Aspect ratios in the slot tests varied from 2 to 20, affording comparison with the skew. Figs (5.1) to (5.33) also reveal that angle measurements, and hence transverse velocity component measurements, were taken at four vertical slices in each main channel cross–section. The resulting transverse components contain both a real transverse velocity for flow passing from right floodplain to left floodplain as well as a recirculating component due to the main channel spiral. The best idea of the recirculating component is therefore to be seen in the magnitude of the reversing flows, moving in the opposite direction to the cross–over flows.

The data used from the reversing recirculating flows in Chapter 5 was V_{rmax}, the maximum reversing recirculating velocity at any point in a cross–section, and V_r, which is the mean recirculating velocity averaged over the reversing part of the flow velocity slices.

For the skewed flow data, it was decided to normalise the recirculating flow data with the normal component of the floodplain flow $U_f \sin\theta$, where the floodplain velocity used could either be, the local value at the junction of channel and floodplain, or alternatively, the value U_{fr} averaged over the entire right floodplain as sketched below.

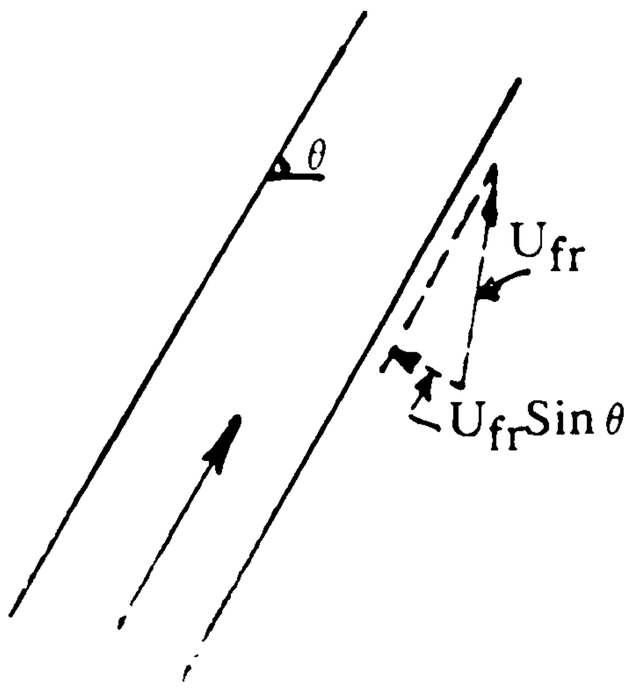

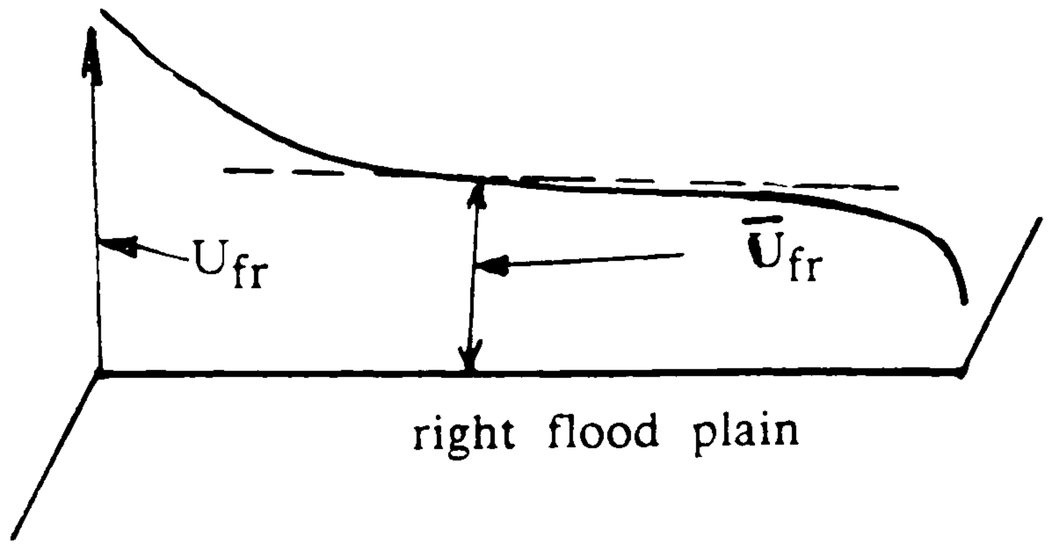

Fig (7.16) shows the mean recirculating velocity in the skewed main channel plotted against relative flow depth, Y_f/Y_c, for the case of the smooth floodplains. Recirculating velocity is normalised using the average right floodplain velocity x $\mathrm{Sin}\,\theta$ rather than the local one. Several conclusions can be drawn from Fig (7.16)

(i) The magnitudes of $V_r/U_{fr}\ \mathrm{Sin}\,\theta$ lie between 0.2 and 0.5 and are substantially higher that the slot test data in Chapter 6, although it should be stated that the lowest slot test Y_f/Y_c was around 0.3. The slot data in Chapter 6 gives typical mean recirculations in the region of $V_r/U_n = 0.1$ to 0.2.

(ii) The magnitude of the recirculating velocity within the main channel decreases in the downstream direction. From Section 1 to Section 3. This is not as evident at larger relative depths.

(iii) At larger relative depths, around 0.4 and 0.5, the magnitude of the recirculations approaches that of the slot tests in Chapter 6. This is probably due to the fact that large relative depths produce little cross–over streamline deviation ($\Phi \longrightarrow 0$) in the smooth floodplain case, and hence the behaviour becomes more and more like the proposed slot analogy.

(iv) At smaller relative depths (around 0.2), the recirculating velocities appear to reach a peak as shown in Fig (7.16). The value of the peak giving normalised recirculations substantially larger than the slot tests.

In fact the highest values of $V_r/U_{fp}\ \mathrm{Sin}\,\theta$ are in the region of 0.5 to 0.6 which is about twice or three times that of comparable slot tests. The reason for this must be connected with the fact that in the skewed flume, flood plain flow can enter the main channel recirculation, adding substantially to the magnitude of the recirculation compared to a slot test. Another reason may be the use of the main right flood plain velocity U_{fr} rather than the local flood plain velocity at the channel/flood plain junction.

Fig (7.17) shows values of the normalised mean recirculating velocities in the main channel for the case of the rough floodplain. It can be seen from Fig(7.17) that the magnitudes of the normalised recirculation velocities are similar to the smooth case, showing a similar trend of slightly reduced recirculating velocities in the downstream direction from Section 1 to Section 3.

Fig (7.17) also reveals a peak in normalised recirculating velocities at a relative depth of 0.3 approximately (compared with 0.2 in the smooth case).
Low and high relative depths produce values of recirculation which are similar to the slot tests.

Again the highest non– dimensional mean recirculations around 0.5 to 0.6 must be a function of the ability of a flood plain flow to bifrucate, and to push some of its flow into the main channel spiral adding to the recirculating velocities, compared to a slot.

It was agreed that such high ratios might be a function of employing the mean right flood plain velocity as a normalising factor and hence it was decided to use the local flood plain velocity at the channel/flood plain interface.

Fig (7.18) is a significant graph comparing slot recirculations from Chapter 6 with skewed channel recirculations (Chapter 5). In both cases the maximum value of recirculating velocity ($V_{r\ max}$) is used. This is the maximum value found at any of the vertical slices in the slot tests and the skewed tests.

It was decided in this case to normalise the maximum recirculations with the <u>local</u> flood plain velocity at the channel/flood plain junction, rather than the mean right flood plain velocity as used in **Fig (7.16)** and **(7.17)**. The skewed data shown in **Fig (7.18)** is for the smooth case only for clearity. The following points can be made.

(i) The maximum recirculating velocities in the slot are between 0.1 and 0.3 of the upstream velocity U_n.

(ii) The range depends of the aspect ratio of the slot. The smallest aspect ratio (2) gives the largest non– dimensional ratios around 0.3.

(iii) These values correspond approximately to the slot data of other authors.

(iv) The smooth skewed channel maximum recirculating velocities are in the ratio 0.2 to 0.4 relative to the local flood plain velocity. That is, the highest flood plain velocity just at the junction of main channel and flood plain U_{fr} $Sin\theta$, rather than the mean for the whole flood plain.

(v) It is clear from **Fig (7.18)** that the maximum recirculating velocities in the skew, with aspect ratio 2.4, are approximately the same as the slot with aspect ratio 2, provided the maximum flood plain velocity is used to normalise the data.

This figure produces strong evidence of the comparability of slot and skewed recirculations.

At this point it was considered to produce theoretical estimates of the magnitudes of recirculating velocities at least for the slot case, and thus test for the influence of boundary roughness, relative depth, or slot aspect ratio.

7.7.3. Theoretical Review of Recirculating Flows at a Step in a Channel Flow

A complete solution of a two–dimensional recirculating flow requires the numerical solution of steady–state continuity and force/momentum equations. A definition of the term is given below

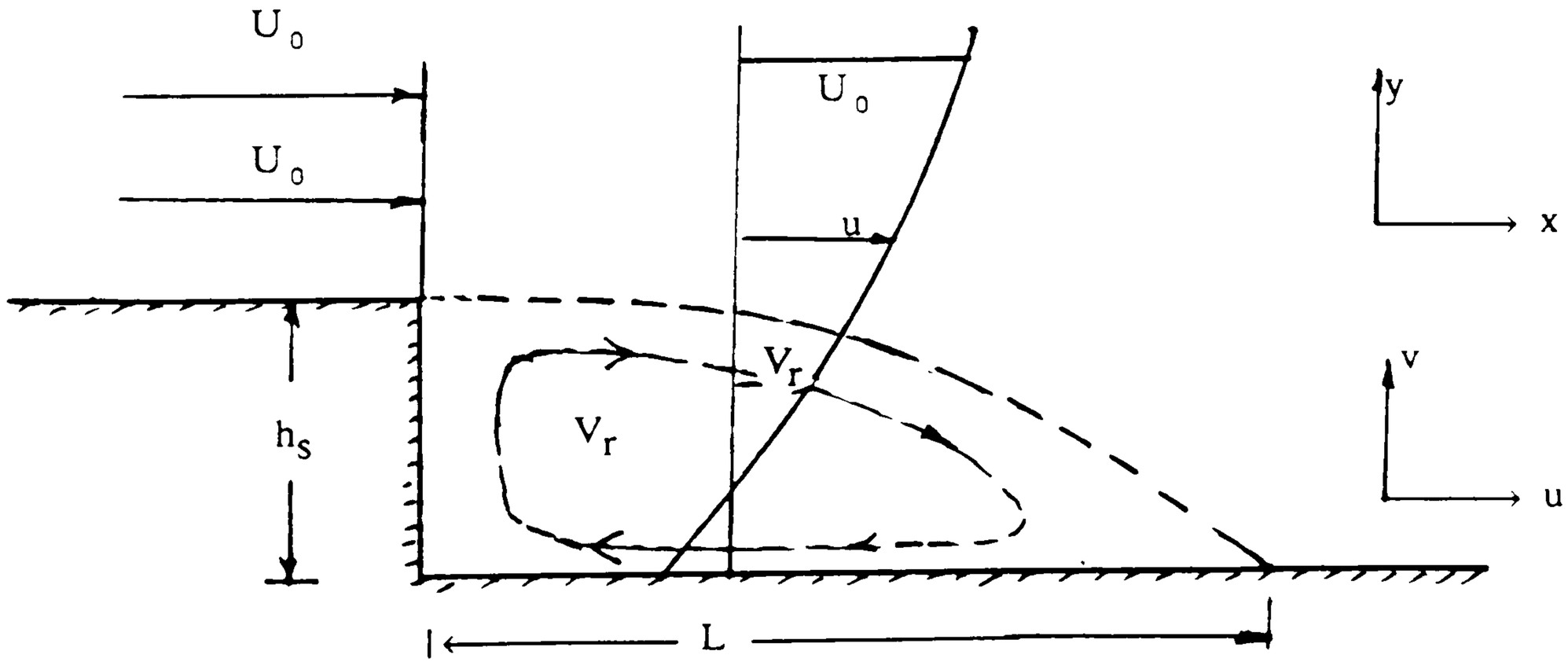

(i) Approximate Analysis of Recirculating Flows for Large Boundary Roughness

Rather than attempting a solution of the full 2–dimensional equations, it was decided to derive a simplified analysis for the case of a friction dominated recirculating shear layer. This has been carried out for the idealised geometry below.

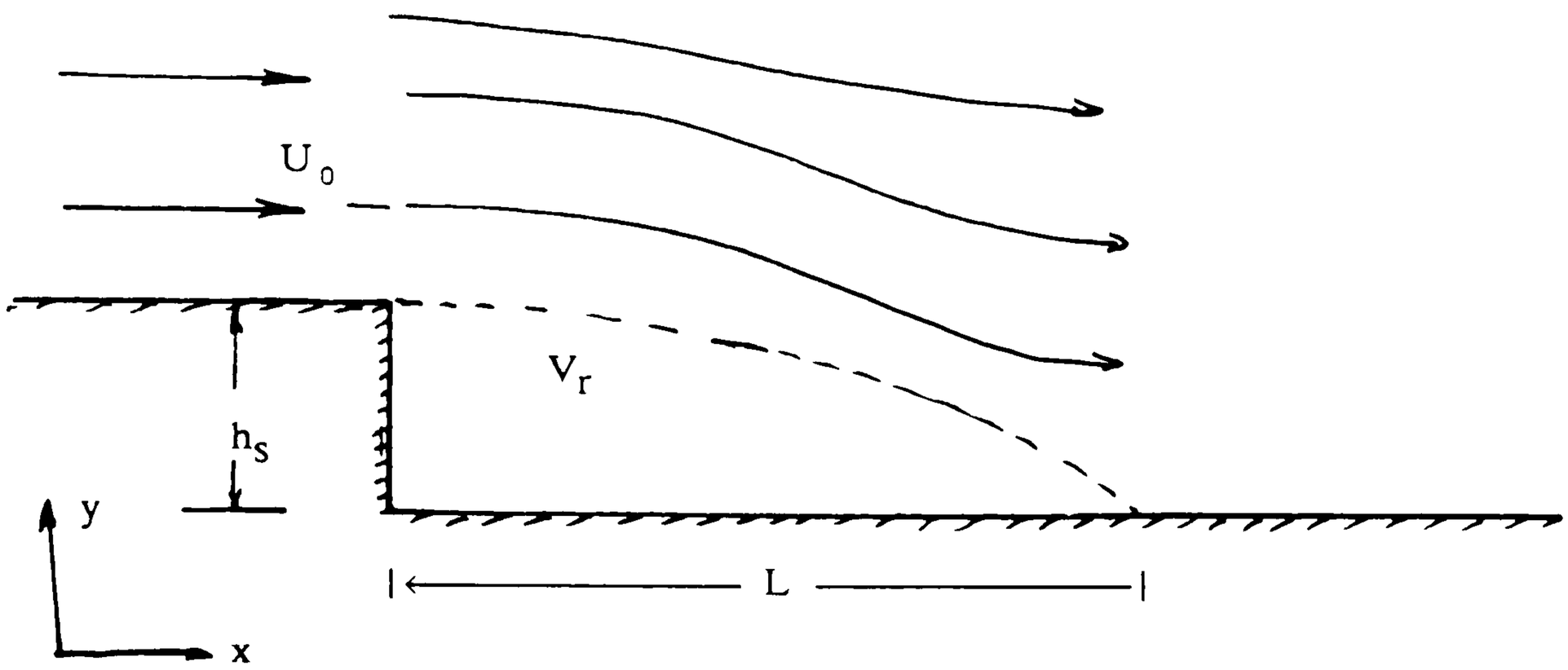

The production of turbulence in the shear layer is given by

$$\tau_{x,y} \frac{du}{dy} = \rho \epsilon \left(\frac{du}{dy} \right)^2 \qquad (7.12)$$

where ϵ is the turbulent eddy viscosity, given by

$$\epsilon = \frac{x}{2R} U_0 \quad \text{(where R =288) (after Lean \& Weare)} \qquad (7.13)$$

Assuming a bed friction dominance so that the turbulent shear stress within the shear layer can be related to the bed shear stress

$$\text{where} \quad \tau = \tau_0 = \rho U_*^2 \qquad (U_* = \text{shear velocity}) \qquad (7.14)$$

From equations (7.13) and (7.14) above, we obtain

$$\frac{du}{dy} = \frac{U^2_*}{U_0} \frac{2R}{x} \qquad (7.15)$$

Since $\frac{U_0}{U_*} = 2 \frac{C}{\sqrt{g}}$ where C = Chezy coefficient

then $$\frac{du}{dy} = \left(\frac{Rg}{2C^2}\right) \frac{U_0}{x} \qquad (7.16)$$

or

$$V_r/U_0 = (A)\ y/x + B \qquad (7.17)$$

An estimate of the value of B can be obtained by appealing to the points where u = 0 is shown in the sketch overleaf, by the dashed line.
Along this dashed line u = 0, and the distance from the wall is given by <u>half</u> the distance to the curved shear layer (solid line).

$$y = \frac{h_s}{2} \sqrt{1 - (x/L)^2}$$

where $\left(\frac{y}{h_s} \sqrt{1 - (x/L)^2}\right)$

is the shape of elliptical shear layer.

Therefore the final expressions is

$$\frac{V_r}{U_0} = \left|\frac{8R}{2C^2}\right|\left|\frac{y}{x} - \frac{h_s}{2x}\right| \Big/ \overline{1 - (x/L)^2}\ \Big| \qquad (7.18)$$

Clearly for the recommended value of R = 288, and Chezy $C^2 = 8g/\lambda$, where λ is the Darcy friction factor, then

$$\frac{V_r}{U_0} = 18\,\lambda\,\left|\frac{y}{x} - \frac{h_s}{2x}\right| \Big/ \overline{1 - (x/L)^2}\ \Big| \qquad (7.19)$$

revealing that the normalised recirculating velocity increases with friction factor for a given step geometry and distance downstream. This is an interesting observation implying that ratios of V_r/U_0 will be greater in the Series D rough case than the Series A smooth case.

It is also of interest to note that the maximum value of V_r occurs at approximately x/L = 0.5 and $h_s/x = 1/3$ giving a ratio of V_{rmax}/U_0 of the order of 0.5 which is in broad agreement with experimental values quoted in Fig (7.18). This corresponds to Mannings 'n' of 0.03 giving $\lambda = 8gn^2/R^{1/3} = 0.2$).

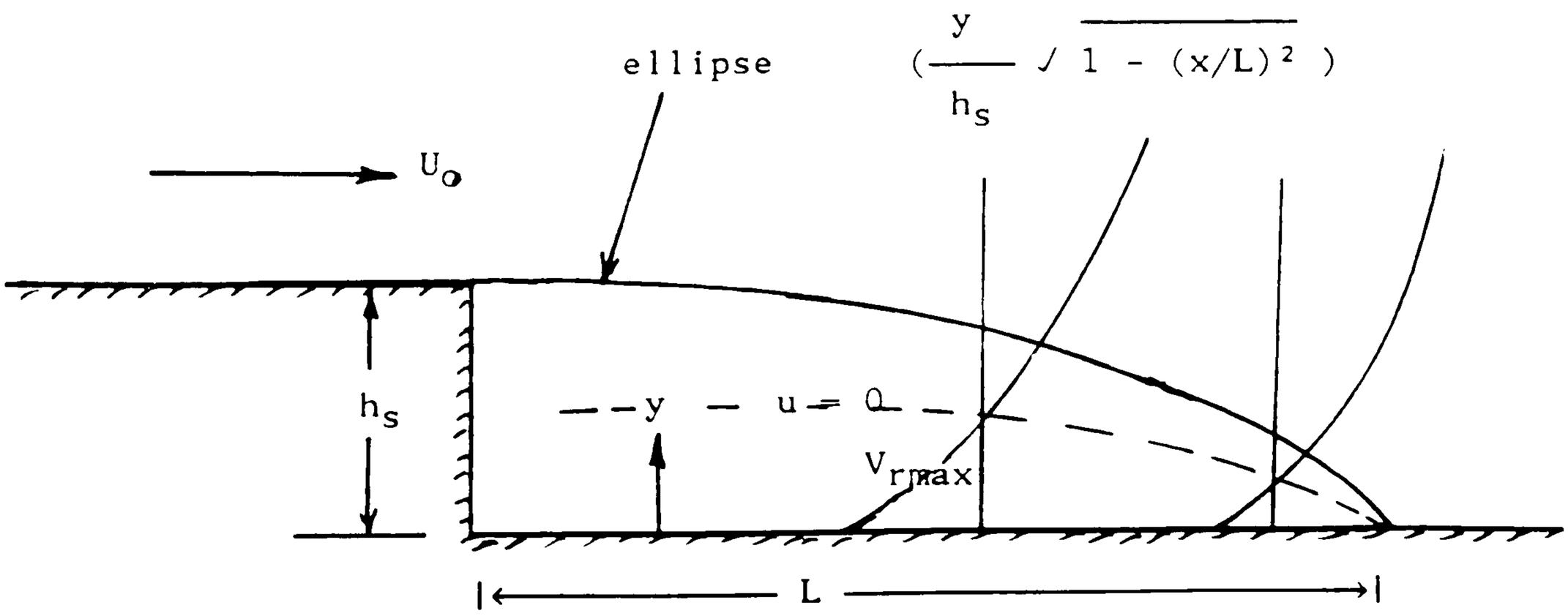

(ii) Approximate Analysis for Recirculation with no Boundary Friction But Only Shear Layer Turbulence.

In this case we assume that shear layer turbulence dominates over boundary shear. Again the production of turbulence in the shear layer is given by

$$\tau = \rho \epsilon (du/dy)^2 \qquad (7.20)$$

where ϵ is the turbulent eddy viscosity.

The problem now arises to find an approximation for τ (as in the rough case) so that a solution may be found for u. In fact, no such approximation exists, so resort was made to the concept of entrainment velocity as sketched overleaf.

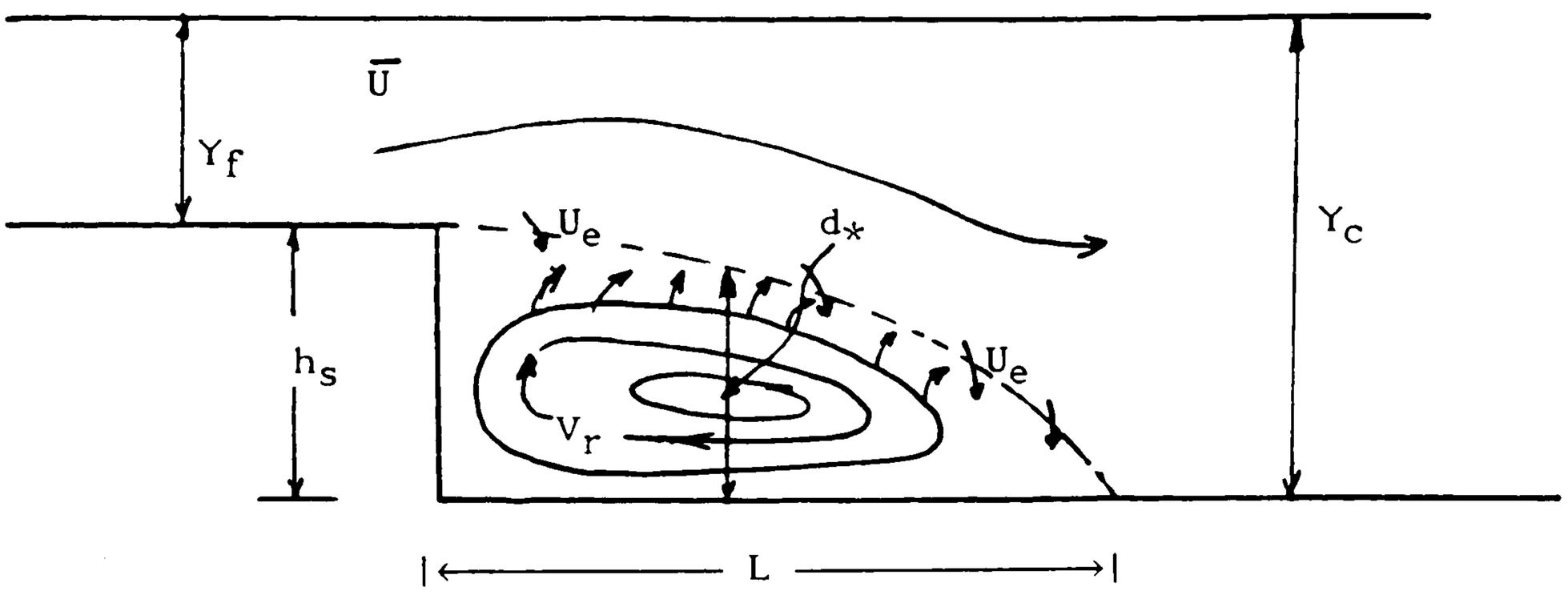

Considering the shear layer like an expanding plane jet then from Rajaratnam (1981), the entrainment velocity U_e

$$\frac{U_e}{U} = 0.026 \qquad (7.21)$$

for a closed recirculation there is no net inflow or outflow from the shear layer, so we could consider Ue to be acting over half the shear layer length (L/2) i.e. inflow into shear layer from recirculation = outflow from shear layer to recirculation region.

Thus the recirculating discharge per unit width

$$q_r = U_e \; L/2 \approx 0.026 \; U \; L/2 \approx 0.013 \; U \; L \qquad (7.22)$$

Also assume that $\sum q_r$ in recirculating region = 0, and the $V_{r\ max}$ occurs at section d_* shown (overleaf above)

Assume $d_* \approx h_s$

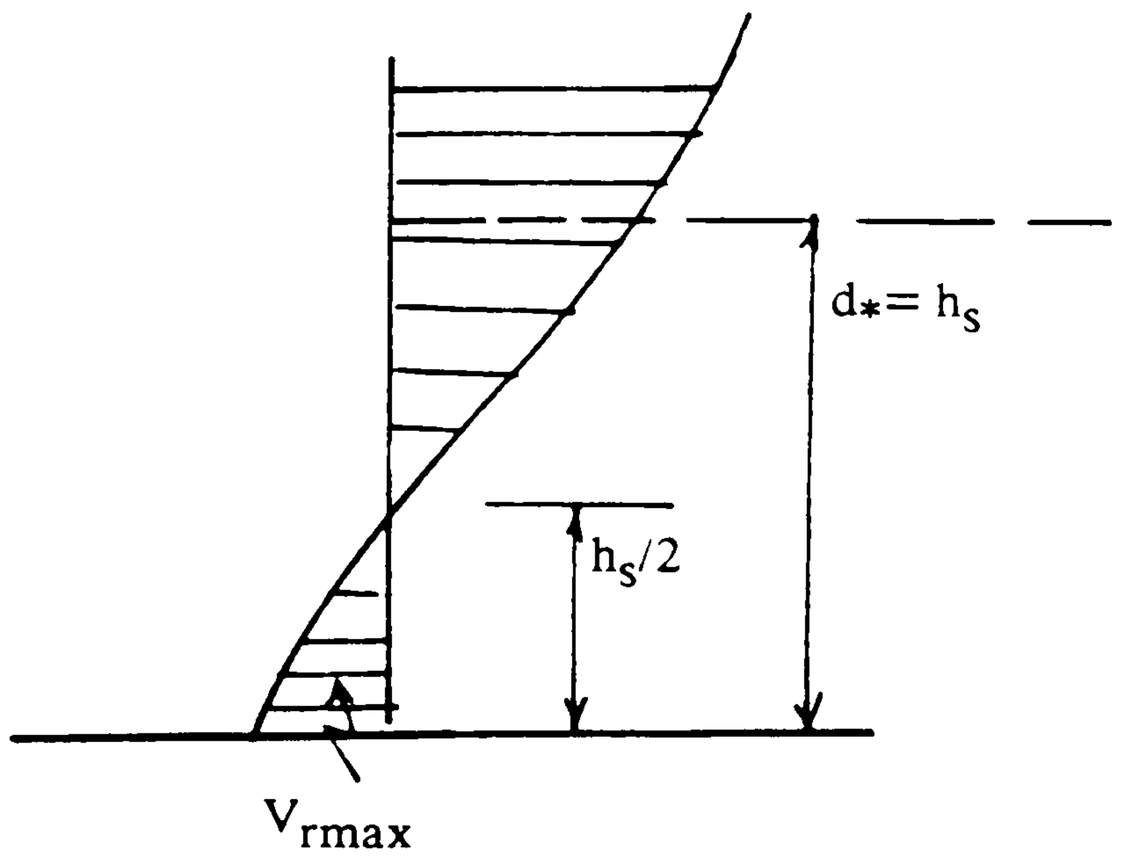

$$q_r \approx V_{r\ max}/2 \; h_s/2 = 0.013 \; U \; L \qquad (7.23)$$

or

$$\frac{V_{r\ max}}{U} = 0.052 \; \frac{L}{h_s} \qquad (7.24)$$

now highest value of $L/h_s \approx 6$

$$\frac{V_{r\ max}}{U} = 0.3 \qquad (7.25)$$

Again this is in broad agreement with smooth results shown in Fig (7.18)

7.7.4 CONCLUSION ON RECIRCULATING FLOWS

The Following tentative conclusions may be drawn from the mixture of experimental data and theoretical analysis in sections 7.7.2 and 7.7.3.

(i) There is considerable relationship between recirculating velocities in the skewed main channel and that of a slot. The relationship is not perfect as the two flow mechanisms are different.

(ii) Skewed channel recirculations appear to have higher recirculating velocities V_r compared with a comparable slot test. This may be due to the fact that flood plain flow is materially added to the skewed main channel spiral, whereas this is not the case in the slot tests.

It may also be a function of which flood plain velocity is used to normalise the recirculating velocities. Maximum flood plain velocities give better correlation with slot tests.

(iii) Experiments show that recirculations increase and then decrease with increasing relative depth of flow.

(iv) Experiments show that recirculations increase with decreasing aspect ratio of the main channel. (slot tests).

(v) Theory shows that recirculations increase with increasing boundary roughness.

These conclusions show that the slot energy loss (horizontal shear) can not be applied perfectly to skewed compound channel tests because it ignores the increased spiral velocities in the skew caused by flood plain flow being diverted.

7.8 DEPTH– AVERAGED LONGITUDINAL VELOCITIES IN SKEWED TWO–STAGE CHANNEL AND VARIATION IN THE DOWNSTREAM DIRECTION

7.8.1 The Depth Averaged Longitudinal Velocity Profile.

Figs (5.1) to (5.33) in chapter 5 reveal the variation of depth–averaged longitudinal velocity in a skewed compound section for a range of relative depths of flow (Y_f/Y_c), distances along the flume (Section 1, 2, 3) and for both flood plain roughness values. The results have been discussed in detail in Chapter 5.

One of the main conclusions from Chapter 5, is that the nature of the skewed main channel depth–averaged velocity profile is completely different from the straight/parallel case. The main features are sketched below showing the very distinct asymmetry of the velocity profile. This phenomenon occurs even at a point of symmetry in the skewed geometry, as has also been confirmed by Elliot and Sellin (1990) shown in Fig (7.19)

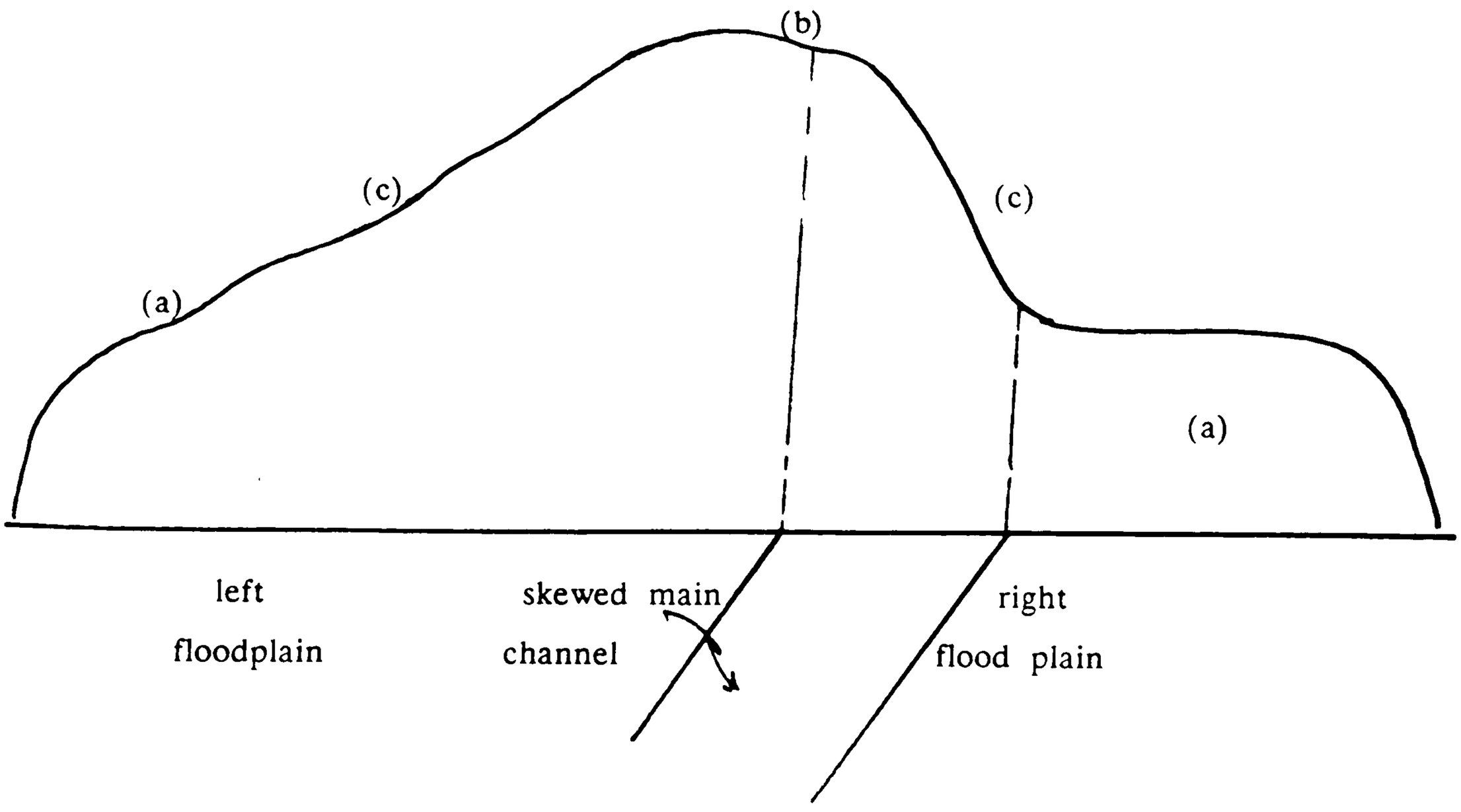

The first and most abvious point which arises from the sketch above is that the mean velocity on the right (converging) flood plain is less than the mean velocity on the left (diverging) flood plain. This is true for all relative depths tested, for all three cross–sections and for both flood plain roughness. A comparsion of the left and right flood plain mean velocities is given in Fig (7.20) for all experimental test runs. It is clear from Fig (7.20) that the left flood plain velocities are significantly higher than the right by afactor of 20%–30% but sometimes as high as 50%. The pattern is consistent for both smooth and rough flood plain boundaries, albeit for a narrower range of velocity on the rough flood plains.

The most significant aspect of this behaviour is the fact that left flood plain velocities are larger than right flood plain velocities even at a point of symmetry in the flume, at section 1 (see Fig (7.21) where the width of both flood plains are equal. This is also shown very clearly at the point of symmetry on the skewed SERC flume, described in the recent paper by Elliot and Sellin (1990) and shown in Fig (7.19).

The reason for this phenomenon must be sought carefully, because it is clear from the nature of the Glasgow flume geometry, that sections downstream of the point of symmetry are likely to have higher velocities on the left compared with the right, simply because the main direction of the flow along the flume, effectively moves the flood from right to left. This is true downstream of the point of symmetry, but at the point of symmetry a more uniform distribution of velocity would be expected.

One possible explanation is that lateral momentum transfer occurs in the same fashion as the straight/parallel flood plain case, caused by turbulent shear between the co–flowing main channel and flood plain. In this skewed case such lateral shear momentum transfer occurs, but is modified by the natural cross–flow from right to left flood plain. i.e. flow from the right flood plain enters the skewed main channel region and lateral enters the left flood plain. The natural right to left flow in the skew simply pushes the maximum velocity filament to the left side of the main channel (or even onto the left flood plain) with co–flowing shear happening around the maximum velocity filament axis rather than the centre of the main channel, as is normally the case. This explanation, based on a combination of lateral shear and natural right to left flows, does not offer a complete explanation for the velocity asymmetry at the point of geometrical symmetry.

A full explanation is more likely to be found in the sketch below covering the full flume length. A sketch of a typical depth averaged velocity is shown at the flume entrance, clearly revealing an asymmetrical entrance profile simply because the deeper main channel is on the left side of the flume. This is an inbuilt asymmetry of velocity.

Further more at section 3, near the end of the skew, the maximum velocity filament has been found to move to the left wall of the main channel or unto the left flood plain at layer flow depths. This means that the line of maximum velocity filament along the flume length (shown dashed) moves along a line whose angle is less than θ, and is therefore bound to produce an asymmetry even at the point of symmetry (Section 1).

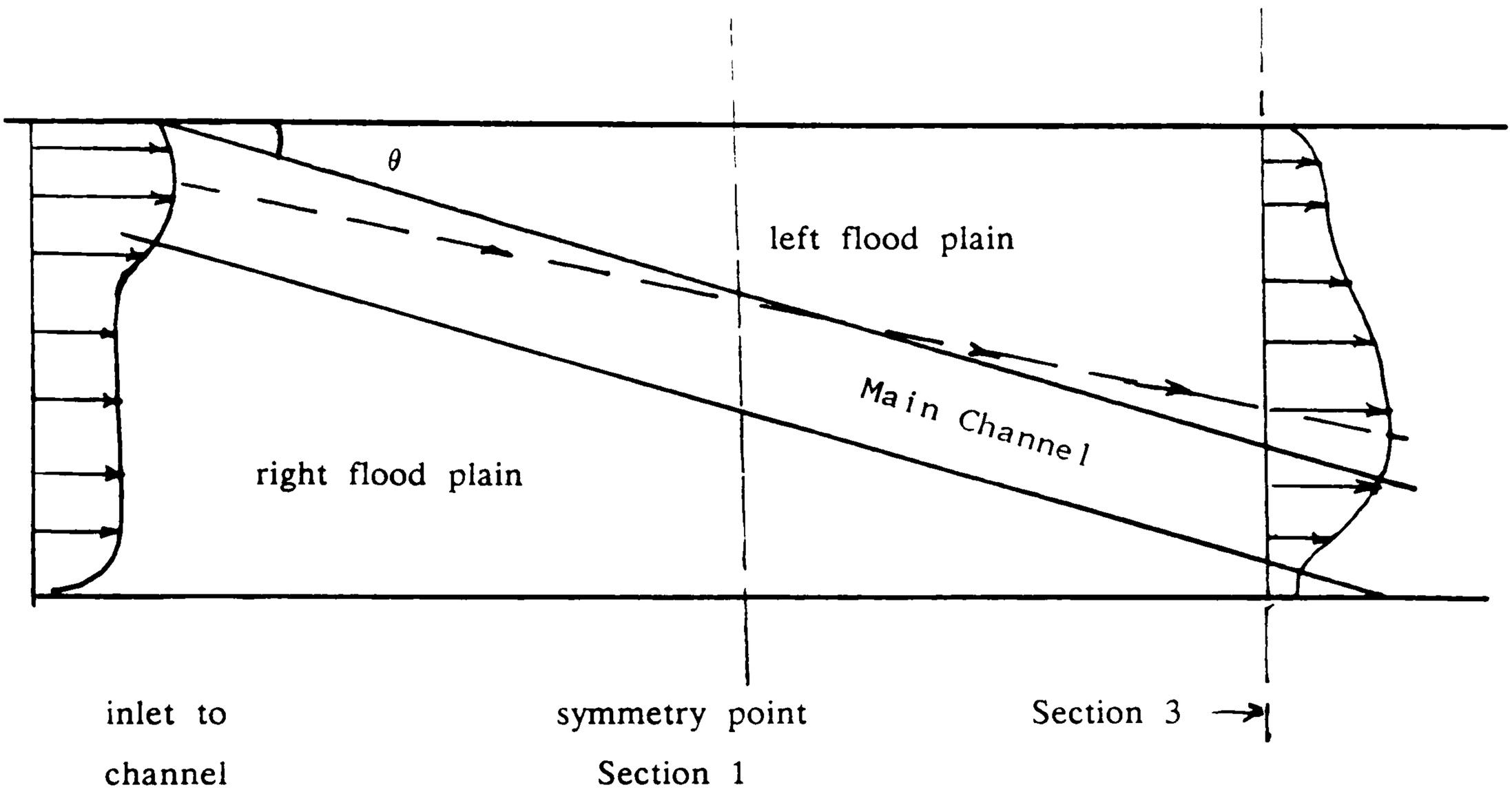

distribution of typical depth– averged velocities along flume length

7.8.2 Position of the Maximum Velocity Filament.

A plot of the position of the maximum velocity filament is shown in Fig (7.20) for the case of the smooth flood plains. Fig (7.20) is a plan view of the flume between section 1 and section 3 indicating both the line of the skewed main

channel, as well as the centre– line of the overall flume. The dashed lines on Fig (7.22) show the position of the maximum velocity filament for a range of relative flow depths from $Y_f/Y_c = 0.15$ to $Y_f/Y_c = 0.5$.

Low relative depths indicate a maximum velocity filament which lies within the skewed main channel, but moving towards the left side of the skewed main channel. High relative depths of flow reveal the position of the maximum velocity filament to be to the left of the skewed main channel, and in fact in the general vicinity of the centre line of the flume. Intermediate flood plain depths reveal a maximum velocity filament to be at the left wall of the skewed main channel or just on the left flood plain.

This means that cross– flows push the maximum velocity filament towards the left of the main channel. At high relative depths the flow is dominated by the flood plain geometry, with the main channel having little or no effect on cross over flows which become much more centrally orientated around the centreline of the flume.

This may have a significant effect on the longer term development of 2– stage channels in the sense that sediment movements are likely to occur on the left bank of the main channel, moving the skew to the left and in fact tending to cause a realignment nearer the straight/parallel case.

The maximum velocity filament position for the rough flood plain case is shown in Fig (7.22), again from section 1 to 3 and for a range of relative depths.

The most significant feature of Fig (7.22) is that the maximum velocity filament is always contained within the skewed main channel, even of large relative flow depths. This is a function of the line of least resistance along the main channel, rather than the rough flood plain, which offers approximately three times more resistance than the main channel.

The other feature of **Fig (7.22)** is that the maximum velocity filament is again on the left side of the main channel (because of cross– over flows) and hence in nature will tend to move the main channel towards the left.

7.8.3 The Width of Lateral Shear Layers in 2–Stage Channels.

The width of the lateral shear layers is greater on the left side than the right flood plain. This is shown in **Fig (7.23)** for the smooth flood plain case. The width of the lateral shear layer is estimated approximately from the depth–averaged velocities, to the point where the velocity remains approximately constant. This point on the left flood plain is shown as solid curves representing a low relative depth and a high relative depth. It is clear that the the left flood plain shear layer increases substantially in width with increasing relative flow depth. The edge of the right shear layer is indicated as a dashed curve on Fig (7.23) for both a low and high relative flow depth. The right shear layer extent barely encroaches unto the right flood plain implying substantial momentum transport from right flood plain to the main channel. This implies little or no scour on the right flood plain, with a good chance of sediment deposition. This represents a major departure from straight/parallel compound flows with their symmetric shear layers on both flood plains. This also presents considerable difficulty in simple turbulence models of lateral eddy viscosity, which would now require to be modelled differently on either flood plain.

Fig (7.24) shows the comparable width of shear layers on the left and right flood plains, for a high and low relative flow depth, for the case of the rough flood plain. Again the left shear layer is much wider than the right, which essentially goes along the right main channel wall. This time the left shear layer width is only about half of that of the smooth boundary case in Fig (7.23), which is to be expected in view of the greatly increased resistance to flow.

7.8.4 Variations in Mean Velocity in Each Sub–Section of the Flow.

It was decided to investigate the variation in mean velocity in each sub–section; right flood plain , left flood plain and the main channel alone, and to investigate their variation in the downstream direction.

(a) Skewed main channel with smooth flood plain.

The variation in the mean velocity on the smooth left flood plain is shown in

Fig (7.25). Plotted against relative depth of flow and at each of the three cross sections. The solid curve in **Fig (7.25)** refers to the flood plain isolated case, using only the accurate boundary friction values determined in Chapter 4.

It is clear from **Fig (7.25)** that left flood plain velocities are greater than the isolated flood plain case. The dashed lines indicate mean velocities at Section 1 to Section 3 and for the most case indicate a slight reduction in mean velocity in the downstream direction but not significantly so.

The variation of the mean velocity on the smooth right flood plain is shown in **Fig (7.26)**. Here it is clear that the mean velocities on the right flood plain are less than the isolated case determined from a knowledge of boundary roughness. Second, there is a clear reduction in mean velocity moving in the downstream direction from Section 1 to Section 3.

The reduction in right flood plain mean velocity in moving downstream has also been shown by **Elliot results Fig (7.19)** and is a function of the flow patterns in the overall flume. The right flood plain is diverging, is being influenced by the flume walls more and more in the downstream direction, and is being influenced by the gradual shifting of velocity filaments to the left side of the main channel and left flood plain. Thus the net momentum transfer is towards the left flood plain.

The variation in the mean velocity within the main channel sub–section is shown in **Fig (7.27)**. Here it is seen that a very slight reduction of mean velocity occurs in the downstream direction again implying lateral momentum transfer to the left flood plain. This is consistent with the maximum velocity filament moving to the left and also out of the main channel (at higher relative flow depths) unto the left flood plain.

Fig (7.27) in combination with finding on flow bifrucation in Section 7.6 now reduce a significant finding for skewed two–stage channels.

If streamlines from the flood plain swirl down into the main channel spiral as shown is dye tests, and if this occurs right along the right flood plain length, then the mean velocity in the main channel should increase, because it is having flow added materially from the right flood plain. In fact the mean velocity in the main channel shows a slight decrease in the downstream direction. This means that the

spiral must decrease in intensity in the downstream direction. This has already been proved in Section 7.7.2. and shown in **Fig (7.16)**.

This of course raises the question of equilibrium. Is it ever possible to reach an equilibrium condition in a skewed flume where nothing varies in the downstream direction. The answer to this must be no, because by its nature a skew must have a continuousty diverging flood plain on one side and a continuously converging flood plain on the other. Thus dis– equilibrium is assured and completely uniform flow is not feasible.

(b) Skewed main channel with rough flood plain

The variation of the mean velocity on the rough left flood plain is shown in Fig(7.28) and clearly shows an increase in velocity in the downstream direction from Section 1 to Section 3. This indicates a large momentum transfer to the left flood plain although not significantly so at very high relative flow depths.

The variation of mean velocity on the rough right flood plain is shown in Fig(7.29). The picture is confused by a strange result at relative depth around 0.27, but as a general rule, the mean velocities on the right flood plain decrease in the downstream direction.

It is clear from both Fig (7.28) and Fig(7.29) that the mean velocity is substantially higher on the left flood plain compared to the right.

Fig (7.30) shows the variation of mean velocity in the rough main channel sub– section. It is clear from this figure that there is no substantial reduction in velocity between Sections 1 and 3 in the downstream direction.

This implies that momentum added to the main channel from the right flood plain is added to the left flood plain giving little or no reduction in the main channel in the downstream direction. Again this is expected for the rough case as we have already seen that maximum velocity filaments never reach the left flood plain (as in the smooth case) showing that less momentum is lost to the left flood plain compared with the smooth case.

7.9 APPLICATIONS TO THE DESIGN OF 2–STAGE CHANNELS

The desgin of a two–stage channel such as the River Roding **Fig** (1.3), involves predicting how deep to cut the berms producing a lower bank level, and secondly how wide to contruct the berms out to the flood plain side walls. In essence, the designer must be able to predict the stage–discharge relationship for any two–stage channel whether meandering, skewed or straight, for any cross sectional geometry and for any given boundary roughness values.

At present there is no completely accurate method for predicting stage–discharge curves for two–stage channels, but a possible range is as given below.

(a) A two–dimensional numerical model.
(b) A one–dimensional numerical model.
(c) Application of a method proposed by Ervine and Ellis (1987).
(d) Using channel sub–division methods as outlined in section (7.2) and (7.3).
(e) A physical model study of the area involved.

(a) Wark (at the University of Glasgow) has recently developed a two–dimensional model of meandering two–stage channels. The method is a finite element technique to accomodate curved boundaries, and extends the original work of Dr. Paul Samuels (1985). By its nature the model predicts velocities in the x–y directions and is therefore depth–averaged. It does include lateral turbulent shear to simulate lateral momentum transfer.

The work of this thesis, however, shows that a depth averaged model will be inaccurate on two counts. It does not include horizontal shear at cross–over regions, and more importantly, is able to simulate circulations only in plan view. It is clear from this work, and recent work in meandering compound flows, that very substantial circulations occur over the channel depth, both at cross–over regions and at channel bends. These would not be simulated in a depth–averaged model.

The use of a width–averaged 2–D model would not be suitable either because of large variations in conditions with width in a compound cross–section.

(b) One dimensional numerical models of the type devised by **Knight (1988), Wormleaton (1988), Kiely (1989), and Wark** (1990) are even less suitable than two– dimensional models. Although the 1– D models incorporate lateral turbulent shear stress, they omit horizontal shear and recirculations (as in the 2– D case), and they also omit convective acceleration terms (udu/dx) which are necessary for such flow decelearation and acceleration as it passes over the main channel. The 1– D model also omits all transverse components of velocity and hence has a limited application in the area of straight/parallel two stage channels. The one dimensional models of this nature are not applicable to skews either because of substantial recirculations in skewed main channels and deviation of streamlines causing large V components which are ignored.

(c) A one dimensional model was proposed by **Ervine and Ellis (1987)** for the case of a meandering two– stage channel. They divided the compound section into sub– areas and quantified the energy losses associated with each. **Ervine and Ellis** estimated the energy losses for meandering channel with flood plain by dividing the total cross– section into three areas as below:

(1) The main channel below bank level.

(2) Flood plain area 1, which includes the flood plain flow inside the meander belt, of width W_m.

(3) Flood plain area 2, covering the flood plain flow outside the meander belt.

(i) <u>The energy losses from the main channel</u>

(1) Friction losses around the wetted boundary.

Colebrook– White equation and the smooth low equation are used to estimate the appropriate friction factor, Reynolds Number and Darcy– Weisbach equation to determine the mean velocity. This loss was discussed in Chapter 4.

(2) The lateral shear layer is due to the co– flowing shear between the main channel velocity and the longitudinal flood plain velocity component. **Ervine (1987)** suggests that this additional shear stress be treated as an apparant shear stress τ_a acting over the interface area.

(3) The energy losses due to secondary currents.

Meandering bends with outward centrifugal pressures generate transverse currents (V_r). These secondary currents are in effect a large scale turbulent eddy occupying most of the cross–sectional area, giving rise to energy loss, both in the form of internal fluid friction and also boundary resistance due to transverse shear. A method proposed by **Chang (1983)** was used by **Ervine and Ellis (1987)**. For the case of skewed main channel with small skew angle such as 5.843^0 the energy loss due to bend is almost insignificant.

(ii) The energy loss from flood plain flow inside the meander belt.

(1) Frictional losses summed over the wetted area on the flood plain within the meandering width. This loss was discussed in Chapter 4.

(2) Expansion losses due to flood plain flow passing over the main channel flow, where the flood plain flow encounters the sudden drop at the entrance to the main channel. This phenomenon was discussed in detail in Chapter 6.

(3) Contraction losses where the flow encounters an abrupt rise and re–enters the flood plain. A contraction loss coefficient ($C_{L)}$ was determined from the experimental results and also discussed in Chapter 6.

(iii) Energy losses of flood plain outside the meander belt.

The flood plain outside the meander belt is considered to have frictional losses around the wetted perimeter. Colebrook–White equation was used to find the friction factor and Darcy–Weisbach equation used to find the mean velocity.

In the light of the work in this thesis and that by **Kiely (1989)**, **the Ervine and Ellis** model is not very appropriate. Although the model attempts to simulate losses from bend secondary currents and cross–over flows, and ignores lateral turbulent shear, the estimates for bend secondary currents and cross over flows are not accurate. First, the secondary cells at bends rotate in the opposite direction to inbank flows and are of greater magnitude than inbank flows, and secondly, the cross–over flows do not cross–over, like flow over a slot, but instead the

streamlines deviate and bifrucate down in the main channel to be transported off in a different direction to the remainder of the flood plain cross–over flow. This combined with the fact that lateral turbulent shear is ignored, means that the **Ervine and Ellis** model is not useful. Work is at present under way to incorporate the new flow mechanisms into a more physically sound 1–D model which reflects the actual flow mechanisms occuring.

(d) Sub–divided channel methods.

It is clear from Section 7.2 and 7.3 that sub–divided channel methods for discharge assessment are seriously in error for skewed compound flows. For the smooth flood plain case in Section 7.2, the errors can be up to 25 – 30% in discharge estimate at a relative flow depth around 0.15. This pertains to the vertical imaginary wall subdivision method assuming bed friction to be the only energy losing mechanism. For high relative depths around 0.5, the errors would appear to be negligible (Fig 7.1), thus indicating a specific point where the compound flow discharge could be estimated with some accuracy.

A problem arises however for this particular relative depth when the flood plain is rough, as in Fig (7.8) where $n_f/n_c \approx 2$ to 4. The rough flood plain case produces increasing errors with increasing relative depth, reaching values of discharge error of the order of 50 to 60% at higher flow depths. Therefore for the case of rough flood plain, the discharge could not be estimated by a vertical sub–division method, particulary at higher flow depths. Fig (7.8) has shown how this problem can be overcome by placing an imaginary horizontal sub–division with flood plain friction at, or just below the bank full level. As a general rule this reduces errors to below 10%, which is acceptable. This method could now be accepted as a rough guide to discharge assessment provided the flood plain is of the order of 2 to 4 times rougher than the main channel.

For the case of flood plain roughness comparable to the main channel roughness ($n_f/n_c = 1$) and both boundaries relatively smooth, then the problem remains as to how to estimate the errors involved. There are three possibilities :–

– Use the error curves in Fig (7.6) to correct for the discharge over–estimated by the vertical wall sub–division method. This method is approximate but useful as a first guide to the true stage–discharge relationship.

– Determine the apparent shear stress and apply to each sub–section of the flow as per the method of Ervine and Baird (1982). This method is approximately correct for straight/parallel compound flows (Wormleaton and Merrett (1988)), but is completely inadequate for skewed flows. The most recent paper by Elliot and Sellin has shown no consistant pattern in the value of apparent shear stress.

– Devise a system of determing Radokovic type Φ indices to be applied to each subsection of the flow. This has been done for straight/parallel cases (Wormleaton (1988)) but has still not been attempted for either skewed or meandering compound flows.

Thus it is clear that the crude method of applying Fig (7.6) discharge errors to the discharge estimated by the vertical sub–division method, is the best estimate for smooth boundaries at the present.

(e) Physical modelling of compound flows.

Physical modelling of a river/flood plain situation is becoming a less and less popular method of investigating flows in compound channels. This is mainly because of the great expense of the model, plus the fact that scale effects may introduce as many errors as a two dimensional numerical model, such as that described in (a).

Although the work of this thesis involved a small scale compound flow physical model, the purpose of the model was not to investigate a specfic problem, but instead simply to highlight flow mechanisms in order to produce more realistic computer models.

Physical modelling of river–flood plain situations does present some specific problems:–

– The flood plain is usually an order of magnitude wider than the main channel, necessitating a very wide testing area.

– The Reynolds Number of the model flood plain may be also as low as to produce laminar flow, or at least flow which is much less turbulent than nature.

– In order to overcome both problems above, it is common to construct a distorted model often with vertical distortion of the order of 2:1 or 3:1. This provides more realistic Reynolds Numbers in both main channel and flood plain, ensuring that a better degree of bed generated turbulence is achieved.

It is also creates a problem in the sense of simulating large and strong secondary cells such as found in the study. In nature the aspect ratio of the main channel may be 10, typically, with a large secondary cell occupying most of this width. In a distorted model, the main channel may have a typical aspect ratio of 3, which means that the secondary cell is now distorted in shape and probably in magnitude as well. This is important for cross–over flows where the recirculating cell may form naturally to about 6 $\longrightarrow$ 7 bankfull depths into the main channel. This is not physically possible in a distorted model with aspect ratio of 3.

– A further more significant problem is how to simulate flood plain roughness in a scale model. Most river flood plains are composed of grass, reeds, hedges, trees, and are totally different in character to the main channel, which may be composed of sand, silt, stones and cobbles. It is often sufficient to introduce bed roughness in the main channel to simulate natural roughness. However. what is the best type of roughening elements to use on the flood plain? Experience has shown that roughness elements stuck into the flood plain bed does not generate enough turbulence throughout the flood plain flow depth. Hence it is considered more effective to introduce vertical roughening rods such as used in this work. This produces turbulence over the full flood plain flow depth, but it has the side–effect of steadily increasing Mannings 'n' with depth, a phenomenon which does not occur readily in nature. A compromise solution might involve using flexible vertical roughness elements which bend due to the oncoming flow and which become submerged after a certain flood plain flow depth, with decreases in Mannings 'n' values therafter.

(f) Summary

There is at the moment no reliable method of determining stage–discharge curved in a compound skewed or meandering channel. The best method is still physical modelling especially in a large natural scale model with no vertical distortion. Reynolds Number effects should keep scaling errors to within 10% on discharge estimates.

Two– dimensional numerical models are progressing, but because of non– simulation of various features, could not be expected to be any more accurate than _ 20% on discharge estimates for compound flows.

The current range of one– dimensional models are not applicable to skewed and meandering compound flows and hence are unlikely to be reliable to any greater accuracy than _ 20⟶30%. This is essentially because of ommission of secondary cells at cross– overs and bend.

The use of error curves in Section 7.2 and 7.3 should provide a useful first estimate of discharge in a compound channel.

7.10 LONG TERM BEHAVIOUR OF TWO STAGE CHANNELS

Chapter 1 in this thesis commenced with a description of two stage channels and environmental benefits they might be bring to river flooding situations. Providing space is avilable at the sides of a meandering river to cut– out berms and to provide an upper stage of flow, then flooding problems can be minimised elsewhere.

The two– stage channels have been employed in earnest only over the last decade or so, and one of the main questions regarding their performance is how they will behave in the longer term. In praticular, the formation of side berms at a lower bank full level will ensure that more sediment transport will occur on to the side berms, as the largest river sediment movements occur during floods. The question then becomes, "will two– stage channel side berms simply silt– up again?" due to sediment deposit on the flood plains during high flows.

(i) Straight and parallel two– stage channels.

In this case the physical process is dominated by the classical lateral turbulent shear mechanism. During floods there is the distinct possibility of fine bed material being held in suspension. Such fine material might be transported unto the edges of the side berms because lateral momentum transport is present and is therefore capable of lateral transport of fine material.

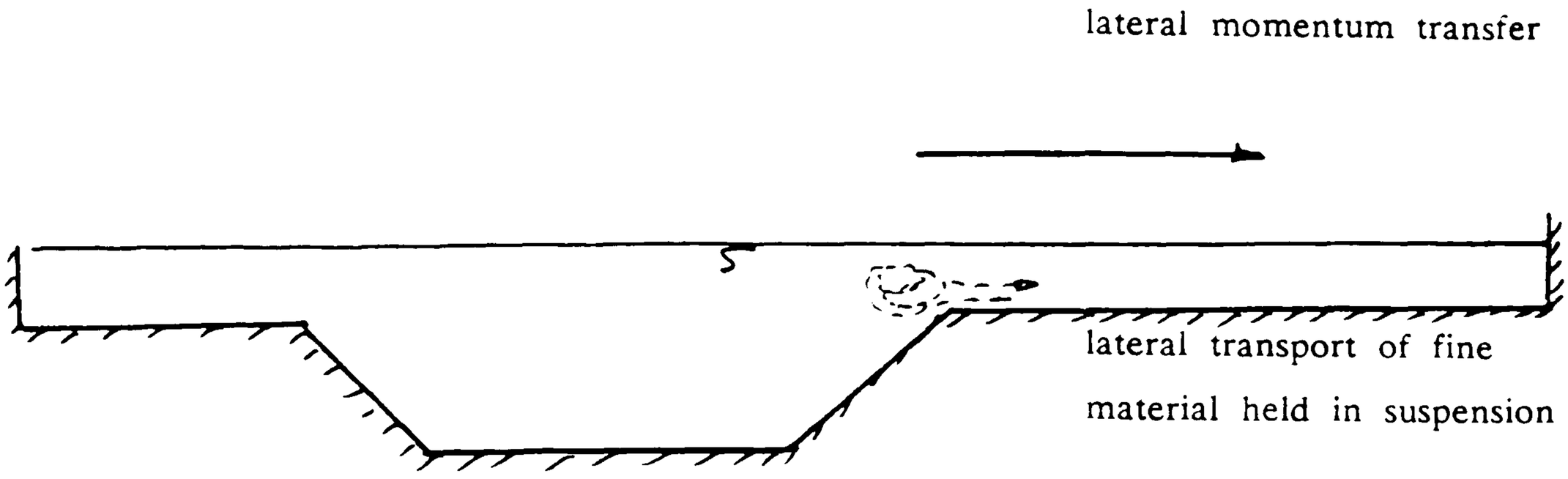

This is most likely to produce sediment deposits at or near the edges of the berm nearest the main channel. This is likely to produce local banks of material in the region eventually raising the bank–full level region.

(ii) Skewed main channel two–stage channel

Some of the physical flow mechanisms discovered in this work are sketched in **Fig (7.31)** in the case of a skewed main channel compound flow. The depth averaged longitudinal velocity is shown together with deviation of mean flood plain streamlines as well as the main channel spiral caused (and added to) by the cross–over flow. What effect are these mechanisms going to have on the longer term behaviour of two stage channels?.

– The most likely effect will be a result of the high velocity along the left side of the skewed main channel which is likely to cause more erosion along that bank relative to the right bank.

– The lower velocities on the right berm compared with the left is likable to lead to differential sediment deposit with more laid down on the right side compared to the left.

– Both these effects will tend to move the skewed main channel to the left and to reduce the effectiveness of the right flood plain as a true two stage channel.

– The large recirculating spiral in the skewed main channel is likely to cause most bed load scour at the point where the recirculation spiral plunges towards the channel bed, usually at a distance of around six times bank–full depth measured

from the right bank. For most channels this is liable to cause scour near the centre of the main channel or on the left side of the main channel.

(iii) Meandering two– stage channels

The case of meandering two– stage channels is further complicated by the presence of river bends. This however is the most common form the two– stage channel and hence is the considerable practical interest. There are two main effects represented in **Fig (7.32) and Fig (7.33)** respectively.

Fig (7.32) shows a diagram from **Goncharov (1964)** giving streamlines in a compound meandering two– stage channel. In this case it can be seen that sediment is likely to be deposited on the flood plains in the region where the streamlines are furthest apart. This differential sediment deposit is likely to produce sediment build– up in the flood plain region between the two cross– overs as in **Fig (7.32)**. This means that more flow will be forced down the existing river channel during flood periods and also a secondary channel may form at the bottom of the diagram, joining up to two bends to give a kind of flood relief channel.

This is a problem of differential sediment deposit changing the nature of the two– stage channel as designed.

A second problem is shown **Fig (7.33)** and concerns the direction of secondary currents at river bends during compound flows. The example shown in **Fig (7.33)** is from the SERIES B SERC flume tests at the apex of a bend. The diagram shows transverse velocities and a large recirculation in the OPPOSITE direction of conventional in– bank flow river bends. The magnitude of the recirculation is also about twice that of an inbank river bend secondary flow. This phenomenon has also been confirmed by **Kiely (1989)** and **Toebes and Sooky (1967)**.

The implication of **Fig (7.33)** is that scour at compound river bends will occur at the inside of the bend rather than the outside of the bend, which means that in two– stage channels, the cross section at the river bend will begin to become deeper at the inside of the bend and give deposits at the outside of the bend. Also the meander pattern will tend to straighten, simply because the inside bends will be scouring thus reducing the overall sinuosity.

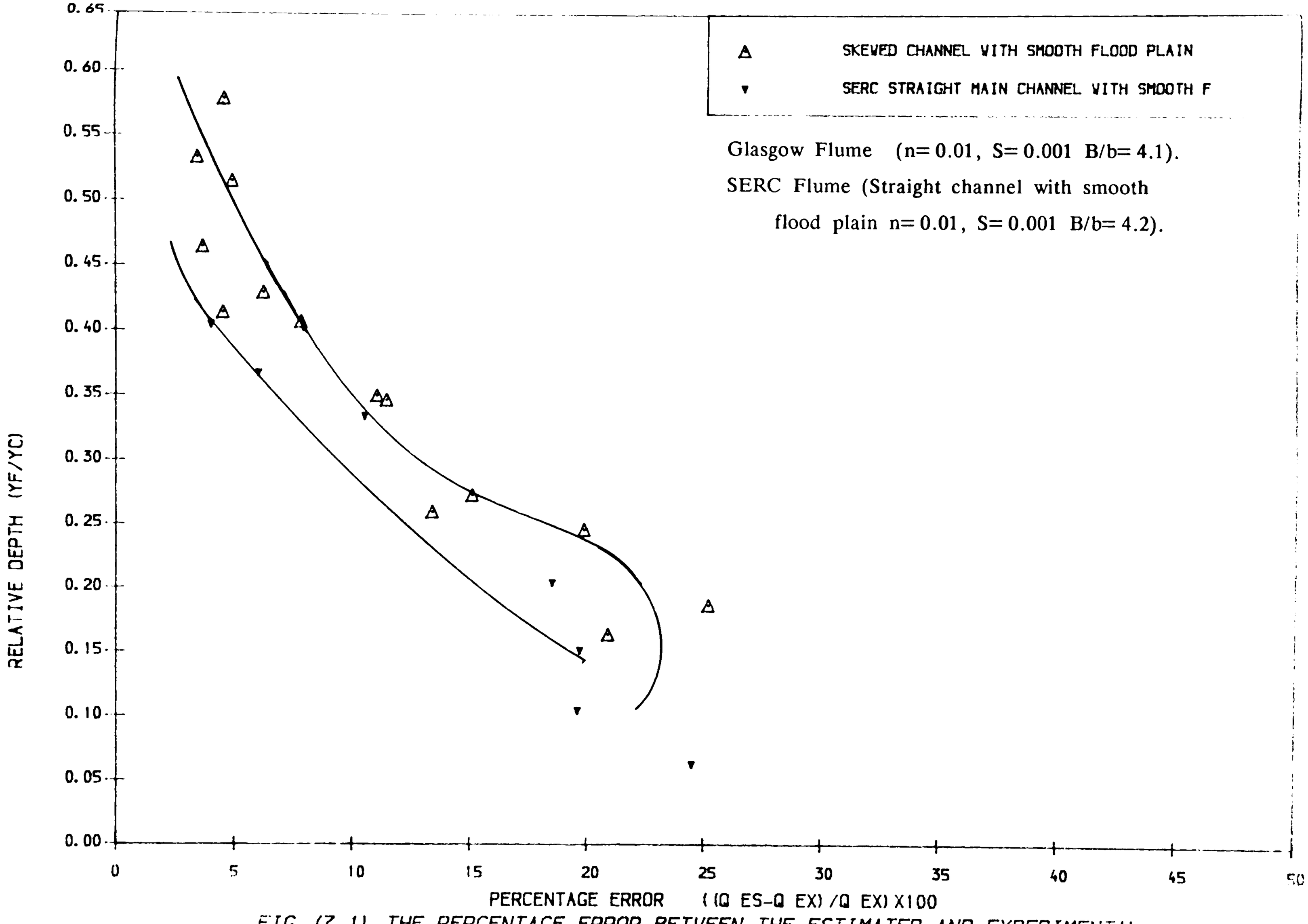

FIG (7.1) THE PERCENTAGE ERROR BETWEEN THE ESTIMATED AND EXPERIMENTAL DISCHARGE WITH THE RELATIVE DEPTH

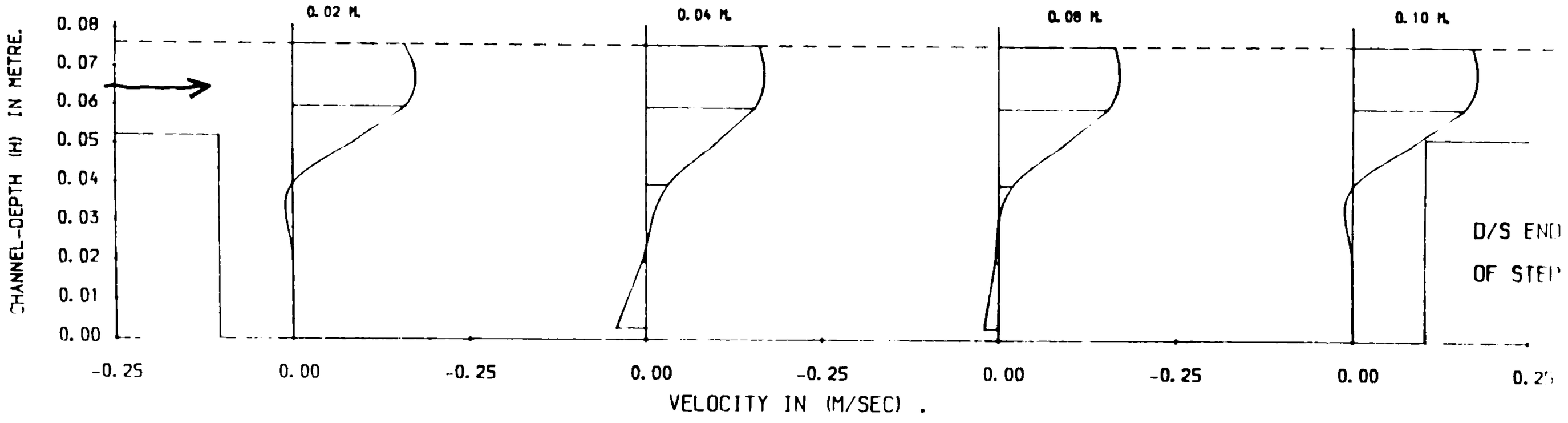

Fig (7.2a) THE VELOCITY PROFILE THROUGH THE SLOT (BC/h=2)

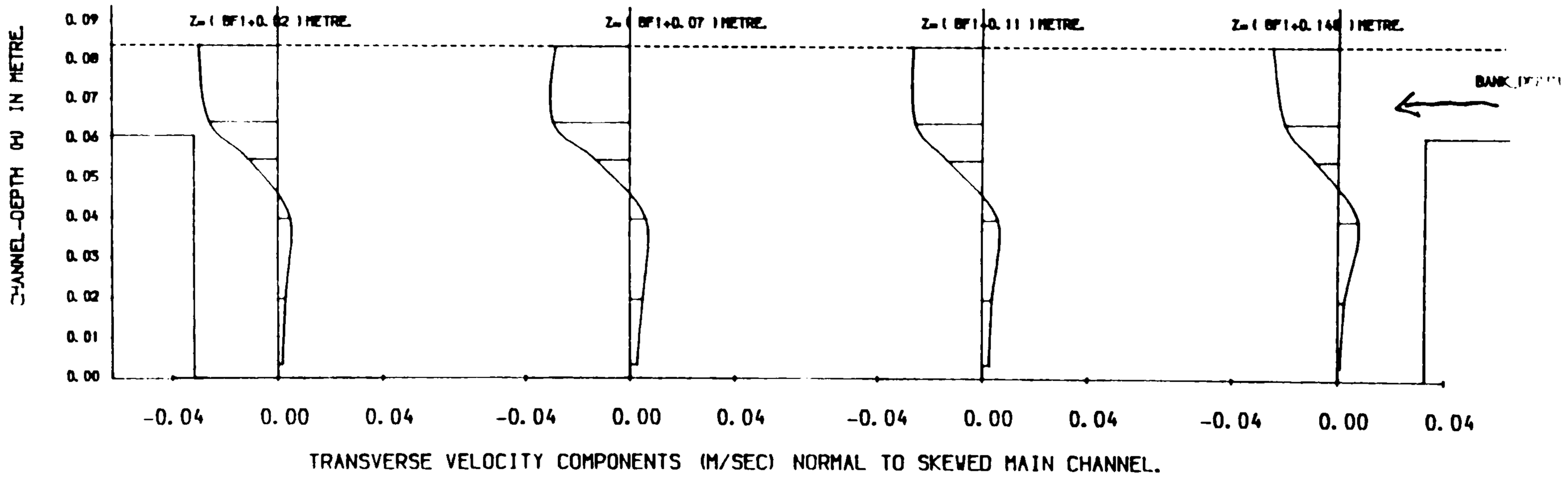

Fig (7.2b) LONGITUDINAL & TRANSVERSE VELOCITYCOMPONENTS IN SKEWED CHANNEL WITH SMOOTH FLOODPLAIN

Fig (7.2) Longitudinal and Transverse Velocity Components in Skewed Main Channel with Smooth Flood Plain and Slot.

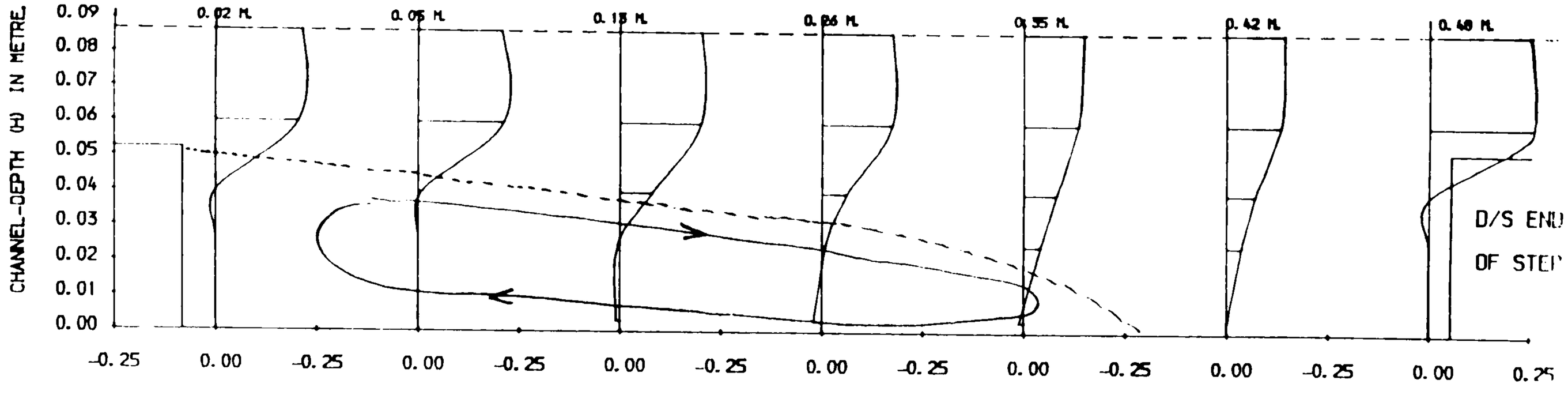

Fig (7.3a) THE VELOCITY PROFILE THROUGH THE SLOT (BC/h=10)

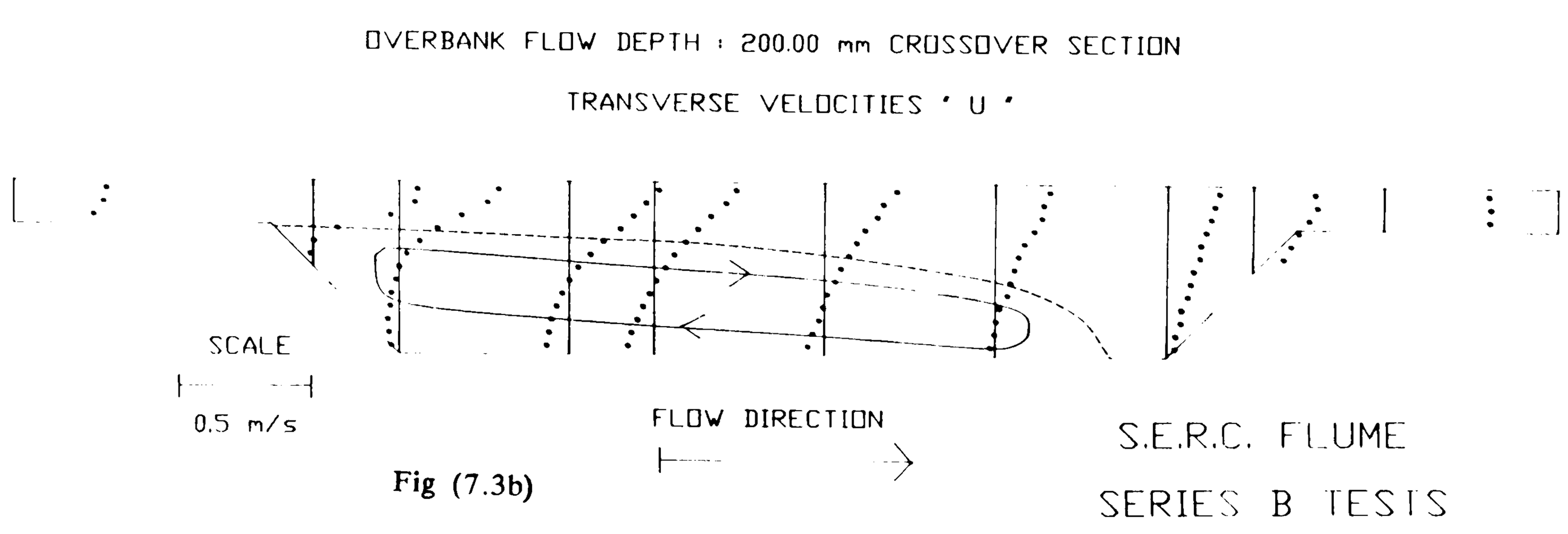

Fig (7.3b)

Fig (7.3) The Recirculation Velocity for the Meandering Channel with Flood Plain (SERC Flume) and Velocity Profile for the Slot

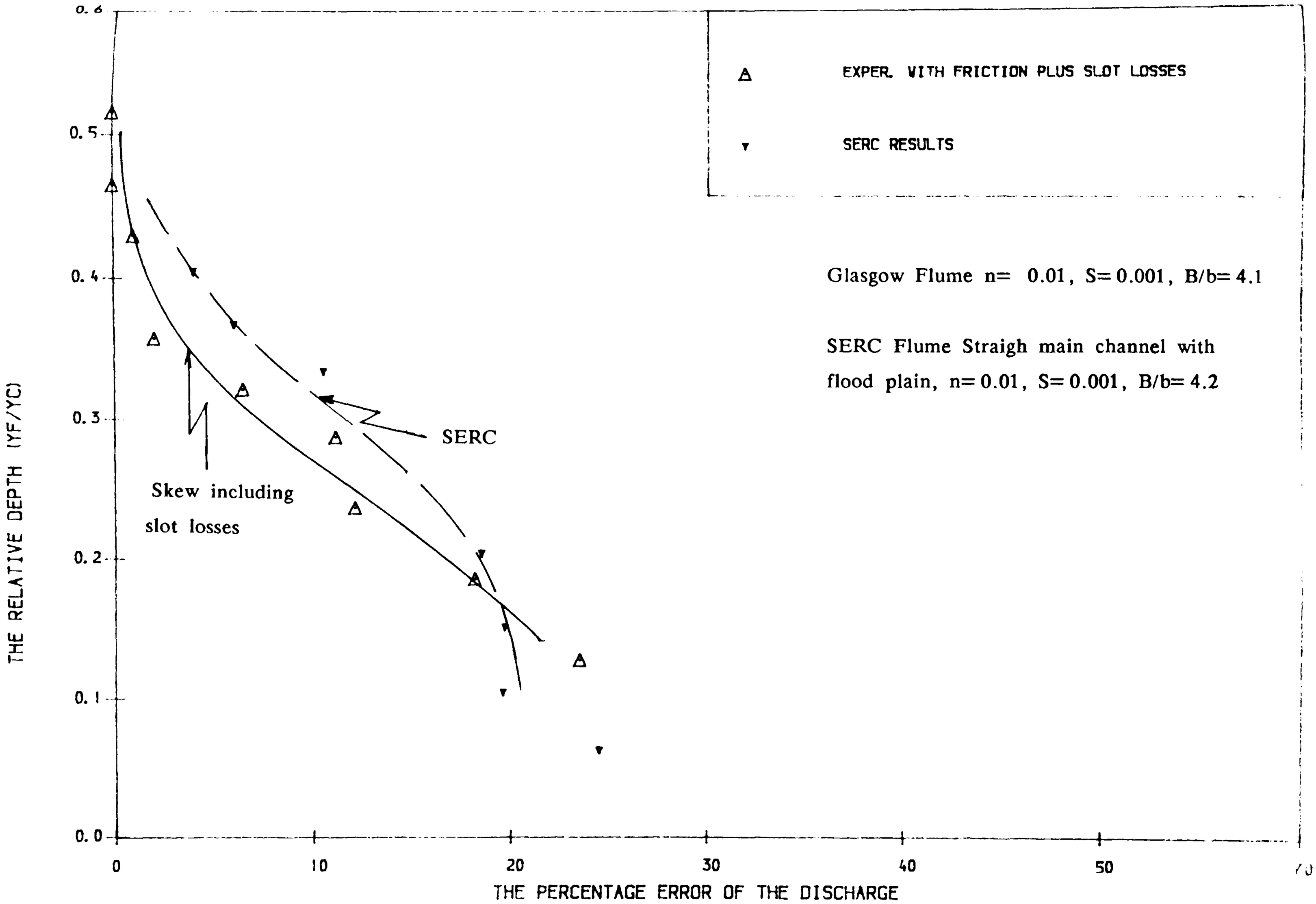

FIG (7.4) PERCENTAGE ERROR RELATIONSHIP OF THE DISCHARGE BETWEEN THE EXPERIMENTAL AND THE THEORETIAL RESULTS

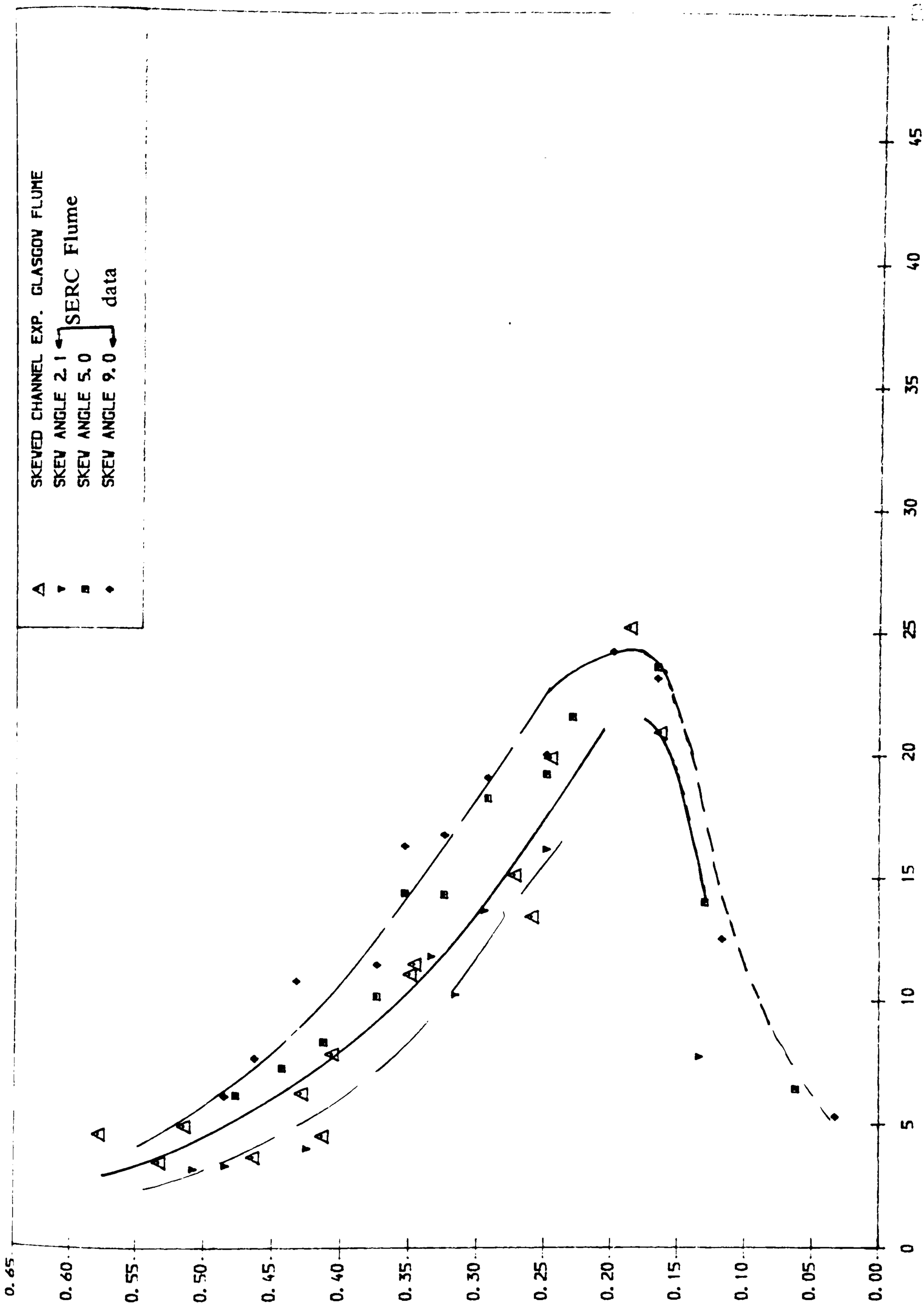

FIG (7.5) THE PERCENTAGE ERROR BETWEEN THE ESTIMATED AND EXPERIMENTAL DISCHARGE WITH THE RELATIVE DEPTH

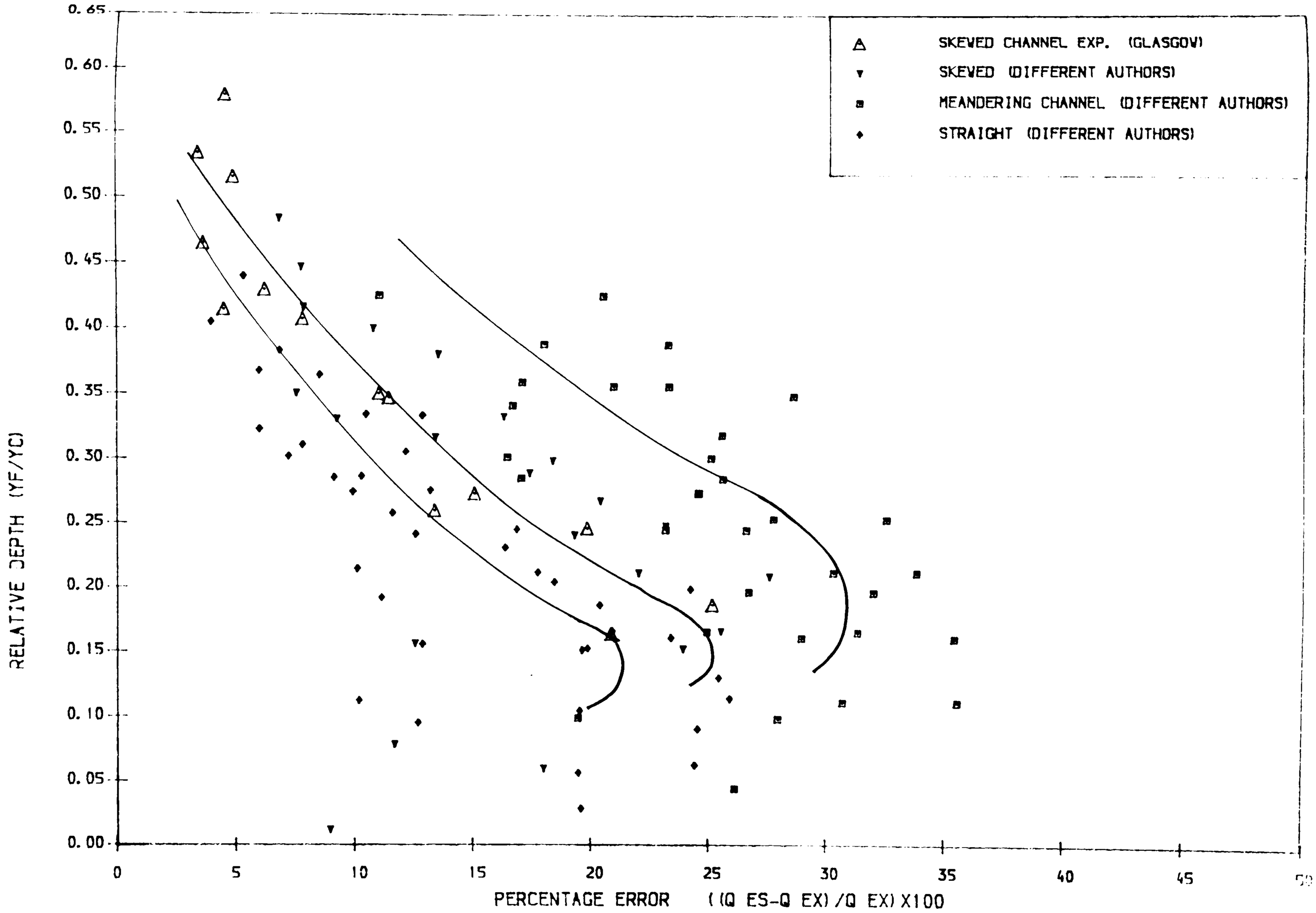

FIG (7.6) THE PERCENTAGE ERROR BETWEEN THE ESTIMATED AND EXPERIMENTAL DISCHARGE WITH THE RELATIVE DEPTH

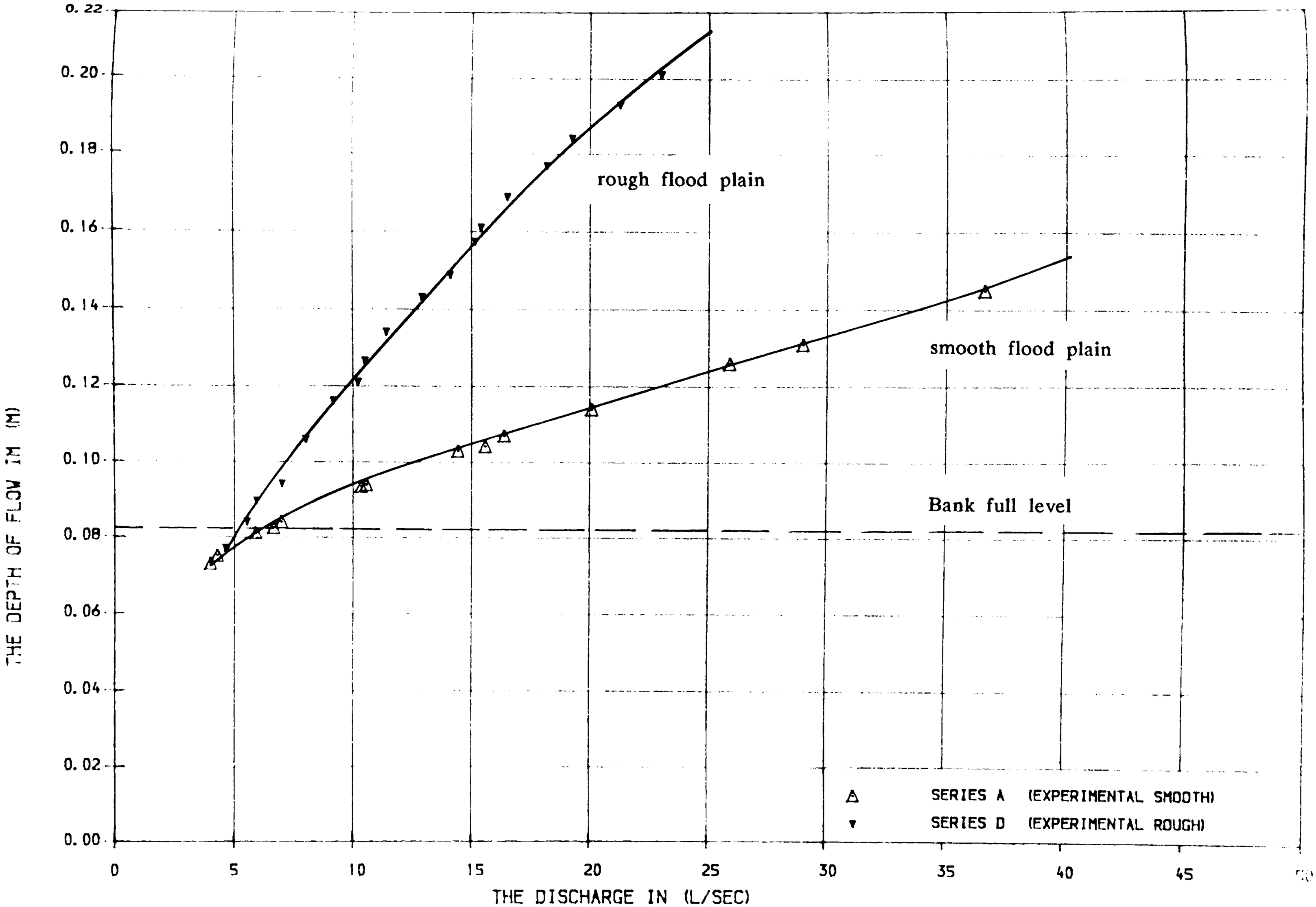

FIG (7.7) A COMPARISON OF STAGE-DISCHARGE CURVES FOR SKEWED GEOMETRY WITH SMOOTH AND ROUGH FLOOD PLAINS. P12

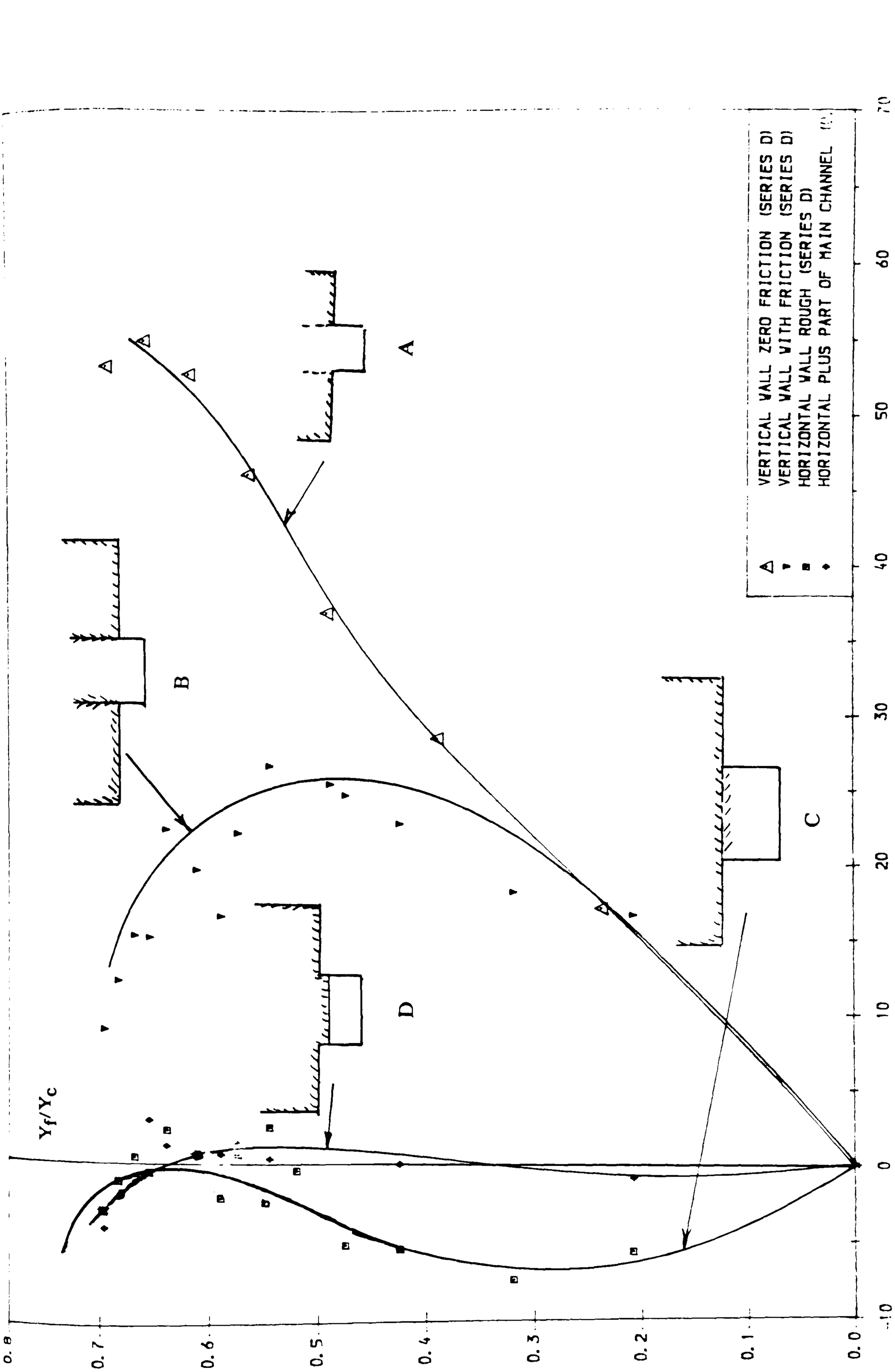

FIG (7.8) THE PERCENTAGE ERROR BETWEEN THE ESTIMATED AND EXPERIMENTAL DISCHARGE WITH THE RELATIVE DEPTH FOR SKEWED CHANNEL WITH ROUGH FLOODPLAIN

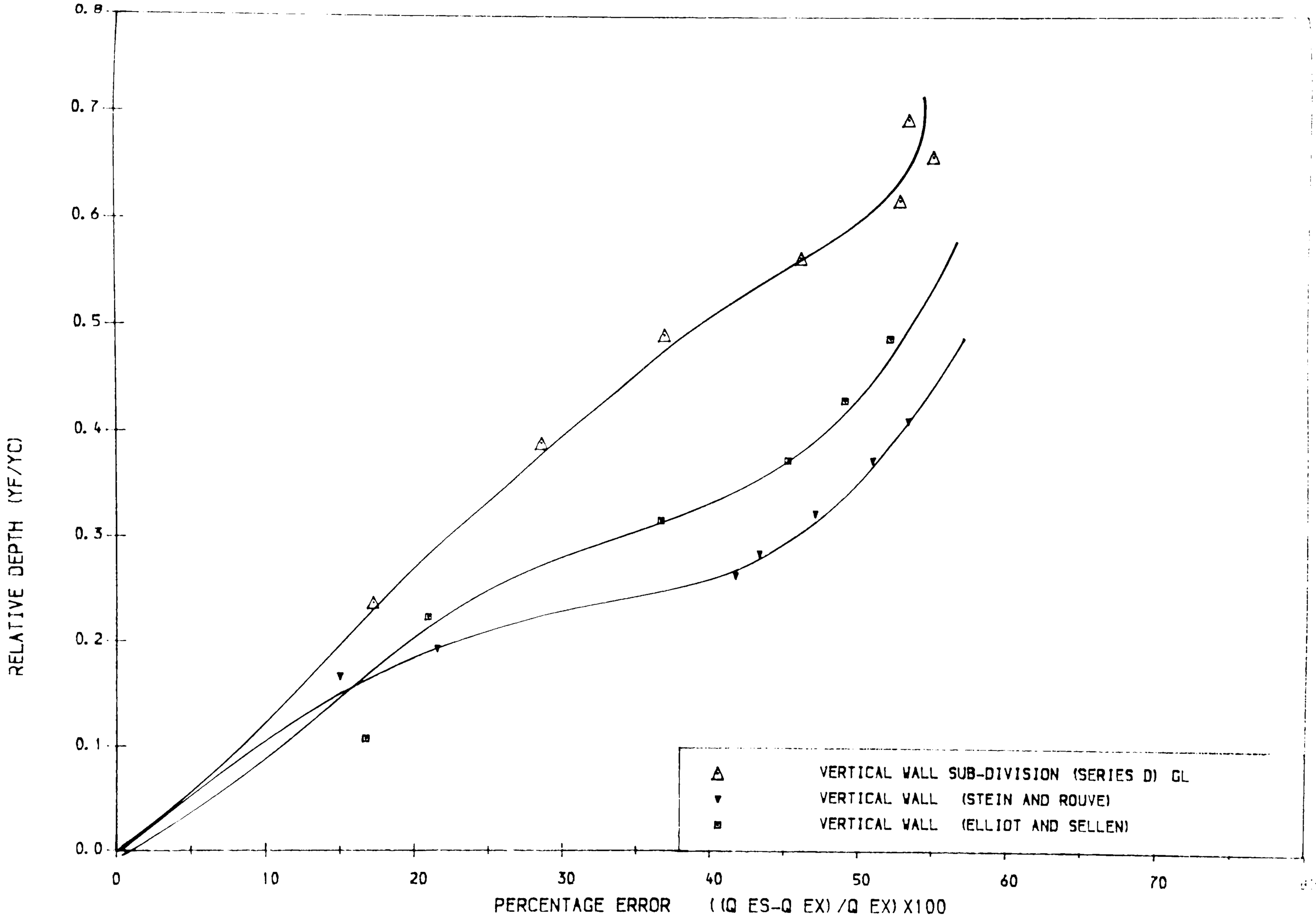

FIG (7.9) THE PERCENTAGE ERROR BETWEEN THE ESTIMATED AND EXPERIMENTAL DISCHARGE WITH RELATIVE DEPTH FOR SKEWED CHANNEL WITH ROUGH FLOODPLAIN

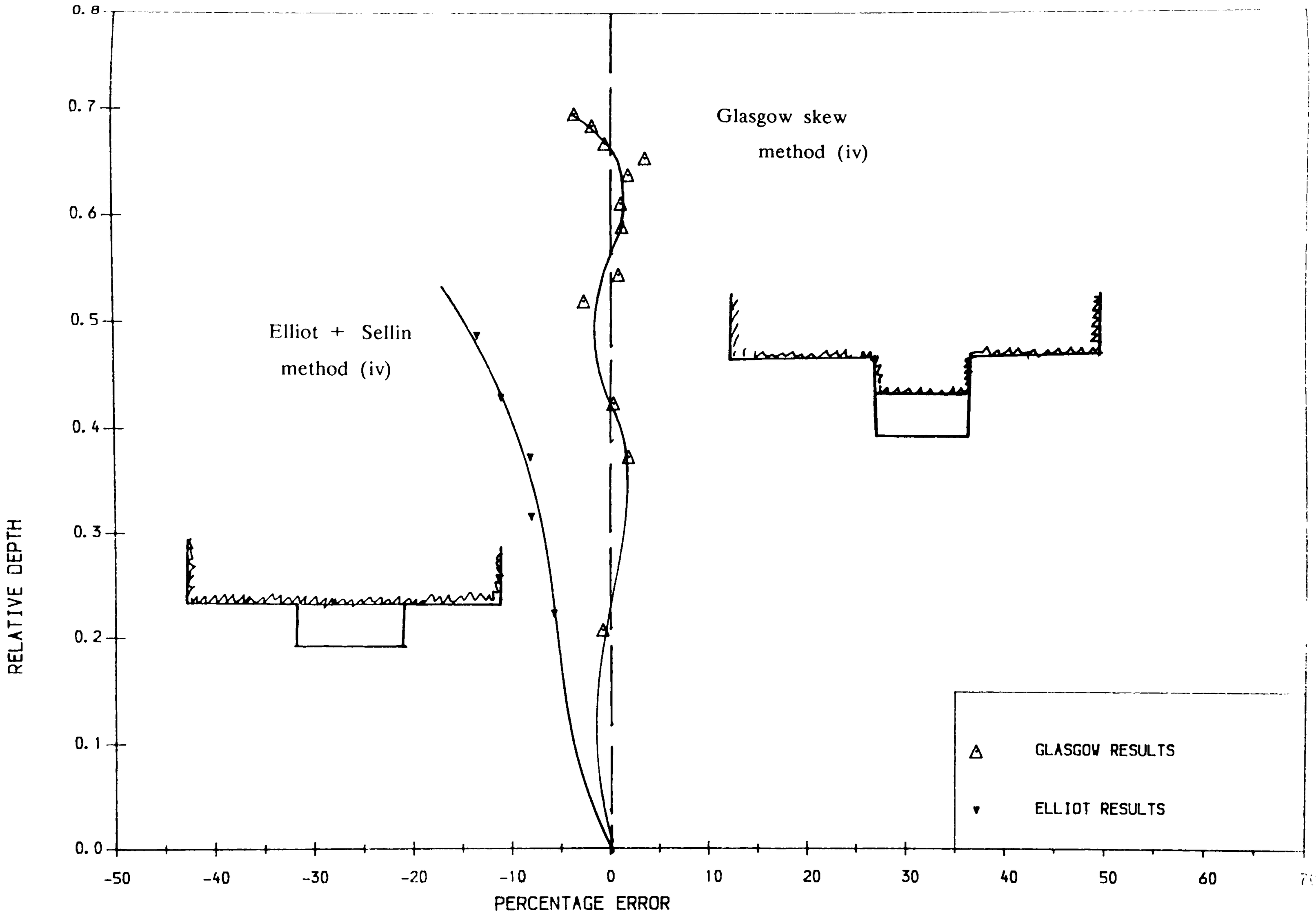

FIG (7.10) *THE PERCENTAGE ERROR RELATIONSHIP BETWEEN THE EXPERIMENTAL AND SUB-DIVIDED METHOD AND RELATIVE DEPTH*

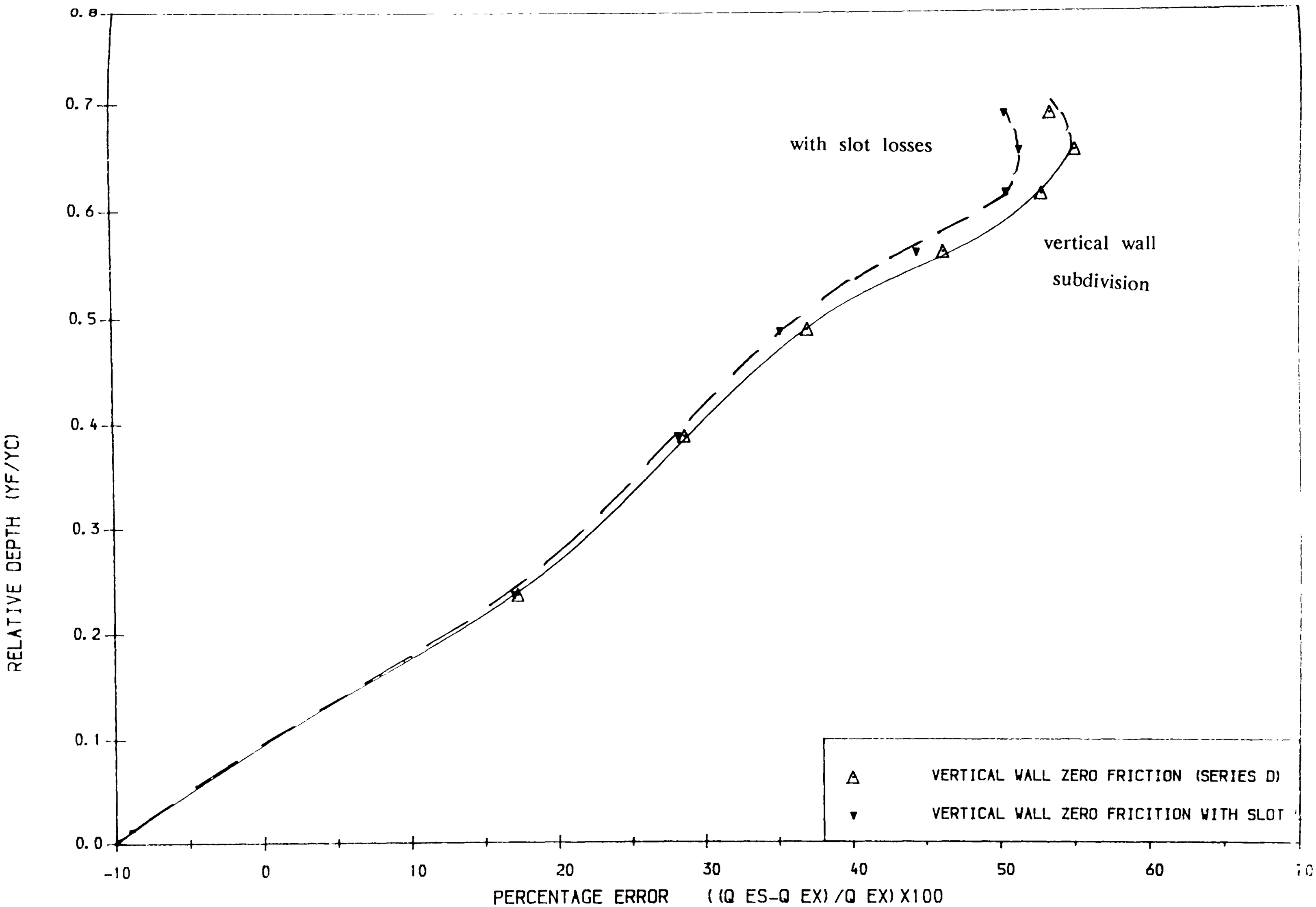

FIG (7.11) THE PERCENTAGE ERROR BETWEEN THE EXPERIMENTAL AND ESTIMATED DISCHARGE WITH THE RELATIVE DEPTH FOR SKEWED CHANNEL WITH ROUGH FLOODPLAIN

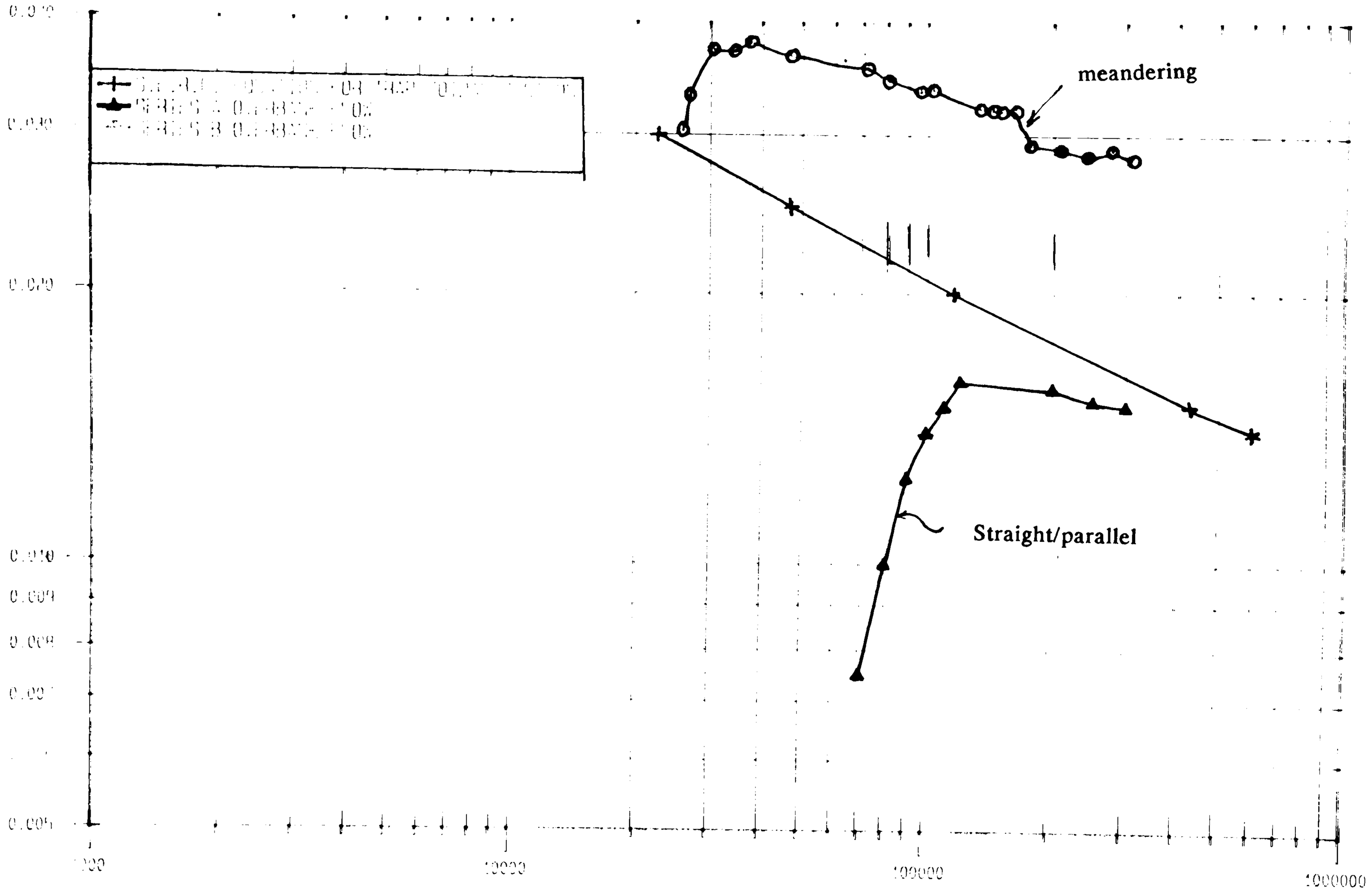

Fig (7.12) VARIATION OF DARCY-WEISBACH RESISTANCE COEFFICIENT WITH REYNOLDS NUMBER

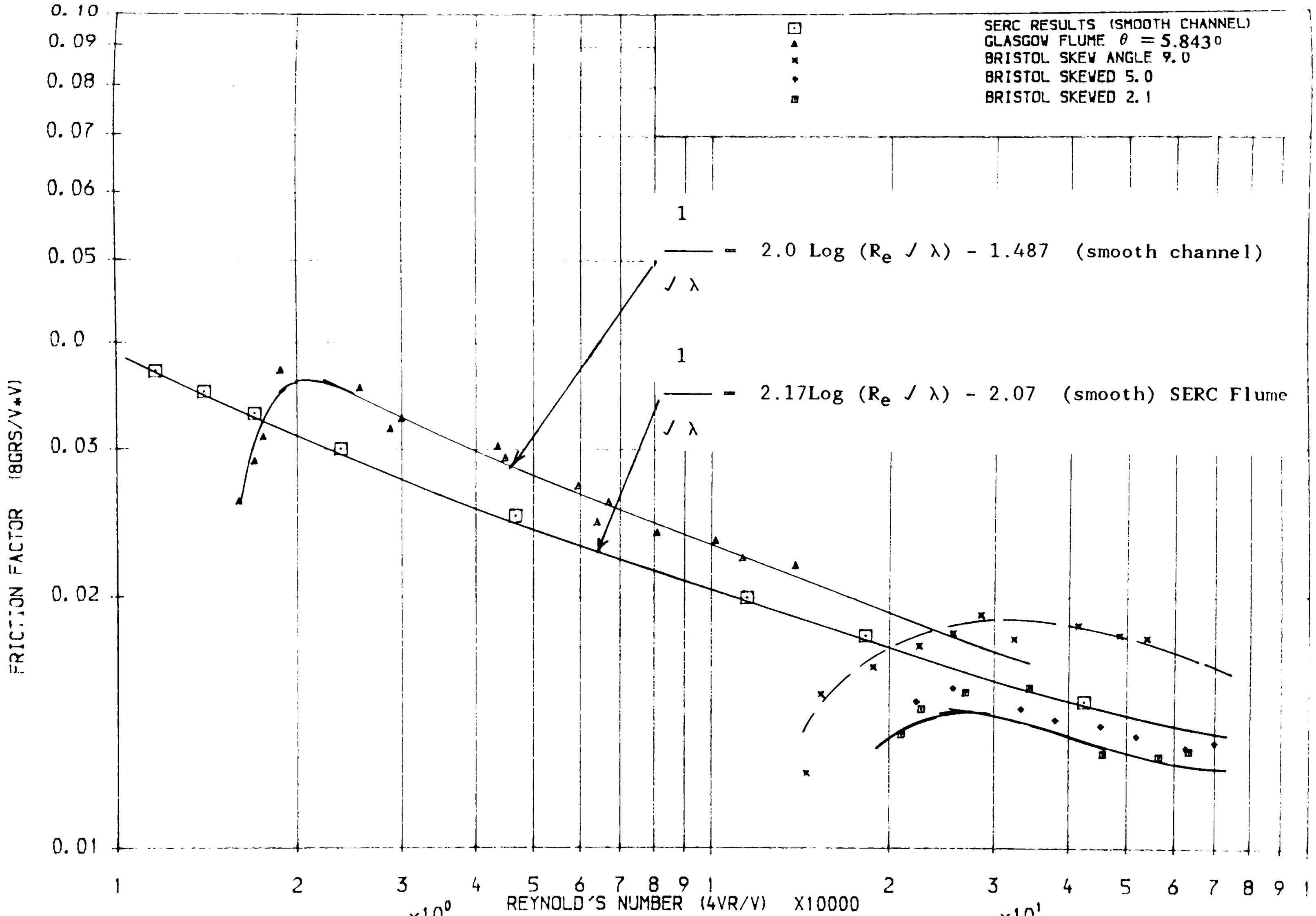

FIG (7.13) THE RELATIONSHIP BETWEEN THE REYNOLD'S NUMBER AND FRICTION FACTOR FOR SKEWED MAIN CHANNEL WITH SMOOTH FLOOD PLAIN.

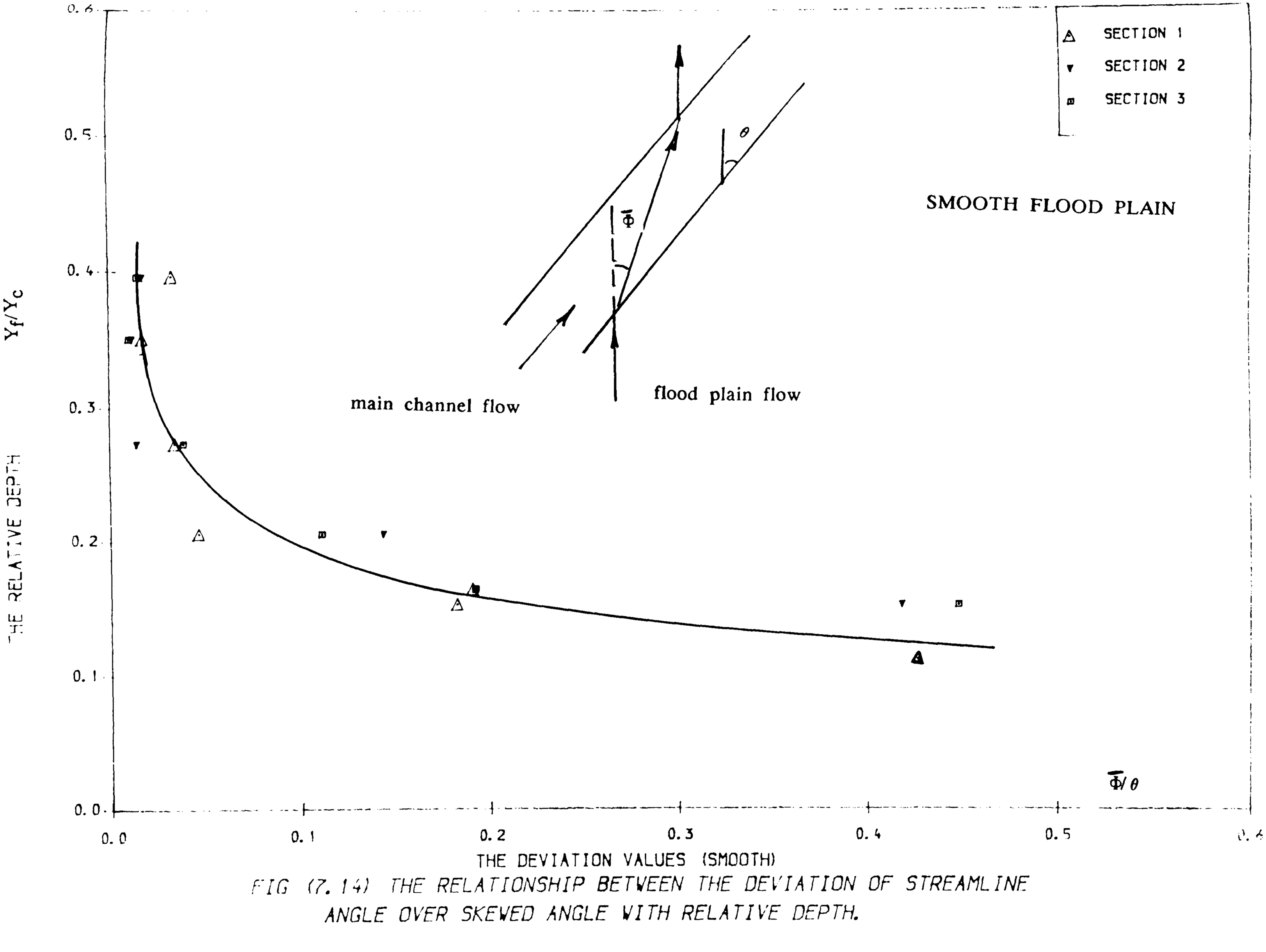

FIG (7.14) THE RELATIONSHIP BETWEEN THE DEVIATION OF STREAMLINE ANGLE OVER SKEWED ANGLE WITH RELATIVE DEPTH.

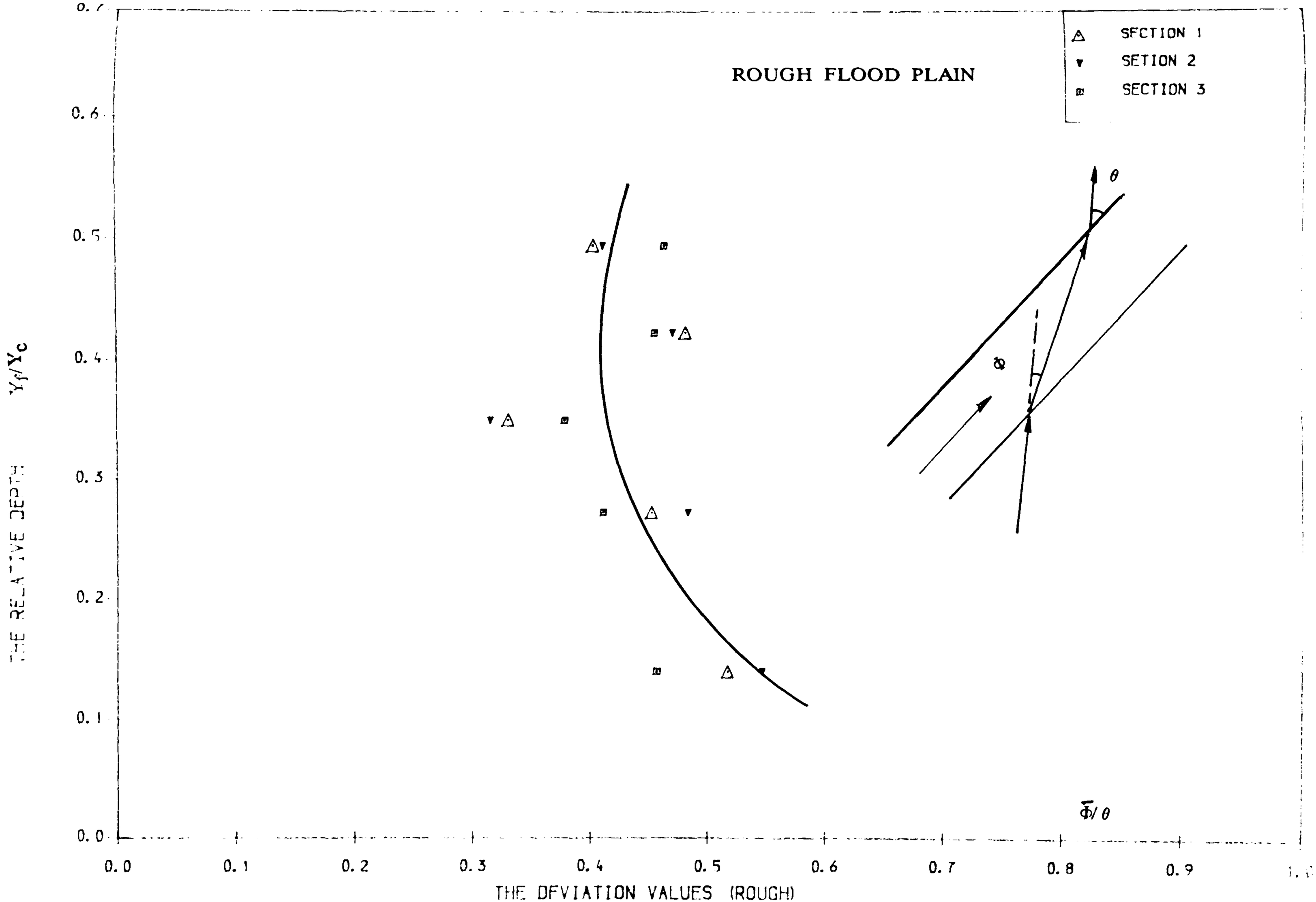

FIG (7.15) THE RELATIONSHIP BETWEEN THE DEVIATION OF STREAMLINE ANGLE OVER SKEWED ANGLE WITH RELATIVE DEPTH.

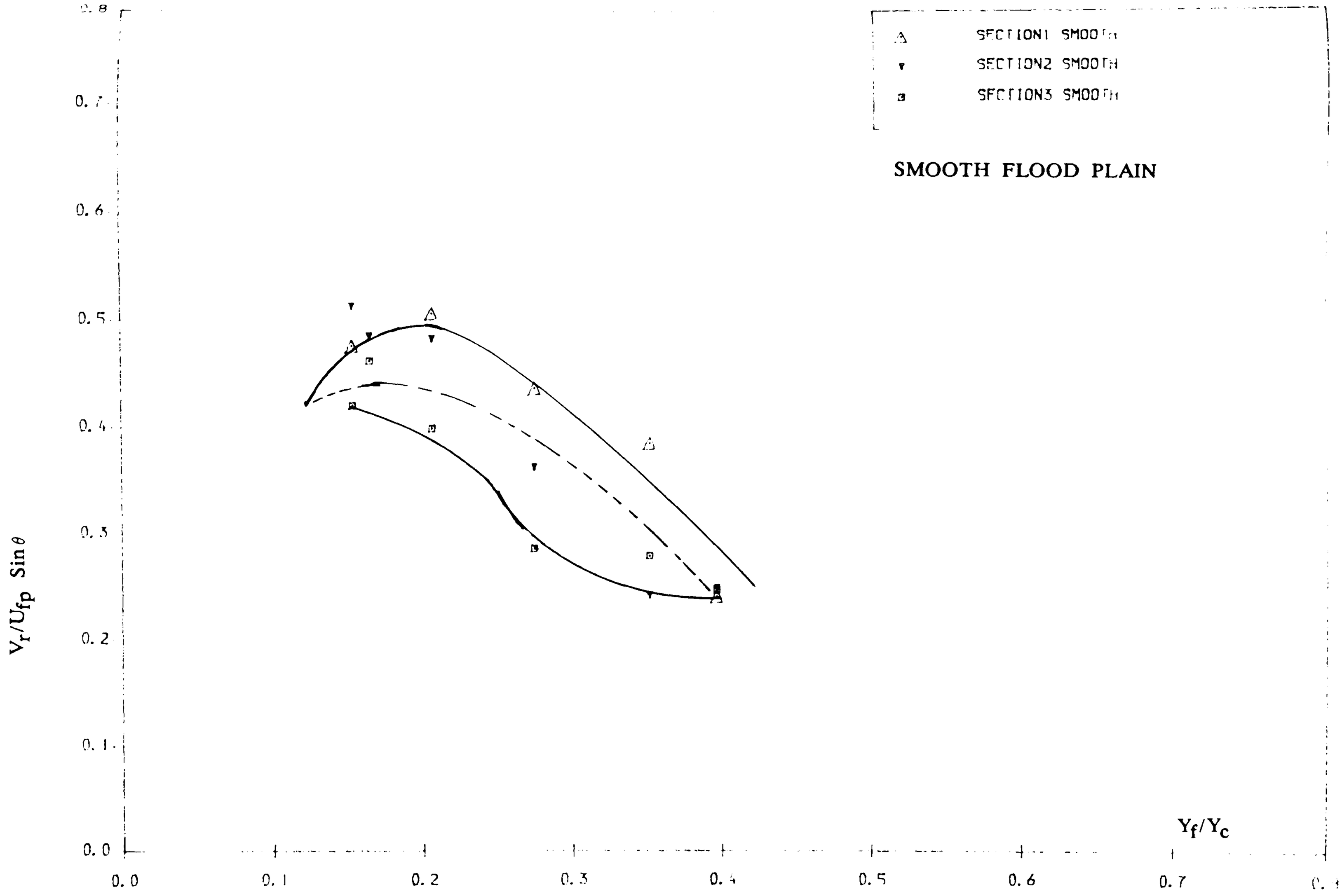

FIG(7.16) THE RELATIONSHIP BETWEEN THE RECIRCULATING VELOCITY TO THE MEAN VELOCITY ON THE FLOODPLAIN, NORMAL TO SKEW.

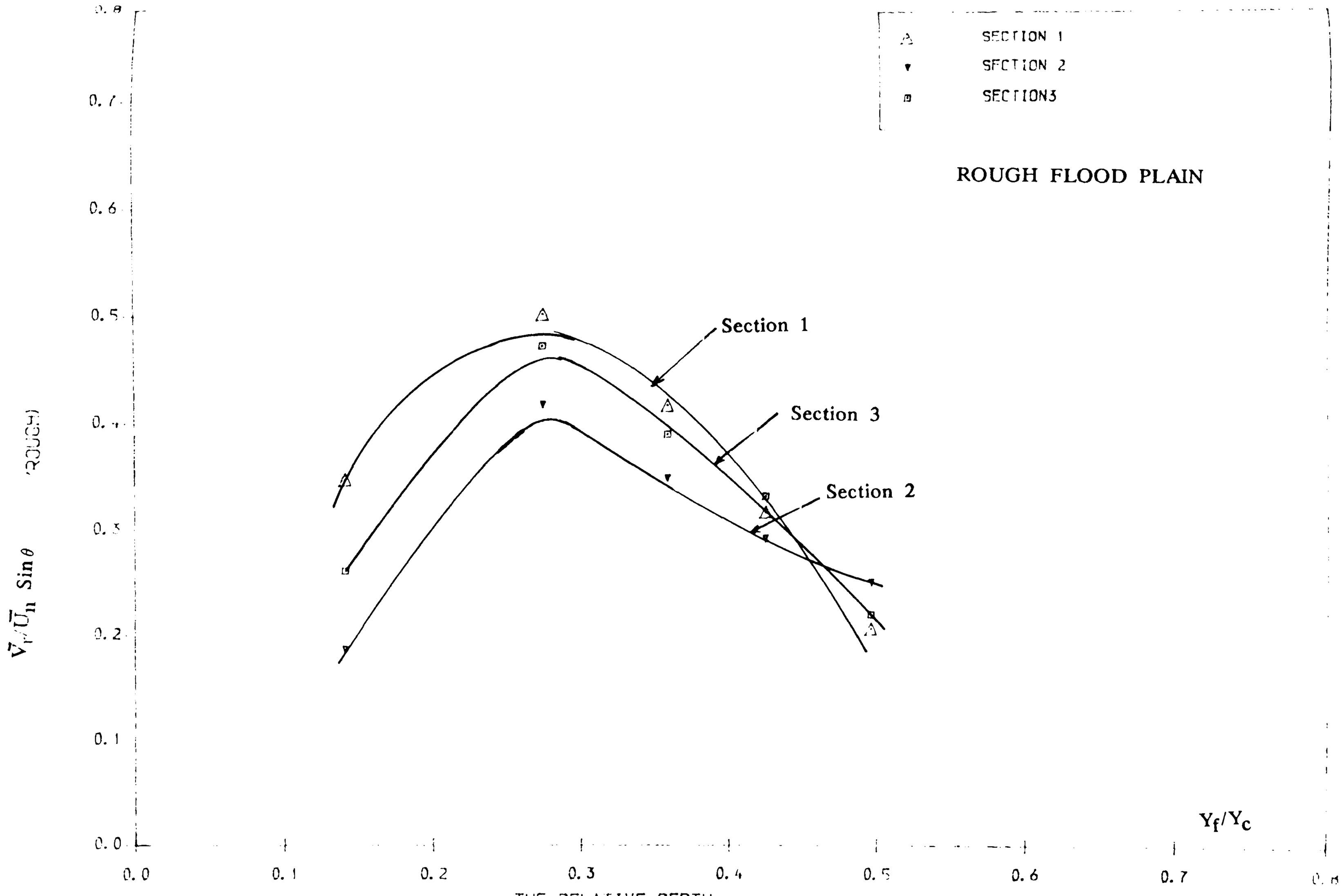

FIG(7.17) THE RELATIONSHIP BETWEEN THE RECIRCULATING VELOCITY TO THE MEAN RIGHT VELOCITY ON THE FLOODPLAIN, NORMAL TO SLOT OR SKEW.

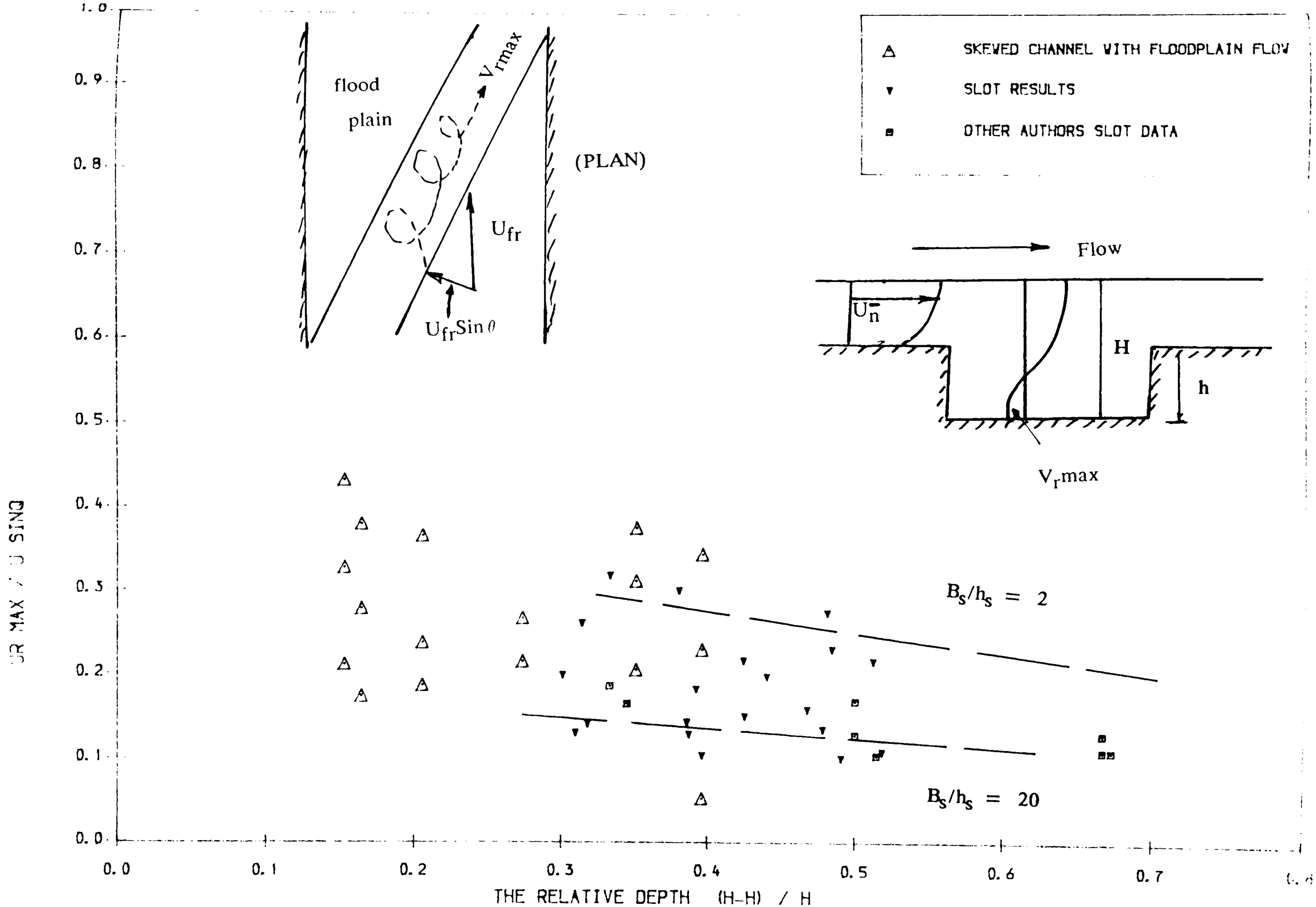

FIG(7.18) THE RELATIONSHIP BETWEEN THE MAXIMUM RECIRCULATING VELOCITY TO THE MEAN VELOCITY ON THE FLOODPLAIN, NORMAL TO SLOT OR SKEW.

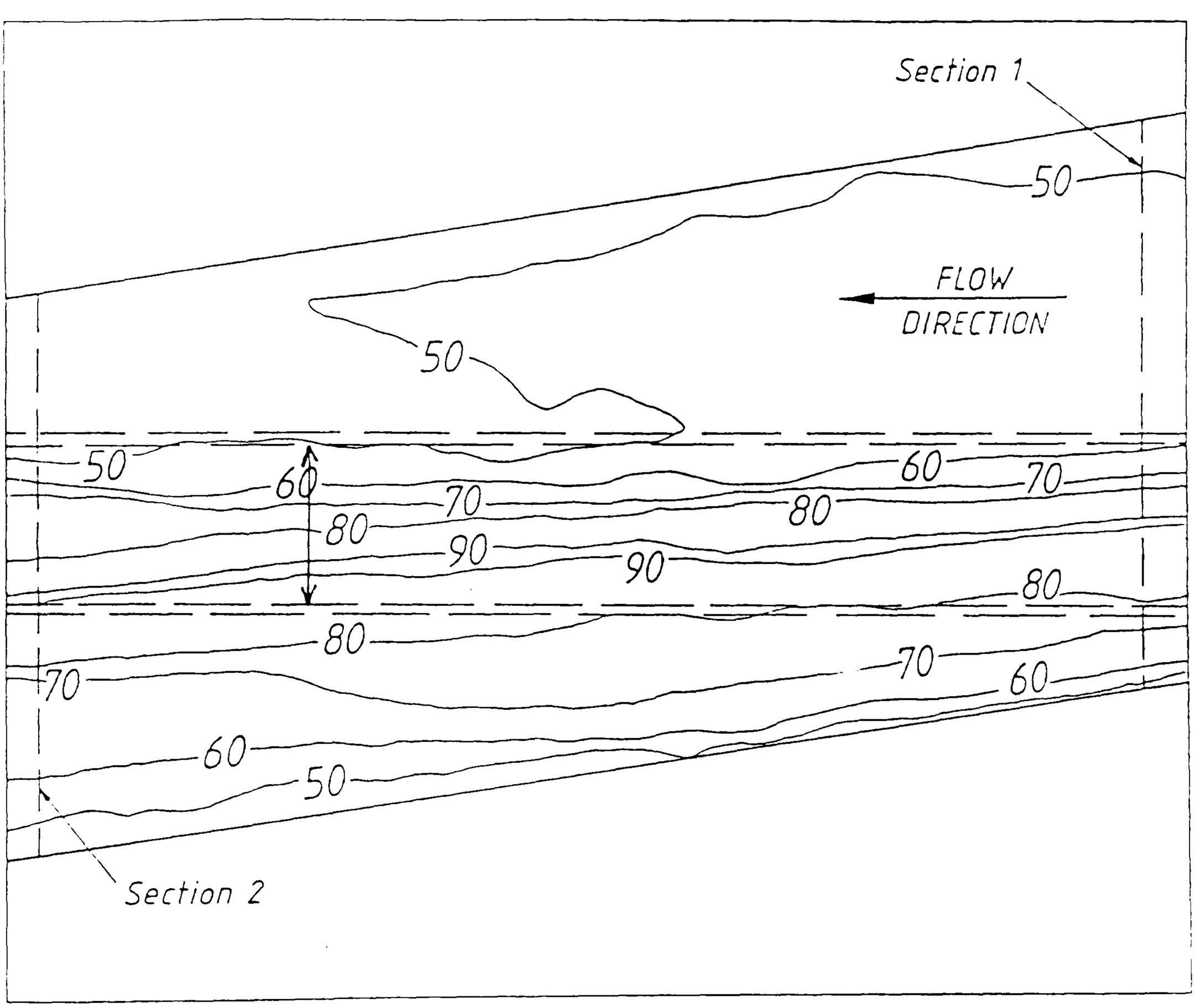

Fig (7.19) Distribution of surface velocities/cm s^{-1}; $\alpha = 9^{o}$; $(H-h)/H = 0.25$

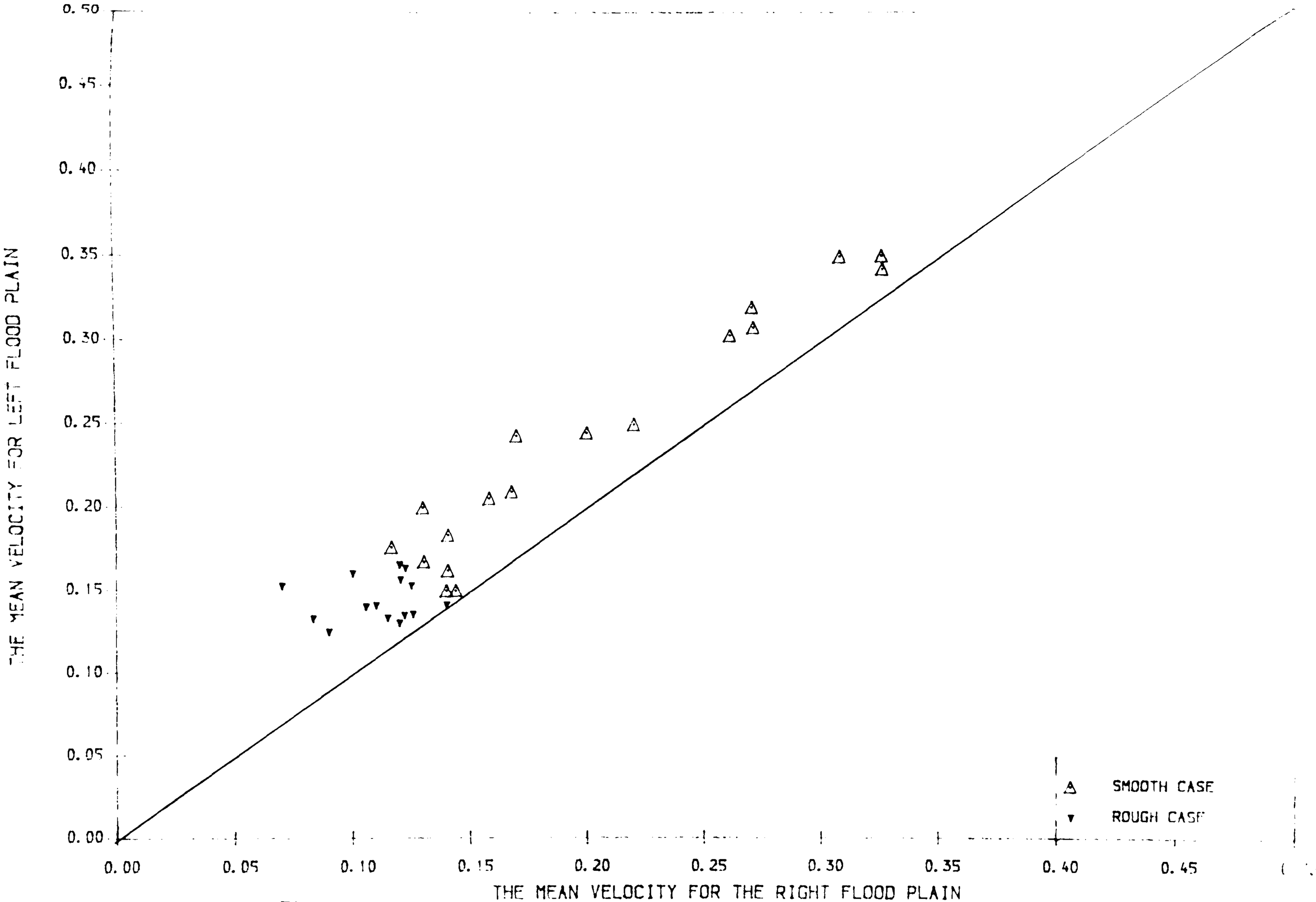

Fig (7.20) *THE RELATIONSHIP BETWEEN THE MEAN VELOCITY FOR THE RIGHT TO THE LEFT FLOOD PLAIN FOR SMOOTH AND ROUGH CASE.*

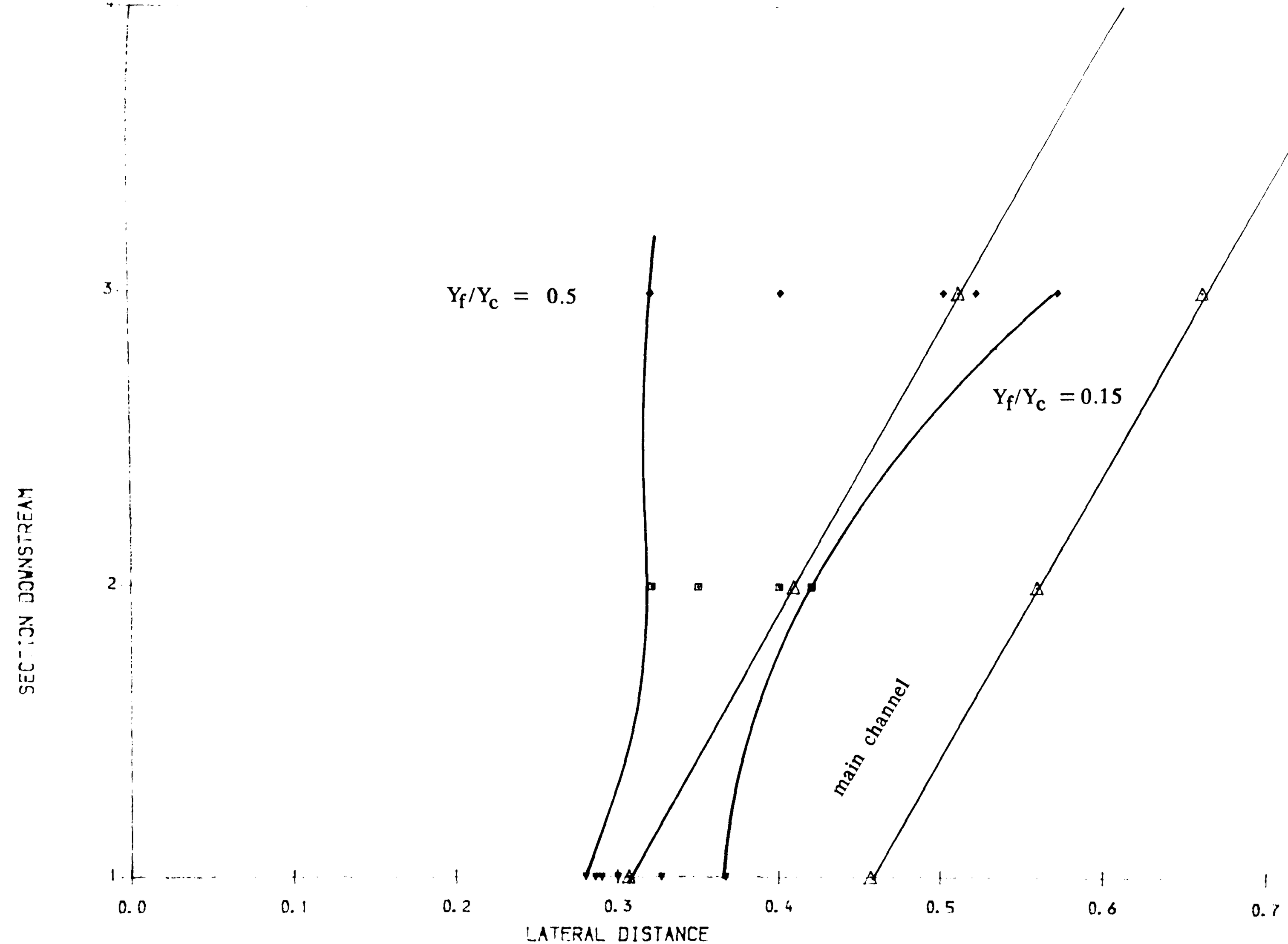

Fig (7.21) *POSITON OF MAXIMUM VELOCITY FILAMENT RELATIVE TO CENTER LINE OF THE SKEWED CHANNEL AND THE FLUME (SMOOTH CASE)*

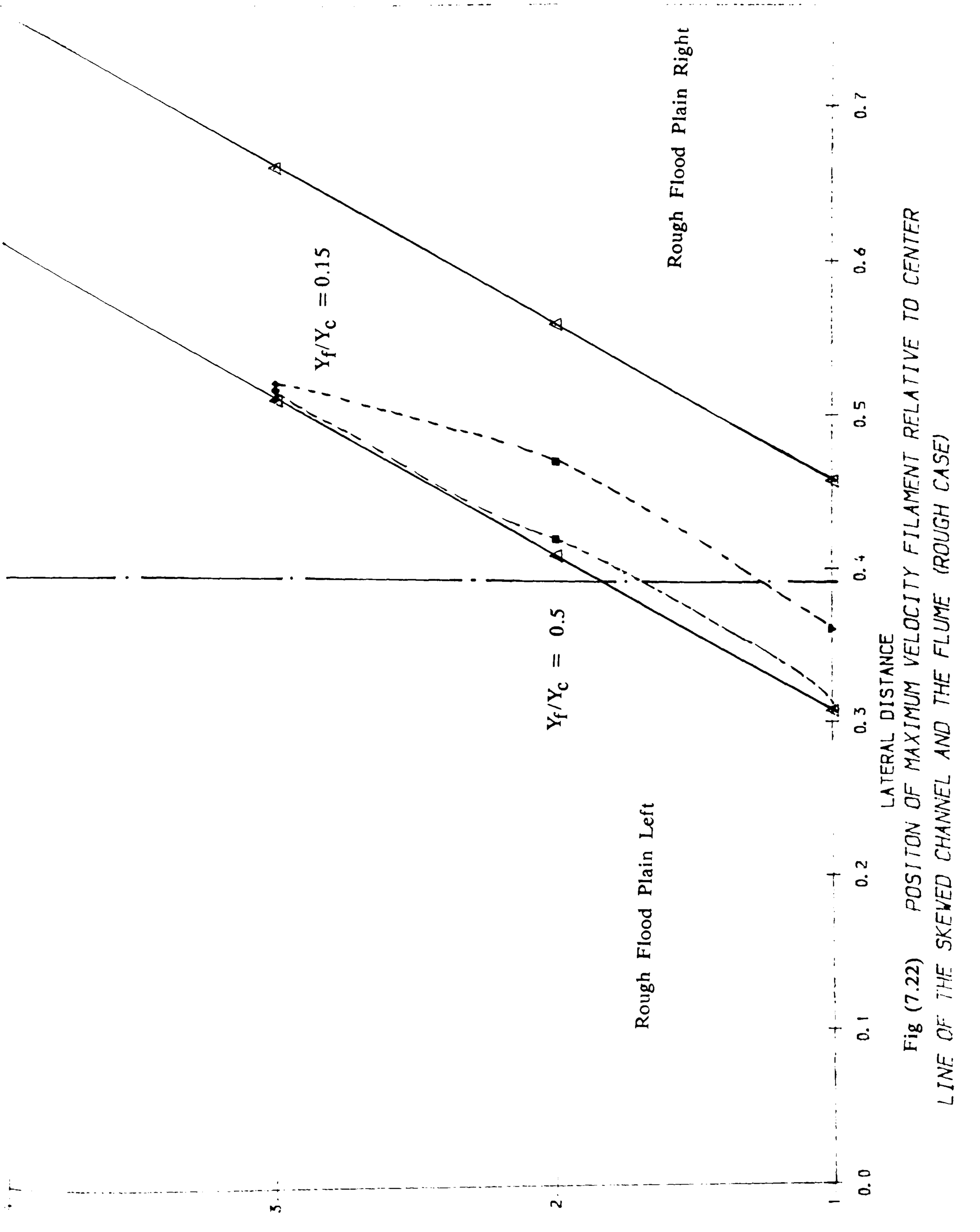

Fig (7.22) *POSITION OF MAXIMUM VELOCITY FILAMENT RELATIVE TO CENTER LINE OF THE SKEWED CHANNEL AND THE FLUME (ROUGH CASE)*

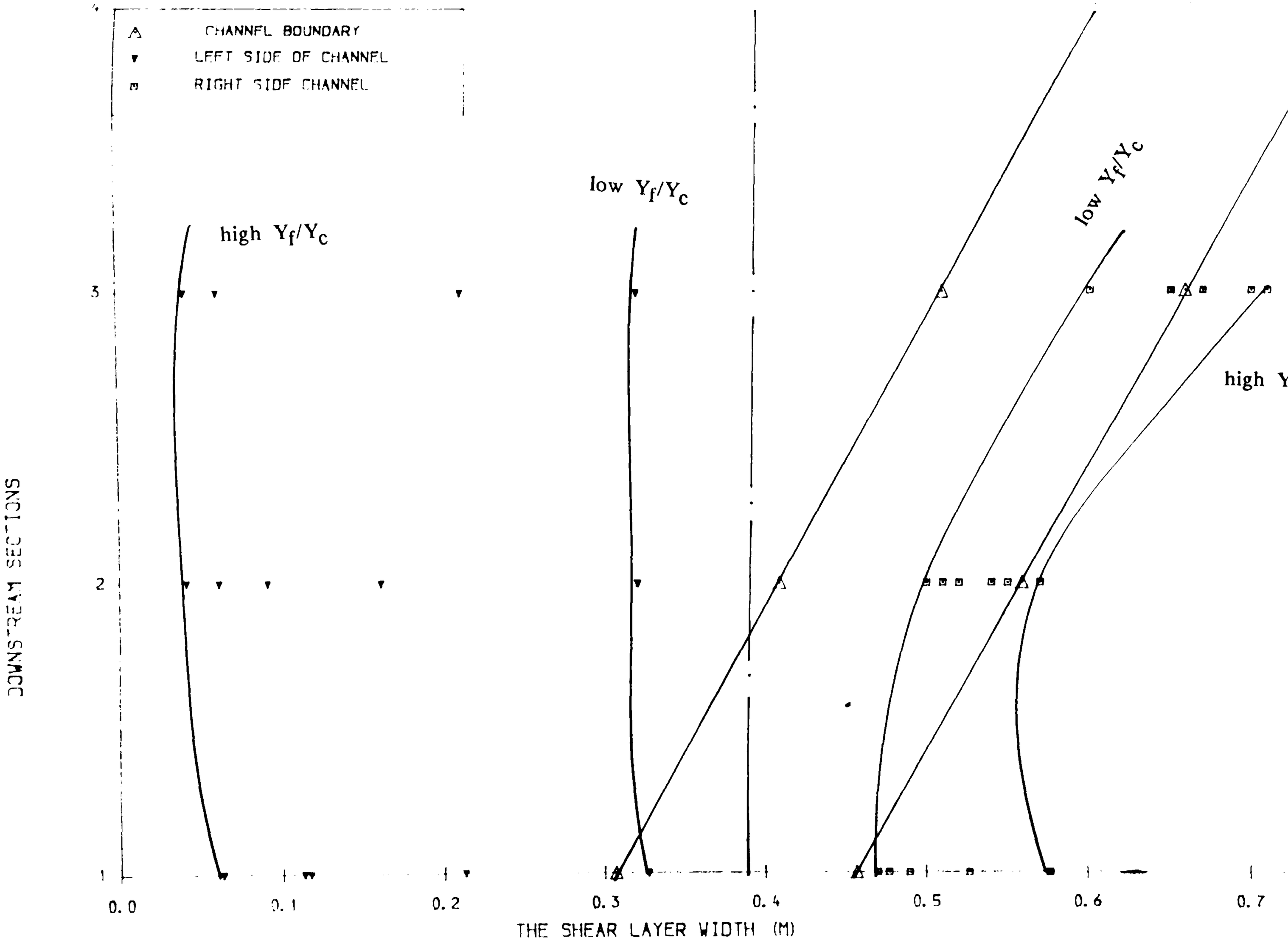

Fig (7.23) *THE RELATIONSHIP BETWEEN SHEAR LAYER DISTANCE FOR LEFT AND RIGHT FLOOD PLAIN AREA RELATIVE TO DOWNSTREAM SECTION FOR SMOOTH CASE*

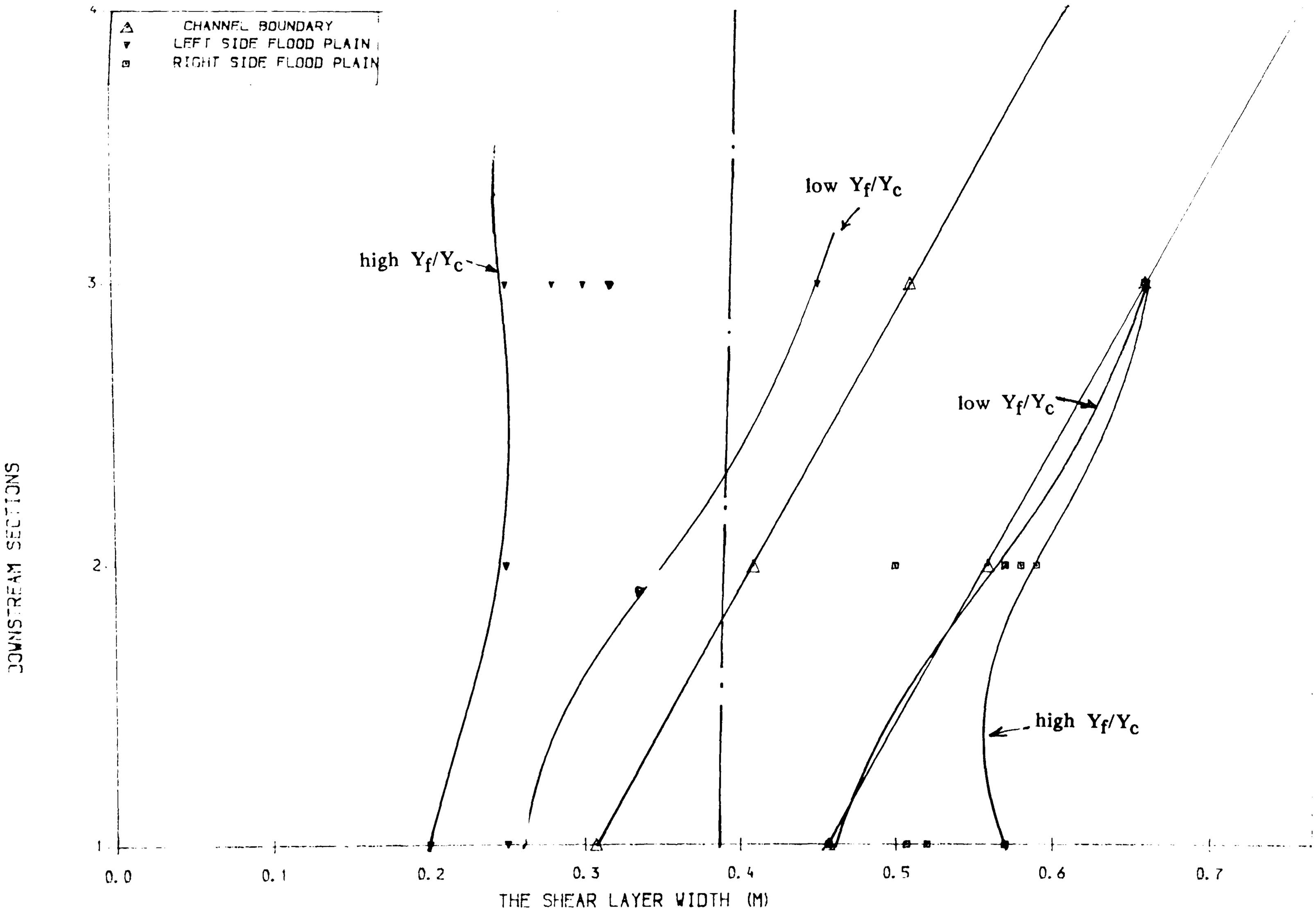

Fig (7.24) *THE RELATIONSHIP BETWEEN SHEAR LAYER DISTANCE FOR LEFT AND RIGHT FLOOD PLAIN AREA RELATIVE TO DOWNSTREAM SECTION FOR ROUGH CASE*

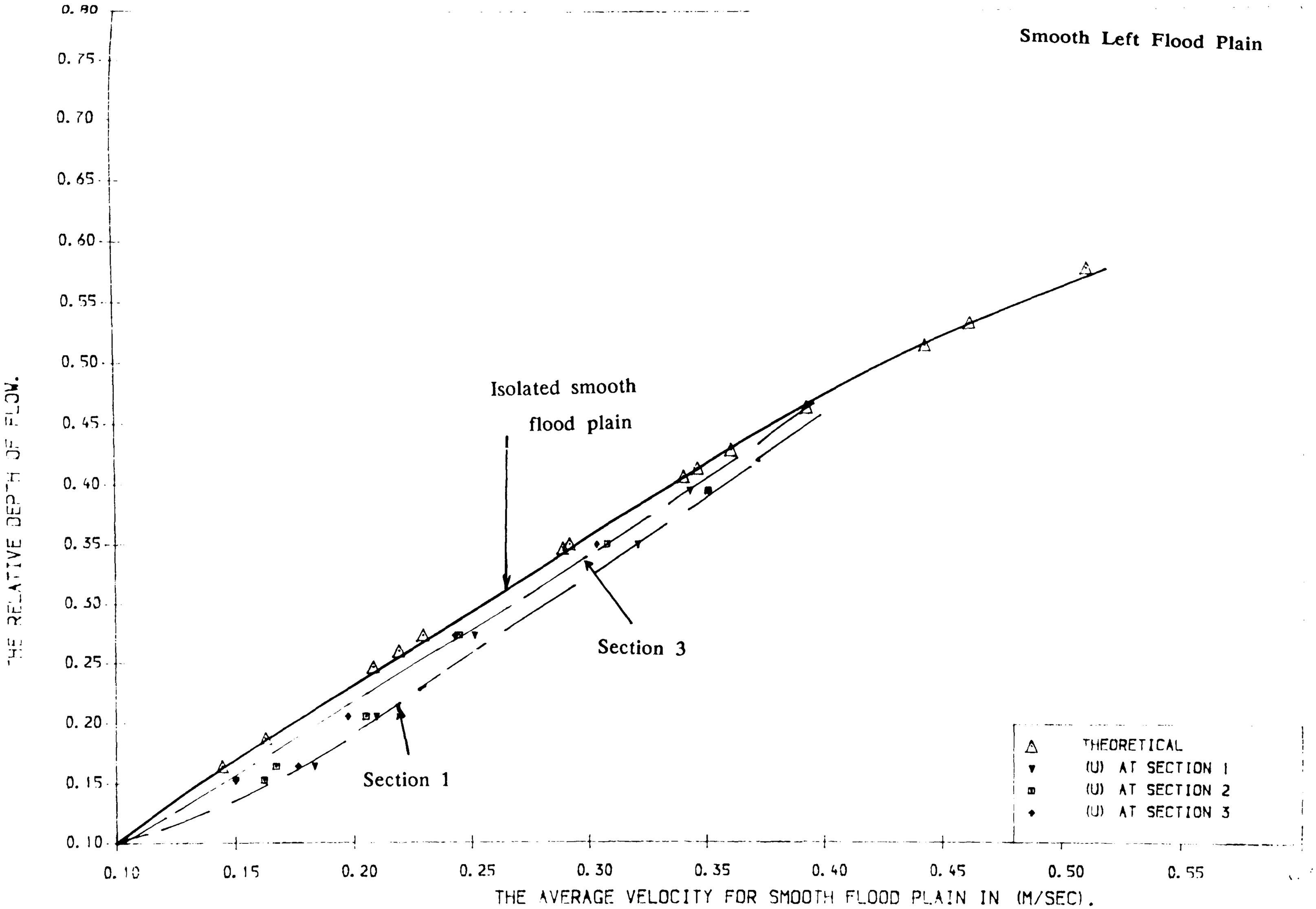

Fig (7.25) *RELATIONSHIP BETWEEN RELATIVE DEPTH OF FLOW AND AVERAGE VELOCITY ON LEFT SIDE FLOODPLAIN AT VARIOUS LENGTHS ALONG THE FLUME*

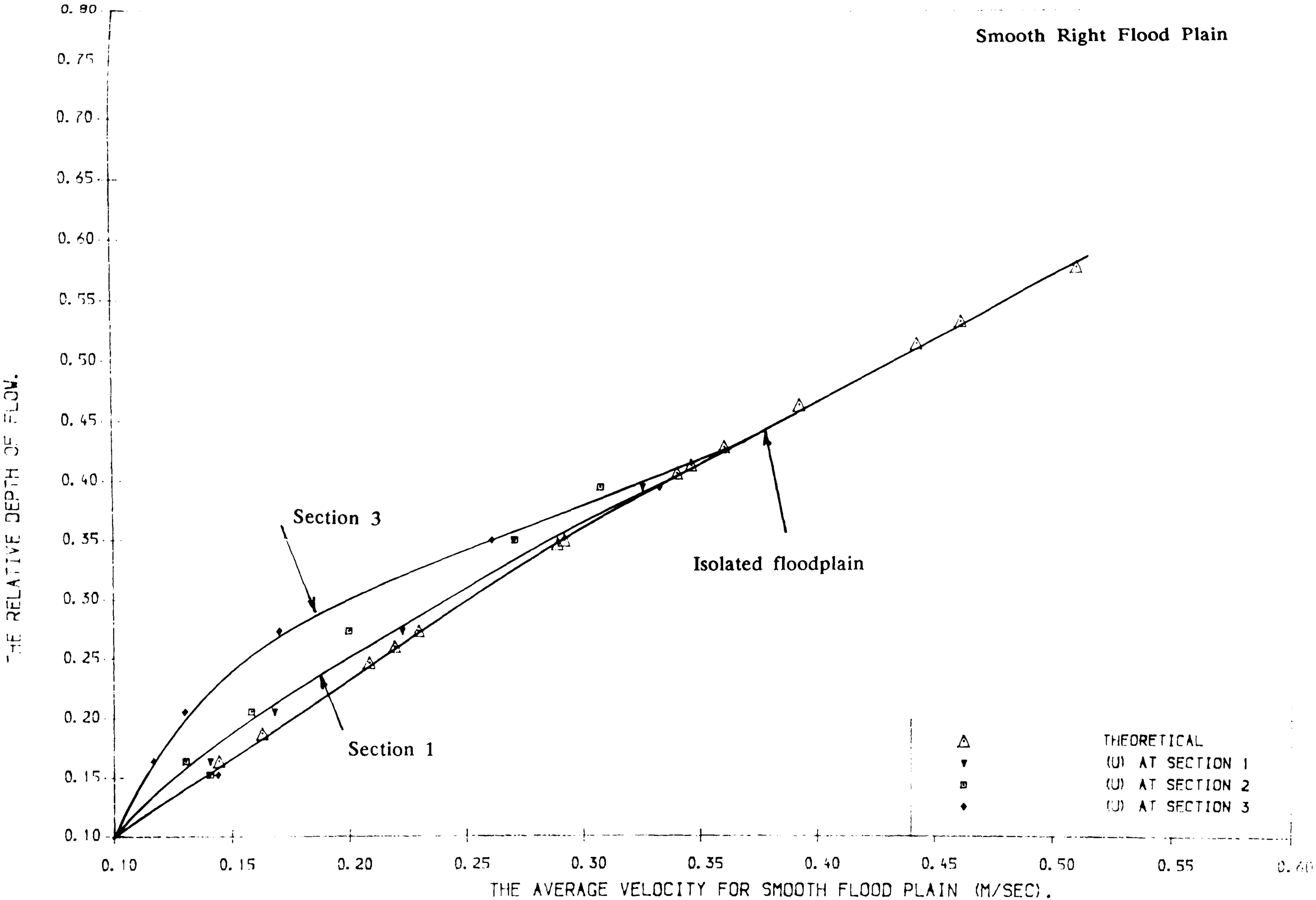

Fig (7.26) *RELATIONSHIP BETWEEN RELATIVE DEPTH OF FLOW AND AVERAGE VELOCITY ON RIGHT SIDE FLOODPLAIN AT VARIOUS LENGTHS ALONG THE FLUME*

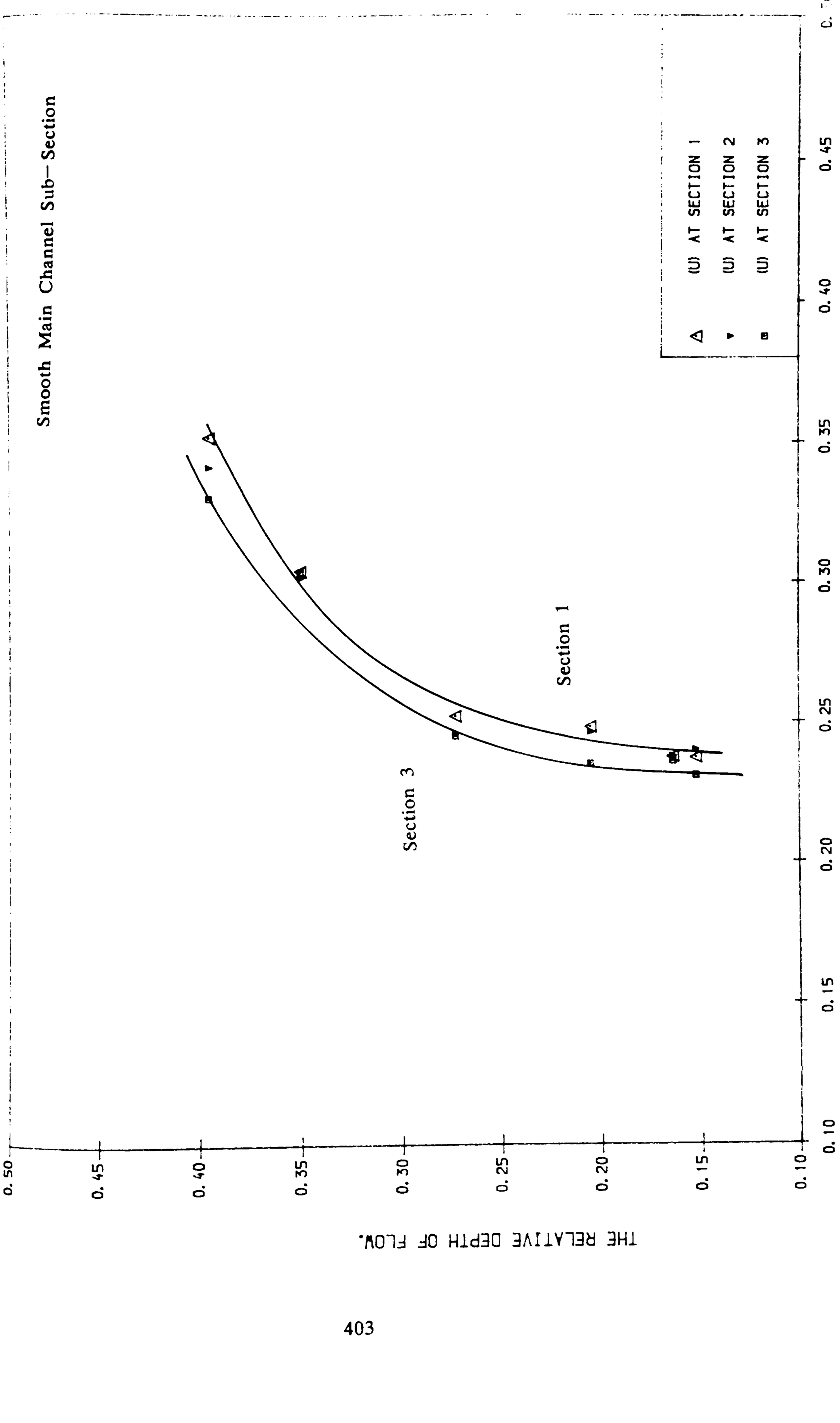

FIG (7.27) RELATIONSHIP BETWEEN RELATIVE DEPTH OF THE FLOW AND AVERAGE VELOCITY IN THE SKEWED MAIN CHANNEL SUB–SECTION AT VARIOUS LENGTHS ALONG THE FLUME.

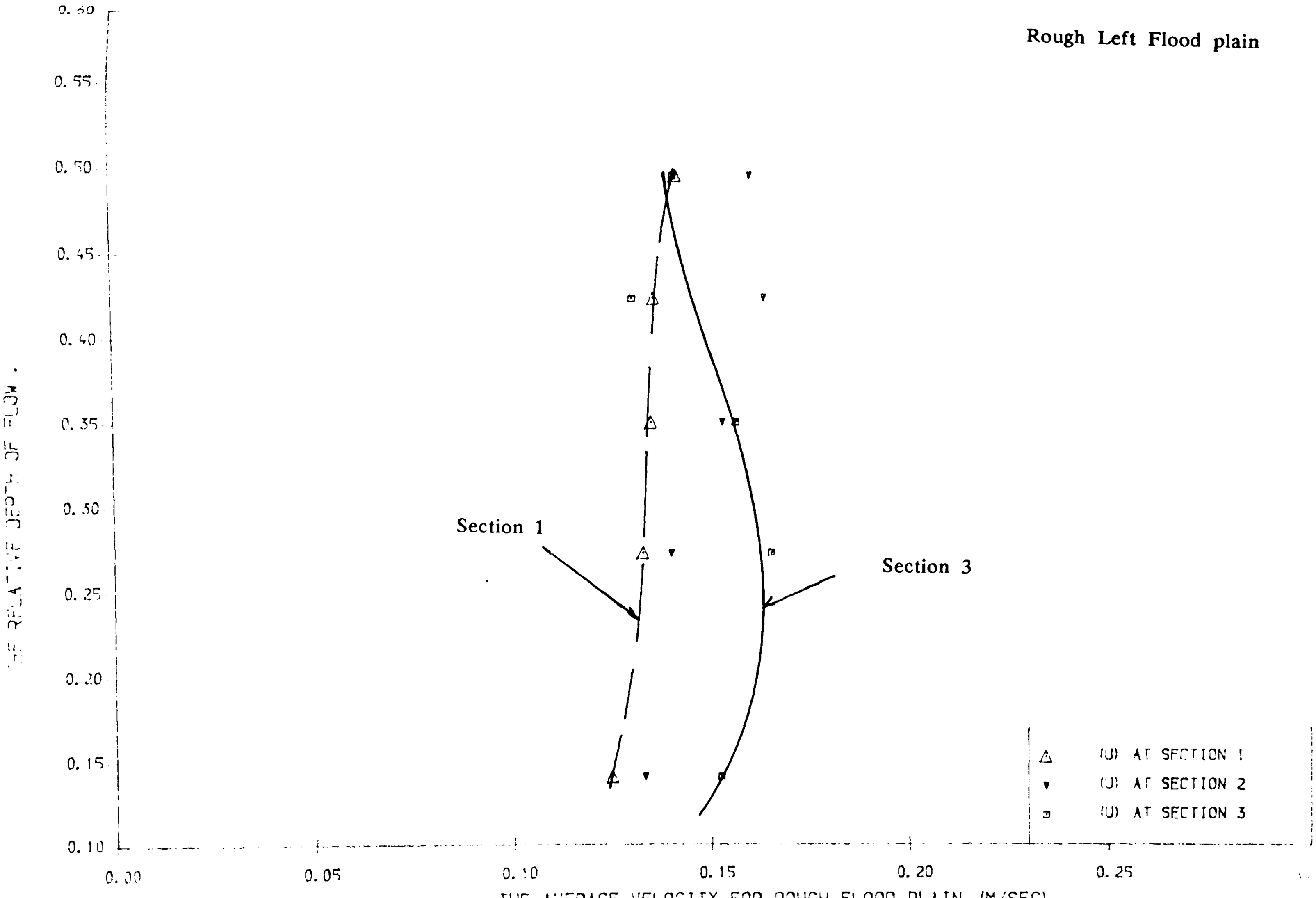

Fig (7.28) *RELATIONSHIP BETWEEN RELATIVE DEPTH OF FLOW AND AVERAGE VELOCITY ON LEFT SIDE FLOODPLAIN AT VARIOUS LENGTHS ALONG THE FLUME*

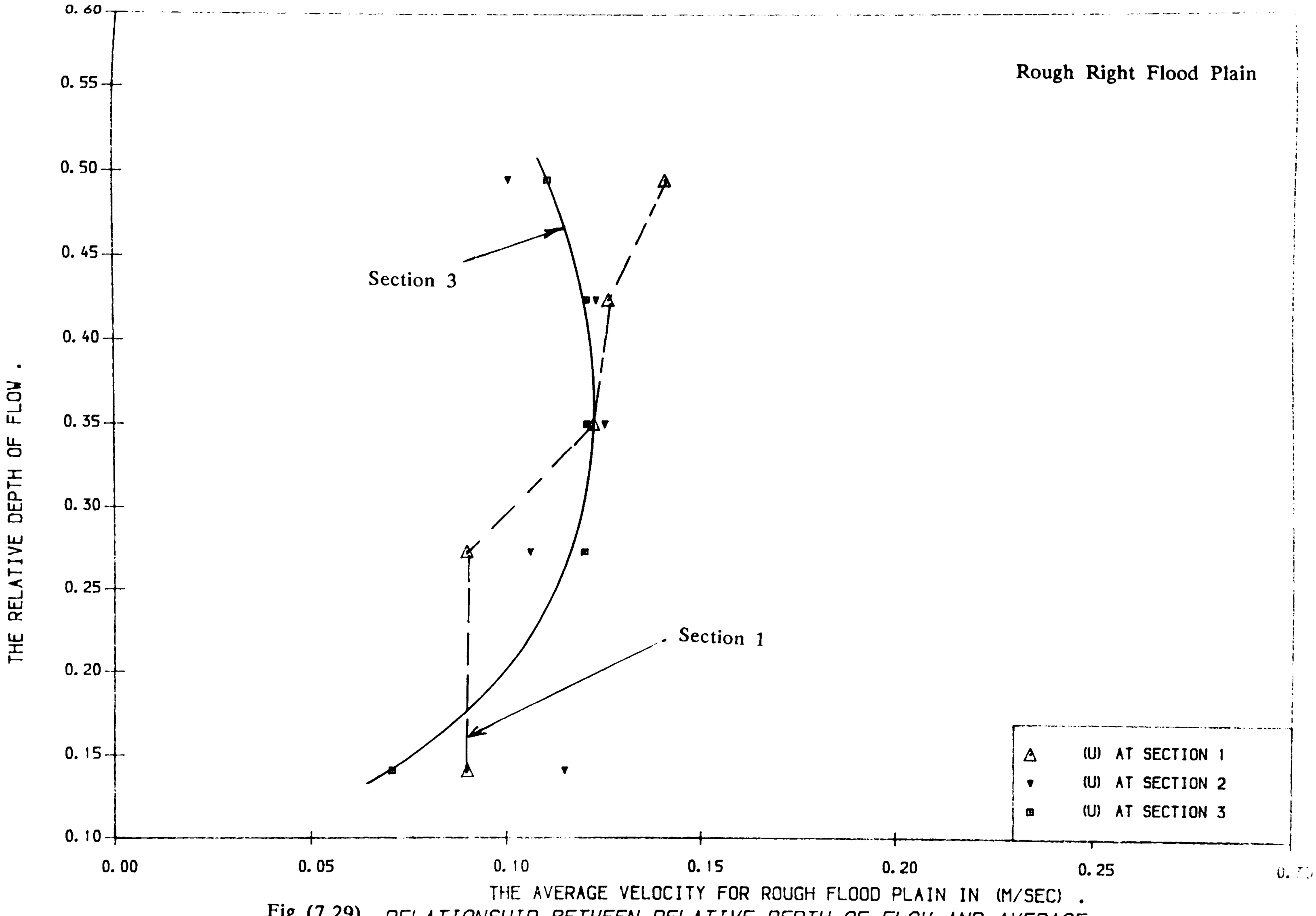

Fig (7.29) *RELATIONSHIP BETWEEN RELATIVE DEPTH OF FLOW AND AVERAGE VELOCITY ON RIGHT SIDE FLOODPLAIN AT VARIOUS LENGTHS ALONG THE FLUME*

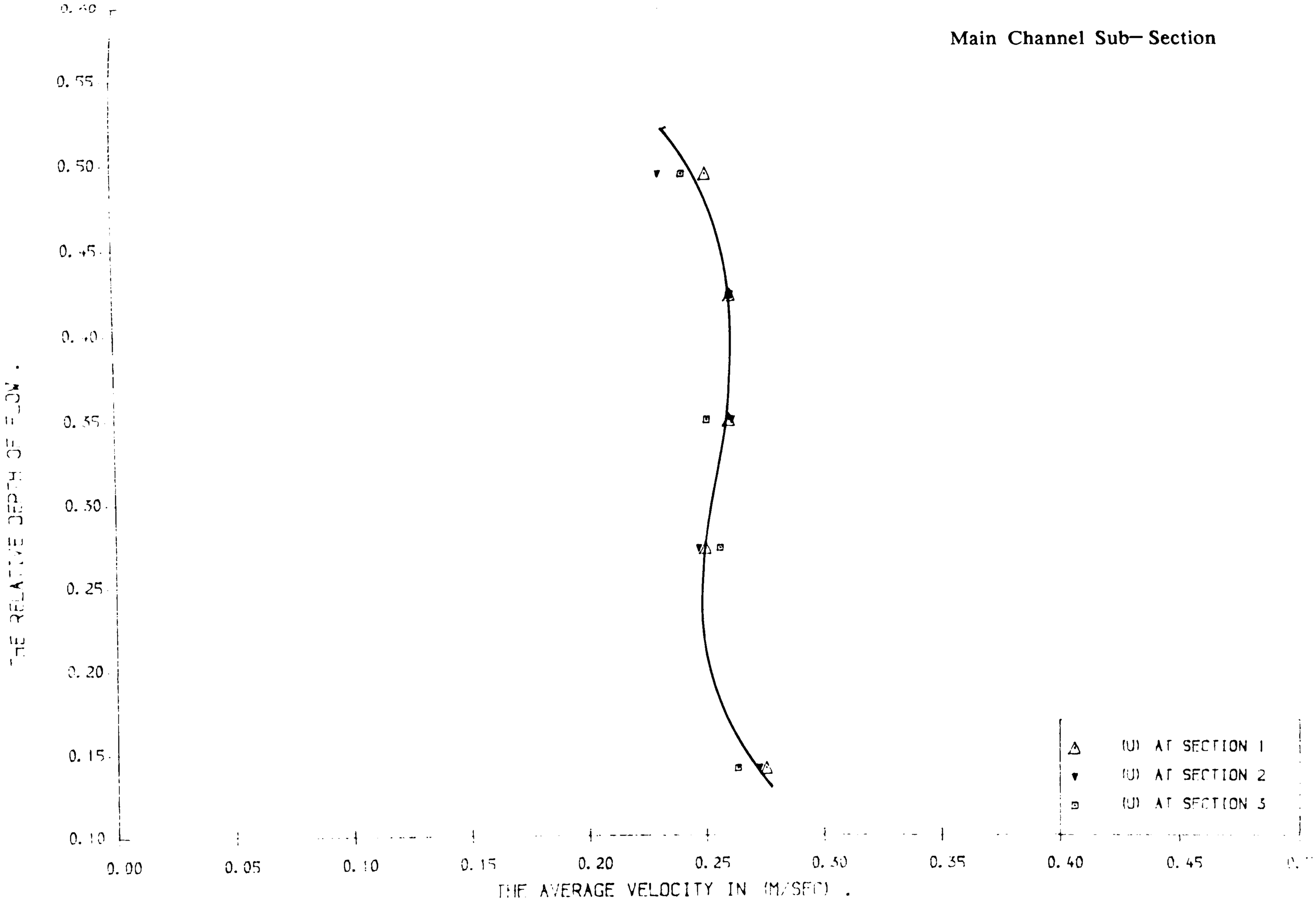

Fig (7.30) *RELATIONSHIP BETWEEN RELATIVE DEPTH OF FLOW AND AVERAGE VELOCITY ON SKEWED MAIN CHANNEL AT VARIOUS LENGTHS ALONG THE FLUME*

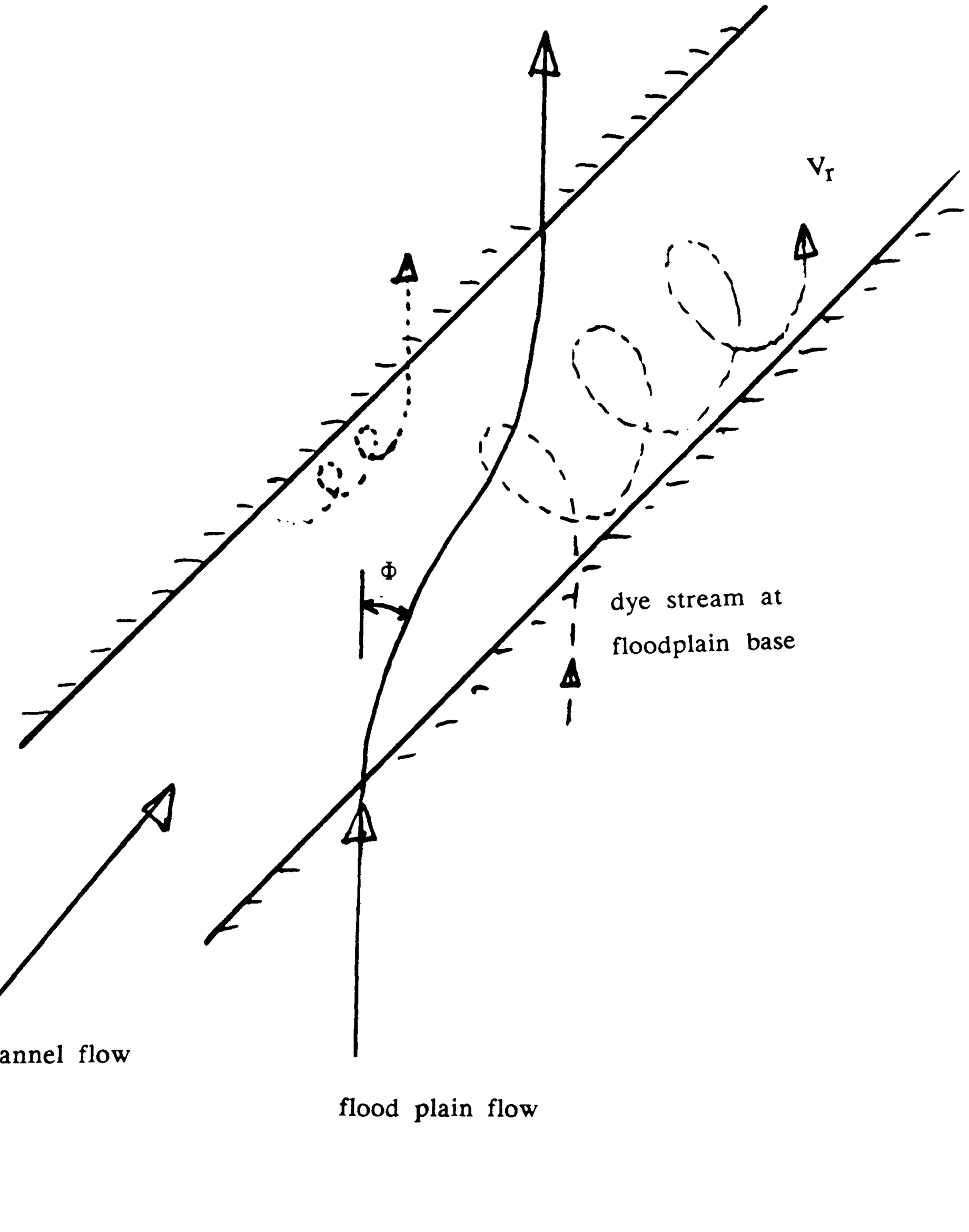

Fig (7.31) The Flow Mechanisms of the Meandering Channel with Flood Plain Flow

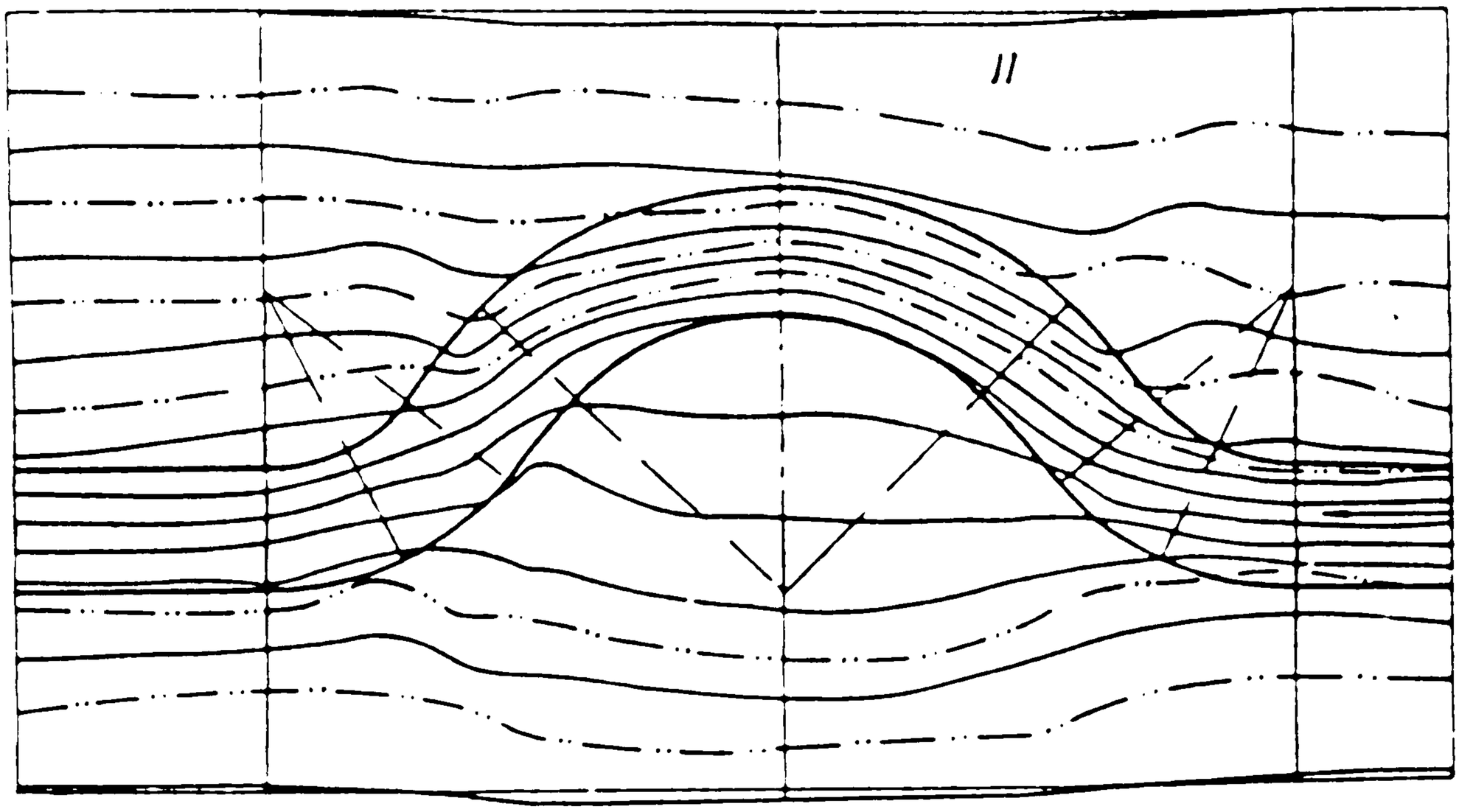

Fig (7.32) The Flow Mechanisms of the Meandering Channel with Flood Plain Flow (Goncharov 1964)

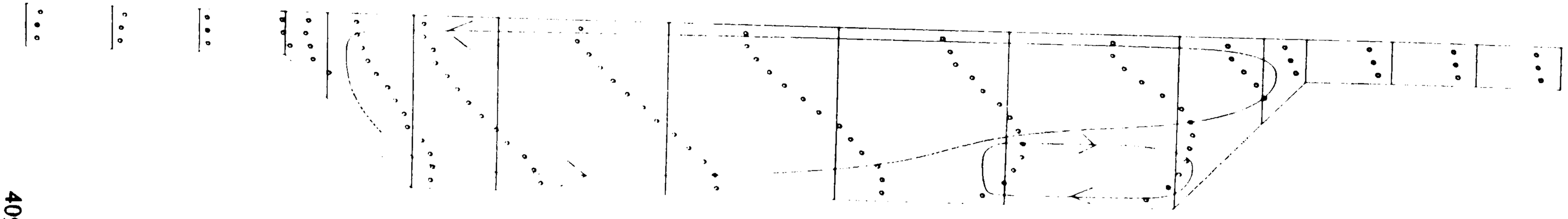

Fig (7.33) The Recirculation Velocity in Meandering Channel During the Flood Plain Flow

CHAPTER 8

CONCLUSIONS

(A) Conclusions on flow resistance

(B) Conclusions on velocity measurements

(C) Conclusions on the slot tes

(D) Recomandations For Future Research

CHAPTER 8

CONCLUSIONS

Several general conclusions can be made before moving to more specific conclusions:

(i) Flow in a skewed compound channel flow, even at a small skew angle less than 6^0, has several characteristics which are dissimilar to the straight / parallel case of compound flow.

(ii) The depth–averaged logitudinal velocity is asymmetric, even at the point of geometric symmetry. The left diverging flood plain has a higher mean velocity and a wider lateral shear layer than the right converging flood plain. The maximum velocity filament is always on the left side of the skewed main channel, and sometimes on the left flood plain, especially at high relative flow depths and smooth flood plains.

(iii) The skewed main channel contains within it, a large magnitude recirculting swirl which is caused by the flood plain flow passing over the skew. This has been proved by removing the flood plain flow. The magnitude of the recirculating swirl produces recirculating velocities which are up to 4% – 5% of the mean longitudinal velocities, or 50% – 60% of the components of flood plain velocity normal to the skew.

(iv) Dye tests reveal that flood plain flow, near to the solid bed, can be entrained down into the main channel swirl and transported–off in the direction of the main channel. This adds materially to the magnitude of the velocities within the swirl, producing larger recirculating velocities than comparable slot tests.

(v) Angle measurements reveal that the mean flood plain streamline deviates by an angle Φ on reaching the skewed main channel. The angle of deviation depends on the relative flow depth and flood plain roughness. For the rough

flood plain case, the deviation Φ is considerable at all relative depths. For the smooth flood plain case, the deviation angle is negligible at relative depths above 0.3.

(vi) Conclusion (iv) and (v) mean that the energy loss estimate from slot tests in Chapter 6, is not directly applicable to skewed compound flows. Thus, the recirculating velocity pattern found in the slot tests in Chapter 6 is not directly applicable either.

(vii) The imaginary vertical wall sub–divided channel method for discharge assessment is not accurate either in the smooth or rough flood plain cases. In the smooth flood plain case the errors involved in using this method can be up to 30%. Inclusion of horizontal shear losses from the slot tests reduces the errors to less than that of a straight/parallel compound flow (where the errors are due to lateral turbulent shear only). Thus reveals that skewed flows contain an element of lateral shear and an element of horizontal shear, as well as large magnitude secondary cells not found in the straight/parallel case.

(viii) For the case of a roughened flood plain, the best method of sub–division for discharge assessment, is an imaginary horizontal wall with flood plain roughness placed on the upper side, and the horizontal sub–division at, or just below bank–full level. This gives errors to within 5% to 10%, which is acceptable.

(ix) Skewed compound flows produce a resistance function on the Darcy Weisbach – Reynolds Number diagram ($\lambda - R_e$), which is between the straight/parallel case and the meandering case. For the straight cases and small angles of skew and the pattern at large relative depths approximates to the isolated channel, whereas for larger skew angles and meanders, the pattern approximates to a channel with definite roughness (k/4R) even if the boundary is smooth.

(x) Because of complex three–dimensional flow patterns in a skewed compound flow, neither one dimensional nor two–dimensional numerical models can accurately simulate flow patterns, energy losses or the stage–discharge relationship.

(xi) The longer term behaviour of skewed two–stage channels may be

governed by scour along the left bank, and differential deposition of sediment mainly on the right flood plain.

More detailed conclusions from each of Chapter 4 to 7 are given below.

(A) Conclusions on flow resistance

(1) The resistance coefficient of the flood plain material is best described by the Darcy Weisbach quasi– smooth function

$$1/\sqrt{\lambda} = 2 \text{ Log } (R_e \sqrt{\lambda}) - 1.487 \qquad (8.1)$$

(2) The resistance coefficient for the skewed main channel is given by

$$1/\sqrt{\lambda} = 2 \text{ Log } (R_e \sqrt{\lambda}) - 1.76 \qquad (8.2)$$

(3) At present we are unable to predict accurately stage and discharge for a skewed main channel interacting with flow on smooth floodplains. The errors in discharge assessment are of order of 25%–30%, because of both lateral shear (coflowing) and horizontal shear.

(4) An attempt has been made to separate drag due to vertical roughening rods, from skin friction, and also to estimate drag coefficients C_d for the experimental set– up. The trends and values of C_d are shown in Fig (4.15) and **Fig (4.16)**.

(5) 10mm roughening rods at 100mm centres both laterally and longitudinally produce Manning's 'n' values around 0.02 to 0.04, increasing with flow depth.

(6) At present we are unable to predict accurately stage and discharge for a skewed main channel with rough flood plains. The best sub– division method appears to be a horizontal sub– division at or just below bank– full level with the sub division having the same roughness as the flood plain. See Fig (4.18) and Fig (4.19).

(7) For the rough flood plain case, flow in the main channel becomes

completely dominated by the flood plain roughness, Fig (4.20), rather than the classical interactive lateral shear which is more the case for smooth flood plains.

(B) Conclusions on velocity measurements

(1) Flow behaviour in a compound skewed channel reveals flow patterns that are much more complex than the straight/parallel compound case. This complexity involves asymmetric velocity profiles and secondary currents derived from horizontal shear.

(2) The maximum longitudinal velocity filament tends to follow the left wall of the main channel, and at higher relative depths moves onto the flood plain as if moving towards the centre– line of the flume. At least this is the case for the smooth flood plains. For the rough flood plain case the maximum velocity filament follows the line of the main channel, again near the left side wall, but does not go unto the left flood plain at higher relative depths.

(3) As a general rule there are no lateral shear layers extending unto the right flood plain. The right shear layer is usually contained within the main channel. The left side shear layers extend a considerable distance unto the left flood plain, certainly further than predicted by conventional formulae. The left shear layer tends to become wider in the downstream direction. This implies large lateral momentum transfer from main channel to left flood plain and no lateral momentum transfer from main channel to right flood plain.

(4) The mean velocity on the right flood plain shows slight decreases in the downstream direction, and sometimes shows increases on the left flood plain moving in the same direction. This is particularly true for the rough flood plain case. The mean velocity in the main channel sub section remains reasonably constant in the downstream direction, but does show slight decreases in the smooth flood plain case in moving from section 1 to section 3. As a general rule the mean velocity on the left flood plain is greater than on the right flood plain.

(5) Flood plain flow streamlines have a tendency to deviate in the same

direction as the main channel, when they approach the main channel region.

For the smooth flood plain case the mean deviation angle is of the order of 1.5^0 to 2.0^0 at the lowest flood plain depth tested. $Y_f/Y_c = 0.15$. The deviation angle tends towards zero for high relative flow depths. For the rough flood plain case, the mean deviation angle is of the order of 2.5^0 to 3.5^0, irrespective of the relative depth of flow.

(6) Flood plain flow passing over the skewed main channel produces secondary recirculations with maximum ratios of transverse to longitudinal velocity around 4%. This ratio is true for both rough and smooth flood plains. The 4% ratio is also much greater than secondary currents in the skewed main channel when isolated from adjacent flood plains, where the ratio is of the order of 1/2% to 1%. The secondary circulation occupies one main cell (at this aspect ratio), rotating in the same sense as the crossing over flood plain flow, and the strength of these secondary cells reduces in the downstream direction.

(7) The magnitude of the recirculating velocities in the skewed main channel is greater than that of a comparable slot test in Chapter 6.

(C) Conclusions on the slot tests

(1) Flow passing over a slot in the channel bed produces a horizontal shear layer with associated energy loss, a recirculation region of maximum length $7h_s$, as well as a rise in the free surface water level Δh.

(2) The rise in free water surface can be predicted reasonably accurately by the application of the force–momentum equation combined with the continuity equation. The maximum rise in water level Δh was 1.7mm giving a non–dimensional rise of $\Delta h/h_s = 0.05$. The rise in free water surface level decreases with decreasing slot width/depth ratio.

(3) Energy losses through the slot in the channel bed comprise of both expansion and contraction losses. The total energy loss coefficient increases with increasing slot width/depth ratio. The energy loss coefficient increases with decreasing relative flow depth (Y_f/Y_c).

The total energy loss can be predicted from conventional expansion and

contraction loss theory, with a correction factor for the width/depth ratio of the slot, B_s/h_s.

(4) Velocity measurements through the slot show a large recirculation, of non−dimensionalised length, L_r/h_s = 5.5 to 7. Maximum recirculation velocities, non−dimensionalised by the mean upstream velocity U_f, gave values of V_{rmax}/U_f between 0.14 and 0.26 depending on the slot width/depth ratio. The patterns of recirculation are different for small B_s/h_s ratios compared with larger B_s/h_s ratios.

(5) The velocity at any point in the recirculation region can be expressed in the form,

$$\frac{v - V_r}{V_m - V_r} = (1 + t)e^{-t} \qquad (8.3)$$

where

$$t = 1.67 \left(Y_c/Y_b \right)^{2.5}$$

(d) Recomandations For Future Research.

For skewed compound channels, the following topics are suggested for future research.

(1) For the same geometry and different skew angles extend the velocity data for more flood plain depths, for smooth and rough flood plain areas.

(2) To carry out 2−D flow visualisation for the overbank flow experiments using possibly the technique suggested by Pender (1985), or Wark (1990).

(3) To modify the model suggested by Ervine and Ellis (1987).

(4) A coordinated effort of a wide group of researchers is needed to address the problem of overbank flow in skewed and meandering channels.

BIBLIOGRAPHY

BIBLIOGRAPHY

Abbott. M.B., Larsen J., and Tao J. " Modelling circulations in depth integrated flows." Part1: The Accumulation of the Evidence, J.of Hyd. Res. Vol.23, No.5, 1985

Abbott M.B. and Larsen J. " Modelling circulations in depth integrated flows." Part2: A Recirculations. J.of Hyd. Res. Vol.23, No.5,1985

Ackers P. " Resistance to fluids flowing in channel and pipes" Hydraulic Research Paper No.1, H.M.S.O., London, England, 1958

Ackers P. " SERC Flood channels facilty." Design manual project, Report no.1, August 1989

Ackers P. " Resistance functions for the Wallingford facility rod roughness." Design manual project, report no.2, November 1989

Agasieva S.I. and Barekyan A.S. " Change in the main velocities in main bed and Chezy's coefficient during floodplain water." Meteorogiai Geologia, No.9, 1961, (Russian)

Arnold U., Pasche E. and Rouve G. " Mixing in rivers with compound sections." 21st I.A.H.R. Congress, Melbourne. 1985

Arnold U., Hottges J. and Rouve G. " Turbulence and mixing mechanisms in compound open channel flow." 23rd I.A.H.R. Congress, Ottawa Aug. 1989

Babarutsi S., Ganoulis J., and Chu V. " Experimental investigation of shallow recirculating flows." Proc.of A.S.C.E , J. Hyd. Eng. Vol.115, No.7, July 1989

Baird J.I. " The hydraulic characteristics of channels with overbank flood plain flow" Thesis submitted to the University of Glasgow for the Degree of Doctor of Philosophy in Department of Civil Engineering, Oct. 1984

Bhowrick N.G. and Demissie M. " Carrying capacity of floodplains." Proc.of A.S.C.E. Jnl Hyd. Div. Vol.108, no.Hy3, March 1982

B.S. 3680:Part 3c:1983 " Methods for determination of stage– discharge relation."

Chang H.H. " Energy expenditure in curved open channels." Proc.of A.S.C.E., Jnl Hyd. Eng. Vol.109 no.Hy7, July 1983

Chang H.H. " Analysis of river meanders" Proc.of A.S.C.E. Jnl Hyd. Eng. Vol.110, no.Hy1, January 1984

Chang H.H. " Regular meander path model." Proc.of A.S.C.E. Jnl Hyd. Eng. Vol.110, no.Hy10, **October 1984**

Chang H.H. " Variation of flow resistance through curved channels." Proc.of A.S.C.E. Jnl Hyd. Eng. Vol.110, no.Hy12, **December 1984**

Chiu C.L. " Effect of secondary flow on sediment transport" Proc A.S.C.E. Jnl Hyd. Div. Vol.92, no.Hy5, **Septemper 1966**

Chiu C.L. " Factors determining the strength of secondary flow." Proc A.S.C.E. Jnl.of Engineering Mechanics Division, EM4, **August 1967**

Chiu C.L. " Method of calculating secondary flow." Water Resource Research, Vol.7, **August 1971**

Chiu C.L. and Hsiung, E.D. " Three dimensional open channel flow." Proc. of A.S.C.E. Jnl Hyd. Div. Vol.104, no.Hy8, **August 1978**

Chiu C.L. and Hsiung, E.D. " Secondary flow, shear stress, and sediment transport." Proc A.S.C.E. Jnl Hyd. Div. Vol.107, no.Hy7, **July 1981**

Chow V.T. " Open channel hydraulics." New York McGraw Hill, **1959**

Cruff R.W. " Cross channel transfer of linear momentum in smooth rectangular channels." U.S Geol. Survey, Water supply paper, **1965**

Einstein H.A. and Li H. " Secondary currents in straight channels." Transactions American Geophysical Union, Vol.39, **1958**

Ervine D.A. and Baird J. I. " Rating curves for rivers with overbank flow." Proc. I.C.E. Part 2, Vol.73, **June 1982**.

Ervine D.A. and Baird J. I. " Analysis of initial results, University of Glasgow **Dec. 1982.**

Ervine D.A " Notes on Meandering flow" **Glasgow University 1986.**

Ervine D.A. and Baird J. I. " Resistance to flow in channels with overbank flood plain flow." Proc of the 1st Int. Conference on Channels and Channel Control Structures, Session 4, A.4.137–4.150, Springer–Verlag, **1984**

Ervine D.A. and Ellis J. " Experimental and computational aspects of overbank flood plain flow." Symposium on Hydrology in Scotland, Royal Soc. of Edinburgh, Edinburgh, **October 1987**

Ervine D.A. and Lorena M. " Meandering channel with floodplain flows." Report submitted to the Civil engineering Dept. Glasgow University, **Dec. 1989**

Etheridge D.W. and Kemp P.H. " Measurement of turbulent flow downstream of a rearward facing step." Jnl Fluid Mechanics, Vol.86 part 3, **1978**

Ghosh S.N. " River flood plain interaction and distribution of boundary shear stress in a meander channel with flood plain." Proc I.C.E., Vol.59, **December 1975**

Goncharov V.N. " Dynamics of channel flow." Israel Program for Scientific Translations, Jerusalem 1964.

Hey R.D. and Thorne C.R. " Secondary flows in river channels." AREA, Vol.7, 1975

Hey R.D. and Thorne C.R. " Secondary flows in river channels." AREA, Vol.8, 1976

Hey R.D. and Thorne C.R. " Direct measurements of secondary currents in river bends." NATURE, Vol.269, October 1977

Holden A.P. and James C.S. " Boundary shear distribution on floodplain." Jnl. of IAHR, Vol 27 , no.1, 1989,

Hollinrake P.G. " The Structure of flow in open channels— a literature search". Vol.2 Report SR96, Hydraulic Research Ltd., Wallingford, England, Jan. 1987.

Hollinrake P.G. " The Structure of flow in open channels— a literature search". Vol.2 Report SR153, Hydraulic Research Ltd., Wallingford, England, Jan. 1988.

Ikeda S. " Flow and profile in meandering sant— silt rivers." Proc A.S.C.E. Jnl Hyd. Eng., Vol.112, no.Hy7, July 1986

James A.L., Chiu C.L. and Miao S.L. " Secondary currents in a corner." Proc.of A.S.C.E. Jnl Hyd. Div. Vol.91, no.Hy6, November 1965

James M. and Brown R.J. " Geometric parameters that influence floodplain flow." US Army Engineers, Waterways Experimental Station, Vicksburg, Mississippi. Research Report H— 77— 1 June 1977

Jeremy P. " Taming the Flood" A History and National History of Rivers and Wetlands, Oxford University Press in Association with Channel Four Television Company 1989.

Johannesson H. and Parker G. " Secondary flow in mildly sinous channel." Proc. A.S.C.E. Journal of Hydraulic Engineering, Vol. 115, No.3. March 1988

Joseph B.F. and Dougherty R.L. " Fluid mechanics with engineering applications." McGraw— Hill, Kogaakusha Lyd. 1965

Kalkwik J.P.Th. and Booijh R. " Adaptation of secondary flow in nearly horizontal flow." I.A.H.R Journal of Hyd. Res. Vol.24, No.1, 1986

Kawahara Y. and Tamai N. " Numerical calculation of turbulent flows in compound channels with an algebraic stress turbulence model." Proc. of 3rd Symp. on Refined Flow Modelling and Turbulence Measurements, Tokyo, 1988

Kawahara Y. and Tamai N. " Mechanism of lateral momentum transfer in compound channel flows." 23rd I.A.H.R. Congress, Ottawa. Aug. 1989

Kazemipour A.K, Apelt C.J. " Shape effects on resistance to uniform flow in open channels" Jour. Hydr. Research, I.A.H.R., Vol.17, No.2, **1979**

Keller R.J. and Rodi W. " Prediction of two dimensional flow characteristics in complex channel cross sections." Hydraulic Engineering Software. Proceedings of The International Conference, Portoroz, Yugoslavia. **September** 1984

Keulegan G.H " Laws of turbulent flow in open channels" Jour. of Research of the National Bureau of Standards, U.S. Dept. of Commerce, Vol.21, Dec 1938

Keller R.J. and Rodi W. " Prediction of Flow Characteristics in main channel and floodplain flows." J. Hyd. Res. Vol.26. No.4. PP.425–441 **1988**

Kiely R.J. " An experimental study of overbank flow in straight and measureming compound channels." PhD thesis submitted to civil engineering department, University College, Cork, Repuplic of Ireland, **September** 1989

Kikkawa H., Ikeda S. and Kitagawa A. " Flow and bed topography in curved open channels." Proc. A.S.C.E. Jnl Hyd. Div. Vol.102, no.Hy9, **September 1976**

Knight D.W. and Demetriou J.D. " Floodplain and main channel flow interaction." Proc. A.S.C.E. Jnl. Hyd. Eng., Vol.109. no.Hy8, **Aug.** 1983

Knight D.W. and Lai C.J. " Turbulent flow in compound channels and ducts." Int. Symp. on refined flow modelling and turbulence measurements., Iowa, U.S.A. **Sep** 1985

Knight D.W. " Compound channel research at Birmingham University." Dept. of Civil Eng. of Birmingham Univ., **April 1986**

Knight D.W. and Sellin R.H.J. " The SERC flood channel facility." J. of the Instituion of Water and Environmental Management, Vol.1.,No.2, 1987

Knight D.W. and Shiono K. " Turbulence measurements in a shear layer Region of a compound channel." J.of Hyd. Res. I.A.H.R. **January** 1989

Krishnappan B.G. " Laboratory verification of turbulent flow model." J. of Hyd Eng., Vol.110, No.4. **April** 1984

Krishnappan B.G. and Lau Y.L. " Turbulence modelling of floodplain flows." Proc A.S.C.E. Jnl Hyd. Eng. Vol.112, no.Hy4, **April 1986**

Larrson R. " Numerical simulation of flow in compound channels." Proc. of 3rd Symp. on Refined Flow Modelling and Turbulence Measurements, Tokyo, PP 537–544, 1988

Larrson R., " Lateral mixing in open channels." 23rd I.A.H.R. Congress, Ottawa. **Aug.** 1989

Lean G.H. and Weare T.J. " Modelling two dimensional circulating flow." Proc.of A.S.C.E. J. of Hyd.Div Vol.105. No. HY1. 1979

Lee H.Y. and Hsieh K.C. " Flow characteristics in an alluvial aiver bend." 23rd International Congress of I.A.H.R. Ottawa, Canada **Sep. 1989**

Leopold L.B. and Wolman M.G. " River channel patterns: Braided, Meandering, and Straight." Geological Survey Professional Paper 282– B, Washington. **1957**

Leopold L.B., Bagnold R.A., Wolman M.G. and Brush L.M. " Flow resistance in sinuous or irregular channels." Gelogical Survey Professional Paper 282– D, Washington. **1960**

McKee P.M., " A study of the tydraulic characteristics of open channels with floodplains." PhD thesis, Queen's University, Belfast. **May 1982**

McKee P.M., Elsawy E.M. and McKeogh E.J. " A study of the hydraulic characteristics of open channels with floodplains." 21st. I.A.H.R. Congress, Melbourne. **Aug. 1985**

McKeogh E.J., Javan M., and Kiely G.K. " A comparison of turbulence measurements in straight, single meander and multiple meander compound channels." International conference on channel flow and catchment runoff, centennial of manning's formula and kuichling's rational formula. University of Virginia. **May 1989**

McKeogh E.J. and Kiely G.K. " A comparison of velocity measurements in straight, single meander and multiple meander compound channels." International Conference on Channel Flow and Catchment Runoff, Centennial of Manning's Formula and Kuichling's Rational Formula. University of Virginia **May 1989**

McKeogh E.J. and Kiely G.K. " Experimental study of the mechanisms of flood flow in meandering channels." 23rd I.A.H.R. Congress, Ottawa. **Aug. 1989**

McKeogh E.J., Kiely G.K., and Javan M. " Velocity and turbulence measurements in a straight channel with interacting floodplains using Laser Doppler Anemometry." Intrnational Conference on Hydraulic and Environmental Modeling of Coastal, Estuarine and River Waters." Bradford, U.K. **Sep. 1989**

McQuivey R.S. and Rinhardson E. " Some turbulence measurements in open channel flow." A.S.C.E. Journal of the Hydraulics Division. Vol.95. No. HY1. **Jan. 1969**

Maclean A.G. and Willets B.B. " Measurement of boundary shear sterss in non– uniform open channel flow." I.A.H.R. Journal of Hyd. Res. Vol.24. No.1. **1986**

Mockmore C.E. " Flow around bends in stable channels." Transactions A.S.C.E., Vol.109, **1944**

Myers W.R.C. and Elsawy E.M. " Boundary shear in channel with

floodplain." Proc.of Journal of Hydraulics Division. A.S.C.E., Vol.101,HY7. 1975

Myers W.R.C. " Momentum transfer in a compound channel." I.A.H.R. J.of Hyd. Res. Vol.16., No.2, 1978

Myers W.R.C. " Flow resistance in smooth compound channels." Experimental Data, Civil Eng. Dept., University of Ulster. **March 1985**

Myers W.R.C. " Velocity and discharge in compound channels." Proc. of Jnl Hyd. Eng., A.S.C.E., Vol.113, no.Hy6, **June 1987**

Myers W.R.C. and Brennan E.K. " Flow resistance in compound channels." draft paper submitted to journal IAHR 1989

Nakagawa H. and Nezu I. " Experimental investigation on turbulent structure of back–ward facing step flow in open channel flow." Jnl Hydraulic Research, Vol.25, no.1 1987

Nalluri C. and Judy N. " Interaction between main channel and floodplain flow." 21st. I.A.H.R. Congress, Melbourne. **Aug. 1985**

Nalluri C. and Judy N. " Flow characteristics in compound channels with vegetated floodplain." Private publication, Civil Eng. Dept., Newcastle 1989

Naot D. and Rodi W. " Applicability of algebraic models based on undirectional flow to duct flow with lateral motions." International Journal of Numerical Methods in Fluids, Vol.1, 1981, pp225–235.

Naot D. and Rodi W. " Numerical simulation of secondary currents in open channel flow with an algebraic stress turbulence model." Report SFB80/T/187, University of Karlsruhe, Karlsruhe, West Germany, **Feb. 1981**

Naot D. and Rodi W. " Calculation of secondary currents in channel flow." Proc. of Jnl Hyd. Div, A.S.C.E., Vol.108, Hyd8, **August 1982**

Nezu I. and Rodi W. " Calculation of secondary currents in open channel flows." Proc. of A.S.C.E. J.of Hyd. Div.,no.HY8. **Aug. 1982**

Nezu I. and Rodi W. " Experimental study on secondary currents in open channel flows." 21st. I.A.H.R. Congress, Melbourne, 1985

Nezu I. and Rodi W. " Open channel flow measurements with a Laser Doppler Aneometer." Proc.of A.S.C.E. J. of Hyd. Eng. HY5. 1986

Nezu I., Nakawaga H. and Rodi W. " Significant differences of secondary currents in closed channels and narrow open channels." 23rd Inter. Congress of I.A.H.R., Ottawa, **Aug. 1989**

Nouh M.A. and Townsend R.D. " Shear–stress distribution in stable channel bends." J. Hydr. Div., ASCE, Vol. 105, No. HY10, proc. paper 14898, 1979

Odgaard A. J. " Transverse bed slope in alluvial channel bends." Proc. of A.S.C.E., J. of Div., No.HY12., **Dec. 1981**

Odgaard A. J. " Bed characteristics in alluvial channel bends." Proc. of A.S.C.E., J. of Hyd. Div. No.HY11., **Nov.** 1982

Odgaard A. J. " Shear induced secondary currents in channel flows." Proc. A.S.C.E., J. of Hyd. Eng., No.7, **July 1984**

Odgaard A. J. " Meander flow model I: Development" Proc A.S.C.E. Jnl. Hyd. Eng. Vol.112, No. Hy12, **December 1986**

Pasche E., Rouve G. and **Evers P.** " Investigations on flow in channels with vegetated floodplain." 21st. I.A.H.R. Congress, Melbourne, **Aug. 1985**

Pasche E. and Rouve G. " Overbank flow with vegetatively roughened floodplains." Proc. A.S.C.E. Jnl. Hyd. Eng. Vol.111, No. Hy9, **September 1985**

Pender G. " The Numerical modelling of tide and flood movement in two– dimensional space using implicit finite difference methods" Thesis Submitted in Fulfilment of the Requirements for the Degree of Doctor of Philosopy, department of Civil Engineering University of Strathclyde, Glasgow, **1985**

Posey C. J. F. " Computation of discharge including overbank flow." Civil Engineering, A.S.C.E. No.CE4, Vol.37, **April 1967**

Ragojkovic M. " Math. modelling of river with flood plains." River, Vol.1, pp 56, **1976**

Ragojkovic M. and Djordjevic S. " Computational of discharge distribution in compound channels." 21st I.A.H.R. Congress, Melbourne **1985**

Rajaratnam N. and Ahmadi R. " Interaction between main channel and floodplain flows." Proc. A.S.C.E. Jnl. Hyd. Div., Vol.105, **1979**

Rajaratnam N. and Ahmadi R. " Hydraulics of Channels with Floodplains." Jnl. Hyd. Research, Vol.19, **1981**

Rajaratnam N. and Ahmadi R. " Meandering channels with floodplains." Proc A.S.C.E. Jnl Hyd. Eng. Vol.109, No. Hy3, **March 1983**

Rao K.K. " Effect of shape on the mean flow characteristcs of turbulent flow through smooth rectangular open channel" Thesis, University of Iwoa, Iwoa City, **1967**

Raspopin G. A. and Kovalyov E.A. " River stream dynamics mathematical modelling in river bed and floodplain." 23rd. I.A.H.R. Congress, Ottawa, **Aug. 1989**

Reinus E " Steady uniform flow in open channels" Transactions, Royal Institue of Technology, Stockholm, Sweden, No.179, **1961**

Rodi W. " Turbulence models and their application in hydraulics." A state of the Art Review. I.A.H.R. Delft. **1984**

Rodi W. " Hydraulic computations with the $\kappa-\epsilon$ turbulence model." Proc.

of the Conf. of Applying Research to Hydraulic Practice, Jackson, U.S.A. 1984

Rozovskii I. L. " Flow of water in bends of open channels." The Israel Program for Scientific Translations, No.OTS 60−51133, Office of Technical Services, U.S. Dept. Comm., Eashington, D.C. 1961

Samuels P.G. " Modelling open channel flow using the finite element method." Hydraulics Research, Wallingford, SR 61. 1985

Samuels P.G " Modelling open channel flow using preissmann's scheme." Hydraulics of Flood and Flood Control." 2nd Int. Conf. Cambridge U.K., **Sep.** 1985

Samuels P.G. " Lateral shear layers in compound channels." International Conference on Fluvial Hydraulics, Budapest, 1988

Sellin R.H.J. "A laboratory Investigation into the interaction between the flow in the channel of river and over its floodplain" La Houille Blanche, 7, 1964

Sellin R.H.J. and Searle D.J. " Developments in the understanding of compound channel flow from the 1950's to 1984's." Report to Civil Eng. Dept. of Bristol. March 1984

Sellin R.H.J. and Searle D.J. " Modelling channel roughness caused by floodplain vegetation." International Conference I.A.H.R. Lausanne 1987

Sellin R.H.J. and Elliott S. " Flow mechanism in skewed channel with overbank flow." Private Publication, Bristol Dep. Civil Engineering, **Jan. 1989**

Sellin R.H.J. and Giles A. " Two stage channel flow." Publication University of Bristol, Dept. Civil Eng. **July 1988**

Sellin R.H.J. and Giles A. " Flow mechanisms in spilling meander channels." 23rd. I.A.H.R. Congress, Ottawa, **Aug. 1989**

Shiono K. and Knight D.W. " Two dimensional analytical solution for a compound channel." 3rd. Int. Symp. on Refined Flow Modelling and Turbulence Measurements." Tokyo, Japan, **July 1988**

Shiono K. and Knight D.W. " Structure of Reynolds stress contribution in the shear layer region of a compound channel." J. Hyd. Res. 1989

Shiono K. and Knight D.W. " Vertical and transverse measurement of reynolds stress in a shear region of a compound channel." Proc. 7th Int. Symp. on Turbulent Shear Flows, Stanford, USA, **Aug. 1989**

Shukry A. " Flow around bends in an open channel." Transactions A.S.C.E., Vol. 115, **1950**

Smith C.D. " Flood stage in a valley with meandering channel." Research Report, Proc A.S.C.E. Jnl Hyd. Div. Vol.104, no.Hy7, **July 1978**

Smith C. D. " Some aspects of floodplain flow in a valley with a meandering channel." 23rd I.A.H.R. Congress, Ottawa. **Aug. 1989**

Smith K.V.H, Hussein A.S.A " Flow and bed deviation angle in curved open channels." J. Hydr. Eng., ASCE, Vol. 111, No. 11, Proc. paper 20133, **1986**

Soliman M. M. and Tinney E. R. " Flow around 180^0 bends in open rectabgular channels." Proc A.S.C.E. Jnl Hyd. Div. Vol.94, No. Hy6, **July 1968** pp893–908.

Spitsin J. P. " On the interaction of the streams of the main river bed and the flood plain." Meterologiai Gidrologia, No.10, **1962** (Russian)

Stein C. J. and Rouve G. " Two dimensional LDV–technique for measuring flow in a meandering channel with wetted floodplains (First Results)." International Conference on Fluvial Hydraulics, Budapest **1988**

Stein C. J. and Rouve G. " 2D depth averaged numerical predictions of the flow in a meandering channel with compound cross section." Computational Mechanics Publications Hydrosoft, Vol.2, No.1, **1989**

Stein C. J. and Rouve G. " Two dimensional depth averaged numerical predictions of the flow in a meandering channels with compound cross section." International Conference on Computational Metheod and Water Resources, Rebat, Morocco, **14–18 March** 1988

Tamai N., Ikeuchi K., and Mohamed A.A. " Evolution of depth averaged flow fields in meandering channels." River Meandering Conference A.S.C.E. Louisianna. **1983**

Task Force, " Friction factors in open channels." Report of the Engr., Vol.89, No.2, pp 97–143, **1963**

Thomson J. " On the origin of winding of rivers in alluvial plains, with remarks in the flow of water around bends in pipes." Proc. Royal Soc. London, England, **Vol.25, 1876**

Thorne C. and Rais S. " Secondary current in a meandering river." River Meandering, River Meandering Louisianna, **1983**

Thorne C., Zevenbergen L.W., Pitlick J.C., Rais S., Bradley J.B. and Julien P.Y. " Direct measurements of secondary currents in a meandering sand–bedded stream." NATURE, Vol.315. PP.746–747. **1985**

Tingsanchali T. and Ackermann N. L. " Effects of overbank flow on flood computations." Proc. A.S.C.E, J. of Hyd. Div. Vol.102, No. HY7. **July 1976**

Toebes G. H. and Sookey A. A. " The hydraulics of meandering rivers with floodplains." Proc. A.S.C.E. Jnl Water Ways and Harbors Div. Vol.73, pp213–236, **1967**

Tominaga A. and Ezaki K. " Hydraulic characteristics of compound channel flow." Proc. of 6th Congress of Asian and Pacific Division, I.A.H.R.,Kyoto, 1988

Tominaga A., Nezu I. and Ezaki K. " Turbulent structure in compound channel flows with rectangular and trapezodial main channel." Proc. of 3rd Symp. on Refined Flow Modelling and Turbulence Measurements, Tokyo, 1988

Tominaga A., Ezaki K. and Nezu I. " An experimental study on three dimensional turbulent structure in a trapezoidal open channel flow." Proc. J.S.C.E, No.381, II.7, PP. 55−63, 1987

Tominaga A., Ezaki K., and Nezu I. " An experimental study on secondary currents in compound open channel flows." 23rd. I.A.H.R. Congress, Ottawa, Aug. 1989

Tominaga A., Ezaki K., Nezu I., and Nakagawa H. " Three dimensional turbulent structure in straight open channel flows." I.A.H.R. J.of Hyd. Res.,Vol.27, No.1, 1989

Tominaga A., Ezaki K. and Nakamura E. " Three dimensional turbulent structures in compound open channel flows." Proc. 42nd Annual Conf. JSCE, II, PP. 372−373 (Japanese) 1987

Tominaga A., Nezu I., and Kobataga S. " Flow measurements in compound Open channels with a fibre optic Laser Doppler Anemometer." Proc. I.A.H.R. Workshop on Instrumentation for Hydraulic Laboratories, Canada Centre for Inland Waterways. Aug. 1989

Townsend R., Prinos P. and Tavoularis S. " Structure of turbulence in Compound channel flows." Proc. A.S.C.E. Jnl Hyd. Eng. Vol.111, No.9, September 1985

Udai K. C. and Sampathiengar N. M. " Flow in 180° open channel rigid boundary bends." Technical Notes, Proc A.S.C.E. Jnl Hyd. Div. Vol.103. No.Hy6, June 1977

Tracy H.J. and Lester C.M. " Resistance coefficients and velocity distribution in smooth rectangular channel" U.S. Geological Survey, Water Supply Paper, Vol.1592− A, 1961

Urban C. and Zielke W. " Steady state solution for 2− D flows in river with floodplains." 2nd. Int. Conf. Cambridge 1985

U.S. Engineers " Hydraulic capacity of meandering channels in straight floodways." Technical Memorandum, No.2− 429 March 1956

Vreugdenhill C.B. " Computation of patterns in rivers." Proc. A.S.C.E. Journal of Hyd. Div., No.HY11 Nov. 1982

Williams D.Y. and Julien P. " Examination of stage discharge relationships

of compound or composite channels." Inte. Conf. on Channel Flow and Catchment Runoff, Centennial of Manning's Formula and Kuichling's Rational Formula, University of Virginia, May 1989

Wark J.B., Ervine D.A. and Samuels P.G. " Apartical method of estimating velocity and discharge in compound channels" Paper submitted to the International Confr. on River Flood Hydraulics, Wallingford, England, **Sept. 1990**

Wormleaton P. R., Allen J. and Hadjipanos P. " Discharge assessment in compound channel flow." Proc. A.S.C.E. Jnl. Hyd. Div. Vol.108, No. Hy9, September 1982

Wormleaton P. R. " Some results of a preliminary investigation of flow in trapezoidal main channel and floodplain." ' Paper Presented to SERC Flood Channels Working Party, **May 1986**

Wormleaton P. R. " Determination of discharge in compound channels using the dynamic equation for lateral velocity distribution." Inter. Conference on Fluvial Hydraulics, Budapest 1988

Yen C. L. and Overton D. E. " Shape effects on resistance in floodplain channels." Proc. A.S.C.E., Jnl. Hyd. Div. Vol 99. No. Hyl, **January 1973**

Yen B. C. " Characteristics of subcritical flow in a meandering channel." Institute of Hydraulic Research, Univ. of Iowa, Iowa City, **1965**

Yen B. C. " Flood flow over meandering channels." River Meandering Conference, Louisianna. **1983**

Yen C.L. and Yen B.C. " Bed topography in meandering mends." River Meandering Conference, Louisanna, **1983**

Zheleznyakov G. V. " Relative deficit of mean velocity of unstable river flow— kinematic effect in river beds with floodplains." Proc. 11th International Congress I.A.H.R Leningrad, 1965

Zheleznyakov G. V. " Interaction of channel and floodplain streams." Proc. 14th International Congress I.A.H.R. Paris, **1971**

Zimmermann C. and Kennedy J. F. " Transverse bed slopes in curved alluvial streams." Proc. A.S.C.E. Jnl. Hyd. Div. Vol.104, No. Hyl, **January 1978**

APPENDICES

APPENDIX A – Computer Program

APPENDIX B – Integration Program

APPENDIX C – Point Velocity Measurements

APPENDIX D – The Angular Point Measurements

APPENDEX A

(Longitudinal Contours, Longitudinal Depth-Average Velocity and Transverse Velocity)

```
      PROGRAM FLOOD
      DIMENSION V(20,20),VEL(20),HEIHT(20)
      DIMENSION RANGE(20),CONT(13),WIDTHY(20)
      DIMENSION VSINT(20,20),VSIN(20),WIDTH(20)
      DIMENSION THETA(20,20),VCOST(20,20),THETA1(20,20)
        DATA CONT /0.1,0.15,0.2,0.25,0.3,0.35,0.4,0.45,0.5,
     1   0.55,0.6,0.65,0.7 /
        READ(5,*)CONT1,CONT2,CONT3,CONT4,CONT5,CONT6,CONT7,CONT8
        READ(5,*)  ISET,FR,YF
        WRITE(6,9993)  ISET,FR,YF
        READ(5,*)  NT,SECT,DH
        WRITE(6,9995)  NT,SECT,DH
        READ(5,*)  H,S,BW,BC,R,BF
        READ(5,*)  LL
        READ(5,*)  (RANGE(I),I=1,LL)
        READ(5,*)  KK
        READ(5,*)  (HEIHT(J),J=1,KK)
        READ(5,*)  N,NBF1,NBC,NBF
        READ(5,*)  (WIDTH(I),I=1,LL-1)
        READ(5,*)  (WIDTHY(J),J=1,KK-1)
        BF1=BW-BC-BF
        DO 12  I=1,LL
        READ(5,*)  (VCOST(I,J),THETA(I,J),J=1,KK)
   12   CONTINUE
        DO 111  I=NBF1+1,NBF1+NBC
        DO 111  J=1,KK
        THETA1(I,J)=(-THETA(I,J)-5.843)
  111   CONTINUE
        PI=4.0*ATAN(1.0)
        RAD=PI/180.0
        DO 15  I=1,LL
        DO 16  J=1,KK
        THETA(I,J)=RAD*THETA(I,J)
        V(I,J)=VCOST(I,J)/COS(THETA(I,J))
   16   CONTINUE
```

```
      WRITE(6,9997) (VCOST(I,J),THETA(I,J),J=1,KK)
 15   CONTINUE
      DO 19 I=1,LL
      WRITE(6,9992) (V(I,J),J=1,KK)
 19   CONTINUE
9999  FORMAT(I2)
9998  FORMAT(6 F10.4)
9997  FORMAT(2F7.3)
9995  FORMAT(I3,4X,'SECT',F3.1,5X,'DH=',F9.5)
9992  FORMAT(12F8.5)
9993  FORMAT(I1,5X,'FR=',F7.5,5X,'YF=',F7.5)
      CALL PAPER(1)
      CALL CTRMAG(8)
      CALL PSPACE(0.15,0.65,0.65,0.91)
      CALL CSPACE(0.05,0.7,0.60,1.0)
      CALL MAP(0.0,0.80+0.05,0.0,H+0.01)
      CALL POSITN(0.0,R)
      CALL JOIN(BF1,R)
      CALL JOIN(BF1,0.0)
      CALL JOIN(BF1+BC,0.0)
      CALL JOIN(BF1+BC,R)
      CALL JOIN(BW,R)
      CALL JOIN(BW,H+0.01)
      CALL POSITN(BW,H)
      CALL JOIN(0.0,H)
      CALL POSITN(0.0,H+0.01)
      CALL JOIN(0.0,0.0)
      CALL AXESSI(0.1,0.01)
      CALL MASK(0.0,BF1,0.0,R)
      CALL MASK(BF1+BC,BW,0.0,R)
      CALL CONTIA(V,1,LL,20,1,KK,20,CONT,1,8,RANGE,HEIHT)
      CALL UNMASK(0)
      CALL CTRMAG(8)
      CALL PLOTCS(BC-0.08,R-0.0080,'RUN   ',4)
      CALL TYPENI(NT)
      CALL PLOTCS(BC-0.08,R-0.016,'H=   ',4)
      CALL TYPENF(H,4)
      CALL PLOTCS(BC-0.08,R-0.024,'BC=   ',4)
      CALL TYPENF(BC,3)
      CALL PLOTCS(BC-0.08,R-0.032,'BF=   ',4)
```

```
      CALL TYPENF(BF,4)
C
C
C                START LATERAL VELOSITY PLOTS
C
      CALL CTRMAG(8)
      CALL PSPACE(0.15,1.32,0.2,0.43)
      CALL CSPACE(0.05,1.45,0.0,0.6)
      CALL MAP(BF1-0.05,(BF1+BC+0.06),0.0,H+0.01)
      CALL PSPACE(0.15,0.2,0.2,0.5)
      CALL MAP(0.0,1.0,0.0,H+0.01)
      CALL YAXISI(0.01)
      CALL CTRMAG(15)
      CALL PSPACE(0.15,1.32,0.2,0.5)
      CALL CSPACE(0.05,1.45,0.0,0.6)
      CALL MAP(BF1-0.05,(BF1+BC+0.06),0.0,H+0.01)
      CALL POSITN(BF1-0.05,0.0)
      CALL JOIN(BF1,0.0)
      CALL POSITN(BF-0.05,R)
      CALL JOIN(BF1-0.035,R)
      CALL JOIN(BF1-0.035,0.0)
      CALL JOIN(BF1+BC+0.04,0.0)
      CALL JOIN(BF1+BC+0.04,R)
      CALL JOIN(BF1+BC+0.055,R)
      CALL FULL
      DO 112 I=NBF1+1,NBF1+NBC
      DO 112 J=1,KK
      THETA1(I,J)=RAD*THETA1(I,J)
      VSINT(I,J)=V(I,J)*SIN(THETA1(I,J))
112   CONTINUE
      PMIN=0.2
      PING=0.118
      DO 90 I=NBF1+1,NBF1+NBC
      PINC=0.173
      CALL CTRMAG(12)
      CALL PSPACE(PMIN,PMIN+PINC,0.2,0.5)
      CALL CSPACE(-1.0,1.0,0.0,0.5)
      CALL MAP(-0.04,0.04,0.0,H+0.01)
      CALL AXESSI(0.04,1.0)
      DO 95 J=1,KK
```

```
95    VSIN(J)=VSINT(I,J)
      CALL CURVEO(VSIN,HEIHT,1,KK)
      PMIN=PMIN+PINC+PING
      DO 34 J=1,KK
      CALL POSITN(0.0,HEIHT(J))
      CALL JOIN(VSIN(J),HEIHT(J))
34    CONTINUE
90    CONTINUE

CCCC   Start with velocity profile in plan

      CALL CTRMAG(8)
      CALL PSPACE(0.75,1.15,0.65,0.91)
      CALL CSPACE(0.75,1.45,0.55,1.0)
      CALL MAP(0.0,0.80+.05,0.0,0.5)
      CALL AXESSI(0.1,0.1)
      CALL CTRMAG(15)
      CALL BROKEN(10,10,10,10)
      CALL POSITN(BF1,0.0)
      CALL JOIN(BF1,0.4)
      CALL POSITN(BF1+BC,0.0)
      CALL JOIN(BF1+BC,0.4)
      CALL POSITN(BW,0.0)
      CALLJOIN(BW,0.4)
      CALL FULL
      CALL CTRFNT(3)

CCC    The average velocity in the left floodplain.

      DO 10 I=1,NBF1
      WRITE(6,*) ' '
      SUM=0.0
      DO 20 J=N+1,KK
      SUM=SUM+V(I,J)
20    CONTINUE
      VEL(I)=SUM/(KK-N)
10    CONTINUE

CCCCCC      The main channel.
```

```
      DO 30 I=NBF1+1,NBF1+NBC
      WRITE(6,*) ' '
      SUM=0.0
      DO 40 J=1,KK
      SUM=SUM+V(I,J)
40    CONTINUE
      VEL(I)=SUM/KK
30    CONTINUE

CCCCCC    Use the right floodplain side
      DO 50 I=NBF1+NBC+1,LL
      WRITE(6,*)  ' '
      SUM=0.0
      DO 60 J=N,KK
      SUM=SUM+V(I,J)
60    CONTINUE
      VEL(I)=SUM/(KK-N)
50    CONTINUE
      JJ=245+J
      CALL CURVEO(RANGE,VEL,1,LL)
      CALL PTPLOT(RANGE,VEL,1,LL,JJ)
88    CONTINUE
      CALL CTRFNT(1)
      CALL CTRMAG(8)
      CALL PLACE(172,10)
      CALL TYPECS('CONT1=0.1M/SEC',24)
      CALL PLACE(172,13)
      CALL TYPECS('CONT2=0.15 M/SEC',25)
      CALL PLACE(172,16)
      CALL TYPECS('CONT3=0.2 M/SEC',25)
      CALL PLACE(172,19)
      CALL TYPECS('CONT4=0.25 M/SEC',25)
      CALL PLACE(172,22)
      CALL TYPECS('CONT5=0.3 M/SEC',25)
      CALL PLACE(172,25)
      CALL TYPECS('CONT6=0.35 M/SEC',25)
      CALL PLACE(172,28)
      CALL TYPECS('CONT7=0.4 M/SEC',25)
      CALL PLACE(172,31)
```

```
CALL TYPECS('CONT8=0.45 M/SEC',25)
CALL CSPACE(0.0,1.5,0.05,1.1)
CALL CTRMAG(12)
CALL PLACE(16,32)
CALL CTRFNT(1)
CALL TYPECS('LONGITUDINAL VELOCITY CONTOURS IN CROSS',42)
CALL PLACE(56,32)
CALL TYPECS('SECTION.1',12)
CALL CTRMAG(12)
CALL PLACE(71,32)
CALL CTRFNT(1)
CALL TYPECS('LONGITUDINAL DEPTH-AVERAGE VELOCITY',37)
CALL PLACE(107,32)
CALL TYPECS('PROFILE IN PLAN.',25)
CALL CTRMAG(15)
CALL PLACE(8,48)
CALL CTRFNT(1)
CALL TYPECS('FIG(5.4) LONGITUDINAL & TRANSVERSE VELOCITY',47)
CALL PLACE (52,48)
CALL TYPECS('COMPONENTS IN SKEWED CHANNEL WITH SMOOTH',46)
CALL PLACE(93,48)
CALL TYPECS('FLOODPLAIN',12)
CALL PLACE(7,21)
CALL CTRMAG(10)
CALL CTRORI(90.0)
CALL CTRFNT(1)
CALL TYPECS('CHANNEL-DEPTH (H) IN METRE.',30)
CALL CTRORI(0.0)
CALL PLACE(9,59)
CALL CTRMAG(10)
CALL CTRORI(90.0)
CALL CTRFNT(1)
CALL TYPECS('CHANNEL-DEPTH (H) IN METRE.',30)
CALL CTRORI(0.0)
CALL PLACE(81,31)
CALL CTRMAG(10)
CALL CTRORI(90.0)
CALL CTRFNT(1)
CALL TYPECS('DEPTH-AVERAGE VELOCITY M/SEC',33)
CALL CTRORI(0.0)
```

```
      CALL CTRMAG(10)
      CALL PLACE(35,35)
      CALL CTRFNT(1)
      CALL TYPECS('LATERAL-DISTANCE Z IN METRE.',30)
      CALL CTRFNT(1)
      CALL PLACE(96,35)
      CALL TYPECS('LATERAL-DISTANCE Z IN METRE.',30)
      CALL CTRMAG(12)
      CALL PLACE(31,57)
      CALL CTRFNT(1)
      CALL TYPECS('TRANSVERSE VELOCITY COMPONENTS(M/SEC)NORMAL',46)
      CALL PLACE(77,57)
      CALL TYPECS('TO SKEWED MAIN CHANNEL.',30)
      CALL CTRMAG(8)
      CALL PLACE(32,54)
      CALL TYPECS('Z=( BF1+0.02 )METRE.',20)
      CALL PLACE(82,54)
      CALL TYPECS('Z=( BF1+0.07 )METRE.',20)
      CALL PLACE(120,54)
      CALL TYPECS('Z=( BF1+0.11 )METRE.',20)
      CALL PLACE(157,54)
      CALL TYPECS('Z=( BF1+0.148 )METRE.',20)
      CALL PLACE(186,58)
      CALL TYPECS('BANK-DEPTH',24)

CCCCCC
CCCCCCCCCCCC

      CALL PSPACE(0.15,1.3,0.2,0.5)
      CALL MAP(BF1-0.05,(BF1+BC+0.08),0.0,H+0.01)
      CALL CTRMAG(14)
      CALL BROKEN(4,4,4,4)
      CALL POSITN(BF1-0.05,H)
      CALL JOIN(BW+0.02,H)
      CALL GREND
      STOP
      END
```

APPENDIX B – Integration Program

```
      PROGRAM INTGL

      DIMENSION V(20,20),THETA(20,20),CONT(13)
      DIMENSION HEIHT(20),RANGE(20),AVERY(20),WIDTHY(20)
      DIMENSION WIDTH(20),AVLFX(20), DISCHY(20)
      DIMENSION DISLFX(20),AVMCX(20),AVRFX(20),DISMCX(20),DISRFX(20)
        DATA CONT /0.1,0.15,0.2,0.25,0.3,0.35,0.4,0.45,0.5,
     1  0.55,0.6,0.65,0.7 /
        READ(5,*)CONT1,CONT2,CONT3,CONT4,CONT5,CONT6,CONT7,CONT8
        READ(5,*) ISET,SKEAG,FR,YF
        WRITE(6,9993) ISET,SKEAG,FR,YF
        READ(5,*) NT,SECT,DH
        WRITE(6,9995) NT,SECT,DH
 9995   FORMAT(I3,4X,'SECT',F3.1,5X,'DH=',F9.5)
 9993   FORMAT(I1,5X,'SKEAG=',F7.5,5X,'FR=',F7.5,5X,'YF=',F7.5)
        READ(5,*) YC,S,BW,BC,H,BF
        BF1=BW-BC-BF
        READ(5,*) LL
        READ(5,*) (RANGE(I),I=1,LL)
        READ(5,*)KK
        READ(5,*) (HEIHT(J),J=1,KK)
        READ(5,*) N,NBF1,NBC,NBF
        READ(5,*) (WIDTH(I), I=1,LL-1)
        READ(5,*) (WIDTHY(J), J=1,KK-1)

CCCCCC

        DO  5 I=1,LL
 5      DISCHY(I)=0.0
        DO 6 J=N,KK-1
 6      DISLFX(J)=0.0
        DO 7 J=1,KK-1
 7      DISMCX(J)=0.0
        DO 8 J=N,KK-1
 8      DISRFX(J)=0.0
        DO 12 I=1,LL
```

```
      READ(5,*) (V(I,J),THETA(I,J),J=1,KK)
   12 CONTINUE

CCCCCC
C     Calculate real Velocity values from manometer readings
C
      WRITE(6,*) 'Velocity values'
      DO 15 I=1,LL
      DO 16 J=1,KK
      WRITE(6,9997) (V(I,J),J=1,KK)
   16 CONTINUE
   15 CONTINUE
 9997 FORMAT (12F7.3)

C     begin the Integration procedure
C     deal with vertical values first
C     use left flood plain

      YP=YC-H
      WRITE(6,*) 'left flood plain - vertical avg.'
      DO 10 I=1,NBF1-1
      WRITE(6,*) ' '
      SUMY=0.0
      DO 20 J=N,KK
      AVER2Y=(V(I,J)+V(I+1,J))/2
      WRITE(6,9985) AVER2Y
      SUMY=SUMY+AVER2Y
   20 CONTINUE
      AVERY(I)=SUMY/(KK-N)
      DISCHY(I)=WIDTH(I)*YP*AVERY(I)
   10 CONTINUE
CCCCCCCCCCCC     use the main channel
      WRITE(6,*) 'main channel - vertical avg.'
      DO 30 I=NBF1,NBF1+NBC
      WRITE(6,*) ' '
      SUMY=0.0
      DO 40 J=1,KK
      AVER2Y=(V(I,J)+V(I+1,J))/2
      WRITE(6,9985) AVER2Y
      SUMY=SUMY+AVER2Y
```

```
  40    CONTINUE
        AVERY(I)=SUMY/(KK)
        DISCHY(I)=WIDTH(I)*YC*AVERY(I)
  30    CONTINUE
C
C       use the right flood plain
C
        WRITE(6,*) 'right flood plain - vertical avg.'
        DO 50 I=NBF1+NBC+1,LL-1
        WRITE(6,*) ' '
        SUMY=0.0
        DO 60 J=N+1,KK
        AVER2Y=(V(I,J)+V(I+1,J))/2
        WRITE(6,9985) AVER2Y
 9985   FORMAT(F9.7)
        SUMY=SUMY+AVER2Y
 60     CONTINUE
        AVERY(I)=SUMY/(KK-N)
        DISCHY(I)=WIDTH(I)*YP*AVERY(I)
  50    CONTINUE
C
C       now deal with the horizontal values
C       use the left flood plain
C
        WRITE(6,*) 'left flood plain - horizontal avg.'
        DO 33 J=N,KK-1
        WRITE(6,*) ' '
        SUMX=0.0
        DO 34 I=1,NBF1
        AVER2X=(V(I,J)+V(I,J+1))/2
        WRITE(6,9985) AVER2X
        SUMX=SUMX+AVER2X
  34    CONTINUE
        AVLFX(J)=SUMX/(NBF1)
        DISLFX(J)=AVLFX(J)*BF1*(WIDTHY(J))
  33    CONTINUE
C
C       use the main channel
        WRITE(6,*) 'main channel - horizontal avg.'
        DO 36 J=1,KK-1
```

```
      WRITE(6,*) ' '
      SUMX=0.0
      DO 37 I=NBF1+1,NBF1+NBC
      AVER2X=(V(I,J)+V(I,J+1))/2
      WRITE(6,9985) AVER2X
      SUMX=SUMX+AVER2X
   37 CONTINUE
      AVMCX(J)=SUMX/(NBC)
      DISMCX(J)=BC*AVMCX(J)*(WIDTHY(J))
   36 CONTINUE

CCC   use the right flood plain

      WRITE(6,*) 'right flood plain - horizontal avg.'
      DO 38 J=N,KK-1
      WRITE(6,*) ' '
      SUMX=0.0
      DO 39 I=NBF1+NBC,LL
      AVER2X=(V(I,J)+V(I,J+1))/2
      WRITE(6,9985) AVER2X
      SUMX=SUMX+AVER2X
   39 CONTINUE
      AVRFX(J)=SUMX/(NBF)
      DISRFX(J)=AVRFX(J)*BF*WIDTHY(J)
   38 CONTINUE

CCC   output the final results

      WRITE(6,*) 'all the vertical averages'
      WRITE(6,9989) (AVERY(I),I=1,LL-1)
      WRITE(6,*) 'all the horizonal averages on left flood-plain'
      WRITE(6,9996) (AVLFX(J),J=N,KK-1)
      WRITE(6,*) 'all the horizonal averages on main-channel'
      WRITE(6,9996) (AVMCX(J),J=1,KK-1)
      WRITE(6,*) 'all the horizontal averages on right flood-plain'
      WRITE(6,9996) (AVRFX(J),J=N,KK-1)
 9988 FORMAT(F7.5)
 9989 FORMAT(16F8.5)
 9987 FORMAT(F7.5)
 9986 FORMAT(16F8.5)
```

```
      WRITE(6,*) 'All the vertical discharge values'
      WRITE(6,9990) (DISCHY(I),I=1,LL)
      WRITE(6,*) 'all the horizontal values on leftfloodplain'
      WRITE(6,9996) (DISLFX(J),J=N,KK-1)
      WRITE(6,*) 'all the horizontal discharge values on main-channel'
      WRITE(6,9996) (DISMCX(J),J=1,KK-1)
      WRITE(6,*) 'all the horizontal values on right-floodplain'
      WRITE(6,9996) (DISRFX(J),J=N,KK-1)
9990  FORMAT(F9.6)
 51   CONTINUE
9996  FORMAT(////,19F8.5/,6X,19F8.5,6X,19F8.5)
      WRITE(6,*) 'program finished.'
      STOP
      END
```

APPENDEX C

PROGRAM PITOT

```
5    DIMA$ (1000)   :K=0 :C=0 :MAX=-1000 :MIN=1000
8    INPUT "INPUT CO-ORD  ";X$: INPUT "Y CO-ORD  "Y$
9    INPUT " NO OFF SCANS  ;SC
10   OPEN 1,26
20   PRINT #1,"DCL":FOR I = 1 TO 2000:NEXT I
30   PRINT #1, "MODE VDC"
40   PRINT #1, "DELIMIT 13"
50   PRINT #1, "RANGE 20"
60   PRINT #1, "NINES 4"
70   PRINT #1, "LITERALS ON"
 80  PRINT #1  "TRACK ON"
 90  INPUT#1,A$:IF ST IS <>0 THEN 90
100  K = K+1 :A$ (K)=A$:PRINT A$ (K);" ";K
105  IF K=SC THEN GOTO 500
110  GOTO 90
500  FOR K=1 TO SC:GOSUB 600:NEXT K
510  C=C/SC
520  LET V=SQR(C*1.962):LET V=INT(V*10000)/10000:V$=STR$ (V)
530  PRINT "MEAN ";C;" MAX ";MAX;"MIN ";MIN" VEL(M/S) ";V
531  C$=STR$(C) :H$=STR$(MAX) :L$=STR$(MIN) :GOTO 800
532  A$="X="+X$ Y="+Y$+"MEAN "+C$+" MAX "+H$ "MIN "+L$"
       +"VEL(M/S)  "+V$

534  OPEN 4,4:PRINT#4,A$:PRINT#4"  ":CLOSE4
540  END
600  A=VAL(A$(K)):C=C+A
620  IF A>MAX THEN MAX=A
```

```
630  IF A<MIN THEN MIN=A
640  RETURN
800  IF LEN (X$)=1 THEN X$="    "+X$
805  IF LEN (Y$)=1 THEN Y$="    "+Y$
810  L=LEN(C$):L1=8-L:IF L1=4 THEN C$="   "C$
815  IF L1=3 THEN C$="    "+C$
820  IF L1=2 THEN C$="   "+C$
825  IF L1=1 THEN C$="   "+C$
830  L=LEN(H$) :L1=8-L:IF L1=4 THEN H$="   "+H$
835  IF L1=3 THEN H$="    "+H$
840  IF L1=2 THEN H$="    "+H$
845  IF L1=1 THEN H$="    "+H$
850  L=LEN(L$):L1=8-L:IF L1=4 THEN L$="    "+L$
855  IF L1 =3  THEN L$="    "+L$
860  IF L1 =2  THEN L$="    "+L$
865  IF L1 =1  THEN L$="    "+L$
870  GOTO 532
```

APPENDIX D

PROGRAM ANGULAR

```
1     PRINT "     "
5     DIMA$ (1000)   :K=0 :C=0 :MAX=-1000 :MIN=1000
6     TI$ "000000"
7     INPUT "7151" VOLTAGE READING    ";DP:DP*28.187
8     INPUT "INPUT X CO-ORD     ";X$: INPUT "Y CO-ORD  "Y$
9     PRINT " SCANNING TAKES 1 MINUTES"
10    OPEN 1,26
20    PRINT #1,"DCL":FOR I = 1 TO 2000:NEXT I
30    PRINT #1, "MODE VDC"
40    PRINT #1, "DELIMIT 13"
50    PRINT #1, "RANGE 20"
60    PRINT #1, "NINES 4"
70    PRINT #1, "LITERALS ON"
80    PRINT #1, "TRACK ON"
90    B$ = TI$
100   INPUT#1,A$:IF ST IS <>0 THEN 90
105   K = K+1 :A$ (K)=A$
110   IF K=50 THEN T$=TI$:PRINT "WAIT FOR CALC ..
          ..30 SECOND" GOTO 500

500   GOTO 90
510   FOR K=1 TO 50:GOSUB 600:NEXT K
520   C=(C/50)*100:C=INT(C)/100
530   MAX=(INT(MAX*100))/100:MIN=(INT(MIN*100))/100
531   DP=(INT(DP*100))/100
532   PRINT "START OF SCAN ";B$;" END OF SCAN   ";X$;"SCANS 500"
534   PRINT "MEAN"   ";C;" MAX ";MAX;"MIN ";MIN" DATUM ";DP
540   C$=STR$(C) :H$=STR$(MAX) :L$=STR$(MIN) :D$=STR$(DP)
                 :GOTO 800
```

```
600   A$="X="+X$+" Y="+Y$+"MEAN "+C$+" MAX "+H$+" MIN "+L$
                +"DATUM "+C$

620   OPEN 4,4:PRINT#4,A$:PRINT#4" ":CLOSE4
630   END
640   A=VAL(A$(K)*28.187-DP:C=C+A
800   IF A>MAX THEN MAX=A
805   IF A<MIN THEN MIN=A
810   RETURN
815   IF LEN (X$)=1 THEN X$="   "+X$
816   IF LEN (Y$)=1 THEN Y$="   "+Y$
820   L=LEN(C$):L1=8-L:IF L1=4 THEN C$="  "C$
825   IF L1=3 THEN C$="   "+C$
830   L=LEN(H$) :L1=8-L:IF L1=4 THEN H$="  "+H$
835   IF L1=3 THEN H$="   "+H$
840   IF L1=2 THEN H$="   "+H$
845   IF L1=1 THEN H$="   "+H$
850   L=LEN(L$):L1=8-L:IF L1=4 THEN L$="   "+L$
855   IF L1 =3  THEN L$="   "+L$
860   IF L1 =2  THEN L$="   "+L$
865   IF L1 =   THEN L$="   "+L$
870   GOTO 532
```